Dipl.-Ing. Dr.techn. Martin Steinberger

Analysis and Design of Networked Feedback Loops: A packet-based Approach

Habilitation Thesis

Institute of Automation and Control
Graz University of Technology
Head: Univ.-Prof. Dipl.-Ing. Dr.techn. Martin Horn

Graz, July 2021

Dedicated to
Stefanie, Georg and Klemens,
my parents and Peter

Abstract

The scientific field of Networked Control plays a more and more important role in control engineering. The conventional wired connections between the plant and the controller are replaced by (wireless) communication networks to enable novel control architectures. This is especially important, e.g., if the plant and hence the actuators and sensors are spatially distributed as it is the case in large factories. But also low-level feedback loops where, for example, the sensors are placed on rotating parts are possible applications for Networked Control Systems (NCS).

The main challenge in such feedback loops is to design controllers and perform a stability analysis in the presence of network imperfections such as time-varying delays of the transmitted packets. The present work thus contributes to tackle this field of research.

First, the modeling and simulation of NCS is considered, where special emphasis is placed on the fact, that each transmitted data packet experiences an individual delay in communication channels. This packetized character is often either neglected or not explicitly incorporated in existing approaches, although it might have a significant impact on the closed loop performance.

Based on that, different techniques are proposed for NCS that depend on a trade-off between achievable properties and the assumptions made for the considered networked connections. This means that, for example, a buffering mechanism is used in one approach to mitigate the effect of time-varying delays. Consequently, the introduced conservatism with respect to the network allows to fully exploit the properties of sliding mode techniques to get robust controllers that might also be spatially distributed over the network.

The other extreme case treated in this work is given by NCS with networked channels, where arbitrary but bounded time-varying packet delays can occur. Thus, the actual packet skipping, packet dropping and hold mechanisms at the receiver side play important roles for the stability of the closed loop system. Different criteria for packetized NCS are proposed that allow to prove the stability under the presence of time-varying packet delays and uncertainties in the plant model description.

The third setup constitutes an intermediate case between the previously mentioned cases, where the assumptions are less strict than in the case with arbitrarily varying packet delays. Adaptive control approaches are proposed for such situations in which, e.g., the delays depend on the current task classes in the communication links.

In summary, this work sheds light on effects caused by time-varying packet delays in networked systems and proposes novel methods for the robust stability analysis and controller design of packetized feedback loops. The presented techniques allow to further push the technology towards robust and reliable networked systems.

Kurzfassung

Das Forschungsgebiet der vernetzten Regelung erlangt einen immer größeren Stellenwert in der Regelungstechnik. Konventionelle verdrahtete Verbindungen zwischen Regelstrecke und Regler werden hierbei durch (drahtlose) Netzwerkverbindungen ersetzt, um neuartige Regelkreis-Architekturen zu ermöglichen. Dies ist beispielsweise für Strecken mit örtlich verteilten Sensoren und Aktuatoren, wie in großen Produktionsstraßen, wichtig. Es bietet aber auch neue Einsatzmöglichkeiten in unterlagerten Regelkreisen, in denen zum Beispiel die Sensoren an rotierenden Teilen angebracht sind.

Die größten Herausforderungen stellen der Reglerentwurf und die Stabilitätsanalyse unter Berücksichtigung der Unzulänglichkeiten von Netzwerkverbindungen dar. Die in dieser Arbeit vorgestellten Verfahren dienen vor allem der Berücksichtigung von zeitlich veränderlichen Verzögerungen (Totzeiten) einzelner übertragener Datenpakete.

Zuerst wird die Modellierung und Simulation vernetzter Regelkreise betrachtet, wobei besonders auf die paketbasierte Datenübertragung Wert gelegt wird, wie sie in realen Netzwerken vorkommt. In existierenden Ansätzen wird der paketbasierte Charakter oft vernachlässigt oder nicht explizit berücksichtigt, obwohl er einen erheblichen Einfluss auf den Regelkreis haben kann.

Aufbauend darauf werden verschiedene Methoden für vernetzte Regelkreise entwickelt. Ausschlaggebend ist dabei immer eine Abwägung zwischen den Annahmen über das Netzwerk und den, durch die Regelung, erreichbaren Eigenschaften. Beispielsweise wird bei einem vorgestellten Ansatz ein Pufferungs-Mechanismus verwendet, um die Effekte durch zeitlich veränderliche Verzögerungen zu verringern. Durch diese Erweiterung können, wie in der Arbeit gezeigt, Sliding Mode Methoden zum Entwurf robuster Regelkreise verwendet werden und zusätzlich die Regler auch örtlich über das Netzwerk verteilt sein.

In einem anderen betrachteten Extremfall können in den Netzwerkverbindungen beliebige, aber beschränkte zeitliche Veränderungen der Verzögerungen auftreten. In diesem Fall spielen die implementierten Mechanismen zur Auswahl und/oder zum Verwerfen der Pakete auf Empfängerseite eine wichtige Rolle im Regelkreis. Verschiedene neuartige Kriterien erlauben einen Stabilitätsbeweis für den vernetzten Regelkreis unter Berücksichtigung des paketbasierten Charakters der Netzwerkverbindung und Unsicherheiten in der mathematischen Streckenbeschreibung.

Zusätzlich wird eine weitere Konfiguration eines vernetzen Regelkreises betrachtet, die - bezüglich der Annahmen über das Netzwerk und der erreichbaren Eigenschaften - zwischen den zuvor behandelten Fällen liegt. Für Netzwerke in denen die Verzögerungszeiten von der aktuellen Task-Klasse abhängen können, werden adaptive Regelungsmethoden vorgeschlagen.

Somit erlaubt die vorliegende Arbeit eine Betrachtung von vernetzten Regelkreisen mit paketbasierten Datenübertragungen. Es werden neue Methoden zur robusten Stabilitätsanalyse sowie zum Reglerentwurf vorgestellt, die einen weiteren Schritt in Richtung zuverlässiger, robuster, vernetzter Systeme ermöglichen.

Contents

Notation

$\mathbb{N}$	set of natural numbers including zero
$\mathbb{R}$	set of real numbers
$\mathbb{R}_+$	set of non-negative real numbers
$\mathbb{R}^{\alpha \times \beta}$	set of real matrices with α rows and β columns
$0_{\alpha \times \beta}$	zero matrix with α rows and β columns
I_α	identity matrix with α rows and columns
(y_k)	sequence $(y_0, y_1, y_2, \ldots)$. One element is written as y_k using the iteration index $k \in \mathbb{N}$.
$\lvert\lvert(y_k)\rvert\rvert_2$	2-norm of sequence (y_k)
$\mathcal{Z}\left\{(y_k)\right\}$	z-transformation of sequence (y_k)
$G(z)$	discrete-time transfer function
$\lvert\lvert G(z)\rvert\rvert_\infty$	infinity norm of $G(z)$. Maximal amplitude of the Bode magnitude plot corresponding to $G(z)$ evaluated for $z = e^{j\omega h}$, frequencies $\omega \in [0, \pi/h)$ and sampling interval h.
$\lfloor \alpha \rfloor$	floor operator; largest integer smaller than α
$\lceil \alpha \rceil$	ceil operator; smallest integer larger than α
$\lvert\lvert A\rvert\rvert_F$	Frobenius norm of matrix A
$\rho(A)$	spectral radius of matrix A
$\mathcal{R}(A)$	right nullspace of matrix A
$A \prec 0$	matrix $A = A^{\mathrm{T}}$ is negative definite
$A \preceq 0$	matrix $A = A^{\mathrm{T}}$ is negative semi-definite
$\operatorname{diag}(A, B)$	diagonal matrix composed of elements A and B in the main diagonal. The resulting matrix is in block diagonal form if the arguments are matrices.

Chapter 1

Introduction

In classical control, the systems to be controlled - also referred to as plants - are linked to sensors, actuators and controllers via fixed wired connections. Over the last decades this rigid feedback loop has been replaced by more flexible structures, so-called networked control systems.

In Networked Control Systems (NCS), plants are controlled over a (shared) communication medium. Figure 1.1 shows an example of such a feedback loop, where the measured states $x(t) \in \mathbb{R}^n$ of the continuous-time plant are sampled (S) using a constant sampling interval h such that $x_k = x(kh)$ for all $k \geq 0$. The measured and sampled state vectors x_k are sent in separate data packets from a transmitter at the sensor side (T^{S}) to a receiver at the controller side (R^{C}). The controller provides actuating signals that are forwarded from the transmitter at the controller (T^{C}) to the receiver (R^{A}) at the actuator side of the plant. A zero-order hold block (H) converts the arriving sequence of packets into a continuous-time actuation signal $u(t)$ that is actually applied to the plant. The sample element S and the hold element H have to work in a synchronized fashion. Each data packet j experiences an individual packet delay between sensor and controller τ_j^{sc} and controller and actuator τ_j^{ca} due to the used communication network, see Figure 1.1.

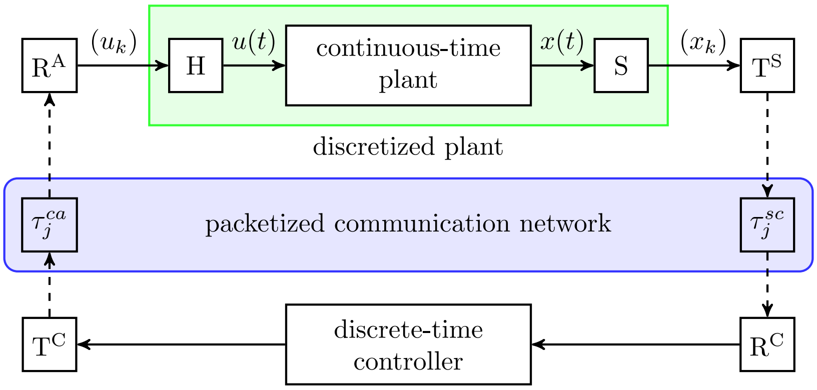

R^{A}
(u_k)
H
$u(t)$
continuous-time plant
$x(t)$
S
(x_k)
T^{S}
discretized plant
τ_j^{ca}
packetized communication network
τ_j^{sc}
T^{C}
discrete-time controller
R^{C}

Figure 1.1: Networked feedback loop with a packetized communication network, hold element H and sampling element S. Transmitters T and receivers R are used at the controller as well as at the actuator and sensor side of the plant.

The networked structure of the feedback loop offers a huge variety of new possibilities. NCS can be used in low level control loops where, e.g., the sensors are mounted on rotating parts or for the supervisory control of, e.g., paper mills or large chemical plants, where a large number of sensor and actuators are spatially distributed over long distances. If, for example, multi-hop wireless networks are utilized one can reduce the wiring effort and increase the flexibility to add and replace components of the infrastructure without drastically changing the control architecture. It is also possible to keep sensor and actuator nodes simple and exploit central (or distributed) controller nodes with high computational power.

All these nice possibilities are traded for new challenges related to the controller design and stability analysis. The most important ones are effects due to time-varying packet delays and packet losses in the transmission channels. Also the power and communication constraints may play an important role in NCS, since it might not always be possible, e.g., for a sensor to transmit the data at any time instant resulting in an increased packet delay. In addition, the question of the used protocol has to be addressed. Either protocols with reduced overhead as, for example, the User Datagram Protocol (UDP) [Pos81] or more dependable protocols like WirelessHART for industrial wireless networks [SXLC15] can be used. This choice also affects the characteristics of packet losses and transmission delays.

Extensive overviews of important aspects in NCS are provided in [PEF$^+$18, ZSWY17, HvdW10, GC10, HNX07] and the references therein. A more detailed discussion of the state of the art that is relevant for this work is presented in Section 1.2 before the main contributions of this work are described briefly in Section 1.3. In the subsequent section, a motivating example of reduced complexity is use to show that the effects of time-varying packet delays and different network protocols might have a strong impact on the closed feedback loop and, thus, have to be considered in the controller design and stability analysis in NCS.

1.1 A motivating Example

Consider an unstable, single-input single-output, continuous-time plant with a constant delay and transfer function [SH20]

$$P(s) = \frac{0.1}{20s-1}e^{-5s}\,. \tag{1.1}$$

A discrete-time representation of $P(s)$ is given by

$$P(z) = \frac{\mathcal{Z}\big\{(y_k)\big\}}{\mathcal{Z}\big\{(u_k)\big\}} = \hat{P}(z)z^{-\hat{d}} = \frac{0.0051271}{z-1.051}z^{-5}\,, \tag{1.2}$$

where the input sequence and output sequence are symbolized by (u_k) and (y_k), respectively and the constant sampling interval is set to $h = 1\,s$. Relation $\mathcal{Z}\big\{(y_k)\big\}$ represents the z-transform of sequence (y_k). Transfer function $P(z)$ consists of a delay-free part $\hat{P}(z)$ and a constant nominal delay equal to $\hat{d} = 5$ sampling steps. The goal is to design a controller that allows to track a reference sequence (r_k) despite the time delay in the plant, see Figure 1.2.

A classical approach for the controller design of stable plants with constant time delays was originally proposed by O. Smith [Smi59]. It consists of a copy of the plant model that is used in parallel to the real world plant (green block in Figure 1.3) to generate an error signal that is added to the feedback of a nominal control loop consisting of

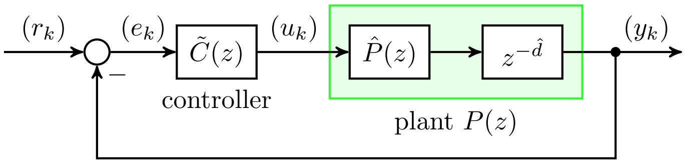

Figure 1.2: Unity feedback loop with a linear controller $\tilde{C}(z)$, nominal plant $\hat{P}(z)$ and a nominal delay of $\hat{d}$ time steps.

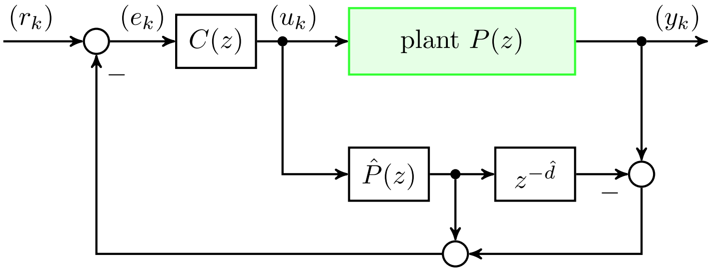

Figure 1.3: Classical Smith predictor structure.

a nominal controller $C(z)$ and the nominal, delay-free plant model $\hat{P}(z)$ as shown in Figure 1.3. However, this classical Smith predictor structure can only be utilized for stable plants, as explained in detail in Appendix A.

Several extensions of the classical predictor as in Figure 1.3 exist in literature as, for example, in [NRC09] that introduces a filtered Smith predictor to robustly stabilize uncertain unstable plants subject to constant time delays. A specific choice of the introduced transfer functions $H(z)$ and $F(z)$ allows to achieve an internally stable [DFT09] feedback loop as detailed in Appendix A. Figure 1.4 depicts the structure of

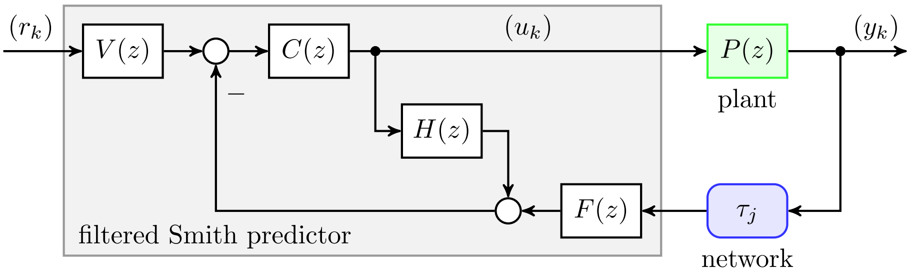

Figure 1.4: Filtered Smith predictor structure.

the resulting feedback loop, where, in contrast to [NRC09], an additional networked induced packet delay τ_j (blue block) is present in the transmission of output sequence (y_k). This delay is set to zero, i.e. $\tau_j = 0$ for all packets j, for the first investigations but will be changed later on. Transfer function $H(z)$ is specified depending on the nominal plant and filter transfer function

$$\hat{P}(z) = \frac{\hat{\mu}(z)}{\hat{\nu}(z)} \qquad \text{and} \qquad F(z) = \frac{\mu_F(z)}{\nu_F(z)} \tag{1.3}$$

and the nominal delay $\hat{d}$ such that

$$H(z) = \hat{P}(z)\left(1 - z^{-\hat{d}}F(z)\right) = \frac{\hat{\mu}(z)\left(z^{\hat{d}}\nu_F(z) - \mu_F(z)\right)}{z^{\hat{d}}\hat{\nu}(z)\nu_F(z)} \tag{1.4}$$

is fulfilled. Since the plant has unstable poles, one chooses

$$z^{\hat{d}}\nu_F(z) - \mu_F(z) = 0\ , \qquad \forall z \quad \big| \quad \hat{\nu}(z) = 0 \quad \wedge \quad |z| \geq 1 \tag{1.5}$$

to get a stable $H(z)$. The zeros of $\nu_F(z)$ can, e.g., be fixed at the same positions $z = \lambda$ with $0 \leq \lambda < 1$. In [NRC09] it is shown that one can also design (1.4) to compensate for stable but "too slow" poles of $\hat{P}(z)$. Parameter λ is a tuning parameter to balance the disturbance rejection against the robustness to uncertain plant information. The use of $H(z)$ as designed in (1.4), (1.5) and filter transfer function (1.3) leads to an internally stable feedback loop shown in Figure 1.4. See Appendix A for a more detailed explanation.

For the example plant model in (1.2), a nominal controller $C(z)$ is designed by algebraic synthesis [Che06, FPW97], where the poles of the nominal, delay-free closed loop system are assigned to $p_1 = p_2 = 0.95$. Additionally, the controller should be able to compensate for constant disturbances and therefore includes an integral action. This results in

$$C(z) = \frac{29.504(z - 0.9835)}{z - 1}\ , \tag{1.6}$$

which is used together with a prefilter transfer function

$$V(z) = \frac{0.16527(z - 0.9)}{z - 0.9835} \tag{1.7}$$

to decrease the overshoot for step responses of the feedback loop shown in Figure 1.4. The corresponding step responses for the case with and without prefilter are shown in Figure 1.5. Due to $V(z)$, the nominal design causes no overshoot and a reduced actuating signal u_k. The filter transfer function for the given example is selected as

$$F(z) = \frac{1.561(z - 0.968)}{z - 0.95}\ , \tag{1.8}$$

see Appendix A for details.

Often, the considered structure is also used in scenarios, where the nominal delay is not precisely known or changes, e.g., due to additional time delays introduced in NCS. For example, the authors of [BJ18] proposed to use an adaptive Smith predictor approach in that sense that a classical Smith predictor is used but the nominal plant delay is roughly estimated online and used in the predictor. Surprisingly, the effect of time-varying delays is not explicitly taken into account in the approach and no stability analysis is presented. However, already the simple example presented in this section will show that the time-varying packet delays of the transmitted data packets have to be taken into account for the stability analysis.

To see this, we first introduce additional constant packet delays $\tau_j \neq 0$ in the feedback loop depicted as blue block in Figure 1.4. The framework proposed in [STHJ20] and explained in detail in Chapter 3 is utilized for all subsequent simulations that include time-varying delays. Figure 1.6 show the resulting control signal u_k and output y_k for

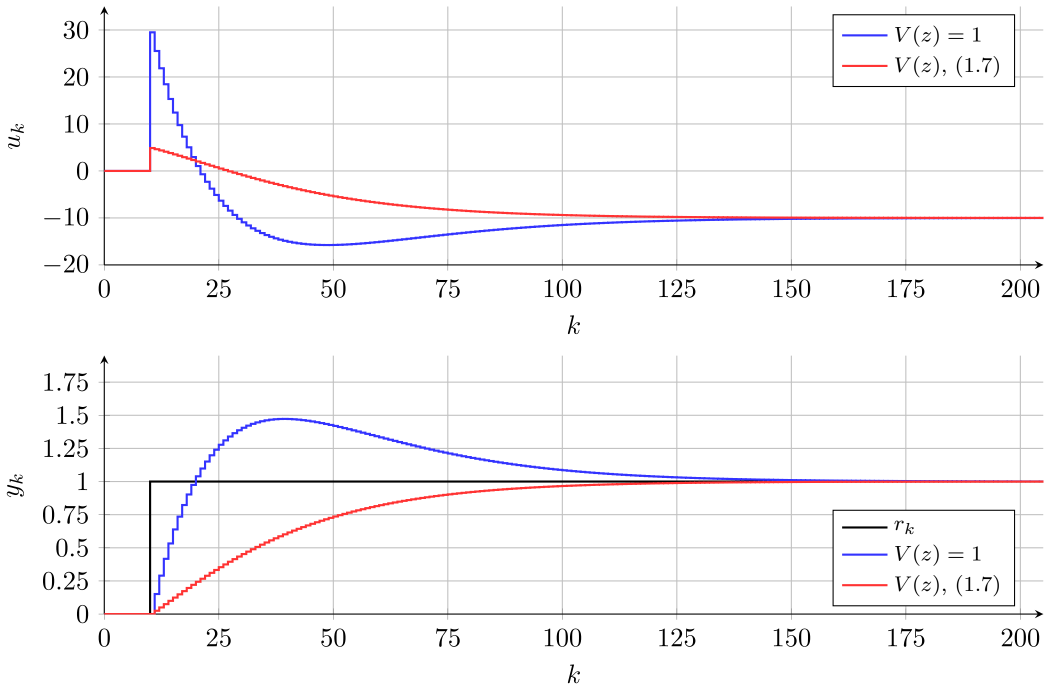

Figure 1.5: Example: Actuating signal u_k (top); reference r_k and output y_k (bottom) for the nominal design for the case without (blue) and with prefilter $V(z)$ (red), respectively.

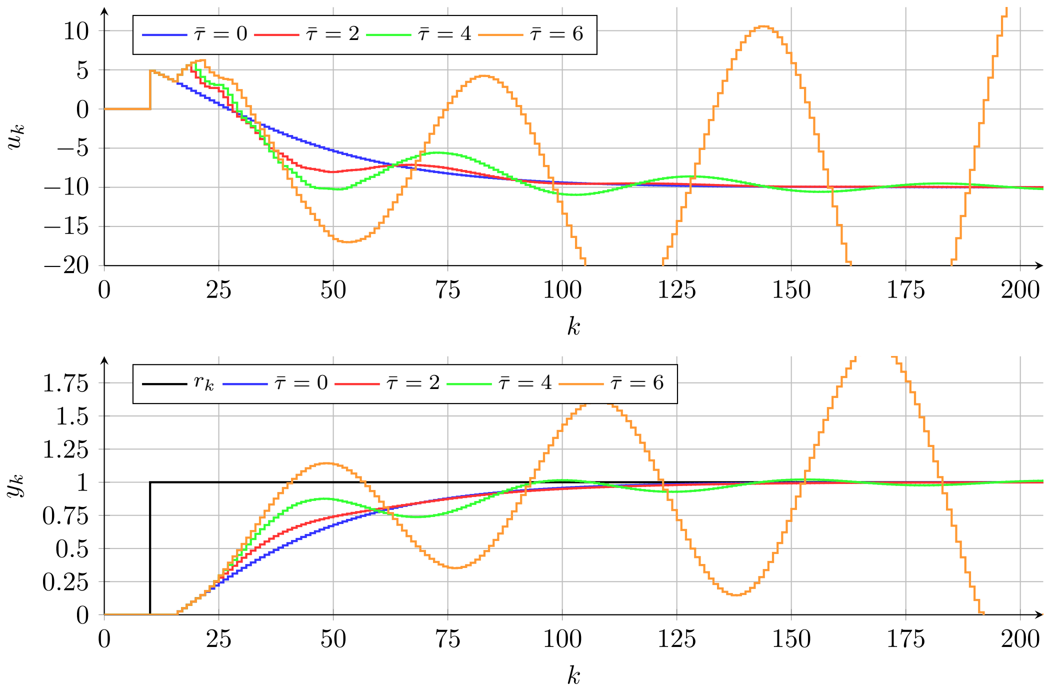

Figure 1.6: Example: Actuating signal u_k (top); reference r_k and output y_k (bottom) for different constant network delays $\tau_j = \bar{\tau}$ for all packets j.

different constant network delays, i.e. $\tau_j = \bar{\tau}$ for all packets j. As expected, the case $\bar{\tau} = 0$ yields a time-shifted version of the nominal, delay-free response (represented by the red curve in Figure 1.5) seen in blue in Figure 1.6. For $\bar{\tau} = 2$ and $\bar{\tau} = 4$, it is still possible to track the desires reference r_k. The closed loop stability is lost for constant network delays of $\bar{\tau} = 6$. It is now tempting to conclude that a packet delay of $\bar{\tau} = 4$ is the maximal admissible delay for the introduced network connection. This is supported by the simulation result in Figure 1.7, where random packet delays τ_j between $\underline{\tau} = 0$ and $\bar{\tau} = 4$ are present. Due to the time-varying delays, there are time instances, where

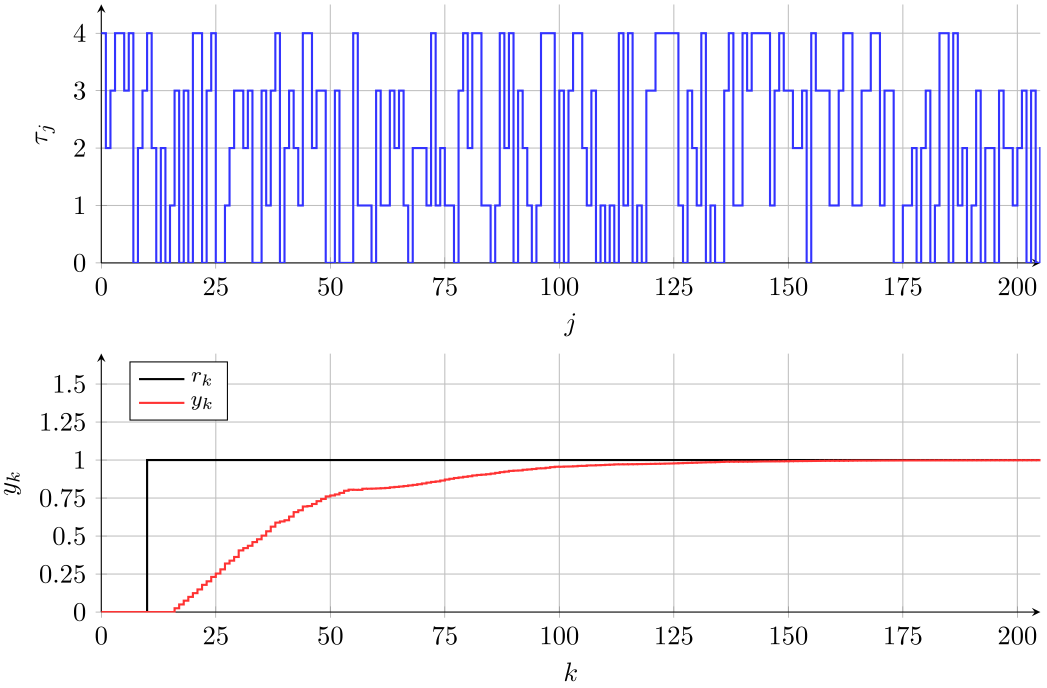

Figure 1.7: Example: Random delay pattern for $0 \leq \tau_j \leq 4$ (top); reference r_k and corresponding output y_k (bottom). The newest packet is selected if more packets are available at the same time instant.

no packet arrives and hence the packet received last is used. The most recent packet is selected if more packets arrive at the same time instant.

However, the situation changes whenever other protocols are used. If, for example, no packet synchronization nor packet numbering is used in low-cost realizations of NCS the actual packet selection and skipping mechanism may have a strong impact on the closed loop dynamics. This is exemplified in Figure 1.8 for the case of a repeating delay pattern with a minimum delay of $\underline{\tau} = 0$ and a maximum delay of $\bar{\tau} = 4$. The selection of the oldest packet leads to instability for the case with variable time delays, although stability can be achieved for constant delays of $\tau_j = 4$ for all j.

To conclude, it is evident that the stability of the closed loop system as well as the control performance significantly depends on the time-varying delays due to the network connections and the considered protocols, i.e. packet selection, skipping and hold mechanisms. However, this packetized nature of real-world network transmissions is often neglected in literature. It triggers the need of advanced control concepts that allow to consider the packetized communication networks in Figures 1.1 and 1.4. In addition, the network protocol has to be included in the stability analysis as pointed out in this work.

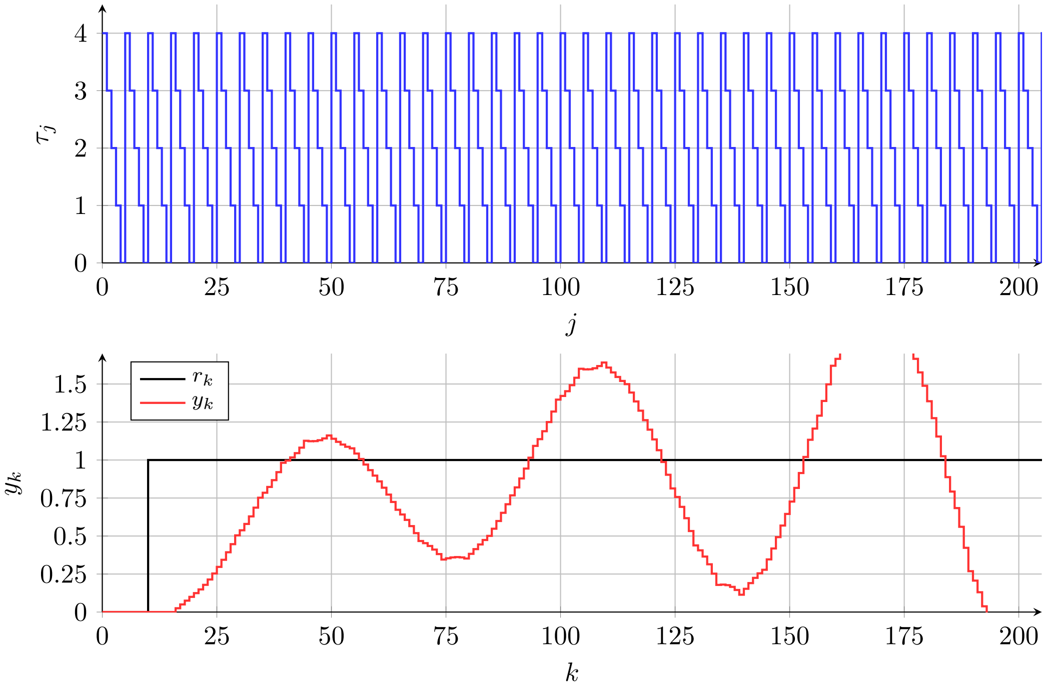

Figure 1.8: Example: Repeating delay pattern for $0 \leq \tau_j \leq 4$ (top); reference r_k and corresponding output y_k. The oldest packet is selected if more packets are available at the same time instant.

1.2 State of the Art

As indicated at the beginning of this chapter, the challenges in NCS are manifold. Reliable transmissions can be, for example, be achieved by using protocols like the Transmission Control Protocol (TCP) [Pos80]. Data losses are automatically detected and retransmissions of the data packets ensure that the data is received in the end. This might lead to larger variable time delays in the network. An alternative is to use the User Datagram Protocol (UDP) [Pos81] to reduce the overhead and the delay in NCS. However, reliable transmissions cannot be guaranteed in this case.

The example of the two mentioned protocols already shows that there is always a trade-off between many aspects in (possibly multi-hop wireless) networked control systems. Consequently, the literature is very rich as can, e.g., be seen by inspecting the survey papers [PEF^{+}18, ZSWY17, ZHY16, HvdW10, GC10, HNX07] and the references therein. Various methods and approaches for the analysis and controller design respecting the different network properties are available. The main issues are the effects of variable packet delays (communication delays) and packet dropouts (packet losses) in combination with packet discard mechanisms, e.g., to skip old packets if more recent data packets are available. Also the energy consumption plays a role in wireless NCS. One possible approach to account for this aspect is to reduce the power consumption by event-triggered approaches, where variable sampling/transmission intervals are utilized. This also allows to include the effect of communication constraints such as situations in which the transmitter is not allowed to send data at any time instant. Nevertheless, the consideration of time-varying delays is not straight forward for such approaches. In addition to the presented network imperfections, quantization effects might be of interest for the realization of low-cost network connections.

For example, [PEF$^+$18] is more focused on protocols and first steps towards a co-design of the transmission network and the controller; [ZSWY17] presents an overview of input delay approach and methods based on switched systems. Network based filtering, as, e.g., the estimation of state variable over networks subject to imperfections, is described in [ZHY16].

It is important to note that this section does not provide a complete overview of available methods. There is always a trade-off between the complexity of the considered network model and the corresponding control design approaches. Hence, only a small selection of methods and approaches are presented subsequently, which are of interest in the context of the techniques proposed in this work.

Stochastic Approaches

One major distinction between different existing approaches is in terms of the assumptions on the delays and packet dropouts. Stochastic properties as delay distributions are the basis of, e.g., [PSH21, SSF$^+$07, XL07] and [Azi03].

The authors of [SSF$^+$07] provide an overview of the design and analysis of lossy networks where TCP- and UDP-like protocols, i.e. protocols with and without acknowledgment signals, are used. A Kalman filter in combination with a linear state controller is employed in the stochastic dropout setting. Packet losses with a specific packet dropping rate and its influence on the mean square stability are tackled in [Azi03]. In [XL07], a packet-loss dependent Lyapunov approach is proposed for different loss processes, e.g., represented by Markov models. An optimal control law for NCS is presented in [PSH21], where networks between the sensors and the controller as well as between the controller and the actuators are considered. Random delays and packet dropouts are modeled as independent Markov decision processes. Methods from stochastic optimal control are combined in [XJL12] with ideas from machine learning for unknown linear NCS with known probability distribution functions for the delays.

However, stochastic approaches are not the focus of the present work. Instead methods only assuming the boundedness of the time-varying delays and the subsequent number of packet dropouts as, e.g., in [HvdW10] are considered. Please note that although no delay distributions are assumed, the resulting network feedback loops do not represent deterministic settings since the delays are subject to not foreseen, and not influenceable changes, within given bounds.

Modeling and Simulation

Modeling the effects of delays and dropouts is one crucial aspect in NCS. As pointed out in [HvdW10], there are in principle three different approaches:

(a) In the discrete-time approach, a discretized continuous-time plant that is linked via sample and hold elements to a transmitter and receiver is considered. Consequently, linear systems are used in most of the works because they allow for an exact discretization. For nonlinear systems, more sophisticated discretization methods have to be utilized.

(b) The continuous-time approach (or emulation approach) rests on the design and analysis of a continuous-time controller in closed loop with a continuous-time plant in the absence of network effects. A stability analysis then allows to derive conditions, e.g., for the maximal allowable delay and the maximal allowable sampling and transmission interval. Hybrid system modeling is often applied to enable an analysis of the resulting properties of the networked loop.

(c) In the sampled-data approach, continuous-time plant models are used without any form of discretization. The stability analysis and controller design take into account the fact that, e.g., the control signal provided by a discrete-time controller can only be changed (updated) at specific sampling instances. The analysis is challenging and can be done, e.g., by different forms of the Lyapunov-Krasovskii functional approach.

In the present work, the discrete-time approach is followed. It allows to include the properties of the transmission channel in a nice way in the design and analysis. This is vital since real-word communication is discrete by nature in networked feedback loops. At the same time, it enables one to reduce the mathematical complexity and to include a bounded number of subsequent packet dropouts in the framework as, for example, shown in [vDHv10].

An important aspect that is directly linked to the modeling of a NCS is its simulation. State of the art simulation tools are, for example, TrueTime [Tru, CHL+03] and OMNeT++ [OMN]. They aim to include properties of the transmission channels based on implemented communication protocols and physical effect as, for example, fading channel effects and the actual locations of the network nodes. However, models that are employed for the analysis and design of NCS are usually not so detailed to render model-based approaches manageable. Often, simulation approaches using Matlab standard blocks [ZY12] and the Matlab toolbox TrueTime [CHL+03] are applied for the direct validation of derived stability criteria and design techniques. Especially Matlab standard blocks are the basis of lots of simulation examples since they provide the possibility to arbitrary define bounded time-varying channel delays. As it will be pointed out in Chapter 3, such simulations have to be carried while respecting the packetized nature of real transmission channels. This means that the individual packet delays that may, e.g., depend on the actually present network load and task priorities, have to be included in the simulation to avoid incorrect results.

Disordering and Reordering

In wireless multi-hop networks, packet disordering can occur. This means that packets containing older data are available at the receiver side after packets with more recent information have been received. Two possibilities to alleviate the effects of packet disordering are presented in [LZY+15] and [WZ18]. In the first paper, a packet reordering method is introduced such that a sufficient condition for the NCS to be exponentially stable can be stated. An alternative packet reordering mechanism, which makes use of the assumed Markovian delays, is proposed in [WZ18] for nonlinear networked systems with medium access constraints. Conditions based on Linear Matrix Inequalities (LMIs) can be stated as in [LZL18] to integrate packet disordering by using Markov jump systems in the analysis.

Smith Predictor Approaches

Various extensions of the original Smith predictor [Smi59] can be found in literature for NCS. For example, a version of a filtered Smith predictor is introduced for the robust stabilization of unstable plants with constant time delays in [NRC09] and extended in

[STNR16] to multivariable systems with individual constant time delays in the different output channels.

Smith predictors are also utilized in the context of NCS with variable time delays. The authors of [LH10] make use of the original Smith predictor and a PI-controller. The round trip time, i.e. the difference between the sending time at the sensor and the receive time at the actuator, is measured for a network with an Ethernet and Controller Area Network (CAN) connection. The measured delay is directly used as nominal delay in the predictor.

In [RMQF14], the mean value of an estimated network delay is utilized in a Smith predictor with PI-controller. Adaptive buffers avoid packet dropouts due to late arrivals and packet disordering. The average delay for successfully transmitted packets are employed in a Smith predictor for IEEE 802.15.4 wireless personal area networks in [GSRA16]. Similarly, the authors of [BJ18] apply the classical Smith predictor approach for an optical oven, where the feedback loop is closed via the internet and CAN connections. In all the previously mentioned papers, standard Smith predictors and average values for the time-varying delays are used in the networked context but no stability analysis is conducted.

A robust stability analysis of the filtered Smith predictor proposed in [NRC09] for time-varying delay processes is presented in [NRGG12]. Delay dependent Linear Matrix Inequality (LMI) conditions are used to prove the closed loop stability for the case with norm-bounded uncertainties. In [BSG17], polytopic over-approximation techniques and LMI conditions are utilized for the stability analysis of the standard Smith predictor. Nevertheless, the important aspect of packetized transmissions is not included in any of the referenced works. This aspect was already mentioned in the introduction and will be further addressed in subsequent chapters of this work.

Predictive Approaches

A natural way to handle time-varying delays and dropouts is given by predictive approaches as, e.g., in [ZMW19, QN11, Liu10, LMRC06] and [MLR05]. This is possible since the future actuating signals are calculated based on an internal plant model in the Model Predictive Control (MPC) framework. The entire predicted sequence of actuating signals can then be sent over a network to a receiver, which selects the most recent data out of the received packets depending on the actual time instant.

Generalized predictive control (GPC) is combined in [MLR05] with a modified Smith predictor to compensate for fixed delays in the feedback channel, i.e. between sensor and controller, and time-varying delays in the forward channel, i.e. between controller and actuator. In [LMRC06], analytical criteria are obtained for both fixed and random communication time delays. An application to a servo motor control system points out the main features of the proposed approach. An alternative way if followed in [Td06], where generalized predictive controller is extended by a minimum-effort estimator to deduce missing or delayed sensor data. The proposed control structure is implemented on a dual-axis hydraulic position system of an industrial fish-processing machine and allows to compensate for transmission delays.

An MPC based network controller is proposed in [QN11] for constrained nonlinear plants that are subject to disturbances. For a bounded number of consecutive packet dropouts, input-to-state stability is shown for a suitable choice of the controller parameters. The authors of [ZMW19] introduce a predictive approach for a NCS with quantizers using an event-driven strategy to compensate for delays in the forward and the backward channel. A proper design of the event generator at the sensor side allows to state sufficient stability conditions using LMIs.

As for the conventional MPC, it is easy to include constraints, e.g., of the inputs or states in the controller design. This advantage induces the need of more computational power to solve the online optimization problems involved.

Event-triggered Approaches

One way to reduce the energy consumption in wireless multi-hop networks is to reduce the operation time of the corresponding network nodes. A reduction of the number of data transmissions is possible by introducing event-triggered and self-triggered control approaches, see [HJT12] for an overview. The reduced network load should indirectly yield smaller time delays and fewer packet dropouts. Examples can, e.g., be found in [DH12] and [LL10]. Also the issue of scheduling can be tackled in an event-triggered framework as shown in [Tab07] to guarantee a predefined performance of the networked feedback loop. The stability of systems with aperiodic sampling is investigated in [HFO$^+$17].

Gain Scheduling

In [TC04], gain scheduling is used to modify the output of an existing controller (e.g. PI-controller) with respect to the current network traffic conditions. An estimator provides network parameters like the mean delay or the loss rate as a basis for the scheduling of the control parameters.

Gain scheduling state feedback integral controllers are designed in [LSCS11] where the control parameters depend on the round trip time. The controller calculates a set of control signals for different delays. This allows to formulate the feedback loop as a switched system with different outputs and use delay-dependent LMI conditions for the stability analysis. An optimization problem is formulated to calculate the controller gains within the stable region provided by the LMI conditions.

LMI-based Approaches

The theory of time delay systems (TDS) play an important role in networked control, see, e.g., [Ric03]. A nice introduction to time delay systems can be found in [Fri14]. It deals with retarded time delay systems, i.e. systems with delayed states in the differential equations, and with neural type time delay systems, where the delay is present in the highest state derivative with respect to time. As described in [Fri14], time delay systems can be represented by classical transport partial differential equations.

Since continuous-time time delay systems are infinite dimensional, generalizations of the classical Lyapunov-based stability analysis are necessary. Lyapunov functionals are used in the Krasovskii approach to take into account the initial state function of TDS. For example, the delay-induced stability of second-order systems is presented in [FS16] with the resulting LMI conditions that are found via a model transformation-based approach.

An alternative technique is the Razumikhin approach, where Lyapunov functions are employed instead of Lyapunov functionals as in the Krasovskii approach. Consequently, the time derivative of the Lyapunov function and an additional Razumikhin condition can be checked in an easier way. However, the results are often more conservative [Fri14]. In the Lyapunov-Krasovskii as well as the Lyapunov-Razumikhin approach one makes extensive use of LMI conditions that might be delay independent or delay dependent. Because delay-independent conditions are usually limited to either slowly varying delays or stable systems, delay dependent criteria have been proposed that prevent such limitations.

The key for such methods are different model transformations such as, e.g., in [KR99] that are exploited in the analysis. The authors of [GN01] showed that these model transformations lead to conservative results. An improvement of the approaches is possible by using the descriptor model transformation proposed in [Fri01]. For example, [FS03] make use of the Krasovskii method to analyze TDS with fast varying delays.

Both the Lyapunov-Krasovskii and the Lyapunov-Razumikhin method are also available for discrete-time delay systems. The discrete-time nature enables one to use state augmentation techniques for the finite dimensional TDS. Again, delay independent and delay dependent LMI conditions can be formulated for the discrete-time case [Fri14]. It is shown in the following chapters of the present work that it is quite challenging to include effects due to the packetized nature of real-world data transmissions within the analysis when using this framework. Nevertheless, techniques based on LMI conditions are widespread in literature and offer a lot of nice possibilities in the context of NCS.

An alternative path to follow is the time-delay approach to sampled-data systems, where a continuous-time plant receives an updated piece-wise constant input signal whenever new data arrives via the network. Usually, old packets are skipped whenever new data is available. The analysis is based on a formulation of the closed loop system with a piecewise continuous time-varying delay, see [Fri14] and references therein for more details.

Additional examples of LMI-based approaches are [LFH12, LF12] and [Liu10]. The controller design for TDS using linear quadratic regulators and H_∞ approaches are presented, e.g., in [Fri14]. An approach using over-approximation techniques is proposed in [CHvdW$^+$10] to deal with time-varying network delays. This work will form the basis of the nominal controller design in Chapter 4.

Adaptive Approaches

For the case with constant or slowly varying time delays, approaches from adaptive control [GS84, AW08, NA12] can be used, see also [Tao14] for an overview of adaptive approaches for multivariable systems. In [ACK19, ASP20], adaptive methods are used in the context of event-triggered networked control. The output regulation of linear systems with known input time delays is presented in [GJ18]. Bounded but unknown delays in the states can be handled, e.g., using the adaptive approach in [LLL15].

For unknown time delays, [ASP20] introduces a technique for continuous-time systems by employing a reduction approach, where the assumptions on the input delay are very restrictive. Less restrictive assumptions can be used in the work of [TTY18] that suggests to use a multi-model approach with a set of adaptive controllers that are selected depending on a certain performance index.

Sliding Mode Approaches

Since each control architecture is, in the end, dedicated to operate under real-world conditions, the effect of perturbations should be considered also in the context of networked systems. One nice way to incorporate disturbance rejection properties in a robust controller design is given by sliding mode techniques [SEFL15, ES98, Utk92]. Usually, only the worst case bound of the perturbation or its time-derivative is given whereas the actual time-varying perturbation is unknown. Different steps towards networked sliding mode control were followed in the last years.

Event-triggered sliding mode approaches are proposed in [IFM17, BB16] and [IF16]. A smart sensor acts as an event generator that uses information about the states or the sliding variable. Depending on the actual realization, nominal models can be used to calculate the control signal at the actuator side if no new information is transmitted via the network. No guarantees on the stability for the case with time delays can be given because network imperfections are not directly included in the analysis. An experimental evaluation of event-triggered sliding mode control strategies can be found in [SSGH20].

In [XZL$^+$10], robust adaptive sliding mode techniques are considered for discrete-time delay systems where the states as well as the delayed state are present in the systems description. Sufficient LMI conditions are derived for the case of norm bounded disturbances and uncertainties. Also continuous-time sliding mode methods are introduced for systems with input and output or only output delays to track the desired output [COC14, LZS09] or to estimate the present time delay [DLR$^+$20].

A buffering approach is incorporated in combination with discrete-time sliding mode techniques by the author of this work in [LSR$^+$17] and extended in [LSH$^+$18] by introducing different switching and non-switching reaching laws. This allows to compensate the time-varying delays via the buffer and fully exploit the advantages of sliding mode techniques with respect to the rejection of external perturbations in NCS. This forms the basis for the presented networked sliding mode approaches presented in Chapter 4.

Adaptive sliding mode techniques are shown to be very effective to accomplish a desired behavior of the feedback loop as, e.g., presented in [HLD97, CHCL03]. Various formulations for continuous-time systems exist, where different adaptation strategies are followed. For example, the gains are only increased in [MNTF16], increased and decreased [BLP$^+$13] or derived through the equivalent control signal in [UP13, ES16] and [OCH16]. Model Reference Adaptive Control (MRAC) is utilized in [ORF18]; adaptive methods based on barrier functions [OFLH18] are presented for continuous-time systems with an uncertain bound of the perturbations.

Interestingly, only a few discrete-time versions are available although real-world NCS sent separate packets at discrete instances. The ideal notions of continuous-time sliding modes are replaced by quasi-sliding modes in this discrete-time setting, where a sliding variable is driven to a band around zero in a finite number of steps. This is also referred to as discrete-time sliding mode, see [CB16, Bar98, BFU95]. Design techniques based on discrete-time MRAC and a gain adaptation using the equivalent control can be, e.g., be found in [BFU95] and [LO98] respectively. Adaptive sliding mode designs resting on transfer function models are, for example, published in [Cha97].

An alternative, computationally cheap, adaptive approach for network control systems with unknown transmission delays is presented in Chapter 5.

Additional Methods for the Stability Analysis

As mentioned above, the stability analysis of NCS may be based on continuous-time, discrete-time or hybrid formulations, see also [HvdW10]. Different LMI-based approaches can be used to show the stability of discrete-time formulations as, e.g., in [SGF15, LG11] and papers mentioned above in this section. One major aspect in such stability criteria is to reduce the number of variables in the LMIs to allow computationally cheaper computations while proving stability for an admissible transmission delay that is as large as possible.

An alternative way for the stability analysis of linear systems subject to time delays was introduced in [KL04], where the small gain theorem [Vid02, Sas99] was applied to feedback loops with variable time delays. This has the benefit that the calculations are computationally inexpensive and can be done in a straight forward way.

However, the packetized character of networked transmissions is usually not included in the analysis. Appropriate modeling and simulation techniques as well as stability criteria are needed to incorporate packet transmission in NCS as shown in Chapters 2, 3, 6, 7 and 8.

1.3 Contributions of this Habilitation Thesis

The focus of this work is the controller design and the stability analysis for packetized networked systems as depicted in Figure 1.9.

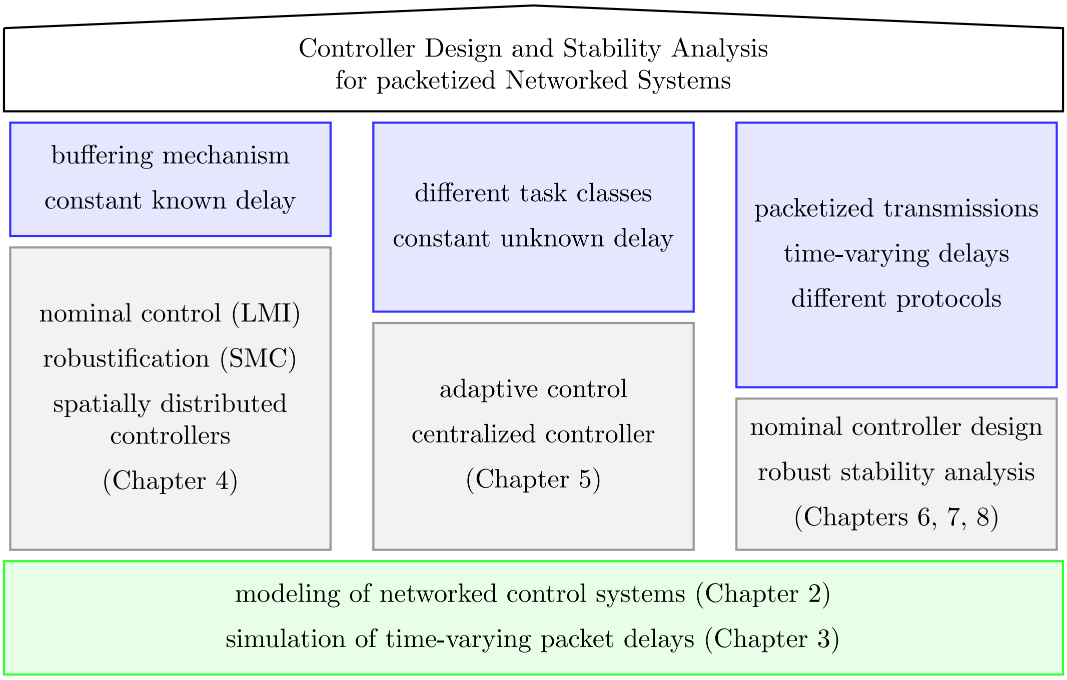

Figure 1.9: Properties of the considered networks (blue) and corresponding controllers (gray) for three different approaches.

Chapters 2 and 3 deal with the modeling of NCS and the accurate simulation of transmission channels with time-varying delays, respectively. Hence, they form the basis for all subsequent chapters and are adopted from

[STHJ20] M. Steinberger, M. Tranninger, M. Horn, K.H. Johansson: *How to Simulate Networked Control Systems with Variable Time Delays?*, IFAC PapersOnLine 53 (2), pp. 3098-3103, 2020 to some extent. Modeling techniques are reviewed and commented with respect to packetized NCS. Techniques to accurately simulate networked control systems with bounded time-varying delays are presented to link delays in transmission channels to individual packets. In addition, effects like packet disordering that may occur in wireless multi-hop networks can be included. Simulation examples underline the features of the proposed approach and illustrate why other simulation and modeling approaches may fail.

Chapters 4 to 8 present different approaches for NCS where a trade-off between the assumed properties of the network connections and the achievable properties of the control system is made, see Figure 1.9. This means that, e.g., the use of a buffering mechanism in Chapter 4 reduces the complexity using time-varying delays in the network (see blue boxes), and make more sophisticated control approaches possible as visualized in Figure 1.9 using gray boxes. This makes it possible to design even spatially distributed controllers that are robust with respect to external perturbations. At the same time, it introduces some conservatism due to the involved buffering.

In the case of packetized transmissions subject to time-varying delays and different protocols, the network model is much more sophisticated. Hence, the variability in the network is interchanged with a more challenging controller design. A nominal controller design, i.e. a design for a nominal constant time delay, is used together with an additional robust stability analysis to prove the admissible range for the time-varying packet delays as shown in Chapters 6 to 8. The middle column in Figure 1.9 represents an intermediate case, where the assumptions on the network are less restrictive compared to Chapters 6 to 8 and makes it possible to adopt adaptive control methods.

In Chapter 4, the robust control of buffered networked systems is covered as published in

[LSH$^+$18] J. Ludwiger, M. Steinberger, M. Horn, G. Kubin, A. Ferrara: *Discrete Time Sliding Mode Control Strategies for Buffered Networked Systems*, IEEE Conference on Decision and Control, pp. 6735-6740, 2018

[LSH19] J. Ludwiger, M. Steinberger, M. Horn: *Spatially Distributed Networked Sliding Mode Control*, IEEE Control Systems Letters, 3, pp. 972-977, 2019

and preliminary works in [LSR$^+$17] and [LRSH19]. The main contribution is an approach that robustly stabilizes a networked feedback loop subject to external perturbations. The effect of time-varying packet delays is compensated via a buffering mechanism that converts the delay into a time-invariant one. On the basis of that, a combination of a nominal controller (designed using LMI conditions) and an additional discrete-time integral sliding mode part is proposed. The algorithm is designed such that the m controllers of the considered multivariable system with m inputs can be implemented in a spatially distributed fashion, without any communication links between them. Matched perturbations, i.e. disturbances that can be, in principle, be compensated, are rejected by the algorithm.

Adaptive control approaches are considered in Chapter 5, which are adopted from

[SHF19] M. Steinberger, M. Horn, A. Ferrara: *Discrete-time Model Reference Adaptive Sliding Mode Control for Systems in State-Space Representation*, IEEE Conference on Decision and Control, pp. 6007-6012, 2019.

[SHF21] M. Steinberger, M. Horn, A. Ferrara: *Adaptive Control of Multivariable Networked Systems with uncertain Time Delays*, IEEE Transactions on Automatic Control, early access, DOI: 10.1109/TAC.2021.3083563, 2021.

Based on the idea of model reference adaptive control, adaptive laws are derived for uncertain linear multivariable networked systems in state-space form. They allow to control a plant over a network connection with unknown but (piece-wise) constant[1] delays. This enables one to reduce the conservativeness, which is usually present whenever the time delays are unknown. Two different approaches are presented and compared to a non-adaptive solution. In contrast to Chapter 4, the controller has to be implemented in a centralized way.

Chapters 6, 7 and 8 rest on the following publications:

[SH21b] M. Steinberger, M. Horn: *A Stability Criterion for Networked Control Systems with Packetized Transmissions*, IEEE Control System Letters, 5 (3), pp. 911-916, 2021

[SH20] M. Steinberger, M. Horn: *From classical to Networked Control: Retrofitting the Concept of Smith Predictors*, arXiv:2010.05486, submitted for journal publication

[SH21a] M. Steinberger, M. Horn: *A Less-Conservative Stability Criterion for Networked Control Systems with Time-Varying Packet Delays*, arXiv:2103.16514, revised version submitted for journal publication

Several stability criteria are proposed for networked feedback loops with packetized transmissions characterized by bounded time-varying packet delays. The plant, which is modeled by a transfer function, transmits its output through a network. A nominal controller design forms the basis to perform trajectory tracking despite an uncertain time-varying communication.

Different protocols, i.e. different packet selection and packet skipping mechanisms, are included in the stability analysis. The derived criteria can easily be checked in frequency domain without adopting any computationally expensive algorithms. An extension to uncertain plant models facilitate a robust stability analysis with respect to time-varying packet delays and uncertainties in the model description. The presented approaches are exemplified for a NCS consisting of a filtered Smith predictor, and an unstable plant model and a packetized transmission network.

The analysis points out clearly, that the packetized character of the network has to be considered explicitly, as it is evident in the modeling and simulation of networked systems, as presented Chapters 2 and 3. In Chapter 8, the criteria are improved to yield less conservative results. This is possible by exploiting a splitting of the considered feedback loop into a causal and an acausal part for the purpose of analysis. In addition, conditions for the optimal choice of a nominal time delay (out of a bounded interval) are given, which can be utilized for the nominal controller design. Consequently, it is shown that one can prove the closed loop stability with respect to a larger maximal admissible variable time delay.

[1] From a practical point of view, it is also possible to utilize this approach for sufficiently slowly varying delays.

Hence, the present work provides different control approaches that are robust with respect to uncertain network delays. The complexity and capabilities of the different approaches strongly depend in the properties (and thus also assumptions) about the transmission network. This is also highlighted in Chapter 9, where an outlook is given.

Chapter 2

Modeling of packetized Networked Control Systems

This chapter presents all steps to model networked control systems that are relevant for the subsequent chapters. The modeling takes into account the packetized transmission channels and is adopted from [STHJ20, SHF21, SH20] and [SH21a].

It forms the basis for the later introduced techniques for the analysis and controller design of networked feedback loops. First, basic assumptions concerning the plant and the transmission channels, including the considered protocols, are stated. Then, a mathematical model for the combination of a plant and a network is shown. Variable time delays and packet dropouts imply that the corresponding system matrices are unknown and time-varying.

2.1 Considered Network Feedback Loop

The feedback loop consists of a continuous-time plant, i.e. a real-world system to be manipulated, and a discrete-time controller that are connected via two transmission channels as shown in Figure 2.1, where the transmitter and receiver blocks at the plant and the controller sides (see T and R in Figure 1.1) are omitted.

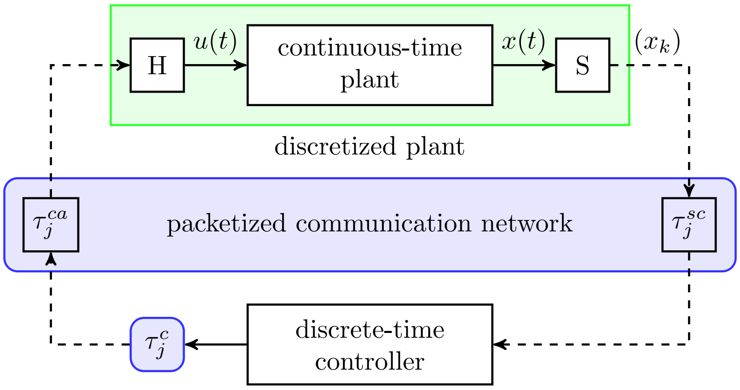

Figure 2.1: Networked control system with a plant that is connected to a controller via a packetized communication network.

The plant is modeled as a linear time-invariant multivariable system

$$\frac{\mathrm{d}x}{\mathrm{d}t} = \tilde{A}x(t) + \tilde{B}u(t) \tag{2.1}$$

with state vector $x(t) = \begin{bmatrix} x_1(t) & x_2(t) & \dots & x_n(t) \end{bmatrix}^{\mathrm{T}} \in \mathbb{R}^n$, input vector $u(t) = \begin{bmatrix} u_1(t) & u_2(t) & \dots & u_m(t) \end{bmatrix}^{\mathrm{T}} \in \mathbb{R}^m$ and system matrices $\tilde{A} \in \mathbb{R}^{n \times n}$ and $\tilde{B} \in \mathbb{R}^{n \times m}$. All states $x(t)$ are sampled with a constant sampling period h at the transmitter on the plant side (S in Figure 2.1) resulting in a sequence (x_k) with elements $x_k = x(kh)$ for $k \in \mathbb{N}$. The transmission of the j^{th} data packet containing x_k towards the receiver on the controller side is subject to a time-varying delay symbolized by τ_j^{sc}.

The discrete-time state feedback controller acts in an event-triggered fashion, i.e. it determines the control signal as soon as a new packet arrives, where τ_j^c represents the corresponding calculation time. A transmitter on the controller side sends packet j with a time-varying delay τ_j^{ca} to the receiver at the plant side. A zero-order-hold mechanism is employed at the actuator (receiver) side of the plant to obtain a continuous control signal $u(t)$, see Figure 2.1.

> **Assumption 2.1** (Plant). *The pair $(\tilde{A}, \tilde{B})$ in* (2.1) *is controllable. Sampling is done with a non-pathological sampling period h in the sense of [KHN63] so that the full rank of the input matrix as well as the controllability are preserved during discretization.*

Details about non-pathological sampling are presented, e.g., in [KHN63] and [Lud20].

> **Assumption 2.2** (Network delays). *The data is transmitted in separate packets j that experience an individual bounded packet delay τ_j^N such that*
>
> $$0 \le \underline{\tau}^N \le \tau_j^N \le \bar{\tau}^N \tag{2.2}$$
>
> *with $\underline{\tau}^N, \tau_j^N, \bar{\tau}^N \in \mathbb{R}_+$ for the sensor-to-controller and controller-to-actuator delay, i.e. $N \in \{sc, ca\}$.*

Please note that there are no further assumptions on the delay distribution nor on the maximal admissible delay change rate between two subsequently sent packets. The upper bounds $\bar{\tau}^{sc}$ and $\bar{\tau}^{ca}$ may be larger than the sampling period h, which is sometimes referred to as large delay case in literature. It is important to note that one distinguishes between packet index j and index k to be able to link delays to packets, i.e. τ_j is not the delay at a certain time k but the delay of a specific packet. This allows to also consider situations, where packets might take different routes between sender and receiver, e.g., depending on blocked paths or time-varying network traffic conditions and may arrive at the same time or out of order.

> **Assumption 2.3** (Computational delays). *The time for evaluating the control law in the controller is bounded such that*
>
> $$0 \le \underline{\tau}^c \le \tau_j^c \le \bar{\tau}^c \tag{2.3}$$
>
> *with $\underline{\tau}^c, \tau_j^c, \bar{\tau}^c \in \mathbb{R}_+$.*

This computational delay is very small for the algorithms presented in this work because they are designed also considering this aspect. However, τ_j^c can be relevant if, for example, model predictive controllers are utilized in the networked feedback loop.

2.2 Simplifications

In Figure 2.1, three independent delays are considered in the sensor-to-controller and controller-to-actuator path. However, there are situations in which one can lump the individual delays to one single delay

$$\tau_j = \tau_j^{sc} + \tau_j^{c} + \tau_j^{ca} \tag{2.4}$$

for the analysis as shown in Figure 2.2. This delay is often referred to as round trip time or round trip delay. To see the concrete assumptions that have to hold in this case, one considers a general formulation of a dynamic discrete-time controller that calculates the control signal u_k based on the state x_k and some of its previous values, i.e.

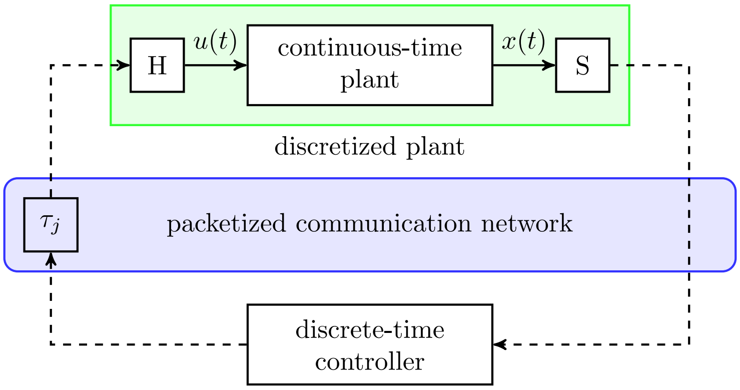

Figure 2.2: Feedback loop, where the network is described by one lumped time delay τ_j.

$$u_k = \mathcal{C}\left(x_k, x_{k-1}, x_{k-2}, \ldots\right) . \tag{2.5}$$

Control law (2.5) can only be evaluated if all necessary states $x_k, x_{k-1}, x_{k-2}, \ldots$ are available at the actual time, as explained, e.g., in [Lud20]. Figure 2.3 depicts the underlining configuration with three independent delays, where the notation $x|_t$ means that a packet containing x arrives at time t at the indicated position. Hence, the control law can only be applied whenever

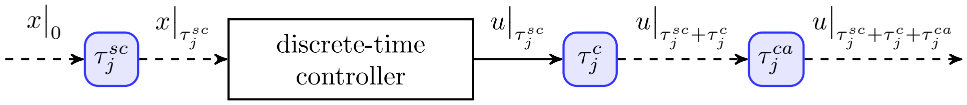

Figure 2.3: Three independent delays.

$$\tau_j^{sc} \geq \tau_{j-1}^{sc} - h \qquad \text{and so} \qquad \tau_{j-1}^{sc} - \tau_j^{sc} \leq h \tag{2.6}$$

hold for all packets j. In other words, packet j has to arrive not before packet $j-1$ at the controller side to not introduce an additional waiting delay. Control signal u related to packet j is then sent to the actuator with time delay $\tau_j^{sc} + \tau_j^{c}$ and experiences an additional delay of τ_j^{ca}. Consequently, Figure 2.3 is equivalent to Figure 2.4 if condition (2.6) is fulfilled because no overtaking packets can occur in the channel from the sensor to the controller.

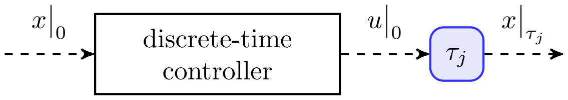

Figure 2.4: One lumped delay between controller and actuator.

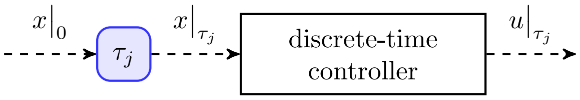

Figure 2.5: One lumped delay between sensor and controller.

An alternative situation is shown in Figure 2.5, where the three delays τ_j^{sc}, τ_j^{c} and τ_j^{ca} are lumped at the sensor side to τ_j. As a result, control law (2.5) can only be evaluated if condition (2.6) holds and the states that are delayed by τ_j have been received, which is ensured by condition

$$\tau_j \geq \tau_{j-1} - h \qquad \text{and so} \qquad \tau_{j-1} - \tau_j \leq h \tag{2.7}$$

for all packets j.

Please note that all three structures in Figures 2.3, 2.4 and 2.5 are equivalent for static controllers

$$u_k = \mathcal{C}\left(x_k\right) \tag{2.8}$$

since the control signal can be calculated immediately after packet arrival. Whenever the delays are lumped in the subsequent chapters, one combines them between the controller and the actuator to benefit from less restrictive conditions about the delays.

Assumption 2.4 (Lump delays at actuator side)**.** *At least one of the following two conditions holds to lump the delays in the channel between controller and actuator:*

(a) a dynamic control law (2.5) *is used and the sensor-to-controller delay fulfills* (2.6)*, i.e.* $\tau_j^{sc} \geq \tau_{j-1}^{sc} - h$.

(b) a static control law (2.8) *is used.*

Consequently, the following assumption holds for the simplified structure presented in Figure 2.4:

Assumption 2.5 (Round trip delay)**.** *The round trip delay* $\tau_j = \tau_j^{sc} + \tau_j^{c} + \tau_j^{ca}$ *of each individual packet* j *is bounded by*

$$0 \leq \underline{\tau} \leq \tau_j \leq \bar{\tau} \tag{2.9}$$

with $\underline{\tau}, \tau_j, \bar{\tau} \in \mathbb{R}_+$.

The violation of condition (2.6) yields situations, where overtaking of sent packets occurs. This non-trivial effect has to be explicitly taken into account in the stability analysis of the closed loop system as shown in Chapters 6 to 8.

2.3 Mathematical Model

In this section, a mathematical model is derived for the network structure presented in Figure 2.1 where Assumption 2.4 holds. Hence the network structure is equivalent to Figure 2.4 and the round trip delay is bounded as stated in Assumption 2.5. In addition, it is assumed that old packets are skipped, i.e. packets that are related to previously sampled values are skipped at the receiver side if more recent data packets are available, see [HvdW10] for more details. A formal definition of such a protocol is given in the subsequent section as protocol $\mathcal{P}_1$.

Two important entities are defined based on the upper bound $\bar{\tau}$ and the lower bound $\underline{\tau}$ as the largest integer smaller than $\underline{\tau}/h$ and the smallest integer larger than $\bar{\tau}/h$, i.e.

$$\underline{d} = \left\lfloor \frac{\underline{\tau}}{h} \right\rfloor \qquad \text{and} \qquad \bar{d} = \left\lceil \frac{\bar{\tau}}{h} \right\rceil . \tag{2.10}$$

Thus, $\underline{d}$ stands for the number of sampling instants, after which a transmitted packet can arrive in principle at the receiver (under-estimation of the minimum delay). Parameter $\bar{d}$ is the maximal number of sampling instances after which a transmitted packet has been arrived for sure at the receiver (over-estimation of the maximum delay).

A simple example of a scalar system

$$\frac{\mathrm{d}x}{\mathrm{d}t} = \tilde{a}x(t) + \tilde{b}u(t) \tag{2.11}$$

with $x \in \mathbb{R}$, $u \in \mathbb{R}$, $\tilde{a}, \tilde{b} \in \mathbb{R}$ and bounded packet delays $0 \leq \tau_j \leq 2h$ is considered to point out properties that are relevant to the modeling process. As a result, one gets $\underline{\tau} = 0$, $\bar{\tau} = 2h$ and so $\underline{d} = 0$ and $\bar{d} = 2$. Figures 2.6 and 2.7 depict all arriving patterns of (u_k) that can occur between two sampling steps s_k and $s_{k+1} = s_k + h$ for bounded packet delays $0 \leq \tau_{j-1} \leq 2h$ and $0 \leq \tau_j \leq 2h$.

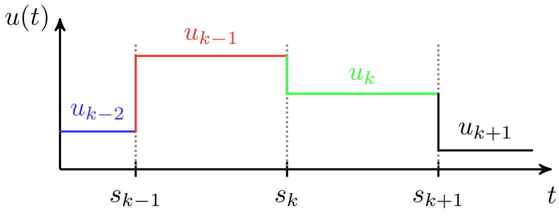

(a) Delay free case: $\tau_{j-1} = 0$ and $\tau_j = 0$.

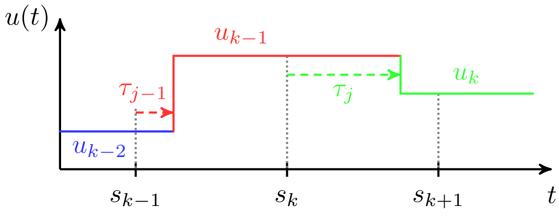

(b) Case $0 \leq \tau_{j-1} \leq h$ and $0 \leq \tau_j \leq h$.

Figure 2.6: Actually employed actuating signal $u(t)$ depending on different packet delays $0 \leq \tau_{j-1} \leq 2h$ and $0 \leq \tau_j \leq 2h$ (part 1).

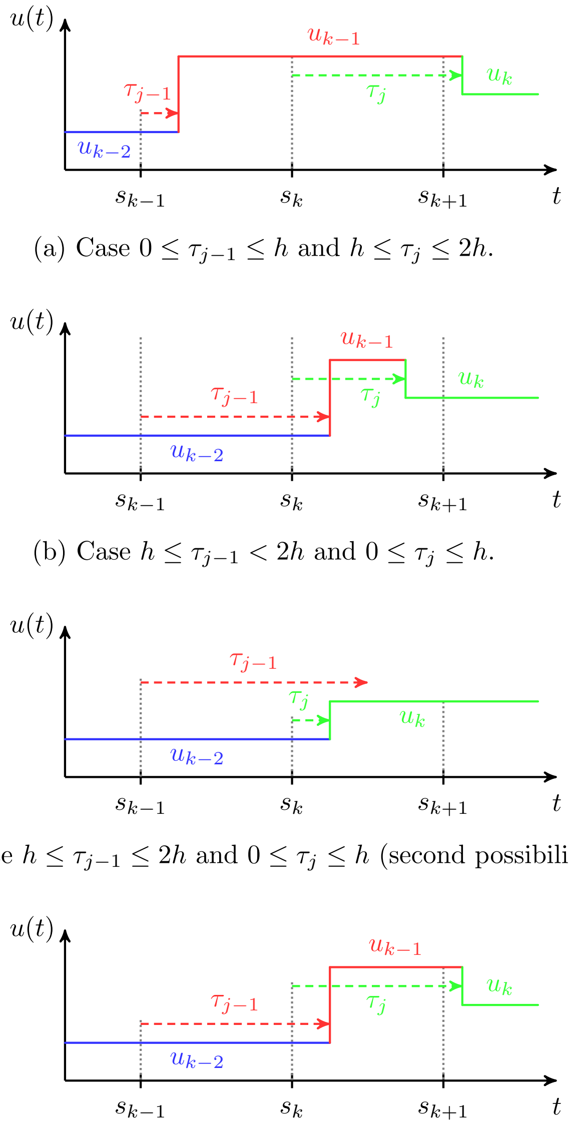

(a) Case $0 \leq \tau_{j-1} \leq h$ and $h \leq \tau_j \leq 2h$.

(b) Case $h \leq \tau_{j-1} < 2h$ and $0 \leq \tau_j \leq h$.

(c) Case $h \leq \tau_{j-1} \leq 2h$ and $0 \leq \tau_j \leq h$ (second possibility).

(d) Case $h \leq \tau_{j-1} \leq 2h$ and $h \leq \tau_j \leq 2h$.

Figure 2.7: Actually employed actuating signal $u(t)$ depending on different packet delays $0 \leq \tau_{j-1} \leq 2h$ and $0 \leq \tau_j \leq 2h$ (part 2).

Subplot 2.6a shows the delay-free case, whereas different packet delays τ_j and τ_{j-1} are used in the remaining subplots in Figures 2.6 and 2.7. There are cases, where only one u_{k-i}, $i \in \{0, 1, 2\}$ is present between s_k and s_{k+1}, see Figures 2.6a, 2.7a as well as 2.7c for $\tau_{j-1} = 2h$ and $\tau_j \geq h$. Figures 2.6b, 2.7c and 2.7d show situations, in which only one transition is visible between u_{k-1} to u_k, u_{k-2} to u_k and u_{k-2} to u_{k-1}, respectively. At maximum two changes can be present between two sampling instants as show in Figure 2.7b. Consequently, at maximum $\bar{d} - \underline{d} + 1 = 3$ packets containing u_k, u_{k-1} and u_{k-2} may be received. Out of order arrival as, e.g., u_{k-2}, u_k and u_{k-1} are not considered in the modeling since old packets are skipped as stated in the next section for protocol $\mathcal{P}_1$.

Figure 2.8 shows a zoom of Figure 2.7b for the derivation of the mathematical description. In the following, the solution of (2.11) at time instant $k + 1$ is calculated based

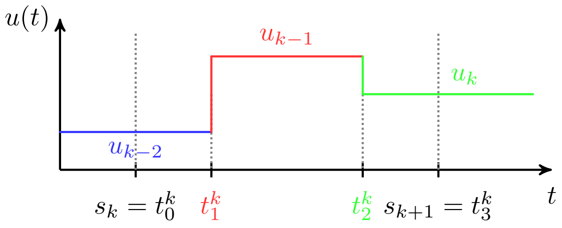

Figure 2.8: Zoom of Figure 2.7b for one sampling interval.

on the state vector x_k at time instant k and the input signal as in Figure 2.8. The linearity of the system allows one to write the solution as

$$x_{k+1} = e^{\tilde{a}h} x_k + \int_{t_0^k}^{t_1^k} e^{\tilde{a}(h-\nu)} \tilde{b} \, \mathrm{d}\nu \, u_{k-2} + \int_{t_1^k}^{t_2^k} e^{\tilde{a}(h-\nu)} \tilde{b} \, \mathrm{d}\nu \, u_{k-1} + \int_{t_2^k}^{t_3^k} e^{\tilde{a}(h-\nu)} \tilde{b} \, \mathrm{d}\nu \, u_k \tag{2.12}$$

and with a change of coordinates $\eta = h - \nu$ as

$$x_{k+1} = e^{\tilde{a}h} x_k + \underbrace{\int_{h-t_1^k}^{h-t_0^k=h} e^{\tilde{a}\eta} \tilde{b} \, \mathrm{d}\eta}_{m_0(\tau_j)} \, u_{k-2} + \underbrace{\int_{h-t_2^k}^{h-t_1^k} e^{\tilde{a}\eta} \tilde{b} \, \mathrm{d}\eta}_{m_1(\tau_j)} \, u_{k-1} + \underbrace{\int_{h-t_3^k=0}^{h-t_2^k} e^{\tilde{a}\eta} \tilde{b} \, \mathrm{d}\eta}_{m_2(\tau_j)} \, u_k \, , \tag{2.13}$$

where $t_0^k = 0$ and $t_3^k = h$ are used in addition. All integrals in (2.13) are functions of the time instances t_1^k and t_2^k, which depend on the actual packet delays τ_j for all relevant packets j. This is also emphasized by the notation $m_i(\tau_j)$ for $i \in \{0, 1, 2\}$.

After defining a new extended (lifted) state vector

$$\xi_k = \begin{bmatrix} x_k & u_{k-1} & u_{k-2} \end{bmatrix}^{\mathrm{T}} , \tag{2.14}$$

one can state an extended (lifted) state space model

$$\begin{bmatrix} x_{k+1} \\ u_k \\ u_{k-1} \end{bmatrix} \begin{bmatrix} e^{\tilde{a}h} & m_1(\tau_j) & m_0(\tau_j) \\ 0 & 0 & 0 \\ 0 & 1 & 0 \end{bmatrix} \begin{bmatrix} x_k \\ u_{k-1} \\ u_{k-2} \end{bmatrix} + \begin{bmatrix} m_2(\tau_j) \\ 1 \\ 0 \end{bmatrix} u_k \, , \tag{2.15}$$

which is a linear system

$$\xi_{k+1} = \mathcal{A} \xi_k + \mathcal{B} u_k \tag{2.16}$$

with a time-varying dynamic matrix $\mathcal{A}$ and input vector $\mathcal{B}$ as

$$\mathcal{A} = \begin{bmatrix} e^{\tilde{a}h} & m_1(\tau_j) & m_0(\tau_j) \\ 0 & 0 & 0 \\ 0 & 1 & 0 \end{bmatrix} \quad \text{and} \quad \mathcal{B} = \begin{bmatrix} m_2(\tau_j) \\ 1 \\ 0 \end{bmatrix} \tag{2.17}$$

that depend on the actual packet delays. Please note that there are only two independent time-varying parameters in (2.17) because

$$m_0(\tau_j) = \int_{h-t_1^k}^{h} e^{\tilde{a}\eta} \tilde{b} \, \mathrm{d}\eta = \int_0^h e^{\tilde{a}\eta} \tilde{b} \, \mathrm{d}\eta - \underbrace{\int_0^{h-t_2^k} e^{\tilde{a}\eta} \tilde{b} \, \mathrm{d}\eta}_{m_2(\tau_j)} - \underbrace{\int_{0-t_2^k}^{h-t_1^k} e^{\tilde{a}\eta} \tilde{b} \, \mathrm{d}\eta}_{m_1(\tau_j)} \tag{2.18}$$

holds and the first integral on the right hand side of (2.18) is a known constant. Parameters m_i for $i \in \{0, 1, 2\}$ can also be zero as can be seen, e.g., in Figure 2.7a, where $m_0(\tau_j) = 0$ as u_{k-1} does not arrive in the considered interval between s_k and s_{k+1} but before that.

The scalar case presented above is now generalized to multivariable dynamic systems as stated in (2.1) with $x \in \mathbb{R}^n$, $u \in \mathbb{R}^m$ and bounded packet delays $0 \leq \underline{\tau} \leq \tau_j \leq \bar{\tau}$ according to Assumption 2.5. Due to the definition of $\underline{d}$ and $\bar{d}$ in (2.10), the packet containing the oldest data $u_{k-\bar{d}}$ arrives for sure in the considered interval; the newest packet that might be received may contain $u_{k-\underline{d}}$. Consequently, at maximum $\bar{d} - \underline{d} + 1$ packets have to be considered as depicted in Figure 2.9. The number of arriving packets between s_k and s_{k+1} might be smaller if packets are received before or after this interval. In addition, out of order arrivals reduce the number of relevant packets due to the skipping mechanism for older packets. This yields the generalization of (2.13) to multivariable systems such that

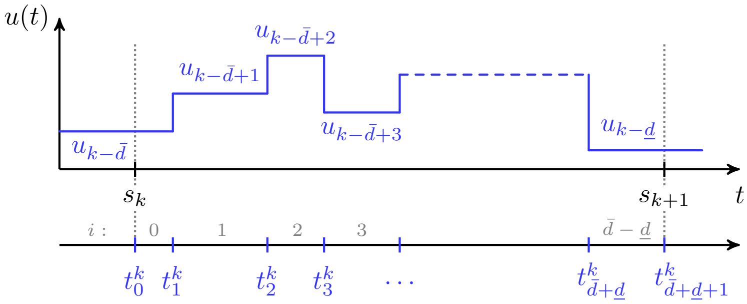

Figure 2.9: Maximal number of packets i that might arrive between sampling instants s_k and s_{k+1}.

$$\begin{aligned} x_{k+1} = e^{\tilde{A}h} x_k + \int_{h-t_1^k}^{h-t_0^k=h} e^{\tilde{A}\eta} \tilde{B} \,\mathrm{d}\eta \, u_{k-\bar{d}} + \int_{h-t_2^k}^{h-t_1^k} e^{\tilde{A}\eta} \tilde{B} \,\mathrm{d}\eta \, u_{k-\bar{d}+1} + \\ \ldots + \int_{h-t_{\bar{d}-\underline{d}}^k}^{h-t_{\bar{d}-\underline{d}-1}^k} \tilde{B} \,\mathrm{d}\eta \, u_{k-\underline{d}-1} + \int_{h-t_{\bar{d}-\underline{d}+1}^k=0}^{h-t_{\bar{d}-\underline{d}}^k} e^{\tilde{A}\eta} \tilde{B} \,\mathrm{d}\eta \, u_{k-\underline{d}} \end{aligned} \tag{2.19}$$

holds. Analogously to the scalar case, one can introduce matrices $M_i(\tau_j)$ depending on the unknown network delays τ_j (for all relevant packets j) as

$$M_i(\tau_j) = \begin{cases} \displaystyle\int_{h-t_{i+1}^k}^{h-t_i^k} e^{\tilde{A}\eta} \tilde{B} \,\mathrm{d}\eta & \text{for} \quad 0 \leq i \leq \bar{d} - \underline{d} \\ 0 & \text{for} \quad \bar{d} - \underline{d} < i \leq \bar{d} \end{cases} \tag{2.20}$$

and thus

$$\begin{aligned} x_{k+1} = e^{\tilde{A}h} x_k + M_0(\tau_j)\, u_{k-\bar{d}} + M_1(\tau_j)\, u_{k-\bar{d}+1} + \ldots + M_{\bar{d}-\underline{d}}(\tau_j)\, u_{k-\underline{d}} + \\ \ldots + M_{\bar{d}-1}(\tau_j)\, u_{k-1} + M_{\bar{d}}(\tau_j)\, u_k \,. \end{aligned} \tag{2.21}$$

Note that the most recent data packet contains $u_{k-\underline{d}}$ as shown in Figure 2.9. As a result, all M_i with $i \in \left\{\bar{d} - \underline{d} + 1, \bar{d} - \underline{d} + 2, \ldots, \bar{d} - 1, \bar{d}\right\}$ are equal to zero, i.e. u_k, u_{k+1} up to $u_{k-\underline{d}-1}$ does not play any role in the solution for the considered time interval.

The plant states and the inputs u_{k-1} to $u_{k-\bar{d}}$ are combined an extended (lifted) state vector

$$\xi_k = \begin{bmatrix} x_k^{\mathrm{T}} & u_{k-1}^{\mathrm{T}} & u_{k-2}^{\mathrm{T}} & \cdots & u_{k-\bar{d}}^{\mathrm{T}} \end{bmatrix}^{\mathrm{T}} \in \mathbb{R}^{n+m\bar{d}}. \tag{2.22}$$

Hence, a model of the sampled plant in combination with a lumped variable network delay shown in Figure 2.2 can be stated as

$$\xi_{k+1} = \mathcal{A}\xi_k + \mathcal{B}u_k \tag{2.23}$$

with matrices

$$\mathcal{A} = \begin{bmatrix} e^{\tilde{A}h} & M_{\bar{d}-1}(\tau_j) & M_{\bar{d}-2}(\tau_j) & \cdots & M_2(\tau_j) & M_1(\tau_j) & M_0(\tau_j) \\ 0 & 0 & 0 & \cdots & 0 & 0 & 0 \\ 0 & I_m & 0 & \cdots & 0 & 0 & 0 \\ 0 & 0 & I_m & \ddots & 0 & 0 & 0 \\ \vdots & \vdots & \ddots & \ddots & \ddots & \vdots & \vdots \\ 0 & 0 & 0 & \ddots & I_m & 0 & 0 \\ 0 & 0 & 0 & \cdots & 0 & I_m & 0 \end{bmatrix} \tag{2.24a}$$

and

$$\mathcal{B} = \begin{bmatrix} M_{\bar{d}}(\tau_j)^{\mathrm{T}} & I_m & 0 & 0 & \cdots & 0 & 0 \end{bmatrix}^{\mathrm{T}}. \tag{2.24b}$$

Constant I_m symbolizes the identity matrix with dimension m. System matrix $\mathcal{A} \in \mathbb{R}^{(n+m\bar{d})\times(n+m\bar{d})}$ and input matrix $\mathcal{B} \in \mathbb{R}^{(n+m\bar{d})\times m}$ are unknown because of the unknown network delay where only the bounds are known as stated in Assumption 2.5. Note that the matrix dimensions increase with the maximal admissible network delay $\bar{\tau}$ and thus with $\bar{d}$. At least in simulation, the packet arrival times t_i^k can be calculated as

$$\begin{aligned} t_i^k \quad = \quad \min\Bigg\{ & \max\Big\{0, \tau_{j+i-\bar{d}} - \sum_{\ell=k+i-\bar{d}}^{k-1} h\Big\}, \\ & \max\Big\{0, \tau_{j+i-\bar{d}+1} - \sum_{\ell=k+i-\bar{d}+1}^{k-1} h\Big\}, \\ & \qquad \vdots \\ & \max\Big\{0, \tau_{j-\underline{d}} - \sum_{\ell=k-\underline{d}}^{k-1} h\Big\},\ h\Bigg\} \end{aligned} \tag{2.25}$$

for $i \in \{0, 1, \ldots, \bar{d} - \underline{d} + 1\}$ with $0 = t_0^k \leq t_1^k \leq \ldots \leq t_{\bar{d}-\underline{d}}^k \leq t_{\bar{d}-\underline{d}+1}^k = h$, see [HvdW10] for details.

For the simple example (2.11) presented above with the corresponding Figures 2.6, 2.7, it follows that $\bar{d} = 2$, $\underline{d} = 0$, and consequently

$$t_i^k = \min\Bigg\{ \max\Big\{0, \tau_{j+i-2} - \sum_{\ell=k+i-2}^{k-1} h\Big\}, \tag{2.26}$$

$$\max\Big\{0, \tau_{j+i-1} - \sum_{\ell=k+i-1}^{k-1} h\Big\},$$

$$\max\Big\{0, \tau_{j+i}\Big\},\ h\Bigg\} \tag{2.27}$$

for $i \in \{0, 1, 2, 3\}$. This yields

$$t_0^k = \min\Big\{ \max\big\{0, \tau_{j-2} - 2h\big\}, \tag{2.28a}$$

$$\max\big\{0, \tau_{j-1} - h\big\},$$

$$\max\big\{0, \tau_j\big\},\ h\Big\} = 0$$

$$t_1^k = \min\Big\{ \max\big\{0, \tau_{j-1} - h\big\}, \tag{2.28b}$$

$$\max\big\{0, \tau_j\big\},\ h\Big\}$$

$$t_2^k = \min\Big\{ \max\big\{0, \tau_j\big\},\ h\Big\} \tag{2.28c}$$

$$t_3^k = \min\Big\{h\Big\} = h \tag{2.28d}$$

In principle, it is also possible to extend the presented mathematical description to NCS with time-varying sampling intervals h_k as explained in [HvdW10]. However, this is not relevant for the present work.

It is also possible to extend the formulation to include the effects of packet dropouts. The main idea [HvdW10] is to constrain the number of subsequent dropouts $\bar{\delta}$. Mathematically, this means that a variable m_j is introduced such that

$$m_j = \begin{cases} 0 & \text{if packet } j \text{ is successfully received} \\ 1 & \text{if packet } j \text{ is dropped} \end{cases} \tag{2.29}$$

and $\bar{\delta}$ is given by

$$\sum_{\ell=j-\bar{\delta}}^{j} m_\ell \leq \bar{\delta}\,. \tag{2.30}$$

For example, $\bar{\delta} = 2$ yields $m_{j-2} + m_{j-1} + m_j \leq 2$, which implies that at maximum two out of three subsequent packets might be dropped.

The maximum number of subsequent packet dropouts $\bar{\delta}$ acts as an additional time delay for the networked plant. Hence, $\bar{d}$ is replaced by $\bar{d} + \bar{\delta}$ in Figure 2.9 and relations (2.20) to (2.25).

2.4 Protocols

The main point to consider for the networked connections is, apart from of the bounded time-varying delay according to Assumption 2.2 and the computational delay as in Assumption 2.3, the packetized character of the transmitted sequences. Such sequences can represent states (x_k), actuating signals (u_k) but also output signals (y_k) for the case of output regulation treated in Chapters 6 to 8. Subsequently, only the case for the transmission of the states (x_k) as, e.g., in Figure 2.1 is considered.

In the following, the packetized nature of real communication channels is taken into account by including a network policy (protocol) consisting of specific packet selection, skipping and hold mechanisms in the analysis. This is done in a discrete-time framework for simplicity reasons to convey the main points. However, similar protocol definitions can also be done for continuous-time delays as in Assumption 2.2.

The packet delays can also take continuous values within the considered interval such that several packets may arrive between two sampling instants at the receiver side. However, they are associated with the next sampling instant by the discrete-time controller. Thus, only delays that are multiples of the sampling interval have to be considered in real-world implementations of the controller as well as for the actuator interfaces.

Assumption 2.6 (Discrete network delays)**.** *The samples of a sequence, as e.g. (x_k), are transmitted in separate packets j that experience an individual bounded packet delay $\tau_j^N h$ that is in integer multiple of the sampling interval h such that*

$$0 \leq \underline{\tau}^N \leq \tau_j^N \leq \bar{\tau}^N \tag{2.31}$$

with $\underline{\tau}^N, \tau_j^N, \bar{\tau}^N \in \mathbb{N}$.

Remark 2.7. Please note that (2.31) describes the relation between the respective integer multiples of the sampling interval. This yields packet delays $\tau_j^N h$, which are lower and upper bounded by $\underline{\tau}^N h$ and $\bar{\tau}^N h$ respectively.

Three different protocols are formally introduced in the following. A packet containing output sample x_k is sent at instant k. It is received at the controller at sampling instant

$$r^{(k)} \in \left\{k + \underline{\tau}^N, k + \underline{\tau}^N + 1, \dots, k + \bar{\tau}^N - 1, k + \bar{\tau}^N\right\} \tag{2.32}$$

depending on the actual packet delay τ_j^N. Since the maximal packet delay is bounded, the packet containing x_k reaches the receiver at the controller side at the latest at $r^{(k)} = k + \bar{\tau}^N$. The packet including x_{k+1} arrives at

$$r^{(k+1)} \in \left\{k + \underline{\tau}^N + 1, k + \underline{\tau}^N + 2, \dots, k + \bar{\tau}^N, k + \bar{\tau}^N + 1\right\}. \tag{2.33}$$

Consequently, the arrival instant of the packet containing $x_{k+\bar{\tau}^N}$ equals

$$r^{(k+\bar{\tau}^N)} \in \left\{k + \underline{\tau}^N + \bar{\tau}^N, k + \underline{\tau}^N + \bar{\tau}^N + 1, \dots, k + 2\bar{\tau}^N - 1, k + 2\bar{\tau}^N\right\}. \tag{2.34}$$

At instant $p = k + \bar{\tau}^N \in \mathbb{N}$, at most $\bar{\tau}^N - \underline{\tau}^N + 1$ packets may arrive that contain

$$\begin{aligned} &x_{k+\underline{\tau}^N} && \text{if} \quad r^{(k+\underline{\tau}^N)} = p\,, && \text{(2.35a)}\\ &x_{k+\underline{\tau}^N+1} && \text{if} \quad r^{(k+\underline{\tau}^N+1)} = p\,, && \text{(2.35b)}\\ &\quad\vdots && \qquad\vdots && \\ &x_{k+\bar{\tau}^N} && \text{if} \quad r^{(k+\bar{\tau}^N)} = p && \text{(2.35c)} \end{aligned}$$

Hence, the set of all received packets at instant p is

$$\mathcal{Y}(p) = \left\{ x_{k+i} \;\middle|\; r^{(k+i)} = p,\; i = \underline{\tau}^N, \underline{\tau}^N + 1, \ldots, \bar{\tau}^N \right\} \tag{2.36}$$

and the set of all indices of received samples is

$$\mathcal{I}(p) = \left\{ \kappa \;\middle|\; r^{(\kappa)} = p,\; \kappa = k + \underline{\tau}^N, k + \underline{\tau}^N + 1, \ldots, k + \bar{\tau}^N \right\}. \tag{2.37}$$

This allows one to define several protocols that differ in the corresponding packet selection and packet skipping mechanisms.

> **Definition 2.8** (Protocols)**.** *The receiver chooses a submitted sample $\hat{x}_p$ at time instant $p \in \mathbb{N}$ depending on the protocol such that for*
>
> *(i) protocol $\mathcal{P}_1$:*
>
> $$\hat{x}_p = \begin{cases} x_{\bar{\kappa}_p},\; \bar{\kappa}_p = \max\limits_{\kappa \in \mathcal{I}(p)} \kappa & \textit{if } \mathcal{I}(p) \neq \{\} \;\wedge\; \bar{\kappa}_p > \bar{\kappa}_{p-1} \\ \hat{x}_{p-1} & \textit{otherwise} \end{cases} \tag{2.38a}$$
>
> *(ii) protocol $\mathcal{P}_2$:*
>
> $$\hat{x}_p = \begin{cases} x_{\bar{\kappa}_p},\; \bar{\kappa}_p = \max\limits_{\kappa \in \mathcal{I}(p)} \kappa & \textit{if } \mathcal{I}(p) \neq \{\} \\ \hat{x}_{p-1} & \textit{otherwise} \end{cases} \tag{2.38b}$$
>
> *(iii) protocol $\mathcal{P}_3$:*
>
> $$\hat{x}_p = \begin{cases} x_{\bar{\kappa}_p},\; \bar{\kappa}_p = \operatorname*{any}\limits_{\kappa \in \mathcal{I}(p)} \kappa & \textit{if } \mathcal{I}(p) \neq \{\} \\ \hat{x}_{p-1} & \textit{otherwise} \end{cases} \tag{2.38c}$$

The cases using $\hat{x}_{p-1}$ in (2.38a) to (2.38c) constitute a zero order hold mechanism for each packet that is active whenever no packet is received at the actual time instant p, i.e. $\mathcal{I}(p) = \{\}$. The protocols differ in terms of the packet selection mechanisms.

In Protocol $\mathcal{P}_1$ (2.38a), the newest available packet with the corresponding index $\bar{\kappa}_p$ is selected. Sample $x_{\bar{\kappa}_p}$ is only employed if the actual available packet at time instant p is newer than the packet used at the previous time instant $\bar{\kappa}_{p-1}$, i.e. $\bar{\kappa}_p > \bar{\kappa}_{p-1}$. As a consequence, packets that are older than the previously selected packet are skipped. Note that a unique packet number has to be attached to each sent packet but no synchronization, e.g., using [IEE08], is needed, e.g., between the transmitter at the sensor side and the receiver at the controller side.

Protocol $\mathcal{P}_2$ (2.38b) selects the newest packet with the corresponding index $\bar{\kappa}_p$ if more packets are available but does not implement any skipping mechanism. Consequently, out of order arrivals are tolerated.

In situations where no packet numbering is implemented for simplicity reasons, protocol $\mathcal{P}_3$ (2.38c) is applied. It selects any of the actual received packets at time instant p, e.g., based on the position in the internal packet buffer. This represents the most reduced network transmission approach with the least possible overhead. Consequently, it constitutes the worst case for the stability analysis because the order of arriving packets is unknown and any arriving packet may be selected at the receiver side. More details about the impact of the selected protocols are presented in Chapters 6 to 8.

Chapter 3

Simulation of time-varying Packet Delays

This chapter highlights important aspects for the simulation of NCS subject to packetized transmissions. The presented simulation approaches are adopted from [STHJ20].

It is illustrated that existing NCS simulation tools might give inconsistent results for loops with bounded time-varying delays, which is exemplified for a single packetized transmission channel. Consequently, two new approaches of how such simulations could be performed are proposed that make use of specific packet delay models. The first technique is limited to delays equal to an integer multiple of the sampling interval, while the second technique is also applicable for simulating arbitrary delays. The results can be extended to simple models of networks with packet dropouts, but does not cover more detailed network protocols or physical-layer models. Both techniques extend basic Matlab/Simulink [MAT] and TrueTime [Tru, CHL$^+$03] blocks to accurately simulate packetized transmission channels with time-varying delays. Simulation examples provide insights to the properties of the different approaches and compare the outcomes to simulation results based on models from [LG11], [GC07] and [HvdW10].

Figure 3.1 shows a basic communication channel, where an input sequence (v_k) is sent from a transmitter (T) to a receiver (R). The arriving packets containing w_k experience variable transmission delays τ_j.

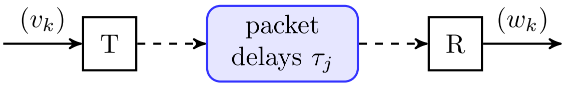

Figure 3.1: Communication channel with transmitter T, time-varying packet delays τ_j and receiver R.

In a test scenario, a ramp signal $v(t)$ is sampled with a sampling interval of $h = 1$ and sent over the channel with corresponding time delays τ_j as depicted in the top plot of Figure 3.2. For simplicity reasons, the time-varying delay is assumed to be a multiple of the sampling time. The signal $v(t)$ and its sampled version v_k are shown in blue in Figure 3.2. Packet 0 should be delayed by 1, packet 1 by 3, packet 2 by 5, and so on. The correct, i.e. the accurately simulated, arriving packets w_k at the receiver are plotted in gray in Figure 3.2. Note that several packets could arrive at the same time (e.g., at $t = 6$) yielding by definition a value of w_k according to the most recent packet (e.g. packet 5 at $t = 6$). Also note that packet disordering is possible at the receiver,

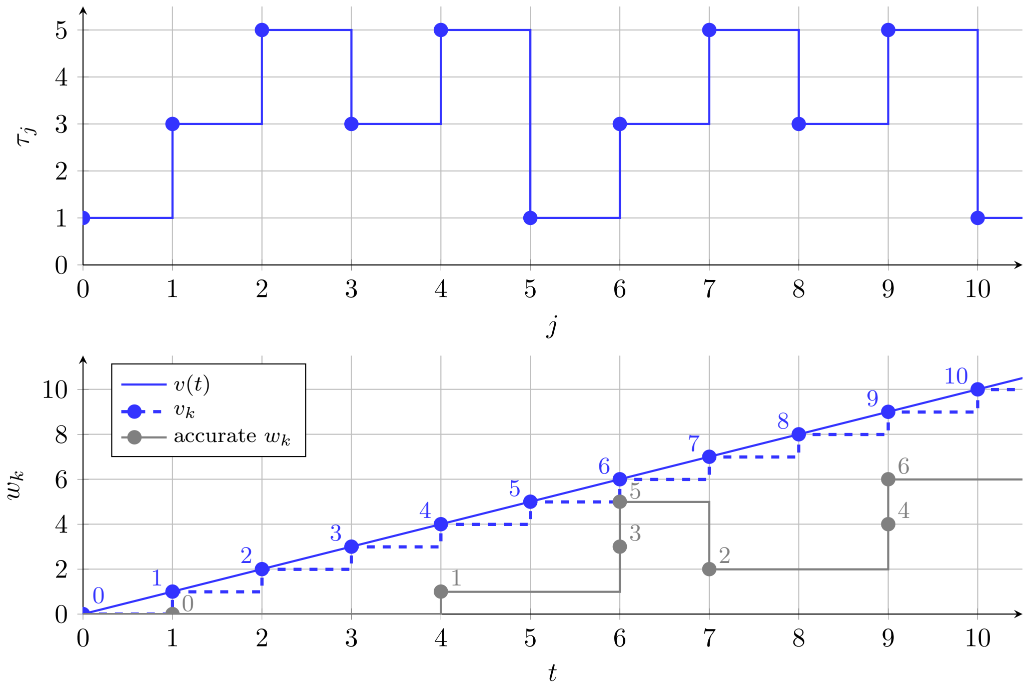

Figure 3.2: Example for the evaluation of simulation methods for a transmission channel with variable time delay τ_j (top plot): continuous-time signal to be transmitted $v(t)$, transmitted packets v_k (blue) and accurately received packets w_k (gray).

which can be seen in Figure 3.2, where packets 1, 5, 2 and 6 are received subsequently. In the following, approaches based on standard simulation blocks are analyzed and extended.

3.1 Simulations with Simulink Standard Blocks

A natural way to simulate time-varying delays is to exploit the Simulink built-in blocks *Variable Integer Delay* or *Variable Time Delay*. The block *Variable Transport Delay* must not be used in the context of NCS because it relates to physical processes where a medium is transported with a specified speed as pointed out in [ZY12]. This is

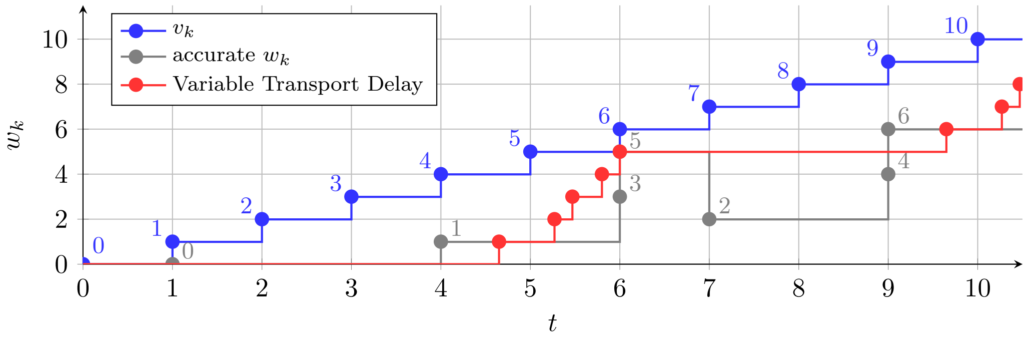

Figure 3.3: Comparison of the accurate result (gray) with results from simulations using the Simulink *Variable Transport Delay* block (red).

also visible in Figure 3.3, where the simulated signal w_k (using a variable-step solver) strongly deviates from the accurate (gray) plot.

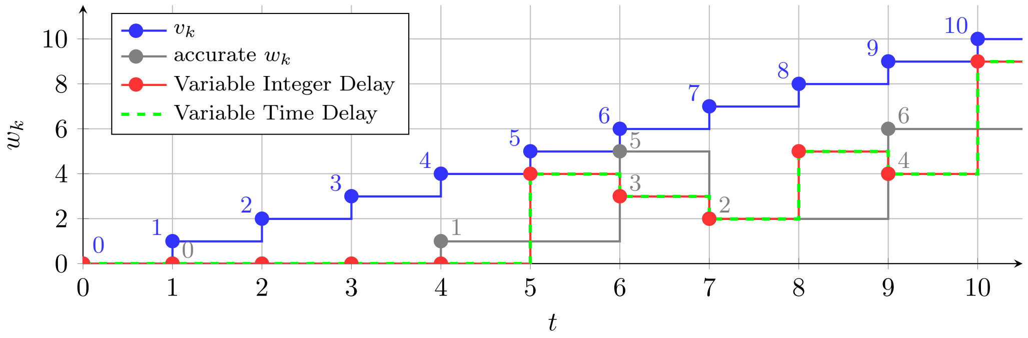

Figure 3.4: Comparison of the accurate result (gray) with results from simulations using the Simulink *Variable Integer Delay* (red) and *Variable Time Delay* block (green).

More surprisingly, also the simulation results using the *Variable Integer Delay* or *Variable Time Delay* blocks yield non-accurate results as shown in Figure 3.4. This can be explained, e.g., for the *Variable Integer Delay* block as follows. The internal structure of the *Variable Integer Delay* block is a tapped delay line in combination with a switching mechanism to realize a variable time delay as depicted in Figure 3.5. In the example presented in Figure 3.4, all delay blocks in Figure 3.5 are initialized with zero. The input sequence v_k increases by one in each sampling interval h and is transferred to the five delay blocks with internal states $x_1, x_2, \dots, x_5$, as shown in Table 3.1.

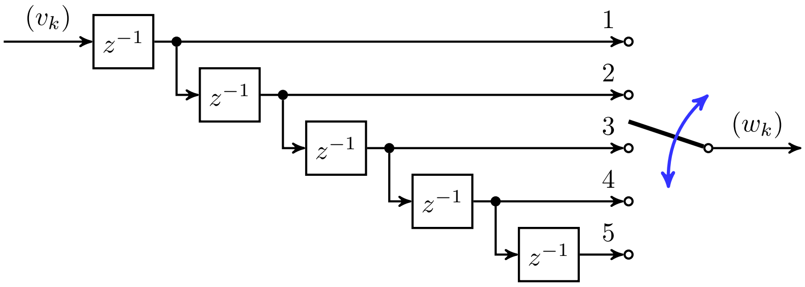

Figure 3.5: Functional principle of the Simulink *Variable Integer Delay* block.

Table 3.1: Results for the simulation example plotted in Figure 3.4 for the case with the Simulink *Variable Integer Delay* block.

t	0	1	2	3	4	5	6	7	8	9
x_1	$\boxed{0}$	0	1	2	3	$\boxed{4}$	5	6	7	8
x_2	0	0	0	1	2	3	4	5	6	7
x_3	0	$\boxed{0}$	0	$\boxed{0}$	1	2	$\boxed{3}$	4	$\boxed{5}$	6
x_4	0	0	0	0	0	1	2	3	4	5
x_5	0	0	$\boxed{0}$	0	$\boxed{0}$	0	1	$\boxed{2}$	3	$\boxed{4}$
τ_k	1	3	5	3	5	1	3	5	3	5

The internal switch selects port 1 to 5 depending on the specified delay τ_j for the actual sampling step depicted in the top plot of Figure 3.2. The resulting sequence

w_k is visualized in Table 3.1 by using blue boxes. These values coincide with the presented red and green signals in Figure 3.4. Non-integer values for the desired delays are truncated in this Simulink implementation.

Hence, the desired delay should not directly be used as an input signal to the Simulink *Variable Integer Delay* block. Instead the proposed Algorithm 1, which extends the Simulink built-in block, can be used to link the packets to the desired packet delays to achieve accurate simulation results. The key element is a packet buffer of length $\bar{d}+1$ (see (2.10) for the definition of $\bar{d}$) that allows to keep track of all packets and corresponding packet delays on the way between transmitter and receiver.

Algorithm 1 Pseudo code for the delay input signal generation for the Simulink *Variable Integer Delay* block.

```
Algorithm: Input generation for the Simulink Variable Integer Delay Block
Initialize packet buffer (length: $\bar{d}+1$);
while simulation is running do
    Shift elements in buffer by 1;
    Subtract $h$ from all delays in the packet buffer;
    Get actual packet delay (round to multiples of $h$);
    Write actual packet delay at first position in buffer;
    if skip old packets then
        Replace negative delays in buffer by 0;
    end
    Choose most recent packet with delay 0 from buffer;
end
```

It also features the possibility to skip old packets in the case that newer packets are available. Algorithm 1 is implemented in the *compute_index* block in Figure 3.6 to provide a proper index, i.e. a selection of the correct multiplexer signal in Figure 3.5. In the case where old packets are skipped, the corresponding delay values in the buffer are set to zero to keep them in play for the next time steps. Otherwise, negative delay values will be assigned for the subsequent time steps (because h is subtracted in each iteration) and, as a result, they will never be selected any more.

An additional case selection block at the output implements the necessary hold mechanism that is active, whenever no new packet is received, see Figure 3.6.
The simulation results for the considered example utilizing Algorithm 1 and the extension of the Simulink *Variable Integer Delay* block as in Figure 3.6 is shown in Figure 3.7 for the case without skipping (red) and with skipping mechanism (black). It is evident that the introduced extension allows to correctly simulate packetized transmission channels, i.e. link individual delays to its corresponding packets.

An alternative, and more flexible, solution for the simulation of a channel is shown in Figure 3.8. It does not incorporate any standard delay blocks, but uses Algorithm 2 to easily implement protocols $\mathcal{P}_1$, $\mathcal{P}_2$ and $\mathcal{P}_3$ from Section 2.4 and can easily be extended to, e.g., choose a random packet if more packets are available at one time instant. This will become valuable in Chapters 6 to 8 with the focus on the stability analysis.

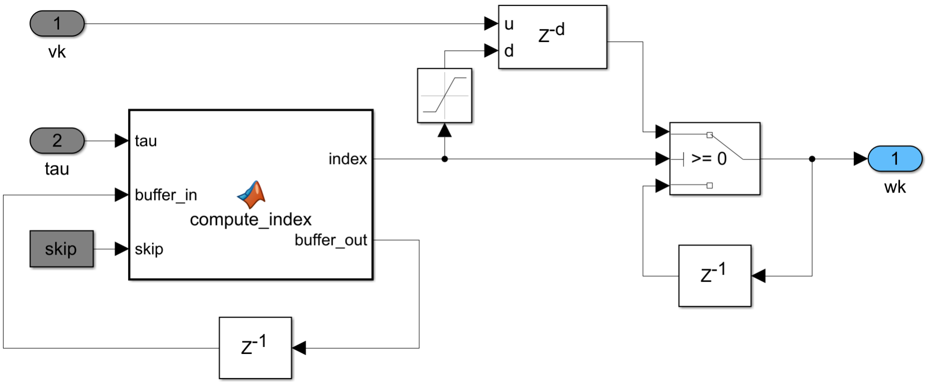

Figure 3.6: Extension of the Simulink *Variable Integer Delay* block to account for packetized transmissions.

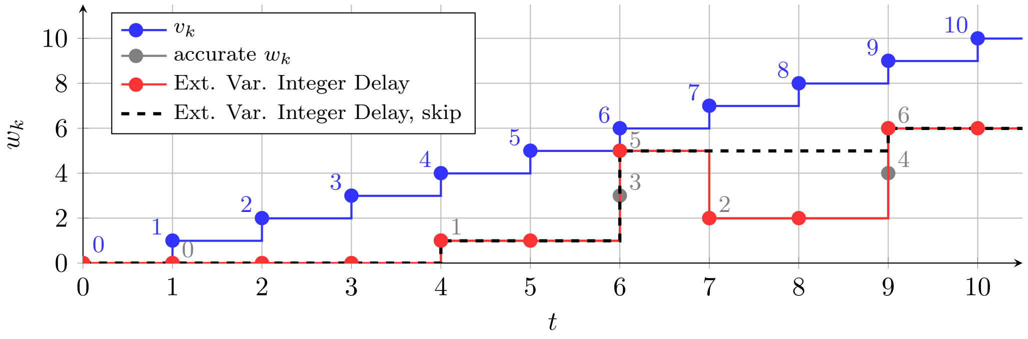

Figure 3.7: Comparison of the accurate result (gray) with results from simulations using the Extension for the Simulink *Variable Integer Delay* block without skipping (red) and with skipping mechanism (black) for old packets.

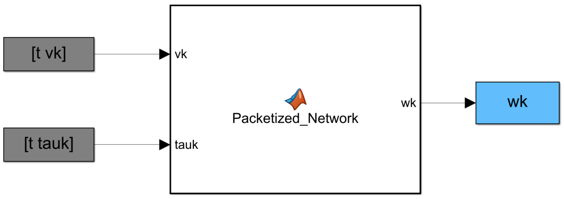

Figure 3.8: Implementation of a packetized network connection using Algorithm 2.

Algorithm 2 Pseudo code for a network connection with time-varying packet delays.

```
Algorithm: Packetized Network
Initialize packet buffer (length: $\overline{d} + 1$);
while simulation is running do
    // include new packet and packet delay in buffer
    Shift elements in buffer by 1;
    Subtract $h$ from all delays in the packet buffer;
    Get actual packet delay (round to multiples of $h$);
    Write actual packet and packet delay at first position in buffer;

    // skipping mechanism
    if skip old packets then
        Replace negative delays in buffer by 0;
    end

    // packet selection and hold mechanism
    if number if delays equal to zero in buffer $\neq 0$ then (packet arrival)
        find indices of arriving packets;
        switch packet selection do
            case choose newest do
                choose packet with minimal index;
            case choose oldest do
                choose packet with maximal index;
            case choose rand do
                choose packet with random index;
            end
        end
        Send chosen packet to output;
    else (no packet arrival)
        hold previous output value;
    end
end
```

3.2 Simulations using TrueTime

A possibility to simulate a time-varying channel is to use the Matlab toolbox TrueTime [CHL$^+$03]. It was developed to enable a co-simulation of controller tasks in real-time kernels, continuous plant dynamics and network transmissions including task scheduling. A big variety of different (wireless) network configurations and protocols can be chosen within the simulation toolbox.

Figure 3.9 shows the packets that are sent (blue) and received (green) when a basic TrueTime simulation (TT) is used. Since no additional network traffic is simulated in this example, the green packets immediately appear at the receiver. Hence, an extension of TrueTime to specify individual packet delays is necessary to enable, e.g., simulations to verify stability criteria that provide a certain range of admissible time-varying delays.

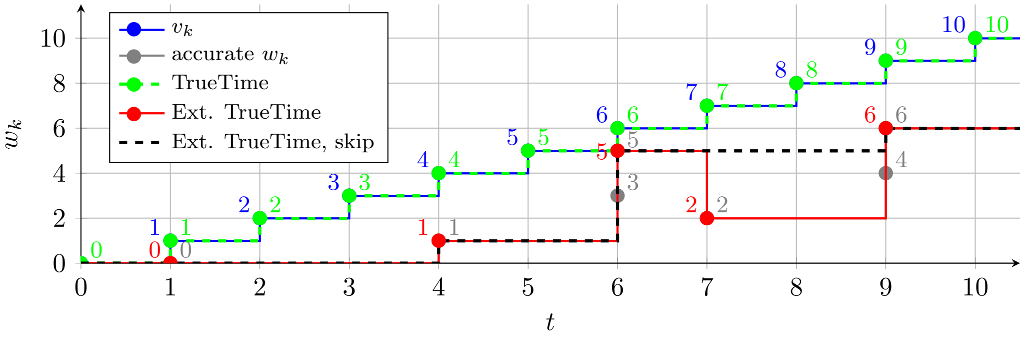

Figure 3.9: Comparison of the accurate result (gray) with results from simulations using a basic TrueTime setting as well as an extended TrueTime setup for the case without skipping (red) and with skipping mechanism (black) for old packets.

The link between specified delays and the individual packets can be established by the following proposed extension for TrueTime. It introduces an additional block (Network Delay Node) between transmitter (Send Node) and receiver (Receive Node) as shown in Figure 3.10. This node schedules the arriving packets in the considered transmission

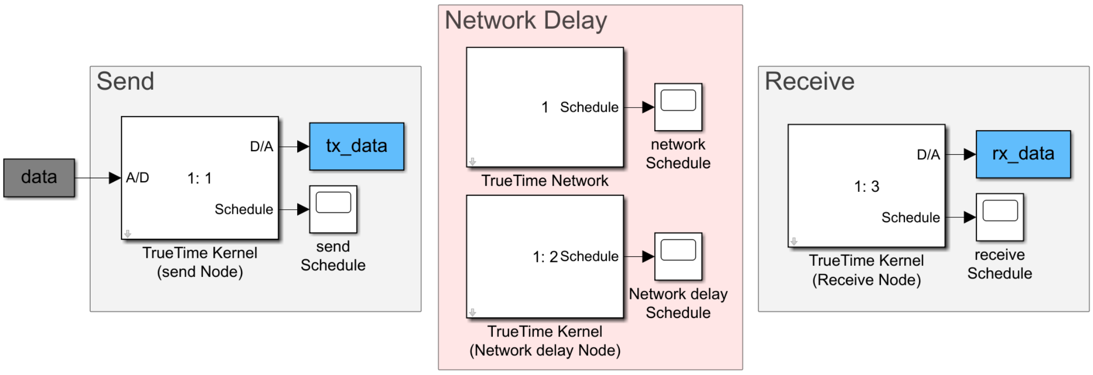

Figure 3.10: TrueTime implementation of a packetized communication channel. The key ingredient is the *Network Delay Node* that links packets to its corresponding time delays.

channel. Packets on the way are stored in an internal list with size $\bar{d} - \underline{d} + 1$, where

Algorithm 3 Pseudo code for the network delay node that schedules the packet arrivals in the transmission channel.

```
Algorithm: Network Delay Node
Initialize packet list (length: $\bar{d} - \underline{d} + 1$);
while simulation is running do
    Get actual packet (to be scheduled for time $t^*$) from transmitter;
    Read actual delay job (next packet that has already been scheduled to be received
    next) from list;
    if no packet has already been scheduled for $t^*$ then
        // not scheduled
        if time $t^*$ less than next planned packet arrival at receiver then
            Cancel running delay job (next packet to be received);
            Include actual packet at first position in list;
            Move other packets backward in the list;
            Start new delay job for the actual packet;
        else
            Include actual packet in list;
            Sort list based on the planned arrival times;
        end
    else
        // already scheduled
        Replace packet in list (that was scheduled for time $t^*$) with the actual packet;
    end
end
```

integers $\underline{d}$ and $\bar{d}$ depend on the sampling interval h as well as on the minimal delay $\underline{\tau}^N$ and maximal delay $\bar{\tau}^N$ respectively, due to the definitions in (2.10).

Algorithm 3 is implemented in the *Network Delay Node* to schedule the packets that should be sent with individual specified delays τ_j. In addition, a delay job is used that sleeps until the packet related to the first entry in the list is sent to the receiver. Then, the first element is removed and a new delay job corresponding to the next packet in the list is started.

Figure 3.9 shows the results (in red) using this proposed extended TrueTime simulation approach. It perfectly reproduces the accurate (gray) behavior of the packetized transmission channel. A slight modification of the code of the receiving node allows to skip old packets in the case that newer packets are available, see black signal in Figure 3.9. Please note that a newer packet replaces an older packet in the packet list if they are scheduled for the very same arrival time. However, this can be changed easily as desired.

One advantage of the presented approach is that it is also capable to deal with variable packet delays, where the delays are not multiples of the sampling instant. The downside is its larger effort with respect to the implementation compared to the solution presented in the previous section.

3.3 Comparison of NCS models for variable time delays

This section compares the approaches for the simulation of time-varying delays in the context of networked feedback loop as in Figure 2.1 using a linear state feedback controller

$$u_k = L\, x_{k-\tau_k} \tag{3.1}$$

with constant gain L that uses the delayed plant state $x_{k-\tau_k}$. For static controllers, the time-varying delays can be combined to one round-trip-delay $\tau_k = \tau_k^{sc} + \tau_k^{c} + \tau_k^{ca}$ as described in Section 2.2. The simulation is carried out for a configuration, where the delay is present between sensor and controller only. Two different ways to model the closed loop are evaluated with respect to the simulation approaches shown in the previous section. The delay is denoted as τ_k as it is often done in literature. This means that there is no link between packets and corresponding delays, in contrast to the modeling steps presented in Chapter 2. The implications of such an approach are highlighted below.

A first possibility to model the closed loop is to directly discretize the continuous-time plant from (2.1) such that

$$x_{k+1} = Ax_k + Bu_k \tag{3.2}$$

with

$$A = e^{\tilde{A}h} \qquad \text{and} \qquad B = \int_0^h e^{\tilde{A}\eta}\tilde{B}\, d\eta \tag{3.3}$$

hold and to combine it with controller (3.1) yielding

$$x_{k+1} = Ax_k + BL\, x_{k-\tau_k} \tag{3.4}$$

as, for example, described in [LG11] and [GC07]. The model for the closed loop (3.4) combines the actual states x_k and the delayed states $x_{k-\tau_k}$; the delay is assumed to be an integer-multiple of the sampling interval. This model is referred to as *Model with Time Delay* in the following.

An alternative way to model the considered networked feedback loop is on the basis of the *Lifted Model* as presented in Chapter 2, with the lifted state vector

$$\xi_k = \begin{bmatrix} x_k^{\mathrm{T}} & u_{k-1}^{\mathrm{T}} & u_{k-2}^{\mathrm{T}} & \cdots & u_{k-\bar{d}}^{\mathrm{T}} \end{bmatrix}^{\mathrm{T}} \in \mathbb{R}^{n+m\bar{d}} \tag{3.5}$$

and the closed loop model

$$\xi_{k+1} = \mathcal{A}\xi_k + \mathcal{B}u_k \tag{3.6}$$

with matrices $\mathcal{A}$ and $\mathcal{B}$ as defined in (2.24) and a state control law

$$u_k = L\, x_k = \begin{bmatrix} L & 0_{m\times m\bar{d}} \end{bmatrix} \xi_k\,. \tag{3.7}$$

Note that the effect of the time-varying delays and protocol $\mathcal{P}_1$ are implicitly embedded into model formulation (3.6), as described in Chapter 2 in detail.

A simple simulation example is considered next, to compare the *Model with Time Delay* and the *Lifted Model* for the closed loop system, where the plant dynamics is given by a double integrator represented by matrices

$$\tilde{A} = \begin{bmatrix} 0 & 1 \\ 0 & 0 \end{bmatrix} \qquad \text{and} \qquad \tilde{B} = \begin{bmatrix} 0 \\ 1 \end{bmatrix} \tag{3.8}$$

and a linear state controller with gain L is designed as proposed in [CHvdW$^+$10]. It stabilizes the feedback loop under the presence of a bounded but time-varying delay, where $h = 1$, $\underline{d} = 0$, $\bar{d} = 4$ and controller design parameter $\gamma = 0.001$ are used. The initial states of the plant and the initial conditions of the network are chosen equal to $x(t = 0) = [2\ -1]^{\mathrm{T}}$ and zero respectively. The packet delays are defined by a repeating sequence that is shown in Figure 3.11.

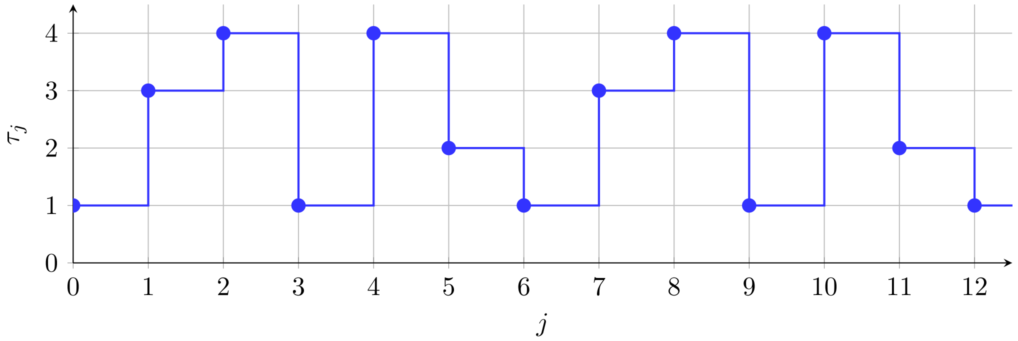

Figure 3.11: Simulation example for the closed NCS: Repeating sequence of time-varying delays τ_j for packets j.

Figure 3.12 depicts the simulation results for the proposed extended TrueTime simulation where, in addition, old packets are skipped (Ext. TrueTime, skip). The plots show the control signal as well as the transmitted (tx) and received (rx) states. It can be seen, that the lifted model yields identical results when compared to the continuous plant states at the sampling instants.

In contrast, deviations from these accurate (gray) signals can be seen in Figure 3.13 where the extended TrueTime simulation without the skipping mechanism for old packets is used, which becomes evident by inspecting the transmitted signals shown in blue in Figure 3.13.

Figure 3.14 reinforces the statements from the previous sections that the Simulink built-in block *Variable Integer Delay* is not suitable for solving the considered task. Interestingly, the *Model with Time Delay* (3.4) yields the same results as indicated in Figure 3.14. This is due to the fact that the desired delays (see Figure 3.11) should be related to a specific packet, but are actually associated with the iteration index instead of the individual packets.

For the *Model with Time Delay*, the relations between packets and simulated delays are lost. In contrast, the *Lifted Model* exactly reproduces the expected results for the case that old packets are discarded whenever newer packets are available. This is possible due to the calculation of the arrival times t_j^k in simulation. However, the lifted model is not valid any more if different protocols as, e.g., protocols $\mathcal{P}_2$ and $\mathcal{P}_3$ from Chapter 2 are considered.

To sum up, the simulation of packetized transmissions with individual time-varying delays for each packet should be done with care and the inclusion of individual packet delays is vital to get accurate simulation results. Therefore, two different simulation approaches are proposed in this chapter: (i) an extension of TrueTime to simulate packet delays that are not integer multiples of the sampling time and (ii) an extension of the Simulink *Variable Integer Delay* block as well as an easy-to-use and easy-to-implement

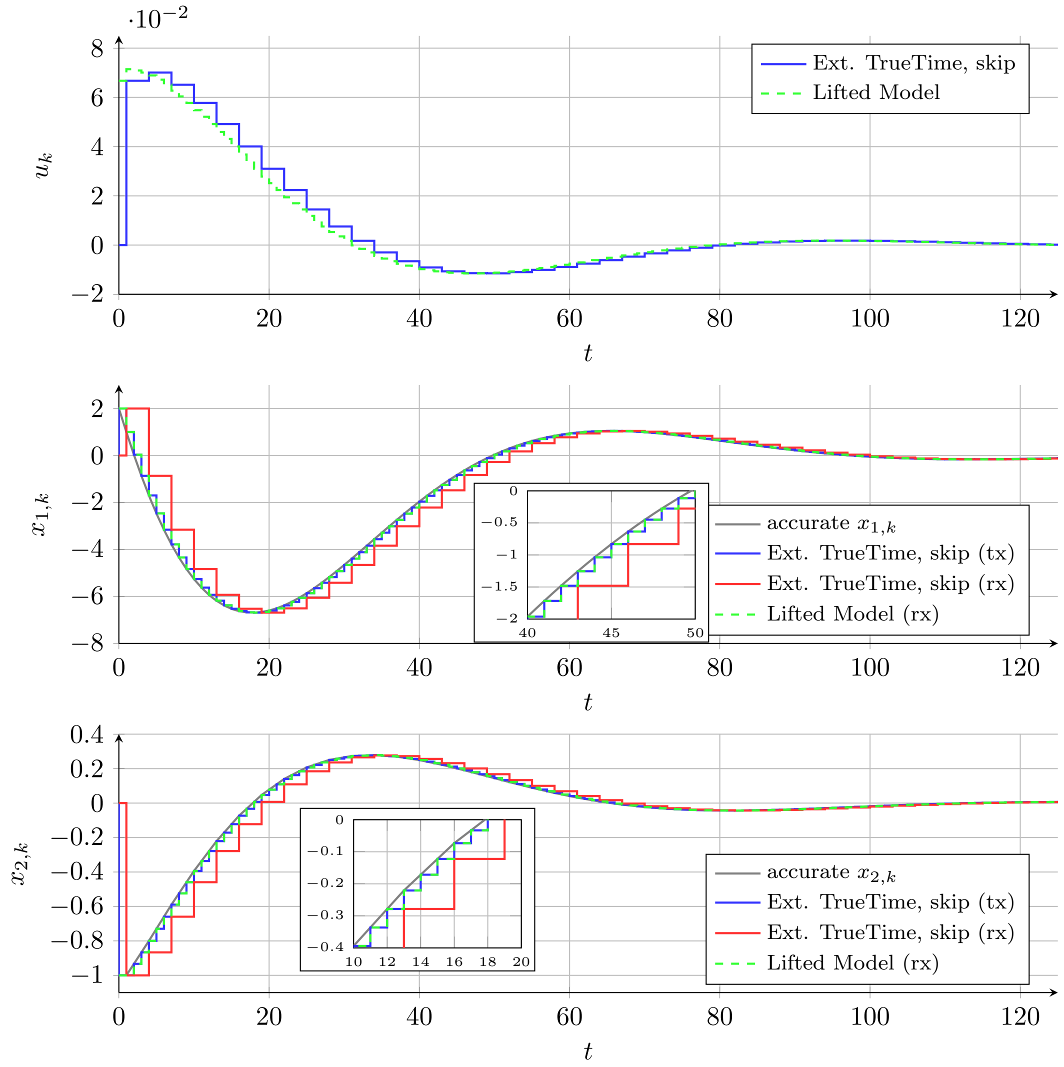

Figure 3.12: Simulation example for the closed NCS: Extended TrueTime simulation with a mechanism to skip old packets. Comparison of the accurate continuous-time signal, the transmitted (tx) and received (rx) signal, as well as the lifted states corresponding to (3.6).

Packetized Network simulation block for packetized transmissions with variable time delays. All versions allow to also easily include different packet skipping and hold mechanisms.

The presented simulation approaches can easily be extended to incorporate packet dropouts in transmission channels of networked systems with variable time delays by excluding the packets to be dropped from the packet buffer or packet list depending on the actually chosen simulation approach.

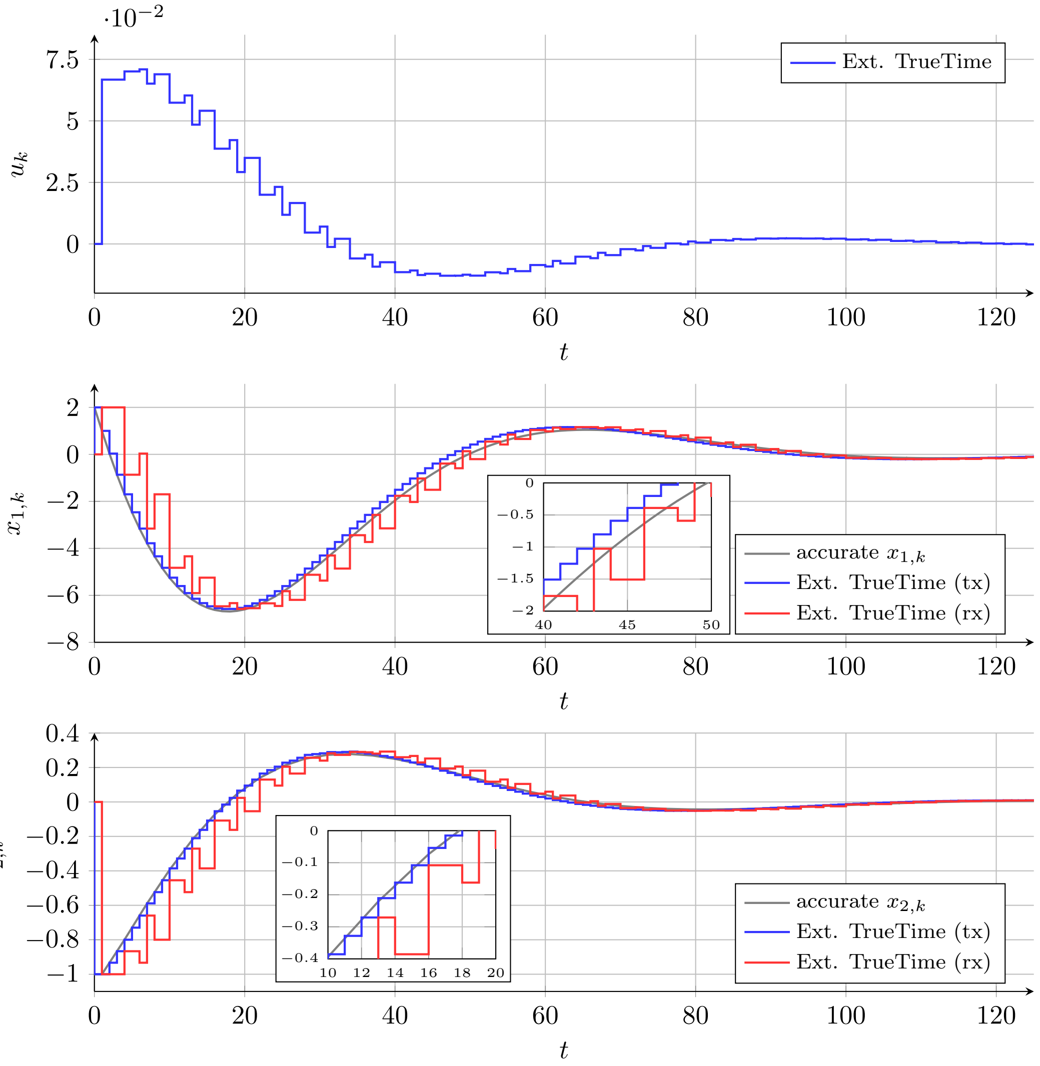

Figure 3.13: Simulation example for the closed NCS: Extended Truetime simulation without skipping mechanism. Comparison of the accurate continuous-time signal, the transmitted (tx) and received (rx) signals.

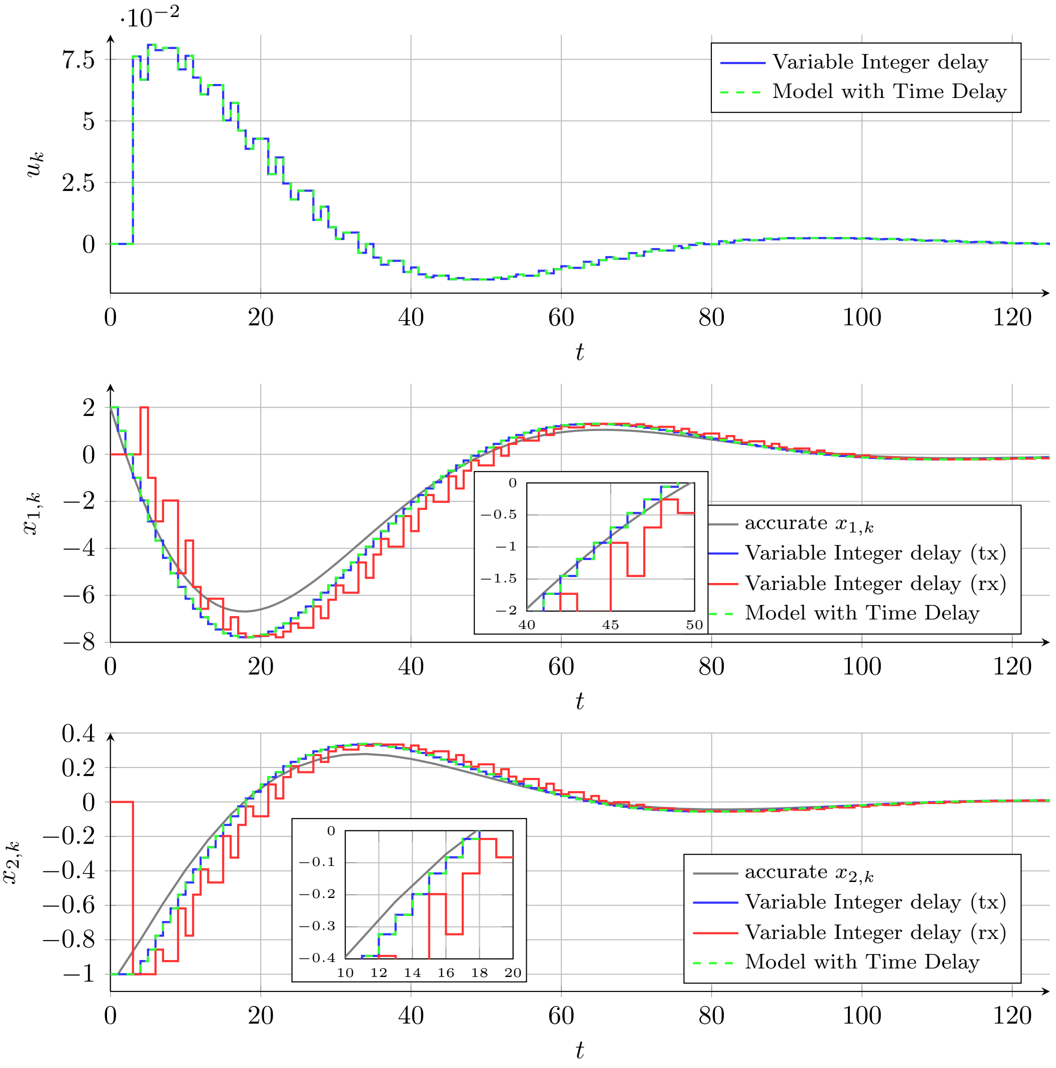

Figure 3.14: Simulation example for the closed NCS: Simulation with the Simulink *Variable Integer Delay* block. Comparison of the accurate continuous-time signal, the transmitted (tx) and received (rx) signal as well as the states corresponding to (3.4).

Chapter 4

Robust Control of Buffered Networked Systems

This chapter introduces a control approach for multivariable networked plants exploiting buffering mechanisms and is adopted from [LSH19] that rests on [LRSH19, LSH$^+$18].

Integral sliding mode techniques allow to design robust controllers that are insensitive with respect to matched perturbations, i.e. external perturbations that act in the input channels. The proposed approach makes it possible to implement m controllers for the distributed plant with m inputs in a spatially distributed way without any communications between the corresponding controllers. This yields simpler communication architectures and offers the possibility to, e.g., utilize different task classes for the individual control loops resulting in different induced time-varying network delays.

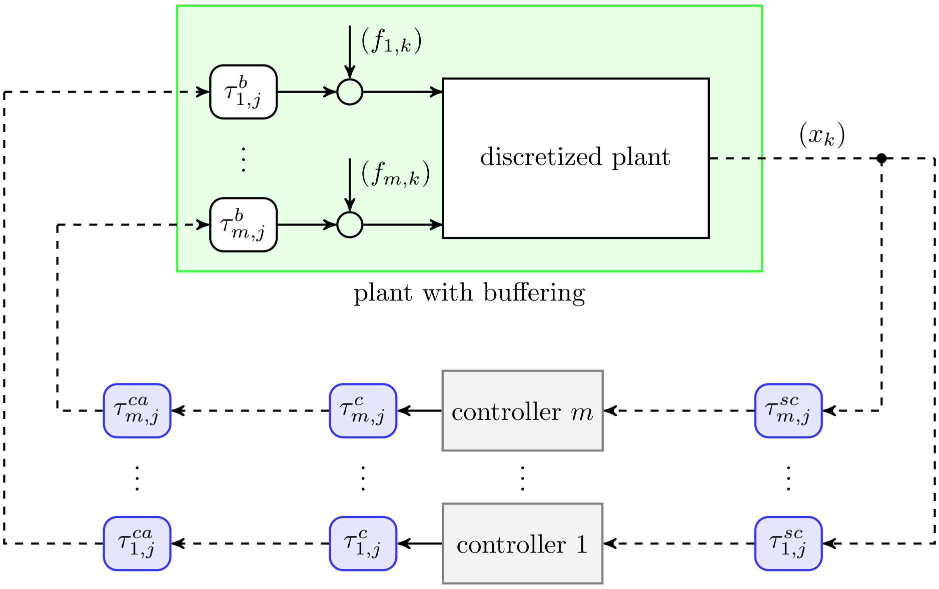

Figure 4.1: Feedback loop for the buffered networked plant that is subject to external perturbations $(f_{i,k})$ in each input channel $i \in \{1, 2, \dots, m\}$.

Figure 4.1 depicts the underlying structure of the feedback loop, which is a generalization of Figure 2.1 from Chapter 2. It is assumed that the external perturbations $(f_{i,k})$ with $i \in \{1, 2, \dots, m\}$ act in all input channels of the discretized plant (2.1), which fulfills the basic Assumption 2.1 about the controllability.

All m controllers are linked via network connections to the buffered plant as shown in Figure 4.1. The i^{th} control loop is associated with time-varying computational delays $\tau_{i,j}^{c}$, sensor-to-controller delays $\tau_{i,j}^{sc}$ and controller-to-actuator delays $\tau_{i,j}^{ca}$. Parameter j represents the index that is attached to each packet at the sensor side. In addition, buffers with the corresponding time delays $\tau_{i,j}^{b}$ are needed in the input channels to ensure constant round trip delays as explained subsequently in detail.

Buffering techniques are also used by the author in [LSR$^+$17, LSH$^+$18] and recently in [SSLH21] in combination with switching, non-switching and predictive discrete-time sliding mode approaches. See also [Lud20] for more details. However, the defined sliding variables exhibit relative degrees larger than one and, thus, make the controller design task more challenging. In contrast, the methods presented in this chapter are based on discrete-time integral sliding modes and facilitate a straight forward design of a nominal controller in combination with an additional robustification designated for relative degree one systems. It also allows to spatially distribute the controllers, which is not possible in the other buffered approaches mentioned above.

4.1 Buffered Networked System

The basis for the subsequent controller design is the mathematical description of the networked plant (that is subject to external perturbations) together with the buffering mechanisms.

Assumption 4.1 (Perturbations)**.** *The perturbations act on the m inputs of the discretized plant and are bounded in their change rate such that*

$$\sup\left|\frac{f_{i,k+1}-f_{i,k}}{h}\right| = L_i < \infty \tag{4.1}$$

for all $i \in \{1,2,\dots,m\}$, with h being the sampling interval and L_i the Lipschitz constant of perturbation $(f_{i,k})$ in the i^{th} input channel.

Furthermore, the assumptions on the delays presented in Chapter 2 are generalized to account for the structure in Figure 4.1.

Assumption 4.2 (Network and computational delays)**.**

(a) The samples of sequence (x_k) are time-stamped at the sensor and transmitted in separate packets j that experience individual bounded packet delays $\tau_{i,j}^{N}$ such that

$$0 \leq \underline{\tau}_i^{N} \leq \tau_{i,j}^{N} \leq \bar{\tau}_i^{N} \tag{4.2}$$

for $i \in \{1,2,\dots,m\}$ with $\underline{\tau}_i^{N}, \tau_{i,j}^{N}, \bar{\tau}_i^{N} \in \mathbb{R}_+$ for the sensor-to-controller and controller-to-actuator delays, i.e. $N \in \{sc, ca\}$.

(b) The time for the evaluation of the control laws in the controllers are bounded such that

$$0 \leq \underline{\tau}_i^{c} \leq \tau_{i,j}^{c} \leq \bar{\tau}_i^{c} \tag{4.3}$$

for $i \in \{1, 2, \dots, m\}$ *with* $\underline{\tau}_i^c, \tau_{i,j}^c, \bar{\tau}_i^c \in \mathbb{R}_+$.

It is possible to lump the individual delays in the ith channel at the actuator side if either the change rate of the sensor-to-controller delay is restricted or a static control law is used as explained in Section 2.2. The focus of this work is on the design feedback laws respecting the overall round trip delays $\tau_{i,j}$ for the simplified network structure shown in Figure 4.2.

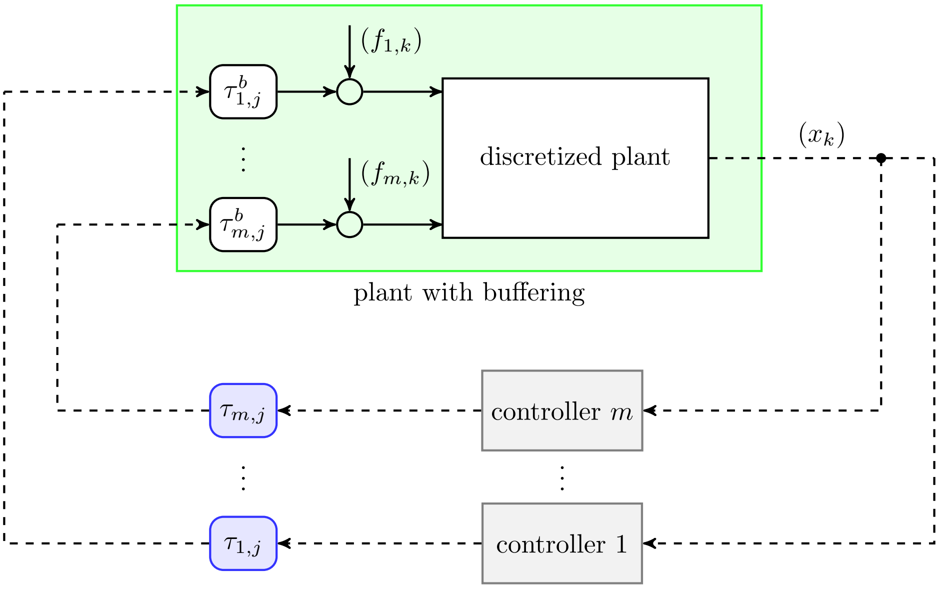

Figure 4.2: Simplified structure of the spatially distributed networked feedback loop with m inputs.

Assumption 4.3 (Combined delays)**.**

(a) *The round trip delays* $\tau_{i,j} = \tau_{i,j}^{sc} + \tau_{i,j}^c + \tau_{i,j}^{ca}$ *of each individual packet* j *in all channels* $i \in \{1, 2, \dots, m\}$ *are bounded by*

$$0 \leq \underline{\tau}_i \leq \tau_{i,j} \leq \bar{\tau}_i \tag{4.4}$$

with $\underline{\tau}_i, \tau_{i,j}, \bar{\tau}_i \in \mathbb{R}_+$.

(b) *The sensor-to-controller delays fulfill* $\tau_{i,j}^{sc} \geq \tau_{i,j-1}^{sc} - h$ *to allow lumping the delays at the actuator side.*

The key elements in the feedback loop as shown in Figure 4.2 are the buffers that introduce additional time delays $\tau_{i,j}^b$ to keep the round trip delay constant in each channel i. This is possible, since a time stamp is attached to each transmitted packet (see Assumption 4.2(a)) at the sensor side, which render compensations of the time-varying delays possible. This packet, containing x_k, is used in the ith controller to calculate the corresponding control signal for actuator i, which is forwarded to the plant. The original time stamp that is attached at the sensor side is not changed in the controller block. Hence, the actual packet delay $\tau_{i,j}$ can be determined at the receiver side of the plant, because the actual time is known at the buffer. The i buffers induce additional packet delays

$$\tau_{i,j}^{b} = \delta_i h - \tau_{i,j} \tag{4.5}$$

for $i \in \{1, 2, \ldots, m\}$, where

$$\delta_i = \left\lceil \frac{\bar{\tau}_i}{h} \right\rceil \tag{4.6}$$

represents the largest integer multiple of the sampling interval that is needed to dominate the maximum delay stated in Assumption 4.3. Consequently, all arriving packets are stored in the buffers and forwarded to the plant after a time equal to $\delta_i h$, i.e. after a constant round trip delay time.

This buffering mechanism is quite common in classical communication technologies like IP telephony and packetized audio applications as, e.g., shown in [AL06, NKMP05, RKTS94]. It has also found applications in the control community as, for example, in [QN11, ABL08] and [Lib06]. It allows to convert the time-varying packet delays into a known constant round trip delay in the present work. The buffers make it also possible to introduce a packet reordering mechanism to correct out-of-order arrivals at the receiver side. It is important to note that a time synchronization between sensors and the actuators is vital and can, e.g., be done by the flooding time synchronization protocol introduced in [MKSL04].

To sum up, the established buffers shown in Figure 4.2 at the actuator sides of the plant introduce additional delays (4.5) to ensure that control signal $(u_{1,k})$ is delayed by δ_1 time steps, $(u_{2,k})$ is delayed by δ_2 time steps, and so on. Thus, the vector of control signals

$$u_k = \begin{bmatrix} u_{1,k} & u_{2,k} & \cdots & u_{m,k} \end{bmatrix}^{\mathrm{T}} \quad \in \mathbb{R}^m \tag{4.7}$$

arrives in a delayed fashion

$$u_k^{\delta} = \begin{bmatrix} u_{1,k-\delta_1} & u_{2,k-\delta_2} & \cdots & u_{m,k-\delta_m} \end{bmatrix}^{\mathrm{T}} \tag{4.8}$$

at the discretized plant. The discrete-time formulation of the networked plant including the buffering mechanisms for the m channels is then given by

$$x_{k+1} = Ax_k + B\left(u_k^{\delta} + f_k\right) , \tag{4.9}$$

where $x_k = \begin{bmatrix} x_{1,k} & x_{2,k} & \ldots & x_{n,k} \end{bmatrix}^{\mathrm{T}} \in \mathbb{R}^n$ and

$$f_k = \begin{bmatrix} f_{1,k} & f_{1,k} & \cdots & f_{m,k} \end{bmatrix}^{\mathrm{T}} \quad \in \mathbb{R}^m \tag{4.10}$$

represent external perturbations acting on the plant as shown in Figure 4.2. The dynamic matrix A and input matrix B follow from the discretization of the continuous-time plant (2.1) such that

$$A = e^{\tilde{A}h} \qquad \text{and} \qquad B = \int_0^h e^{\tilde{A}\eta}\tilde{B}\,\mathrm{d}\eta = \begin{bmatrix} b_1 & b_2 & \cdots & b_m \end{bmatrix} \tag{4.11}$$

with $b_i \in \mathbb{R}^n$.

Similar to (2.22) in Section 2.3, one can now introduce an extended (lifted) state vector for the buffered plant as

$$\begin{aligned} \xi_k = \Big[\; x_k^{\mathrm{T}} \;\Big|\; u_{1,k-1} \quad u_{1,k-2} \quad \cdots \quad u_{1,k-\delta_1} \;\Big|\; u_{2,k-1} \quad u_{2,k-2} \quad \cdots \quad u_{2,k-\delta_2} \;\Big|\; \cdots \\ \cdots \;\Big|\; u_{m,k-1} \quad u_{m,k-2} \quad \cdots \quad u_{m,k-\delta_m} \;\Big]^{\mathrm{T}} . \end{aligned} \tag{4.12}$$

Please note that the number of delayed $u_{i,k}$ depends on the corresponding buffer lengths δ_i. In contrast to (2.22), where for example $u_{1,k-1}, u_{2,k-1}, \dots, u_{m,k-1}$ are used consecutively, relation (4.12) groups the delayed versions of one control input as, e.g., $u_{1,k-1}, u_{1,k-2}, \dots, u_{m,k-\delta_1}$ in one block. This is necessary to facilitate the design of spatially distributed controllers as explained below.

The final structure of the lifted state space model with states ξ_k (4.12) is an alternative description of (4.9), where u_k^δ (4.8) is replaced by u_k (4.7), i.e. the buffers are explicitly included in the mathematical description. This yields

$$\xi_{k+1} = \mathcal{A}\xi_k + \mathcal{B}u_k + \mathcal{B}_f f_k \tag{4.13}$$

with system matrix

$$\mathcal{A} = \left[\begin{array}{c|cc|cc|c|cc}
A & 0_{n\times\delta_1-1} & b_1 & 0_{n\times\delta_2-1} & b_2 & \cdots & 0_{n\times\delta_m-1} & b_m \\ \hline
0_{1\times n} & 0 & 0 & 0 & 0 & \cdots & 0 & 0 \\
0_{\delta_1-1\times n} & \boxed{I_{\delta_1-1}} & 0_{\delta_1-1\times 1} & 0 & 0 & \cdots & 0 & 0 \\ \hline
0_{1\times n} & 0 & 0 & 0 & 0 & \cdots & 0 & 0 \\
0_{\delta_2-1\times n} & 0 & 0 & \boxed{I_{\delta_2-1}} & 0_{\delta_2-1\times 1} & \cdots & 0 & 0 \\ \hline
\vdots & \vdots & \vdots & \vdots & \vdots & \ddots & \vdots & \vdots \\ \hline
0_{1\times n} & 0 & 0 & 0 & 0 & \cdots & 0 & 0 \\
0_{\delta_m-1\times n} & 0 & 0 & 0 & 0 & \cdots & \boxed{I_{\delta_m-1}} & 0_{\delta_m-1\times 1}
\end{array}\right] \tag{4.14a}$$

and input matrices

$$\mathcal{B} = \left[\begin{array}{c|c|c|c}
0_{n\times 1} & 0_{n\times 1} & \cdots & 0_{n\times 1} \\ \hline
\boxed{1} & 0 & \cdots & 0 \\
0_{\delta_1-1\times 1} & 0 & \cdots & 0 \\ \hline
0 & \boxed{1} & \cdots & 0 \\
0_{\delta_2-1\times 1} & 0 & \cdots & 0 \\ \hline
\vdots & \vdots & \ddots & \vdots \\ \hline
0 & 0 & \cdots & \boxed{1} \\
0_{\delta_m-1\times 1} & 0 & \cdots & 0
\end{array}\right] \quad \text{and} \quad \mathcal{B}_f = \left[\begin{array}{c}
B \\ \hline
0 \\
0_{\delta_1-1\times 1} \\ \hline
0 \\
0_{\delta_2-1\times 1} \\ \hline
\vdots \\ \hline
0 \\
0_{\delta_m-1\times 1}
\end{array}\right] \tag{4.14b}$$

related to u_k and the disturbance vector f_k, respectively, in which the dimensions of the zero matrices are only mentioned where necessary. The segmentation of the matrices is in accordance with (4.12) to also emphasize the effects of the individual buffers modeled by the blue parts in (4.14). All actuating signals u_k enter via matrix $\mathcal{B}$ and pass through the buffers of different lengths δ_i as indicated in matrix $\mathcal{A}$ before they affect the plant states x_k via the input vectors b_i. The dimensions of $\mathcal{A} \in \mathbb{R}^{(n+\Delta)\times(n+\Delta)}$ and $\mathcal{B}, \mathcal{B}_f \in \mathbb{R}^{(n+\Delta)\times m}$ depend on the sum over all buffer lengths

$$\Delta = \sum_{i=1}^{m} \delta_i \tag{4.15}$$

and the number of plant states n. The same is true for $\xi_k \in \mathbb{R}^{n+\Delta}$.

Please note that f_k is not matched as defined, e.g., in [Utk92] for the lifted model (4.13) with states ξ_k because

$$\operatorname{rank}\begin{bmatrix}\mathcal{B} & \mathcal{B}_f\end{bmatrix} \neq \operatorname{rank}\mathcal{B}\,. \tag{4.16}$$

However, the perturbation is matched with respect to the original plant states x_k as can be seen in (4.9). As a result, it is possible to robustly stabilize the plant only, which meets the goals of the present approach.

Also note that a perturbation $f(t)$ is assumed to act on the continuous-time plant in [LSH19] such that

$$\frac{\mathrm{d}x}{\mathrm{d}t} = \tilde{A}x(t) + \tilde{B}\big(u(t) + f(t)\big)\,. \tag{4.17}$$

This leads to the additional assumption in [LSH19] that the perturbation is piece-wise constant over one sampling interval. Otherwise, additional unmatched perturbations would be present that cannot be rejected in principle by using the actuators and thus would also affect the states.

4.2 Integral Sliding Mode Control

This section summarizes the basic idea of integral sliding mode control that can be found, e.g., in [US96] and [SEFL15] and is available for continuous-time as well as for discrete-time systems. It will be utilized in the subsequent sections for the considered buffered networked system.

Figure 4.3 depicts the general structure consisting of an outer control loop and an inner control loop. A nominal controller, which is designed for the ideal, disturbance free plant model, is employed in the outer loop to provide the nominal actuating signal $(\bar{u}_k)$. The additional inner loop serves as a robustification of the nominal behavior against external perturbations (f_k). One possibility is to use an MPC as nominal controller in that context as proposed by [RRFM11] and [RRJ+15]. This idea was extended by the author of this work in [SCHF20] to the case of robust output regulation based on output integral sliding mode techniques [FPB14]. In this work, the nominal controller is designed using LMI conditions.

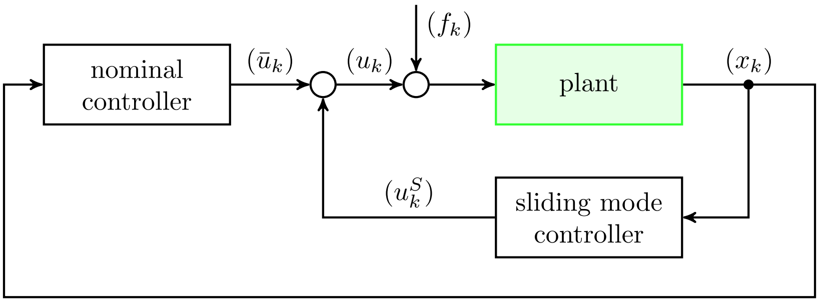

Figure 4.3: Basic structure for integral sliding mode techniques with an outer (nominal) and inner (robustifying) loop.

Control signal (u_k) that is actually applied to the plant is the sum of $(\bar{u}_k)$ and the signal (u_k^S) provided by the sliding mode controller, i.e.

$$u_k = \bar{u}_k + u_k^S\,. \tag{4.18}$$

The principle idea is now briefly explained for a discrete-time system with one input only, which is given by

$$x_{k+1} = Ax_k + b\,(u_k + f_k) \tag{4.19}$$

with $x_k \in \mathbb{R}^n$, $u_k \in \mathbb{R}$, $f_k \in \mathbb{R}$ and system data A, b with appropriate dimensions. For the unperturbed plant, which follows from (4.19) for $f_k = 0$ for all $k \in \mathbb{N}$, one gets

$$x_{k+1} = Ax_k + b\bar{u}_k \, , \tag{4.20}$$

if only the nominal control signal $\bar{u}_k$ is used. A discrete-time sliding variable σ_k is defined as

$$\sigma_k = m^{\mathrm{T}} \big(\underbrace{x_k}_{(i)} - \underbrace{(Ax_{k-1} + b\bar{u}_{k-1})}_{(ii)} \big) \, , \tag{4.21}$$

with a constant parameter vector $m \in \mathbb{R}^n$. Part (i) stands for the solution of the perturbed system with input $u_k = \bar{u}_k + u_k^S$, whereas part (ii) models the effect of the nominal control signal u_k^S on the unperturbed plant as in (4.20). In continuous-time integral sliding mode versions, part (ii) is given by the solution of the nominal response using a convolution integral, see [SEFL15].

Relation (4.21) is equivalent to

$$\sigma_k = m^{\mathrm{T}} x_k + w_k \tag{4.22a}$$

$$w_{k+1} = -m^{\mathrm{T}} \left(Ax_k + b\bar{u}_k \right) w_k \, , \tag{4.22b}$$

which, together with (4.18) to (4.20), yields

$$\begin{aligned} \sigma_{k+1} &= m^{\mathrm{T}} \big(Ax_k + b \left(u_k + f_k \right) - Ax_k + b\bar{u}_k \big) \\ &= m^{\mathrm{T}} \Big(b \left(u_k^S + f_k \right) \Big) \end{aligned} \tag{4.23}$$

In ideal sliding motion, i.e. $\sigma_k = 0$ and thus also $\sigma_{k+1} = 0$ for all $k \geq k^\star$ with some $k^\star \in \mathbb{N}$, one obtains from (4.21) that the control signal u_k^S provided by the sliding mode controller exactly compensates for the perturbation f_k so that

$$u_k^S = -f_k \, . \tag{4.24}$$

However, only a specific band around $\sigma_k = 0$ (quasi sliding mode band) is achieved in reality due to the discrete-time sliding mode algorithms, see, e.g., [Lud20, LRSH19, LSH$^+$18, Bar98] and references therein for details. This will also be evident in the simulation example at the end of this chapter.

4.3 Networked Control via Integral Sliding Modes

This sections extends the basic integral sliding mode approach to networked buffered systems shown in Figure 4.2. First, a nominal controller is designed using LMI conditions. Then, a properly defined sliding variable allows to decouple the sliding mode controller design for the individual channels $i = 1, 2, \ldots, m$.

4.3.1 Nominal Control

The nominal controller design should render a spatially distribution of the individual controllers possible. This implies that each controller should only access the measured and transmitted states as well as its own previous control signals. For example, controller 1 is only allowed to use x_k, $u_{1,k-1}$, $u_{1,k-2}$ and so on but not $u_{2,k-1}$. This avoids mutual transmissions between the corresponding controllers.

The starting point is the nominal lifted model, i.e. model (4.13) evaluated for $f_k = 0$ for all $k \in \mathbb{N}$ and $u_k = \bar{u}_k$. The inner control loop is deactivated such that $u_k^S = 0$ for all k. This yields the mathematical description of the nominal buffered plant such that

$$\bar{\xi}_{k+1} = \mathcal{A}\bar{\xi}_k + \mathcal{B}\bar{u}_k \tag{4.25}$$

with the nominal lifted state vector

$$\begin{aligned}\bar{\xi}_k = \Big[\; x_k^{\mathrm{T}} \;\Big|\; \bar{u}_{1,k-1} \quad \bar{u}_{1,k-2} \quad \cdots \quad \bar{u}_{1,k-\delta_1} \;\Big|\; \bar{u}_{2,k-1} \quad \bar{u}_{2,k-2} \quad \cdots \quad \bar{u}_{2,k-\delta_2} \;\Big|\; \cdots \\ \cdots \;\Big|\; \bar{u}_{m,k-1} \quad \bar{u}_{m,k-2} \quad \cdots \quad \bar{u}_{m,k-\delta_m} \;\Big]^{\mathrm{T}} \quad \in \mathbb{R}^{n+\Delta}\,.\end{aligned} \tag{4.26}$$

The following theorem rests on LMI-based design techniques as, e.g., presented in [CHvdW$^+$10] and [HvdW10] for the case with bounded time-varying delays. In the present work, the delay variation is made uniform and known due to the buffers involved. However, the LMI approach allows to also specify the structure of the developed controllers, which is important for the proposed approach.

Theorem 4.4 (Nominal, spatially distributed controller design [LSH19]). *Consider the buffered networked feedback loop in Figure 4.2 with $i = 1, 2, \ldots, m$ controllers and the buffered plant described by* (4.25) *with state vector* (4.26) *and matrices $\mathcal{A}$ and $\mathcal{B}$ as defined in* (4.14)*. Buffers* (4.5) *ensure that the round trip delays equal $\delta_i h$, where h is the sampling interval and δ_i the length of buffer i. Let Assumptions 2.1 and 4.3 hold.*

The combination of the individual nominal controllers is given by

$$\bar{u}_k = \bar{K}\bar{\xi}_k = \begin{bmatrix} K_x & K_u \end{bmatrix} \bar{\xi}_k \quad \in \mathbb{R}^m \tag{4.27}$$

with $K_x \in \mathbb{R}^{m\times n}$ and

$$K_u = \begin{bmatrix} k_1^T & 0 & \cdots & 0 & 0 \\ 0 & k_2^T & \ddots & 0 & 0 \\ \vdots & \ddots & \ddots & \ddots & \vdots \\ 0 & 0 & \ddots & k_{m-1}^T & 0 \\ 0 & 0 & \cdots & 0 & k_m^T \end{bmatrix}, \qquad \textit{where} \qquad k_i^T \in \mathbb{R}^{1\times\delta_i}\,. \tag{4.28}$$

Let there exist a symmetric positive definite matrix $Y \in \mathbb{R}^{(n+\Delta)\times(n+\Delta)}$ with Δ as in (4.15)*, matrix $Z = \begin{bmatrix} Z_x & Z_u \end{bmatrix}$ with $Z_x \in \mathbb{R}^{m\times n}$,*

$$Z_u = \begin{bmatrix} z_1^T & 0 & \cdots & 0 & 0 \\ 0 & z_2^T & \ddots & 0 & 0 \\ \vdots & \ddots & \ddots & \ddots & \vdots \\ 0 & 0 & \ddots & z_{m-1}^T & 0 \\ 0 & 0 & \cdots & 0 & z_m^T \end{bmatrix}, \tag{4.29}$$

where $z_i^T \in \mathbb{R}^{1\times\delta_i}$*, and matrix*

$$X = \begin{bmatrix} X_1 & 0 \\ X_2 & X_3 \end{bmatrix} \tag{4.30}$$

with $X_1 \in \mathbb{R}^{n\times n}$*,* $X_2 \in \mathbb{R}^{\Delta\times n}$*,*

$$X_3 = \begin{bmatrix} \bar{X}_{3,1} & 0 & \cdots & 0 & 0 \\ 0 & \bar{X}_{3,2} & \ddots & 0 & 0 \\ \vdots & \ddots & \ddots & \ddots & \vdots \\ 0 & 0 & \cdots & \bar{X}_{3,m-1} & 0 \\ 0 & 0 & \cdots & 0 & \bar{X}_{3,m} \end{bmatrix}, \tag{4.31}$$

with $\bar{X}_{3,i} \in \mathbb{R}^{\delta_i\times\delta_i}$ *and a scalar* γ *bounded by* $0 \le \gamma < 1$ *that satisfy*

$$\left[\begin{array}{c|c} X + X^T - Y & X^T\mathcal{A}^T - Z^T\mathcal{B}^T \\ \hline \mathcal{A}X - \mathcal{B}Z & (1-\gamma)Y \end{array}\right] > 0\,. \tag{4.32}$$

Then, the nominal closed loop system is globally asymptotically stable and the control gains (4.27) *are given by*

$$K_u = Z_u X_3^{-1} \qquad \textit{and} \qquad K_x = \left(Z_x - K_u X_2\right) X_1^{-1}\,. \tag{4.33}$$

In addition, only local information, i.e. delayed values of the own control signals $u_{i,k}$*, is used in the* i*th controller together with* x_k*.*

Proof. The control gain matrix $\bar{K}$ (4.27) multiplied by (4.30) while considering (4.33) yields

$$\begin{aligned} \bar{K}X &= \begin{bmatrix} K_x X_1 + K_u X_2 & K_u X_3 \end{bmatrix} \\ &= \begin{bmatrix} \left(Z_x - K_u X_2\right) X_1^{-1} X_1 + K_u X_2 & K_u X_3 \end{bmatrix} \\ &= \begin{bmatrix} \left(Z_x - Z_u X_3^{-1} X_2\right) + Z_u X_3^{-1} X_2 & Z_u X_3^{-1} X_3 \end{bmatrix} \end{aligned} \tag{4.34}$$

and thus

$$\bar{K}X = \begin{bmatrix} Z_x & Z_u \end{bmatrix} = Z\,. \tag{4.35}$$

Inserting (4.34) and its transpose $Z^{\mathrm{T}} = X^{\mathrm{T}}\bar{K}^{\mathrm{T}}$ into (4.32) results in

$$\left[\begin{array}{c|c} X + X^{\mathrm{T}} - Y & X^{\mathrm{T}}\left(\mathcal{A} - \mathcal{B}\bar{K}\right)^{\mathrm{T}} \\ \hline \left(\mathcal{A} - \mathcal{B}\bar{K}\right) X & (1-\gamma)Y \end{array}\right] > 0\,, \tag{4.36}$$

which is the same form as in Theorem 3 of [DB01] for $N = 1$, $G_1 = X$, $S_1 = Y$ and $A_1 = \mathcal{A} - \mathcal{B}\bar{K}$. Consequently, following [DB01], the considered feedback system is globally asymptotically stable.

In addition, the i$^{\mathrm{th}}$ controller only used local information and x_k as can be seen by combining (4.27), (4.28) and (4.26) such that

$$u_{i,k} = k_{x,i}^{\mathrm{T}} x_k + k_i^{\mathrm{T}} \begin{bmatrix} \bar{u}_{i,k-1} \\ \bar{u}_{i,k-2} \\ \vdots \\ \bar{u}_{i,k-\delta_m} \end{bmatrix} \tag{4.37}$$

where $k_i^{\mathrm{T}} \in \mathbb{R}^{1\times\delta_i}$. Vector $k_{x,i}^{\mathrm{T}} \in \mathbb{R}^{1\times n}$ symbolizes the i$^{\text{th}}$ row of matrix K_x, which completes the proof. ■

Assumption 4.3(b) on the change rates of the sensor-to-controller delays might be limiting in some situations. Thus the following corollary can be utilized to get rid of this assumption.

Corollary 4.5 (Nominal, spatially distributed controller design without restrictions of the change rate of the sensor-to-controller delays)**.** *Consider the setup as stated in Theorem 4.4 where Assumption 4.3(b) on the sensor-to-controller delays is removed. Let matrix* (4.29) *be zero, i.e.* $Z_u = 0 \in \mathbb{R}^{m\times\Delta}$*, and* $X_3 \in \mathbb{R}^{\Delta\times\Delta}$ *a fully occupied matrix.*

Then, the nominal closed loop system is globally asymptotically stable and the gain matrix $\bar{K} \in \mathbb{R}^{m\times(n+\Delta)}$ *in* (4.27) *is given by*

$$\bar{K} = \begin{bmatrix} K_x & 0_{m\times\Delta} \end{bmatrix} \tag{4.38}$$

and the i controllers are static, i.e. they use the plant states x_k *only but no actuating signals from previous time steps or other controllers* $\nu \neq i$ *for* $i, \nu \in \{1, 2, \dots, m\}$*.*

Proof. The proof is a direct consequence of the proof of Theorem 4.4 because the choice of $Z_u = 0$ removes the dependency of $u_{i,k}$ on $u_{i,k-1}$, $u_{i,k-2}$ up to $u_{i,k-\delta_i}$. Thus, the mathematical model (4.13) remains valid also for arbitrary time delays within the intervals specified in Assumption 4.3(b) as explained in detail in Section 2.2 because the controllers are static. ■

Please note that matrix X_3 might be a fully occupied matrix in Corollary 4.5, since the specific structure in (4.31) was only specified to decouple controller i from the other controllers. This in now done by $Z_u = 0$, which, however, yields more restrictive results compared to Theorem 4.4.

4.3.2 Sliding Mode Control

In the next step, a sliding mode controller is designed to render the nominal closed loop system insensitive to external perturbations (f_k) following the steps presented in Section 4.2 for the buffered networked plant model. In addition, a specific definition of the sliding surface allows to decouple the individual control loops shown in Figure 4.2.

Theorem 4.6 (Robustifying, spatially distributed controller design [LSH19])**.** *Consider the buffered networked feedback loop in Figure 4.2 with* $i = 1, 2, \dots, m$ *controllers and the buffered plant described by* (4.13) *with state vector* (4.12) *and matrices* $\mathcal{A}$ *and* $\mathcal{B}$ *as defined in* (4.14)*. Buffers* (4.5) *ensure that the round trip delays equal* $\delta_i h$*, where* h *is the sampling interval and* δ_i *the length of buffer i. Let Assumptions 2.1, 4.1 and 4.3 hold.*

The overall control signal is given by

$$u_k = \bar{u}_k + u_k^S \quad \in \mathbb{R}^m \tag{4.39}$$

where $\bar{u}_k$ *stems from a nominal controller design for* $f_k = 0 \ \forall k \in \mathbb{N}$ *and the* i^{th}

component of $u_k^S = \begin{bmatrix} u_{1,k}^S & u_{2,k}^S & \dots & u_{m,k}^S \end{bmatrix}^T$ *is*

$$u_{i,k}^S = \sigma_{i,k} - h\alpha_i \sqrt{|\sigma_{i,k}|}\,\mathrm{sign}\,\sigma_{i,k} + hz_{i,k} \tag{4.40a}$$

$$z_{i,k+1} = z_{i,k} - h\beta_i\,\mathrm{sign}\,\sigma_{i,k} \tag{4.40b}$$

where

$$\alpha_i = 1.5\sqrt{\Lambda_i}\,, \qquad \beta_i = 1.1\Lambda_i\,, \qquad \textit{and} \qquad \Lambda_i \geq \frac{L_i}{h} \tag{4.41}$$

with change rates L_i *as in Assumption 4.1. The discrete-time integral sliding variable is specified depending on the lifted state* ξ_k (4.12) *such that*

$$\sigma_k = \begin{bmatrix} \sigma_{1,k} & \sigma_{2,k} & \dots & \sigma_{m,k} \end{bmatrix}^T = M\xi_k + w_k \tag{4.42a}$$

$$w_{k+1} = \begin{bmatrix} w_{1,k} & w_{2,k} & \dots & w_{m,k} \end{bmatrix}^T = -M\left(\mathcal{A}\xi_k + \mathcal{B}\bar{u}_k\right) \tag{4.42b}$$

with

$$M = \left[\begin{array}{c|cc|cc|c|cc} p_1^T & \boxed{1} & 0_{1\times\delta_1-1} & 0 & 0_{1\times\delta_2-1} & \cdots & 0 & 0_{1\times\delta_m-1} \\ \hline p_2^T & 0 & 0_{1\times\delta_1-1} & \boxed{1} & 0_{1\times\delta_2-1} & \cdots & 0 & 0_{1\times\delta_m-1} \\ \hline \vdots & \vdots & \vdots & \vdots & \vdots & \ddots & \vdots & \vdots \\ \hline p_m^T & 0 & 0_{1\times\delta_1-1} & 0 & 0_{1\times\delta_2-1} & \cdots & \boxed{1} & 0_{1\times\delta_m-1} \end{array}\right] \tag{4.43}$$

where the left inverse of input matrix B *is used to find* $p_i \in \mathbb{R}^n$ *as*

$$\begin{bmatrix} p_1 & p_2 & \cdots & p_m \end{bmatrix}^T = B^+ = \left(B^TB\right)^{-1} B \quad \in \mathbb{R}^{m\times n}\,. \tag{4.44}$$

Then, the plant states x_k *are ultimately bounded and* (u_k^S) *compensates for* (f_k)*. In addition, only local information, i.e. delayed values of the own control signals* $u_{i,k}$*, is used in the* i^{th} *controller together with* x_k*.*

Proof. The ultimate boundedness of the plant states is shown first in the proof. Hence, the forward increment of the sliding variable (4.42a) is considered in combination with (4.13), (4.39) and (4.42b) yielding

$$\begin{aligned} \sigma_{k+1} &= M\left(\mathcal{A}\xi_k + \mathcal{B}u_k + \mathcal{B}_f f_k\right) + w_{k+1} \\ &= M\mathcal{A}\xi_k + M\mathcal{B}\left(\bar{u}_k + u_k^S\right) + M\mathcal{B}_f f_k - M\left(\mathcal{A}\xi_k + \mathcal{B}\bar{u}_k\right) \\ &= M\mathcal{B}u_k^S + M\mathcal{B}_f f_k \end{aligned} \tag{4.45}$$

The left inverse (4.44) of B exists because the controllability of the plant is not lost through sampling and B has full column rank due to Assumption 2.1. Consequently, one get

$$M\mathcal{B} = \left[\begin{array}{c|cc|cc|c|cc} p_1^\mathrm{T} & \boxed{1} & 0 & 0 & 0 & \cdots & 0 & 0 \\ \hline p_2^\mathrm{T} & 0 & 0 & \boxed{1} & 0 & \cdots & 0 & 0 \\ \hline \vdots & \vdots & \vdots & \vdots & \vdots & \ddots & \vdots & \vdots \\ \hline p_m^\mathrm{T} & 0 & 0 & 0 & 0 & \cdots & \boxed{1} & 0 \end{array}\right] \left[\begin{array}{c|c|c|c} 0 & 0 & \cdots & 0 \\ \hline \boxed{1} & 0 & \cdots & 0 \\ 0 & 0 & \cdots & 0 \\ \hline 0 & \boxed{1} & \cdots & 0 \\ 0 & 0 & \cdots & 0 \\ \hline \vdots & \vdots & \ddots & \vdots \\ \hline 0 & 0 & \cdots & \boxed{1} \\ 0 & 0 & \cdots & 0 \end{array}\right] = I_m \tag{4.46}$$

and

$$M\mathcal{B}_f = \left[\begin{array}{c|cc|cc|c|cc} p_1^{\mathrm{T}} & \boxed{1} & 0 & 0 & 0 & \cdots & 0 & 0 \\ \hline p_2^{\mathrm{T}} & 0 & 0 & \boxed{1} & 0 & \cdots & 0 & 0 \\ \hline \vdots & \vdots & \vdots & \vdots & \vdots & \ddots & \vdots & \vdots \\ \hline p_m^{\mathrm{T}} & 0 & 0 & 0 & 0 & \cdots & \boxed{1} & 0 \end{array}\right] \left[\begin{array}{c} B \\ \hline 0 \\ 0 \\ \hline 0 \\ 0 \\ \hline \vdots \\ \hline 0 \\ 0 \end{array}\right] = B^{+}B = I_m \tag{4.47}$$

which simplifies (4.45) to

$$\sigma_{i,k+1} = u_{i,k}^{S} + f_{i,k} \tag{4.48}$$

This means that the i$^{\mathrm{th}}$ sliding variable $\sigma_{i,k+1}$ solely depends on entities from channel i. Consequently, individual sliding mode controllers can be designed for each channel, which are discretized super-twisting controllers in the present work. Therefore, consider a continuous-time integrator with input $u_i(t)$, i.e.

$$\frac{\mathrm{d}\sigma_i}{\mathrm{d}t} = u_i(t) + \phi_i(t) \tag{4.49}$$

with perturbation $\phi_i(t)$ that has a bounded time-derivative of

$$\sup\left(\left|\frac{\mathrm{d}\phi_i(t)}{\mathrm{d}t}\right|\right) = L_{\phi_i} < \infty\,. \tag{4.50}$$

The application of the super-twisting algorithm introduced in [Lev93] as

$$u_i(t) = -\alpha_i\sqrt{\sigma_i(t)}\,\operatorname{sign}\sigma_i(t) + z_i(t) \tag{4.51a}$$

$$\frac{\mathrm{d}z_i}{\mathrm{d}t} = -\beta_i\,\operatorname{sign}\sigma_i(t) \tag{4.51b}$$

to (4.49) yields the finite-time stable feedback loop

$$\frac{\mathrm{d}\sigma_i}{\mathrm{d}t} = -\alpha_i\sqrt{\sigma_i(t)}\,\operatorname{sign}\sigma_i(t) + z_i(t) + \phi_i(t) \tag{4.52a}$$

$$\frac{\mathrm{d}z_i}{\mathrm{d}t} = -\beta_i\,\operatorname{sign}\sigma_i(t) \tag{4.52b}$$

if the parameters α_i and β_i properly tuned [Lev93]. One classical tuning rule is

$$\alpha_i = 1.5\sqrt{\Phi_i} \qquad \text{and} \qquad \beta_i = 1.1\Phi_i \qquad \text{with} \qquad \Phi_i \geq L_{\phi_i} \tag{4.53}$$

to ensure stability as proven in [SH17]. Applying transformation $\nu_i(t) = z_i(t) + \phi_i(t)$ to relation (4.52) yields

$$\frac{\mathrm{d}\sigma_i}{\mathrm{d}t} = -\alpha_i\sqrt{\sigma_i(t)}\,\operatorname{sign}\sigma_i(t) + \nu_i(t) \tag{4.54a}$$

$$\frac{\mathrm{d}\nu_i}{\mathrm{d}t} = \frac{\mathrm{d}z_i}{\mathrm{d}t} + \frac{\mathrm{d}\phi_i}{\mathrm{d}t} = -\beta_i\,\operatorname{sign}\sigma_i(t) + \frac{\mathrm{d}\phi_i}{\mathrm{d}t} \tag{4.54b}$$

as the continuous-time representation of the closed loop system.

Relations (4.40) in Theorem 4.6 represent the Euler forward discretized equations (4.51) of the super-twisting algorithm. Inserting (4.40) into (4.48) results in

$$\begin{aligned}\sigma_{i,k+1} &= u^S_{i,k} + f_{i,k} = \sigma_{i,k} - h\alpha_i\sqrt{|\sigma_{i,k}|}\operatorname{sign}\sigma_{i,k} + hz_{i,k} + f_{i,k} \\ &= \sigma_{i,k} - h\alpha_i\sqrt{|\sigma_{i,k}|}\operatorname{sign}\sigma_{i,k} + h\left(z_{i,k} + \frac{f_{i,k}}{h}\right) && \text{(4.55a)} \\ z_{i,k+1} &= z_{i,k} - h\beta_i \operatorname{sign}\sigma_{i,k} && \text{(4.55b)}\end{aligned}$$

and thus, using the additional variable $\nu_{i,k} = z_{i,k} + \frac{f_{i,k}}{h}$,

$$\begin{aligned}\sigma_{i,k+1} &= \sigma_{i,k} - h\alpha_i\sqrt{|\sigma_{i,k}|}\operatorname{sign}\sigma_{i,k} + h\nu_{i,k} && \text{(4.56a)} \\ \nu_{i,k+1} &= z_{i,k+1} + \frac{f_{i,k+1}}{h} = z_{i,k} - h\beta_i\operatorname{sign}\sigma_{i,k} + \frac{f_{i,k+1}}{h} \\ &= \nu_{i,k} - \frac{f_{i,k}}{h} - h\beta_i\operatorname{sign}\sigma_{i,k} + \frac{f_{i,k+1}}{h} \\ &= \nu_{i,k} - h\beta_i\operatorname{sign}\sigma_{i,k} + \frac{f_{i,k+1} - f_{i,k}}{h}\,. && \text{(4.56b)}\end{aligned}$$

Relation (4.56b) is equivalent to

$$\frac{\nu_{i,k+1} - \nu_{i,k}}{h} = -\beta_i\operatorname{sign}\sigma_{i,k} + \frac{f_{i,k+1} - f_{i,k}}{h^2}\,, \tag{4.57}$$

which is the Euler forward discretized form of (4.56b). Thus, conditions (4.41) follow from (4.53) and

$$L_{\phi_i} = \sup\left(\left|\frac{f_{i,k+1} - f_{i,k}}{h^2}\right|\right) = \frac{1}{h}\sup\left(\left|\frac{f_{i,k+1} - f_{i,k}}{h}\right|\right) = \frac{L_i}{h} \tag{4.58}$$

with L_i as in Assumption 4.1. Due to this equivalence, the ultimate boundedness of the sliding variables $\sigma_{i,k}$ and states x_k is ensured, see [LL14].

In the second part of the proof it is necessary to show that the i controllers use local information only. The sliding variable σ_k and the additional variable w_k are given by (4.42) as

$$\begin{aligned}\sigma_k &= \begin{bmatrix}\sigma_{1,k} & \sigma_{2,k} & \cdots & \sigma_{m,k}\end{bmatrix}^{\mathrm{T}} = M\xi_k + w_k && \text{(4.59a)} \\ w_{k+1} &= \begin{bmatrix}w_{1,k} & w_{2,k} & \cdots & w_{m,k}\end{bmatrix}^{\mathrm{T}} = -M\mathcal{A}\xi_k - M\mathcal{B}\bar{u}_k\,, && \text{(4.59b)}\end{aligned}$$

where $M\xi_k$ and $M\mathcal{A}\xi_k$ can be simplified by means of the structures of the involves matrices, cf. (4.14), (4.43) such that

$$M\mathcal{A} = \left[\begin{array}{c|cc|cc|c|cc} p_1^{\mathrm{T}} & \boxed{1} & 0 & 0 & 0 & \cdots & 0 & 0 \\ \hline p_2^{\mathrm{T}} & 0 & 0 & \boxed{1} & 0 & \cdots & 0 & 0 \\ \hline \vdots & \vdots & \vdots & \vdots & \vdots & \ddots & \vdots & \vdots \\ \hline p_m^{\mathrm{T}} & 0 & 0 & 0 & 0 & \cdots & \boxed{1} & 0 \end{array}\right] \left[\begin{array}{c} x_k \\ \hline u_{1,k-1} \\ u_{1,k-2} \\ \vdots \\ u_{1,k-\delta_1} \\ \hline u_{2,k-1} \\ u_{2,k-2} \\ \vdots \\ u_{2,k-\delta_2} \\ \hline \vdots \\ \hline u_{m,k-1} \\ u_{m,k-2} \\ \vdots \\ u_{m,k-\delta_m} \end{array}\right] = \left[\begin{array}{c} p_1^{\mathrm{T}} x_k + u_{1,k-1} \\ \hline p_2^{\mathrm{T}} x_k + u_{2,k-1} \\ \hline \vdots \\ \hline p_m^{\mathrm{T}} x_k + u_{m,k-1} \end{array}\right] \tag{4.60}$$

and

$$\begin{aligned} M\mathcal{A}\xi_k &= \\ &= \left[\begin{array}{c|cc|cc|c|cc} p_1^{\mathrm{T}} & \boxed{1} & 0 & 0 & 0 & \cdots & 0 & 0 \\ \hline p_2^{\mathrm{T}} & 0 & 0 & \boxed{1} & 0 & \cdots & 0 & 0 \\ \hline \vdots & \vdots & \vdots & \vdots & \vdots & \ddots & \vdots & \vdots \\ \hline p_m^{\mathrm{T}} & 0 & 0 & 0 & 0 & \cdots & \boxed{1} & 0 \end{array}\right] \left[\begin{array}{c|cc|cc|c|cc} A & 0 & b_1 & 0 & b_2 & \cdots & 0 & b_m \\ \hline 0 & 0 & 0 & 0 & 0 & \cdots & 0 & 0 \\ 0 & \boxed{I} & 0 & 0 & 0 & \cdots & 0 & 0 \\ \hline 0 & 0 & 0 & 0 & 0 & \cdots & 0 & 0 \\ 0 & 0 & 0 & \boxed{I} & 0 & \cdots & 0 & 0 \\ \hline \vdots & \vdots & \vdots & \vdots & \vdots & \ddots & \vdots & \vdots \\ \hline 0 & 0 & 0 & 0 & 0 & \cdots & 0 & 0 \\ 0 & 0 & 0 & 0 & 0 & \cdots & \boxed{I} & 0 \end{array}\right] \xi_k \\ &= \left[\begin{array}{c|cc|cc|c|cc} p_1^{\mathrm{T}} A & 0_{1\times\delta_1-1} & p_1^{\mathrm{T}} b_1 & 0_{1\times\delta_2-1} & p_1^{\mathrm{T}} b_2 & \cdots & 0_{1\times\delta_m-1} & p_1^{\mathrm{T}} b_m \\ \hline p_2^{\mathrm{T}} A & 0 & p_2^{\mathrm{T}} b_1 & 0 & p_2^{\mathrm{T}} b_2 & \cdots & 0 & p_2^{\mathrm{T}} b_m \\ \hline \vdots & \vdots & \vdots & \vdots & \vdots & \ddots & \vdots & \vdots \\ \hline p_m^{\mathrm{T}} A & 0 & p_m^{\mathrm{T}} b_1 & 0 & p_m^{\mathrm{T}} b_2 & \cdots & 0 & p_m^{\mathrm{T}} b_m \end{array}\right] \xi_k \qquad (4.61) \\ &= \begin{bmatrix} p_1^{\mathrm{T}} \\ p_2^{\mathrm{T}} \\ \cdots \\ p_m^{\mathrm{T}} \end{bmatrix} A x_k + \begin{bmatrix} p_1^{\mathrm{T}} \\ p_2^{\mathrm{T}} \\ \cdots \\ p_m^{\mathrm{T}} \end{bmatrix} \begin{bmatrix} b_1 & b_2 & \cdots & b_m \end{bmatrix} \begin{bmatrix} u_{1,k-\delta_1} \\ u_{2,k-\delta_2} \\ \cdots \\ u_{m,k-\delta_m} \end{bmatrix} = B^{+} A \xi_k + \underbrace{B^{+} B}_{I_m} \begin{bmatrix} u_{1,k-\delta_1} \\ u_{2,k-\delta_2} \\ \cdots \\ u_{m,k-\delta_m} \end{bmatrix} \end{aligned}$$

Combining (4.59) with (4.46), (4.60) and (4.61) results in the equations evaluated by the i$^{\mathrm{th}}$ controller as

$$\sigma_{i,k} = p_i^{\mathrm{T}} x_k + u_{i,k-1} + w_{i,k} \tag{4.62a}$$

$$w_{i,k+1} = -p_i^{\mathrm{T}} A x_k - u_{i,k-\delta_i} - \bar{u}_{i,k}\,. \tag{4.62b}$$

This shows that controller i only uses local information and the states x_k but no delayed control signals of other channels. This completes the proof. ■

Please note that the main contribution of Theorem 4.6 is the robustification of the nominal control together with the decoupling of the sliding mode controllers in the individual channels i. It offers the possibility to use any sliding mode control algorithm for relative degree one systems to get u_k^S. In the current work, a Euler forward discretized version of the super-twisting algorithm was used as an example. However, many other discrete-time algorithms or discretized versions of continuous-time algorithms can be utilized. For example, a super-twisting algorithm that is discretized via the matching approach [KR19] is employed in [Lud20].

4.4 Simulation Example

The properties of the approach that is proposed in this chapter are highlighted using a simulation example [LSH19] for an unstable continuous-time plant with four states and three inputs. Dynamic matrix $\tilde{A}$ and input matrix $\tilde{B}$ are given by

$$\tilde{A} = \begin{bmatrix} -3 & -3 & -2 & 1 \\ 2 & -3 & -2 & 2 \\ 1 & 2 & -3 & 1 \\ -3 & -3 & 3 & 0 \end{bmatrix} \quad \text{and} \quad \tilde{B} = \begin{bmatrix} -1 & -3 & 0 \\ 1 & 3 & 1 \\ -3 & 3 & -1 \\ -2 & -3 & 2 \end{bmatrix}, \tag{4.63}$$

respectively. A sampling interval of $h = 0.1\,s$ is chosen and the maximal round trip delays equal $\delta_i h$ with $\delta_1 = 3$, $\delta_2 = 7$ and $\delta_3 = 6$ provided by the buffers of channels $i = 1, 2, 3$, see Figure 4.2. The actual time-varying transmission delays are important to a lesser extent, as long as they comply with Assumption 4.3, since the buffers make the round trip delays uniform.

The matched perturbation consists of two sinusoidal functions with offset specified as

$$f_k = \begin{bmatrix} 1 \\ 2 \\ 3 \end{bmatrix} \sin\left(\begin{bmatrix} 0.1 \\ 0.2 \\ 0.3 \end{bmatrix} kh \right) + \begin{bmatrix} 3 \\ 2 \\ 1 \end{bmatrix} \sin\left(\begin{bmatrix} 0.1 \\ 0.2 \\ 0.3 \end{bmatrix} \pi kh \right) + \begin{bmatrix} 1 \\ 2 \\ 3 \end{bmatrix} \tag{4.64}$$

in the simulation as shown in Figure 4.4. Please note that the frequencies of the two sinusoidal functions are not integer multiples (they are multiplied by π in the present case) of each other to avoid periodic disturbances.

In a first step, Theorem 4.4 is evaluated. A choice of parameter $\gamma = 0.98$ yields the solution of the LMI conditions (4.32) such that the nominal control signal $\bar{u}_k$ depends on the states and the previous actuating signals as can be seen in (4.27). Matrix

$$K_x = \begin{bmatrix} 0.25000 & -0.02240 & -0.48700 & -0.50900 \\ -0.00241 & 0.00110 & 0.00261 & 0.00405 \\ -0.00449 & 0.00172 & 0.00553 & 0.00655 \end{bmatrix} \in \mathbb{R}^{m \times n} \tag{4.65}$$

weights the states in $\bar{u}_k = \begin{bmatrix} \bar{u}_{1,k} & \bar{u}_{2,k} & \bar{u}_{3,k} \end{bmatrix}^{\mathrm{T}}$. Matrix $K_u \in \mathbb{R}^{m \times \Delta}$ with $m = 3$ and $\Delta = \delta_1 + \delta_2 + \delta_3 = 17$ is composed of vectors

$$\begin{aligned} k_1^{\mathrm{T}} &= \begin{bmatrix} 0.461 & 0.365 & 0.213 \end{bmatrix} && \in \mathbb{R}^{1 \times \delta_1} \\ k_2^{\mathrm{T}} &= \begin{bmatrix} 80.50 & 57.90 & 32.00 & 16.50 & 9.08 & 4.68 & 2.19 \end{bmatrix} \cdot 10^{-3} && \in \mathbb{R}^{1 \times \delta_2} \\ k_3^{\mathrm{T}} &= \begin{bmatrix} 47.30 & 33.00 & 20.90 & 12.60 & 6.77 & 2.88 \end{bmatrix} \cdot 10^{-3} && \in \mathbb{R}^{1 \times \delta_3} \end{aligned} \tag{4.66}$$

that are arranged as in (4.28).

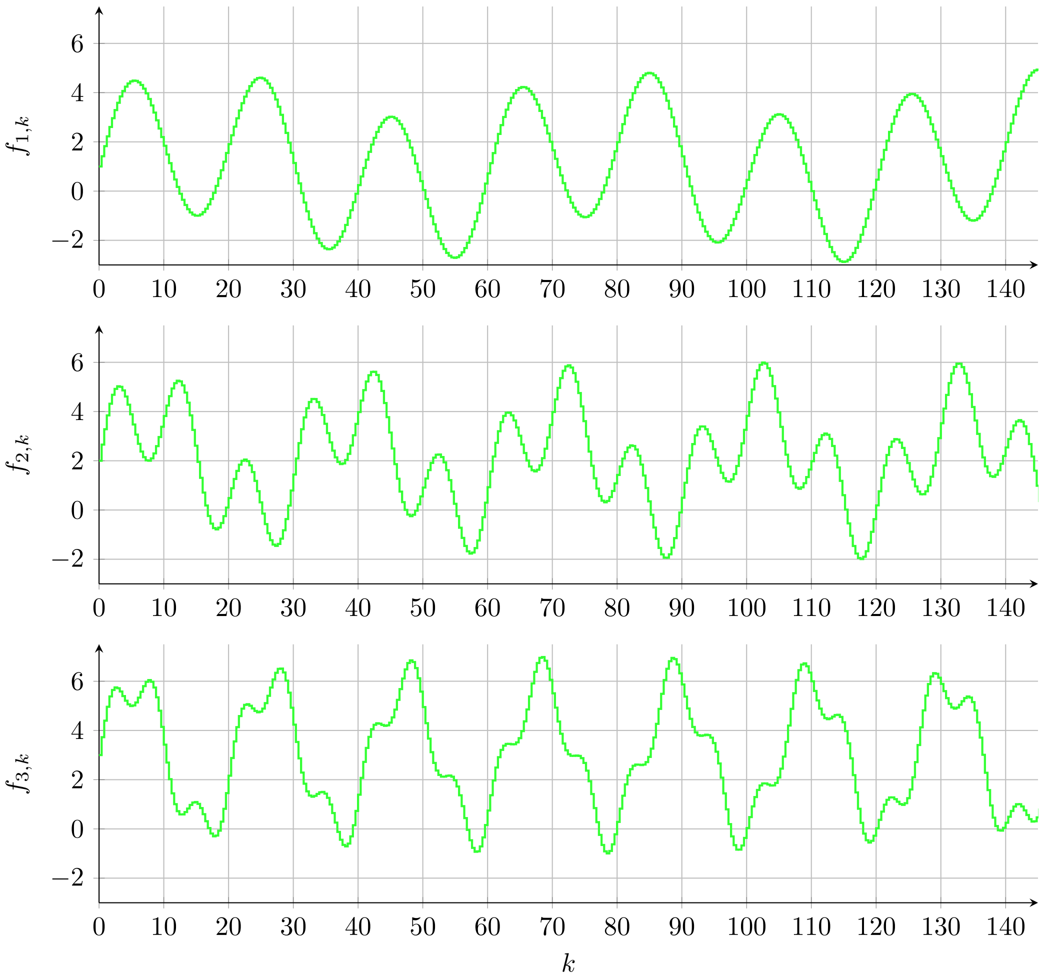

Figure 4.4: Simulation example: perturbations $f_{i,k}$ with $i \in \{1, 2, 3\}$.

In a second step, the sliding mode part is designed as stated in Theorem 4.6. Hence, the maximal change rates (4.1) of perturbations (4.64) are calculated as

$$L = \begin{bmatrix} L_1 & L_2 & L_3 \end{bmatrix}^{\mathrm{T}} = \begin{bmatrix} 1.04 & 1.66 & 1.84 \end{bmatrix}^{\mathrm{T}} \tag{4.67}$$

to find the parameter settings (4.41) for the three individual sliding mode controllers for channels 1, 2 and 3, see Table 4.1. The integral sliding surface is designed as in (4.42), which together with (4.11), yields

Table 4.1: Simulation example: parameters for the $m = 3$ sliding mode controllers

i	Λ_i	α_i	β_i
1	10.6	4.88	11.66
2	16.8	6.15	18.48
3	18.6	6.47	20.46

$$B^{+} = \begin{bmatrix} p_1^{\mathrm{T}} \\ p_2^{\mathrm{T}} \\ p_3^{\mathrm{T}} \end{bmatrix} = \begin{bmatrix} -0.384 & 0.661 & -2.240 & -1.310 \\ -1.380 & 1.140 & 1.070 & -0.302 \\ -1.280 & 3.550 & -1.260 & 3.050 \end{bmatrix} \tag{4.68}$$

and so three independent sliding variables

$$\begin{aligned}\sigma_{1,k} &= p_1^{\mathrm{T}} x_k + u_{1,k-1} + w_{1,k} \\ w_{1,k+1} &= \begin{bmatrix}0.0121 & -0.5220 & 2.0900 & 1.4300\end{bmatrix} x_k - u_{1,k-3} - \bar{u}_{1,k}\,,\end{aligned} \tag{4.69}$$

$$\begin{aligned}\sigma_{2,k} &= p_2^{\mathrm{T}} x_k + u_{2,k-1} + w_{2,k} \\ w_{2,k+1} &= \begin{bmatrix}0.6840 & -1.3000 & -0.6970 & 0.0633\end{bmatrix} x_k - u_{1,k-7} - \bar{u}_{2,k}\end{aligned} \tag{4.70}$$

and

$$\begin{aligned}\sigma_{3,k} &= p_3^{\mathrm{T}} x_k + u_{3,k-1} + w_{3,k} \\ w_{3,k+1} &= \begin{bmatrix}1.4000 & -2.0000 & 0.3300 & -3.3800\end{bmatrix} x_k - u_{1,k-6} - \bar{u}_{3,k}\,.\end{aligned} \tag{4.71}$$

The first terms on the right hand sides of $w_{i,k+1}$ in (4.69), (4.70) and (4.71) are equal to $-p_i^{\mathrm{T}} A x_k$ for $i \in \{1, 2, 3\}$ as stated in (4.62).

Figures 4.5 to 4.7 present the simulation results obtained for an initial state vector of $x_0 = \begin{bmatrix}-7 & 7 & 3 & -3\end{bmatrix}^{\mathrm{T}}$. A convergence to the quasi-sliding mode band is reached after approximately $4\,s$ as visible in Figure 4.5 in all channels.

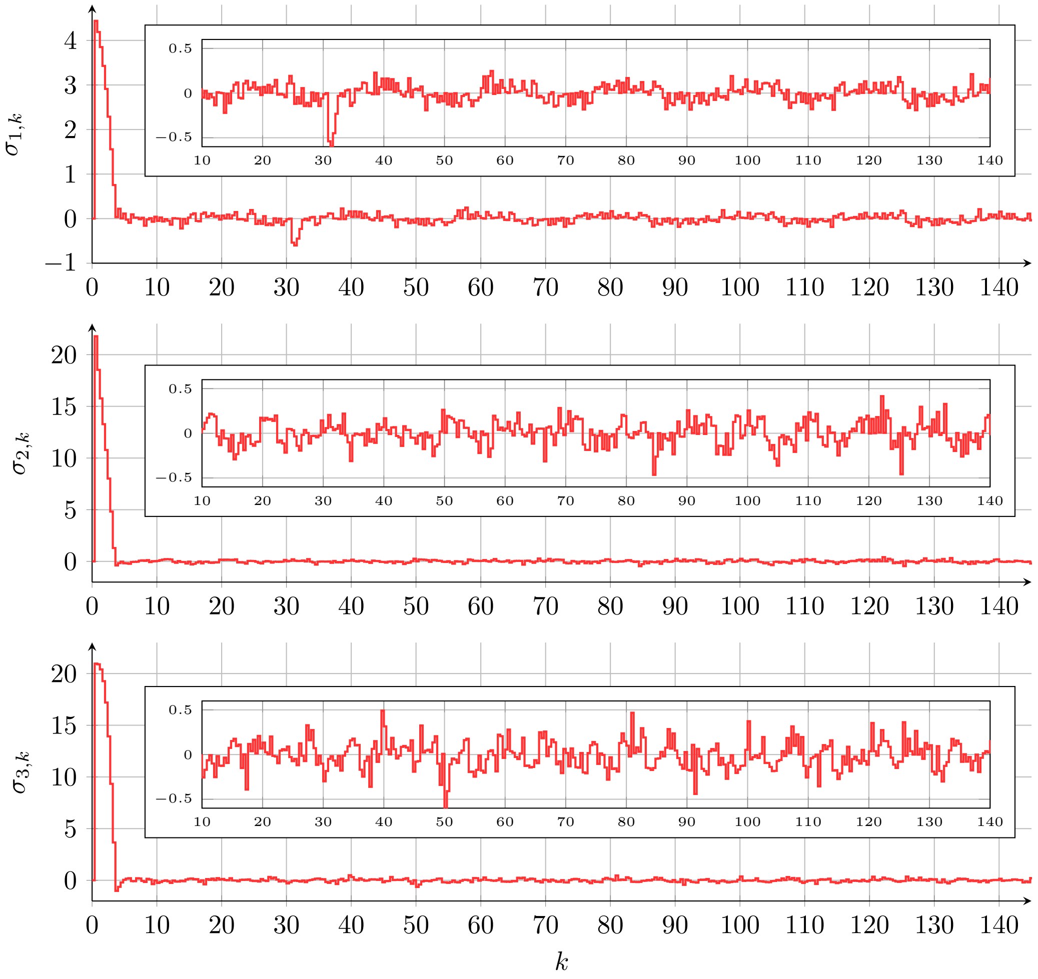

Figure 4.5: Simulation example: sliding variables σ_k for the channels 1, 2 and 3.

The effect of the additional inner integral sliding mode controllers in Figure 4.2 is evident in the plots for the states x_k and the corresponding control signals u_k in Figures 4.6 and 4.7 respectively. The blue signals equal the results for the nominal case, i.e. $u_k = \bar{u}_k$. In contrast, the use of the additional robustification, i.e. $u_k = \bar{u}_k + u_k^S$, allows to drastically attenuate the effects caused by the external perturbations. This is possible since in ideal discrete-time sliding motion, i.e. for $\sigma_{i,k} = 0$ for all $k \geq k^\star$ with some $k^\star \in \mathbb{N}$, the actuating signal compensates for the perturbations such that $u_{i,k}^S = -f_{i,k}$ as also shown in (4.24) and visible in (4.48). The discretized super-twisting algorithm forces the sliding variables to quasi-sliding mode bands only (and not exactly to zero) as depicted in Figure 4.5. Hence, the compensation is not exact as presented in Figure 4.7, where the green plots stand for the perturbations multiplied by minus one.

The simulation example underpins that the proposed integral sliding mode based control approach makes it possible to robustly control networked plants, which are connected via transmissions networks to i separate and possibly spatially distributed controllers for the i actuators. The introduced buffering mechanisms convert the time-varying packet delays in the network connections into constant and known round trip delays in the individual channels $i = \{1, 2, \dots, m\}$.

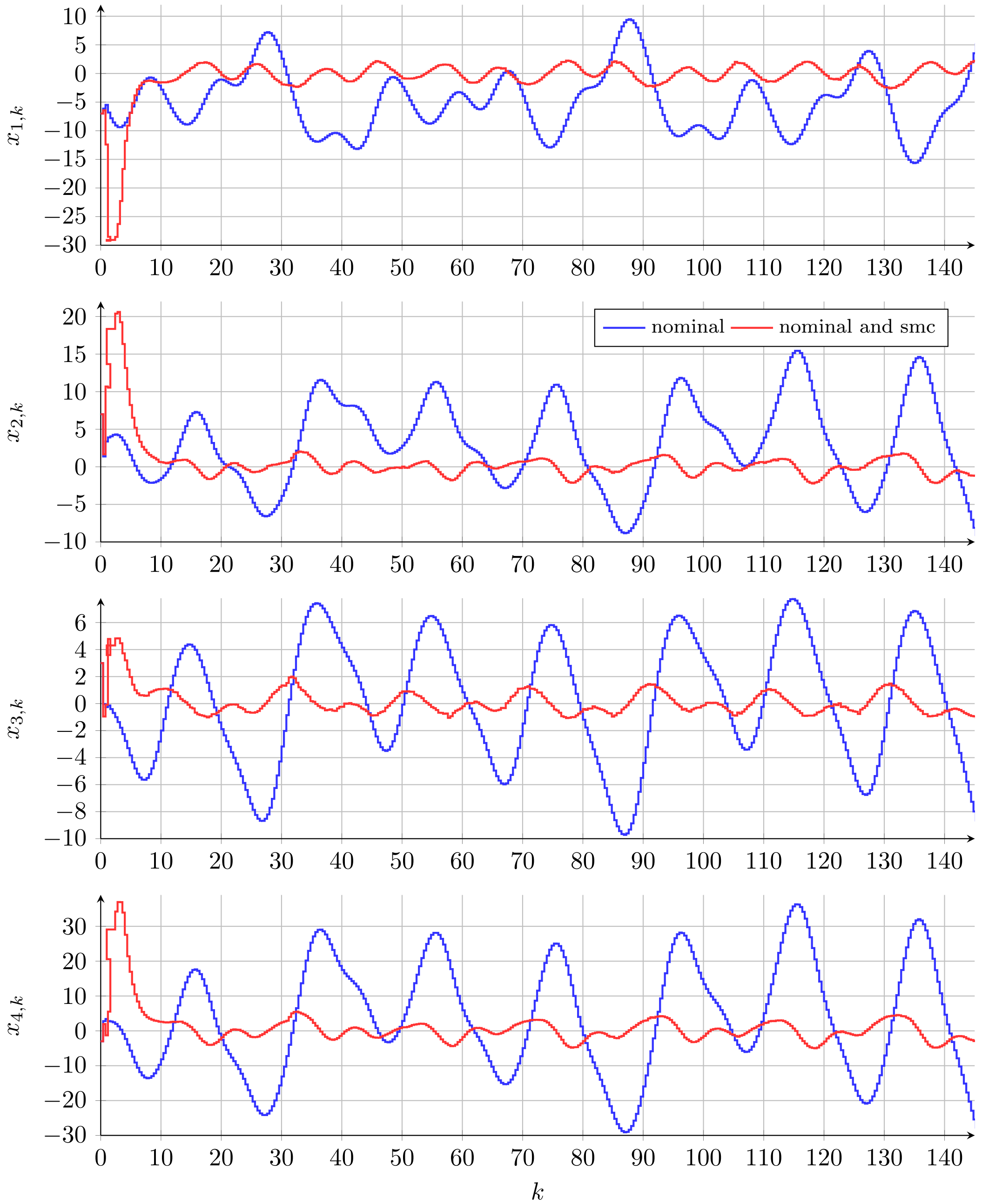

Figure 4.6: Simulation example: states x_k for the case with nominal part only (blue) and for the case with the nominal and sliding mode part (red).

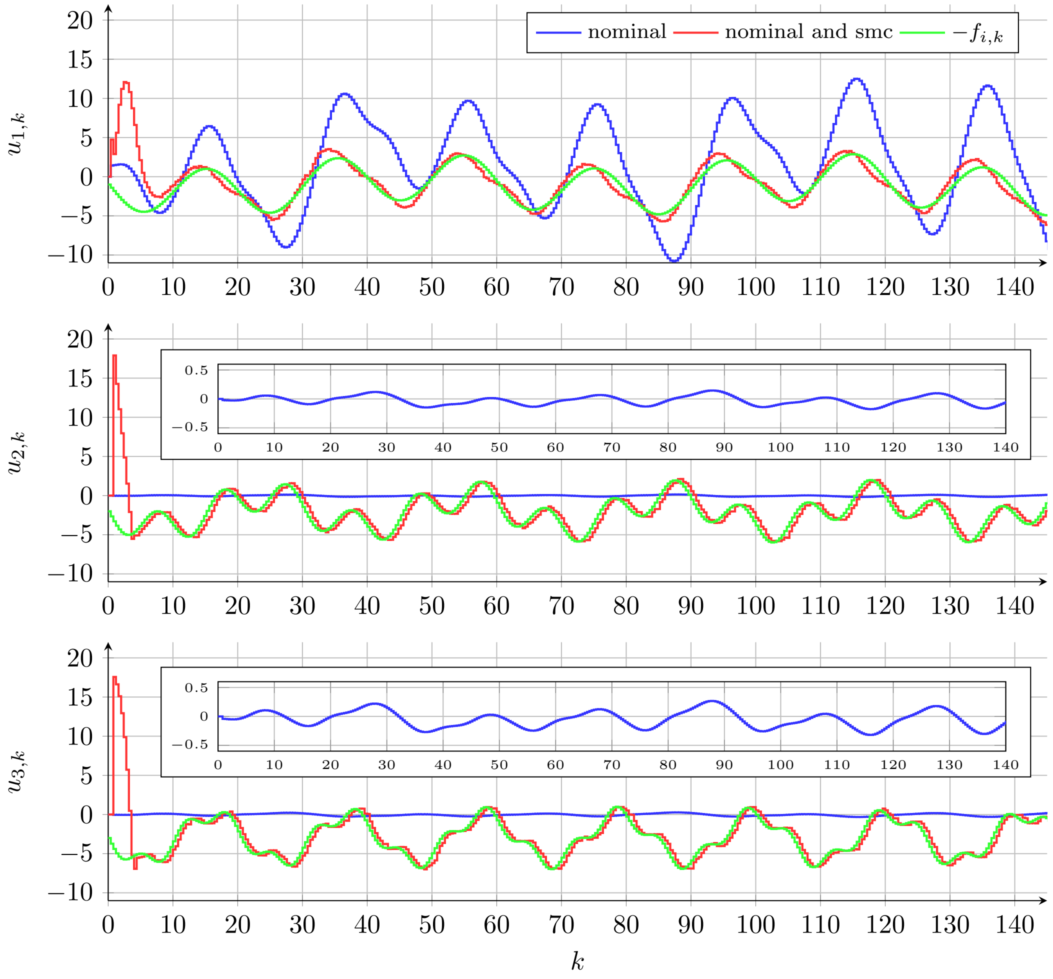

Figure 4.7: Simulation example: control signals u_k for the case with nominal part $\bar{u}_k$ only (blue) and for the case with the nominal and sliding mode part $\bar{u}_k + u_k^S$ (red).

Chapter 5

Adaptive Control of Networked Systems

This chapter is adopted from [SHF19], [SHF21] and presents adaptive control approaches for multivariable networked systems in state space form. The transmission channels are characterized by uncertain time delays.

First, the considered plant description and assumptions on the network are introduced. Adaptive laws are proposed in the following on the basis of the fundamental idea of model reference adaptive control. The key element is the definition of a virtual output variable, which can be, from a sliding mode perspective, regarded as a sliding variable. As a result, the dynamics of the closed loop system can be split into a part related to the virtual output, which is forced to zero, and a remaining part. It is shown in this chapter, how to design the adaptive laws and prove the stability of the system consisting of the adaptive controller, the multivariable plant and the communication network. This allows to control the plant via the transmission network that exhibits unknown time delays in the communication links.

In contrast to classical adaptive approaches, it features computationally cheap implementations since the controller operates in a reduced dimension. Two different approaches are presented to either track desired references for the virtual outputs or to stabilize the virtual outputs at zero. It is also shown, how the two introduced methods can be extended to further improve the control performance. Finally, simulation examples facilitate comparisons between the presented adaptive techniques as well as to a non-adaptive approach.

The starting point is a continuous-time linear time-invariant multivariable plant as in (2.1), i.e.

$$\frac{\mathrm{d}x(t)}{\mathrm{d}t} = \tilde{A}x(t) + \tilde{B}u(t) \tag{5.1}$$

with states $x(t) \in \mathbb{R}^n$ and input vector $u(t) \in \mathbb{R}^m$ at time t.

> **Assumption 5.1** (Plant)**.** *The constant matrices $\tilde{A} \in \mathbb{R}^{n\times n}$ and $\tilde{B} \in \mathbb{R}^{n\times m}$ in* (5.1) *might be known, completely unknown or partially unknown due to some uncertain parameters. The pair $(\tilde{A}, \tilde{B})$ is controllable and the sampling is carried out with a non-pathological sampling interval h in the sense of [KHN63] to preserve the full rank of the discretized input matrix.*

The controller is connected to the plant via a network connection between sensor and controller as well as between controller and actuator, as shown in Figure 2.1.

> **Assumption 5.2** (Round trip delay)**.** *The round trip delay* $\tau = \tau^{sc} + \tau^{c} + \tau^{ca} \in \mathbb{R}$ *is constant for all packets* j*, i.e.* $\tau_j = \tau \ \forall j$ *but unknown. It is bounded such that*
>
> $$h \leq \underline{\tau} \leq \tau \leq \bar{\tau} \tag{5.2}$$
>
> *and* $\underline{\tau}, \tau, \bar{\tau} \in \mathbb{R}_+$ *.*

Assumption 5.2 is reasonable because of the existence of a minimum time for transmission of data packets in real networks due to physical constraints and the used protocols. Unstable plants should be controlled over reliable networks, e.g., using WirelessHART [SXLC15] that ensures constant delays for a specific task class. The delay only changes in situations, where, e.g., additional tasks with higher priority are started or stopped.

Since the round trip delay is constant, one can lump all delays to a combined delay between controller and actuator as depicted in Figure 2.2. It is also not necessary to either assume a bounded changes rate for the sensor-to-controller delays or to use a static controller only as in Assumption 2.4, which is explained in detail in Section 2.2.

The main goals in this chapter are to design control algorithms that

(a) allow the plant states x_k to track given reference values $\hat{x}_k$ under the presence of unknown but constant time delays induced by the network and unknown system matrices $\tilde{A}$ and $\tilde{B}$,

(b) minimizes the computational complexity and the corresponding number of adaptation laws to a minimum by splitting the dynamics into two parts and

(c) ensures the stability of the closed loop system for the networked plant for all times.

The basic ideas are explained in the next section, which forms the basis for the extensions presented in Sections 5.2 and 5.4.

5.1 Adaptive Tracking

A control algorithm based on the idea of model reference adaptive control [NL80, GS84, NA12] for multivariable networked systems described by the lifted model (2.23) with matrices $\mathcal{A}$ and $\mathcal{B}$ (2.24) is considered first. This classical approach [NL80] uses a reference model

$$\xi_{M,k+1} = \mathcal{A}_M \xi_{M,k} + \mathcal{B}_M r_k \ , \tag{5.3}$$

with desired matrices $\mathcal{A}_M$ and $\mathcal{B}_M$, state vector $\xi_{M,k} \in \mathbb{R}^{n+m\bar{d}}$ and a given reference signal $r_k \in \mathbb{R}^m$. The goal is to design a linear time-varying state controller

$$u_k = \theta_{1,k}\xi_k + \theta_{2,k} r_k \tag{5.4}$$

to enforce the convergence of the error $e_k = \xi_k - \xi_{M,k}$ between the consider system states and the reference system states to zero such that $e_k \to 0$ for $k \to \infty$. Hence, a nominal controller $u_k = \bar{\theta}_1 \xi_k + \bar{\theta}_2 r_k$ with constant matrices $\bar{\theta}_1$ and $\bar{\theta}_2$ is designed in a first step. The closed loop system

$$\xi_{k+1} = \left(\mathcal{A} + \mathcal{B}\,\bar{\theta}_1\right) \xi_k + \mathcal{B}\,\bar{\theta}_2\, r_k \, , \tag{5.5}$$

is requested to be equal to the reference dynamics (5.3) for $e_k \to 0$, i.e. $\xi_k \to \xi_{M,k}$. This results in conditions

$$\mathcal{A} + \mathcal{B}\,\bar{\theta}_1 = \mathcal{A}_M \qquad \text{and} \qquad \mathcal{B}\,\bar{\theta}_2 = \mathcal{B}_M \tag{5.6}$$

for the nominal parameters $\bar{\theta}_1$ and $\bar{\theta}_2$. A second step is necessary to stabilize the closed loop system with the help of a law for adapting $\theta_{1,k}$ and $\theta_{2,k}$ in (5.4), because $\mathcal{A}$ and $\mathcal{B}$ are constant but unknown because $\tilde{A}$ and $\tilde{B}$ are unknown according to Assumption 5.1. Details of the classical adaptation law design can be found, e.g., in [NL80]. However, conditions (5.6) cannot always be fulfilled. In addition, the dimension of the state space for $\xi_{M,k} \in \mathbb{R}^{n+m\bar{d}}$ depends on $\bar{d}$ (2.10) and, as a consequence, on the upper bound on the delay $\bar{\tau}$ as stated in Assumption 5.2. Consequently, the resulting adaptive law has a large dimension that leads to an increased computational effort.

Adaptive discrete-time sliding mode control approaches based on ideas of [BFU95] are proposed in the following to overcome the mentioned limitations. Hence, the extended (lifted) state vector defined in (2.22) is rearranged such that

$$z_k = \left[\begin{array}{c|c} z_{1,k}^{\mathrm{T}} & z_{2,k}^{\mathrm{T}} \end{array}\right]^{\mathrm{T}} \quad \in \mathbb{R}^{n+m\bar{d}} \tag{5.7a}$$

with

$$z_{1,k} = \begin{bmatrix} x_k^{\mathrm{T}} & u_{k-\bar{d}}^{\mathrm{T}} & u_{k-\bar{d}+1}^{\mathrm{T}} & \cdots & u_{k-3}^{\mathrm{T}} & u_{k-2}^{\mathrm{T}} \end{bmatrix}^{\mathrm{T}} \quad \in \mathbb{R}^{n+m(\bar{d}-1)}, \tag{5.7b}$$

$$z_{2,k} = u_{k-1} \quad \in \mathbb{R}^{m}\,. \tag{5.7c}$$

This yields the mathematical description

$$z_{k+1} = \mathcal{A}_z z_k + \mathcal{B}_z u_k \tag{5.8}$$

with matrices

$$\mathcal{A}_z = \left[\begin{array}{cccccc|c} e^{\tilde{A}h} & M_0(\tau) & M_1(\tau) & M_2(\tau) & \cdots & M_{\bar{d}-2}(\tau) & M_{\bar{d}-1}(\tau) \\ 0 & 0 & I_m & 0 & \ddots & 0 & 0 \\ \vdots & \vdots & \ddots & \ddots & \ddots & \vdots & \vdots \\ 0 & 0 & 0 & 0 & \ddots & 0 & 0 \\ 0 & 0 & 0 & 0 & \ddots & I_m & 0 \\ 0 & 0 & 0 & 0 & \cdots & 0 & I_m \\ \hline 0 & 0 & 0 & 0 & \cdots & 0 & 0 \end{array}\right], \quad \mathcal{B}_z = \left[\begin{array}{c} M_{\bar{d}}(\tau) \\ 0 \\ \vdots \\ 0 \\ 0 \\ 0 \\ \hline I_m \end{array}\right] \tag{5.9}$$

and sub-matrices $M_i(\tau) \in \mathbb{R}^{n \times m}$ with $i = 0, 1, \ldots, \bar{d}$ that depend on the uncertain time delay τ as defined in (2.20). Matrix $M_{\bar{d}}$ in (5.9) is identical to zero because of Assumption 5.2 and yields, as a consequence, a perfectly known input matrix $\mathcal{B}_z$ in (5.9) although $\tilde{B}$ is not known. Based on that, one can write (5.8) with (5.7) and (5.9) as

$$\begin{bmatrix} z_{1,k+1} \\ z_{2,k+1} \end{bmatrix} = \begin{bmatrix} A_{11} & A_{12} \\ A_{21} & A_{22} \end{bmatrix} \begin{bmatrix} z_{1,k} \\ z_{2,k} \end{bmatrix} + \begin{bmatrix} B_1 \\ B_2 \end{bmatrix} u_k \tag{5.10}$$

where $B_1 = 0_{(n+m(\bar{d}-1))\times m}$ due to Assumption 5.2. This assumption will be relaxed for single-input plants as shown below. Matrices A_{11}, A_{12}, A_{21} and A_{22} represent sub-matrices of $\mathcal{A}_z$ in accordance with the dimensions of (5.7).

A virtual output variable

$$\sigma_k = C_1 z_{1,k} + I_m z_{2,k} = \begin{bmatrix} C_1 & I_m \end{bmatrix} \begin{bmatrix} z_{1,k} \\ z_{1,k} \end{bmatrix} = C z_k \quad \in \mathbb{R}^m \tag{5.11}$$

is designed by specifying matrix $C \in \mathbb{R}^{m \times (n+m\bar{d})}$ such that $C\mathcal{B}_z$ has full rank. The resulting dynamics is given by

$$\sigma_{k+1} = A_1 z_{1,k} + A_2 \sigma_k + C\mathcal{B}_z\, u_k \tag{5.12}$$

with matrices

$$A_1 = A_{21} - A_{22}C_1 + C_1 A_{11} - C_1 A_{12} C_1 \ , \tag{5.13a}$$
$$A_2 = A_{22} + C_1 A_{12} \ . \tag{5.13b}$$

In accordance with (5.12), one can specify the reference dynamics

$$\sigma_{M,k+1} = A_{M1} z_{1,k} + A_M \sigma_{M,k} + B_M r_k \tag{5.14}$$

with respect to $z_{1,k}$ and $\sigma_{M,k}$. A reference $r_k \in \mathbb{R}^m$ for $\sigma_{M,k}$ is included via a non-singular input matrix B_M and the error between actual and desired output is defined as

$$e_k = \sigma_k - \sigma_{M,k} \quad \in \mathbb{R}^m \,. \tag{5.15}$$

From a sliding mode perspective, a so-called discrete-time quasi sliding motion is achieved for $A_{M1} = 0$, $A_M = 0$ and $B_M = I_m$ as, e.g., in [CB16] for the single-input case. This can be regarded as a non-switching discrete-time reaching law that forces the virtual output to zero in a finite number of steps. As shown in [LSH+18], non-switching reaching laws may have some advantages for networked sliding mode control. Especially, the achievable size of the resulting quasi sliding mode band is reduced for the non-switching approach in [LSH+18], whereas the considered switching reaching law yields a larger band.

5.1.1 Nominal control

Following the idea of discrete-time model reference adaptive control as, e.g., in [NA12], a nominal controller is designed first for the dynamics related to the virtual output. Combining (5.8), (5.11), (5.14) and (5.15) yields the error dynamics

$$e_{k+1} = A_M e_k + (A_1 - A_{M1})\, z_{1,k} + (A_2 - A_M)\, \sigma_k - B_M r_k + C\mathcal{B}_z u_k \ . \tag{5.16}$$

that should not explicitly depend on the states and references. A nominal control law

$$\bar{u}_k = \bar{\theta}_1 z_{1,k} + \bar{\theta}_2 \sigma_k + \bar{\theta}_3 r_k \quad \in \mathbb{R}^m \tag{5.17}$$

with matrices

$$\bar{\theta}_1 \;=\; -\left(C\mathcal{B}_z\right)^{-1}(A_1 - A_{M1}) \quad \in \mathbb{R}^{m \times (n+m(\bar{d}-1))}\,, \tag{5.18a}$$
$$\bar{\theta}_2 \;=\; -\left(C\mathcal{B}_z\right)^{-1}(A_2 - A_M) \quad \in \mathbb{R}^{m \times m}\,, \tag{5.18b}$$
$$\bar{\theta}_3 \;=\; \left(C\mathcal{B}_z\right)^{-1} B_M \quad \in \mathbb{R}^{m \times m} \tag{5.18c}$$

is designed to achieve that goal. Relation (5.17) can be written as

$$u_k = \bar{\theta}\omega_k + \bar{\theta}_3\, r_k \,, \tag{5.19}$$

with

$$\bar{\theta} = \begin{bmatrix}\bar{\theta}_1 & \bar{\theta}_2\end{bmatrix} \quad \in \mathbb{R}^{m\times(n+m\bar{d})} \qquad \text{and} \qquad \omega_k = \begin{bmatrix} z_{1,k} \\ \sigma_k \end{bmatrix} \quad \in \mathbb{R}^{n+m\bar{d}} \tag{5.20}$$

where matrix $\bar{\theta}$ depends on the actual values of A_1, A_2 that are unknown because $\mathcal{A}_z$ is unknown. Parameter $\bar{\theta}_3$ is independent of the unknown delay as can be seen from (5.9) and (5.11) since $B_1 = 0$ due to Assumption 5.2. Vector ω_k consists of known entities only.

An implementable version of control law (5.19) is

$$u_k = \theta_k \omega_k + \bar{\theta}_3\, r_k \quad \in \mathbb{R}^m\,, \tag{5.21}$$

where θ_k can be seen as the sum of $\bar{\theta}$, which is unknown due to the unknown network delay τ, and an additional part

$$\phi_k = \begin{bmatrix}\phi_{1,k} & \phi_{2,k}\end{bmatrix} \tag{5.22}$$

such that

$$\theta_k = \begin{bmatrix}\theta_{1,k} & \theta_{2,k}\end{bmatrix} = \bar{\theta} + \phi_k \quad \in \mathbb{R}^{m\times(n+m\bar{d})}\,. \tag{5.23}$$

The implementable control law can be chosen slightly different for the case with one input only, which is detailed below.

The use of (5.21) and (5.23) instead of the nominal control law (5.19) results in the error dynamics

$$e_{k+1} = A_M e_k + C\mathcal{B}_z\, \phi_k \omega_k\,, \tag{5.24}$$

which is written as

$$e_k = W_M\left[B_M^{-1} C\mathcal{B}_z \phi_k \omega_k\right] \tag{5.25}$$

using a $(m \times m)$ transfer matrix

$$W_M(z) = \left(zI_m - A_M\right)^{-1} B_M\,. \tag{5.26}$$

Notation $W_M[\cdot]$ in (5.25) symbolize the calculation of error e_k via a linear time-invariant discrete-time system with system matrix A_M, input matrix B_M and m input signals $B_M^{-1} C\mathcal{B}_z \phi_k \omega_k$. Hence, (5.25) is the equivalent representation of (5.24) using transfer matrix (5.26).

> **Assumption 5.3** (Properties of W_M)**.** *Transfer matrix $W_M(z)$ is stable and diagonal with identical entries, i.e.*
>
> $$A_M = a_M I_m \qquad \text{and} \qquad B_M = b_M I_m \tag{5.27}$$
>
> *with $0 \leq a_M < 1$ and $b_M = 1 - a_M$.*

Due to Assumption 5.3, matrix $W_M(z)$ features a dc-gain equal to one in each of the m channels from input $B_M^{-1} C\mathcal{B}_z \phi_k \omega_k$ to output e_k. In addition, the structure in (5.27) is given in the form of decoupled individual channels $i = 1, 2, \ldots, m$.

5.1.2 Adaptive Law

In a second step, an adaptive law for the parameters in θ_k is designed to guarantee that e_k converges to zero asymptotically. The following proposition is needed as a fundamental requirement for that purpose.

> **Proposition 5.4** (Controllability of (A_{11}, A_{12}) [SHF21])**.** *Let Assumptions 5.1 and 5.2 hold. Then, the pair (A_{11}, A_{12}) is controllable for any value of the bounded but unknown round trip delay τ.*

Proof. Sub-matrices $A_{11} \in \mathbb{R}^{(n+m(\bar{d}-1))\times(n+m(\bar{d}-1))}$ and $A_{12} \in \mathbb{R}^{(n+m(\bar{d}-1))\times m}$ are parts of (5.8), (5.9) as defined in (5.10) such that

$$A_{11} = \begin{bmatrix} e^{\tilde{A}h} & M_0(\tau) & M_1(\tau) & M_2(\tau) & \cdots & M_{\bar{d}-2}(\tau) \\ 0 & 0 & I_m & 0 & \ddots & 0 \\ \vdots & \vdots & \ddots & \ddots & \ddots & \vdots \\ 0 & 0 & 0 & 0 & \ddots & 0 \\ 0 & 0 & 0 & 0 & \ddots & I_m \\ 0 & 0 & 0 & 0 & \cdots & 0 \end{bmatrix}, \quad A_{12} = \begin{bmatrix} M_{\bar{d}-1}(\tau) \\ 0 \\ \vdots \\ 0 \\ 0 \\ I_m \end{bmatrix}. \tag{5.28}$$

The controllability matrix $S \in \mathbb{R}^{(n+m(\bar{d}-1))\times(n+m(\bar{d}-1))m}$ for the pair (A_{11}, A_{12}) is given by

$$S = \begin{bmatrix} A_{12} & A_{11}A_{12} & A_{11}^2 A_{12} & \cdots & A_{11}^{(n+m(\bar{d}-1))-1} A_{12} \end{bmatrix}. \tag{5.29}$$

Exploiting the specific structure of (5.28) yields

$$A_{11}A_{12} = \begin{bmatrix} K_1^{\mathrm{T}} & 0 & \cdots & 0 & 0 & I_m & 0 \end{bmatrix}^{\mathrm{T}}, \qquad K_1 = e^{\tilde{A}h} M_{\bar{d}-1}(\tau) + M_{\bar{d}-2}(\tau), \tag{5.30a}$$

$$A_{11}^2 A_{12} = \begin{bmatrix} K_2^{\mathrm{T}} & 0 & \cdots & 0 & I_m & 0 & 0 \end{bmatrix}^{\mathrm{T}}, \qquad K_2 = e^{\tilde{A}h} K_1 + M_{\bar{d}-3}(\tau) \tag{5.30b}$$

and so on, up to

$$A_{11}^{\bar{d}-1} A_{12} = \begin{bmatrix} K_{\bar{d}-1}^{\mathrm{T}} & 0 & \cdots & 0 & 0 & 0 & 0 \end{bmatrix}^{\mathrm{T}}, \qquad K_{\bar{d}-1} = e^{\tilde{A}h} K_{\bar{d}-2} + M_0(\tau). \tag{5.30c}$$

Consequently, matrices K_j depend on matrices M_ℓ, where $\ell \in \{0, 1, \dots, \bar{d}-1\}$ in the form of

$$K_j = \sum_{i=0}^{j} e^{i\tilde{A}h} M_{\bar{d}-1-j+i}(\tau) \tag{5.31}$$

as can be seen by combining (5.30a) to (5.30c). Hence, matrix S exhibits a special structure such that

$$S = \begin{bmatrix} M_{\bar{d}-1} & K_1 & \cdots & K_{\bar{d}-3} & K_{\bar{d}-2} & K_{\bar{d}-1} & \tilde{K} \\ 0 & 0 & \cdots & 0 & I_m & 0 & 0 \\ 0 & 0 & \iddots & I_m & 0 & 0 & 0 \\ \vdots & \iddots & \iddots & \iddots & \vdots & \vdots & \vdots \\ 0 & I_m & 0 & 0 & 0 & 0 & 0 \\ I_m & 0 & 0 & 0 & 0 & 0 & 0 \end{bmatrix} \tag{5.32}$$

with a matrix $\tilde{K}$ considered later. Matrices $\tilde{B}$, $e^{\tilde{A}h}$ and, thus also, matrices M_ℓ (2.20) are either zero or full rank, due to Assumption 5.1. Matrix $K_{\bar{d}-1}$ consists of the summation of different K_j multiplied by integer powers of $e^{\tilde{A}h}$, yielding, for example,

$$K_4 = M_0 + e^{\tilde{A}h}M_1 + e^{2\tilde{A}h}M_2 + e^{3\tilde{A}h}M_3 + e^{4\tilde{A}h}M_4 \ . \tag{5.33}$$

for $\bar{d} = 5$. Since τ is constant, either (i) one M_ℓ or (ii) two matrices M_ℓ and $M_{\ell-1}$ can be different from zero. In case of (i), e.g., $e^{\tilde{A}h}M_1$ with $e^{\tilde{A}h} \in \mathbb{R}^{n\times n}$ and $M_1 \in \mathbb{R}^{n\times m}$, which are full rank. Hence, $e^{\tilde{A}h}M_1$ has also rank m because of the rank properties of a matrix product [Ber09], i.e.

$$\begin{aligned} \operatorname{rank} e^{\tilde{A}h} + \operatorname{rank} M_1 - n \quad &\leq \quad \operatorname{rank}\left(e^{\tilde{A}h}M_1\right) \\ &\leq \quad \min\left\{\operatorname{rank} e^{\tilde{A}h}, \operatorname{rank} M_1\right\} \ . \end{aligned} \tag{5.34}$$

This holds for all ℓ in (i) because $\operatorname{rank} e^{\tilde{A}h}e^{\tilde{A}h} = \operatorname{rank} e^{\tilde{A}h}$ and at least one $M_\ell \neq 0$ whenever $\tau > 0$, which is fulfilled in Assumption 5.2. The reader is referred to Chapter 2 for more details about the matrices M_ℓ and their dependency on the considered network delay τ.

In case (ii) two matrices M_ℓ and $M_{\ell-1}$ are different from zero as, for example, $M_0 + e^{\tilde{A}h}M_1$. Then, M_0 can be subtracted of the first n rows in matrix S (5.32), which again leads to case (i). As a result, $K_{\bar{d}-1}$ has full rank, independent of the unknown τ.

All remaining columns of (5.32) follow from multiplications of $K_{\bar{d}-1}$ by integer powers of $e^{\tilde{A}h}$ such that

$$\begin{bmatrix} K_{\bar{d}-1} & \tilde{K} \end{bmatrix} = \begin{bmatrix} I_n & e^{\tilde{A}h} & \cdots & e^{(((n+m(\bar{d}-1))-\bar{d})\tilde{A}h} \end{bmatrix} K_{\bar{d}-1}. \tag{5.35}$$

The exponent of the exponential function on the right of (5.35) includes the number $(n+m(\bar{d}-1))-\bar{d}$. This is because matrix S has a dimension of $(n+m(\bar{d}-1))\times(n+m(\bar{d}-1))m$ and the sub-matrix from the left of S to $K_{\bar{d}-1}$ has dimension $(n+m(\bar{d}-1)\times m\bar{d})$, see (5.32). Thus, the remaining number of columns in $\tilde{K}$ is $(n+m(\bar{d}-1))m - m\bar{d} = (n+m(\bar{d}-1)-\bar{d})m$. Since matrices $K_{\bar{d}-1}$ (with m columns) and $\tilde{K}$ are formed by multiplications of $e^{\tilde{A}h}$, one gets (5.35). Consequently, matrix S has full rank for any value of τ because $h \neq 0$ and $A \neq 0$ due to Assumption 5.1. This shows that the pair (A_{11}, A_{12}) is controllable and completes the proof. ■

Proposition 5.4 serves as a basis for the following theorem for adaptive tracking.

Theorem 5.5 (Adaptive tracking [SHF21]). *Let Assumptions 5.1 and 5.2 hold for the networked control system with m inputs represented by* (5.8) *and* (5.9). *The desired transfer matrices $W_M(z)$ with dimension $m\times m$ and $W_N(z)$ with dimension $(n+m\bar{d})\times(n+m\bar{d})$ are specified as in Assumption 5.3.*

(a) A virtual output (5.11) *is designed by selecting matrix $C = [C_1 \ I_m]$ such that $(A_{11} - A_{12}C_1)$ is Schur for all delays τ corresponding to Assumption 5.2.*

(b) Adaptation laws

$$\theta_{k+1} = \theta_k - \epsilon_k\xi_k^T\Gamma_1 \qquad \in \mathbb{R}^{m\times(n+m\bar{d})}, \tag{5.36a}$$

$$\Upsilon_{k+1} = \Upsilon_k + B_M^{-1}C\mathcal{B}_z\epsilon_k\eta_k^T\Gamma_2 \qquad \in \mathbb{R}^{m\times m} \tag{5.36b}$$

with

$$
\begin{aligned}
\xi_k &= W_N(z)\,[\omega_k] \quad \in \mathbb{R}^{n+m\bar{d}}, && (5.37a)\\
\eta_k &= W_M(z)\,[\theta_k\omega_k] - \theta_k W_N(z)\,[\omega_k] \quad \in \mathbb{R}^{m}, && (5.37b)\\
\epsilon_k &= \frac{e_k - \Upsilon_k\eta_k}{1+\alpha\tilde{\xi}_k^T\Gamma\tilde{\xi}_k} \quad \in \mathbb{R}^{m}, && (5.37c)\\
\tilde{\xi}_k &= [\xi_k^T \quad \eta_k^T]^T \quad \in \mathbb{R}^{n+m\bar{d}+m}, && (5.37d)
\end{aligned}
$$

$$
\Gamma = \begin{bmatrix}\Gamma_1 & 0\\ 0 & \Gamma_2\end{bmatrix}, \qquad \Gamma_1 = \Gamma_1^T > 0\,, \qquad \Gamma_2 = \Gamma_2^T > 0 \tag{5.37e}
$$

are considered with $\Gamma_1 \in \mathbb{R}^{(n+m\bar{d})\times(n+m\bar{d})}$ *and* $\Gamma_2 \in \mathbb{R}^{m\times m}$*. The positive constant* α *is tuned such that*

$$
2\alpha I_m > B_M^{-1} C \mathcal{B}_z \tag{5.38}
$$

is fulfilled.

Then, the closed loop system consisting of the networked plant (5.8) *and controller* (5.21) *is stable despite unknown system data* $\mathcal{A}_z$*. The tracking error* e_k (5.15) *tends to zero asymptotically under the presence of an unknown network delay* $\underline{\tau} \le \tau \le \bar{\tau}$*. The parameter matrices* θ_k *and* Υ_k *tend to constant values.*

Figure 5.1 visualizes the principle structure of the proposed adaptive scheme. The specified reference sequence (r_k) is incorporated in the reference model as well as in the adaptive laws and the controller. The difference between the virtual output σ_k of the plant and the virtual output $\sigma_{M,k}$ provided by the reference dynamics establishes the basic error signal utilized in the adaptive controller. The plant can be seen in its rearranged form as in (5.10), (5.11) or, as an alternative, in its original form (2.23),

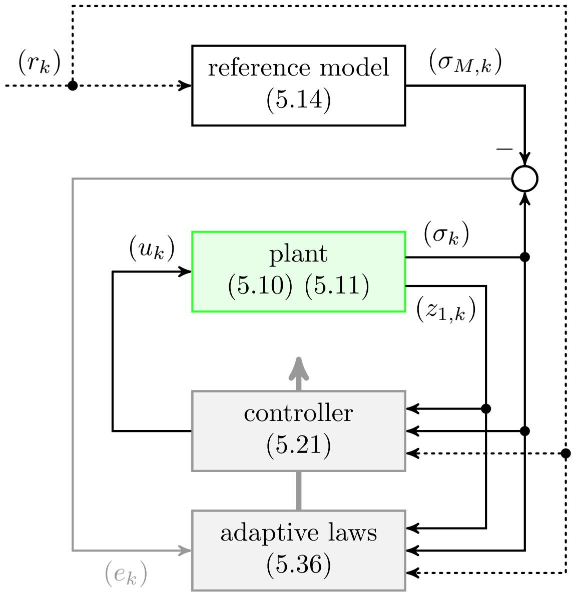

Figure 5.1: Structure of the control loop including reference model, plant, controller and the adaptation laws for the case of tracking the virtual outputs σ_k.

(2.24) in combination with a transformation accounting for the reordering of the state variables (5.7).

Proof. The proof is given in three parts where in (i) the error dynamics is modified, in (ii) it is shown that the error e_k tends to zero asymptotically, and in (iii) the properties of the remaining dynamics as well as concluding manipulations are presented. It follows the main ideas as in [LN80] that has been extended in [SHF19] but takes care of additional aspects that arise due to the considered networked multi-input system.

Part (i): An auxiliary signal $\sigma_{A,k}$ is defined such that

$$\sigma_{A,k} = \Upsilon_k \eta_k + \varphi_k \quad \in \mathbb{R}^m \tag{5.39}$$

with time-varying matrix $\Upsilon_k \in \mathbb{R}^{m \times m}$, η_k as in (5.37b) and vector $\varphi_k \in \mathbb{R}^m$ to be defined later. It is used to stabilize error dynamics (5.24) utilizing an auxiliary error signal

$$\epsilon_k = e_k - \sigma_{A,k} \quad \in \mathbb{R}^m \ . \tag{5.40}$$

Combining (5.25), (5.39) and (5.40) results in

$$\epsilon_k = W_M \left[B_M^{-1} C \mathcal{B}_z \phi_k \omega_k \right] - \Upsilon_k \eta_k - \varphi_k \ . \tag{5.41}$$

Next, the first term on the right hand side in (5.41) is reformulated, which is equivalent to (5.24). Multiplying both sides of difference equation (5.24) with $(C\mathcal{B}_z)^{-1} B_M$ yields

$$\begin{aligned} \underbrace{(C\mathcal{B}_z)^{-1} B_M e_{k+1}}_{\tilde{e}_{k+1}} &= (C\mathcal{B}_z)^{-1} B_M A_M e_k + (C\mathcal{B}_z)^{-1} B_M C\mathcal{B}_z \, \phi_k \omega_k \\ &= A_M \underbrace{(C\mathcal{B}_z)^{-1} B_M e_k}_{\tilde{e}_k} + B_M \, \phi_k \omega_k \end{aligned} \tag{5.42}$$

where a new error variable $\tilde{e}_k$ such that

$$\tilde{e}_k = W_M \left[\phi_k \omega_k \right] \tag{5.43}$$

is introduced. Rearranging the order of the matrices in (5.42) is possible because $C\mathcal{B}_z = I_m$ for the case with more inputs, i.e. $m > 1$, due to the requirement of a minimal delay of $\underline{\tau} \geq h$ as stated in Assumption 5.2. Nevertheless, the product $C\mathcal{B}_z$ is still kept in the proof to allow to state slightly different conditions for the case with only one input, i.e. $m = 1$, as shown below.

From the definition of $\tilde{e}_k$ in (5.42) and the fact that matrix $(C\mathcal{B}_z)^{-1} B_M$ is constant and invertible, one gets

$$e_k = C\mathcal{B}_z B_M^{-1} \tilde{e}_k = B_M^{-1} C\mathcal{B}_z \, W_M \left[\phi_k \omega_k \right] \tag{5.44}$$

and (5.41) changes into

$$\epsilon_k = B_M^{-1} C\mathcal{B}_z \Big\{ W_M \left[\phi_k \omega_k \right] - (C\mathcal{B}_z)^{-1} B_M \Upsilon_k \eta_k \Big\} - \varphi_k \, . \tag{5.45}$$

Combining a new variable

$$\psi_k = I_m - (C\mathcal{B}_z)^{-1} B_M \Upsilon_k \tag{5.46}$$

with (5.23), (5.37b) and (5.45) yields

$$
\begin{aligned}
\epsilon_k &= B_M^{-1} C \mathcal{B}_z \Big\{ W_M \left[\phi_k \omega_k\right] - W_M(z) \left[\theta_k \omega_k\right] + \theta_k W_N(z) \left[\omega_k\right] + \psi_k \eta_k \Big\} - \varphi_k \\
&= B_M^{-1} C \mathcal{B}_z \Big\{ W_M \left[\phi_k \omega_k\right] - W_M(z) \left[\bar{\theta} \omega_k\right] - W_M(z) \left[\phi_k \omega_k\right] + \bar{\theta} W_N(z) \left[\omega_k\right] \\
&\qquad\qquad + \phi_k W_N(z) \left[\omega_k\right] + \psi_k \eta_k \Big\} - \varphi_k \\
&= B_M^{-1} C \mathcal{B}_z \Big\{ - W_M(z) \left[\bar{\theta} \omega_k\right] + \bar{\theta} W_N(z) \left[\omega_k\right] + \phi_k W_N(z) \left[\omega_k\right] + \psi_k \eta_k \Big\} - \varphi_k \, . \qquad (5.47)
\end{aligned}
$$

Due to the fact that $\bar{\theta} \in \mathbb{R}^{m \times (n+m\bar{d})}$ is constant and Assumption 5.3 is introduced, relation

$$
W_M(z) \left[\bar{\theta} \omega_k\right] = \bar{\theta} W_N(z) \left[\omega_k\right] \qquad (5.48)
$$

holds. This can be seen by using (5.24) in (5.48) such that

$$
\left(z I_m - A_M\right)^{-1} B_M \bar{\theta} \mathcal{Z}\{\omega_k\} = \bar{\theta} \left(z I_n - A_N\right)^{-1} \tilde{B}_N \mathcal{Z}\{\omega_k\} \, , \qquad (5.49)
$$

where $\mathcal{Z}\{\omega_k\}$ symbolizes the z-transformation applied component by component to vector ω_k. Because relation (5.49) has to hold for all $\mathcal{Z}\{\omega_k\}$,

$$
\begin{bmatrix}
W_1 & 0 & \cdots & 0 & 0 \\
0 & W_2 & \ddots & 0 & 0 \\
\vdots & \ddots & \ddots & \ddots & \vdots \\
0 & 0 & \ddots & W_{m-1} & 0 \\
0 & 0 & \cdots & 0 & W_m
\end{bmatrix}
\bar{\theta} = \bar{\theta}
\begin{bmatrix}
W_1 & 0 & \cdots & \cdots & 0 & 0 \\
0 & W_2 & \ddots & \ddots & 0 & 0 \\
\vdots & \ddots & \ddots & \ddots & \ddots & \vdots \\
\vdots & \ddots & \ddots & \ddots & \ddots & \vdots \\
0 & 0 & \ddots & \ddots & W_{n+m\bar{d}-1} & 0 \\
0 & 0 & \cdots & \cdots & 0 & W_{n+m\bar{d}}
\end{bmatrix}
\qquad (5.50)
$$

has hold for all non-square matrices $\bar{\theta} \in \mathbb{R}^{m \times (n+m\bar{d})}$ and $W_i = \frac{b_M}{1-a_M}$ for $i = 1, 2, \ldots, n+m\bar{d}$. According to Assumption 5.3, the diagonal elements of W_M and W_N are equal and the left diagonal matrix in (5.50) multiplies the rows of $\bar{\theta}$ and the right diagonal matrix multiplies the columns of $\bar{\theta}$. Hence, (5.50) is fulfilled and (5.47) turns into

$$
\begin{aligned}
\epsilon_k &= B_M^{-1} C \mathcal{B}_z \Big\{ \phi_k W_N(z) \left[\omega_k\right] + \psi_k \eta_k \Big\} - \varphi_k \\
&= B_M^{-1} C \mathcal{B}_z \tilde{\phi}_k \tilde{\xi}_k - \alpha \, \tilde{\xi}_k^{\mathrm{T}} \Gamma \tilde{\xi}_k \, \epsilon_k \qquad (5.51)
\end{aligned}
$$

with

$$
\varphi_k = \alpha \, \tilde{\xi}_k^{\mathrm{T}} \Gamma \tilde{\xi}_k \, \epsilon_k \qquad \text{and} \qquad \tilde{\phi}_k = \begin{bmatrix} \phi_k & \psi_k \end{bmatrix} \in \mathbb{R}^{m \times (n+m\bar{d}+m)} \, . \qquad (5.52)
$$

Vector $\tilde{\xi}_k$ is stated in (5.37d) and matrix Γ is defined in (5.37e).

Part (ii): An adaptation law depending on the auxiliary error ϵ_k and $\tilde{\xi}_k$ is defined as

$$
\Delta \tilde{\phi}_k = \tilde{\phi}_{k+1} - \tilde{\phi}_k = -\epsilon_k \tilde{\xi}_k^{\mathrm{T}} \Gamma \quad \in \mathbb{R}^{m \times (n+m\bar{d}+m)} \, . \qquad (5.53)
$$

To show stability, the Frobenius norm $|| \cdot ||_F$ is used, which is defined for a matrix $K \in \mathbb{R}^{n \times m}$ as the sum over the squared absolute values of the elements k_{ij} for all rows i and columns j, i.e. $\left|\left|K\right|\right|_F = \sqrt{\sum_{i=1}^{n} \sum_{j=1}^{m} |k_{ij}|^2} = \sqrt{\mathrm{trace}\,(K^{\mathrm{T}} K)} = \sqrt{\mathrm{trace}\,(K K^{\mathrm{T}})}$.

In the present case, one uses the squared Frobenius norm of the weighed parameter matrix $\tilde{\phi}_k$ as a Lyapunov function candidate, i.e.

$$V_k = \left\|\tilde{\phi}_k L\right\|_F^2 = \operatorname{trace}\left(\tilde{\phi}_k L L^{\mathrm{T}} \tilde{\phi}_k^{\mathrm{T}}\right) \;, \tag{5.54}$$

with $\Gamma^{-1} = LL^{\mathrm{T}} > 0$. Such a separation of Γ^{-1} is always possible because Γ is assumed to be positive definite. The forward difference of V_k taking into account (5.53) and symmetry properties of the trace operator is given by

$$\begin{aligned}\Delta V = V_{k+1} - V_k &= \operatorname{trace}\left(\tilde{\phi}_{k+1}\Gamma^{-1}\tilde{\phi}_{k+1}^{\mathrm{T}} - \tilde{\phi}_k\Gamma^{-1}\tilde{\phi}_k^{\mathrm{T}}\right)\\ &= \operatorname{trace}\left(2\Delta\tilde{\phi}_k\Gamma^{-1}\tilde{\phi}_k^{\mathrm{T}} + \Delta\tilde{\phi}_k\Gamma^{-1}\Delta\tilde{\phi}_k^{\mathrm{T}}\right)\\ &= \operatorname{trace}\left(-2\epsilon_k\tilde{\xi}_k^{\mathrm{T}}\tilde{\phi}_k^{\mathrm{T}} + \epsilon_k\tilde{\xi}_k^{\mathrm{T}}\Gamma\tilde{\xi}_k\epsilon_k^{\mathrm{T}}\right) \;.\end{aligned} \tag{5.55}$$

This results in

$$\Delta V = \operatorname{trace}\left(-2\frac{B_M^{-1}C\mathcal{B}_z\tilde{\phi}_k\tilde{\xi}_k\left(\tilde{\phi}_k\tilde{\xi}_k\right)^{\mathrm{T}}}{1+\alpha\,\tilde{\xi}_k^{\mathrm{T}}\Gamma\tilde{\xi}_k} + \frac{B_M^{-1}C\mathcal{B}_z\tilde{\phi}_k\tilde{\xi}_k\tilde{\xi}_k^{\mathrm{T}}\Gamma\tilde{\xi}_k\left(\tilde{\phi}_k\tilde{\xi}_k\right)^{\mathrm{T}}\left(B_M^{-1}C\mathcal{B}_z\right)^{\mathrm{T}}}{\left(1+\alpha\,\tilde{\xi}_k^{\mathrm{T}}\Gamma\tilde{\xi}_k\right)^2}\right), \tag{5.56}$$

where (5.51) is used in the calculations. Definitions

$$P_k = B_M^{-1}C\mathcal{B}_z\tilde{\phi}_k\tilde{\xi}_k\big(\tilde{\phi}_k\tilde{\xi}_k\big)^{\mathrm{T}} \qquad \text{and} \qquad N = 2\alpha I_m - B_M^{-1}C\mathcal{B}_z \tag{5.57}$$

allow further simplifications resulting in

$$\begin{aligned}\Delta V =& \frac{1}{\left(1+\alpha\,\tilde{\xi}_k^{\mathrm{T}}\Gamma\tilde{\xi}_k\right)^2}\operatorname{trace}\left(P_k\Big\{-2I_m - \tilde{\xi}_k^{\mathrm{T}}\Gamma\tilde{\xi}_k\left(2\alpha I_m - \big(B_M^{-1}C\mathcal{B}_z\big)^{\mathrm{T}}\right)\Big\}\right)\\ =& -\frac{2}{\left(1+\alpha\,\tilde{\xi}_k^{\mathrm{T}}\Gamma\tilde{\xi}_k\right)^2}\operatorname{trace}\left(P_k\right) - \frac{\tilde{\xi}_k^{\mathrm{T}}\Gamma\tilde{\xi}_k}{\left(1+\alpha\,\tilde{\xi}_k^{\mathrm{T}}\Gamma\tilde{\xi}_k\right)^2}\operatorname{trace}\left(P_k N^{\mathrm{T}}\right) \;.\end{aligned} \tag{5.58}$$

Due to condition (5.38) in Theorem 5.5 and the required lower bound of the round trip delay τ as in Assumption 5.2, matrix N is positive definite and symmetric because $C\mathcal{B}_z$ is positive definite and symmetric. This makes it possible to split matrix $B_M^{-1}C\mathcal{B}_z$ into

$$B_M^{-1}C\mathcal{B}_z = X^{\mathrm{T}}X > 0\,. \tag{5.59}$$

Exploiting the properties of the trace operator [Ber09] yields

$$\operatorname{trace}\left(P_k\right) = \operatorname{trace}\left(X\tilde{\phi}_k\tilde{\xi}_k\tilde{\xi}_k^{\mathrm{T}}\tilde{\phi}_k^{\mathrm{T}}X^{\mathrm{T}}\right) \geq 0 \tag{5.60}$$

and for the second term on the right hand side of equation (5.58)

$$\begin{aligned}\operatorname{trace}\left(P_k N\right) &= \operatorname{trace}\left(NB_M^{-1}CB\tilde{\phi}_k\tilde{\xi}_k\left(\tilde{\phi}_k\tilde{\xi}_k\right)^{\mathrm{T}}\right)\\ &= \operatorname{trace}\left(Y^{\mathrm{T}}Y\tilde{\phi}_k\tilde{\xi}_k\tilde{\xi}_k^{\mathrm{T}}\tilde{\phi}_k^{\mathrm{T}}\right) = \operatorname{trace}\left(Y\tilde{\phi}_k\tilde{\xi}_k\tilde{\xi}_k^{\mathrm{T}}\tilde{\phi}_k^{\mathrm{T}}Y^{\mathrm{T}}\right) \geq 0\,.\end{aligned} \tag{5.61}$$

Hence, (5.58) in combination with (5.61) yields

$$\Delta V \leq -\frac{2}{\left(1+\alpha\,\tilde{\xi}_k^{\mathrm{T}}\Gamma\tilde{\xi}_k\right)^2}\operatorname{trace}\left(P_k\right) \leq 0 \tag{5.62}$$

so that $\tilde{\phi}_k$ is bounded for any bounded initial value $\tilde{\phi}_0$.

V_k is non-increasing and bounded below and has, therefore, a limit V_∞ as $k \to \infty$, i.e.

$$\lim_{k\to\infty} \left\|\tilde{\phi}_k L\right\|_F^2 = V_\infty < \infty \ , \tag{5.63}$$

and so, the squared Frobenius norm of scaled matrix $\tilde{\phi}_k$ converges to a limit. The difference between initial value V_0 and this limit is

$$\lim_{k\to\infty} \sum_{i=1}^{k} |\Delta V_i| = V_0 - V_\infty < \infty \, , \tag{5.64}$$

causing that ΔV_i has to tend to zero. Implied by this, P_k has to approach zero as can be seen in the first line of (5.58). According to the definition of P_k in (5.57) and the fact that $B_M^{-1} C\mathcal{B}_z$ is non-singular, it follows that this is only possible if $\tilde{\phi}_k \tilde{\xi}_k$ tends to zero. Then ϵ_k is zero for $k \to \infty$ as can be seen from (5.51), $\Delta\tilde{\phi}_k \to 0$. Parameter matrix $\tilde{\phi}_k$ tends to a constant value.

Part (iii): As a result of (ii), parameter matrix $\tilde{\theta}_k$ tends to a constant value θ_c. Combining (5.39), (5.40) and (5.52) results in

$$\epsilon_k = e_k - \Upsilon_k \eta_k - \alpha \, \tilde{\xi}_k^{\mathrm{T}} \Gamma \tilde{\xi}_k \, \epsilon_k \ , \tag{5.65}$$

see (5.37c) in Theorem 5.5. In addition,

$$\eta_k = W_M(z) \left[\theta_k \omega_k\right] - \theta_k W_N(z) \left[\omega_k\right] \to 0 \qquad \text{as} \qquad \theta_k \to \theta_c \tag{5.66}$$

and $\epsilon_k \to 0$. This means that the error $e_k \to 0$ for $k \to \infty$ and $\sigma_k \to \sigma_{M,k}$. The remaining dynamics reads as

$$z_{1,k+1} = (A_{11} - A_{12}C_1) z_{1,k} + A_{12}\sigma_{M,k} + B_1 u_k \tag{5.67}$$

where (5.10) and (5.11) are used. Input matrix B_1 is zero due to Assumption 5.2. Matrix $(A_{11} - A_{12}C_1)$ in (5.67) has to be Schur for all delays to assure bounded-input bounded-state stability, which is assured by the assumptions made in Theorem 5.5. Combining (5.37d), (5.37e), (5.52) and (5.53) yields

$$\tilde{\phi}_{k+1} - \tilde{\phi}_k = -\epsilon_k \begin{bmatrix} \xi_k^{\mathrm{T}} & \eta_k^{\mathrm{T}} \end{bmatrix} \begin{bmatrix} \Gamma_1 & 0 \\ 0 & \Gamma_2 \end{bmatrix} \ , \tag{5.68}$$

and so

$$\phi_{k+1} - \phi_k = -\epsilon_k \xi_k^{\mathrm{T}} \Gamma_1 \ , \tag{5.69}$$

as in (5.36a) and

$$\psi_{k+1} - \psi_k = -\epsilon_k \eta_k^{\mathrm{T}} \Gamma_2 \tag{5.70}$$

that is converted into (5.36b) using (5.46) so that

$$\Upsilon_{k+1} - \Upsilon_k = B_M^{-1} C\mathcal{B}_z \, \epsilon_k \eta_k^{\mathrm{T}} \Gamma_2 \, . \tag{5.71}$$

This completes the proof. ■

Remark 5.6. Please note that $C\mathcal{B}_z = I_m$ holds due to the structure of (5.9), the definition of σ_k (5.11), and Assumption 5.2. As a consequence, a strict positive real requirement as in [BFU95] is not needed.

The adaptive laws are inspired by [NL80] and extended to multivariable systems with additional uncertain network delays under consideration of a suitably constructed virtual output σ_k.

Relations (5.36a) and (5.36b) are of lower dimension than classical ones, cf. [Tao14], because only the dynamics related to the virtual output is stabilized in this approach. For $\sigma_k = 0$, which is reached for the first time at $k^\star$, the remaining dynamics for $k \geq k^\star$ is fixed by the choice of matrix $C = [C_1 \ I_m]$. Matrix C_1 is designed such that $(A_{11} - A_{12}C_1)$ is Schur for all round trip delays τ and, e.g., the corresponding spectral radius is minimized. This is also shown for simulation examples in the next section.

5.1.3 Single-input case

The restriction of Theorem 5.5 to the single-input case, i.e. $m = 1$, leads to a similar algorithm that comes along with a relaxation of Assumption 5.2 such that the lower bound is allowed to be smaller than the sampling interval h.

Assumption 5.7 (Round trip delay, single-input case)**.** *The round trip delay $\tau = \tau^{sc} + \tau^c + \tau^{ca} \in \mathbb{R}$ is constant for all packets j, i.e. $\tau_j = \tau \ \forall j$ but unknown. It is bounded such that*

$$0 < \underline{\tau} \leq \tau \leq \bar{\tau} \tag{5.72}$$

and $\underline{\tau}, \tau, \bar{\tau} \in \mathbb{R}_+$.

As a consequence of Assumption 5.7, Matrix $M_{\bar{d}}$ in (5.9) is unknown and, thus, vector $\mathcal{B}_z$ is an unknown as well. This makes it necessary to modify control law (5.21) such that

$$u_k = \theta_k \omega_k \tag{5.73}$$

using parameter vector

$$\theta_k = \begin{bmatrix} \theta_{1,k} & \theta_{2,k} & \theta_{3,k} \end{bmatrix} \quad \in \mathbb{R}^{1\times(n+\bar{d}+1)} \tag{5.74}$$

with a nominal vector $\bar{\theta} = \begin{bmatrix} \bar{\theta}_1 & \bar{\theta}_2 & \bar{\theta}_3 \end{bmatrix}$ and an additional parameter vector $\phi_k = \begin{bmatrix} \phi_{1,k} & \phi_{2,k} & \phi_{3,k} \end{bmatrix}$ such that

$$\theta_k = \bar{\theta} + \phi_k \tag{5.75}$$

and column vector

$$\omega_k = \begin{bmatrix} z_{1,k} \\ \sigma_k \\ r_k \end{bmatrix} \in \mathbb{R}^{n+\bar{d}+1} \tag{5.76}$$

is built only from known entities.

Assumption 5.8 (Condition on $C\mathcal{B}_z$, single-input case)**.** *The sign condition*

$$\operatorname{sign}(C\mathcal{B}_z) = \operatorname{sign} B_M \tag{5.77}$$

holds for all round trip delays τ in Assumption 5.7.

This assumption is necessary to also allow small delays, i.e. $\tau < h$. It is still less restrictive than the strictly positive real condition as in [BFU95].

Corollary 5.9 (Adaptive tracking, single-input case)**.** *Let Assumptions 5.1, 5.7 and 5.8 hold for the single input networked control system represented by* (5.8) *and* (5.9)*. The desired transfer function $W_M(z)$ for a system with one input and one output comply with Assumption 5.3 for $m = 1$.*

(a) A virtual output variable (5.11) *is designed such that $(A_{11} - A_{12}C_1)$ is Schur for all delays τ corresponding to Assumptions 5.7.*

(b) Adaptation laws

$$\begin{aligned} \theta_{k+1} &= \theta_k - \epsilon_k \xi_k^T \Gamma_1 \quad \in \mathbb{R}^{1\times(n+\bar{d})}, && (5.78a)\\ \Upsilon_{k+1} &= \Upsilon_k + \epsilon_k \eta_k \Gamma_2 \quad \in \mathbb{R} && (5.78b) \end{aligned}$$

with

$$\begin{aligned} \xi_k &= W_N(z)\,[\omega_k] \quad \in \mathbb{R}^{n+\bar{d}}, && (5.79a)\\ \eta_k &= W_M(z)\,[\theta_k\omega_k] - \theta_k W_M(z)\,[\omega_k] \quad \in \mathbb{R}, && (5.79b)\\ \epsilon_k &= \frac{e_k - \Upsilon_k\eta_k}{1+\alpha\tilde{\xi}_k^T\Gamma\tilde{\xi}_k} \quad \in \mathbb{R}, && (5.79c)\\ \tilde{\xi}_k &= [\xi_k^T \quad \eta_k]^T \quad \in \mathbb{R}^{n+\bar{d}+1}, && (5.79d) \end{aligned}$$

$$\Gamma = \begin{bmatrix} \Gamma_1 & 0 \\ 0 & \Gamma_2 \end{bmatrix}, \qquad \Gamma_1 = \Gamma_1^T > 0\,, \qquad \Gamma_2 > 0\,, \tag{5.79e}$$

are considered with $\Gamma_1 \in \mathbb{R}^{(n+\bar{d})\times(n+\bar{d})}$ and $\Gamma_2 \in \mathbb{R}$. The positive constant α is tuned such that

$$\alpha > \frac{1}{2} B_M^{-1} C \mathcal{B}_z \tag{5.80}$$

is fulfilled.

Then, the closed loop system consisting of augmented plant (5.8), (5.9) *and controller* (5.73) *is stable despite unknown system data $\mathcal{A}_z$, $\mathcal{B}_z$ and the tracking error e_k* (5.15) *tends to zero asymptotically under the presence of an unknown network delay $0 < \tau \leq \bar{\tau}$. Parameter vectors θ_k and Υ_k tend to constant values.*

Please note the main differences between Theorem 5.5 and Corollary 5.9:

(a) A minimum delay of $\underline{\tau} > 0$ is allowed that might be smaller than the sampling interval, i.e. $\underline{\tau} < h$.

(b) Matrix $B_M^{-1} C \mathcal{B}_z$ in (5.78b) can be skipped in the adaptation law as can be seen in the proof.

(c) Condition (5.80) has to hold for all admissible delays corresponding to Assumption 5.7, which is different when compared to Theorem 5.5, where (5.38) is independent of the round trip delay τ.

Proof. The proof follows the same line as in the multi-input case as shown the previous subsection for Theorem 5.5. The differences are that $M_{\bar{d}}(\tau)$ may not be zero and

$B_M^{-1} C\mathcal{B}_z$ is now scalar. Assumption 5.8 ensures that $B_M^{-1} C\mathcal{B}_z$ is positive for all considered τ and can be pulled out in relation (5.56) resulting in an adaptive law (5.78b) that is independent of B_M, C and $\mathcal{B}_z$. ■

5.2 Adaptive Stabilization

In the previous section, adaptive tracking of a virtual output related to model (5.8), (5.9) is considered. An alternative approach is to define the virtual output with respect to a desired reference vector for the states $\hat{z}_k$ of the networked plant, i.e.

$$\sigma_k = C\left(z_k - \hat{z}_k\right) = \begin{bmatrix} C_1 & I_m \end{bmatrix} \left(z_k - \hat{z}_k\right) \quad \in \mathbb{R}^m \,, \tag{5.81}$$

and aim for stabilizing $\sigma_k = 0$. Signals $\hat{z}_k$ are chosen such that they are consistent for (5.8) as shown, e.g., in [SCHF20] and exemplified in the next section. Subsequently, the same line of calculations as in the tracking case is followed to get dynamics

$$\sigma_{k+1} = A_1 z_{1,k} + A_2 \sigma_k + C\mathcal{B}_z\, u_k - C\hat{z}_{k+1} \tag{5.82}$$

and the dynamics of error (5.15) as

$$e_{k+1} = A_M e_k + \left(A_1 - A_{M1}\right) z_{1,k} + \left(A_2 - A_M\right) \sigma_k - B_M r_k + C\mathcal{B}_z u_k - C\hat{z}_{k+1} \,, \tag{5.83}$$

with matrices A_1, A_2 according to (5.13) and the reference dynamics specified in (5.14). The nominal control is then given by

$$\bar{u}_k = \bar{\theta}_1 z_{1,k} + \bar{\theta}_2 \sigma_k + \bar{\theta}_3 \hat{z}_{k+1} + \bar{\theta}_4 r_k \tag{5.84}$$

where

$$\bar{\theta}_1 = -\left(C\mathcal{B}_z\right)^{-1}\left(A_1 - A_{M1}\right) \quad \in \mathbb{R}^{m\times(n+m(\bar{d}-1))} \,, \tag{5.85a}$$

$$\bar{\theta}_2 = -\left(C\mathcal{B}_z\right)^{-1}\left(A_2 - A_M\right) \quad \in \mathbb{R}^{m\times m} \,, \tag{5.85b}$$

$$\bar{\theta}_3 = \left(C\mathcal{B}_z\right)^{-1} C \quad \in \mathbb{R}^{m\times(n+m\bar{d})} \,, \tag{5.85c}$$

$$\bar{\theta}_4 = \left(C\mathcal{B}_z\right)^{-1} B_M \quad \in \mathbb{R}^{m\times m} \,. \tag{5.85d}$$

Using control law

$$u_k = \theta_k \omega_k + \bar{\theta}_4\, r_k \quad \in \mathbb{R}^m \tag{5.86}$$

with

$$\theta_k = \bar{\theta} + \phi_k \,, \qquad \text{and} \qquad \omega_k = \begin{bmatrix} z_{1,k} \\ \sigma_k \\ \hat{z}_{k+1} \end{bmatrix} \quad \in \mathbb{R}^{2(n+m\bar{d})} \,, \tag{5.87}$$

where

$$\theta_k = \begin{bmatrix} \theta_{1,k} & \theta_{2,k} & \theta_{3,k} \end{bmatrix} \,, \tag{5.88a}$$

$$\bar{\theta} = \begin{bmatrix} \bar{\theta}_1 & \bar{\theta}_2 & \bar{\theta}_3 \end{bmatrix} \,, \tag{5.88b}$$

$$\phi_k = \begin{bmatrix} \phi_{1,k} & \phi_{2,k} & \phi_{3,k} \end{bmatrix} \,, \tag{5.88c}$$

yields the same structure of error dynamics as in relation (5.24) but with different dimensions of the matrices involved. This is stated in the following corollary that is a direct consequence of Theorem 5.5.

Corollary 5.10 (Adaptive stabilization [SHF21])**.** *Consider Theorem 5.5 where the control law is replaced by* (5.81)*, controller* (5.86)*,* $\theta_k \in \mathbb{R}^{m\times 2((n+m\bar{d})+m\bar{d})}$ *and* $\omega_k \in \mathbb{R}^{2(n+m\bar{d})}$ *as in* (5.87)*,* $\tilde{\xi}_k \in \mathbb{R}^{2n+m}$*,* $\Gamma \in \mathbb{R}^{(2(n+m\bar{d})+m)\times(2(n+m\bar{d})+m)}$*, and transfer matrix* $W_N(z)$ *of dimension* $(2(n+m\bar{d}) \times 2(n+m\bar{d}))$*. Let condition* (5.38) *hold.*

Then, the closed networked control system consisting of augmented plant (5.8)*,* (5.9) *and controller* (5.86) *is stable despite unknown system data* $\mathcal{A}_z$*. The tracking error* e_k (5.15) *tends to zero asymptotically under the presence of an unknown network delay* $\underline{\tau} \leq \tau \leq \bar{\tau}$*. Parameter matrices* θ_k *and* Υ_k *tend to constant values.*

Proof. The proof directly follows by the same considerations as for Theorem 5.5, which are adopted to the use of (5.81) and the different matrix dimensions involved. As the remaining dynamics for $\sigma_k \to \sigma_{M,k}$ is

$$z_{1,k+1} = (A_{11} - A_{12}C_1)\, z_{1,k} + A_{12}\sigma_{M,k} + B_1 u_k + A_{12}C\hat{z}_{k+1} \tag{5.89}$$

with $B_1 = 0$, the same considerations have to be taken into account as in Theorem 5.5 to achieve stability. The reference $\hat{z}_{k+1}$ for the states acts as a bounded input signal. ■

Note that one have to deal with a larger matrix $\theta \in \mathbb{R}^{m\times 2(n+m\bar{d})}$ in (5.36a) instead of $\theta \in \mathbb{R}^{m\times(n+m\bar{d})}$ in Theorem 5.5 and the desired reference for the states in the next time instant $\hat{z}_{k+1}$ has to be specified.

In the single-input case, one can utilize control law

$$u_k = \theta_k \omega_k \tag{5.90}$$

with

$$\theta_k = \begin{bmatrix}\theta_{1,k} & \theta_{2,k} & \theta_{3,k} & \theta_{4,k}\end{bmatrix} \quad \in \mathbb{R}^{1\times(n+\bar{d}+1)} \tag{5.91a}$$

and

$$\omega_k = \begin{bmatrix} z_{1,k} \\ \sigma_k \\ \hat{z}_{k+1} \\ r_k \end{bmatrix} \quad \in \mathbb{R}^{2(n+\bar{d})+1}\,. \tag{5.91b}$$

Corollary 5.11 (Adaptive stabilization, single-input case)**.** *Consider Corollary 5.10 where the control law is replaced by* (5.81) *and* (5.90)*,* $\theta_k \in \mathbb{R}^{1\times 2(n+\bar{d})}$ *and* $\omega_k \in \mathbb{R}^{2(n+\bar{d})}$ *as in* (5.91)*,* $\tilde{\xi}_k \in \mathbb{R}^{2(n+\bar{d})+1}$ *and* $\Gamma \in \mathbb{R}^{(2(n+\bar{d})+1)\times(2n+1)}$*. Let condition* (5.38) *hold.*

Then, the closed loop system consisting of augmented plant (5.8)*,* (5.9) *and* (5.90) *is stable despite unknown system data* $\mathcal{A}_z$*,* $\mathcal{B}_z$ *and the tracking error* e_k (5.15) *tends to zero asymptotically under the presence of an unknown network delay* $0 < \tau \leq \bar{\tau}$*. Parameter vectors* θ_k *and* Υ_k *tend to constant values.*

Proof. The proof is a direct consequence of the proof of Corollary 5.10 adopted to the use of (5.81) and the changed matrix dimensions. ■

5.3 Simulation Examples

In this section, two examples are used to show the differences between the adaptive tracking and adaptive stabilization approach presented for NCS in Sections 5.1 and 5.2, respectively.

5.3.1 Example with fast Plant Dynamics

First, a continuous-time plant with fast dynamics specified by matrices

$$\tilde{A} = \begin{bmatrix} 1.2 & -0.5 & 0.5 \\ -1.0 & -0.4 & -1.2 \\ 0.2 & -0.8 & -1.0 \end{bmatrix}, \quad \tilde{B} = \begin{bmatrix} 0.3 & 1.5 \\ -1.2 & -1.7 \\ 0.4 & 0.4 \end{bmatrix} \tag{5.92}$$

and a sampling interval of $h = 0.1\,s$ is considered. The eigenvalues of the continuous-time plant are $s_1 = 1.6562$, $s_2 = -0.1362$ and $s_3 = -1.7200$. The nominal values of $\bar{\theta}$ and $\bar{\Upsilon}$ are calculated for $\tau = h$ since the real values of the round trip delay is unknown but they are needed for the initialization of the adaptive laws (5.36a) and (5.36b). Matrix $\bar{\theta}$ follows from (5.20) and (5.18); matrix $\bar{\Upsilon}$ is selected such that the new variable ϕ_k as stated in (5.46) is equal to zero.

Desired values for the first two plant states $(x_{1,k})$ and $(x_{2,k})$ of the discretized plant (5.1) are converted into references (r_k) for (σ_k) as described in [SCHF20]. This means that in the present case only two states can be specified to get consistent results for the remaining states, which can be checked by Proposition 3 in [SCHF20] that depends on the number of inputs m. The resulting plant states (x_k) and corresponding reference signals (r_k) are depicted in Figures 5.5 and 5.2, respectively.

Parameter $a_M = 0$ and gain α is chosen as $\underline{\alpha} + 1$, where $\underline{\alpha}$ corresponds to the minimal value of α given by condition (5.5).

Matrix C_1 is designed such that $(A_{11} - A_{12}C_1)$ is Schur for all network delays τ. This is achieved by solving an optimization problem in which the corresponding spectral radius, i.e. the largest absolute value of the eigenvalues of $(A_{11} - A_{12}C_1)$, is minimized to accomplish a fast convergence of the remaining dynamics for all considered τ. In addition to that, the largest imaginary part is penalized in the optimization to avoid strong oscillations during parameter adaptation. This yields

$$C_1 = \begin{bmatrix} -1.1874 & -1.2464 & 1.6324 & -0.1117 & 0.0917 & 0.3373 & 0.1862 \\ 2.2515 & -0.1870 & -0.0927 & 0.0077 & 0.0050 & 0.1552 & 0.4451 \end{bmatrix} \tag{5.93}$$

for the design of the virtual output (5.11).

Figures 5.2 to 5.5 show the sequences of artificial output variable (σ_k), the control signal (u_k) as well as error (e_k) and the plant states (x_k) for the considered simulation example when the adaptive tracking approach is utilized. The tracking of the desired reference for the virtual output (see black signals in Figure 5.2) enables one to track desired reference signals for the plant states as shown in Figure 5.5 for all considered network delays $\tau \in \{0.10, 0.15, 0.20, 0.25, 0.30\}\,s$. The relative change of the adapted parameters $\theta_{1,k}$, $\theta_{2,k}$, Υ_k to their nominal values are shown in Figure 5.6 for the case $\tau = 0.15\,s$. Stability is achieved for all considered delays, (σ_k) converges to its desired reference and the adaptation parameters converge to constant values as ensured by Theorem 5.5.

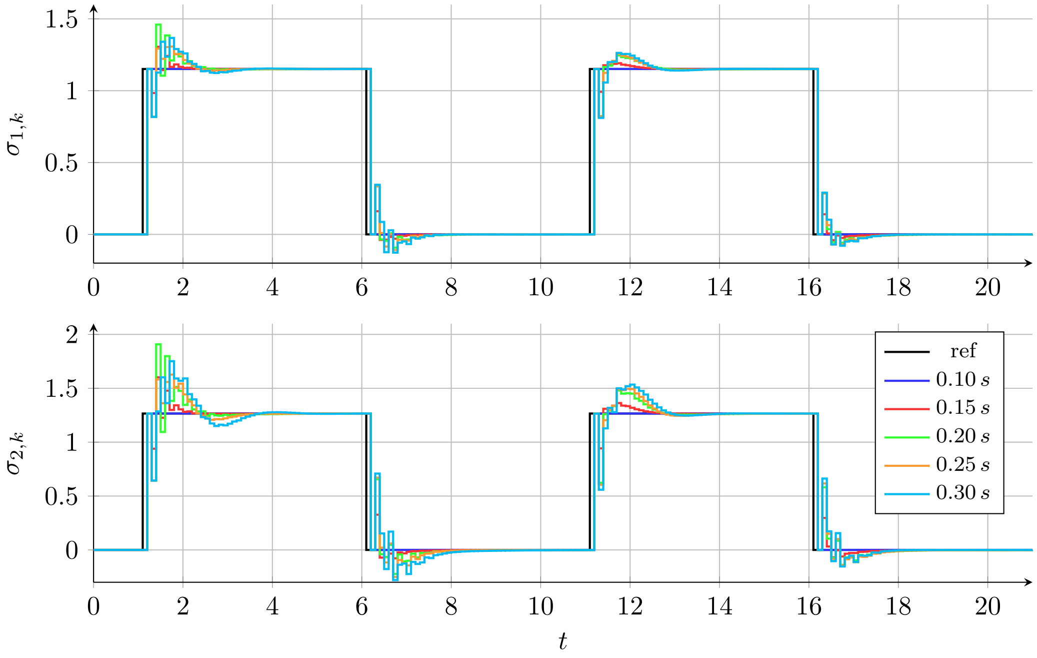

Figure 5.2: Example with fast dynamics (tracking of r_k): Tracking of virtual outputs σ_k for different network delays τ.

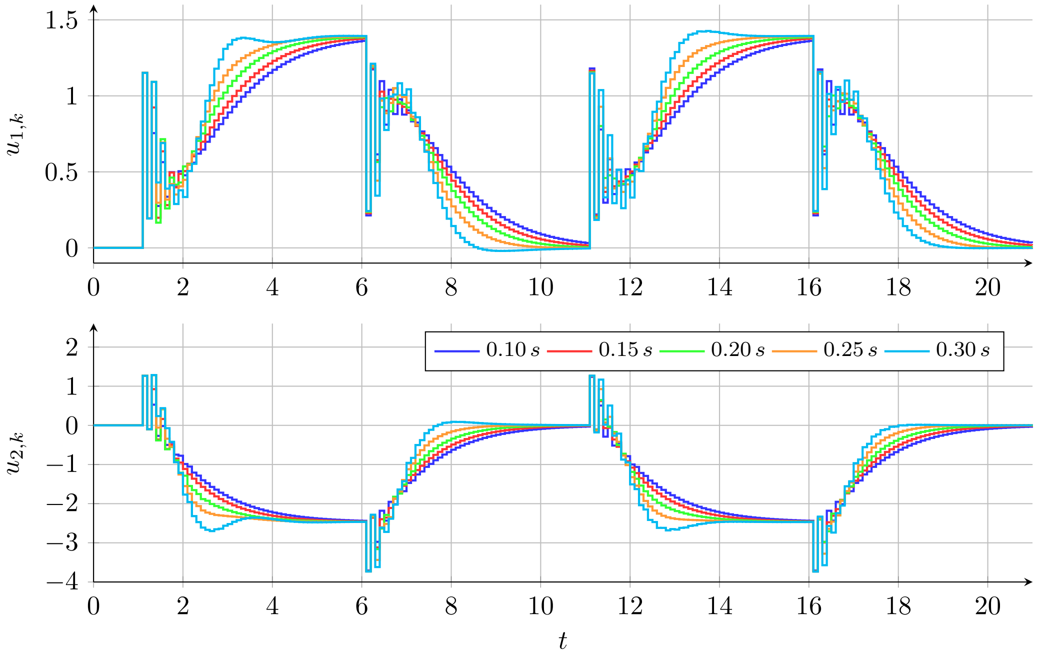

Figure 5.3: Example with fast dynamics (tracking of r_k): Control signals u_k for different network delays τ.

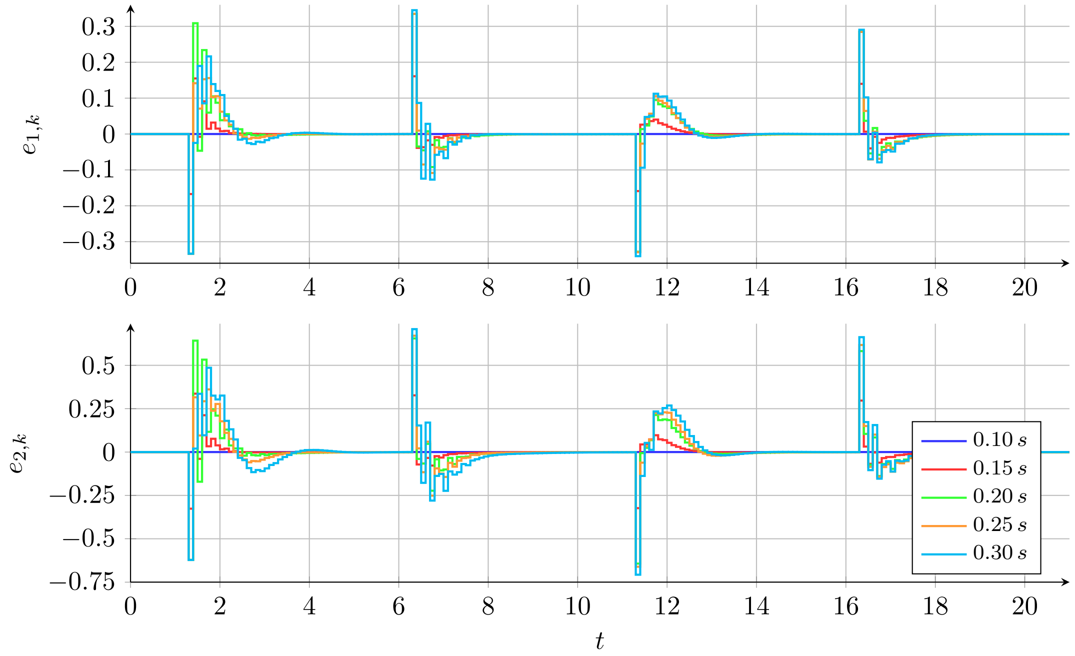

Figure 5.4: Example with fast dynamics (tracking of r_k): Error signals e_k for different network delays τ.

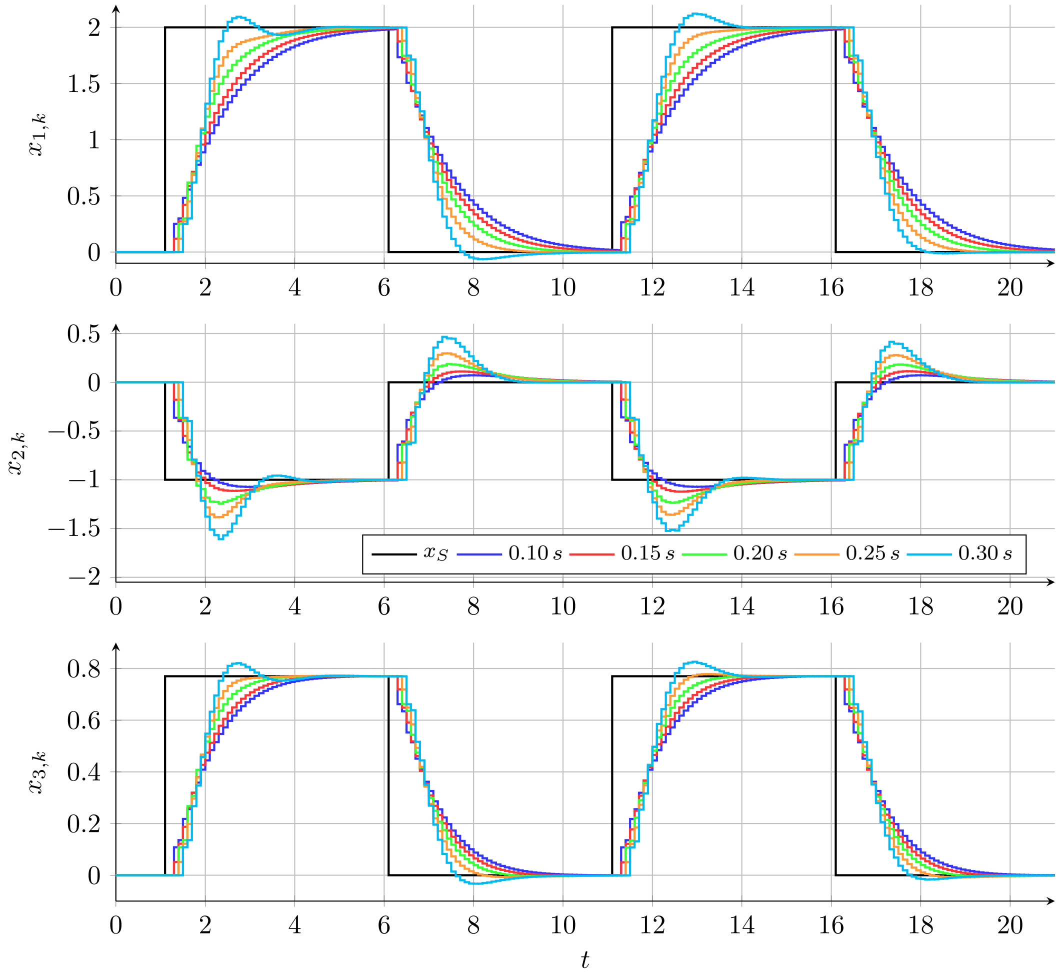

Figure 5.5: Example with fast dynamics (tracking of r_k): States x_k for different network delays τ.

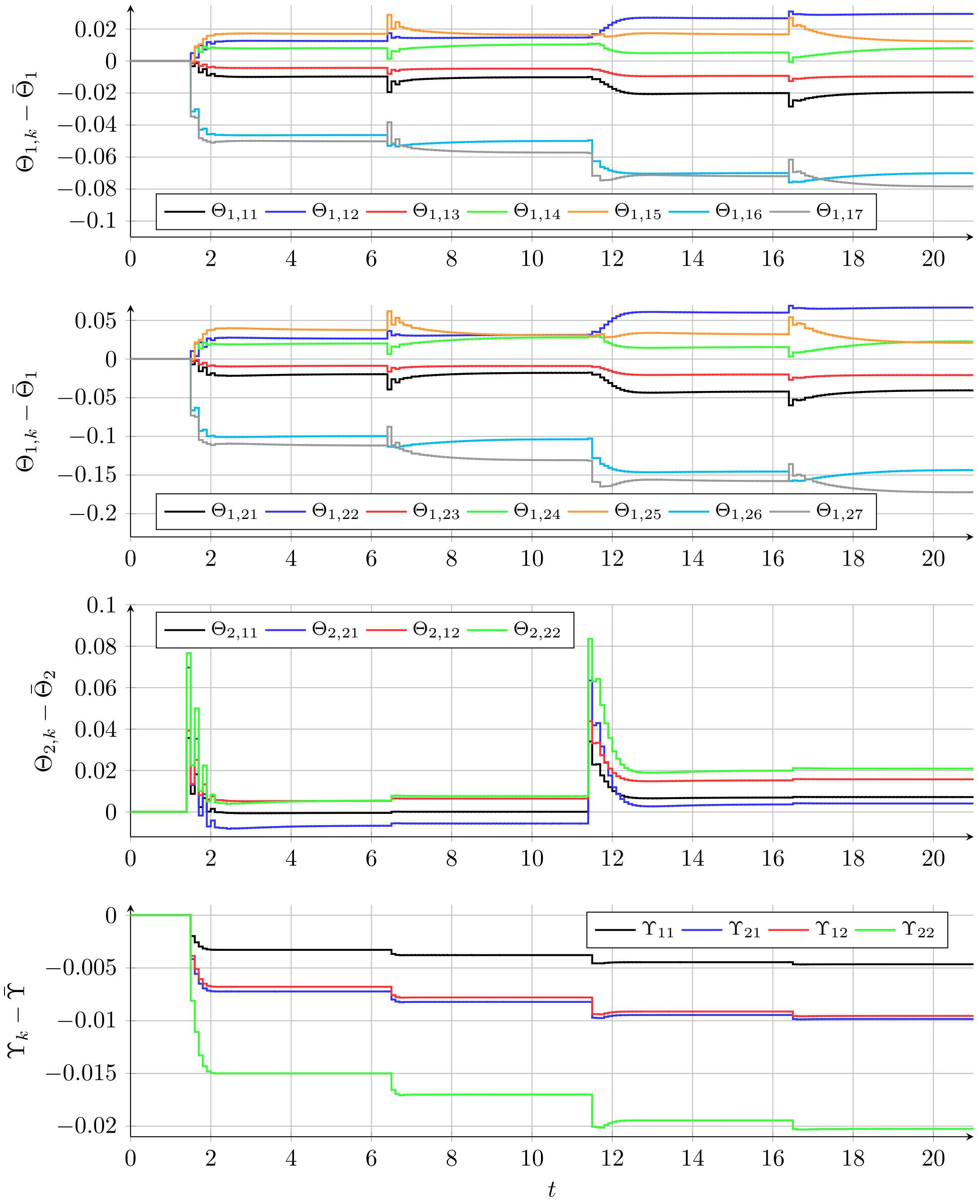

Figure 5.6: Example with fast dynamics (tracking of r_k): Relative changes in the adaptation parameters, i.e. $\Theta_{i,rc}$, $i \in \{1, 2\}$, and Υ_{rc} where r and c are the numbers of the corresponding rows and columns in matrices $\Theta_i = \Theta_{i,k} - \bar{\Theta}_i$ and $\Upsilon = \Upsilon_k - \bar{\Upsilon}$ for a network delay of $\tau = 0.15\,s$.

In addition, Figures 5.7 to 5.12 present the corresponding results for the case, when the second approach is used that stabilizes $\sigma_k = 0$ as stated in Corollary 5.10.

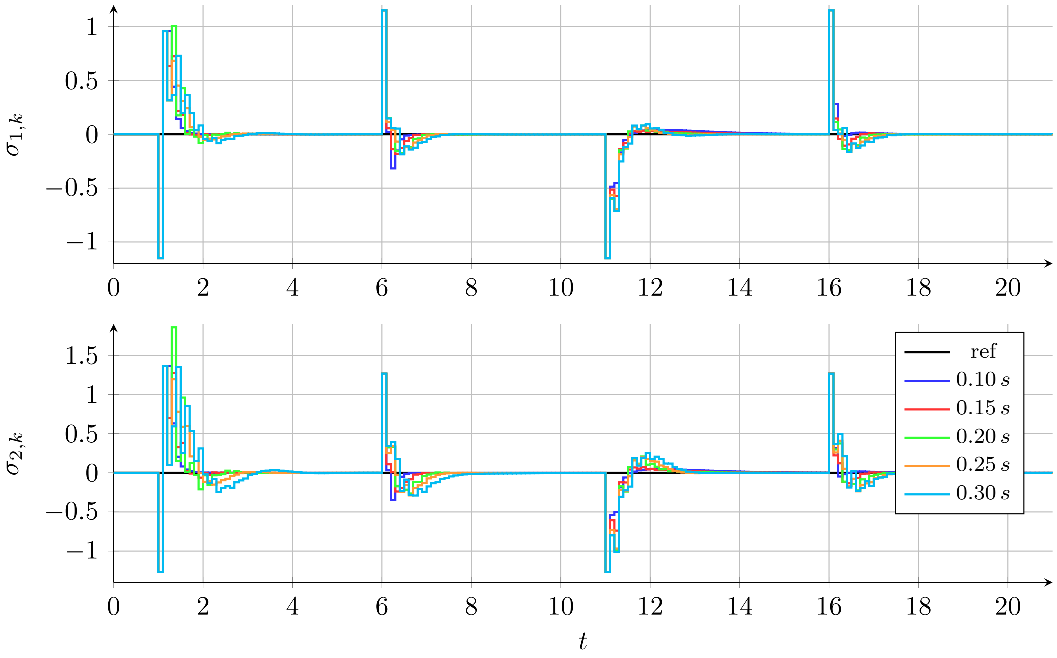

Figure 5.7: Example with fast dynamics (stabilization of $\sigma_k = 0$): Tracking of virtual outputs σ_k for different network delays τ.

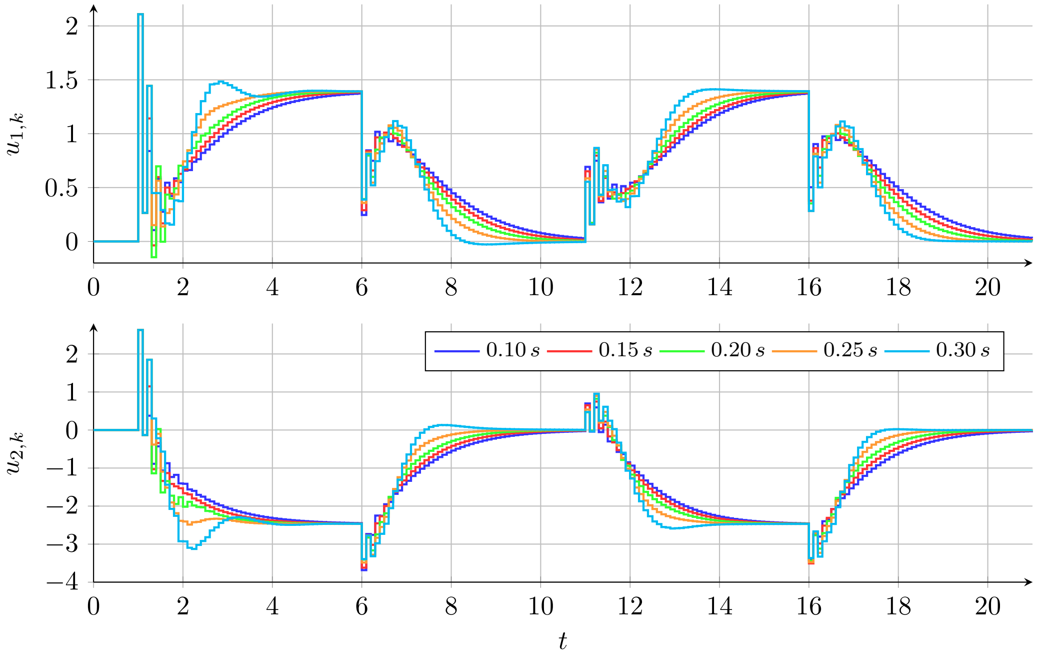

Figure 5.8: Example with fast dynamics (stabilization of $\sigma_k = 0$): Control signals u_k for different network delays τ.

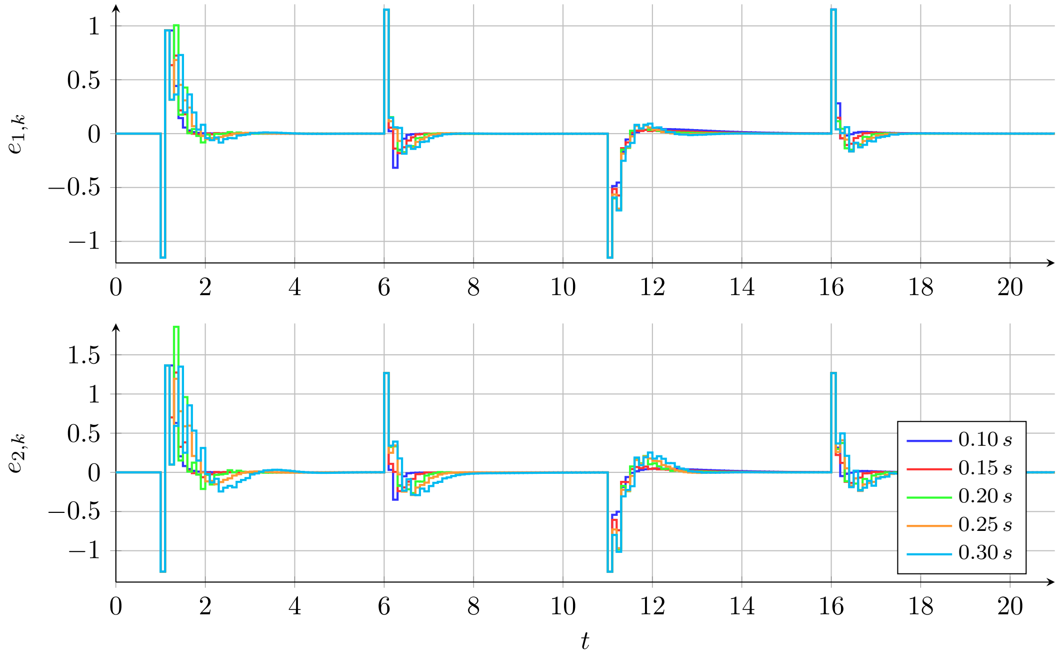

Figure 5.9: Example with fast dynamics (stabilization of $\sigma_k = 0$): Error signals e_k for different network delays τ.

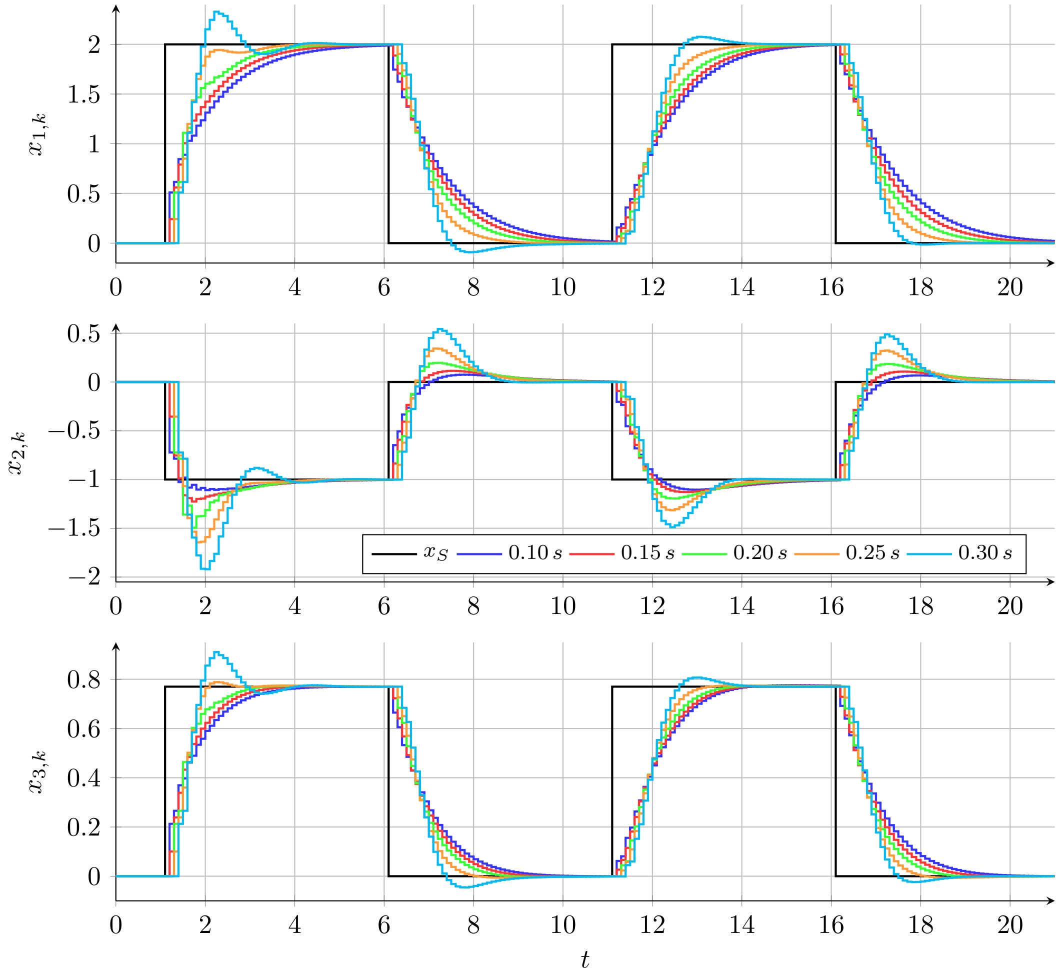

Figure 5.10: Example with fast dynamics (stabilization of $\sigma_k = 0$): States x_k for different network delays τ.

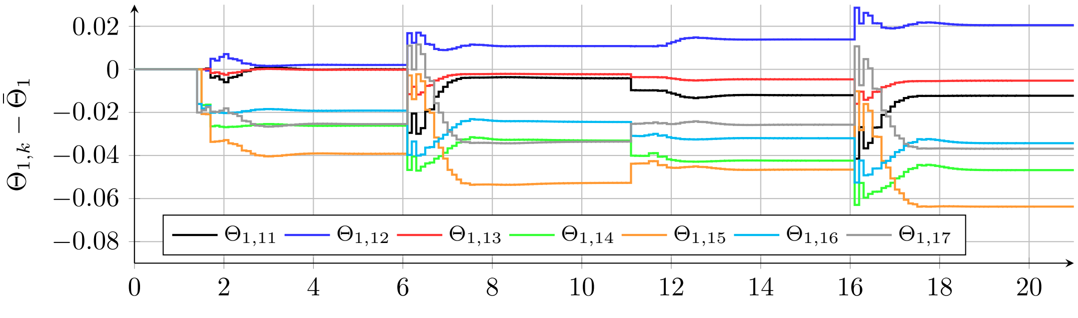

Figure 5.11: Example with fast dynamics (stabilization of $\sigma_k = 0$): Relative changes in the adaptation parameters, i.e. $\Theta_{i,rc}$, $i \in \{1, 2\}$, and Υ_{rc} where r and c are the numbers of the corresponding rows and columns in matrices $\Theta_i = \Theta_{i,k} - \bar{\Theta}_i$ and $\Upsilon = \Upsilon_k - \bar{\Upsilon}$ for a network delay of $\tau = 0.15\,s$ (part 1).

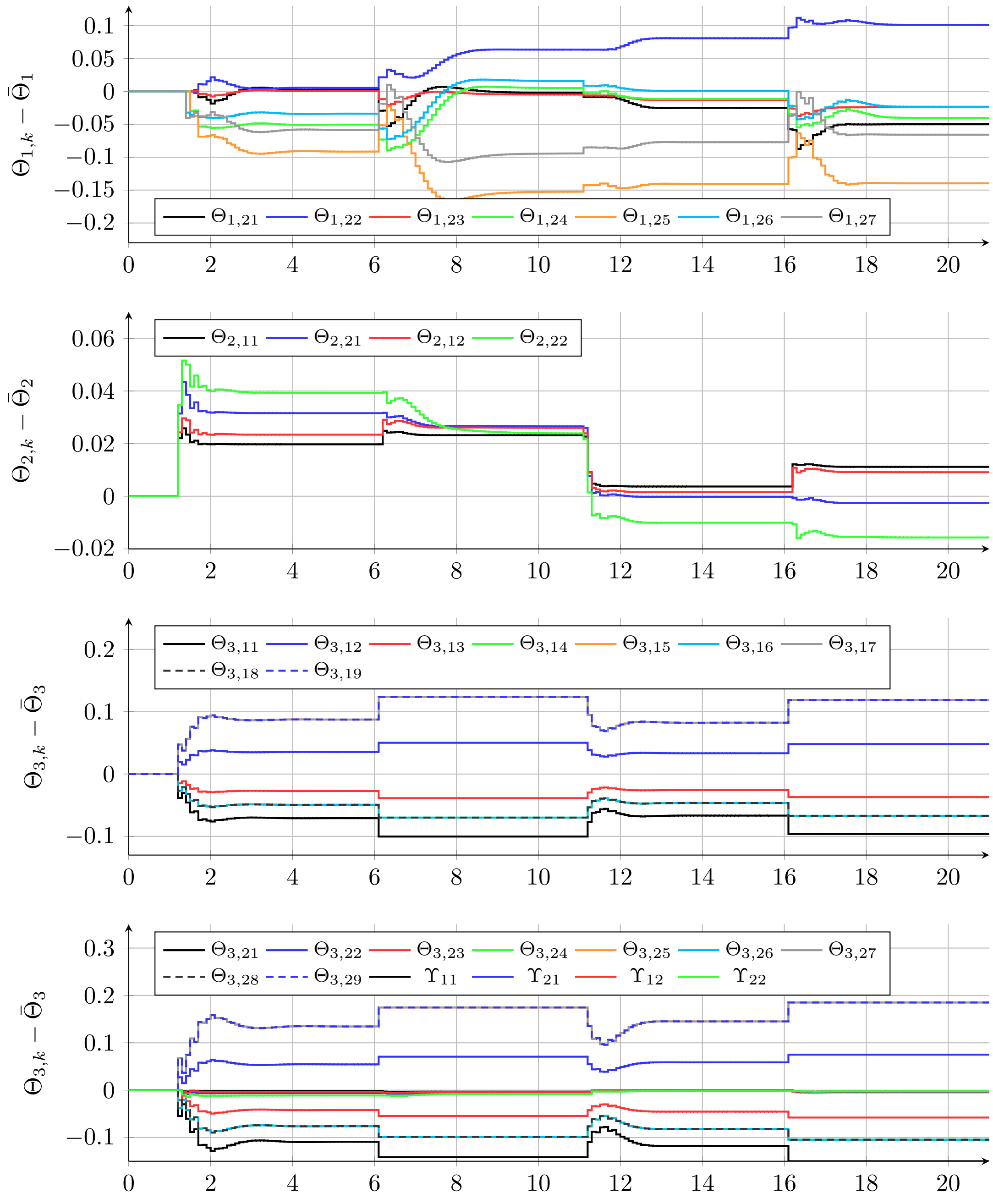

Figure 5.12: Example with fast dynamics (stabilization of $\sigma_k = 0$): Relative changes in the adaptation parameters, i.e. $\Theta_{i,rc}$, $i \in \{1, 2\}$, and Υ_{rc} where r and c are the numbers of the corresponding rows and columns in matrices $\Theta_i = \Theta_{i,k} - \bar{\Theta}_i$ and $\Upsilon = \Upsilon_k - \bar{\Upsilon}$ for a network delay of $\tau = 0.15\,s$ (part 2).

A comparison of the proposed approaches to a non-adaptive approach is presented in Figure 5.13. This non-adaptive controller

$$u_k = -\mathcal{C} z_k \tag{5.94}$$

is designed similar to C_1 for the remaining dynamics as detailed above to minimize the spectral radius of $(\mathcal{A}_z - \mathcal{C}\mathcal{B}_z)$, where $\mathcal{A}_z$ and $\mathcal{B}_z$ represent the system data of the networked system in the transformed version (5.8) and (5.9). For the actual example, one gets a gain controller gain matrix $\mathcal{C}$ as

$$\mathcal{C} = \begin{bmatrix} \mathcal{C}_1 & \mathcal{C}_2 \end{bmatrix} \quad \text{with} \tag{5.95a}$$

$$\mathcal{C}_1 = \begin{bmatrix} -0.4182 & -0.1019 & 0.1413 & 0.0265 & 0.0025 & -0.2342 & -0.0413 \\ 0.9119 & -0.6272 & 0.6983 & -0.2356 & -0.0395 & -0.2535 & -0.2207 \end{bmatrix}, \tag{5.95b}$$

$$\mathcal{C}_2 = \begin{bmatrix} -0.4097 & -0.0877 \\ 1.4873 & 0.6780 \end{bmatrix}. \tag{5.95c}$$

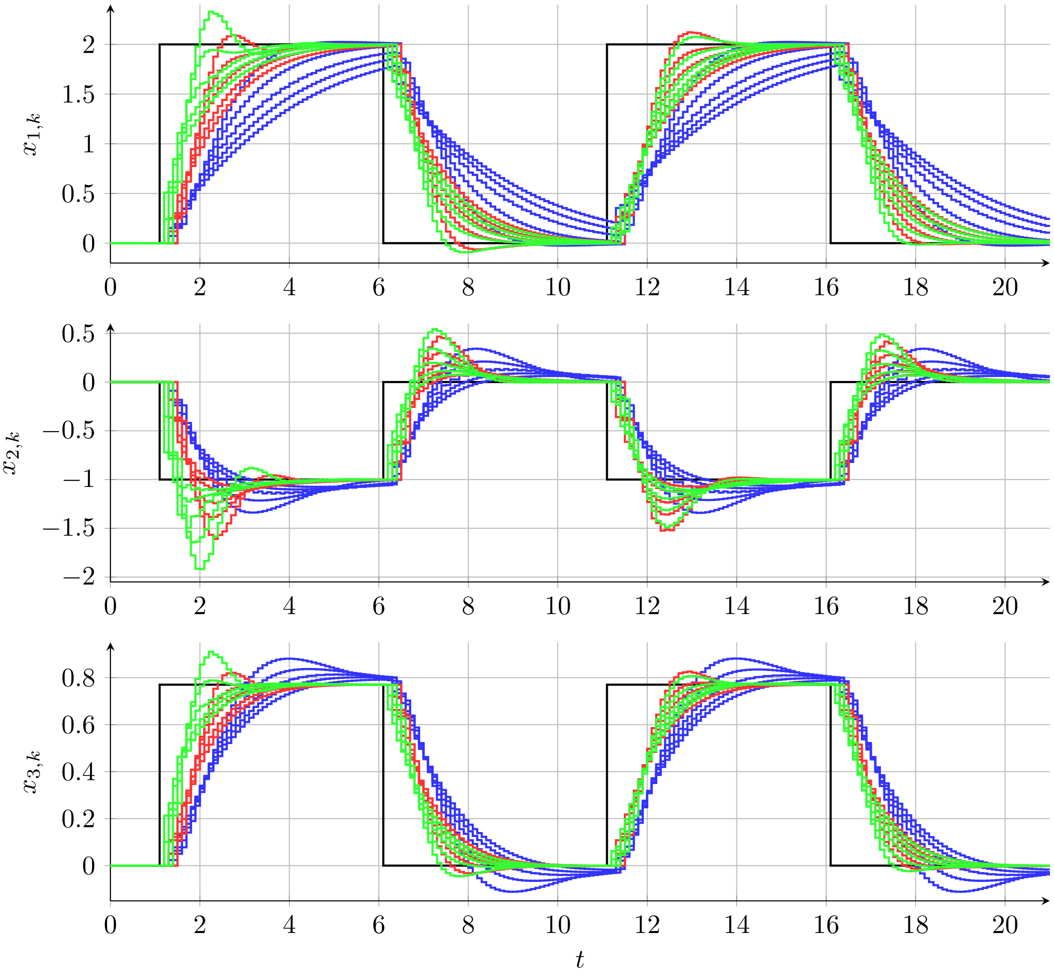

Figure 5.13: Example with fast dynamics: Comparison of the tracking approach (red) and stabilization approach (green) with a non-adaptive approach (blue).

As can be seen in Figure 5.13, the adaptive tracking approaches improve the performance when compared to the basic, non-adaptive controller, which is conservative because it has to stabilize the loop for all considered round trip delays τ. Using the stabilization approach allows to further speed up the response time of the closed loop system but results in a larger overshoot. The differences become clearly visible by inspecting the resulting error between desired $\hat{x}_k$ and actual plant states x_k, using measure $\sqrt{\sum(x_k - \hat{x}_k)^2}$ as well as the related control energy as shown in Table 5.1.

Table 5.1: Example with fast dynamics: Results for the non-adaptive controller (non-ad) in comparison to adaptive tracking (track) and adaptive stabilization (stab) in terms of tracking error and control energy.

approach	non-ad	track	stab	non-ad	track	stab
$\sqrt{\sum (x_k - \hat{x}_k)^2}$	32.55	26.91	24.43	100.0 %	82.6 %	75.0 %
$\sqrt{\sum u_k^2}$	54.24	59.59	60.66	100.0 %	109.8 %	111.8 %

Please note that the maximal admissible overshoot of the step responses is not taken into account in the design of C_1. Hence, various alternative methods to design the remaining dynamics may lead to an improved performance.

5.3.2 Example with slow Plant Dynamics

In contrast to the previous example, a plant with slower dynamics is considered next. It is given by a dynamic matrix $\tilde{A}$ and an input matrix $\tilde{B}$ as

$$\tilde{A} = \begin{bmatrix} -0.5 & -1.0 & 1.1 \\ -0.7 & -0.8 & -1.9 \\ 0.5 & 0.1 & 1.8 \end{bmatrix} \qquad \text{and} \qquad \tilde{B} = \begin{bmatrix} -0.9 & 1.3 \\ 0.6 & -0.5 \\ 1.0 & 0.0 \end{bmatrix} \tag{5.96}$$

with corresponding eigenvalues of the continuous-time plant as $s_1 = 2.0903$, $s_2 = -1.3501$ and $s_3 = -0.2402$. The very same references as before are used to evaluate the proposed algorithms for the actual plant model. Matrices C_1 and $\mathcal{C}$ follow in this case as

$$C_1 = \begin{bmatrix} 0.7421 & 0.5091 & 4.5167 & 0.1126 & 0.1105 & 0.5165 & -0.0267 \\ 0.6677 & -1.4529 & 1.3999 & -0.3724 & -0.3453 & -0.2667 & 0.3712 \end{bmatrix} \tag{5.97}$$

and

$$\mathcal{C} = \begin{bmatrix} \mathcal{C}_1 & \mathcal{C}_2 \end{bmatrix} \qquad \text{with} \tag{5.98a}$$

$$\mathcal{C}_1 = \begin{bmatrix} 0.4712 & -0.0585 & 2.2877 & 0.1350 & 0.0515 & -0.4450 & 0.1242 \\ 0.1582 & -0.0520 & 0.7915 & -0.0836 & -0.2484 & -0.0432 & -0.7940 \end{bmatrix}, \tag{5.98b}$$

$$\mathcal{C}_2 = \begin{bmatrix} 0.2467 & 0.0724 \\ 0.1016 & 0.3033 \end{bmatrix}. \tag{5.98c}$$

The plots for (σ_k) and (u_k) in Figures 5.14 to 5.17 underline the outcomes of the proposed approaches for the plant with slow dynamics. Especially Figure 5.18 emphasizes the fact that the presented adaptive approaches allow to significantly improve the closed loop performance when compare to a non-adaptive algorithm that has to be designed for the worst case scenario. This also becomes evident in Table 5.2 by a considerable improvement in the tracking error that is traded for an enlarged control energy.

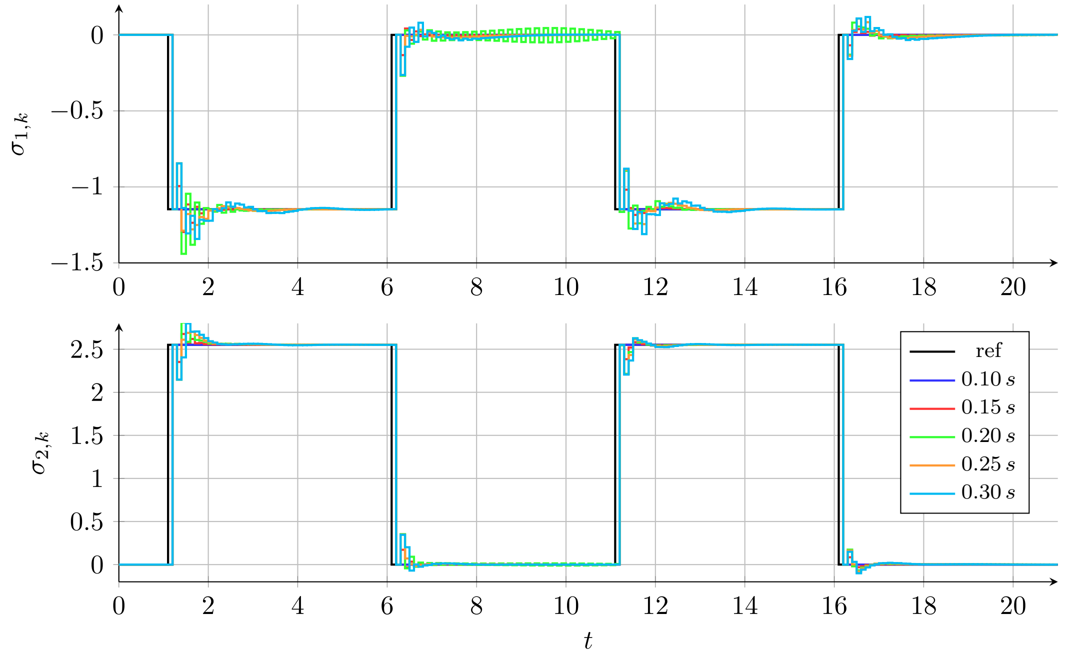

Figure 5.14: Example with slow dynamics (tracking of r_k): Tracking of virtual outputs σ_k for different network delays τ.

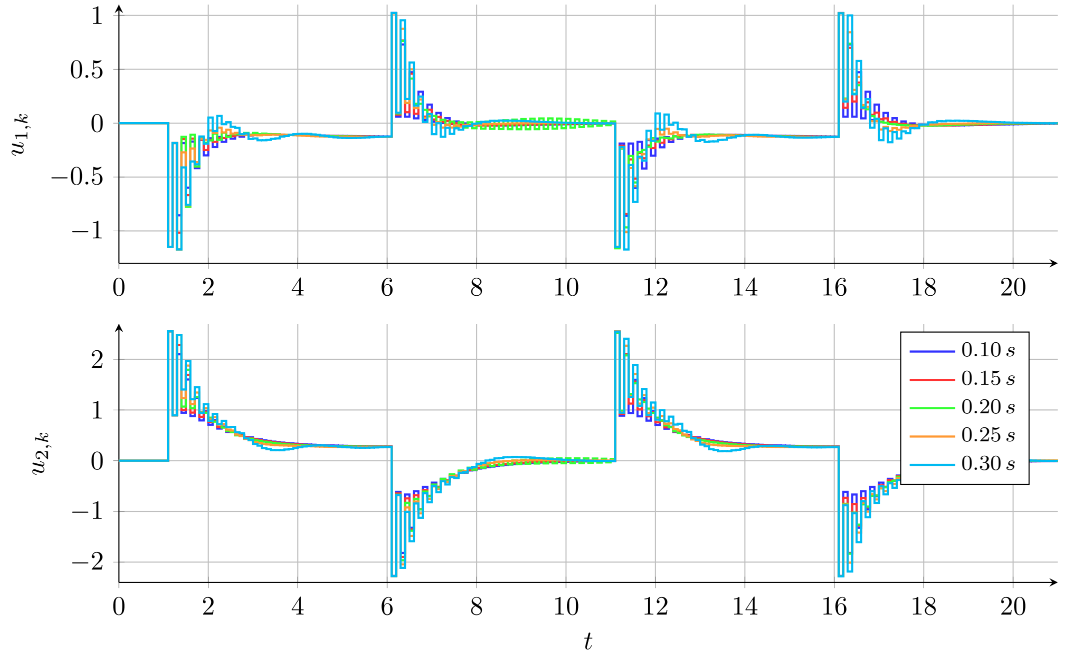

Figure 5.15: Example with slow dynamics (tracking of r_k): Control signals u_k for different network delays τ.

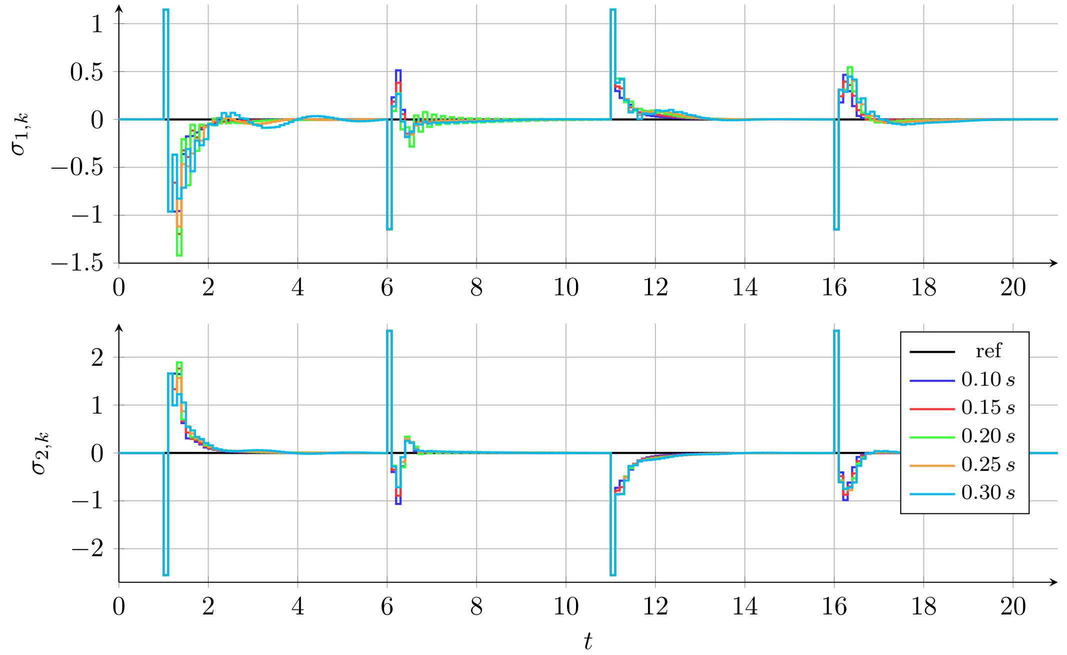

Figure 5.16: Example with slow dynamics (stabilization of $\sigma_k = 0$): Tracking of virtual outputs σ_k for different network delays τ.

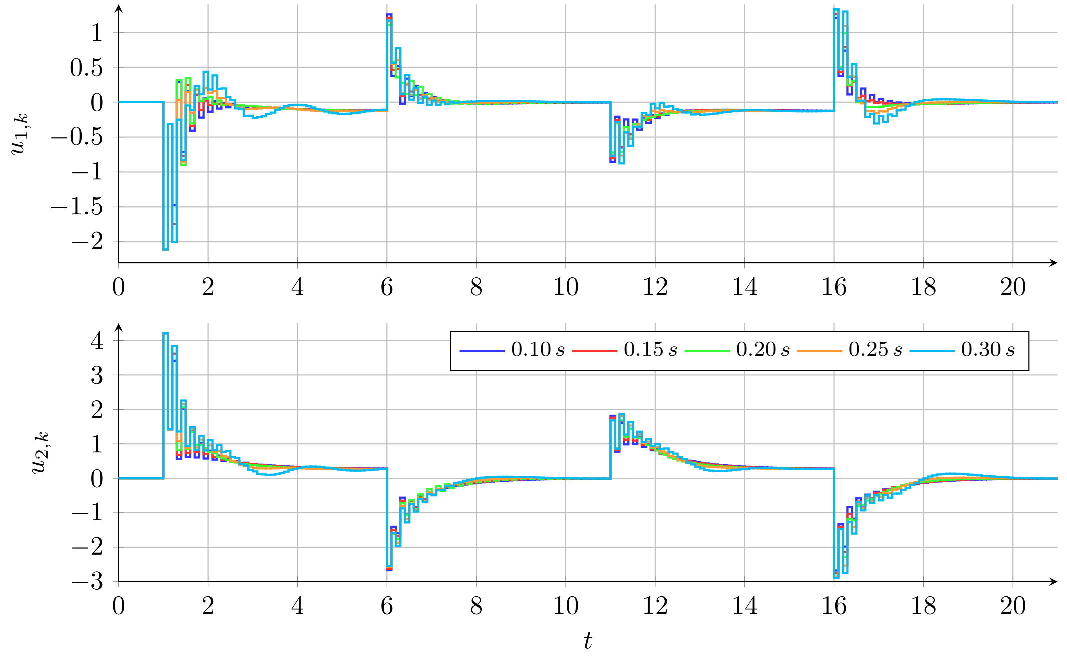

Figure 5.17: Example with slow dynamics (stabilization of $\sigma_k = 0$): Control signals u_k for different network delays τ.

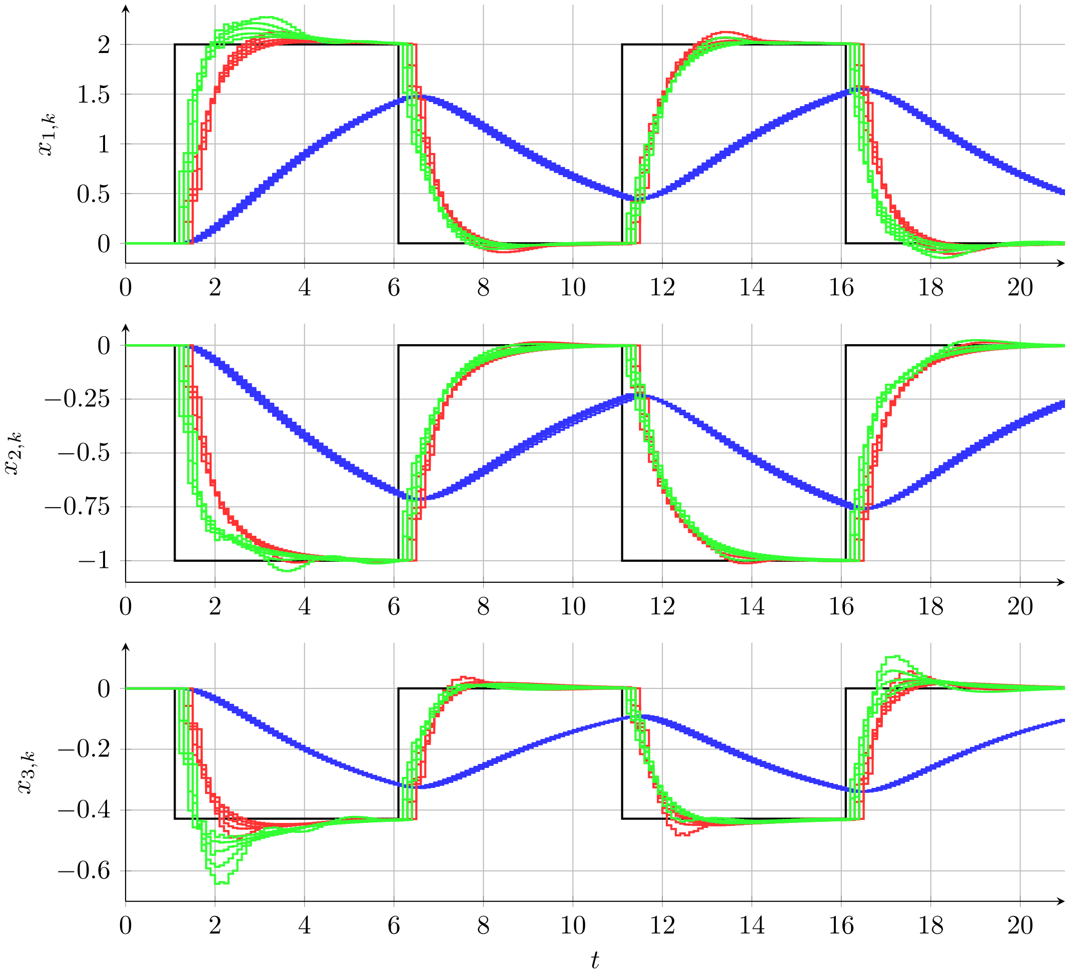

Figure 5.18: Example with slow dynamics: Comparison of the tracking approach (red) and stabilization approach (green) with a non-adaptive approach (blue).

Table 5.2: Example with slow dynamics: Results for the non-adaptive controller (non-ad) in comparison to adaptive tracking (track) and adaptive stabilization (stab) in terms of tracking error and control energy.

approach	non-ad	track	stab	non-ad	track	stab
$\sqrt{\sum (x_k - \hat{x}_k)^2}$	42.13	2.303	19.83	100.0 %	54.6 %	47.0 %
$\sqrt{\sum u_k^2}$	7.618	22.43	25.39	100.0 %	294.3 %	333.2 %

5.4 Extended Formulation

Several extensions of the approaches presented in the sections above are possible. One example is to, e.g., include the plant states x_k into $z_{2,k}$ and define $z_{1,k}$ (5.7) in a different way such that

$$z_{1,k} = \begin{bmatrix} u_{k-2}^{\mathrm{T}} & u_{k-3}^{\mathrm{T}} & \cdots & u_{k-\bar{d}+1}^{\mathrm{T}} & u_{k-\bar{d}}^{\mathrm{T}} \end{bmatrix}^{\mathrm{T}} \quad \in \mathbb{R}^{m(\bar{d}-1)}, \tag{5.99a}$$

$$z_{2,k} = \begin{bmatrix} x_k^{\mathrm{T}} & u_{k-1}^{\mathrm{T}} \end{bmatrix}^{\mathrm{T}} \quad \in \mathbb{R}^{n+m}. \tag{5.99b}$$

This results in a new partitioning of the system description (5.10) with the partitioning of matrix $\mathcal{A}_z$ as

$$A_{11} = \begin{bmatrix} 0 & 0 & \cdots & 0 & 0 & 0 \\ I_m & 0 & \cdots & 0 & 0 & 0 \\ 0 & I_m & \ddots & \vdots & \vdots & \vdots \\ 0 & \ddots & \ddots & 0 & 0 & 0 \\ 0 & \ddots & \ddots & I_m & 0 & 0 \\ 0 & \cdots & \cdots & 0 & I_m & 0 \end{bmatrix}, \qquad A_{12} = \begin{bmatrix} 0 & I_m \\ 0 & 0 \\ \vdots & \vdots \\ 0 & 0 \\ 0 & 0 \\ 0 & 0 \end{bmatrix}, \tag{5.100a}$$

$$A_{21} = \begin{bmatrix} M_{\bar{d}-2}(\tau) & M_{\bar{d}-3}(\tau) & \cdots & M_1(\tau) & M_0(\tau) \\ 0 & 0 & \cdots & 0 & 0 \end{bmatrix}, \qquad A_{22} = \begin{bmatrix} e^{\tilde{A}h} & M_{\bar{d}-1}(\tau) \\ 0 & 0 \end{bmatrix}, \tag{5.100b}$$

and the sub-matrices of $\mathcal{B}_z$ in the form of

$$B_1 = 0 \qquad \text{and} \qquad B_2 = \begin{bmatrix} M_{\bar{d}}(\tau) \\ 0 \end{bmatrix} \tag{5.101}$$

with appropriate dimensions. This implies that the uncertain matrices $M_\ell(\tau)$ do not directly influence the states $z_{1,k}$.

Relying on this new representation, a modified virtual output

$$\sigma_k = C z_k = \begin{bmatrix} C_1 & C_2 \end{bmatrix} \begin{bmatrix} z_{1,k} \\ z_{2,k} \end{bmatrix} = C_1 z_{1,k} + C_2 z_{2,k} \in \mathbb{R}^m \tag{5.102}$$

with $C_1 \in \mathbb{R}^{m \times (m(\bar{d}-1))}$ and $C_2 \in \mathbb{R}^{m \times (n+m)}$ is designed allowing to further improve the performance at the price of a more sophisticated design problem for C_1 and C_2. One can, in principle, follow the same steps described in Section 5.1 for the design of the adaptive laws and the stability analysis. However, some aspects require special attention due to the changed dimensions of C_1 and C_2.

To see this, one defines a new variable s_k for the rightmost part in (5.102) such that

$$s_k = C_2 z_{2,k} \quad \in \mathbb{R}^m, \tag{5.103}$$

where $C_2 \in \mathbb{R}^{m \times (n+m)}$ is assumed to be full rank, i.e. $\operatorname{rank} C_2 = m$. Since, the dimension of $z_{2,k} \in \mathbb{R}^{n+m}$ is larger than the dimension of s_k, the complementary part of s_k is given by

$$s_k^{\perp} = C_2^{\perp} z_{2,k} \quad \in \mathbb{R}^n \tag{5.104}$$

with a matrix $C_2^{\perp} \in \mathbb{R}^{n\times(n+m)}$ that is constructed in a way to form a regular transformation stated as

$$\begin{bmatrix} s_k^{\perp} \\ s_k \end{bmatrix} = \begin{bmatrix} C_2^{\perp} \\ C_2 \end{bmatrix} z_{2,k}\,, \tag{5.105}$$

where the transformation matrix $\begin{bmatrix} C_2^{\perp\mathrm{T}} & C_2^{\mathrm{T}} \end{bmatrix}^{\mathrm{T}}$ has dimension $((n+m)\times(n+m))$. Matrix $C_2^{\perp}$ can be constructed as

$$C_2^{\perp} = \mathcal{R}\left(C_2\right)^{\mathrm{T}}\,, \tag{5.106}$$

in which $\mathcal{R}(C_2)$ stands for the right nullspace of matrix $C_2 \in \mathbb{R}^{m\times(n+m)}$ such that $C_2\mathcal{R}\left(C_2\right) = 0$ with $\mathcal{R}\left(C_2\right) \in \mathbb{R}^{(n+m)\times(n+m-\mathrm{rank}(C_2))}$. The right inverse of matrix C_2, i.e.

$$C_2^{+} = C_2^{\mathrm{T}}\left(C_2C_2^{\mathrm{T}}\right)^{-1} \quad \in \mathbb{R}^{(n+m)\times m}\,, \tag{5.107}$$

exists such that $C_2C_2^{+} = I_m$ because it is assumed to be full rank. Since also $C_2^{\perp}$ has full row rank due its particular construction, on gets the corresponding right inverse

$$C_2^{\perp+} = C_2^{\perp\mathrm{T}}\left(C_2^{\perp}C_2^{\perp\mathrm{T}}\right)^{-1} \quad \in \mathbb{R}^{(n+m)\times n} \tag{5.108}$$

such that $C_2^{\perp}C_2^{\perp+} = I_n$ is fulfilled. Hence,

$$z_{2,k} = \begin{bmatrix} C_2^{\perp+} & C_2^{+} \end{bmatrix}\begin{bmatrix} s_k^{\perp} \\ s_k \end{bmatrix} \tag{5.109}$$

is constructed based on the new variable s_k and its complementary part $s_k^{\perp}$. This becomes evident by combining (5.105) and (5.109) yielding

$$\begin{bmatrix} s_k^{\perp} \\ s_k \end{bmatrix} = \begin{bmatrix} C_2^{\perp} \\ C_2 \end{bmatrix}\begin{bmatrix} C_2^{\perp+} & C_2^{+} \end{bmatrix}\begin{bmatrix} s_k^{\perp} \\ s_k \end{bmatrix} = I_{n+m}\begin{bmatrix} s_k^{\perp} \\ s_k \end{bmatrix} \tag{5.110}$$

and, as a consequence,

$$z_{2,k} = C_2^{\perp+}s_k^{\perp} + C_2^{+}s_k = C_2^{\perp+}C_2^{\perp}z_{2,k} + C_2^{+}C_2^{\perp}z_{2,k} \tag{5.111}$$

with

$$C_2^{\perp+}C_2^{\perp} + C_2^{+}C_2^{\perp} = I_{n+m}\,. \tag{5.112}$$

Thus, the virtual output variable σ_k can be written as

$$\sigma_k = C_1z_{1,k} + C_2z_{2,k} = C_1z_{1,k} + s_k\,, \tag{5.113}$$

in which definition (5.103) is incorporated. The mathematical description of the rearranged system equation for the networked plant model (5.10) with states z_k is transformed to an alternative representation, which uses the constructed virtual output σ_k and $s_k^{\perp}$, i.e.

$$z_k = \begin{bmatrix} z_{1,k} \\ z_{2,k} \end{bmatrix} \qquad \Rightarrow \qquad \begin{bmatrix} z_{1,k} \\ s_k^{\perp} \\ \sigma_k \end{bmatrix} \quad \in \mathbb{R}^{m(\bar{d}-1)+n+m}\,. \tag{5.114}$$

Based on (5.10) and (5.100), one can derive a difference equation for $z_{1,k+1}$ such that

$$\begin{aligned} z_{1,k+1} &= A_{11}z_{1,k} + A_{12}z_{2,k} \\ &= \left(A_{11} - A_{12}C_2^{+}C_1\right)z_{1,k} + A_{12}C_2^{\perp+}s_k^{\perp} + A_{12}C_2^{+}\sigma_k\,, \end{aligned} \tag{5.115}$$

as well es for the complementary part of s_k as

$$\begin{aligned} s_{k+1}^{\perp} &= C_2^{\perp} z_{2,k+1} \\ &= \left(C_2^{\perp} A_{21} - C_2^{\perp} A_{22} C_2^{+} C_1 \right) z_{1,k} + C_2^{\perp} A_{22} C_2^{\perp \mathrm{T}} s_k^{\perp} + C_2^{\perp} A_{22} C_2^{+} \sigma_k + C_2^{\perp} B_2 u_k \end{aligned} \tag{5.116}$$

and for the virtual output σ_k in the form of

$$\begin{aligned} \sigma_{k+1} &= C_1 z_{1,k+1} + C_2 z_{2,k+1} \\ &= C_1 A_{11} z_{1,k} + C_1 A_{12} z_{2,k} + C_2 A_{21} z_{1,k} + C_2 A_{22} z_{2,k} + C_2 B_2 u_k \\ &= A_1 z_{1,k} + A_2 s_k^{\perp} + A_3 \sigma_k + C \mathcal{B}_z u_k \end{aligned} \tag{5.117}$$

with

$$A_1 = C_1 A_{11} - C_1 A_{12} C_2^{+} C_1 + C_2 A_{21} - C_2 A_{22} C_2^{+} C_1 \tag{5.118a}$$

$$A_2 = C_1 A_{12} C_2^{\perp +} + C_2 A_{22} C_2^{\perp +} \tag{5.118b}$$

$$A_3 = C_1 A_{12} C_2^{+} + C_2 A_{22} C_2^{+} \,. \tag{5.118c}$$

Following again the main idea of model reference adaptive control for a virtual output σ_k, a reference model

$$\sigma_{M,k+1} = A_{M1} z_{1,k} + A_{M2} s_k^{\perp} + A_M \sigma_k + B_M r_k \quad \in \mathbb{R}^m \tag{5.119}$$

is defined in accordance with the actual dynamics (5.117). Consequently, the dynamics of error

$$e_k = \sigma_k - \sigma_{M,k} \quad \in \mathbb{R}^m \tag{5.120}$$

is given by

$$\begin{aligned} e_{k+1} = A_M e_k &+ \left(A_1 - A_{M1} \right) z_{1,k} + \left(A_2 - A_{M2} \right) s_k^{\perp} \\ &+ \left(A_3 - A_M \right) \sigma_k - B_M r_k + C \mathcal{B}_z u_k \,. \end{aligned} \tag{5.121}$$

The reference dynamics (5.119) is identical to the actual dynamics (5.117), if the a nominal controller

$$\begin{aligned} \bar{u}_k &= \bar{\theta}_1 z_{1,k} + \bar{\theta}_2 s_k^{\perp} + \bar{\theta}_3 \sigma_k + \bar{\theta}_4 r_k \\ &= \bar{\theta} \omega_k + \bar{\theta}_4 r_k \end{aligned} \tag{5.122}$$

with

$$\bar{\theta} = \begin{bmatrix} \bar{\theta}_1 & \bar{\theta}_2 & \bar{\theta}_3 \end{bmatrix} \quad \in \mathbb{R}^{m \times (n + m\bar{d})} \,, \qquad \omega_k = \begin{bmatrix} z_{1,k} \\ s_k^{\perp} \\ \sigma_k \end{bmatrix} \quad \in \mathbb{R}^{n + m\bar{d}} \tag{5.123}$$

and

$$\bar{\theta}_1 = - \left(C \mathcal{B}_u \right)^{-1} \left(A_1 - A_{M1} \right) \quad \in \mathbb{R}^{m \times (m(\bar{d}-1))} \tag{5.124a}$$

$$\bar{\theta}_2 = - \left(C \mathcal{B}_u \right)^{-1} \left(A_2 - A_{M2} \right) \quad \in \mathbb{R}^{m \times n} \tag{5.124b}$$

$$\bar{\theta}_3 = - \left(C \mathcal{B}_u \right)^{-1} \left(A_3 - A_M \right) \quad \in \mathbb{R}^{m \times m} \tag{5.124c}$$

$$\bar{\theta}_4 = \left(C \mathcal{B}_u \right)^{-1} B_M \quad \in \mathbb{R}^{m \times m} \tag{5.124d}$$

is utilized. Hence, adaptive laws can be constructed and the stability of the closed loop networked system can be shown by following the same ideas as in Section 5.1, where parameter matrix

$$\theta_k = \bar{\theta} + \phi_k \tag{5.125}$$

appears because the nominal values for $\bar{\theta}$ are unknown. The corresponding dimensions of the involved variables are as follows:

$$\begin{array}{ll} \theta_k \in \mathbb{R}^{m\times(n+m\bar{d})} & \varepsilon_k \in \mathbb{R}^{m} \\ \Upsilon_k \in \mathbb{R}^{m\times m} & \tilde{\xi}_k \in \mathbb{R}^{n+m\bar{d}+m} \\ \omega_k \in \mathbb{R}^{(n+m\bar{d})} & \Gamma_1 \in \mathbb{R}^{(n+m\bar{d})\times(n+m\bar{d})} \\ \xi_k \in \mathbb{R}^{(n+m\bar{d})} & \Gamma_2 \in \mathbb{R}^{m\times m} \\ \eta_k \in \mathbb{R}^{m} & \end{array} \tag{5.126}$$

The transfer matrices $W_N[\cdot]$ and $W_M[\cdot]$ needed for the adaptive laws in Theorem 5.5 comply with Assumption 5.3 and have $(n + m\bar{d})$ and m inputs (and outputs), respectively.

The remaining dynamics, i.e. the dynamics for $\sigma_k = 0$ for all $k \geq k^\star$, follows for the extended formulation as

$$\begin{aligned} \begin{bmatrix} z_{1,k+1} \\ s^\perp_{k+1} \end{bmatrix} &= \begin{bmatrix} A_{11} - A_{12}C_2^+C_1 & A_{12}C_2^{\perp\mathrm{T}} \\ C_2^\perp A_{21} - C_2^\perp A_{22}C_2^+C_1 & C_2^\perp A_{22}C_2^{\perp\mathrm{T}} \end{bmatrix} \begin{bmatrix} z_{1,k} \\ s^\perp_k \end{bmatrix} \\ &\quad + \begin{bmatrix} A_{12}C_2^+ \\ C_2^\perp A_{22}C_2^+ \end{bmatrix} \sigma_{M,k} + \begin{bmatrix} 0 \\ C_2^\perp B_2 \end{bmatrix} u_k \,. \end{aligned} \tag{5.127}$$

It is beneficial for the design of matrix C_2 to split it into two parts as

$$C_2 = \begin{bmatrix} C_x & C_u \end{bmatrix} , \tag{5.128}$$

where matrix C_x that weights the plant states x_k in (5.99) and C_u the actuation signals u_{k-1} from the previous sampling step. A possible choice for the design of C_2 is to fix $C_u = I_m$.

It is also possible in a straight forward way to state the corresponding versions of Corollaries 5.9, 5.10 and 5.11 for the presented extended formulation.

5.5 Simulation Example for the extended Formulation

A continuous-time plant characterized by matrices

$$\tilde{A} = \begin{bmatrix} 0.7 & 0.9 & 0.7 \\ 0 & 0.4 & 0.3 \\ 0 & 0 & 0.5 \end{bmatrix} , \quad \tilde{B} = \begin{bmatrix} 0.8 & 0.8 \\ 0.3 & 1.0 \\ 0.1 & 0.6 \end{bmatrix} \tag{5.129}$$

is considered to compare the proposed approaches for adaptive tracking of (r_k) and the stabilization of (σ_k) for the original as well as for their extended formulations introduced in the previous section. The sampling interval h and the reference signals are the same as in Section 5.3. Matrix

$$C_1 = \begin{bmatrix} 0.8068 & 0.3654 & 0.7866 & -0.5883 & 0.8022 & 0.1834 & -0.3658 \\ 0.1180 & -0.3008 & 1.0316 & 0.1115 & -0.1572 & -0.0564 & -0.4567 \end{bmatrix} \tag{5.130}$$

is used for the original approaches, while

$$\mathcal{C} = \begin{bmatrix}\mathcal{C}_1 & \mathcal{C}_2\end{bmatrix} \qquad \text{with} \tag{5.131a}$$

$$\mathcal{C}_1 = \begin{bmatrix}0.3783 & 0.3130 & 0.5234 & 0.0036 & 0.2826 & -0.4114 & 0.3323\\ 0.4684 & -0.2055 & 1.7776 & 0.0484 & -0.3248 & 0.2499 & -0.5093\end{bmatrix}, \tag{5.131b}$$

$$\mathcal{C}_2 = \begin{bmatrix}-0.2183 & -0.1658\\ 0.0340 & 0.7120\end{bmatrix}, \tag{5.131c}$$

is the gain matrix of the non-adaptive controller. For the extended formulations, one gets

$$C = \begin{bmatrix}C_1 & C_2\end{bmatrix} \qquad \text{with} \tag{5.132a}$$

$$C_1 = \begin{bmatrix}0.1952 & 0.5920 & -0.2475 & 0.0619\\ 0.3751 & -0.1439 & -0.1181 & -0.0657\end{bmatrix}, \tag{5.132b}$$

$$C_2 = \begin{bmatrix}1.5259 & -0.0297 & 1.7081 & 1.0000 & 0\\ 0.6553 & -1.0143 & 3.2051 & 0 & 1.0000\end{bmatrix}. \tag{5.132c}$$

following the same design approach that minimizes the spectral radius of the respective remaining closed loop dynamics.

Figure 5.19 and Table 5.3 summarize the results for the different approaches. It is clearly visible that the proposed methods allow to achieve faster convergence of the states when compared to the non-adaptive controller. The extended formulations of the adaptive algorithms (red and green curves) as presented in Section 5.4 yield even faster responses compared to the original formulation from Sections 5.1 and 5.2. However, the improved tracking performance results a more sophisticated design of the virtual output variable, which can be done by using an offline optimization problem.

Table 5.3: Example for the extended Formulation: Results for the non-adaptive controller (non-ad) in comparison to adaptive tracking (track), adaptive stabilization (stab), extended tracking (ext track) and extended stabilization (ext stab) in terms of tracking error and control energy.

approach	non-ad	track	stab	ext track	ext stab
$\sqrt{\sum (x_k - \hat{x}_k)^2}$	61.44	49.32	48.25	39.35	36.76
$\sqrt{\sum u_k^2}$	21.47	38.33	37.88	47.88	47.39
$\sqrt{\sum (x_k - \hat{x}_k)^2}$	100.0 %	80.2 %	78.5 %	64.0 %	59.8 %
$\sqrt{\sum u_k^2}$	100.0 %	178.5 %	176.4 %	223.0 %	220.7 %

It is also visible in Figure 5.19 and especially in Table 5.3 that the stabilization approaches (green and cyan) result in slightly faster responses as the approaches to track a desired reference r_k for the virtual output σ_k (red and orange), see the root mean square errors $\sqrt{\sum (x_k - \hat{x}_k)^2}$ in the table.

The shape of the corresponding virtual output variables and actuating signals are depicted in Figures 5.20 and 5.21 for the tracking approaches; and in Figures 5.22 and 5.23 for the stabilization approaches.

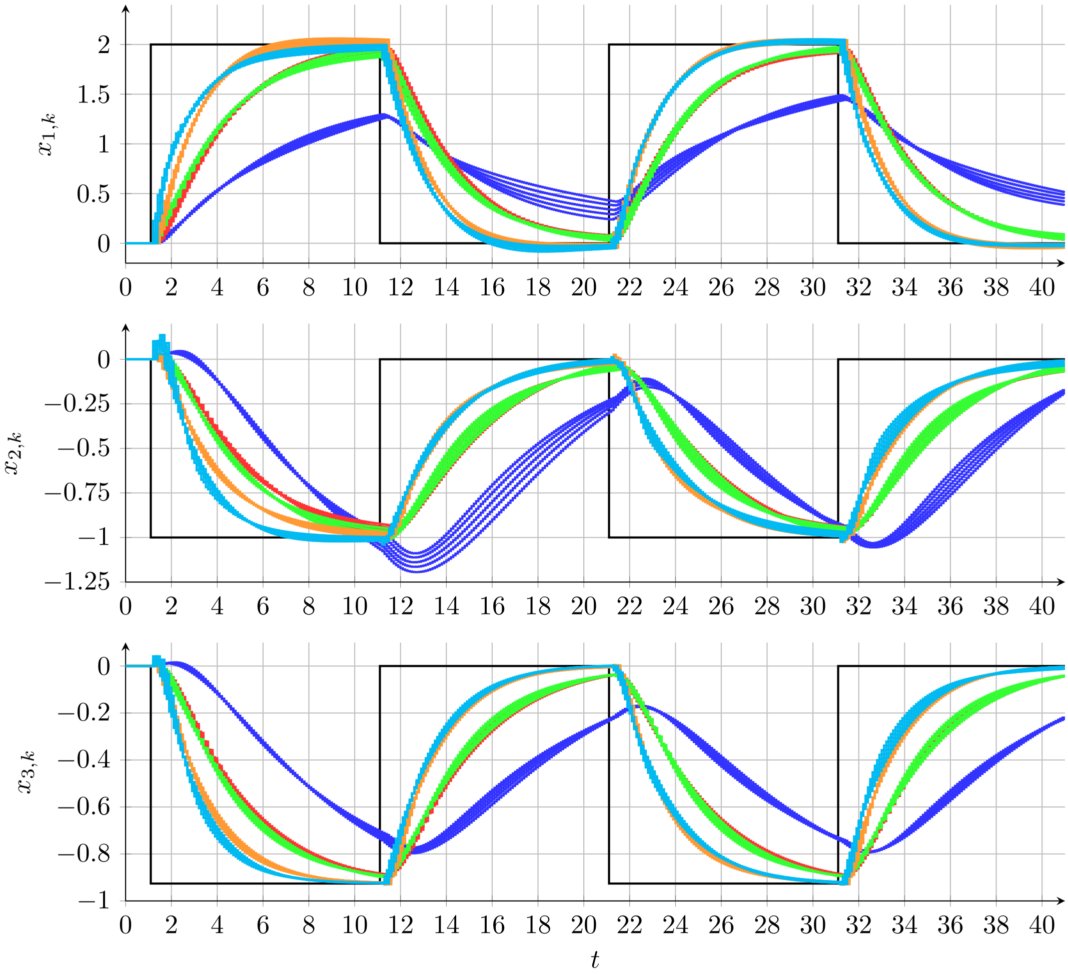

Figure 5.19: Example for the extended Formulation: Comparison of the states x_k for the tracking approach (red) and stabilization approach (green) as well as the extended tracking approach (orange) and extended stabilization approach (cyan) with a non-adaptive approach (blue).

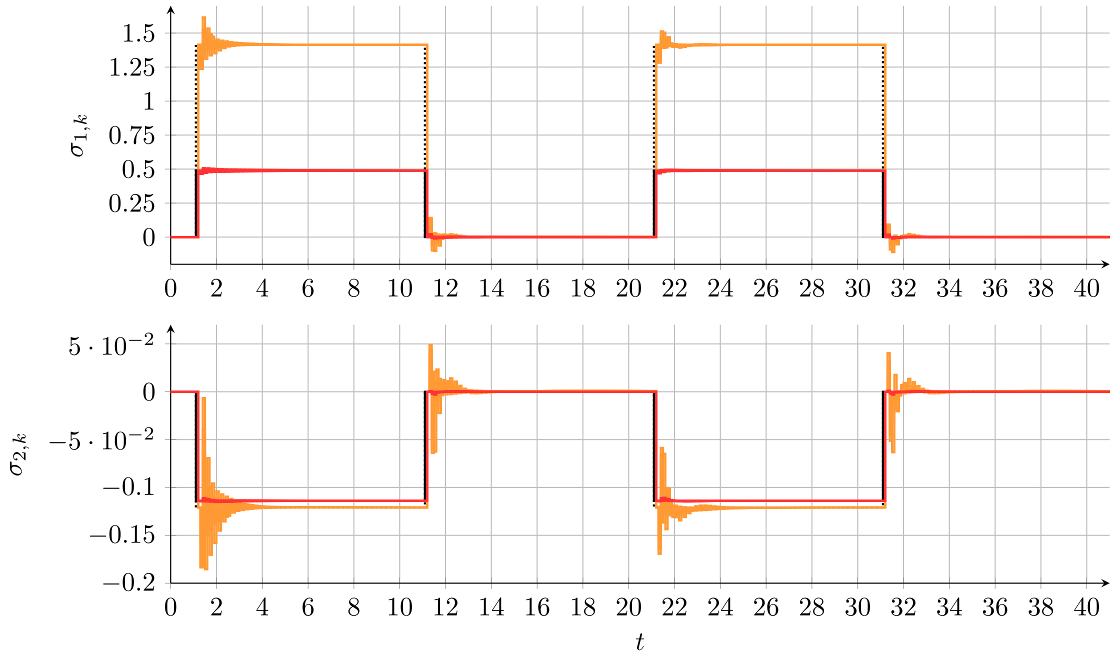

Figure 5.20: Example for the extended Formulation (tracking of r_k): Virtual output σ_k for different network delays τ for the tracking (red) and extended tracking approach (orange).

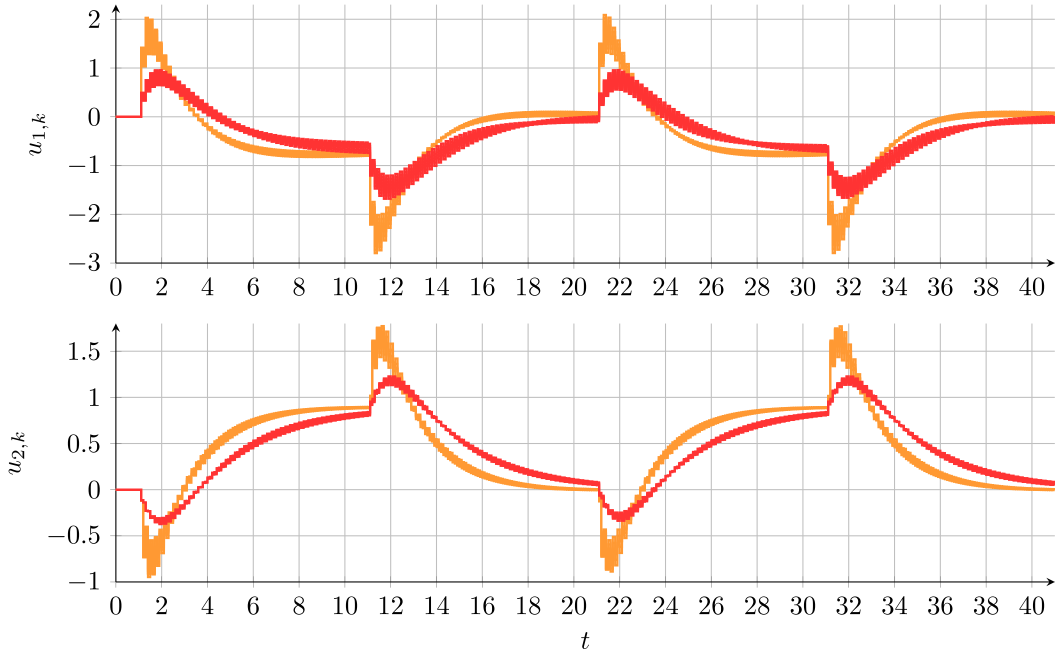

Figure 5.21: Example for the extended Formulation (tracking of r_k): Control signals u_k for different network delays τ for the tracking (red) and extended tracking approach (orange).

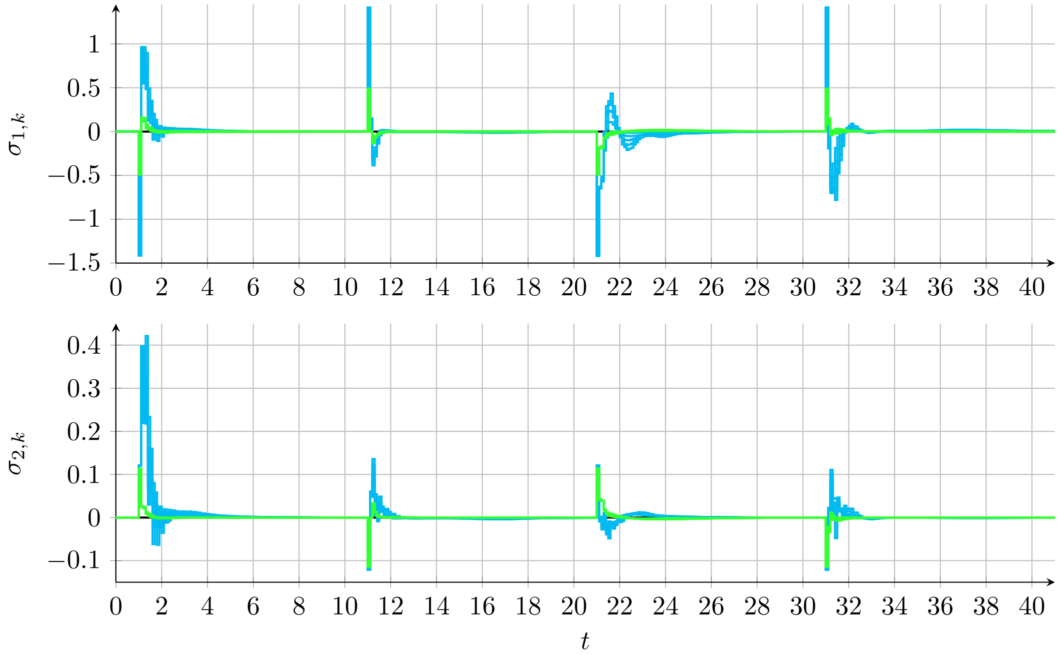

Figure 5.22: Example for the extended Formulation (stabilization of $\sigma_k = 0$): Virtual output σ_k for different network delays τ for the tracking (green) and extended tracking approach (cyan).

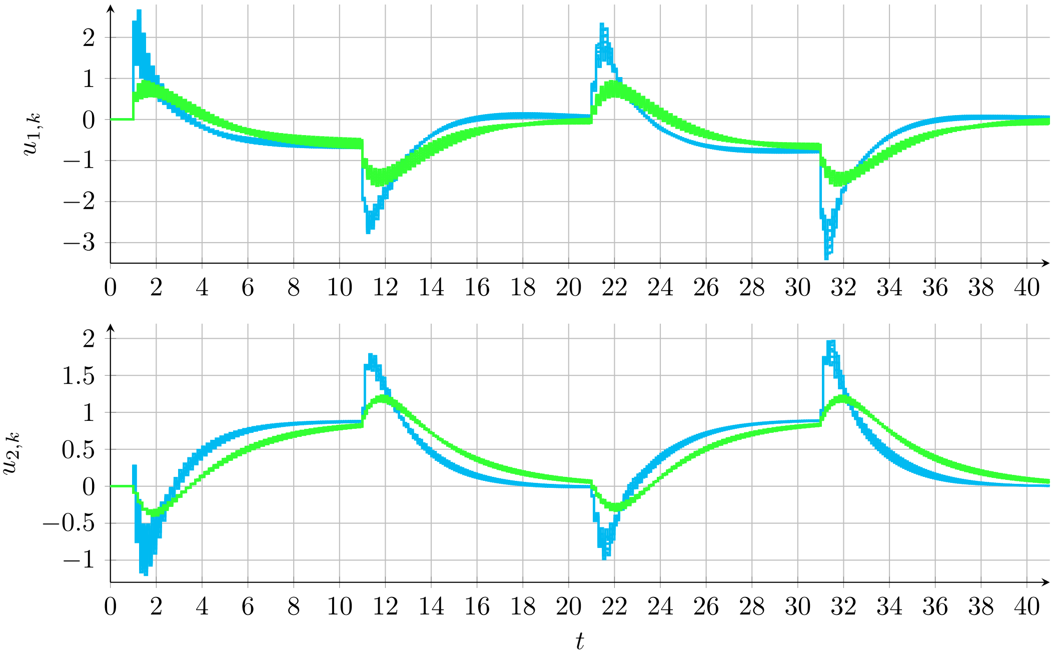

Figure 5.23: Example for the extended Formulation (stabilization of $\sigma_k = 0$): Control signals u_k for different network delays τ for the tracking (green) and extended tracking approach (cyan).

Chapter 6

Stability of packetized Networked Control Systems

In contrast to the previous chapters, no buffering mechanism as in Chapter 4 or adaptation algorithms as in Chapter 5 are considered now. Actually, basic control loops are in focus, where the time-varying packet delays in the transmission network are bounded, but are not restricted in other ways. This implies that the chosen network protocols introduced in Chapter 2, i.e. the active packet skipping and hold mechanisms, play a vital role in the analysis. The present chapter is adopted from [SH20], [SH21a] and [SH21b].

First, the problem setup together with the assumptions on the controller, the plant and the network connection are described. An example of a filtered Smith predictor is introduced and used throughout this and the two subsequent chapters to show the properties of LMI-based as well as of the proposed stability criteria, presented in Chapters 7 and 8. Then, it is illustrated that the packetized nature of the transmissions has to be taken into account in the analysis. The accurate simulation of networked systems subject to packet-based transmissions as introduced in Chapter 3 allows to check the stability criteria.

At the end of this chapter, basic definitions and different versions of the small gain theorem (SGT) [Sas99, Vid02] are recalled and compared. They form the foundation for the SGT-based stability criteria introduced in Chapters 7 and 8.

6.1 Problem setup

The considered feedback loop consists of a spatially distributed plant, a network subject to packetized transmissions and a linear controller as depicted in Figure 6.1. The plant with input sequence (u_k) and output sequence (y_k) is given as

$$P(z) = \hat{P}(z)z^{-\hat{d}}, \tag{6.1}$$

where $\hat{P}(z)$ is a delay-free nominal discrete-time transfer function and $\hat{d} \in \mathbb{N}$ represents a nominal constant plant delay.

The measured output samples y_k are sent over a, possibly wireless and multi-hop, network to the controller.

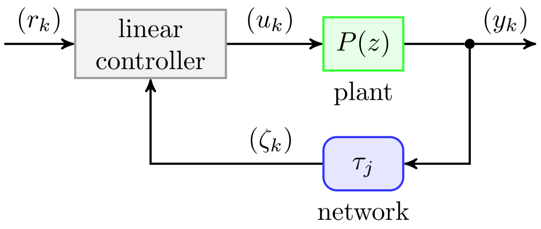

Figure 6.1: Feedback loop that is closed by means of a communication network with time-varying delays τ_j for the transmitted packets j.

Assumption 6.1 (Discrete network delays)**.** *The samples of sequence (y_k) are transmitted in separate packets j experiencing an individual bounded packet delay $\tau_j^N h$ that is an integer multiple of the sampling interval h such that*

$$0 \leq \underline{\tau}^N \leq \tau_j^N \leq \bar{\tau}^N \tag{6.2}$$

with $\underline{\tau}^N, \tau_j^N, \bar{\tau}^N \in \mathbb{N}$.

Overtaking of subsequently packets may occur since no additional restrictions on the variable time delays such as, e.g., a bounded change rate, are assumed. More detailed explanations of such effects can be found in Chapter 2. For the subsequent analysis, the overall time delay present in the feedback loop is split into two parts. Transfer function

$$\hat{D}(z) = z^{-\hat{d}-\underline{\tau}^N} = z^{-\hat{\tau}} \qquad \text{with} \qquad \hat{\tau} = \hat{d} - \underline{\tau}^N \tag{6.3}$$

combines the constant plant delay $\hat{d}$ (6.1) and the lower bound of the network delay $\underline{\tau}^N$ stated in Assumption 6.1. Please note that the delay $\hat{\tau}$ is a known constant.

The remaining time-varying delay τ_j follows from (6.2) such that

$$0 \leq \underbrace{\tau_j^N - \underline{\tau}^N}_{\tau_j} \leq \bar{\tau}^N - \underline{\tau}^N = \bar{\tau}\,. \tag{6.4}$$

Consequently, one can state the following assumption about the involved variable time delays that will be vital in the remaining part of this work.

Assumption 6.2 (Variable time delays)**.** *The time-varying delays in the networked feedback loop in Figure 6.1 are bounded by the maximal time delay $\bar{\tau}$ such that*

$$0 \leq \tau_j \leq \bar{\tau} \tag{6.5}$$

with $\tau_j, \bar{\tau} \in \mathbb{N}$. Each delay τ_j is associated with a corresponding packet j, which is transmitted over the communication channel.

Any linear controller in the form of

$$\tilde{u}(z) = -R(z)\tilde{\zeta}(z) + R_V(z)\tilde{r}(z) \tag{6.6}$$

can be utilized in the feedback loop shown in Figure 6.1. It combines a given reference sequence (r_k) and the transmitted, and thus also delayed, output sequence (y_k)

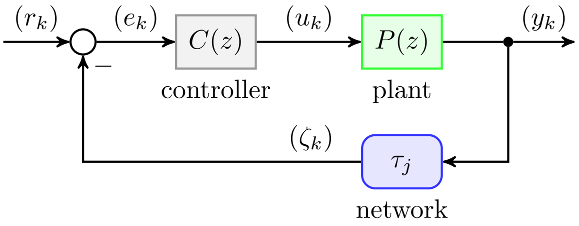

Figure 6.2: Unity feedback loop with delayed output (y_k) that is sent via a transmission network subject to bounded time-varying packet delays τ_j.

symbolized by sequence (ζ_k) by using transfer functions $R_V(z)$ and $R(z)$. One example of a special case of the structure in Figure 6.1 is the unity feedback loop depicted in Figure 6.2, where

$$\tilde{u}(z) = C(z)\left(\tilde{r}(z) - \tilde{\zeta}(z)\right) = -C(z)\tilde{\zeta}(z) + C(z)\tilde{r}(z)\,, \tag{6.7}$$

and thus, $R(z) = C(z)$ and $R_V(z) = C(z)$ hold.

Example: Feedback loop with filtered Smith predictor

Another example that fits into the structure of Figure 6.1 is the filtered Smith predictor, which was already considered as an introductory example in Chapter 1. Figure 6.3 shows the underlying configuration with the corresponding controller described by

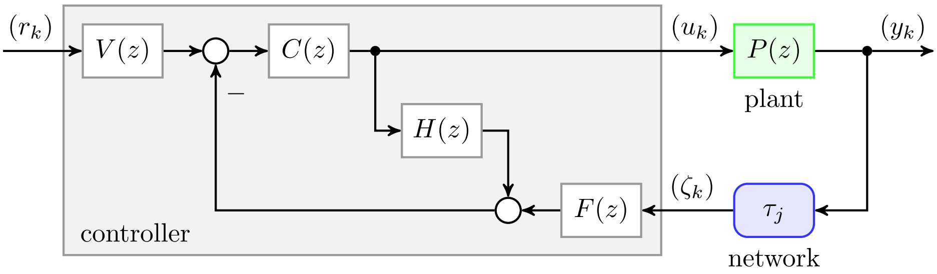

Figure 6.3: Networked feedback loop with filtered Smith predictor (gray), plant (green) and packetized transmission network (blue).

$$\tilde{u}(z) = -\underbrace{\frac{C(z)F(z)}{1 + C(z)H(z)}}_{R(z)}\tilde{\zeta}(z) + \underbrace{\frac{C(z)V(z)}{1 + C(z)H(z)}}_{R_V(z)}\tilde{r}(z)\,, \tag{6.8}$$

where $C(z)$ is the nominal controller designed for the delay-free feedback loop. Transfer functions

$$F(z) = \frac{\mu_F(z)}{\nu_F(z)} \tag{6.9}$$

and

$$H(z) = \hat{P}(z)\left(1 - z^{-\hat{d}}F(z)\right) = \frac{\hat{\mu}(z)\left(z^{\hat{d}}\nu_F(z) - \mu_F(z)\right)}{z^{\hat{d}}\hat{\nu}(z)\nu_F(z)} \tag{6.10}$$

are designed for the first-order unstable plant (1.2) with a nominal plant delay of $\hat{d} = 5$ while respecting condition

$$z^{\hat{d}}\nu_F(z) - \mu_F(z) = 0\ , \qquad \forall z \quad \Big| \quad \hat{\nu}(z) = 0 \quad \wedge \quad |z| \geq 1\,. \tag{6.11}$$

Details about the nominal controller design as well as the design of the transfer functions $F(z)$ and $H(z)$ can be found in Sections 1.1 and in Appendix A. This example is used in this chapter to show results for a LMI-based analysis and in Chapters 7 and 8 for the proposed SGT-based approaches.

6.2 LMI-based Stability Analysis

The literature is very rich in terms of LMI-based stability concepts for time delay systems as mentioned in Section 1.2. In this section, only one specific approach proposed by [LG11] is utilized as a basis for the stability analysis of the feedback loop with filtered Smith predictor presented in the previous section.

6.2.1 LMI-based Stability Criterion

The stability criterion presented in [LG11] is extended to the NCS in Figure 6.3. For that purpose, all related transfer functions, i.e. $P(z)$, $H(z)$, $F(z)$ and $C(z)$ are written as minimal state-space realizations such that

$$P(z)\ \begin{cases} x_{k+1} = Ax_k + bu_k \\ \quad y_k = c^{\mathrm{T}}x_{k-\hat{d}} \end{cases} \tag{6.12a}$$

$$H(z)\ \begin{cases} x_{H,k+1} = A_H x_{H,k} + b_H u_k \\ \quad y_{H,k} = c_H^{\mathrm{T}} x_{H,k} \end{cases} \tag{6.12b}$$

$$F(z)\ \begin{cases} x_{F,k+1} = A_F x_{F,k} + b_F y_{k-\tau_k^N} \\ \quad y_{F,k} = c_F^{\mathrm{T}} x_{F,k} + d_F y_{k-\tau_k^N} \end{cases} \tag{6.12c}$$

and

$$C(z)\ \begin{cases} x_{C,k+1} = A_C x_{C,k} - b_C\left(y_{H,k} + y_{F,k}\right) \\ \quad y_{C,k} = c_C^{\mathrm{T}} x_{C,k} - d_C\left(y_{H,k} + y_{F,k}\right) \end{cases} \tag{6.12d}$$

with state vectors $x_k \in \mathbb{R}^n$, $x_{H,k} \in \mathbb{R}^{n_H}$, $x_{F,k} \in \mathbb{R}^{n_F}$, $x_{C,k} \in \mathbb{R}^{n_C}$. Dynamic matrices, input vectors, output vectors and direct feedthroughs are denoted by A_i, b_i, c_i^{T} and d_i with $i \in \{H, F, C\}$ respectively. No indices are used for the plant data in (6.12a).

Please note that the nominal, constant plant delay $\hat{d}$ is modeled at the output of the plant (6.12a). The time-varying network delay τ_k^N is bounded by

$$1 \leq \underline{\tau}^N \leq \tau_k^N \leq \bar{\tau}^N \tag{6.13}$$

as commonly done in LMI-based approaches. It is important to note the difference in (6.2) and (6.13) in terms of the indices j (packet index) and k (iteration index). Usually, the variable time delay τ_k^N is used in LMI approaches, i.e. the packed-based nature of network transmissions is not directly considered. This is also the case in (6.12c), which is chosen to be able to follow the analysis in [LG11].

The combination of all sub-models (6.12) as visualized in Figure 6.3 yields the description of the closed loop system as

$$\xi_{k+1} = \tilde{A}\xi_k + \tilde{A}_d \xi_{k-\hat{d}-\tau_k^N} \tag{6.14}$$

with state vector

$$\xi_k^{\mathrm{T}} = \begin{bmatrix} x_k^{\mathrm{T}} & x_{H,k}^{\mathrm{T}} & x_{F,k}^{\mathrm{T}} & x_{C,k}^{\mathrm{T}} \end{bmatrix} \in \mathbb{R}^{n_\xi} \tag{6.15}$$

where $n_\xi = n + n_H + n_F + n_C$, system matrix

$$\tilde{A} = \begin{bmatrix} A & -b\, d_C\, c_H^{\mathrm{T}} & -b\, d_C\, c_F^{\mathrm{T}} & b\, c_C^{\mathrm{T}} \\ 0 & A_H - b_H\, d_C\, c_H^{\mathrm{T}} & -b_H\, d_C\, c_F^{\mathrm{T}} & b_H\, c_C^{\mathrm{T}} \\ 0 & 0 & A_F & 0 \\ 0 & -b_C\, c_H^{\mathrm{T}} & -b_C\, c_F^{\mathrm{T}} & A_C \end{bmatrix}, \tag{6.16a}$$

and matrix

$$\tilde{A}_d = \begin{bmatrix} -b\, d_C\, d_F\, c^{\mathrm{T}} & 0 & 0 & 0 \\ -b_H\, d_C\, d_F\, c^{\mathrm{T}} & 0 & 0 & 0 \\ b_F\, c^{\mathrm{T}} & 0 & 0 & 0 \\ -b_C\, d_F\, c^{\mathrm{T}} & 0 & 0 & 0 \end{bmatrix} \tag{6.16b}$$

that weights the delayed state vector (6.15) in (6.14). Consequently, one can state the following stability criterion based on [LG11] and the model description (6.14) to (6.16).

Theorem 6.3 (LMI stability criterion [SH20]). *Consider the networked filtered Smith predictor as shown in Figure 6.3, where transfer functions $V(z)$ and $C(z)$ are designed to stabilize the nominal, delay-free plant $\hat{P}(z)$. The nominal constant time delay is given by $\hat{\tau} = \hat{d} + \underline{\tau}^N > 0$ as in* (6.3)*. Transfer functions $F(z)$ and $H(z)$ are selected corresponding to* (6.9)*, and* (6.10)*,* (6.11)*, respectively. Matrices $\tilde{A}$ and $\tilde{A}_d$ are given by* (6.16)*.*

Then, the closed loop system is asymptotically stable for all bounded time-varying network delays τ_k^N (6.13) *if one of the following conditions holds for a scalar constant $0 < \gamma < 1$:*

(i) There exist positive definite symmetric matrices $P \in \mathbb{R}^{(\hat{d}+\bar{\tau}^N+1)n_\xi \times (\hat{d}+\bar{\tau}^N+1)n_\xi}$ and $S \in \mathbb{R}^{n_\xi \times n_\xi}$ so that

$$G^T \Theta_1 G - \Theta_2 \prec 0 \tag{6.17}$$

with matrices $\Theta_1 = \mathrm{diag}\,(P, S)$, $\Theta_2 = \mathrm{diag}\,(P, \gamma^2 S)$ and

$$G = \begin{bmatrix} \Psi_1 & \frac{1}{2}\tilde{A}_d & \frac{\bar{\tau}^N - \underline{\tau}^N}{2}\tilde{A}_d \\ I_{(\hat{d}+\bar{\tau}^N)n_\xi} & (0)_3 & (0)_3 \\ \Psi_2 & \frac{1}{2}\tilde{A}_d & \frac{\bar{\tau}^N - \underline{\tau}^N}{2}\tilde{A}_d \end{bmatrix} \tag{6.18}$$

where

$$\Psi_1 = \begin{bmatrix} \tilde{A} & (0)_1 & \frac{1}{2}\tilde{A}_d & (0)_2 \end{bmatrix}, \tag{6.19a}$$

$$\Psi_2 = \begin{bmatrix} \tilde{A} - I_{n_\xi} & (0)_1 & \frac{1}{2}\tilde{A}_d & (0)_2 \end{bmatrix}, \tag{6.19b}$$

$$(0)_1 = 0_{n_\xi \times (\hat{d}+\underline{\tau}^N-1)n_\xi}, \tag{6.19c}$$

$$(0)_2 = 0_{n_\xi \times (\bar{\tau}^N-\underline{\tau}^N-1)n_\xi}, \tag{6.19d}$$

$$(0)_3 = 0_{(\hat{d}+\bar{\tau}^N)n_\xi \times n_\xi}. \tag{6.19e}$$

(ii) There exist positive definite matrices P, Q_1, Q_2, R_1, R_2 and $S \in \mathbb{R}^{n_\xi \times n_\xi}$ such that

$$\begin{bmatrix} \Phi_1 & \Psi \\ * & \operatorname{diag}(-P, -R_1, -R_2, -S) \end{bmatrix} \prec 0 \tag{6.20}$$

where

$$\Phi_1 = \begin{bmatrix} \Phi_{11} & \begin{bmatrix} R_1 & R_2 & 0_{n_\xi} \end{bmatrix} \\ * & \operatorname{diag}\left(\Phi_{12}, \Phi_{13}, -\gamma^2 S\right) \end{bmatrix}, \tag{6.21a}$$

$$\Phi_{11} = -P + Q_1 + Q_2 - R_1 - R_2 \,, \tag{6.21b}$$

$$\Phi_{12} = -Q_1 - R_1 \,, \tag{6.21c}$$

$$\Phi_{13} = -Q_2 - R_2 \,, \tag{6.21d}$$

$$\Psi = \begin{bmatrix} \Phi_2^T P & \left(\hat{d} + \underline{\tau}^N\right) \Phi_3^T R_1 & \left(\hat{d} + \bar{\tau}^N\right) \Phi_3^T R_2 & \Phi_3^T S \end{bmatrix}, \tag{6.21e}$$

$$\Phi_2 = \begin{bmatrix} \tilde{A} & \frac{1}{2}\tilde{A}_d & \frac{1}{2}\tilde{A}_d & \frac{\bar{\tau}^N - \underline{\tau}^N}{2}\tilde{A}_d \end{bmatrix}, \tag{6.21f}$$

$$\Phi_3 = \begin{bmatrix} \tilde{A} - I_{n_\xi} & \frac{1}{2}\tilde{A}_d & \frac{1}{2}\tilde{A}_d & \frac{\bar{\tau}^N - \underline{\tau}^N}{2}\tilde{A}_d \end{bmatrix}. \tag{6.21g}$$

Proof. The proof is a direct consequence of Corollary 1 in [LG11] evaluated for (6.14), (6.16), $h_1 = \hat{\tau} = \hat{d} + \underline{\tau}^N$, $h_2 = \hat{d} + \bar{\tau}^N$, and $h_{12} = \bar{\tau}^N - \underline{\tau}^N$. ■

Note that Theorem 6.3 differs from the stability criterion presented in [NRGG12] in several ways. The main difference is that the time-varying delay is modeled in the input channel of the plant in [NRGG12]. It is not equivalent the situation presented in Figure 6.3, where the output sequence is transmitted via a time-varying network channel in separate packets. In addition, a different Lyapunov-Krasovskii functional is employed in the proof to get the LMI conditions.

6.2.2 Simulation Example

Theorem 6.3 is evaluated for the filtered Smith predictor example from the beginning of this chapter. Hence, it is necessary to convert the involved LMIs such that they can be solved in a numerically reliable way. Hence, e.g., relation (6.17) is converted into

$$G^{\mathrm{T}} \Theta_1 G - \Theta_2 \preceq \nu I \tag{6.22}$$

with $\nu < 0$ to avoid strict LMIs as, for example, explained in [Ber09]. The goal is to find the maximal admissible network delay bound $\bar{\tau}^N$ such that the closed loop system is asymptotically stable. The minimal value of τ_j^N is zero, i.e. $\underline{\tau}^N = 0$, in the simulation example.

Theorem 6.3 is evaluated for different scalars γ and maximal admissible variable time delays. The solution is influenced by a proper selection of parameter ν (6.22) that allows to account for numerical errors in the solution finding of the related LMIs. In the present case, MOSEK [MOS] is utilized as solver and is accessed via YALMIP [YAL] with the setting $\nu = 10^{-8}$.

Figure 6.4 shows the results of the evaluation of conditions (i) and (ii) in Theorem 6.3. Situations in which no feasible solution can be found are depicted using red circles and crosses for Theorem 6.3(i) and 6.3(ii), respectively. It can be clearly seen that conditions (ii) yield a significantly smaller maximal admissible variable time delay $\bar{\tau}^N =$

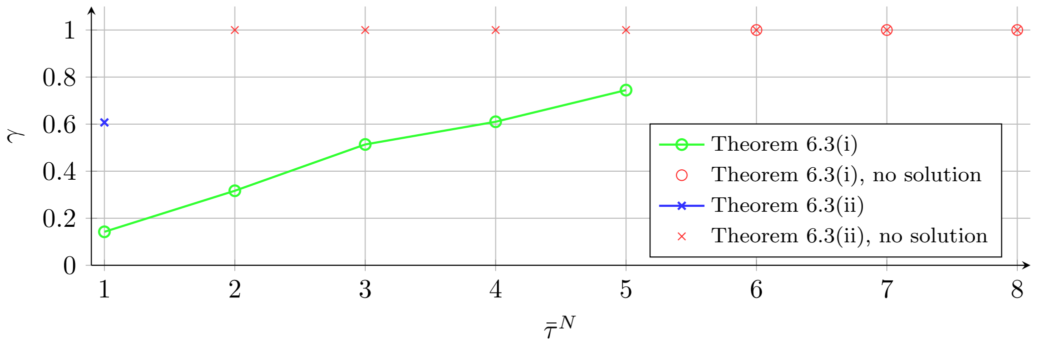

Figure 6.4: Example: Comparison of the maximal admissible delay $\bar{\tau}^N$ and corresponding maximal values for parameter γ resulting from the evaluation of Theorem 6.3.

1 compared to conditions (i) that result in a maximal value of $\bar{\tau}^N = 5$. The blue point and green curve in Figure 6.4 represent the maximal parameter γ, where a solution can be found. This parameter has to be less than one, as indicated in Theorem 6.3, and the difference between γ and 1 can be interpreted as a stability margin. Hence, a decreasing margin can be observed for conditions (ii) when $\bar{\tau}^N$ is increased.

The number of unknowns in the conditions of Theorem 6.3 depend on the dimension of the state vector (6.15) and the maximal overall time delay $\hat{d} + \bar{\tau}^N$. For conditions (i) one gets

$$\underbrace{\frac{\left(\hat{d} + \bar{\tau}^N + 1\right)^2 n_\xi^2 + \left(\hat{d} + \bar{\tau}^N + 1\right) n_\xi}{2}}_{\text{for } P} + \underbrace{\frac{n_\xi^2 + n_\xi}{2}}_{\text{for } S} =$$

$$\frac{1}{2}\left[\left(\hat{d} + \bar{\tau}^N\right)^2 + 2\left(\hat{d} + \bar{\tau}^N\right) + 2\right] n_\xi^2 + \frac{1}{2}\left(\hat{d} + \bar{\tau}^N + 2\right) n_\xi \tag{6.23}$$

unknowns and for Theorem 6.3(ii)

$$\frac{n_\xi^2 + n_\xi}{2}\left(2n_\xi + 2\right) = n_\xi^3 + 2n_\xi^2 + n_\xi \tag{6.24}$$

unknowns because $(2n_\xi + 2)$ matrices $P, Q_1, Q_2, \dots, Q_{n_\xi}, R_1, R_2, \dots, R_{n_\xi}$ and S come into play. The dimension of state vector (6.15) in the present example is $n_\xi = 9$ and the nominal plant delay is given by $\hat{d} = 5$. Consequently, 900 and 8046 unknowns follow for conditions (i) and (ii), respectively. Please note that (6.23) depends on the actual $\bar{\tau}^N$ to be checked, i.e. at maximum $\bar{\tau}^N = 8$ in Figure 6.4. On the contrary, (6.24) does not involve any bound of the time-varying delays.

A simulation of the closed loop system is performed using individual packet delays such that $0 \leq \tau_j \leq 5$, i.e. respecting the maximum of $\bar{\tau}^N = 5$ provided by Theorem 6.3. The network delays τ_j^N, depicted in Figure 6.5, are chosen as random values. Figure 6.6 shows the corresponding actuation signal (top plot) and output sequence (bottom plot) for protocol $\mathcal{P}_1$, when the simulation framework presented in Chapter 3 is used. Although, the packet delays change within the given bounds in a random way, reference signal (r_k) (bottom plot, black) can be tracked successfully. This is in line with the statements from Theorem 6.3.

However, Figures 6.7 and 6.8 exemplify a different setting, where a repeating pattern of packet delays is present with a maximal delay of 4. The reference signal (bottom

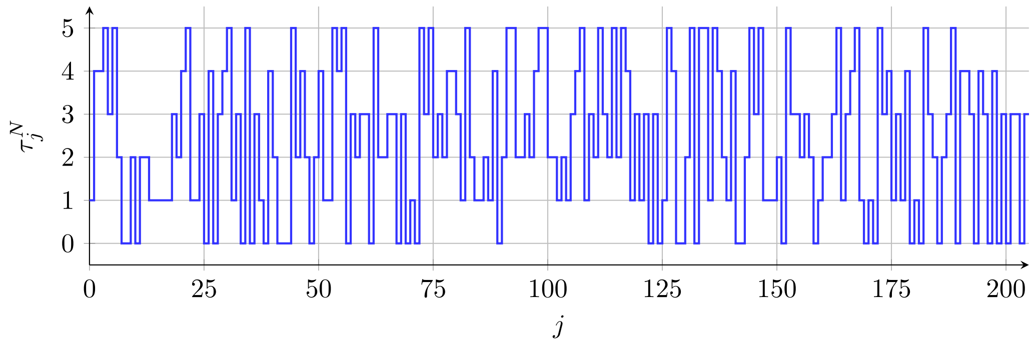

Figure 6.5: Example 1: random packet delays τ_j^N.

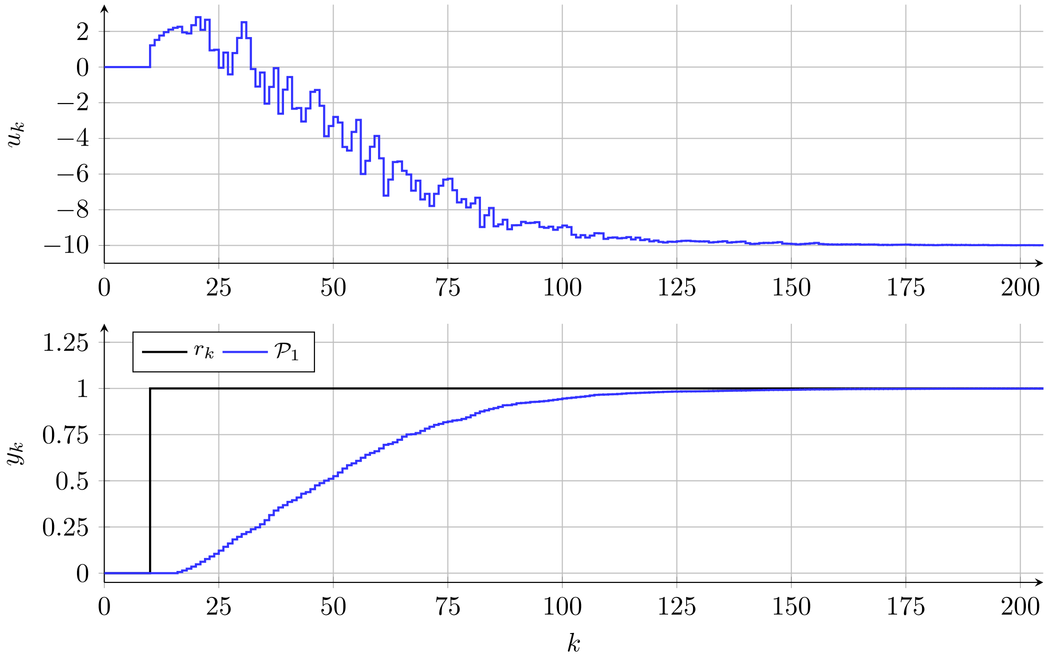

Figure 6.6: Example 1: input sequence (u_k) and output sequence (y_k) for protocol $\mathcal{P}_1$ and random delays as shown in Figure 6.5.

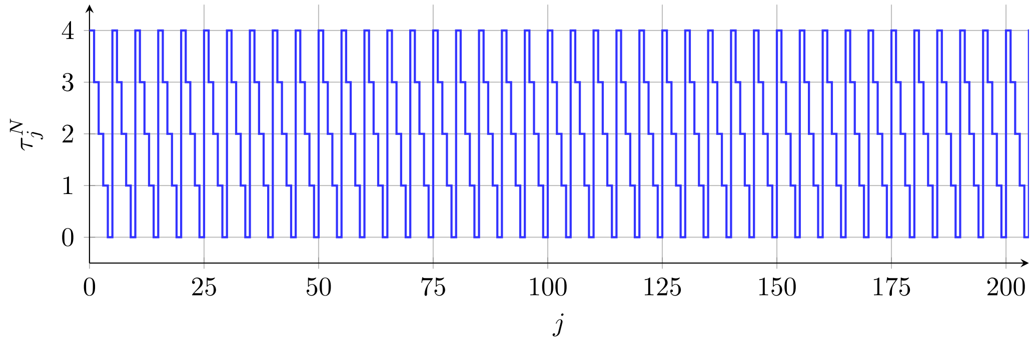

Figure 6.7: Example 2: repeating pattern of packet delays τ_j^N.

plot, black) and the resulting output sequences are visible in Figure 6.8 for the three different protocols $\mathcal{P}_1$, $\mathcal{P}_2$ and $\mathcal{P}_3$ (2.38) introduced in Chapter 2. It can be clearly seen

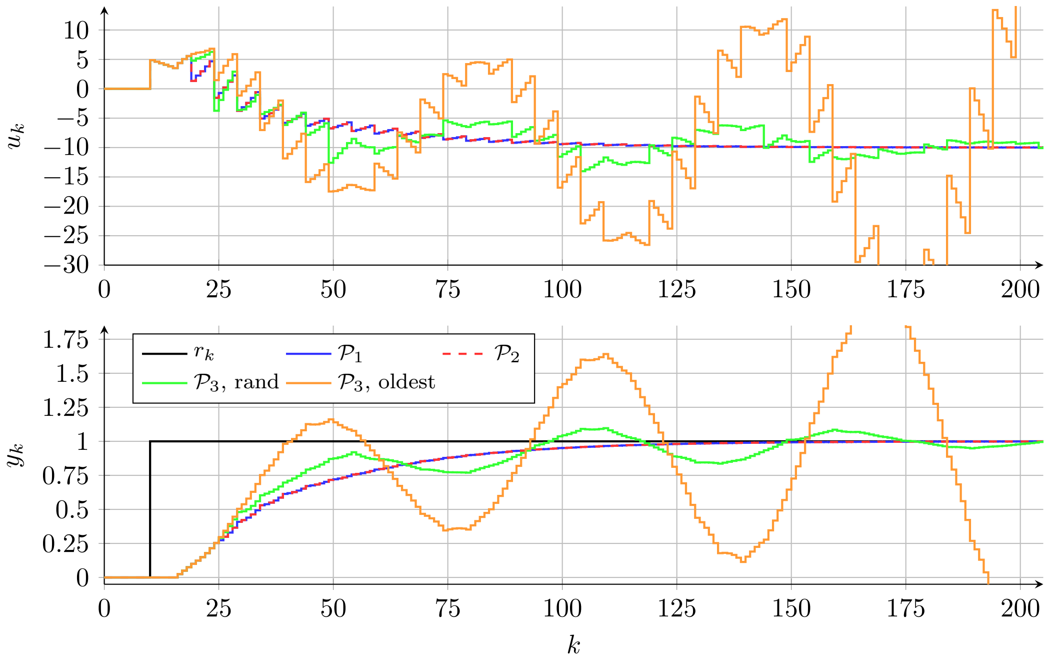

Figure 6.8: Example 2: control signals (u_k) and output signals (y_k) for different protocols (2.38) and packet delays as shown in Figure 6.7. The orange curves represent the worst case scenario.

that the control performance significantly depends on the employed protocol. Protocols $\mathcal{P}_1$ and $\mathcal{P}_2$ yield similar results for the actual simulation experiment. On the contrary, protocol $\mathcal{P}_3$ leads to an oscillating output sequence for the case where a random packet is selected, whenever more packets are available at the same time instant. This is possible due to the characteristics of this third protocol (2.38c) that avoids any form of synchronization or numbering in the networked connection.

If the oldest packet is selected whenever more packets are available at the same time instant, the use of protocol $\mathcal{P}_3$ results in an unstable feedback loop for the networked plant with filtered Smith predictor. This setting constitutes the worst case scenario if a packet numbering mechanism is absent as shown in Chapter 7.

Please note that Figures 6.7 and 6.8 illustrate a situation in which the closed feedback loop is unstable although Theorem 6.3 is fulfilled for $\bar{\tau}^N = 5$, see Figure 6.4. This main issue arises because the actual network protocol is not included in the stability analysis, which is, to the best of the authors knowledge, common in LMI-based approaches in literature and is not a specific feature of the presented theorem.

Consequently, an alternative way to show the stability of feedback loops with time-varying packet delays is necessary. Hence, new stability criteria are introduced in Chapter 7 to explicitly integrate the applied protocol in the analysis. Chapter 8 extends the criteria to render them less conservative.

6.3 Basic definitions and Small Gain Theorems

Some basic definitions are recalled since they provide the basis for the theory developed in the next chapters. They can be found, e.g., in [Sas99] and [Vid02] and are only explicitly mentioned in the definitions below, if there are significant differences. Especially important is the formulation of the small gain theorem (SGT) that is differently introduced in [Sas99] and [Vid02]. This difference is essential for the case with acausal subsystems as presented in Chapter 8.

Definition 6.4 (Truncation of a sequence)**.** *The truncation of sequence $(f_k) : [a, \infty) \to \mathbb{R}$ at a finite time T is defined as*

$$\left(f_k\right)_T = \begin{cases} 0 & \forall k \geq \alpha, \quad \textit{if} \quad T < a \\ f_k & a \leq k \leq T \\ 0 & k > T \geq a \end{cases} \tag{6.25}$$

with $a \in \mathbb{R}$.

Please note that the interval $[a, \infty)$ is considered here as, e.g., in [UI08], because also acausal sequences will be part of the investigations in Chapter 8.

Definition 6.5 (Extended ℓ_p space)**.** *A sequence (f_k) belongs to the $\ell_p[a, \infty)$ space if condition*

$$\sum_{k=a}^{\infty} \left|f_k\right|^p < \infty \tag{6.26}$$

holds for $p \in [1, \infty)$. It belongs to the $\ell_{pe}[a, \infty)$ space, if its truncation belongs to $\ell_p[a, \infty)$, i.e.

$$\left(f_k\right)_T \in \ell_p[a, \infty) \qquad \textit{for all} \quad T \tag{6.27}$$

is fulfilled.

Definition 6.6 (Causality)**.** *A mapping $(y_k) = \mathcal{M}\{(u_k)\} : \ell_{pe}[a, \infty) \mapsto \ell_{pe}[a, \infty)$ is causal if*

$$\left(y_k\right)_T = \left(\mathcal{M}\{(u_k)\}\right)_T = \left(\mathcal{M}\{(u_k)_T\}\right)_T \tag{6.28}$$

for all finite $T > 0$ and $(u_k) \in \ell_{pe}[a, \infty)$.

Definition 6.7 (Finite gain ℓ_p stability [Sas99])**.** *A causal mapping $(y_k) = \mathcal{M}\{(u_k)\} : \ell_{pe}[a, \infty) \mapsto \ell_{pe}[a, \infty)$ is called finite gain ℓ_p stable if*

(a) for a given $(u_k) \in \ell_p[a, \infty)$, it follows that $(y_k) \in \ell_p[a, \infty)$ and

(b) for a given $(u_k) \in \ell_{pe}[a, \infty)$, it implies that there exist constants $\alpha > 0$ and $\beta > 0$ such that the norm of output sequence (y_k) is bounded as

$$\left|\left|\left(y_k\right)_T\right|\right|_p \leq \alpha \left|\left|\left(u_k\right)_T\right|\right|_p + \beta\,, \tag{6.29}$$

for all $T > 0$, where $||(\cdot)_T||_p$ denotes the p-norm of a truncated sequence $(\cdot)_T$. Constant α is referred to as finite ℓ_p gain.

The second condition in Definition 6.7 means that there exists an affine bound on the norm of the (possibly unbounded) output sequence (y_k), which is uniform for all truncations T.

Please note that Definition 6.7 incorporates causal mappings only, which is different to the alternative definition below that does not require causality and does not comprise truncations of sequences.

Definition 6.8 (Finite gain ℓ_p stability [Vid02])**.** *A mapping $(y_k) = \mathcal{M}\{(u_k)\} : \ell_{2e}[a,\infty) \mapsto \ell_{2e}[a,\infty)$ is called finite gain ℓ_p stable if there exist constants $\alpha > 0$ and $\beta > 0$ such that the norm of output sequence (y_k) is bounded as*

$$\big|\big|(y_k)\big|\big|_p \leq \alpha\big|\big|(u_k)\big|\big|_p + \beta \tag{6.30}$$

for $(u_k) \in \ell_p[a,\infty)$ and $(y_k) \in \ell_p[a,\infty)$. The constant α is referred to as the finite ℓ_p gain.

An additional difference is that the space for (u_k) and (y_k) is $\ell_{pe}[a,\infty)$ in Definition 6.7 and $\ell_p[a,\infty)$ in Definition 6.8.

Based on both definitions of finite gain ℓ_p stability, one can define different versions of the small gain theorem for the interconnection of two subsystems as depicted in Figure 6.9 with two inputs $(u_{1,k})$ and $(u_{2,k})$. Each subsystem $i = \{1, 2\}$ is characterized by a mapping $\mathcal{M}_i$ from input $(e_{i,k})$ to output $(y_{i,k})$.

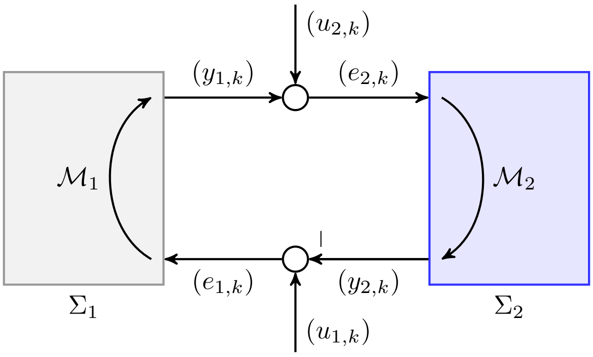

Figure 6.9: Interconnection of two subsystems considered in the SGT.

Theorem 6.9 (Small gain theorem [Sas99])**.** *Consider the feedback loop in Figure 6.9 with inputs $(u_{1,k})$, $(u_{2,k})$, outputs $(y_{1,k})$, $(y_{2,k})$ and signals $(e_{1,k})$, $(e_{2,k})$. The systems Σ_1, Σ_2 described by mappings $(y_{1,k}) = \mathcal{M}_1\{(e_{1,k})\} : \ell_{pe}[a,\infty) \mapsto \ell_{pe}[a,\infty)$, $(y_{2,k}) = \mathcal{M}_2\{(e_{2,k})\} : \ell_{pe}[a,\infty) \mapsto \ell_{pe}[a,\infty)$ are causal and finite gain ℓ_p stable corresponding to Definition 6.7, i.e. there exist constants α_1, α_2, β_1, β_2 such that*

$$\big|\big|(y_{1,k})_T\big|\big|_p \leq \alpha_1\big|\big|(e_{1,k})_T\big|\big|_p + \beta_1 \tag{6.31a}$$

$$\big|\big|(y_{2,k})_T\big|\big|_p \leq \alpha_2\big|\big|(e_{2,k})_T\big|\big|_p + \beta_2 \tag{6.31b}$$

for $(u_{1,k}), (u_{2,k}) \in \ell_{pe}[a, \infty)$ *and* $(y_{1,k}), (y_{2,k}) \in \ell_{pe}[a, \infty)$. *The loop is assumed to be well posed such that* $(e_{1,k}), (e_{2,k}) \in \ell_{pe}$ *are unique. Let condition*

$$\alpha_1 \alpha_2 < 1 \tag{6.32}$$

hold.

Then, the closed loop system is finite gain ℓ_p *stable from* $(u_{1,k})$, $(u_{2,k})$ *to* $(y_{1,k})$, $(y_{2,k})$.

There is also a different version of the SGT in [Sas99] that makes use of the so-called incremental finite gain stability, which is similar to a Lipschitz condition in the continuous-time setting and does not require to assume the well-posed-ness, see [Sas99] for details.

Theorem 6.10 (Small gain theorem [Vid02])**.** *Consider the feedback loop in Figure 6.9 with inputs* $(u_{1,k})$, $(u_{2,k})$, *outputs* $(y_{1,k})$, $(y_{2,k})$ *and signals* $(e_{1,k})$, $(e_{2,k})$. *The systems* Σ_1, Σ_2 *described by mappings* $(y_{1,k}) = \mathcal{M}_1\{(e_{1,k})\} : \ell_{pe}[a, \infty) \mapsto \ell_{pe}[a, \infty)$, $(y_{2,k}) = \mathcal{M}_2\{(e_{2,k})\} : \ell_{pe}[a, \infty) \mapsto \ell_{pe}[a, \infty)$ *are causal and finite gain* ℓ_p *stable corresponding to Definition 6.8, i.e. there exist constants* α_1, α_2, β_1, β_2 *such that*

$$||(y_{1,k})||_p \leq \alpha_1 ||(e_{1,k})||_p + \beta_1 \tag{6.33a}$$

$$||(y_{2,k})||_p \leq \alpha_2 ||(e_{2,k})||_p + \beta_2 \tag{6.33b}$$

for $(u_{1,k}), (u_{2,k}) \in \ell_p[a, \infty)$ *and* $(y_{1,k}), (y_{2,k}) \in \ell_p[a, \infty)$. *Let condition*

$$\alpha_1 \alpha_2 < 1 \tag{6.34}$$

hold.

Then, the closed loop system is finite gain ℓ_p *stable from* $(u_{1,k})$, $(u_{2,k})$ *to* $(y_{1,k})$, $(y_{2,k})$.

Please note that the uniqueness is not directly claimed in Theorem 6.10 but indirectly assumed because all involved mappings are assumed to be binary relations of a specific form as stated in [Vid02].

Causality is the missing link between conditions (6.31) and (6.33) that correspond to Definition 6.7 for $(u_k) \in \ell_p$ and Definition 6.8 for $(u_k) \in \ell_{pe}$, respectively. An evaluation of (6.30), i.e.

$$||(y_k)||_p = ||\mathcal{M}\{(u_k)\}||_p \leq \alpha ||(u_k)||_p + \beta \,, \tag{6.35}$$

for $(u_k)_T \in \ell_p$ yields

$$||\mathcal{M}\{(u_k)_T\}||_p \leq \alpha ||(u_k)_T||_p + \beta \,. \tag{6.36}$$

The use of Definition 6.6 for causality

$$(\mathcal{M}\{(u_k)_T\})_T = (\mathcal{M}\{(u_k)\})_T = (y_k)_T \tag{6.37}$$

allows to state

$$||(\mathcal{M}\{(u_k)_T\})_T||_p \leq ||\mathcal{M}\{(u_k)_T\}||_p \tag{6.38}$$

and, as a consequence,

$$||(y_k)_T||_p \leq \alpha ||(u_k)_T||_p + \beta \,, \tag{6.39}$$

where relations (6.36) and (6.37) are taken into account. This shows, that the Definition 6.7 is equal to (6.33) if causality is assumed. In Chapter 8, the small gain theorem in a modified form of Theorem 6.10 is utilized since not all subsystems in Figure 6.9 are assumed to be causal in that setting.

The definitions and theorems presented here for $p \in [1, \infty)$ are evaluated for the specific choice $p = 2$ in the following chapters.

Chapter 7

SGT-based Stability Analysis

This chapter introduces novel stability criteria, which allow to explicitly incorporate the fact that the data is sent in separate packets over transmission networks. It is adopted from [SH20] and [SH21b].

Different criteria for the robust stability of the networked feedback loops are proposed that allow to explicitly consider the three protocols introduced in Chapter 2 and time-varying packet delays for the case where a packet numbering mechanism is used as well as for the (worst) case without packet numbering nor synchronization between sender and receiver. The criteria are based on the small gain theorem [Sas99, Vid02] as presented in Chapter 6 and make it possible to check the stability in a computationally inexpensive way without involving any optimization algorithms. They are proposed on the basis of the work in [KL04], which is considerably extended in the following.

A basic version of the new stability criteria for packetized networked systems is introduced first for feedback loops with linear controllers and known linear plants. The effects due to different packet skipping and hold mechanisms are included in the derivation of the criterion that, in the end, provides a maximal admissible bound on the time-varying packet delays.

Finally, an extension to networked loops with uncertain plant models is proposed and exemplified for the filtered Smith predictor. It underlines the easy-to-use character of the introduced approaches.

7.1 SGT-based Stability Criterion

To formulate the basic version of the stability criterion, the networked feedback loop depicted in Figure 6.1 is considered. It consists of a linear controller (6.6), a plant represented by its discrete-time transfer function (6.1) and a packetized network connection for the transmission of output sequence (y_k). Following the idea of [KL04], Figure 6.1 is rearranged to get the structure in Figure 7.1, where the input sequence (r_k) is assumed to be identically to zero for all k. The known constant time delay $\hat{\tau}$ (6.3) is included in the nominal part (gray) via transfer function $\hat{D}(z)$, whereas the remaining time-varying delay τ_j (6.5) stated in Assumption 6.2 is associated with the uncertainty, see blue part in Figure 7.1. The artificially introduced discrete-time integrator and differentiator are utilized to reduce the conservatism of the stability criterion as explained below.

In [KL04], the small gain theorem [Sas99] is employed to state a sufficient stability condition for systems with time-varying delays. It is based on the assumption that the

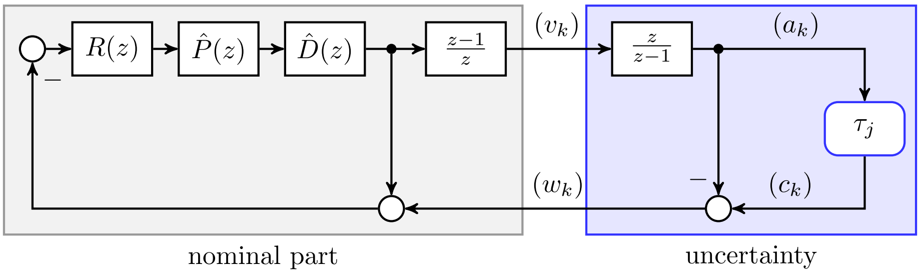

Figure 7.1: Rearranged networked feedback loop with two subsystems representing the nominal control loop (gray) and the uncertainty (blue) representing the effects of the time-varying delays.

uncertainty block with input (v_k) and output (w_k) (see blue block in Figure 7.1) can be represented by

$$w_k = \sum_{i=0}^{k-\tau_k} v_i - \sum_{i=0}^{k} v_i = - \sum_{i=k-\tau_k+1}^{k} v_i \,, \tag{7.1}$$

where the sums follow due to the discrete-time integrator. The first sum in (7.1) stands for the effect of the variable time delay between signal (v_k) and (w_k) via the integrator and the delay block. The second sum follows due to the negative bypass of the delay block. Relation (7.1) is then used to prove the stability criterion in [KL04]. Please note that τ_k and not τ_j is used in (7.1) since the considered time delays are not linked to individual packets in [KL04].

Exactly this missing link between the packets and the corresponding delays is problematic in some cases, as shown in the following figures. Figures 7.2 and 7.3 present the results for a first example, where protocol $\mathcal{P}_2$ is employed. This means that old packets are not skipped and the most recent packet is selected whenever more packets are available.

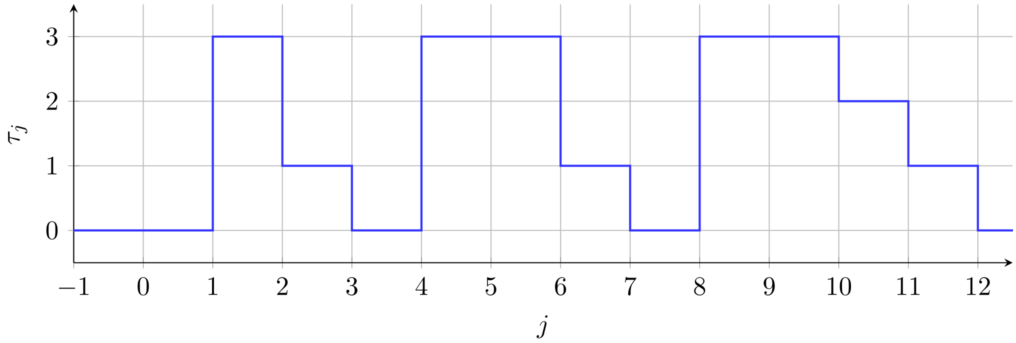

Figure 7.2: Packet delays for the example with protocol $\mathcal{P}_2$.

The packet delay pattern τ_j from Figure 7.2 together with the input sequence (v_k) from Figure 7.3 yields the red curve in the bottom plot in Figure 7.3 if relation (7.1) is applied. However, the use of an accurate simulation framework as presented in Chapter 3 results in the blue curve for (w_k). The visible deviation between the two results underline that relation (7.1) does not allow to correctly reproduce the behavior of transmission channels subject to time-varying packet delays.

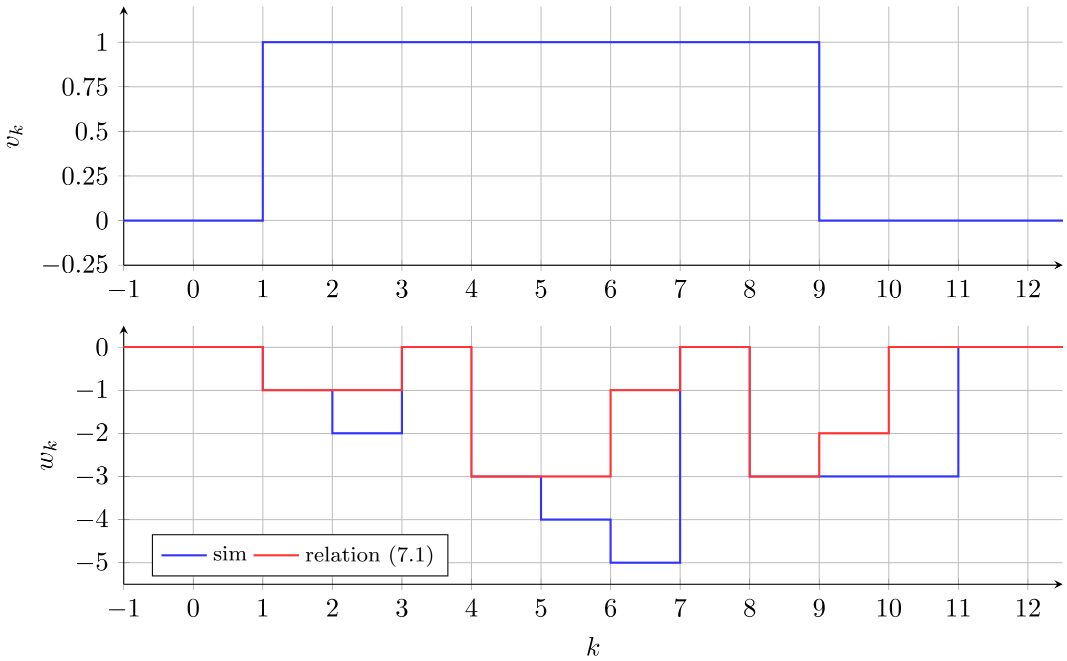

Figure 7.3: Input sequence (v_k) of the uncertainty (top) and output signals (w_k) for a simulation as well as using relation (7.1) for an example with protocol $\mathcal{P}_2$.

This discrepancy can also be observed for other examples and protocols as, e.g., plotted in Figures 7.4 and 7.5, where protocol $\mathcal{P}_1$ is in place, i.e. old packets are skipped if newer information is available and the most recent packet is selected if more packets are available at the same time instant. Deviations between the accurate simulation (including packet skipping and hold mechanisms) result from the calculated results are apparent also for this second example. It underpins the fact, that packet delays have to be linked to their corresponding packet index j.

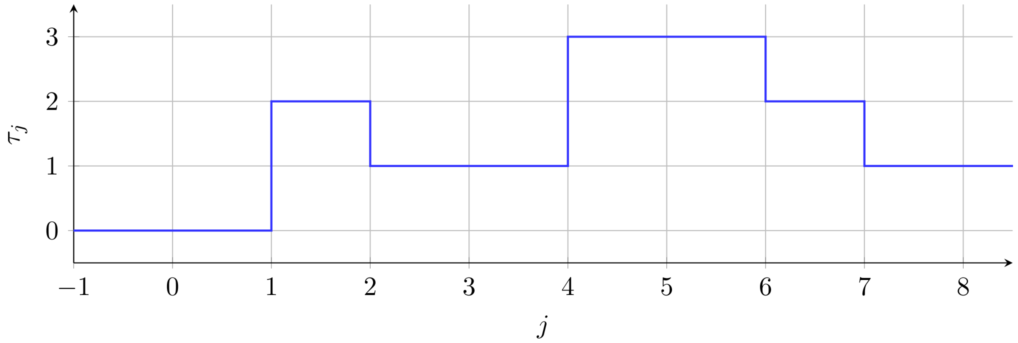

Figure 7.4: Packet delays for the example with protocol $\mathcal{P}_1$.

Consequently, larger values of the finite ℓ_2 gain of the uncertainty in Figure 7.1 are possible for the analyzed feedback structure. This implies that the stability criterion in [KL04] has to be extended to take into account the packetized character of the considered networked feedback loop. Thus, the specific packet skipping, packet selection and hold mechanisms of the considered protocols introduced in Section 2.4 have to be taken into account for the calculation of the finite ℓ_2 gain linked to the uncertainty

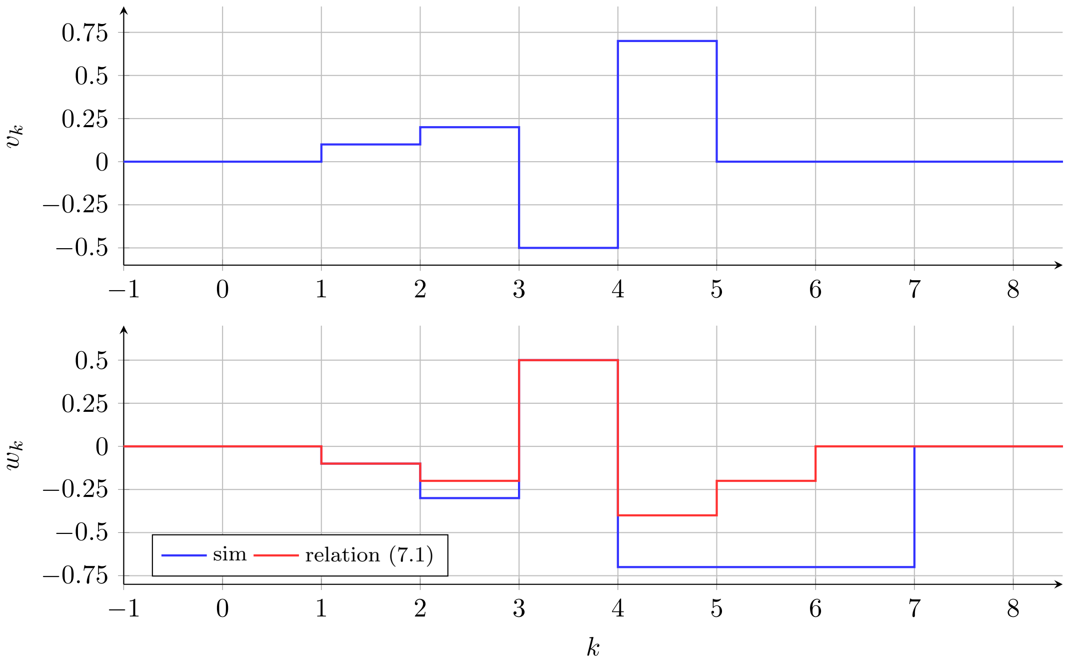

Figure 7.5: Input sequence (v_k) of the uncertainty (top) and output signals (w_k) for a simulation as well as using relation (7.1) for an example with protocol $\mathcal{P}_1$.

shown in Figure 7.1.

The uncertainty block is shown in Figure 7.6 in more detail. It consists of a discrete-time integrator with input (v_k) and output (a_k), and a (blue) block representing the bounded time-varying packet delays $0 \leq \tau_j \leq \bar{\tau}$. For example, an input sequence depicted in Figure 7.7 is given as

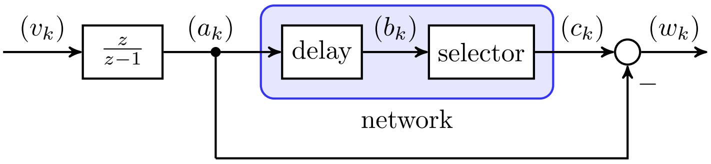

Figure 7.6: Structure of the uncertainty to be analyzed consisting of a discrete-time integrator and a network block (blue) modeling all (delayed) packets on the way as well as a packet selector.

$$v_k = \begin{cases} 1 & 0 \leq k \leq 9 \\ 0 & \text{otherwise} \end{cases}, \tag{7.2}$$

which yields a signal (a_k) such that

$$a_k = \begin{cases} 0 & k < 0 \\ k+1 & 0 \leq k \leq 9 \\ 10 & \text{otherwise} \end{cases} \tag{7.3}$$

as also visible in Figure 7.8. Individual packets containing a_k are sent at time instances k over the transmission channel subject to time delays $0 \leq \tau_j \leq 3$. Each packet might

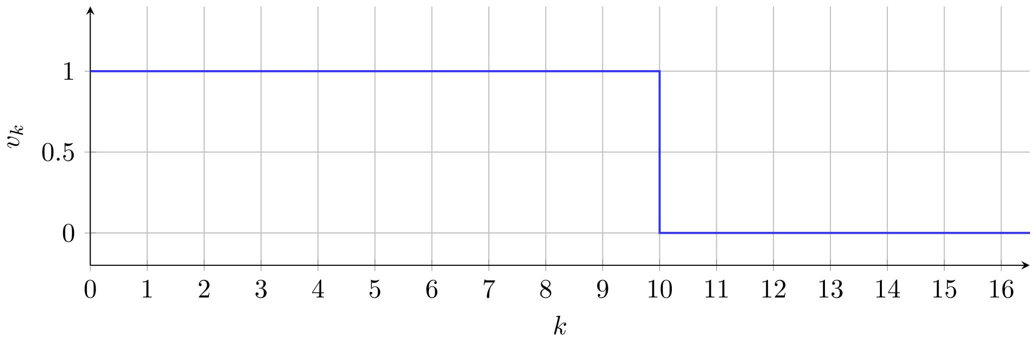

Figure 7.7: Input sequence (v_k) of the uncertainty block as defined in (7.2).

k	0	1	2	3	4	5	6	7	8	9	10	11	12	13	14	15
$b_k^{(0)} = a_k$	1	2	3	4	5	6	7	8	9	10	10	10	10	10	10	10
$b_k^{(1)}$	0	1	2	3	4	5	6	7	8	9	10	11	10	10	10	10
$b_k^{(2)}$	0	0	1	2	3	4	5	6	7	8	9	10	10	10	10	10
$b_k^{(3)}$	0	0	0	1	2	3	4	5	6	7	8	9	10	10	10	10

Figure 7.8: Possible packets on the way that contain a_k for the case $0 \leq \tau_j \leq 3$ and input sequence (7.2). Darker colors stand for more recent data.

be delayed by 0, 1, 2 or 3 time steps in the present example, which is is symbolized by $b_k^{(0)}$, $b_k^{(1)}$, $b_k^{(2)}$ and $b_k^{(3)}$, respectively. Hence, the table in Figure 7.8 visualizes all packets on the way together with all possible arrival times.

The selector in Figure 7.6 implements the protocol dependent packet skipping, selection and hold mechanism to provide sequence (c_k), see Section 2.4 for details. Due to the specific structure of the uncertainty block, the output sequence (w_k) follows from

$$w_k = c_k - a_k \; . \tag{7.4}$$

The following theorem states a sufficient stability criterion that explicitly takes into account the considered protocol by providing protocol-dependent ℓ_2 gains α.

Theorem 7.1 (Stability criterion, nominal plant [SH20, SH21b])**.** *Consider the networked control system in Figure 6.1 consisting of a controller* (6.6) *represented by transfer function $R(z)$, a plant $P(z)$* (6.1) *and a transmission network with bounded time-varying packet delays as in Assumption 6.2. Let condition*

$$\left|\left|M(z)\right|\right|_\infty \alpha = \left|\left|\frac{R(z)\hat{P}(z)}{1 + R(z)\hat{P}(z)\hat{D}(z)} \frac{(z-1)}{z}\right|\right|_\infty \alpha < 1 \tag{7.5}$$

hold for all $\omega \in [0, \pi/h)$ where α is the finite ℓ_2 gain of the uncertainty and h represents the sampling interval. Parameter α is given depending on the network protocol (2.38) *such that*

(a) for protocol $\mathcal{P}_1$ (skip old packets, take newest):

$$\alpha = \bar{\tau} \, , \tag{7.6a}$$

(b) for protocol $\mathcal{P}_2$ (do not *skip old packets, take newest)*

$$\alpha = \max\left\{\sqrt{\frac{\bar{\tau}\,(14\bar{\tau}^2 - 9\bar{\tau} + 1)}{6(\bar{\tau}+1)}}, 1\right\}, \tag{7.6b}$$

(c) for protocol $\mathcal{P}_3$ (no numbering nor synchronization)

$$\alpha = \sqrt{\frac{\bar{\tau}}{6}\,(14\bar{\tau} + 1)}\,. \tag{7.6c}$$

Then, the networked feedback loop is finite gain ℓ_2 stable for all time-varying bounded packet delays $0 \le \underline{\tau}^N \le \tau_j^N \le \bar{\tau}^N$ and $\bar{\tau}^N > \underline{\tau}^N$.

Proof. The proof is presented separately in Section 7.2, since it involves extensive calculations for the individual protocols. ■

Remark 7.2. In Theorem 7.1, the term "skip old packets" means that arriving packets are skipped, whenever more recently sent packets are available at the receiver side. The phrase "take newest" means that the most recent packet is selected whenever more packets are available at the receiver side at the same time instant. Case (c) constitutes the worst case scenario when no numbering nor synchronization is available. According to the definition of protocol $\mathcal{P}_3$, any packet might be selected as stated in condition (2.38c). Hence, gain α has to cover the worst case, which is present if the oldest available packet is selected. This is shown in detail in the proof of Theorem 7.1 in Section 7.2.

Please note that only known information is used in (7.5) to obtain the infinity norm of $M(z)$. Condition (7.5) can be checked easily, e.g., using Bode magnitude plots for a given bound $\bar{\tau}$ of the variable time delays. Bound $\bar{\tau}$ can then be increased step-by-step to find its maximal admissible value. The application of the theorem is presented for a feedback loop with filtered Smith predictor in simulation (Section 7.3) and using a laboratory setup in Section 7.4.

The protocol dependent ℓ_2 gains given by Theorem 7.1 are visualized in Figure 7.9 to point out the relation between the respective ℓ_2 gains α.

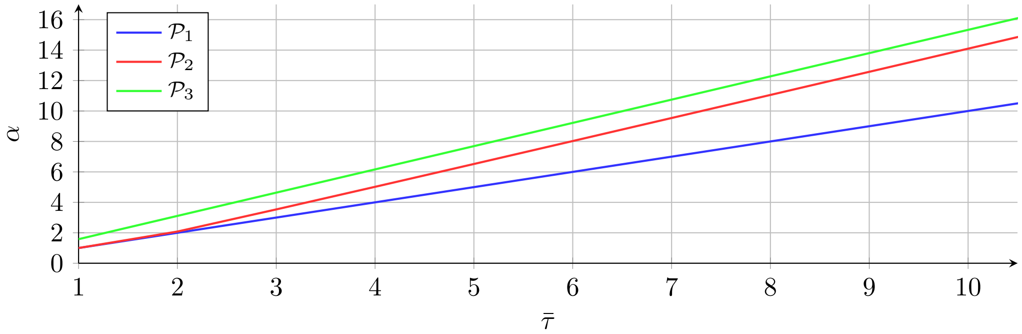

Figure 7.9: Comparison of the finite ℓ_2 gains as a function of the maximal admissible time-varying delay $\bar{\tau}$ for the three protocols.

It is also possible to formulate Theorem 7.1 such that the discrete-time differentiator and the integrator shown in Figure 7.1 are removed. This yields condition

$$\left\| \frac{R(z)\hat{P}(z)}{1 + R(z)\hat{P}(z)\hat{D}(z)} \right\|_{\infty} \tilde{\alpha} < 1 \tag{7.7}$$

and, as a consequence, a different finite ℓ_2 gain $\tilde{\alpha}$. However, this is limiting for the cases where $R(z)$ is designed such that the closed delay-free feedback loop has a dc-gain equal to one.

The proof in Section 7.2 allows the construction of the worst case packet delay patterns, i.e. the sequence of packet delays that lead to the largest 2-norm of the output (w_k) of the uncertainty. Figures 7.10, 7.11 and 7.12 show such sequences for the three protocols, where the input sequence (v_k) depicted in Figure 7.7 is applied to the uncertainty block in Figure 7.1.

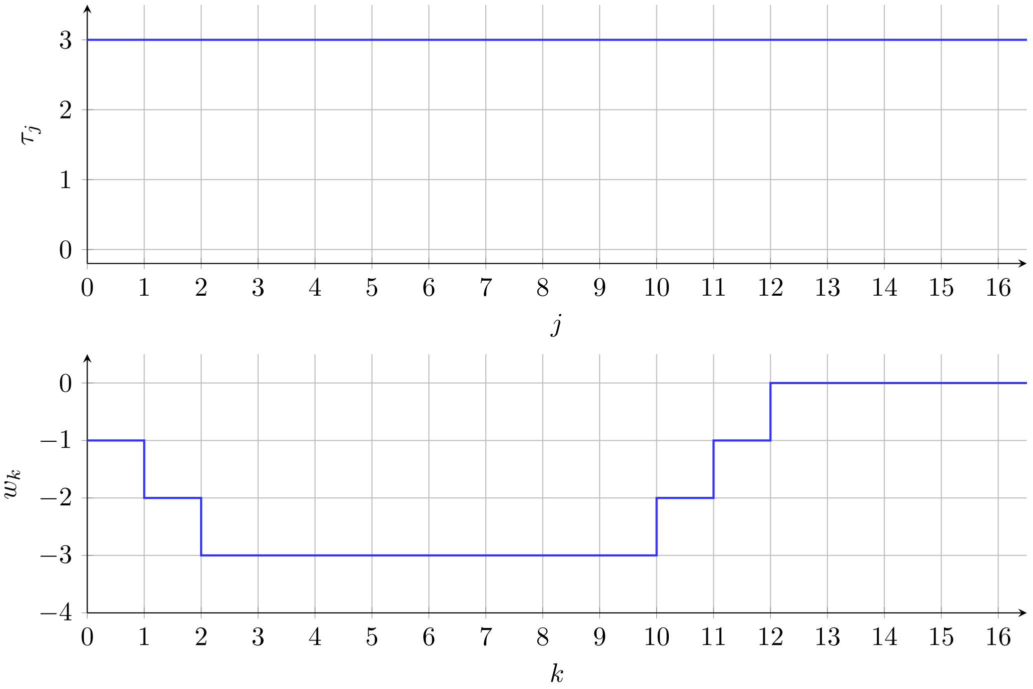

Figure 7.10: Worst case packet delay pattern (top) and output sequence (w_k) of the uncertainty (bottom) for input sequence (v_k) (7.2) and protocol $\mathcal{P}_1$.

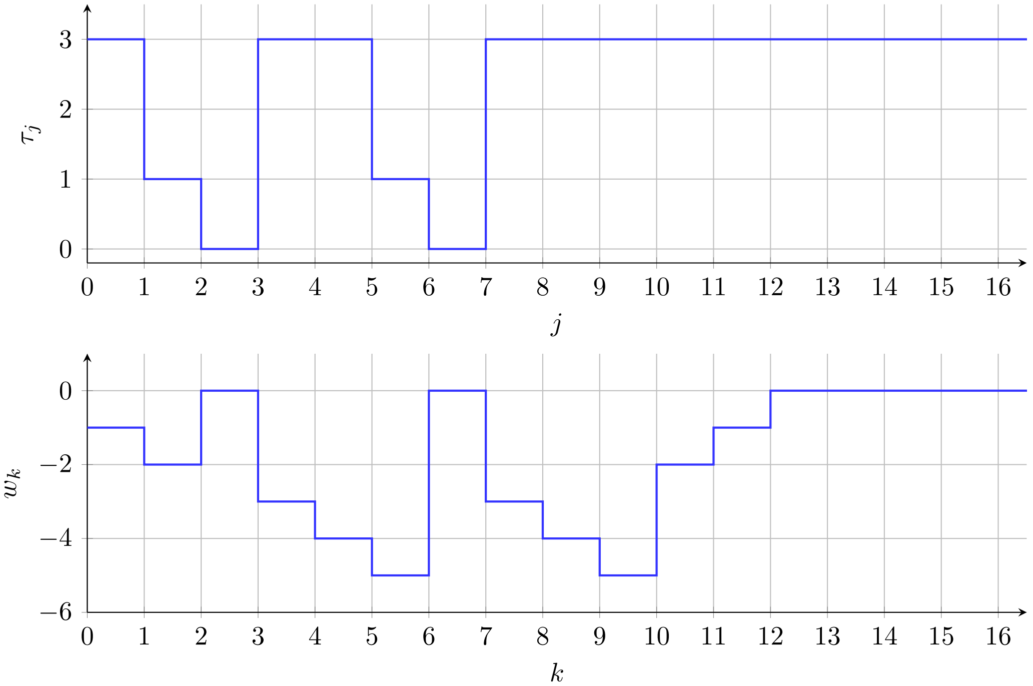

Figure 7.11: Worst case packet delay pattern (top) and output sequence (w_k) of the uncertainty (bottom) for input sequence (v_k) (7.2) and protocol $\mathcal{P}_2$.

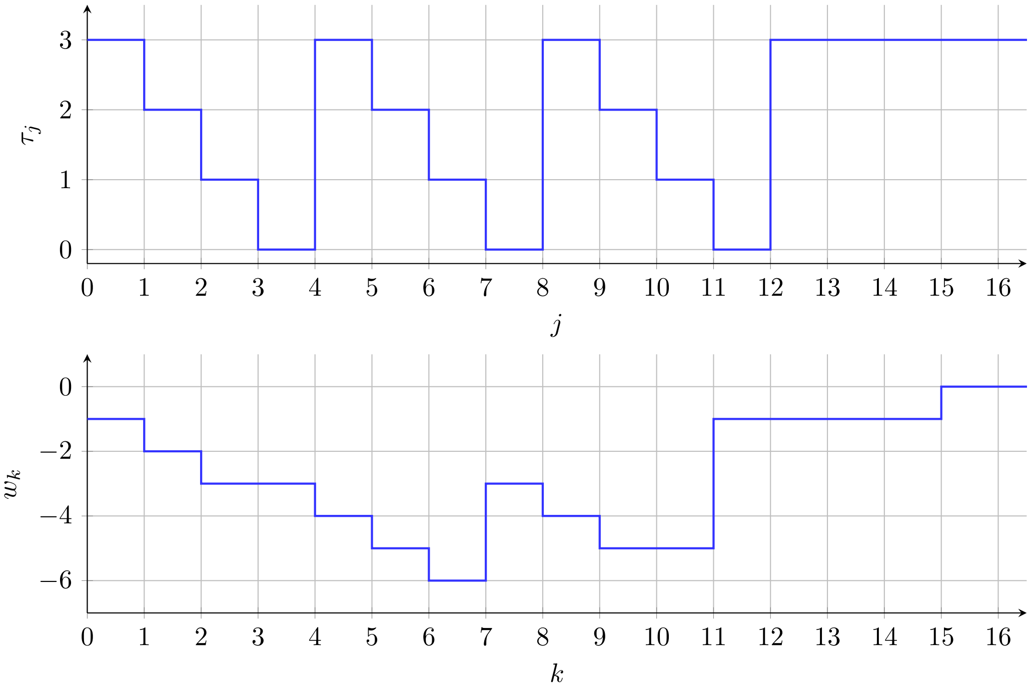

Figure 7.12: Worst case packet delay pattern (top) and output sequence (w_k) of the uncertainty (bottom) for input sequence (v_k) (7.2) and protocol $\mathcal{P}_3$.

7.2 Proof of Theorem 7.1

The proof is based on the small gain theorem [KL04, Sas99], where the feedback loop is split into a nominal part and the remaining uncertainty shown in gray and blue in Figure 7.1, respectively.

The nominal (gray) part in Figure 7.1 with input (w_k) and output (v_k) can be described by transfer function

$$T(z) = \frac{\mathcal{Z}\big\{(v_k)\big\}}{\mathcal{Z}\big\{(w_k)\big\}} = -\frac{R(z)\hat{P}(z)\hat{D}(z)}{1 + R(z)\hat{P}(z)\hat{D}(z)} \frac{z-1}{z}. \tag{7.8}$$

Applying the SGT [Sas99] to the structure in Figure 7.1 yields condition (7.5), where $||D(z)||_\infty = 1$ was taken into account.

The ℓ_2 gains α of the uncertainty depend on the actually used protocols stated in Definition 2.8. This is shown for all protocols $\mathcal{P}_1$, $\mathcal{P}_2$ and $\mathcal{P}_3$ in the subsequent sections, where the 2-norm of output $w_k = c_k - a_k$ (7.4) has to be maximized for the worst case input sequence (v_k) with bounded magnitude. For that purpose, the fact that the considered uncertainty is linear but time-varying is exploited. These properties hold for the uncertainty in Figure 7.6 because it consists of a discrete-time integrator, a delay block and a selector only. To find the gain α, one defines an input sequence

$$(v_k) = \big(v_0, v_1, v_2, \dots\big) = \big(\bar{v}, \bar{v}, \bar{v}, \dots\big) \tag{7.9}$$

for time instants $k \in \mathbb{N}$ and a truncation point T such that

$$\begin{aligned}\big(v_k\big)_T &= \big(v_0, v_1, v_2, \dots, v_T, 0, \dots\big) \\ &= \big(\bar{v}, \bar{v}, \bar{v}, \dots, \bar{v}, 0, 0, \dots\big).\end{aligned} \tag{7.10}$$

Because of the discrete-time integrator in Figure 7.6, it follows that

$$\begin{aligned}\big(a_k\big)_T &= \big(a_0, a_1, a_2, \dots, a_T, a_{T+1}, \dots\big) \\ &= \big(\bar{v}, 2\bar{v}, 3\bar{v}, \dots, (T+1)\bar{v}, (T+1)\bar{v}, \dots\big)\end{aligned} \tag{7.11}$$

that is directly fed to output w_k (and multiplied by -1) as shown in Figure 7.6. In addition, sequence (a_k) passes the blue block in Figure 7.6, which represents the transmission network that is subject to time-varying packet delays. It comprises a transmitter as well as a packet selection and a hold mechanism as specified in (2.38). Thus, each packet a_k might be delayed between 0 and $\bar{\tau}$ time steps as indicated by $b_k^{(0)}, b_k^{(1)}, \dots, b_k^{(\bar{\tau})}$, respectively. This situation with several packets "on the way" is exemplified in Figure 7.8 for $\bar{\tau} = 3$ and $T = 10$.

The selector in Figure 7.6 picks specific packets depending on the used protocol to allow the computation of the output (w_k), which has to be maximized with respect to its absolute value to find the finite ℓ_2 gains stated in Theorem 7.1, i.e.

$$\alpha = \max_{T>0} \alpha_T \tag{7.12}$$

with

$$\alpha_T = \sqrt{\frac{\big|\big|\big(w_k\big)_T\big|\big|_2^2}{\big|\big|\big(v_k\big)_T\big|\big|_2^2}} \tag{7.13}$$

is evaluated for all truncation points T in the following for the different protocols.

Since the goal is to maximize (w_k) for a given input (v_k), the number of samples to consider has to include all samples of (w_k) that are different from zero. The input signal tends to a constant value of $(T+1)\bar{v}$, i.e. after some time, only packets containing $(T+1)\bar{v}$ can arrive at the receiver side. This implies that $w_k = c_k - a_k = 0$ due to the structure of the uncertainty in Figure 7.6.

For protocol $\mathcal{P}_1$, the number of samples $s_{\mathcal{P}_1}$ to be considered for the calculation of the gain is

$$s_{\mathcal{P}_1} = T + 1 + \bar{\tau}\,. \tag{7.14}$$

Figure 7.13a shows the corresponding packet pattern for $\bar{v} = 1$. The cells enclosed by the gray parts represent the packets containing increasing values from 1 to T that might be delayed between 0 and $\bar{\tau}$ steps. The first packet, which contains the maximal value of $T + 1$ is transmitted at time instant $k = T$ and reaches the receiver at the latest at instant $T + \bar{\tau}$. Consequently, the reception of this (blue) packet marks the end of the interesting time interval since no overtaking of packets is allowed in protocol $\mathcal{P}_1$. This yields the number of samples to be considered as stated in (7.14).

Overtaking packets are feasible for protocols $\mathcal{P}_2$ and $\mathcal{P}_3$. Hence, the packet selection mechanism is of importance to determine the number of samples that should be used for the analysis. The largest number of samples follows for $\mathcal{P}_2$ if (i) the packet containing T is received at its latest possible time instant $T + \bar{\tau} - 1$, (ii) no other, previously sent packet arrives at the same time instant or afterwards and (iii) the (red) packet sent at instant $T+\bar{\tau}-1$ reaches the receiver with the maximal admissible delay at time instant $T + 2\bar{\tau} - 1$. This implied that the number of samples to be considered for protocol $\mathcal{P}_2$ is given by

$$s_{\mathcal{P}_2} = T + 2\bar{\tau}\,. \tag{7.15}$$

See Figure 7.13b for a visualization of this scenario. Condition (ii) is necessary because the most recent packet (containing $T+1$) would be selected whenever more packets are available at one sampling instant due to the definition of protocol $\mathcal{P}_2$.

On the contrary, any packet might be selected for protocol $\mathcal{P}_3$ that does not use any numbering of the packets. Thus, also the oldest packet (containing T) at time instant $T + \bar{\tau} - 1$ might be selected at the receiver side although a more recently packet (containing $T+1$) might be available. A (green) packet related to a value of $T+1$ is received for sure at the latest at instant $T + 2\bar{\tau}$, as depicted in Figure 7.13c. As a result

$$s_{\mathcal{P}_3} = T + 2\bar{\tau} + 1 \tag{7.16}$$

samples have to be taken into account to derive the finite ℓ_2 gain for protocol $\mathcal{P}_3$.

k	0	1	2	$\cdots$	$\cdots$	$\bar\tau$	$\bar\tau+1$	$\cdots$	$\cdots$	$T-1$	T	$T+1$	$T+2$	$\cdots$	$T+\bar\tau-1$	$T+\bar\tau$	$\cdots$	$T+2\bar\tau-3$	$T+2\bar\tau-2$	$T+2\bar\tau-1$	$T+2\bar\tau$
$b_k^{(0)}=a_k$	1	2	3	$\cdots$	$\cdots$	$\bar\tau+1$	$\bar\tau+2$	$\cdots$	$\cdots$	T	$T+1$	$T+1$	$T+1$	$\cdots$	$T+1$	$T+1$	$\cdots$	$T+1$	$T+1$	$T+1$	$T+1$
$b_k^{(1)}$	0	1	2			$\bar\tau$	$\bar\tau+1$	$\cdots$	$\cdots$	$T-1$	T	$T+1$	$T+1$	$\ddots$	$T+1$	$T+1$	$\ddots$	$T+1$	$T+1$	$T+1$	$T+1$
$b_k^{(2)}$	0	0	1	$\ddots$		$\bar\tau-1$	$\bar\tau$	$\cdots$	$\cdots$	$T-2$	$T-1$	T	$T+1$	$\ddots$	$T+1$	$T+1$	$\ddots$	$T+1$	$T+1$	$T+1$	$T+1$
$\vdots$	$\vdots$		$\ddots$	$\ddots$	$\ddots$							$\ddots$	$\ddots$	$\ddots$	$\ddots$	$\ddots$	$\ddots$	$\ddots$	$\ddots$	$\ddots$	$\ddots$
$\vdots$	$\vdots$			$\ddots$	$\ddots$	$\ddots$							$\ddots$	$\ddots$	$\ddots$	$\ddots$	$\ddots$	$\ddots$	$\ddots$	$\ddots$	$\ddots$
$b_k^{(\bar\tau)}$	0	0	0	0	0	1	2	$\cdots$	$\cdots$	$T-\bar\tau$	$T-\bar\tau+1$	$T-\bar\tau+2$	$\cdots$	$\cdots$	T	$T+1$	$\cdots$	$T+1$	$T+1$	$T+1$	$T+1$

(a) Protocol $\mathcal{P}_1$

k	0	1	2	$\cdots$	$\cdots$	$\bar\tau$	$\bar\tau+1$	$\cdots$	$\cdots$	$T-1$	T	$T+1$	$T+2$	$\cdots$	$T+\bar\tau-1$	$T+\bar\tau$	$\cdots$	$T+2\bar\tau-3$	$T+2\bar\tau-2$	$T+2\bar\tau-1$	$T+2\bar\tau$
$b_k^{(0)}=a_k$	1	2	3	$\cdots$	$\cdots$	$\bar\tau+1$	$\bar\tau+2$	$\cdots$	$\cdots$	T	$T+1$	$T+1$	$T+1$	$\cdots$	$T+1$	$T+1$	$\cdots$	$T+1$	$T+1$	$T+1$	$T+1$
$b_k^{(1)}$	0	1	2			$\bar\tau$	$\bar\tau+1$	$\cdots$	$\cdots$	$T-1$	T	$T+1$	$T+1$	$\ddots$	$T+1$	$T+1$	$\ddots$	$T+1$	$T+1$	$T+1$	$T+1$
$b_k^{(2)}$	0	0	1	$\ddots$		$\bar\tau-1$	$\bar\tau$	$\cdots$	$\cdots$	$T-2$	$T-1$	T	$T+1$	$\ddots$	$T+1$	$T+1$	$\ddots$	$T+1$	$T+1$	$T+1$	$T+1$
$\vdots$	$\vdots$		$\ddots$	$\ddots$	$\ddots$							$\ddots$	$\ddots$	$\ddots$	$\ddots$	$\ddots$	$\ddots$	$\ddots$	$\ddots$	$\ddots$	$\ddots$
$\vdots$	$\vdots$			$\ddots$	$\ddots$	$\ddots$							$\ddots$	$\ddots$	$\ddots$	$\ddots$	$\ddots$	$\ddots$	$\ddots$	$\ddots$	$\ddots$
$b_k^{(\bar\tau)}$	0	0	0	0	0	1	2	$\cdots$	$\cdots$	$T-\bar\tau$	$T-\bar\tau+1$	$T-\bar\tau+2$	$\cdots$	$\cdots$	T	$T+1$	$\cdots$	$T+1$	$T+1$	$T+1$	$T+1$

(b) Protocol $\mathcal{P}_2$

k	0	1	2	$\cdots$	$\cdots$	$\bar\tau$	$\bar\tau+1$	$\cdots$	$\cdots$	$T-1$	T	$T+1$	$T+2$	$\cdots$	$T+\bar\tau-1$	$T+\bar\tau$	$\cdots$	$T+2\bar\tau-3$	$T+2\bar\tau-2$	$T+2\bar\tau-1$	$T+2\bar\tau$
$b_k^{(0)}=a_k$	1	2	3	$\cdots$	$\cdots$	$\bar\tau+1$	$\bar\tau+2$	$\cdots$	$\cdots$	T	$T+1$	$T+1$	$T+1$	$\cdots$	$T+1$	$T+1$	$\cdots$	$T+1$	$T+1$	$T+1$	$T+1$
$b_k^{(1)}$	0	1	2			$\bar\tau$	$\bar\tau+1$	$\cdots$	$\cdots$	$T-1$	T	$T+1$	$T+1$	$\ddots$	$T+1$	$T+1$	$\ddots$	$T+1$	$T+1$	$T+1$	$T+1$
$b_k^{(2)}$	0	0	1	$\ddots$		$\bar\tau-1$	$\bar\tau$	$\cdots$	$\cdots$	$T-2$	$T-1$	T	$T+1$	$\ddots$	$T+1$	$T+1$	$\ddots$	$T+1$	$T+1$	$T+1$	$T+1$
$\vdots$	$\vdots$		$\ddots$	$\ddots$	$\ddots$							$\ddots$	$\ddots$	$\ddots$	$\ddots$	$\ddots$	$\ddots$	$\ddots$	$\ddots$	$\ddots$	$\ddots$
$\vdots$	$\vdots$			$\ddots$	$\ddots$	$\ddots$							$\ddots$	$\ddots$	$\ddots$	$\ddots$	$\ddots$	$\ddots$	$\ddots$	$\ddots$	$\ddots$
$b_k^{(\bar\tau)}$	0	0	0	0	0	1	2	$\cdots$	$\cdots$	$T-\bar\tau$	$T-\bar\tau+1$	$T-\bar\tau+2$	$\cdots$	$\cdots$	T	$T+1$	$\cdots$	$T+1$	$T+1$	$T+1$	$T+1$

(c) Protocol $\mathcal{P}_3$

Figure 7.13: Length of the sequences to be considered for the derivation of the finite ℓ_2 gains for the different protocols.

7.2.1 Protocol $\mathcal{P}_1$

The maximization of the absolute value of w_k is done element-wise starting at $k = 0$. For each time instant one has check if a certain packet “on the way” $b_k^{(j)}$ should arrive or if no packet should arrive, i.e. the hold mechanism is active such that $c_k = c_{k-1}$, to maximize w_k. This means that for time instant $k = 0$ one possibility is that packet $a_k = 1$ arrives without time delay, i.e. $w_k = b_k^{(0)} - a_k = 0$. A second possibility is that no packet arrives, i.e. $w_k = c_{k-1} - a_k = -1$, as indicated in Figure 7.14. As a consequence, the second possibility maximizes the absolute value of w_k. Variable $c_{k-1} = 0$ for $k = 0$ due to the assumption of vanishing initial conditions.

k	-1	0	1	2	3	4	5	6	7	8	9	10	11	12
$b_k^{(0)} = a_k$	0	$\cancel{1}$	$\cancel{2}$	$\cancel{3}$	$\cancel{4}$	$\cancel{5}$	$\cancel{6}$	$\cancel{7}$	$\cancel{8}$	$\cancel{9}$	$\cancel{10}$	$\cancel{10}$	$\cancel{10}$	10
$b_k^{(1)}$	$\cancel{0}$	$\cancel{0}$	$\cancel{1}$	$\cancel{2}$	$\cancel{3}$	$\cancel{4}$	$\cancel{5}$	$\cancel{6}$	$\cancel{7}$	$\cancel{8}$	$\cancel{9}$	$\cancel{10}$	$\cancel{10}$	10
$b_k^{(2)}$	$\cancel{0}$	$\cancel{0}$	$\cancel{0}$	$\cancel{1}$	$\cancel{2}$	$\cancel{3}$	$\cancel{4}$	$\cancel{5}$	$\cancel{6}$	$\cancel{7}$	$\cancel{8}$	$\cancel{9}$	$\cancel{10}$	10
$b_k^{(3)}$	$\cancel{0}$	$\cancel{0}$	$\cancel{0}$	$\cancel{0}$	1	2	3	4	5	6	7	8	9	10
$b_k^{(0)} - a_k$	0	0	0	0	0	0	0	0	0	0	0	0	0	0
$b_k^{(1)} - a_k$	0	-1	-1	-1	-1	-1	-1	-1	-1	-1	-1	0	0	0
$b_k^{(2)} - a_k$	0	-1	-2	-2	-2	-2	-2	-2	-2	-2	-2	-1	0	0
$b_k^{(3)} - a_k$	0	-1	-2	-3	-3	-3	-3	-3	-3	-3	-3	-2	-1	0
packet arr.	yes	no	no	no	yes	yes	yes	yes	yes	yes	yes	yes	yes	yes
c_k	0	0	0	0	1	2	3	4	5	6	7	8	9	10
w_k	0	-1	-2	-3	-3	-3	-3	-3	-3	-3	-3	-2	-1	0
block		A	A	B	B	B	B	B	B	B	B	C	C	0
τ_j		3	3	3	3	3	3	3	3	3	3	≥ 2	≥ 1	≥ 0

Figure 7.14: Protocol $\mathcal{P}_1$: arriving packets (represented using different colors) that lead to the worst case gain for $\bar{\tau} = 3$ and $T = 9$. Additionally, it shows all inner signals of the structure in Figure 7.6 and the corresponding packet delays τ_j.

This approach is also applied for the remaining time instants. In addition, no overtaking of packets is allowed for this protocol and each packet has to arrive at the latest after $\bar{\tau}$ time steps due to Assumption 6.2. This leads to the worst case pattern of time delays and a specific pattern for the arriving packets at the receiver side as illustrated in Figure 7.14. In addition, it lists all inner signals of the uncertainty corresponding to Figure 7.6. The time evolution of w_k for the worst case τ_j is also shown in Figure 7.10.

The packet delays τ_{10}, τ_{11} and τ_{12} are not uniquely defined because it does not make any difference for the gain calculation whether this packets arrive at $k = 12$ or later. Choosing different values for T result in the same worst case patterns for different maximal delays $\bar{\tau}$ and truncation times T as shown in Figures 7.15, 7.16, and for more cases in Appendix B.1.

k	-1	0	1	2	3	4	5	6	7	8
$b_k^{(0)} = a_k$	0	$\cancel{1}$	$\cancel{2}$	$\cancel{3}$	$\cancel{4}$	$\cancel{5}$	$\cancel{6}$	$\cancel{6}$	$\cancel{6}$	6
$b_k^{(1)}$	$\cancel{0}$	$\cancel{0}$	$\cancel{1}$	$\cancel{2}$	$\cancel{3}$	$\cancel{4}$	$\cancel{5}$	$\cancel{6}$	$\cancel{6}$	6
$b_k^{(2)}$	$\cancel{0}$	$\cancel{0}$	$\cancel{0}$	$\cancel{1}$	$\cancel{2}$	$\cancel{3}$	$\cancel{4}$	$\cancel{5}$	$\cancel{6}$	6
$b_k^{(3)}$	$\cancel{0}$	$\cancel{0}$	$\cancel{0}$	$\cancel{0}$	1	2	3	4	5	6
w_k	0	-1	-2	-3	-3	-3	-3	-2	-1	0
τ_j		3	3	3	3	3	3	≥ 2	≥ 1	≥ 0

Figure 7.15: Protocol $\mathcal{P}_1$: packet receiving pattern for $\bar{\tau} = 3$ and $T = 5$.

k	-1	0	1	2	3	4	5	6	7
$b_k^{(0)} = a_k$	0	$\cancel{1}$	$\cancel{2}$	$\cancel{3}$	$\cancel{4}$	$\cancel{5}$	$\cancel{6}$	$\cancel{6}$	6
$b_k^{(1)}$	$\cancel{0}$	$\cancel{0}$	$\cancel{1}$	$\cancel{2}$	$\cancel{3}$	$\cancel{4}$	$\cancel{5}$	$\cancel{6}$	6
$b_k^{(2)}$	$\cancel{0}$	$\cancel{0}$	$\cancel{0}$	1	2	3	4	5	6
w_k	0	-1	-2	-2	-2	-2	-2	-1	0
τ_j		2	2	2	2	2	2	≥ 1	≥ 0

k	-1	0	1	2	3	4	5	6	7	8	9	10	11
$b_k^{(0)} = a_k$	0	$\cancel{1}$	$\cancel{2}$	$\cancel{3}$	$\cancel{4}$	$\cancel{5}$	$\cancel{6}$	$\cancel{7}$	$\cancel{8}$	$\cancel{9}$	$\cancel{10}$	$\cancel{10}$	10
$b_k^{(1)}$	$\cancel{0}$	$\cancel{0}$	$\cancel{1}$	$\cancel{2}$	$\cancel{3}$	$\cancel{4}$	$\cancel{5}$	$\cancel{6}$	$\cancel{7}$	$\cancel{8}$	$\cancel{9}$	$\cancel{10}$	10
$b_k^{(2)}$	$\cancel{0}$	$\cancel{0}$	$\cancel{0}$	1	2	3	4	5	6	7	8	9	10
w_k	0	-1	-2	-2	-2	-2	-2	-2	-2	-2	-2	-1	0
τ_j		2	2	2	2	2	2	2	2	2	2	≥ 1	≥ 0

Figure 7.16: Protocol $\mathcal{P}_1$: packet receiving pattern for $\bar{\tau} = 2$ and $T = 5$ (top) and $T = 9$ (bottom).

As a result, (w_k) consists of three blocks marked by colors green, orange and red such that

$$
\begin{aligned}
(w_k) = \big(&\underbrace{-\bar{v}, -2\bar{v}, \dots, -(\bar{\tau}-1)\bar{v},}_{\text{block A}} \\
&\underbrace{-\bar{\tau}\bar{v}, -\bar{\tau}\bar{v}, \dots, -\bar{\tau}\bar{v},}_{\text{block B}}\ \underbrace{-(\bar{\tau}-1)\bar{v}, \dots, -2\bar{v}, -\bar{v},}_{\text{block C}}\ 0, 0, \dots\big),
\end{aligned}
\tag{7.17}
$$

see also Figure 7.14. Blocks A and C consist of $\bar{\tau} - 1$ samples each, block B of $(T + 1 + \bar{\tau}) - 2(\bar{\tau} - 1) = T - \bar{\tau} + 2$ samples because the overall number of considered samples is given by (7.14). Hence, the squared 2-norm of the output computes as

$$
\begin{aligned}
\left|\left|(w_k)_T\right|\right|_2^2 &= 2\sum_{i=1}^{\bar{\tau}-1}\left(i^2\bar{v}^2\right) + (T - \bar{\tau} + 2)\bar{\tau}^2\bar{v}^2 \\
&= \left[\frac{(\bar{\tau}-1)\bar{\tau}(2\bar{\tau}-1)}{3} + (T - \bar{\tau} + 2)\bar{\tau}^2\right]\bar{v}^2 \\
&= \frac{\bar{\tau}}{3}\left(-\bar{\tau}^2 + 3\bar{\tau} + 3\bar{\tau}T + 1\right)\bar{v}^2
\end{aligned}
\tag{7.18}
$$

for $(T - \bar{\tau} + 2) \geq 0$, i.e. $T \geq \bar{\tau} - 2$. In the first line of (7.18), the first term relates to blocks A and C; the second term to block B. The gain α_T (7.13) for this worst case setting is calculated using the squared 2-norm of the input sequence

$$
\left|\left|(v_k)_T\right|\right|_2^2 = (1 + T)\bar{v}^2\,. \tag{7.19}
$$

Figure 7.17 presents the calculated gains (crosses) according to (7.13) for different maximal variable delays $\bar{\tau}$ and truncation times T (with $T \geq \bar{\tau} - 2$), and compares them to actual worst case gains. Those actual values are computed by evaluating all possible combinations of time delays τ_j for the considered $\bar{\tau}$ and T while respecting the skipping and hold mechanisms as specified in (2.38). It can be seen that (7.17), (7.19) and (7.12) reproduce the worst case values perfectly.

With relations (7.18) and (7.19), the finite ℓ_2 gain α follows as the upper bound of (7.12)

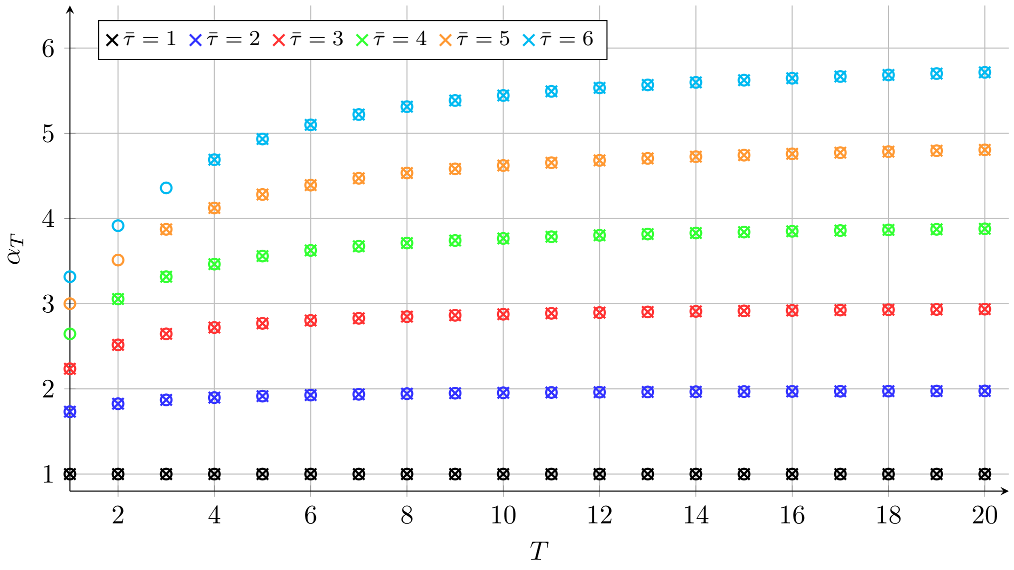

Figure 7.17: Protocol $\mathcal{P}_1$: Comparison of actual (circles) and calculated (crosses) gains α_T for different $\bar\tau$ and T.

for $T \to \infty$ such that

$$\alpha = \sqrt{\lim_{T\to\infty} \frac{\frac{\bar\tau}{3}\left(-\bar\tau^2 + 3\bar\tau + 3\bar\tau T + 1\right)}{(1+T)}} \tag{7.20}$$
$$= \sqrt{\lim_{T\to\infty} \frac{\bar\tau}{3}\left[3\bar\tau + \frac{1-\bar\tau^2}{1+T}\right]} = \bar\tau$$

as stated in (7.6a) in Theorem 7.1. In Figure 7.18, the gains α_T are plotted for different $\bar\tau$ and T (crosses) together with the finite ℓ_2 gain α (dotted lines).

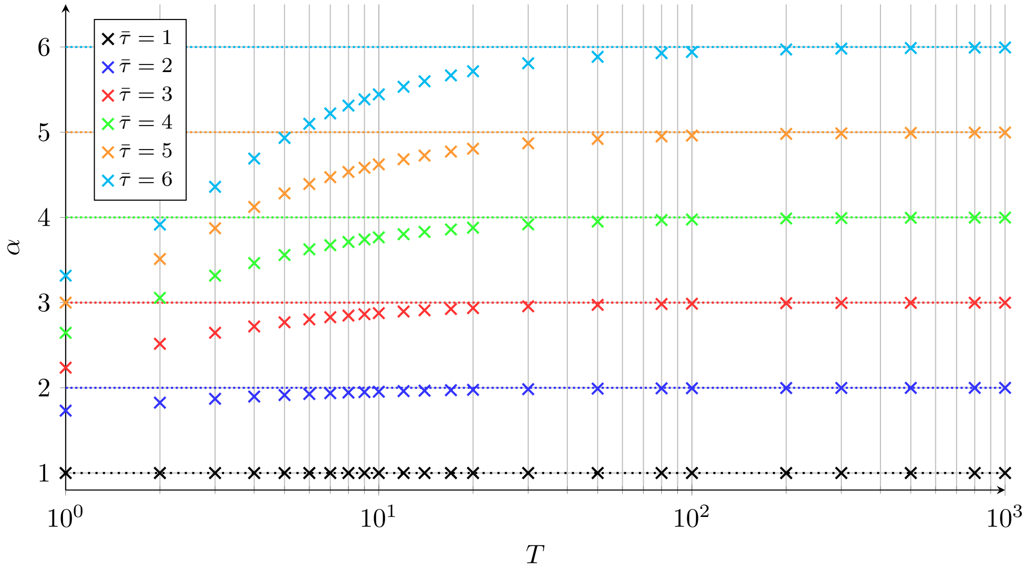

Figure 7.18: Protocol $\mathcal{P}_1$: gains α_T for different $\bar\tau$ and T (crosses). The associated maximal ℓ_2 gains α are shown using dotted lines.

7.2.2 Protocol $\mathcal{P}_2$

The strategy to maximize each element of (w_k) automatically yields non-overtaking packet patterns as shown in the previous subsection. It will be shown next that the finite ℓ_2 gain is larger for the case where old packets are not skipped and overtaking of packets is possible as defined for protocol $\mathcal{P}_2$ defined in (2.38b).

This means that older packets (with smaller signal values in Figure 7.8) have to be used whenever possible to maximize w_k, which is the difference between c_k and a_k. In addition, the effect of newer packets (with larger signal values) should only be used when absolutely necessary, e.g., because the maximal delay has already been reached.

k	-1	0	1	2	3	4	5	6	7	8	9	10	11	12	13	14
$b_k^{(0)} = a_k$	0	$\cancel{1}$	$\cancel{2}$	3	$\cancel{4}$	$\cancel{5}$	$\cancel{6}$	7	$\cancel{8}$	$\cancel{9}$	$\cancel{10}$	$\cancel{10}$	$\cancel{10}$	$\cancel{10}$	$\cancel{10}$	10
$b_k^{(1)}$	$\cancel{0}$	$\cancel{0}$	$\cancel{1}$	2	$\cancel{3}$	$\cancel{4}$	$\cancel{5}$	6	$\cancel{7}$	$\cancel{8}$	$\cancel{9}$	$\cancel{10}$	$\cancel{10}$	$\cancel{10}$	$\cancel{10}$	10
$b_k^{(2)}$	$\cancel{0}$	$\cancel{0}$	$\cancel{0}$	$\cancel{1}$	$\cancel{2}$	$\cancel{3}$	$\cancel{4}$	$\cancel{5}$	$\cancel{6}$	$\cancel{7}$	$\cancel{8}$	$\cancel{9}$	$\cancel{10}$	$\cancel{10}$	$\cancel{10}$	10
$b_k^{(3)}$	$\cancel{0}$	$\cancel{0}$	$\cancel{0}$	$\cancel{0}$	1	$\cancel{2}$	$\cancel{3}$	4	5	$\cancel{6}$	$\cancel{7}$	8	9	10	10	10
$b_k^{(0)} - a_k$	0	0	0	0	0	0	0	0	0	0	0	0	0	0	0	0
$b_k^{(1)} - a_k$	0	-1	-1	-1	-1	-1	-1	-1	-1	-1	-1	0	0	0	0	0
$b_k^{(2)} - a_k$	0	-1	-2	-2	-2	-2	-2	-2	-2	-2	-2	-1	0	0	0	0
$b_k^{(3)} - a_k$	0	-1	-2	-3	-3	-3	-3	-3	-3	-3	-3	-2	-1	0	0	0
packet arr.	yes	no	no	yes	yes	no	no	yes	yes	no	no	yes	yes	yes	yes	yes
c_k	0	0	0	3	1	1	1	7	5	5	5	8	9	10	10	10
w_k	0	-1	-2	0	-3	-4	-5	0	-3	-4	-5	-2	-1	0	0	0
block		A	A	B1	B1	B1	B1	B2	B2	B2	B2	C	C	C	C	C
τ_j		3	1	0	3	3	1	0	3	3	3	≥ 2	≥ 1	≥ 0	≥ 0	≥ 0

Figure 7.19: Protocol $\mathcal{P}_2$: arriving packets (represented using different colors) that lead to the worst case gain for $\bar{\tau} = 3$ and $T = 9$. Additionally, it shows all inner signals of the structure in Figure 7.6 and the corresponding packet delays τ_j.

Figure 7.19 shows an example for $0 \leq \tau_j \leq 3$, $T = 9$ and $\bar{v} = 1$. Packet $a_k = 0 = c_k$ has been already received due to the assumption about the initial conditions. This value $c_k = 0$ has to be kept as long as possible to create the largest distance $c_k - a_k$. Consequently, no packets should arrive in the next time steps. However, packet $a_k = 1$ has to arrive at $k = 3$ at the latest which results in $c_k = 1$. This second smallest possible value should be kept constant as long as possible. This follows if packets $a_k = 2$ and $a_k = 3$ already arrive at time instant $k = 2$ as shown in Figure 7.19. The most recent packet, i.e. $a_k = 3$, is selected as requested for protocol $\mathcal{P}_2$.

By continuing this approach for all subsequent time instants, a repeating pattern (see, e.g., columns $k = 4$ to $k = 7$ in Figure 7.19) for the order of arriving packets can be constructed. The delays for the last $\bar{\tau}$ time instants are only lower bounded because of the same reason as in the case where old packets are skipped in protocol $\mathcal{P}_1$. Packets $a_k = 2$, $a_k = 4$, and $a_k = 6$ are never selected at (c_k). The resulting worst case packet delays τ_j and the corresponding output sequence (w_k) are depicted in Figure 7.11.

Figures 7.20 and 7.21 illustrate examples for resulting packet patterns for different values of T and $\bar{\tau} = 3$ as well as for $\bar{\tau} = 2$. More examples of packet patterns for this protocol can be found in Appendix B.2.

Based on that, the worst case output sequence consists of at most four parts A, B, C and D, which are marked in the colors green, orange, blue and red in Figures 7.19 to 7.21 and Figures B.5 to B.8 in Appendix B.2. Please note that part C (blue) is not present for all combinations of $\bar{\tau}$ and T. The number of samples to be considered in

k	-1	0	1	2	3	4	5	6	7	8	9	10
$b_k^{(0)} = a_k$	0	$\cancel{1}$	$\cancel{2}$	3	$\cancel{4}$	$\cancel{5}$	$\cancel{6}$	$\cancel{6}$	$\cancel{6}$	6	6	6
$b_k^{(1)}$	$\cancel{0}$	$\cancel{0}$	$\cancel{1}$	2	$\cancel{3}$	$\cancel{4}$	$\cancel{5}$	$\cancel{6}$	$\cancel{6}$	6	6	6
$b_k^{(2)}$	$\cancel{0}$	$\cancel{0}$	$\cancel{0}$	$\cancel{1}$	$\cancel{2}$	$\cancel{3}$	$\cancel{4}$	$\cancel{5}$	$\cancel{6}$	6	6	6
$b_k^{(3)}$	$\cancel{0}$	$\cancel{0}$	$\cancel{0}$	$\cancel{0}$	1	$\cancel{2}$	$\cancel{3}$	4	5	6	6	6
w_k	0	-1	-2	0	-3	-4	-5	-2	-1	0	0	0
τ_j		3	1	0	3	3	3	≥ 2	≥ 1	≥ 0	≥ 0	≥ 0

Figure 7.20: Protocol $\mathcal{P}_2$: packet receiving pattern for $\bar{\tau} = 3$ and $T = 5$.

k	-1	0	1	2	3	4	5	6	7	8
$b_k^{(0)} = a_k$	0	$\cancel{1}$	2	$\cancel{3}$	$\cancel{4}$	$\cancel{5}$	$\cancel{6}$	$\cancel{6}$	6	6
$b_k^{(1)}$	$\cancel{0}$	$\cancel{0}$	$\cancel{1}$	$\cancel{2}$	$\cancel{3}$	$\cancel{4}$	$\cancel{5}$	$\cancel{6}$	6	6
$b_k^{(2)}$	$\cancel{0}$	$\cancel{0}$	$\cancel{0}$	1	$\cancel{2}$	3	4	5	6	6
w_k	0	-1	0	-2	-3	-2	-2	-1	0	0
τ_j		2	0	2	2	2	2	≥ 1	≥ 0	≥ 0

k	-1	0	1	2	3	4	5	6	7	8	9	10	11	12
$b_k^{(0)} = a_k$	0	$\cancel{1}$	2	$\cancel{3}$	$\cancel{4}$	5	$\cancel{6}$	$\cancel{7}$	8	$\cancel{9}$	$\cancel{10}$	$\cancel{10}$	10	10
$b_k^{(1)}$	$\cancel{0}$	$\cancel{0}$	$\cancel{1}$	$\cancel{2}$	$\cancel{3}$	$\cancel{4}$	$\cancel{5}$	$\cancel{6}$	$\cancel{7}$	$\cancel{8}$	$\cancel{9}$	$\cancel{10}$	10	10
$b_k^{(2)}$	$\cancel{0}$	$\cancel{0}$	$\cancel{0}$	1	$\cancel{2}$	3	4	$\cancel{5}$	6	7	$\cancel{8}$	9	10	10
w_k	0	-1	0	-2	-3	0	-2	-3	0	-2	-3	-1	0	0
τ_j		2	0	2	2	0	2	2	0	2	2	≥ 1	≥ 0	≥ 0

Figure 7.21: Protocol $\mathcal{P}_2$: packet receiving pattern for $\bar{\tau} = 2$ and $T = 5$ (top) and $T = 9$ (bottom).

the analysis is $T + 2\bar{\tau}$ as stated in (7.15). Block A (green) consists of $\bar{\tau} - 1$ samples. The remaining $(T + 2\bar{\tau}) - (\bar{\tau} - 1) = T + \bar{\tau} + 1$ samples are split into k_1 (orange) blocks B with length $\bar{\tau} + 1$, k_3 (blue) blocks C and one (red) block D at the end.

Parameter k_1 is obtained by subtracting $\bar{\tau} + 1$ from $T + \bar{\tau} + 1$ until the remainder has a length $\leq 3\bar{\tau}$. This yields a remaining part with length $k_2 = T + \bar{\tau} + 1 - k_1(\bar{\tau} + 1)$. Parameter k_3 follows by subtracting $\bar{\tau}+1$ from k_2 as long as $k_2 \geq 6$. The resulting part D has length $k_2 - k_3(\bar{\tau} + 1)$. Consequently, the squared 2-norm of (w_k) is given by

$$\begin{aligned} \left|\left|(w_k)_T\right|\right|_2^2 = & \underbrace{\sum_{i=1}^{\bar{\tau}-1} i^2 \bar{v}^2}_{A} + \\ & \underbrace{\sum_{j=0}^{k_1-1} \left\{ \sum_{i=\bar{\tau}+j(\bar{\tau}+1)}^{2\bar{\tau}-1+j(\bar{\tau}+1)} \left(a_i - a_{j(\bar{\tau}+1)}\right)^2 \right\}}_{B} + \\ & \underbrace{\sum_{j=k_1}^{k_1+k_3-1} \left\{ \sum_{i=\bar{\tau}+j(\bar{\tau}+1)}^{2\bar{\tau}-1+j(\bar{\tau}+1)} \left(a_i - a_{j(\bar{\tau}+1)}\right)^2 \right\}}_{C} + \\ & \underbrace{\sum_{i=\bar{\tau}-1+(k_1+k_3)(\bar{\tau}+1)}^{T+2\bar{\tau}-1} \left(a_i - a_{i-\bar{\tau}}\right)^2}_{D} \end{aligned} \tag{7.21}$$

where the contribution of the individual blocks is indicated. The corresponding sequence of worst case packet delays is

$$(\tau_j) = \Big(\underbrace{\bar{\tau}, \bar{\tau}-2, \bar{\tau}-3, \dots, 1,}_{\bar{\tau}-1 \text{ elements}} \underbrace{\underbrace{0, \bar{\tau}, \bar{\tau}, \bar{\tau}-2, \bar{\tau}-3, \dots, 1,}_{\bar{\tau}+1 \text{ elements}} \;\dots}_{k_1-1 \text{ blocks}}, 0, \bar{\tau}, \bar{\tau}, \dots\Big) \tag{7.22}$$

for the case without block C present, i.e. $k_3 = 0$, and

$$(\tau_j) = \Big(\underbrace{\bar{\tau}, \bar{\tau}-2, \bar{\tau}-3, \dots, 1,}_{\bar{\tau}-1 \text{ elements}} \underbrace{\underbrace{0, \bar{\tau}, \bar{\tau}, \bar{\tau}-2, \bar{\tau}-3, \dots, 1,}_{\bar{\tau}+1 \text{ elements}} \;\dots}_{k_1 \text{ blocks}}, 0, \bar{\tau}, \bar{\tau}, \dots\Big) \tag{7.23}$$

with block C as, e.g., in Figure B.6 for $T = 8$ and $\bar{\tau} = 3$. Please note that $k_1 - 1$ and k_1 repeating blocks are used after the introductory part A with $\bar{\tau} - 1$ elements in (7.22) and (7.23), respectively.

Subsequently, relations (7.21), (7.19) and (7.13) are employed to get gain α_T that is plotted using plus signs in Figure 7.22 for different $\bar{\tau}$ and T (with $T \geq 3$). It clearly

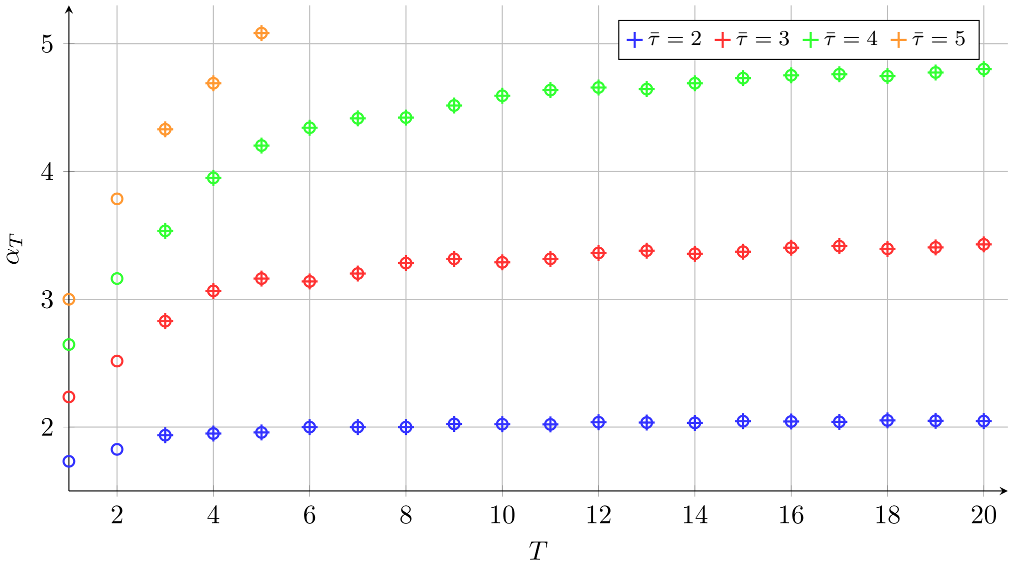

Figure 7.22: Protocol $\mathcal{P}_2$: Comparison of actual (circles) and calculated (plus signs) gains α_T for different $\bar{\tau}$ and T.

points out that the derived relations (plus signs) for α_T correctly reproduce the actual gain values (circles), which are again found through direct calculations for all possible combinations of individual packet delays. Please note that the case $\bar{\tau} = 1$ is not considered here because overtaking of packets cannot occur for this maximal variable time delay and $\mathcal{P}_1$ already yields the worst case gain. Also note that α_T as a function of T is *not* monotonically increasing as for protocol $\mathcal{P}_1$.

The finite ℓ_2 gain α is found for $T \to \infty$ or equivalently $k_1 \to \infty$ such that

$$\alpha = \sqrt{\lim_{T\to\infty} \frac{A+B+C+D}{(1+T)\bar{v}^2}}\,, \tag{7.24}$$

where A, B, C and D correspond to the individual contributions of the blocks to the squared 2-norm of (w_k). The element-wise squared sequences of the $k_1 = \frac{T+1}{\bar{\tau}+1}$ blocks

B are given by

$$\left(\bar{\tau}^2\bar{v}^2, (\bar{\tau}+1)^2\bar{v}^2, (\bar{\tau}+2)^2\bar{v}^2, \ldots, (2\bar{\tau}-1)^2\bar{v}^2\right), \tag{7.25}$$

with a corresponding 2-norm of one B block such that

$$d = \sum_{i=1}^{\bar{\tau}} \left((\bar{\tau}-1)+i\right)^2 \bar{v}^2 = \frac{\bar{\tau}}{6}\left(14\bar{\tau}^2 - 9\bar{\tau} + 1\right)\bar{v}^2 \ . \tag{7.26}$$

The contribution of blocks A, C and D to (7.24) only depend on $\bar{\tau}$, whereas the contribution of block $B = k_1 d$ also depends on T. As direct consequence, it follows that

$$\alpha = \sqrt{\lim_{T\to\infty} \frac{A + \frac{T+1}{\bar{\tau}+1}d + C + D}{(1+T)}} = \sqrt{\frac{d}{\bar{\tau}+1}} \tag{7.27}$$

with d as in (7.26), and thus condition (7.6b) stated in Theorem 7.1. Figure 7.23 presents the derived gains α_T (plus signs) together with the corresponding ℓ_2 gains (7.6b) (dotted lines) for a larger range of truncation times T and maximal time-varying delays $\bar{\tau} \in \{2, 3, 4, 5\}$. Please note that the first element in Figure 7.23 is calculated using the conditions above, which are actually defined for $T \geq 3$. It differs from the first element in Figure 7.22, which follows from the direct iteration of all possible combinations of packet delays. This emphasizes the fact that the conditions derived in this section reproduce gain α_T for $T \geq 3$ (see Figure 7.22). For smaller values of T, the delay pattern from protocol $\mathcal{P}_1$ may lead to larger values for α_T. However, mathematical relations for $T \geq 3$ are sufficient for the calculation of the finite ℓ_2 gain, which follows for $T \to \infty$, as shown in Figure 7.23.

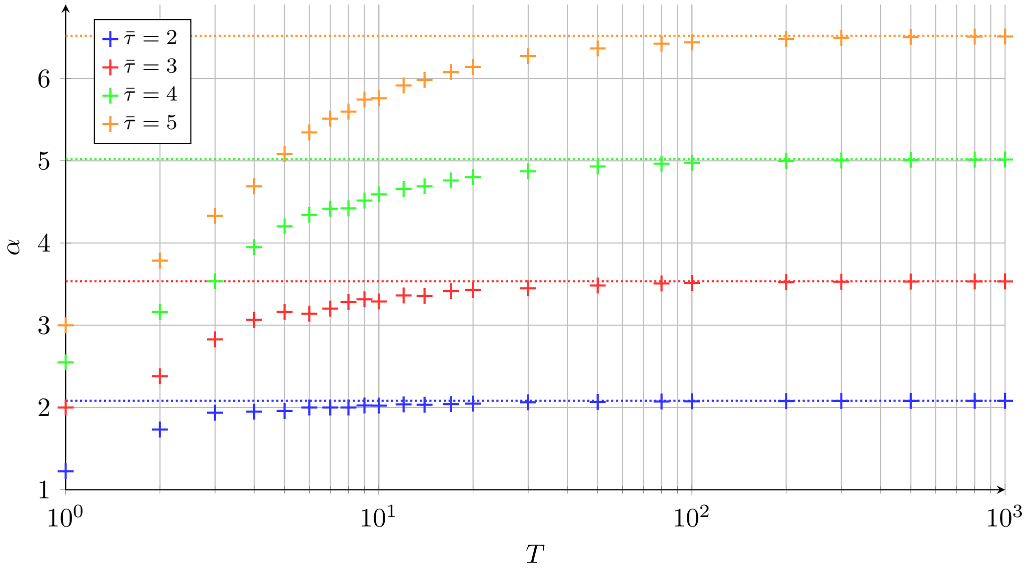

Figure 7.23: Protocol $\mathcal{P}_2$: gains α_T for different $\bar{\tau}$ and T (plus signs). The associated maximal ℓ_2 gains α are shown using dotted lines.

7.2.3 Protocol $\mathcal{P}_3$

The maximal number of samples to consider for protocol $\mathcal{P}_3$ is $T + 2\bar{\tau} + 1$ as stated in (7.16) because they contribute to $w_k = c_k - a_k$. To show that the worst case ℓ_p gain of the uncertainty is (7.6c), one has to maximize the squared 2-norm of output (w_k), while taking into account (2.38c). All initial conditions, as, e.g., c_k for $k = -1$, are assumed to be zero.

Due to the fact that (a_k) is monotonically increasing and the difference between c_k and a_k is used to get w_k, the worst case sequence (w_k) follows if one selects the packets containing the smallest c_k and keep them as long as possible, utilizing the hold mechanism. This can be clearly seen using, for example, $\bar{\tau} = 3$ and $T = 9$ as in Figure 7.24. Sample $a_0 = 1$ is received at the latest possible time instant $k = \bar{\tau} = 3$, which yields $c_k = b_k^{(3)} - a_k = 1$ for $k = 3$. No packet has to arrive for $k = 0, 1, 2$ to maximize (w_k). In addition, $c_3 = 1$ has to be hold as long as possible, i.e. until the next packet has to arrive due to Assumption 6.2. This means, that no packet should arrive at time instants $k = 4, 5, 6$ and $a_4 = 5$ is selected at time instant $k = 7$. Consequently, the packets containing $a_1 = 2$, $a_2 = 3$ and $a_3 = 4$ have to be discarded, which is only possible if they arrive at $k = 3$ and are not selected at this time instant, see Figure 7.24. Next, $c_7 = 5$ has to be kept as long as possible until packet $a_8 = 9$ is selected at $k = 11$. The entire pattern of received packets, all packets "on the way", the resulting worst case sequence (w_k) and the corresponding packet delays τ_j are depicted in Figure 7.24.

k	-1	0	1	2	3	4	5	6	7	8	9	10	11	12	13	14	15
$b_k^{(0)} = a_k$	0	$\cancel{1}$	$\cancel{2}$	$\cancel{3}$	4	$\cancel{5}$	$\cancel{6}$	$\cancel{7}$	8	$\cancel{9}$	$\cancel{10}$	$\cancel{10}$	10	$\cancel{10}$	$\cancel{10}$	$\cancel{10}$	10
$b_k^{(1)}$	$\cancel{0}$	$\cancel{0}$	$\cancel{1}$	$\cancel{2}$	3	$\cancel{4}$	$\cancel{5}$	$\cancel{6}$	7	$\cancel{8}$	$\cancel{9}$	$\cancel{10}$	10	$\cancel{10}$	$\cancel{10}$	$\cancel{10}$	10
$b_k^{(2)}$	$\cancel{0}$	$\cancel{0}$	$\cancel{0}$	$\cancel{1}$	2	$\cancel{3}$	$\cancel{4}$	$\cancel{5}$	6	$\cancel{7}$	$\cancel{8}$	$\cancel{9}$	10	$\cancel{10}$	$\cancel{10}$	$\cancel{10}$	10
$b_k^{(3)}$	$\cancel{0}$	$\cancel{0}$	$\cancel{0}$	$\cancel{0}$	1	$\cancel{2}$	$\cancel{3}$	$\cancel{4}$	5	$\cancel{6}$	$\cancel{7}$	$\cancel{8}$	9	$\cancel{10}$	$\cancel{10}$	$\cancel{10}$	10
$b_k^{(0)} - a_k$	0	0	0	0	0	0	0	0	0	0	0	0	0	0	0	0	0
$b_k^{(1)} - a_k$	0	-1	-1	-1	-1	-1	-1	-1	-1	-1	-1	0	0	0	0	0	0
$b_k^{(2)} - a_k$	0	-1	-2	-2	-2	-2	-2	-2	-2	-2	-2	-1	0	0	0	0	0
$b_k^{(3)} - a_k$	0	-1	-2	-3	-3	-3	-3	-3	-3	-3	-3	-2	-1	0	0	0	0
packet arr.	yes	no	no	no	yes	no	no	no	yes	no	no	no	yes	no	no	no	yes
c_k	0	0	0	0	1	1	1	1	5	5	5	5	9	9	9	9	10
w_k	0	-1	-2	-3	-3	-4	-5	-6	-3	-4	-5	-5	-1	-1	-1	-1	0
block		A	A	A	B	B	B	B	C	C	C	C	C	C	C	C	D
τ_j		3	2	1	0	3	2	1	0	3	2	1	0	3	2	1	0

Figure 7.24: Protocol $\mathcal{P}_3$: arriving packets (represented using different colors) that lead to the worst case gain for $\bar{\tau} = 3$ and $T = 9$. Additionally, it shows all inner signals of the structure in Figure 7.6 and the corresponding packet delays τ_j.

k	-1	0	1	2	3	4	5	6	7	8	9	10	11
$b_k^{(0)} = a_k$	0	$\cancel{1}$	$\cancel{2}$	$\cancel{3}$	4	$\cancel{5}$	$\cancel{6}$	$\cancel{6}$	6	$\cancel{6}$	$\cancel{6}$	$\cancel{6}$	6
$b_k^{(1)}$	$\cancel{0}$	$\cancel{0}$	$\cancel{1}$	$\cancel{2}$	3	$\cancel{4}$	$\cancel{5}$	$\cancel{6}$	6	$\cancel{6}$	$\cancel{6}$	$\cancel{6}$	6
$b_k^{(2)}$	$\cancel{0}$	$\cancel{0}$	$\cancel{0}$	$\cancel{1}$	2	$\cancel{3}$	$\cancel{4}$	$\cancel{5}$	6	$\cancel{6}$	$\cancel{6}$	$\cancel{6}$	6
$b_k^{(3)}$	$\cancel{0}$	$\cancel{0}$	$\cancel{0}$	$\cancel{0}$	1	$\cancel{2}$	$\cancel{3}$	$\cancel{4}$	5	$\cancel{6}$	$\cancel{6}$	$\cancel{6}$	6
w_k	0	-1	-2	-3	-3	-4	-5	-5	-1	-1	-1	-1	0
τ_j		3	2	1	0	3	2	1	0	3	2	1	0

Figure 7.25: Protocol $\mathcal{P}_3$: packet receiving pattern for $\bar{\tau} = 3$ and $T = 5$.

Figures 7.25 and 7.26 present the worst case patterns of arriving packets for the cases with different $\bar{\tau}$ and T. The results for other truncation times T can be found in

k	-1	0	1	2	3	4	5	6	7	8	9
$b_k^{(0)} = a_k$	0	~~1~~	~~2~~	3	~~4~~	~~5~~	6	~~6~~	~~6~~	6	~~6~~
$b_k^{(1)}$	~~0~~	~~0~~	~~1~~	2	~~3~~	~~4~~	5	~~6~~	~~6~~	6	~~6~~
$b_k^{(2)}$	~~0~~	~~0~~	~~0~~	1	~~2~~	~~3~~	4	~~5~~	~~6~~	6	~~6~~
w_k	0	-1	-2	-2	-3	-4	-2	-2	-2	0	0
τ_j		2	1	0	2	1	0	2	1	0	2

k	-1	0	1	2	3	4	5	6	7	8	9	10	11	12	13
$b_k^{(0)} = a_k$	0	~~1~~	~~2~~	3	~~4~~	~~5~~	6	~~7~~	~~8~~	9	~~10~~	~~10~~	10	~~10~~	~~10~~
$b_k^{(1)}$	~~0~~	~~0~~	~~1~~	2	~~3~~	~~4~~	5	~~6~~	~~7~~	8	~~9~~	~~10~~	10	~~10~~	~~10~~
$b_k^{(2)}$	~~0~~	~~0~~	~~0~~	1	~~2~~	~~3~~	4	~~5~~	~~6~~	7	~~8~~	~~9~~	10	~~10~~	~~10~~
w_k	0	-1	-2	-2	-3	-4	-2	-3	-4	-2	-3	-3	0	0	0
τ_j		2	1	0	2	1	0	2	1	0	2	1	0	2	1

Figure 7.26: Protocol $\mathcal{P}_3$: packet receiving pattern for $\bar{\tau} = 2$ and $T = 5$ (top) and $T = 9$ (bottom).

Appendix B.3 for $\bar{\tau} = 3$ and $\bar{\tau} = 2$.

The worst case sequence (w_k) consists of maximal four different blocks A, B, C and D as indicated in the figures using different colors as, e.g. in Figure 7.24. The worst case pattern consists of a (green) introductory part A consisting of $\bar{\tau}$ samples, followed by the remaining $T + \bar{\tau} + 1$ samples that are split into several parts. First, the k_1 (orange) blocks B with length $\bar{\tau} + 1$ are separated from the rest to get $\leq 3\bar{\tau}$ remaining samples. This rest with k_2 elements is split into a (blue) block C with length

$$k_3 = \left\lfloor \frac{k_2}{\bar{\tau} + 1} \right\rfloor, \tag{7.28}$$

which represents the largest integer smaller than $\frac{k_2}{\bar{\tau}+1}$, and a (red) block D with $k_2 - k_3(\bar{\tau} + 1)$ elements. Note that the last element is always equal to zero. Based on this splitting into four parts, one can formalize the 2-norm of the truncated worst case sequence such that

$$\begin{aligned} ||(w_k)_T||_2^2 = &\underbrace{\sum_{i=1}^{\bar{\tau}} i^2 \bar{v}^2}_{A} + \\ &\underbrace{\sum_{j=0}^{k_1-1} \left\{ \sum_{i=\bar{\tau}+j(\bar{\tau}+1)}^{2\bar{\tau}+j(\bar{\tau}+1)} \left(a_i - a_{j(\bar{\tau}+1)}\right)^2 \right\}}_{B} + \\ &\underbrace{\sum_{j=k_1}^{k_1+k_3-1} \left\{ \sum_{i=\bar{\tau}+j(\bar{\tau}+1)}^{2\bar{\tau}+j(\bar{\tau}+1)} \left(a_i - a_{j(\bar{\tau}+1)}\right)^2 \right\}}_{C} + \\ &\underbrace{\sum_{i=\bar{\tau}+(k_1+k_3)(\bar{\tau}+1)}^{T+2\bar{\tau}} \left(a_i - a_{\bar{\tau}+(k_1+k_3)(\bar{\tau}+1)}\right)^2}_{D} \end{aligned} \tag{7.29}$$

with the underlying worst case packet delay pattern

$$(\tau_j) = \Big(\underbrace{\bar{\tau}, \bar{\tau}-1, \bar{\tau}-2, \ldots, 0,}_{\bar{\tau}+1 \text{ elements}} \underbrace{\bar{\tau}, \bar{\tau}-1, \bar{\tau}-2, \ldots, 0,}_{\bar{\tau}+1 \text{ elements}} \ldots\Big). \tag{7.30}$$

Next, the gain α_T is calculated for different $\bar{\tau}$ and T following the steps described for protocols $\mathcal{P}_1$ and $\mathcal{P}_2$. Figure 7.27 compares calculated values for α_T (stars) with the actual results, which are obtained by evaluating the effect of all possible combinations of bounded packet delays τ_j indicated using circles. The derived relations allow to correctly reproduce the accurate results from direct iterations and, thus, provide the basis for the derivation of the finite ℓ_2 gain α (7.12). The limit of α_T for $T \to \infty$ is computed using $||(w_k)_T||_2^2 = A+B+C+D$, where the part corresponding to B consists of k_1 blocks of the form

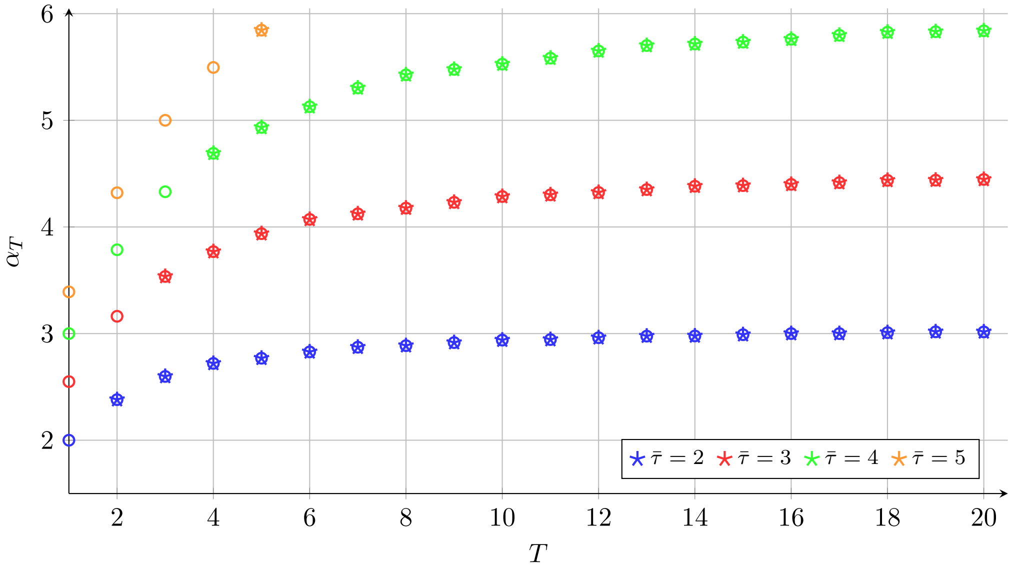

Figure 7.27: Protocol $\mathcal{P}_3$: Comparison of actual (circles) and calculated (stars) gains α_T for different $\bar{\tau}$ and T.

$$\big(-\bar{\tau}\bar{v}, -(\bar{\tau}+1)\bar{v}, -(\bar{\tau}+2)\bar{v}\ldots, -2\bar{\tau}\bar{v}\big) \tag{7.31}$$

with $\bar{\tau}+1$ samples each. One of these blocks B contributes to the overall 2-norm of $(w_k)_T$ with

$$\begin{aligned} d &= \sum_{i=1}^{\bar{\tau}+1} \big((\bar{\tau}-1)+i\big)\bar{v}^2 \\ &= \sum_{i=1}^{\bar{\tau}+1} \big((\bar{\tau}-1)^2 + 2(\bar{\tau}-1)i + i^2\big)\bar{v}^2 \\ &= \left((\bar{\tau}-1)^2 \sum_{i=1}^{\bar{\tau}+1} 1 + 2(\bar{\tau}-1)\sum_{i=1}^{\bar{\tau}+1} i + \sum_{i=1}^{\bar{\tau}+1} i^2 \right)\bar{v}^2 \\ &= \frac{\bar{\tau}+1}{6}\left(14\bar{\tau}^2+\bar{\tau}\right)\bar{v}^2 \,. \end{aligned} \tag{7.32}$$

leading to

$$\big|\big|(w_k)_T\big|\big|_2^2 = A + \frac{T+1}{\bar{\tau}+1}d + C + D\,, \tag{7.33}$$

where blocks A, C and D are constant with respect to T. Consequently, one gets

$$\alpha_T^2 = \frac{A + \frac{T+1}{\bar{\tau}+1}d + C + D}{1+T} = \frac{A+C+D}{1+T} + \frac{d}{1+T} \tag{7.34}$$

and thus

$$\alpha = \lim_{T\to\infty} \alpha_T = \sqrt{\frac{d}{\bar{\tau}+1}} = \sqrt{\frac{14\bar{\tau}^2}{6} + \frac{\bar{\tau}}{6}}\,, \tag{7.35}$$

which is equivalent to (7.6c) in Theorem 7.1. Figure 7.28 depicts the gains α_T for a larger range of truncation times T and maximal time-varying delays $\bar{\tau} \in \{2, 3, 4, 5\}$.

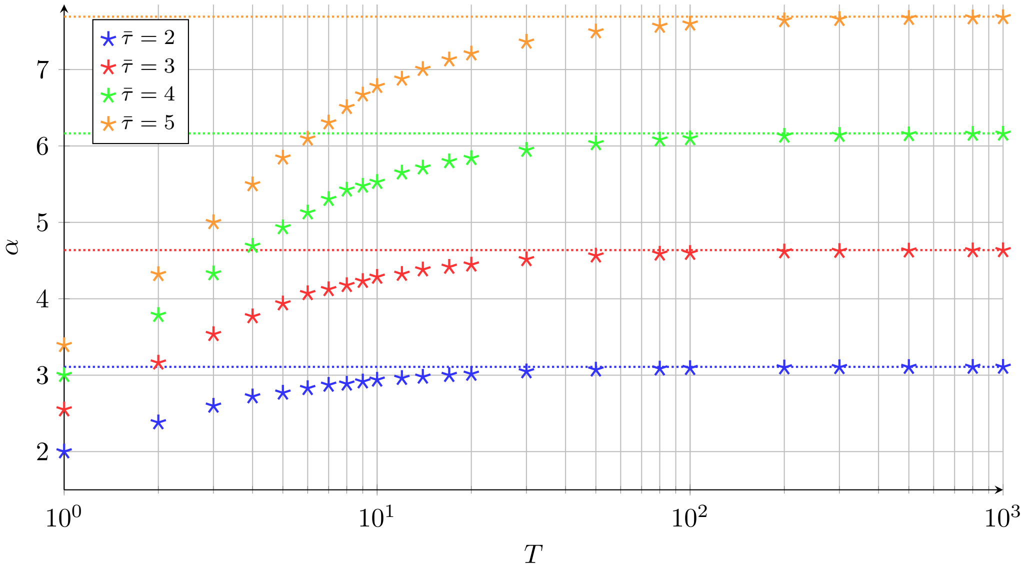

Figure 7.28: Protocol $\mathcal{P}_3$: gains α_T for different $\bar{\tau}$ and T (stars). The associated maximal ℓ_2 gains α are shown using dotted lines.

A comparison of all three protocols is presented in Figure 7.29 to emphasize the relations of the corresponding ℓ_2 gains for $\mathcal{P}_1$, $\mathcal{P}_2$ and $\mathcal{P}_3$.

This completes the proof. ■

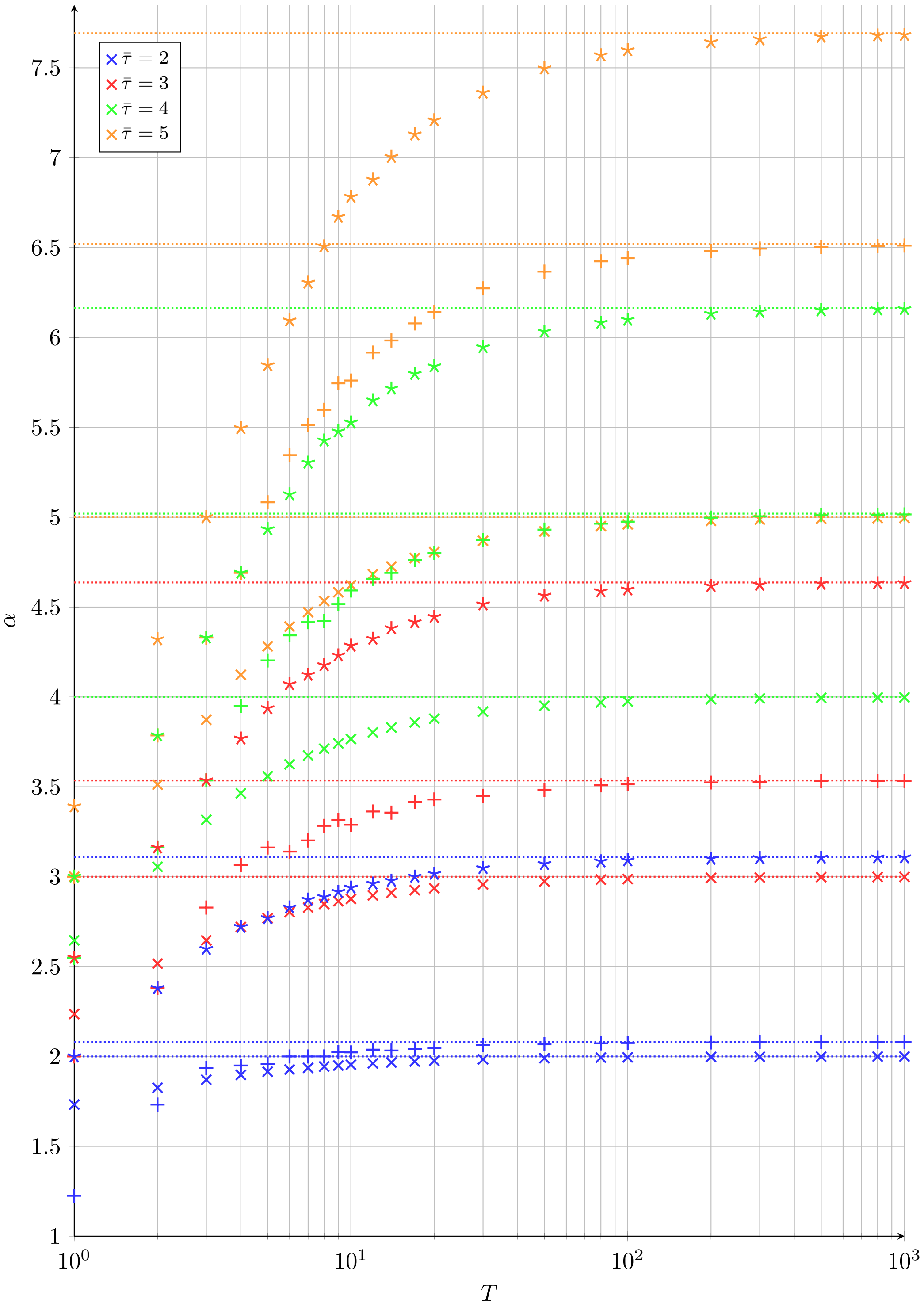

Figure 7.29: Comparison of the gains α_T for different $\bar{\tau}$ and T as well as the corresponding ℓ_2 gains (dotted lines) for all three protocols: $\mathcal{P}_1$ (crosses), $\mathcal{P}_2$ (plus signs) and $\mathcal{P}_3$ (stars).

7.3 Simulation Example

Theorem 7.1 is now applied to the feedback loop with Smith predictor, which was introduced in Chapter 1 and Chapter 6. Hence, condition (7.5) is evaluated with $R(z)$ as defined in (6.8) and

$$\hat{D}(z) = z^{-\hat{d}}. \tag{7.36}$$

The finite ℓ_2 gains α are a function of the maximal admissible variable time delays $\bar{\tau}$ and depend on the actual protocol as stated in (7.6). Figures 7.30, 7.31 and 7.32 present the corresponding magnitude plots of $M(z)\alpha$ for protocols $\mathcal{P}_1$, $\mathcal{P}_2$ and $\mathcal{P}_3$, respectively.

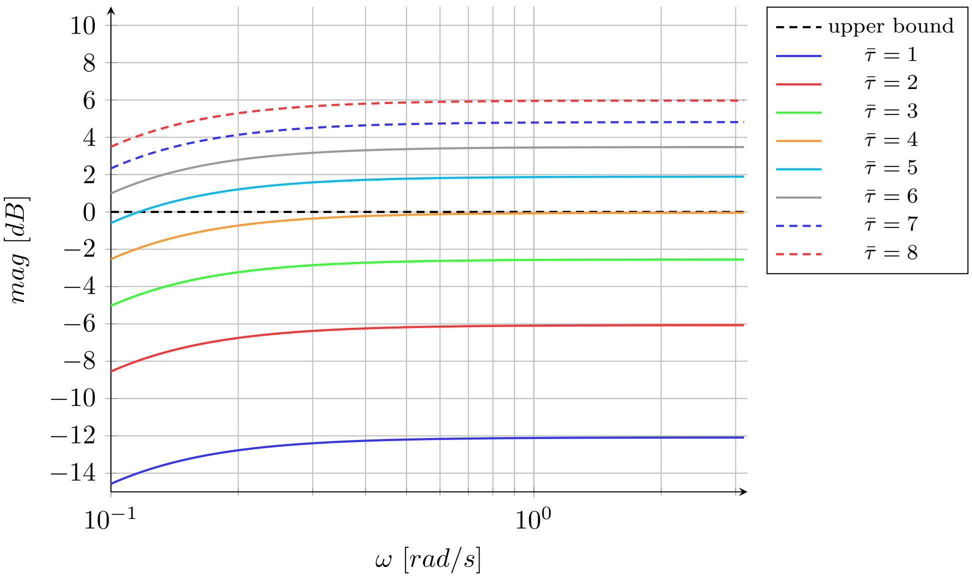

Figure 7.30: Simulation example: Bode magnitude plots of $M(z)\alpha$ in condition (7.5) for protocol $\mathcal{P}_1$.

Since the magnitude plot has to remain below the zero dB line, one gets a maximal time-varying delay of:

(a) $\bar{\tau} = 4$ for protocol $\mathcal{P}_1$ (orange curve in Figure 7.30),

(b) $\bar{\tau} = 3$ for protocol $\mathcal{P}_2$ (green curve in Figure 7.31),

(c) $\bar{\tau} = 2$ for protocol $\mathcal{P}_3$ (red curve in Figure 7.32).

It is evident, that an increased ℓ_2 gain decreases the maximal admissible $\bar{\tau}$.

Figure 7.33 shows the achieved step responses for changes in the reference signal (r_k) of the networked filtered Smith predictor in closed loop with the plant including a nominal delay of $\hat{d} = 5$ and with the worst case pattern τ_j for protocol $\mathcal{P}_3$ as shown in Figure 7.12. Two different scenarios are chosen for $\mathcal{P}_3$ such that either the packet leading to the worst case or a random packet is selected whenever more packets are available at the same time instant.

Please note that Theorem 7.1 provides a more restrictive bound on the time-varying delays when compared to Theorem 6.3. However, the packetized character of the network transmissions is explicitly incorporated into Theorem 7.1 to prevent contradictions between the theoretical statements and actual results for the networked feedback loops if

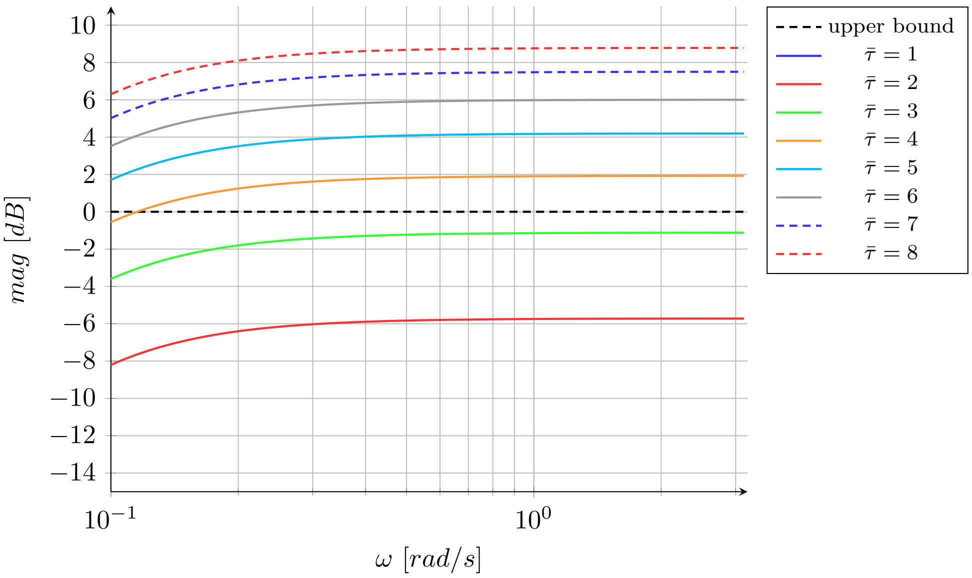

Figure 7.31: Simulation example: Bode magnitude plots of $M(z)\alpha$ in condition (7.5) for protocol $\mathcal{P}_2$.

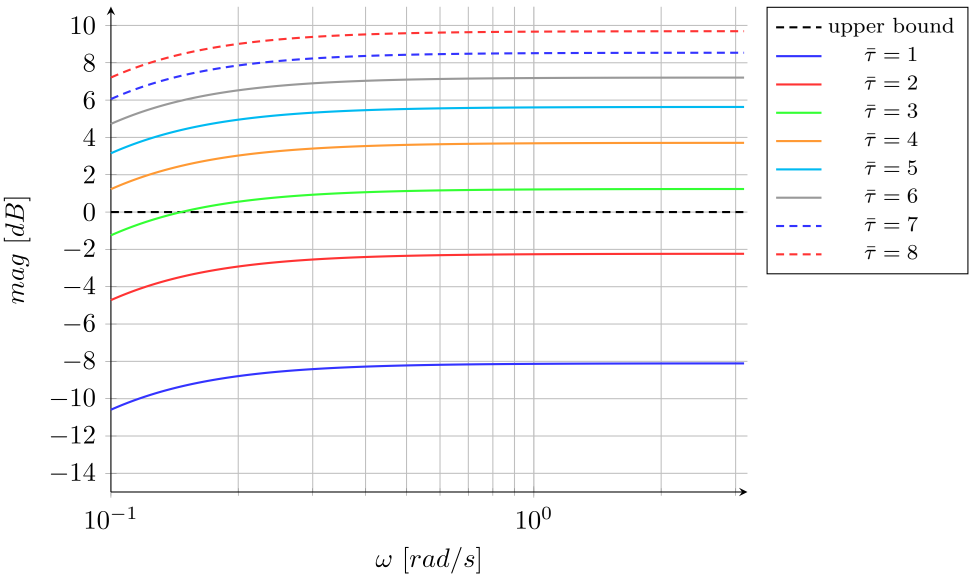

Figure 7.32: Simulation example: Bode magnitude plots of $M(z)\alpha$ in condition (7.5) for protocol $\mathcal{P}_3$.

different protocols are utilized. This is not the case for the LMI-based Theorem 6.3 as can be seen in the simulation example in Section 6.2.2.

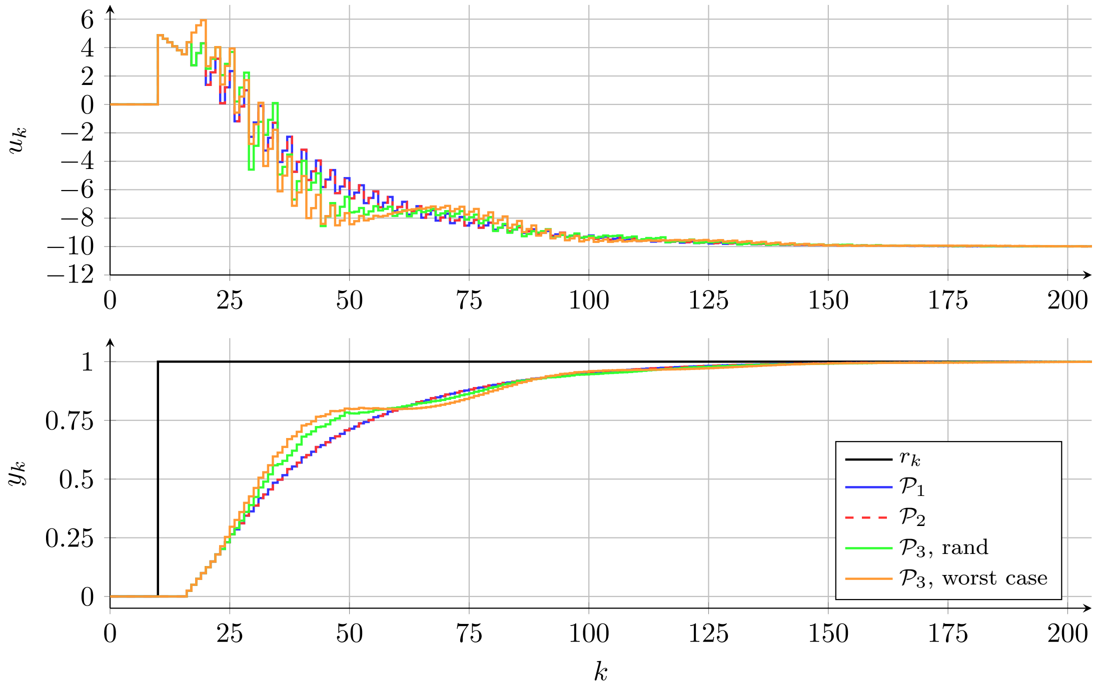

Figure 7.33: Simulation example: step responses of the closed networked loop as in Figure 6.3 for different protocols (2.38) and a network induced packet pattern as in Figure 7.12 with $\bar{\tau} = 2$.

7.4 Laboratory Experiment

The application of Theorem 7.1 is also shown using a real-world laboratory experiment presented in Figure 7.34. It consists of a dc-motor that winds up a cord, which is fixed at the left hand side of a spring with spring constant c. The other side of the spring is attached to another cord that is connected via a pulley with a viscous friction coefficient

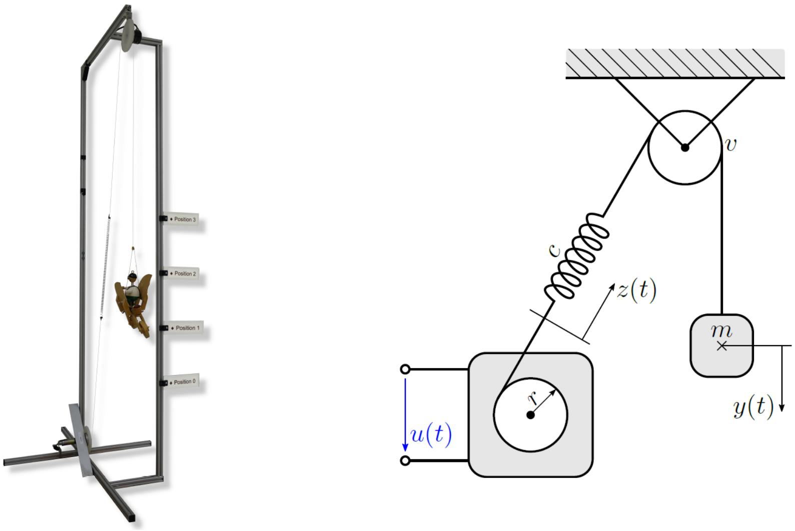

Figure 7.34: Photo and schematic structure of the laboratory setup (form [LRSH19]).

v to a mass m.

The application of an input voltage $-5\,V \leq u(t) \leq 5\,V$ to the motor allows to lift the mass in y-direction as indicated in Figure 7.34. Due to a low level motor controller, the position $z(t)$ at the left hand side of the spring is proportional to the integral of input u via constant V. Newton's second law of motion yields a mathematical model of the considered mass spring system as

$$\frac{\mathrm{d}x(t)}{\mathrm{d}t} = \begin{bmatrix} 0 & 1 & 0 \\ -\frac{c}{m} & -\frac{v}{m} & \frac{c}{m} \\ 0 & 0 & 0 \end{bmatrix} x(t) + \begin{bmatrix} 0 \\ 0 \\ V \end{bmatrix} u(t)\,, \tag{7.37}$$

with state variables $z(t)$, $y(t)$ and $\dot{y}(t)$, i.e.

$$x = \begin{bmatrix} y & \frac{\mathrm{d}y}{\mathrm{d}t} & z \end{bmatrix}^{\mathrm{T}}\,. \tag{7.38}$$

The output variable is defined as the vertical mass position $y(t)$. The mass of $m = 0.19\,kg$ was measured; all other parameters were identified using experimental data and are given by $V = 0.2702\,mV^{-1}s^{-1}$, $c = 5.4285\,Nm^{-1}$ and $v = 0.0489\,kgs^{-1}$. In addition, a nominal plant delay of five time steps, i.e. $\hat{d} = 5$ is introduced. Matlab/Simulink [MAT] with the additional control software QUARC [QUA] is utilized to connect the lab setup to the computer, where the introduced filtered Smith predictor structure is implemented with a sampling interval of $h = 0.1\,s$.

To be able to introduce network induced packed delays in a reproducible way (for all protocols), the simulation framework presented in Chapter 3 is put to use in the laboratory. A nominal controller is designed for the nominal, delay-free, discretized plant

$$\hat{P}(z) = \frac{0.0012604\,(z+3.647)\,(z+0.2707)}{(z-1)\,\left(z^2-1.699z+0.9746\right)} \tag{7.39}$$

such that its weakly damped conjugate complex poles are compensated and replaced by desired ones. This yields the nominal controller

$$C(z) = \frac{18.652(z^2-1.699z+0.9746)}{(z-0.3012)^2}\,, \tag{7.40}$$

which leads to the step response of the nominal closed loop as in Figure 7.35.

The remaining transfer functions $F(z)$ and $H(z)$ needed for the filtered Smith predictor follow from (6.9), (6.10) and (6.11) such that

$$F(z) = \frac{1.5}{(z+0.5)} \tag{7.41}$$

and

$$H(z) = \frac{0.0012604\,(z+1.174)\,(z+3.647)\,(z+0.2707)\,\left(z^2+1.248z+1.217\right)}{z^5\,(z+0.5)} \cdot \frac{\left(z^2-0.9216z+1.05\right)}{\left(z^2-1.699z+0.9746\right)}\,. \tag{7.42}$$

Details about the design can be found in Appendix A.

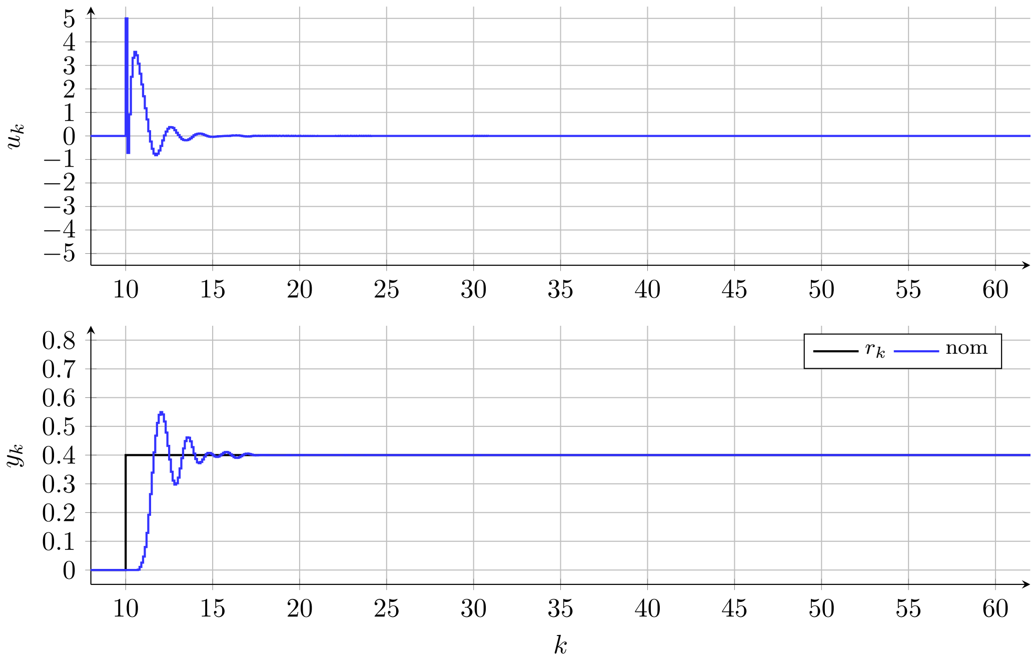

Figure 7.35: Experiment: nominal step response (bottom plot, blue) to reference input (r_k) (black) and the corresponding actuating signal (u_k) (top).

Theorem 7.1 is evaluated in the next step to find the maximal admissible bound $\bar{\tau}$ for the time-varying packet delays τ_j. Figures 7.36 and 7.37 reveal that

(a) $\bar{\tau} = 2$ for protocol $\mathcal{P}_1$ (red curve in Figure 7.36),

(c) $\bar{\tau} = 1$ for protocol $\mathcal{P}_3$ (blue curve in Figure 7.37).

Case (b), i.e. protocol $\mathcal{P}_2$, is not considered here because it represents an intermediate case with respect to the corresponding finite ℓ_2 gain.

Figure 7.38 show measurement results of step responses, where different $\bar{\tau}$ are used. As shown in Section 7.1, constant packet delays constitute the worst case scenario for $\mathcal{P}_1$ and are, thus, realized for this experiment. Larger variable time delays degrade the closed loop performance when compared to the nominal behavior in Figure 7.35 and lead to instability for $\bar{\tau} = 3$, as foreseen by Theorem 7.1.

An evaluation of Theorem 7.1 suggests that the maximal admissible, stabilizing network delay is given by $\bar{\tau} = 1$ for protocol $\mathcal{P}_3$. The corresponding worst case sequence (shown in Figure 7.12) is utilized for the experiments in this case. However, the output (y_k) converges to its desired value in Figure 7.39 for $\bar{\tau} = 2$ as well. An enlarged value of $\bar{\tau} = 3$ results in an unstable behavior. Please note that the introduced theorem is sufficient and therefore might lead to conservative results as for the experimental setup for protocol $\mathcal{P}_3$. A strategy to reduce the introduced conservatism is proposed in Chapter 8.

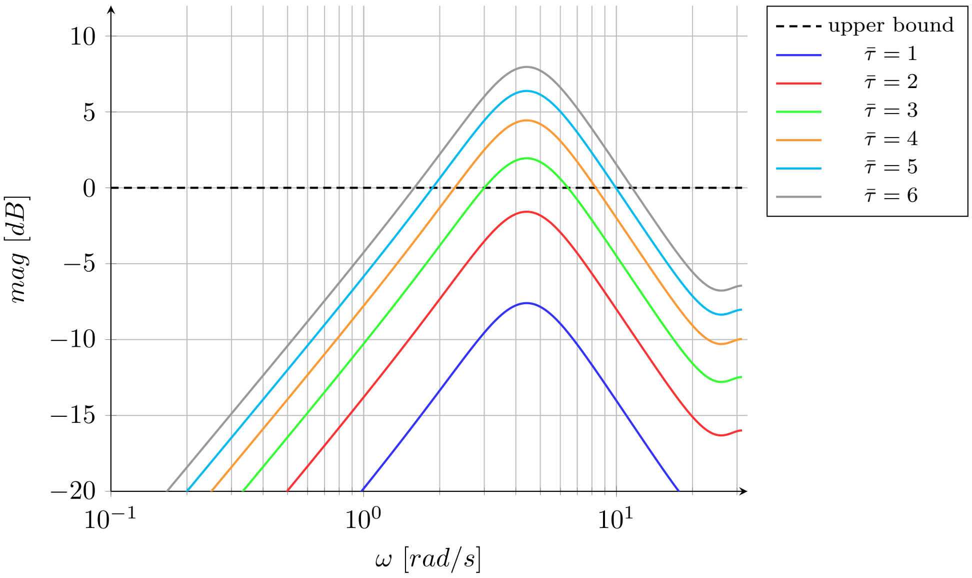

Figure 7.36: Experiment: Bode magnitude plots of $M(z)\alpha$ in condition (7.5) for protocol $\mathcal{P}_1$

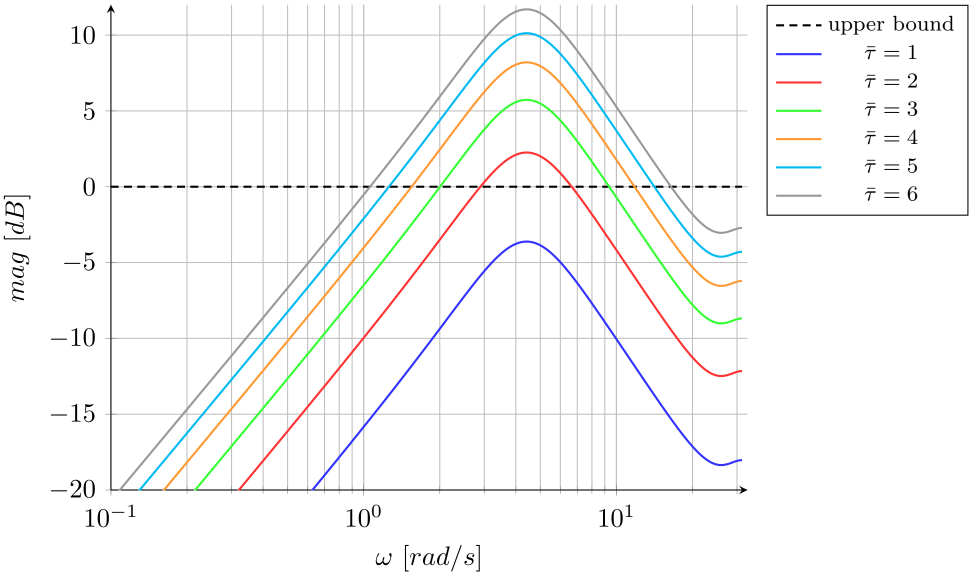

Figure 7.37: Experiment: Bode magnitude plots of $M(z)\alpha$ in condition (7.5) for protocol $\mathcal{P}_3$

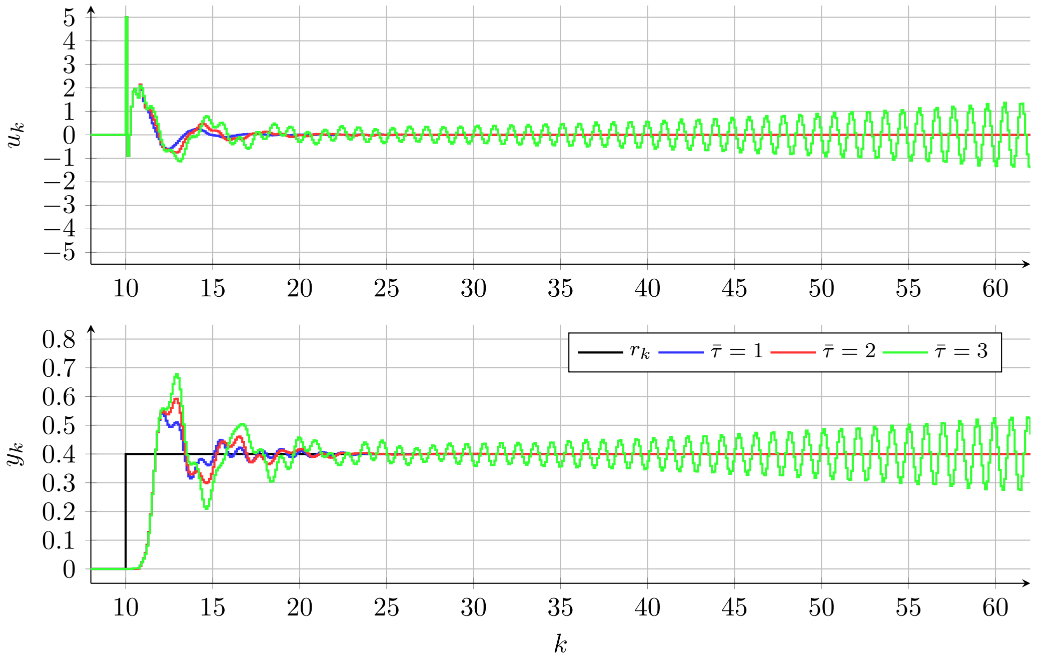

Figure 7.38: Experiment: step responses (y_k) and actuating signals (u_k) for different maximal admissible $\bar{\tau}$ utilizing protocol $\mathcal{P}_1$.

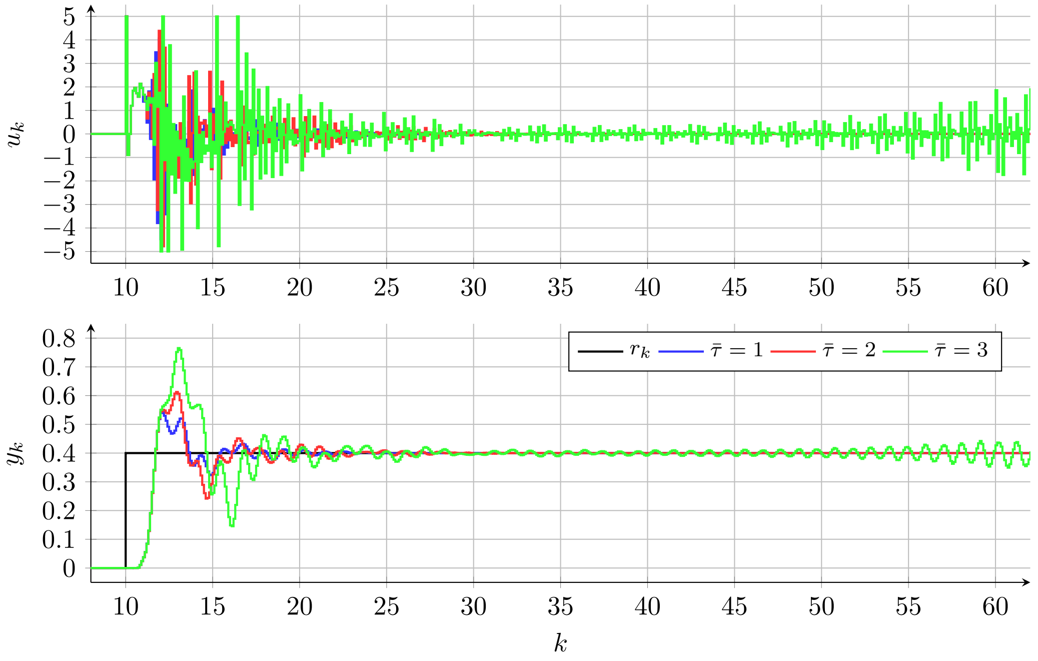

Figure 7.39: Experiment: step responses (y_k) and actuating signals (u_k) for different maximal admissible $\bar{\tau}$ utilizing protocol $\mathcal{P}_3$.

7.5 SGT-based Stability Criterion for uncertain Plants

The stability criterion introduced in Section 7.1 is extended in the following to uncertain plant models. For that purpose, the plant model (6.1) is modified to account for uncertainties such that

$$P(z) = \hat{P}(z)z^{-\hat{d}}\big(1 + \delta P\big)\,, \tag{7.43}$$

consists of a nominal, delay-free part $\hat{P}(z)$, a nominal constant time delay $\hat{d}$ and a multiplicative uncertainty represented by δP.

The underlying stability analysis is then based on the block diagram in Figure 7.40, which is a modification of the structure shown in Figure 7.1. Using sequences $(e_{P,k})$, $(y_{P,k})$ as well as $(e_{\tau,k})$, $(y_{\tau,k})$, Figure 7.40 can be drawn as depicted in Figure 7.41. Additional input signals $(u_{1,k})$, $(u_{2,k})$, $(u_{P,k})$ and (u_{τ_k}) are introduced and exploited in the proof of the following theorem. Parameters α stand for the various ℓ_2 gains between different inputs and outputs of the three considered blocks.

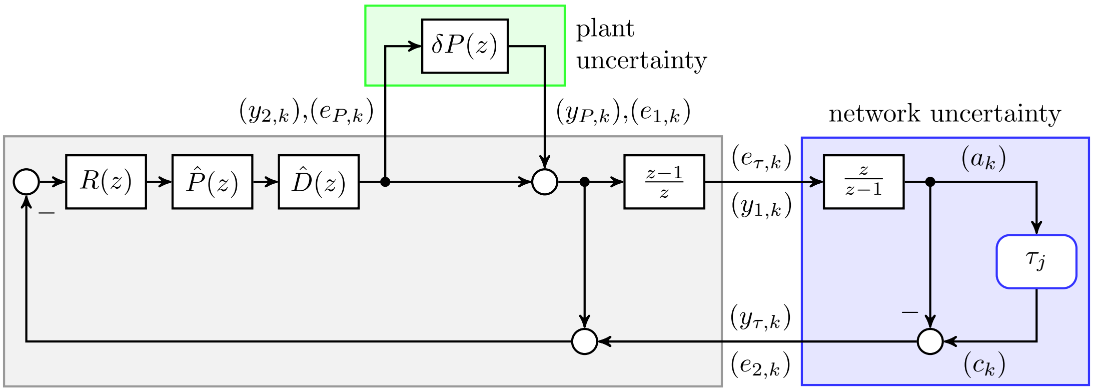

Figure 7.40: Decomposition of the networked feedback loop into a nominal part (gray), one uncertainty related to time-varying packet delays (blue) and a second block δP accounting for plant uncertainties (green).

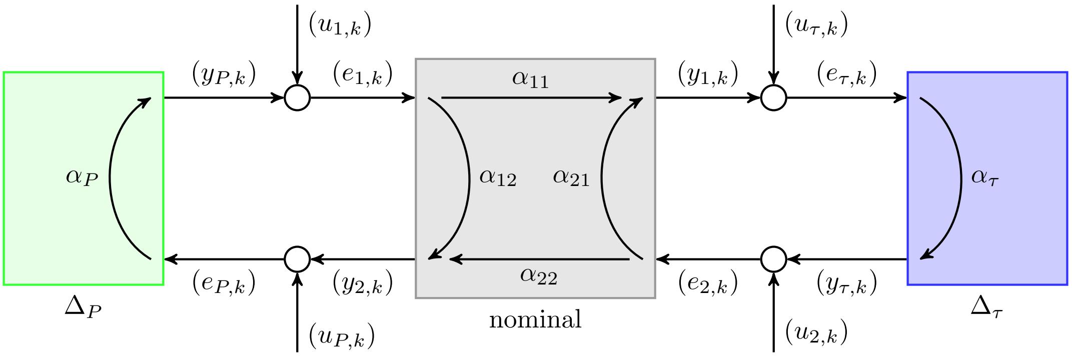

Figure 7.41: Three block structure consisting of a nominal block (gray), a block Δ_P representing the plant uncertainties (green) and a block Δ_τ including the networked induced variable packet delays (blue).

Theorem 7.3 (Stability criterion, uncertain plant [SH20])**.** *Let the same assumptions hold as in Theorem 7.1 except that plant model* (7.43) *is uncertain and* $\left|\left|\delta P\right|\right|_\infty \leq \alpha_P > 0$*. In addition, conditions*

$$\alpha_P \alpha_{12} + \frac{\alpha_P \alpha_\tau \alpha_{11} \alpha_{22}}{1 - \alpha_\tau \alpha_{21}} < 1 \ , \qquad \alpha_\tau \alpha_{21} < 1 \tag{7.44a}$$

$$\alpha_\tau \alpha_{21} + \frac{\alpha_P \alpha_\tau \alpha_{11} \alpha_{22}}{1 - \alpha_P \alpha_{12}} < 1 \ , \qquad \alpha_P \alpha_{12} < 1 \tag{7.44b}$$

hold, where

$$\alpha_{11} = \left|\left|\hat{S}(z)\frac{(z-1)}{z}\right|\right|_\infty , \qquad \alpha_{12} = \left|\left|\hat{T}(z)\right|\right|_\infty \tag{7.45a}$$

$$\alpha_{21} = \left|\left|\hat{T}(z)\frac{(z-1)}{z}\right|\right|_\infty , \qquad \alpha_{22} = \left|\left|\hat{T}(z)\right|\right|_\infty \tag{7.45b}$$

$$\hat{T}(z) = \frac{R(z)\hat{P}(z)}{1 + R(z)\hat{P}(z)} , \qquad S(z) = \frac{1}{1 + R(z)\hat{P}(z)} \tag{7.45c}$$

as shown in Figure 7.41. Parameter α_τ *equals* α *from* (7.6)*, depending on the chosen protocol* (2.38)*.*

Then, the feedback loop in Figure 6.1 consisting of a linear controller $R(z)$*, the uncertain plant* (7.43) *and the packetized transmission network is finite gain* ℓ_2 *stable for all time-varying bounded packet delays* $0 \leq \underline{\tau}^N \leq \tau_j^N \leq \bar{\tau}^N$ *and* $\bar{\tau}^N > \underline{\tau}^N$*.*

Proof. The proof follows the same main idea that is usually used to prove the SGT, see, e.g., [Sas99]. Hence, the structure in Figure 7.41 is analyzed using the corresponding ℓ_2 gains. It is shown that all signals in this three-block structure are bounded as long as all input signals are bounded. The plant uncertainty and the uncertainty due to the time-varying packet delays can be cast into a form as in Definition 6.7 such that

$$\left|\left|(y_{P,k})_T\right|\right|_2 \leq \alpha_P \left|\left|(e_{P,k})_T\right|\right|_2 + \beta_P \, , \tag{7.46a}$$

$$\left|\left|(y_{\tau,k})_T\right|\right|_2 \leq \alpha_\tau \left|\left|(e_{\tau,k})_T\right|\right|_2 + \beta_\tau \tag{7.46b}$$

hold. Due to linearity, the input-output behavior of the nominal block in Figure 7.41 can be written as

$$\left|\left|(y_{1,k})_T\right|\right|_2 \leq \alpha_{11} \left|\left|(e_{1,k})_T\right|\right|_2 + \beta_{11} + \alpha_{21} \left|\left|(e_{2,k})_T\right|\right|_2 + \beta_{21} \, , \tag{7.47a}$$

$$\left|\left|(y_{2,k})_T\right|\right|_2 \leq \alpha_{12} \left|\left|(e_{1,k})_T\right|\right|_2 + \beta_{12} + \alpha_{22} \left|\left|(e_{2,k})_T\right|\right|_2 + \beta_{22} \, . \tag{7.47b}$$

To prove Theorem 7.3, one has to show that all inner signals, as e.g. $e_{1,k} = u_{1,k} + y_{P,k}$, are bounded. Thus, taking into account (7.46a) yields

$$\left|\left|(e_{1,k})_T\right|\right|_2 \leq \left|\left|(u_{1,k})_T\right|\right|_2 + \alpha_P \left|\left|(e_{P,k})_T\right|\right|_2 + \beta_P \tag{7.48}$$

and relation $e_{P,k} = u_{P,k} + y_{2,k}$ results in

$$\left|\left|(e_{P,k})_T\right|\right|_2 \leq \left|\left|(u_{P,k})_T\right|\right|_2 + \alpha_{12} \left|\left|(e_{1,k})_T\right|\right|_2 + \beta_{12} + \alpha_{22} \left|\left|(e_{2,k})_T\right|\right|_2 + \beta_{22} \, . \tag{7.49}$$

Incorporating $e_{2,k} = u_{2,k} + y_{\tau,k}$ and $e_{\tau,k} = u_{\tau,k} + y_{1,k}$ together with relations (7.46b) and (7.47a) yields

$$||(e_{2,k})_T||_2 (1 - \alpha_\tau \alpha_{21}) \leq \delta_1 + \alpha_\tau \alpha_{11} ||(e_{1,k})_T||_2 \tag{7.50}$$

with

$$\delta_1 = ||(u_{2,k})_T||_2 + \alpha_\tau ||(u_{\tau,k})_T||_2 + \beta_\tau + \alpha_\tau (\beta_{11} + \beta_{21}) \tag{7.51}$$

and so

$$||(e_{1,k})_T||_2 \left(1 - \alpha_P \alpha_{21} - \frac{\alpha_P \alpha_\tau \alpha_{11} \alpha_{22}}{1 - \alpha_\tau \alpha_{21}}\right) \leq \delta_2 \tag{7.52}$$

where

$$\delta_2 = ||(u_{1,k})_T||_2 + \beta_P + \alpha_P \left(||(u_{P,k})_T||_2 + \beta_{12} + \beta_{22} + \frac{\alpha_{22}\delta_1}{1 - \alpha_\tau \alpha_{21}}\right). \tag{7.53}$$

As a result, error $(e_{1,k})$ is norm-bounded for bounded input signals $||(u_{1,k})_T||_2$, $||(u_{2,k})_T||_2$, $||(u_{P,k})_T||_2$ and $||(u_{\tau,k})_T||_2$ if

$$1 - \alpha_P \alpha_{21} - \frac{\alpha_P \alpha_\tau \alpha_{11} \alpha_{22}}{1 - \alpha_\tau \alpha_{21}} > 0 \qquad \text{for} \qquad 1 - \alpha_\tau \alpha_{21} > 0 \tag{7.54}$$

that constitute condition (7.44a) in Theorem 7.3. Analogue steps are followed to show that the remaining $||(e_{i,k})_T||_2$ and $||(y_{i,k})||_2$, $i \in \{1, 2, P, \tau\}$, are bounded for bounded inputs $||(u_{i,k})||_2$.

The gains α_{11}, α_{12}, α_{21} and α_{22} (7.45) directly follow by computing the transfer functions corresponding to Figure 7.40. This completes the proof. ■

Please note that conditions (7.44) and (7.45) collapse to condition (7.5) of Theorem 7.1 for the case without uncertainties in the plant, i.e. $\delta P = 0$, or equivalently, $\alpha_P = 0$.

Note that conditions (7.44), (7.45) reduce to the classical formulation of the SGT presented in [Sas99] applied to the filtered Smith predictor if no network with time-varying packet delays is present. In this case, the blue block in Figure 7.40 representing the uncertainty due to the variable time delay is replaced by a direct connection resulting in $\alpha_\tau = 0$.

7.6 Simulation example with uncertain Plant Model

Theorem 7.3 is now applied to the simulation example with filtered Smith predictor that is used for a known plant model, i.e. $\delta P = 0$, in Section 7.3. Therefore, the original, continuous-time plant model

$$P(s) = \frac{0.1}{20s - 1} e^{-5s}. \tag{7.55}$$

is considered as uncertain in either the gain $K = 0.1$ or in the time constant $T = 20$. This means that, e.g., the gain K is multiplied by a factor $0.8 \leq f \leq 1.2$ in the analysis resulting in different transfer functions $P(z)$ such that the plant uncertainty

$$\delta P(z) = \frac{P(z)}{\hat{P}(z)} - 1 \tag{7.56}$$

describes the deviation from the nominal plant transfer function $P(z)$ to determine gain α_P for the analysis.

For the filtered Smith predictor with

$$R(z) = \frac{C(z)F(z)}{1 + C(z)H(z)} \tag{7.57}$$

as defined in (6.8), conditions (7.45) turn into

$$\alpha_{11} = \left|\left|\hat{S}(z)\frac{(z-1)}{z}\right|\right|_\infty, \qquad \alpha_{12} = \left|\left|F(z)\hat{T}(z)\right|\right|_\infty \tag{7.58a}$$

$$\alpha_{21} = \left|\left|F(z)\hat{T}(z)\frac{(z-1)}{z}\right|\right|_\infty, \qquad \alpha_{22} = \left|\left|F(z)\hat{T}(z)\right|\right|_\infty \tag{7.58b}$$

with

$$\hat{T}(z) = \frac{C(z)\hat{P}(z)}{1 + C(z)\hat{P}(z)}F(z) \quad \text{and} \quad \hat{S}(z) = \frac{1 + C(z)H(z)}{1 + C(z)\hat{P}(z)}, \tag{7.59}$$

where the fact that $||\hat{D}(z)|| = 1$ is taken into account. Figure 7.42 presents the maximal $\bar{\tau}$ for the three considered protocols, where a multiplicative factor out of the range between 0.8 and 1.2 is chosen. It can be clearly seen that the achieved shape is symmetric around the nominal gain value. Protocol $\mathcal{P}_1$ yields the largest range for the time varying network delays, whereas $\mathcal{P}_3$ yields the smallest values $\bar{\tau}$, i.e. the largest sensitivity with respect to time-varying delays.

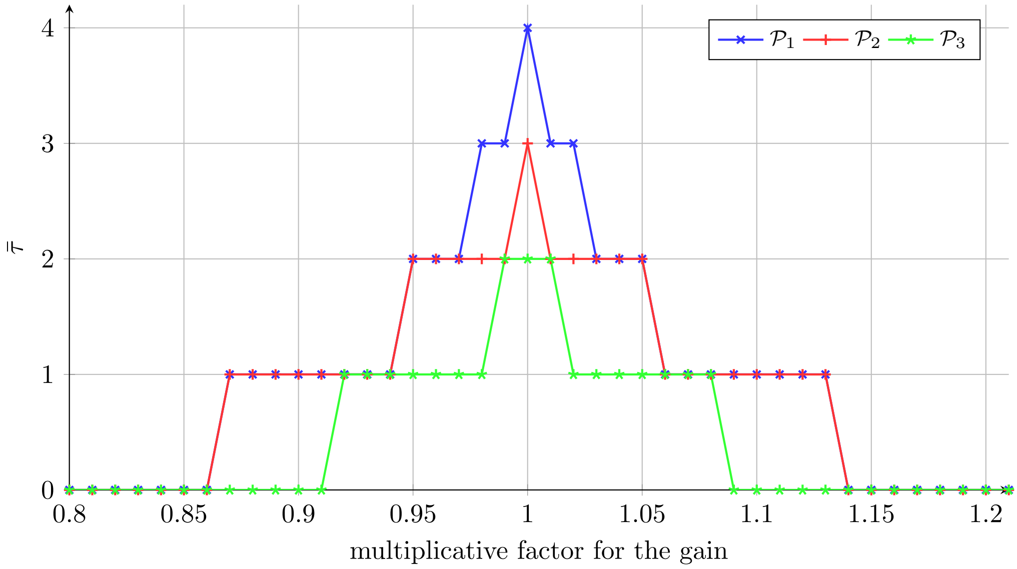

Figure 7.42: Example with uncertain plant model: maximal admissible variable time delay $\bar{\tau}$ for different multiplicative factors for the *gain* and different protocols.

The results for the case with uncertain information of the time constant T is shown in Figure 7.43 for multiplicative factors between 0.8 and 1.2. In contrast to the variation of the gain, a variation of the time constant results in a not symmetric shape. However, the results for $\mathcal{P}_1$ constitute the maximal achievable bound for the variable time delay, whereas $\mathcal{P}_3$ yield the lowest, worst case values for $\bar{\tau}$ according to Theorem 7.3.

The analysis presented for this example can also extended to different $P(z)$ representing other uncertain plant models.

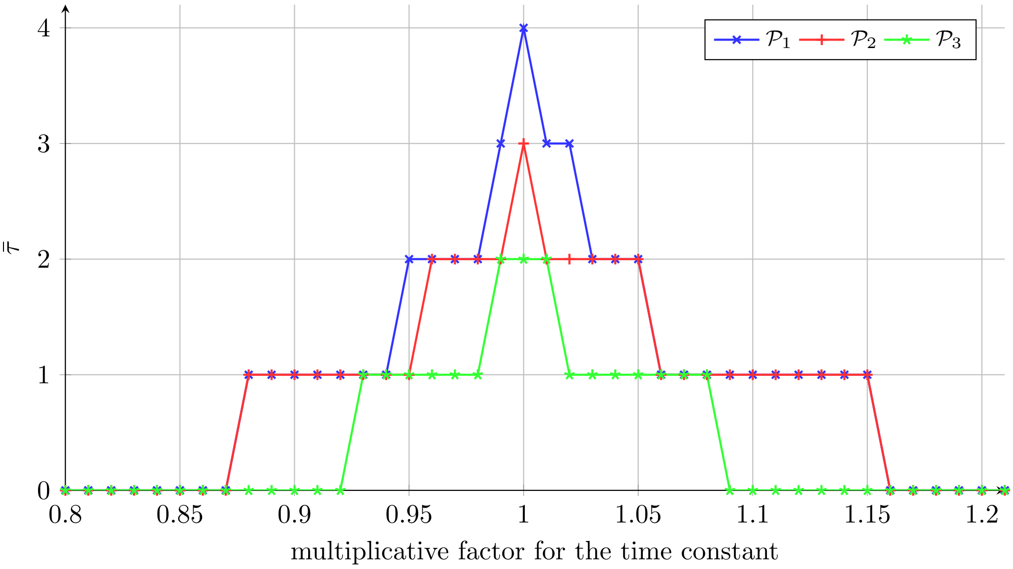

Figure 7.43: Example with uncertain plant model: maximal admissible variable time delay $\bar{\tau}$ for different multiplicative factors for the *time constant* and different protocols.

Chapter 8

SGT-based Stability Analysis using acausal Subsystems

In the previous chapter, sufficient stability criteria for networked feedback loops subject to time-varying packet delays are considered. The results might be conservative in some cases as the criteria are based on the small gain theorem. This chapter aims to reduce the conservatism of the introduced approaches and is adopted from [SH21a].

This is possible via the optimal choice of a nominal constant time delay, which is used in the design of the nominal controller. As a consequence, a splitting of the feedback loop into a causal and an acausal subsystem is used in the derivation of the criterion to minimize the effect of the uncertain variable delay. The enhanced criterion features the same properties as the basic versions such as, e.g., its easy-to-use nature.

8.1 Modified Problem Setup

The original problem setup is described in detail in Section 6.1. Here, only the differences that are needed to reduce the conservatism of Theorem 7.1 are introduced for the case without plant uncertainties, i.e. $\delta P = 0$. A generalization of the theorem presented in this chapter to uncertain plant model follows the same lines of argumentation as Theorem 7.3 and is omitted here.

A combination of plant delay (6.1) and network delay (6.4) results in a constant time delay $\hat{d} + \underline{\tau}_N$ and a time-varying delay that is bounded such that

$$0 \leq \underbrace{\tau_j^N - \underline{\tau}^N}_{\tau_j} \leq \bar{\tau}^N - \underline{\tau}^N = \bar{\tau}\,, \tag{8.1}$$

see also Assumption 6.2. For the nominal controller design and stability analysis presented below, an additional constant acausal time delay $\tau_A \in \mathbb{N}$ is introduced, yielding a modified constant time delay

$$\hat{\tau} = \hat{d} + \underline{\tau}^N + \tau_A \tag{8.2}$$

and a (usually) acausal time-varying delay

$$-\tau_A \leq \tau_j - \tau_A \leq \bar{\tau} - \tau_A \tag{8.3}$$

for the overall delays of plant and communication network. The specific choice of $\tau_A = 0$ constitutes the causal case as presented in Chapter 7.

The task is now to state less conservative stability conditions for protocols $\mathcal{P}_1$ and $\mathcal{P}_3$ when compared to Theorem 7.1. Protocol $\mathcal{P}_2$ is not considered in this chapter because it constitutes an intermediate case between $\mathcal{P}_1$ and $\mathcal{P}_3$. However, the criterion presented below can also be formulated for $\mathcal{P}_2$ using the same ideas.

The main ingredients are the optimal selection for the acausal delay τ_A and the calculation of the resulting finite ℓ_2 gains. This makes it possible to state less conservative conditions that yield a larger range of admissible time-varying packet delays.

8.2 SGT-based Stability Criterion using acausal Subsystems

The proposed stability criterion rests on the separation of the original structure, presented in Figure 6.1 with controller (6.6), into a nominal part (gray in Figure 8.1) and a part characterizing the uncertainty due to the time-varying packet delays (blue block in Figure 8.1). In addition, the reference input (r_k) is zero and the remaining linear controller in Figure 6.1 is represented by transfer function $R(z)$. A discrete-time integrator and differentiator are utilized to avoid issues for the case, where the nominal controller $R(z)$ is designed to achieve a dc-gain equal to one for the nominal loop as explained in Chapter 7. The effect of the known constant time delay $\hat{\tau}$ (8.2) is included in the nominal (gray) part via transfer function

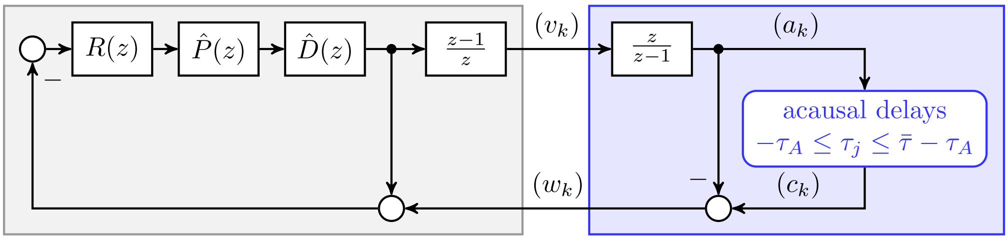

Figure 8.1: Restructured feedback loop that is used for the stability analysis: nominal part (gray) and uncertainty due to the (acausal) time-varying delays (blue).

$$\hat{D}(z) = z^{-\hat{d} - \underline{\tau}^N - \tau_A} = z^{-\hat{\tau}} \, . \tag{8.4}$$

Note that the acausal delay τ_A also appears in (8.4) due to (8.2).

Based on [UI08] where an SGT for continuous-time systems with acausal subsystems is introduced, one can now state the discrete-time SGT for the feedback loop shown in Figure 6.9 with $(u_{1,k}), (u_{2,k}) \in \ell_2[a, \infty)$ and $(e_{1,k}), (e_{2,k}), (y_{1,k}), (y_{2,k}) \in \ell_{2e}[a, \infty)$. The nominal part and the uncertainty are characterized by mappings $(y_{1,k}) = \mathcal{M}_1\{(e_{1,k})\}$ and $(y_{2,k}) = \mathcal{M}_2\{(e_{2,k})\}$ respectively. They are assumed to be finite gain ℓ_2 stable in the sense of Definition 6.8, i.e.

$$\left|\left|(y_{1,k})\right|\right|_2 \leq \alpha_1 \left|\left|(e_{1,k})\right|\right|_2 + \beta_1 \qquad \forall (e_{1,k}) \in \ell_2[a, \infty) \, , \tag{8.5a}$$
$$\left|\left|(y_{2,k})\right|\right|_2 \leq \alpha_2 \left|\left|(e_{2,k})\right|\right|_2 + \beta_2 \qquad \forall (e_{2,k}) \in \ell_2[a, \infty) \; . \tag{8.5b}$$

If both mappings are causal, the classical SGT as stated in [Vid02], [Sas99] can be applied. However, for the stability analysis of networked control systems as considered in this work, it will turn out to be beneficial that one subsystem is acausal.

Theorem 8.1 (Acausal SGT for discrete-time systems [SH21a])**.** *Consider the feedback loop shown in Figure 6.9 with finite ℓ_2 gains* (8.5)*. Let*

$$\alpha_1\alpha_2 < 1 \tag{8.6}$$

and conditions

$$\Big(\mathcal{M}_1\Big\{\mathcal{M}_2\big\{(e_{2,k})\big\}\Big\}\Big)_T = \Big(\mathcal{M}_1\Big\{\mathcal{M}_2\big\{(e_{2,k})_T\big\}\Big\}\Big)_T \tag{8.7a}$$

$$\Big(\mathcal{M}_2\Big\{\mathcal{M}_1\big\{(e_{1,k})\big\}\Big\}\Big)_T = \Big(\mathcal{M}_2\Big\{\mathcal{M}_1\big\{(e_{1,k})_T\big\}\Big\}\Big)_T \tag{8.7b}$$

and

$$\left\|\Big(\mathcal{M}_\nu\Big\{(e^{(1)}_{\nu,k}) + (e^{(2)}_{\nu,k})\Big\}\Big)_T\right\|_2 \leq \left\|\Big(\mathcal{M}\}_\nu\Big\{(e^{(1)}_{\nu,k})_T\Big\}\Big)_T\right\|_2 + \left\|\Big(\mathcal{M}_\nu\Big\{(e^{(2)}_{\nu,k})_T\Big\}\Big)_T\right\|_2, \tag{8.7c}$$

hold for all $(e_{\nu,k}), (e^{(1)}_{\nu,k}), (e^{(2)}_{\nu,k}) \in \ell_{2e}[a,\infty)$ *and* $\nu \in \{1,2\}$*.*

Then, the closed loop system is finite gain ℓ_2 stable.

Proof. The proof directly follows as discrete-time counterpart of the continuous-time version from [UI08] evaluated for $n_1 = n_2 = 1$ and $a_1 = a_2 = a$. ■

Conditions (8.7a) and (8.7b) ensure that the cascade connection of $\mathcal{M}_1$ and $\mathcal{M}_2$ (and vice versa) is causal. For example, $(y_{1,k}) = \mathcal{M}_1\{(e_{1,k})\} = \mathcal{M}_1\{(u_{1,k}) + (y_{2,k})\} = \mathcal{M}_1\{(u_{1,k}) + \mathcal{M}_2\{(e_{2,k})\}$ has to be causal according to Definition 6.6 for $(u_{1,k})$ identically to zero as claimed in (8.7a). Please note that condition (8.7c) is automatically fulfilled if both subsystems in Figure 6.9 are linear.

Theorem 8.1 establishes the basis for the proposed stability criterion for feedback loops as depicted in Figure 6.1. The nominal part with input (w_k) and output (v_k) in Figure 8.1 can be described by transfer function

$$M(z) = \frac{-R(z)\hat{P}(z)\hat{D}(z)}{1 + R(z)\hat{P}(z)\hat{D}(z)}\frac{(z-1)}{z} \tag{8.8}$$

with the corresponding finite ℓ_2 gain of $\alpha_1 = ||M(z)||_\infty$. In contrast, it is more challenging to find the ℓ_2 gain $\alpha_2 = \alpha$ of the uncertainty in Figure 8.1. This is because (acausal) time-varying packet delays in combination with protocol $\mathcal{P}_1$ or $\mathcal{P}_3$ have to be considered. Hence, one follows the general procedure proposed in the previous chapter and extends it to include the acausal delay τ_A.

To find the ℓ_2 gain α associated with the uncertainty, on has to maximize the norm of output $w_k = c_k - a_k$, where the sequence (a_k) is the summation of input sequence (v_k). This principle approach is explained in detail in Chapter 7.

Figure 8.2 shows all possible packets on the way for $\bar{\tau} = 3$ and an acausal delay of $\tau_A = 2$. This means that, e.g., the packet containing $a_5 = 6$ might arrive at the receiver side at time instants $k \in \{3,4,5,6\}$ as can be seen in Figure 8.2 (gray packets labeled with number 6). The set of all packets that might arrive at time instant k is $\{b_k^{(-\tau_A)}, b_k^{(-\tau_A+1)}, \dots, b_k^{(\bar{\tau}-\tau_A)}\}$.

k	-3	-2	-1	0	1	2	3	4	5	6	7	8	9	10	11	12	13	14	15	16
$b_k^{(-2)}$	0	1	2	3	4	5	6	7	8	9	10	11	11	11	11	11	11	11	11	11
$b_k^{(1)}$	0	0	1	2	3	4	5	6	7	8	9	10	11	11	11	11	11	11	11	11
$b_k^{(0)} = a_k$	0	0	0	1	2	3	4	5	6	7	8	9	10	11	11	11	11	11	11	11
$b_k^{(1)}$	0	0	0	0	1	2	3	4	5	6	7	8	9	10	11	11	11	11	11	11

Figure 8.2: Packets on the way for $\bar{\tau} = 3$, $\bar{v} = 1$ and $\tau_A = 2$. Darker colors represent more recently received packets.

Depending on the actual protocol, e.g., the most recent packet is selected as c_k and further used. See Definition 2.8 for the properties of the individual protocols as well as relation (7.12) and (7.13) to calculate α_T and the finite ℓ_2 gain α.

Table 8.1 shows the optimal acausal delays τ_A^* that yield a minimization of the related gain α for different maximal delays $\bar{\tau}$ and protocol $\mathcal{P}_3$. With this, we are able to state the main stability criterion for the considered NCS. Details on the calculations of the gains can be found in the proof of Theorem 8.2 in Section 8.3.

Table 8.1: Optimal acausal delays τ_A^* and related ℓ_2 gains $\alpha^* = g(\tau_A^*, \bar{\tau})$ for different maximal admissible variable network delays $\bar{\tau}$ and protocol $\mathcal{P}_3$.

$\bar{\tau}$	α^*	τ_A^*	$\bar{\tau}$	α^*	τ_A^*	$\bar{\tau}$	α^*	τ_A^*
1	1.0000	1	21	19.000	19	41	37.07	37
2	2.0000	2	22	20.000	20	42	38.000	38
3	2.7839	2	23	21.000	21	43	39.000	39
4	3.6878	3	24	21.904	21	44	39.992	39
5	4.6260	4	25	22.784	22	45	40.866	40
6	5.5377	5	26	23.659	23	46	41.738	41
7	6.4254	6	27	24.531	24	47	42.615	42
8	7.3095	7	28	25.411	25	48	43.489	43
9	8.2082	8	29	26.288	26	49	44.362	44
10	9.0921	9	30	27.16	27	50	45.233	45
11	10.000	10	31	28.031	28	51	46.108	46
12	11.000	11	32	29.000	29	52	47.000	47
13	11.955	11	33	30.000	30	53	48.000	48
14	12.845	12	34	30.950	30	54	49.000	49
15	13.734	13	35	31.826	31	55	49.905	49
16	14.614	14	36	32.699	32	56	0.779	50
17	15.488	15	37	33.574	33	57	51.654	51
18	16.369	16	38	34.451	34	58	52.527	52
19	17.250	17	39	35.325	35	59	53.399	53
20	18.125	18	40	36.196	36	60	54.272	54

Theorem 8.2 (Stability criterion for NCS using acausal subsystems [SH21a]). *Consider the networked feedback loop shown in Figure 6.1 with plant* (6.1) *and a packetized transmission network subject to time-varying network delays as in Assumption 6.1. Let the linear controller $\tilde{u}(z) = -\tilde{R}(z)\zeta(z)$ for $(r_k) = 0$ $\forall k$ be designed for a nominal delay $\hat{\tau} = \hat{d} + \underline{\tau}^N + \tau_A^*$ and suppose that acausal delay τ_A^* and the corresponding finite ℓ_2 gain α^* are given such that*

(a) for protocol $\mathcal{P}_1$ (skip old packets, take newest if more packets are available):

$$\tau_A^* = \left\lceil \frac{\bar{\tau}^N + \underline{\tau}^N}{2} \right\rceil \quad or \quad \tau_A^* = \left\lfloor \frac{\bar{\tau}^N + \underline{\tau}^N}{2} \right\rfloor, \tag{8.9a}$$

$$\alpha^* = \alpha_{\mathcal{P}_1}^* = \max\left\{\tau_A^*, \bar{\tau} - \tau_A^*\right\} \tag{8.9b}$$

(b) for protocol $\mathcal{P}_3$ (no numbering nor synchronization, worst case)

$$\alpha^* = \alpha_{\mathcal{P}_3}^* = g\left(\tau_A^*, \bar{\tau}\right) \tag{8.10}$$

and τ_A^* in accordance with the Table 8.1.

The feedback loop is finite gain ℓ_2 stable for all bounded time-varying packet delays $0 \leq \underline{\tau}^N \leq \tau_j^N \leq \bar{\tau}^N$, $\bar{\tau}^N > \underline{\tau}^N$, if condition

$$\left|\left|M(z)\right|\right|_\infty \alpha^* = \left|\left| \frac{R(z)\hat{P}(z)}{1 + R(z)\hat{P}(z)\hat{D}(z)} \frac{(z-1)}{z} \right|\right|_\infty \alpha^* < 1 \tag{8.11}$$

is fulfilled. Constant τ_A^* is the optimal acausal time delay that minimizes the finite ℓ_2 gain α^* for a given $\bar{\tau}$.

Note that relation (8.10) cannot be stated explicitly, as it is also visible in Table 8.1. The steps, how to numerically find optimal values τ_A^* and α^*, are detailed in the next section. However, it is possible to over-estimate the non-linear characteristics in Table 8.1 using results from protocol $\mathcal{P}_1$ so that

$$\tau_A = \bar{\tau} \qquad \text{and} \qquad \alpha = \alpha_{\mathcal{P}_1}\big|_{\tau_A = \bar{\tau}} = \bar{\tau} \tag{8.12}$$

hold for protocol $\mathcal{P}_3$ as depicted in Figure 8.3.

The specific patterns of packet delays leading to the ℓ_2 gains for both protocols are presented in the proof of Theorem 8.2, which is shown in Section 8.3.

For the causal case, i.e. for $\tau_A = 0$, one obtains the same conditions as in Chapter 7. A generalization of the Theorem 8.2 to uncertain plant models of the form $P(z) = \hat{P}(z)z^{-\hat{d}}\big(1 + \delta P\big)$, similar to Theorem 7.3, can be done in a straight forward way.

Please note that the evaluation of Theorem 8.2 follows the same simple principal steps as for Theorem 7.1. The only difference is that a specific selection of $\bar{\tau}$ to be checked leads to a specific acausal delay τ_A^* and, as a consequence, to a new design for the nominal controller $R(z)$ due to (8.4).

Note that both choices of τ_A^* in (8.9a) yield the very same gain α^* (8.9). However, the resulting maximal admissible $\bar{\tau}$ might be different as τ_A^* is included in $D(z)$ and, as a consequence, has an impact on the nominal controller $R(s)$.

The application of Theorem 8.2 is presented for a simulation example in Section 8.4 and for a laboratory experiment in Section 8.5.

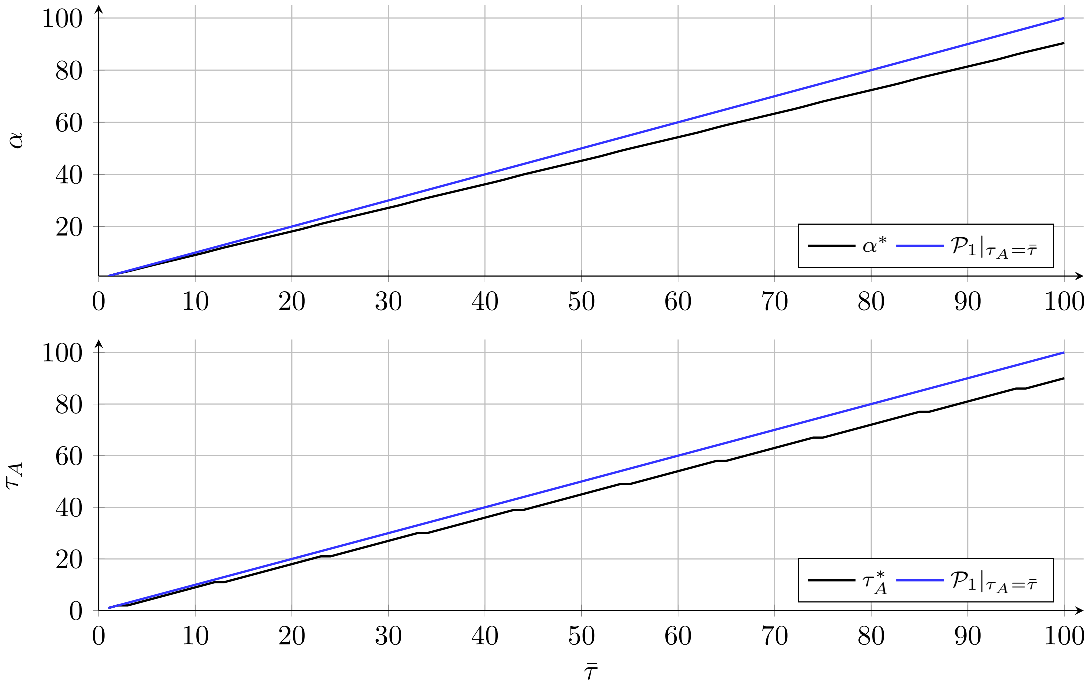

Figure 8.3: Optimal acausal time delay τ_A^* and gain α^* for protocol $\mathcal{P}_3$ (black) and a possible over-estimation (blue).

8.3 Proof of Theorem 8.2

The proof is based on the application of Theorem 8.1 to the feedback structure shown in Figure 8.1. Hence, the gains of the nominal part and the uncertainty due to the time-varying delays are considered. Gain α_1, as defined in (8.5a), is given by

$$\alpha_1 = ||M(z)||_\infty \, , \tag{8.13}$$

where (8.8) is used for the description of the nominal part. Condition (8.7c) is fulfilled for the considered NCS because both subsystems (nominal part and uncertainty) are linear as explained Section 7.2. Since Figure 6.1 is equivalent to Figure 8.1 for $(r_k) = (0, 0, \ldots)$, the cascade connections of both subsystems are causal, as requested by conditions (8.7a) and (8.7b). Consequently, only the calculation of the finite ℓ_2 gain $\alpha^* = \alpha_2$ for the uncertainty remains to show (8.9) and (8.10) in Theorem 8.2. This is done below for the blue subsystem in Figure 8.1 with input v_k (with $\bar{v} = 1$) and output w_k considering protocols $\mathcal{P}_1$ and $\mathcal{P}_3$.

8.3.1 Protocol $\mathcal{P}_1$

Figure 8.4 shows all inner signals as well as the output w_k of the uncertainty for a maximal admissible variable time delay $\bar{\tau} = 3$ and an additional acausal delay $\tau_A = 2$. The input sequence (v_k) and (a_k), are truncated at $T = 10$. To maximize the norm of w_k, all possible packets on the way $\{b_k^{(-\tau_A)}, b_k^{(-\tau_A+1)}, \ldots, b_k^{(\bar{\tau}-\tau_A)}\}$, shown in Figure 8.2, are considered. For example at time instant $k = 0$, the packet containing 3 yields the largest absolute value for $w_k = b_k^{(-2)} - a_k$. Consequently, $a_2 = 3$ has to arrive at time instant $k = 0$, i.e. two time instants before it is sent. Its corresponding packet delay is $\tau_3 = -2$.

k	-3	-2	-1	0	1	2	3	4	5	6	7	8	9	10	11	12	13	14	15	16
$b_k^{(-2)}$	0	1	2	3	4	5	6	7	8	9	10	11	11	11	11	11	11	11	11	11
$b_k^{(1)}$	0	0	1	2	3	4	5	6	7	8	9	10	11	11	11	11	11	11	11	11
$b_k^{(0)} = a_k$	0	0	0	1	2	3	4	5	6	7	8	9	10	11	11	11	11	11	11	11
$b_k^{(1)}$	0	0	0	0	1	2	3	4	5	6	7	8	9	10	11	11	11	11	11	11
$b_k^{(-2)}$	0	1	2	3	4	5	6	7	8	9	10	11	11	11	11	11	11	11	11	11
$b_k^{(-1)}$	0	0	$\cancel{1}$	$\cancel{2}$	$\cancel{3}$	$\cancel{4}$	$\cancel{5}$	$\cancel{6}$	$\cancel{7}$	$\cancel{8}$	$\cancel{9}$	$\cancel{10}$	$\cancel{11}$	$\cancel{11}$	$\cancel{11}$	$\cancel{11}$	$\cancel{11}$	$\cancel{11}$	$\cancel{11}$	$\cancel{11}$
$b_k^{(0)} = a_k$	0	0	0	$\cancel{1}$	$\cancel{2}$	$\cancel{3}$	$\cancel{4}$	$\cancel{5}$	$\cancel{6}$	$\cancel{7}$	$\cancel{8}$	$\cancel{9}$	$\cancel{10}$	$\cancel{11}$	$\cancel{11}$	$\cancel{11}$	$\cancel{11}$	$\cancel{11}$	$\cancel{11}$	$\cancel{11}$
$b_k^{(1)}$	0	0	0	0	$\cancel{1}$	$\cancel{2}$	$\cancel{3}$	$\cancel{4}$	$\cancel{5}$	$\cancel{6}$	$\cancel{7}$	$\cancel{8}$	$\cancel{9}$	$\cancel{10}$	$\cancel{11}$	$\cancel{11}$	$\cancel{11}$	$\cancel{11}$	$\cancel{11}$	$\cancel{11}$
$b_k^{(-2)} - a_k$	0	1	2	2	2	2	2	2	2	2	2	2	1	0	0	0	0	0	0	0
$b_k^{(-1)} - a_k$	0	0	1	1	1	1	1	1	1	1	1	1	1	0	0	0	0	0	0	0
$b_k^{(0)} - a_k$	0	0	0	0	0	0	0	0	0	0	0	0	0	0	0	0	0	0	0	0
$b_k^{(1)} - a_k$	0	0	-0	-1	-1	-1	-1	-1	-1	-1	-1	-1	-1	-1	0	0	0	0	0	0
packet arr.	no	yes	yes	yes	yes	yes	yes	yes	yes	yes	yes	yes	yes	yes	yes	yes	yes	yes	yes	yes
c_k	0	1	2	3	4	5	6	7	8	9	10	11	11	11	11	11	11	11	11	11
w_k	0	1	2	2	2	2	2	2	2	2	2	2	1	0	0	0	0	0	0	0
block		A	B	B	B	B	B	B	B	B	B	B	C	0	0	0	0	0	0	0
τ_j				-2	-2	-2	-2	-2	-2	-2	-2	-2	-2	-2	-2	-2	-2	-2	-2	-2

Figure 8.4: Packet pattern and inner signals of the uncertainty for $\mathcal{P}_1$, $\bar{\tau} = 3$, $T = 10$ and $\tau_A = 2$.

In addition, one has to take into account the fact, that each packet can only be received once at the receiver side and, as defined for protocol $\mathcal{P}_1$, the most recent packet is chosen if more packets are available. The packet received at the last time instant, i.e. c_{k-1}, is used if no packet is received at instant k. Figure 8.4 presents the resulting packet pattern that results in a maximization of the norm of (w_k). The worst case delay pattern is $\tau_j = -2$ for all j.

Figures 8.5 and 8.6 extends the analysis to different $\bar{\tau}$, T and acausal delays τ_A, where also the minimal delay $-\tau_A$ and maximal delay $\bar{\tau} - \tau_A$ are indicated. More resulting packet patterns are shown in Appendix C.1 for different maximal bounds on the time-varying delays $\bar{\tau}$ and truncation times T.

$\bar{\tau}$	min	max	k	-4	-3	-2	-1	0	1	2	3	4	5	6	7	8	9	10	11	12	13	14	15	16	17	18
2	0	2	τ_j					2	2	2	2	2	2	2	2	2	2	2	2	2						
			w_k			0	0	-1	-2	-2	-2	-2	-2	-2	-2	-2	-2	-2	-1	0						
2	-1	1	τ_j					1	1	1	1	1	1	1	1	1	1	1	1	1						
			w_k			0	0	-1	-1	-1	-1	-1	-1	-1	-1	-1	-1	-1	0	0						
2	-2	0	τ_j					-2	-2	-2	-2	-2	-2	-2	-2	-2	-2	-2	-2	-2						
			w_k			1	2	2	2	2	2	2	2	2	2	2	1	0	0	0						
3	0	3	τ_j					3	3	3	3	3	3	3	3	3	3	3	3	3	3					
			w_k		0	0	0	-1	-2	-3	-3	-3	-3	-3	-3	-3	-3	-3	-2	-1	0					
3	-1	2	τ_j					2	2	2	2	2	2	2	2	2	2	2	2	2	2					
			w_k		0	0	0	-1	-2	-2	-2	-2	-2	-2	-2	-2	-2	-2	-1	0	0					
3	-2	1	τ_j					-2	-2	-2	-2	-2	-2	-2	-2	-2	-2	-2	-2	-2	-2					
			w_k		0	1	2	2	2	2	2	2	2	2	2	2	1	0	0	0	0					
3	-3	0	τ_j					-3	-3	-3	-3	-3	-3	-3	-3	-3	-3	-3	-3	-3	-3					
			w_k		1	2	3	3	3	3	3	3	3	3	3	2	1	0	0	0	0					
4	0	4	τ_j					4	4	4	4	4	4	4	4	4	4	4	4	4	4	4				
			w_k	0	0	0	0	-1	-2	-3	-4	-4	-4	-4	-4	-4	-4	-4	-3	-2	-1	0				
4	-1	3	τ_j					3	3	3	3	3	3	3	3	3	3	3	3	3	3	3				
			w_k	0	0	0	0	-1	-2	-3	-3	-3	-3	-3	-3	-3	-3	-3	-2	-1	0	0				
4	-2	2	τ_j					2	2	2	2	2	2	2	2	2	2	2	2	2	2	2				
			w_k	0	0	0	0	-1	-2	-2	-2	-2	-2	-2	-2	-2	-2	-2	-1	0	0	0				
4	-3	1	τ_j					-3	-3	-3	-3	-3	-3	-3	-3	-3	-3	-3	-3	-3	-3	-3				
			w_k	0	1	2	3	3	3	3	3	3	3	3	3	2	1	0	0	0	0	0				
4	-4	0	τ_j					-4	-4	-4	-4	-4	-4	-4	-4	-4	-4	-4	-4	-4	-4	-4				
			w_k	1	2	3	4	4	4	4	4	4	4	4	3	2	1	0	0	0	0	0				

Figure 8.5: Resulting delay patterns (τ_j) and worst case output sequences (w_k) for $\mathcal{P}_1$, $\bar{\tau} \in \{2, 3, 4\}$ and $T = 10$.

All resulting delay patterns and output sequences show a similar structure as for the causal case, with the important differences that:

$\bar{\tau}$	min	max	k	−4	−3	−2	−1	0	1	2	3	4	5	6	7	8	9	10	11	12	13	14	15	16	17	18
2	0	2	τ_j					2	2	2	2	2														
			w_k			0	0	−1	−2	−2	−1	0														
2	−1	1	τ_j					1	1	1	1	1														
			w_k			0	0	−1	−1	−1	0	0														
2	−2	0	τ_j					−2	−2	−2	−2	−2														
			w_k			1	2	2	1	0	0	0														
3	0	3	τ_j					3	3	3	3	3	3													
			w_k		0	0	0	−1	−2	−3	−2	−1	0													
3	−1	2	τ_j					2	2	2	2	2	2													
			w_k		0	0	0	−1	−2	−2	−1	0	0													
3	−2	1	τ_j					−2	−2	−2	−2	−2	−2													
			w_k		0	1	2	2	1	0	0	0	0													
3	−3	0	τ_j					−3	−3	−3	−3	−3	−3													
			w_k		1	2	3	2	1	0	0	0	0													
4	0	4	τ_j					4	4	4	4	4	4	4												
			w_k	0	0	0	0	−1	−2	−3	−3	−2	−1	0												
4	−1	3	τ_j					3	3	3	3	3	3	3												
			w_k	0	0	0	0	−1	−2	−3	−2	−1	0	0												
4	−2	2	τ_j					2	2	2	2	2	2	2												
			w_k	0	0	0	0	−1	−2	−2	−1	0	0	0												
4	−3	1	τ_j					−3	−3	−3	−3	−3	−3	−3												
			w_k	0	1	2	3	2	1	0	0	0	0	0												
4	−4	0	τ_j					−4	−4	−4	−4	−4	−4	−4												
			w_k	1	2	3	3	2	1	0	0	0	0	0												

Figure 8.6: Resulting delay patterns (τ_j) and worst case output sequences (w_k) for $\mathcal{P}_1$, $\bar{\tau} \in \{2, 3, 4\}$ and $T = 2$.

(a) a maximal relative delay

$$\bar{\tau}^* = \max\left\{\tau_A, \bar{\tau} - \tau_A\right\} \tag{8.14}$$

is relevant;

(b) the norm of the output sequence for the introductory part A (green), main part B (orange) and remaining part C (red) is given by

$$\begin{aligned} \left|\left|\left(w_k\right)_T\right|\right|_2^2 &= A + B + C = 2A + B \\ &= 2\sum_{i=1}^{\bar{\tau}-1} i^2 \bar{v}^2 + \left(T - \bar{\tau} + 2\right) \bar{\tau}^2 \bar{v}^2 \end{aligned} \tag{8.15}$$

for $T - \bar{\tau} + 2 \geq 0$, i.e. $T \geq \bar{\tau} - 2$.

Evaluating (7.13) with (8.15) yields α_T as depicted in Figure 8.7 for different acausal delays τ_A (blue plus signs). The black circles are the resulting worst case gains found numerically by direct variation of all possible combinations of packet delays τ_j. Hence, one can mathematically reproduce the true worst case gains α_T that tend to $\alpha = \bar{\tau}$ for $T \to \infty$, see dashed lines in Figure 8.7 and Appendix C.2.

An alternative way to plot the results from Figure 8.7, and also for different $\bar{\tau}$ is presented in Figures 8.8 to 8.10. Circles indicate the different values for α_T for different T and the black dashed line visualizes α as a function of τ_A.

Consequently, an optimal choice of the acausal delay τ_A is possible to minimize the corresponding ℓ_2 gain as shown in Figures 8.11 to 8.13. The optimal choice for the acausal delay (black dots) is equivalent to relation (8.9a) in Theorem 8.2 resulting in $\bar{\tau}^* = \max\left\{\tau_A^*, \bar{\tau} - \tau_A^*\right\}$ and $\alpha^* = \bar{\tau}^*$ as in (8.9b). The corresponding worst case delay pattern is given by

$$\tau_j = \begin{cases} \bar{\tau}^* & \text{if} \quad \bar{\tau}^* = \bar{\tau} - \tau_A^* \\ -\bar{\tau}^* & \text{otherwise} \end{cases} \tag{8.16}$$

as can be seen in Appendix C.1.

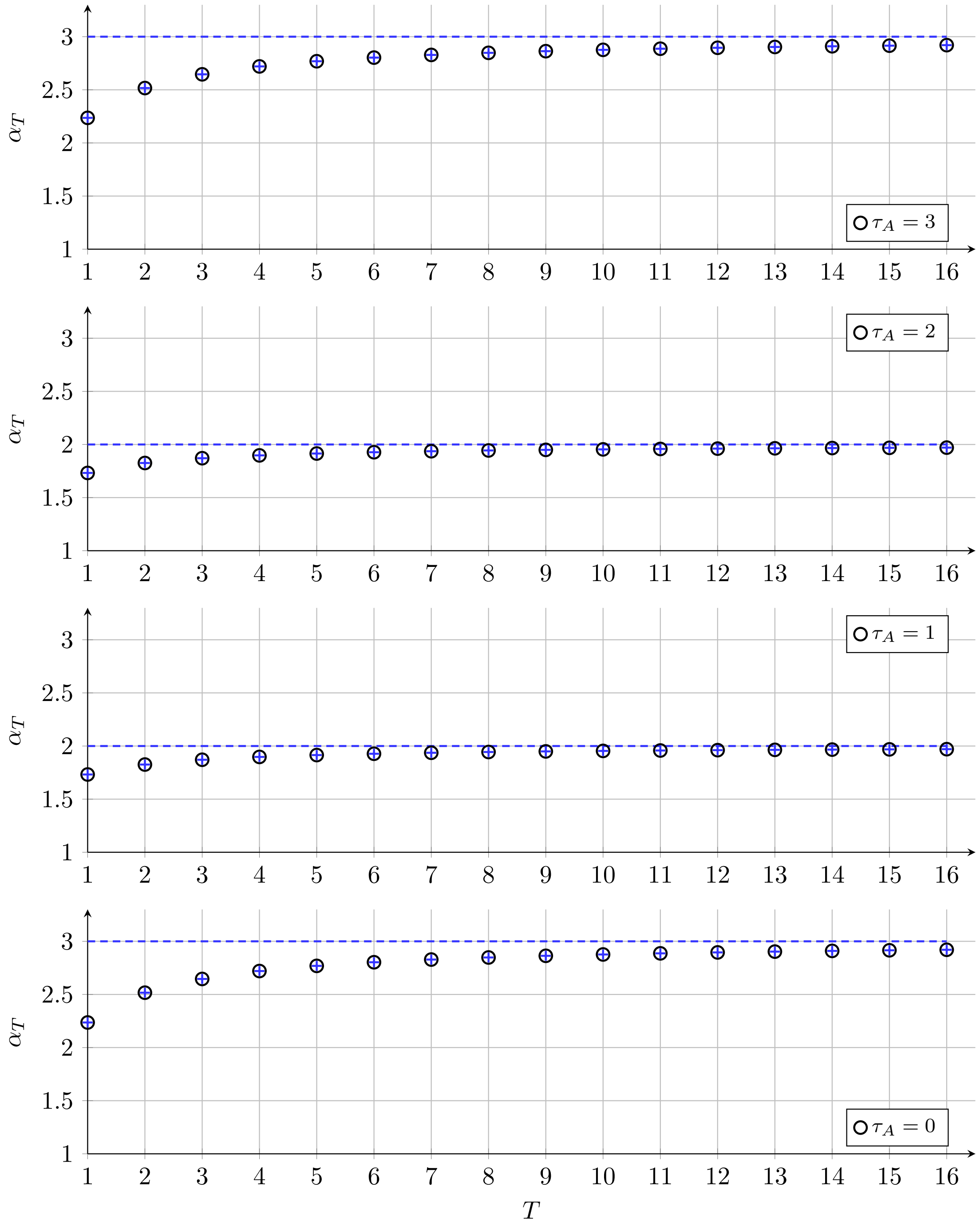

Figure 8.7: Gains α_T as a function of truncation times T for $\mathcal{P}_1$, $\bar{\tau} = 3$ and different acausal delays τ_A. The dashed lines represent the corresponding ℓ_2 gains α.

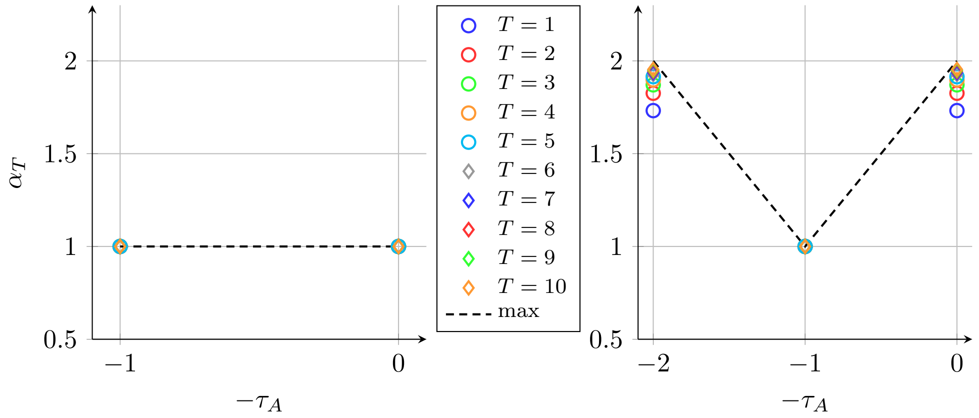

Figure 8.8: Gains α_T for different T and τ_A as well as ℓ_2 gains α (dashed lines) for $\mathcal{P}_1$, $\bar{\tau} = 1$ (left) and $\bar{\tau} = 2$ (right).

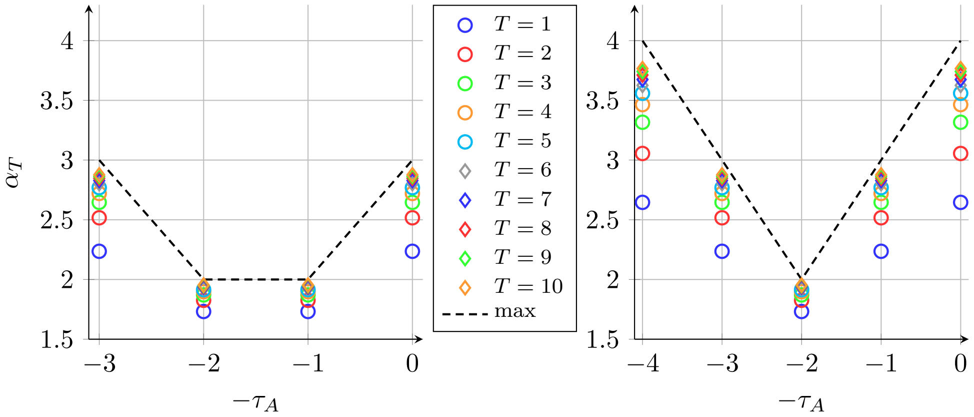

Figure 8.9: Gains α_T for different T and τ_A as well as ℓ_2 gains α (dashed lines) for $\mathcal{P}_1$, $\bar{\tau} = 3$ (left) and $\bar{\tau} = 4$ (right).

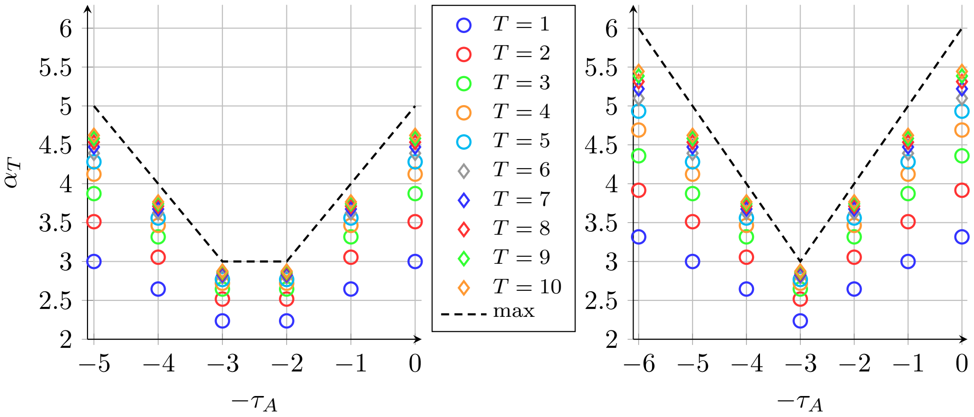

Figure 8.10: Gains α_T for different T and τ_A as well as ℓ_2 gains α (dashed lines) for $\mathcal{P}_1$, $\bar{\tau} = 5$ (left) and $\bar{\tau} = 6$ (right).

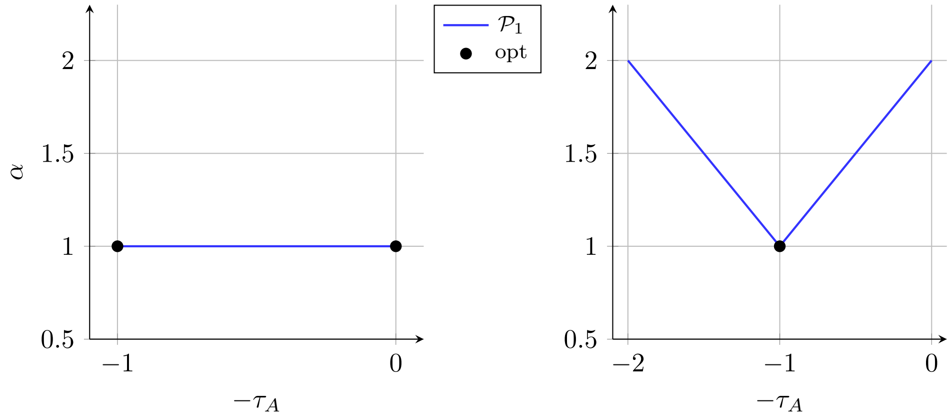

Figure 8.11: Finite ℓ_2 gain α (blue) and the optimal choice of the acausal delay τ_A (black dots) for $\mathcal{P}_1$, $\bar{\tau} = 1$ (left) and $\bar{\tau} = 2$ (right).

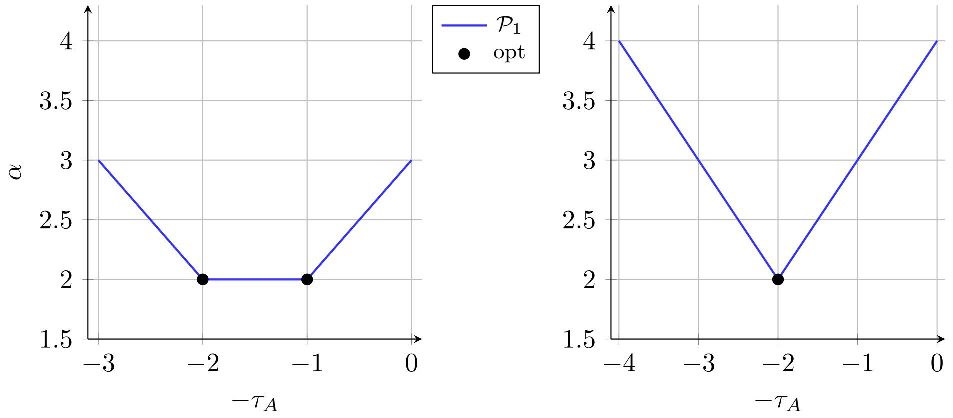

Figure 8.12: Finite ℓ_2 gain α (blue) and the optimal choice of the acausal delay τ_A (black dots) for $\mathcal{P}_1$, $\bar{\tau} = 3$ (left) and $\bar{\tau} = 4$ (right).

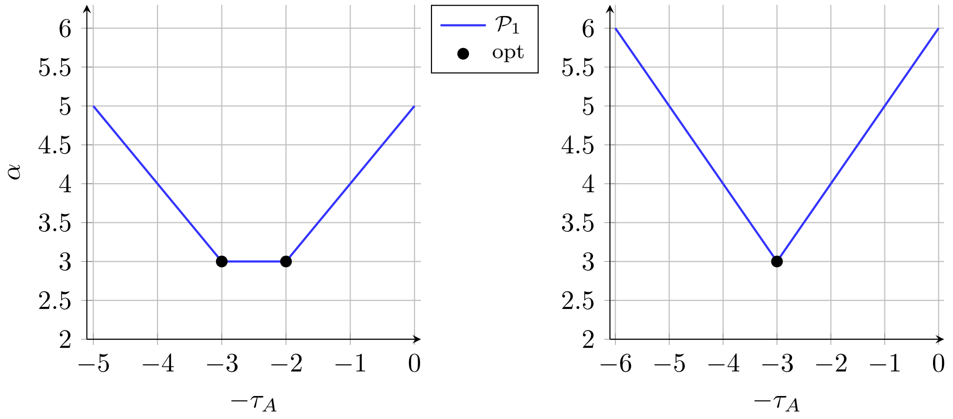

Figure 8.13: Finite ℓ_2 gain α (blue) and the optimal choice of the acausal delay τ_A (black dots) for $\mathcal{P}_1$, $\bar{\tau} = 5$ (left) and $\bar{\tau} = 6$ (right).

8.3.2 Protocol $\mathcal{P}_3$

The calculation of α^* is more demanding for protocol $\mathcal{P}_3$, because the delay patterns from the previous section only partially reproduce gains α_T, e.g., for $\mathcal{P}_3$ and $\tau_A = \bar{\tau}$. This is visualized in Figure 8.14 and in Appendix C.3 using blue plus signs.

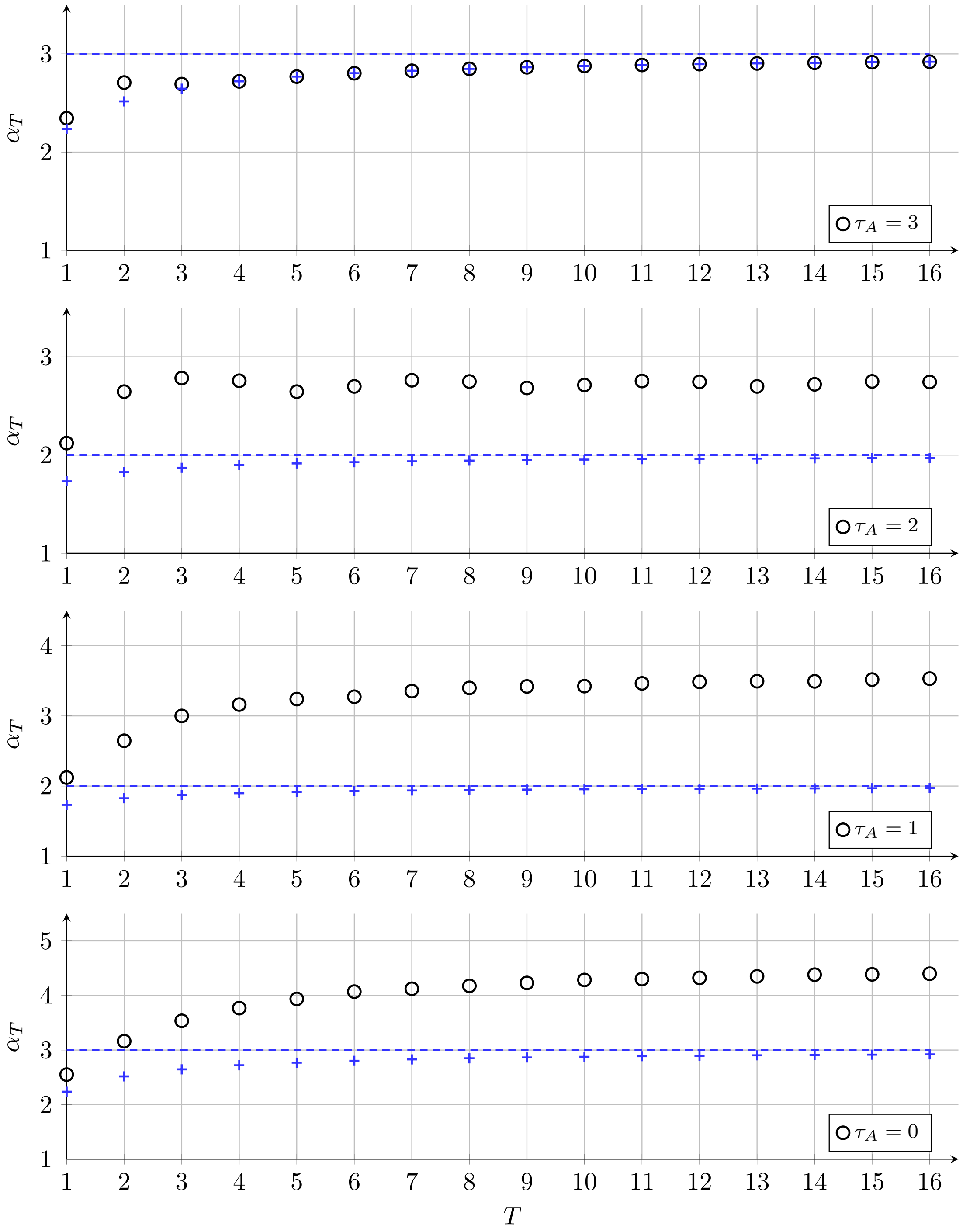

Figure 8.14: Comparison of the actual values of α_T found by direct iteration for $\mathcal{P}_3$ and $\bar{\tau} = 3$ (black circles) as well as the calculated gain values for $\mathcal{P}_1$ (blue plus signs), for different acausal delays τ_A.

An analysis of the delay patterns that correspond to the numerically found worst case gains α_T reveals that three different delay patterns $\mathcal{P}_3'$, $\mathcal{P}_3''$ and $\mathcal{P}_3'''$ have to be considered to mathematically describe the gains related to protocol $\mathcal{P}_3$.

Delay Pattern $\mathcal{P}_3'$

The first packet arrival pattern is based on the causal case of $\mathcal{P}_3$. Figure 8.15 shows the associated delay pattern, inner signals of the uncertainty and the worst case output sequence for $\bar{\tau} = 3$, $T = 10$ and $\tau_A = 2$.

k	-3	-2	-1	0	1	2	3	4	5	6	7	8	9	10	11	12	13	14	15	16
$b_k^{(-2)}$	0	1	2	3	4	5	6	7	8	9	10	11	11	11	11	11	11	11	11	11
$b_k^{(1)}$	0	0	1	2	3	4	5	6	7	8	9	10	11	11	11	11	11	11	11	11
$b_k^{(0)} = a_k$	0	0	0	1	2	3	4	5	6	7	8	9	10	11	11	11	11	11	11	11
$b_k^{(1)}$	0	0	0	0	1	2	3	4	5	6	7	8	9	10	11	11	11	11	11	11
$b_k^{(-2)}$	0	$\cancel{1}$	$\cancel{2}$	$\cancel{3}$	4	$\cancel{5}$	$\cancel{6}$	$\cancel{7}$	8	$\cancel{9}$	$\cancel{10}$	$\cancel{11}$	11	$\cancel{11}$	$\cancel{11}$	$\cancel{11}$	11	$\cancel{11}$	$\cancel{11}$	$\cancel{11}$
$b_k^{(-1)}$	0	0	$\cancel{1}$	$\cancel{2}$	3	$\cancel{4}$	$\cancel{5}$	$\cancel{6}$	7	$\cancel{8}$	$\cancel{9}$	$\cancel{10}$	11	$\cancel{11}$	$\cancel{11}$	$\cancel{11}$	11	$\cancel{11}$	$\cancel{11}$	$\cancel{11}$
$b_k^{(0)} = a_k$	0	0	0	$\cancel{1}$	2	$\cancel{3}$	$\cancel{4}$	$\cancel{5}$	6	$\cancel{7}$	$\cancel{8}$	$\cancel{9}$	10	$\cancel{11}$	$\cancel{11}$	$\cancel{11}$	11	$\cancel{11}$	$\cancel{11}$	$\cancel{11}$
$b_k^{(1)}$	0	0	0	0	1	$\cancel{2}$	$\cancel{3}$	$\cancel{4}$	5	$\cancel{6}$	$\cancel{7}$	$\cancel{8}$	9	$\cancel{10}$	$\cancel{11}$	$\cancel{11}$	11	$\cancel{11}$	$\cancel{11}$	$\cancel{11}$
$b_k^{(-2)} - a_k$	0	1	2	2	2	2	2	2	2	2	2	2	1	0	0	0	0	0	0	0
$b_k^{(-1)} - a_k$	0	0	1	1	1	1	1	1	1	1	1	1	1	0	0	0	0	0	0	0
$b_k^{(0)} - a_k$	0	0	0	0	0	0	0	0	0	0	0	0	0	0	0	0	0	0	0	0
$b_k^{(1)} - a_k$	0	0	0	-1	-1	-1	-1	-1	-1	-1	-1	-1	-1	-1	0	0	0	0	0	0
packet arr.	no	no	no	no	yes	no	no	no	yes	no	no	no	yes	no	no	no	yes	no	no	no
c_k	0	0	0	0	1	1	1	1	5	5	5	5	9	9	9	9	11	11	11	11
w_k	0	0	0	-1	-1	-2	-3	-4	-1	-2	-3	-4	-1	-2	-2	-2	0	0	0	0
block				A	B	B	B	B	B	B	B	B	C	C	C	C	C	C	C	C
τ_j				1	0	-1	-2	1	0	-1	-2	1	0	-1	-2	1	0	-1	-2	1

Figure 8.15: Packet pattern and inner signals of the uncertainty for $\mathcal{P}_3'$, $\bar{\tau} = 3$, $T = 10$ and $\tau_A = 2$.

This is then generalized for different $\bar{\tau}$, T, and τ_A as shown in Figures 8.16, 8.17, and in more detail in Appendix C.4.

$\bar{\tau}$	min	max	k	-4	-3	-2	-1	0	1	2	3	4	5	6	7	8	9	10	11	12	13	14	15	16	17	18
2	0	2	τ_j					2	1	0	2	1	0	2	1	0	2	1	0	2	1	0				
			w_k			0	0	-1	-2	-2	-3	-4	-2	-3	-4	-2	-3	-4	-1	-1	-1	0				
2	-1	1	τ_j					1	0	-1	1	0	-1	1	0	-1	1	0	-1	1	0	-1				
			w_k			0	0	-1	-1	-2	-3	-1	-2	-3	-1	-2	-3	-1	-1	-1	0	0				
2	-2	0	τ_j					0	-1	-2	0	-1	-2	0	-1	-2	0	-1	-2	0	-1	-2				
			w_k			0	0	0	-1	-2	0	-1	-2	0	-1	-2	0	-1	-1	0	0	0				
3	0	3	τ_j					3	2	1	0	3	2	1	0	3	2	1	0	3	2	1	0	3		
			w_k		0	0	0	-1	-2	-3	-3	-4	-5	-6	-3	-4	-5	-6	-2	-2	-2	-2	0	0		
3	-1	2	τ_j					2	1	0	-1	2	1	0	-1	2	1	0	-1	2	1	0	-1	2		
			w_k		0	0	0	-1	-2	-2	-3	-4	-5	-2	-3	-4	-5	-2	-2	-2	-2	0	0	0		
3	-2	1	τ_j					1	0	-1	-2	1	0	-1	-2	1	0	-1	-2	1	0	-1	-2	1		
			w_k		0	0	0	-1	-1	-2	-3	-4	-1	-2	-3	-4	-1	-2	-2	-2	0	0	0	0		
3	-3	0	τ_j					0	-1	-2	-3	0	-1	-2	-3	0	-1	-2	-3	0	-1	-2	-3	0		
			w_k		0	0	0	0	-1	-2	-3	0	-1	-2	-3	0	-1	-2	-2	0	0	0	0	0		
4	0	4	τ_j					4	3	2	1	0	4	3	2	1	0	4	3	2	1	0	4	3	2	1
			w_k	0	0	0	0	-1	-2	-3	-4	-4	-5	-6	-7	-8	-4	-5	-5	-5	-5	0	0	0	0	0
4	-1	3	τ_j					3	2	1	0	-1	3	2	1	0	-1	3	2	1	0	-1	3	2	1	0
			w_k	0	0	0	0	-1	-2	-3	-3	-4	-5	-6	-7	-3	-4	-5	-5	-5	0	0	0	0	0	0
4	-2	2	τ_j					2	1	0	-1	-2	2	1	0	-1	-2	2	1	0	-1	-2	2	1	0	-1
			w_k	0	0	0	0	-1	-2	-2	-3	-4	-5	-6	-2	-3	-4	-5	-5	0	0	0	0	0	0	0
4	-3	1	τ_j					1	0	-1	-2	-3	1	0	-1	-2	-3	1	0	-1	-2	-3	1	0	-1	-2
			w_k	0	0	0	0	-1	-1	-2	-3	-4	-5	-1	-2	-3	-4	-5	0	0	0	0	0	0	0	0
4	-4	0	τ_j					0	-1	-2	-3	-4	0	-1	-2	-3	-4	0	-1	-2	-3	-4	0	-1	-2	-3
			w_k	0	0	0	0	0	-1	-2	-3	-4	0	-1	-2	-3	-4	0	0	0	0	0	0	0	0	0

Figure 8.16: Resulting delay patterns (τ_j) and worst case output sequences (w_k) for $\mathcal{P}_3'$, $\bar{\tau} \in \{2, 3, 4\}$ and $T = 10$.

Hence, the delay pattern

$$(\tau_j) = \Big(\underbrace{(\bar{\tau} - \tau_A), (\bar{\tau} - \tau_A - 1), \ldots, -\tau_A}_{\star},\ \star, \star, \ldots \Big) \tag{8.17}$$

$\bar{\tau}$	min	max	k	-4	-3	-2	-1	0	1	2	3	4	5	6	7	8	9	10	11	12	13	14	15	16	17	18
2	0	2	τ_j					2	1	0	2	1	0	2												
			w_k			0	0	-1	-2	-2	-2	-2	0	0												
2	-1	1	τ_j					1	0	-1	1	0	-1	1												
			w_k			0	0	-1	-1	-2	-2	0	0	0												
2	-2	0	τ_j					0	-1	-2	0	-1	-2	0												
			w_k			0	0	0	-1	-2	0	0	0	0												
3	0	3	τ_j					3	2	1	0	3	2	1	0	3										
			w_k		0	0	0	-1	-2	-3	-2	-2	-2	-2	0	0										
3	-1	2	τ_j					2	1	0	-1	2	1	0	-1	2										
			w_k		0	0	0	-1	-2	-2	-2	-2	-2	0	0	0										
3	-2	1	τ_j					1	0	-1	-2	1	0	-1	-2	1										
			w_k		0	0	0	-1	-1	-2	-2	-2	0	0	0	0										
3	-3	0	τ_j					0	-1	-2	-3	0	-1	-2	-3	0										
			w_k		0	0	0	0	-1	-2	-2	0	0	0	0	0										
4	0	4	τ_j					4	3	2	1	0	4	3	2	1	0	4								
			w_k	0	0	0	0	-1	-2	-3	-3	-2	-2	-2	-2	-2	0	0								
4	-1	3	τ_j					3	2	1	0	-1	3	2	1	0	-1	3								
			w_k	0	0	0	0	-1	-2	-3	-2	-2	-2	-2	-2	0	0	0								
4	-2	2	τ_j					2	1	0	-1	-2	2	1	0	-1	-2	2								
			w_k	0	0	0	0	-1	-2	-2	-2	-2	-2	-2	0	0	0	0								
4	-3	1	τ_j					1	0	-1	-2	-3	1	0	-1	-2	-3	1								
			w_k	0	0	0	0	-1	-1	-2	-2	-2	-2	0	0	0	0	0								
4	-4	0	τ_j					0	-1	-2	-3	-4	0	-1	-2	-3	-4	0								
			w_k	0	0	0	0	0	-1	-2	-2	-2	0	0	0	0	0	0								

Figure 8.17: Resulting delay patterns (τ_j) and worst case output sequences (w_k) for $\mathcal{P}'_3$, $\bar{\tau} \in \{2, 3, 4\}$ and $T = 2$.

yields

$$||(w_k)_T||_2^2 = A + B + C + D \tag{8.18}$$

consisting of four parts A, B, C and D. The introductory (green) part A consists of $\bar{\tau} - \tau_A$ samples. It contributes to $||(w_k)_T||_2^2$ with

$$A = \sum_{i=1}^{\bar{\tau}-\tau_A} \Big(\min\big\{i, T+1\big\}\Big)^2 \bar{v}^2 \tag{8.19}$$

and $T \geq 0$, where this formulation with the min-operator is used to account for cases where $T + 1 < \bar{\tau}$ as, e.g., shown in the Figure 8.17 for $T = 2$, $\bar{\tau} = 4$ and $\tau_A = 0$.

Block B consists of k_1 (orange) blocks of length $\bar{\tau} + 1$, containing a repeating sequence $\big(\bar{\tau} - \tau_A, \bar{\tau} - \tau_A + 1, \ldots, 2\bar{\tau} - \tau_A\big)$ with a squared norm of

$$d = \sum_{i=0}^{\bar{\tau}} \big(\bar{\tau} - \tau_A + i\big)^2 \bar{v}^2 \, . \tag{8.20}$$

The causal case in Chapter 7 provides the basis to generalize the calculation of k_1 for the acausal one. Overall $T + 2\bar{\tau} + 1$ samples (cf. (7.16)) are taken into account in the analysis, where block A contributes with $\bar{\tau} - \tau_A$ samples. To get k_1, one subtracts the length of the repeating sequence $(\bar{\tau}+1)$ from the remaining $T+1+\bar{\tau}+\tau_A$ samples so many times that $\leq 3\bar{\tau}$ samples are left. The remaining samples $k_2 = T+1+\bar{\tau}+\tau_A - k_1(\bar{\tau}+1)$ are split into

$$k_3 = \left\lfloor \frac{k_2}{\bar{\tau}+1} \right\rfloor \tag{8.21}$$

times $\bar{\tau} + 1$ samples (block C, blue) and the left $k_2 - k_3(\bar{\tau} + 1)$ samples shown in red.

This yield

$$\begin{aligned}\big|\big|(w_k)_T\big|\big|_2 = & \underbrace{\sum_{i=1}^{\bar\tau-\tau_A} i^2\bar v^2}_{A} + \underbrace{k_1\sum_{i=0}^{\bar\tau}\big(\bar\tau-\tau_A+i\big)^2\bar v^2}_{B} + \\ & \underbrace{\sum_{j=k_1}^{k_1+k_3-1}\left\{\sum_{i=\bar\tau-\tau_A+j(\bar\tau+1)}^{2\bar\tau-\tau_A+j(\bar\tau+1)}\big(a_i-a_{j(\bar\tau+1)}\big)^2\right\}}_{C} + \\ & \underbrace{\sum_{i=\bar\tau-\tau_A+(k_1+k_3)(\bar\tau+1)}^{T+2\bar\tau}\big(a_i-a_{\bar\tau-\tau_A+(k_1+k_3)(\bar\tau+1)}\big)^2}_{D},\end{aligned} \tag{8.22}$$

which is used in the calculation of α_T. The ℓ_2 gain follows from (7.12), (8.20), (8.22) and

$$\alpha_T^2 = \frac{A+\frac{T+1}{\bar\tau+1}d+C+D}{1+T} = \frac{A+C+D}{1+T}+\frac{d}{\bar\tau+1}\,. \tag{8.23}$$

A comparison of the calculated values α_T for different $\bar\tau$ and T with values from direct iteration are presented in Figures 8.18 and in Appendix C.5.

The finite ℓ_2 gain α follows for $T\to\infty$ such that

$$\begin{aligned} d &= \sum_{i=1}^{\bar\tau}\big(\Delta\tau-1+i\big)^2\bar v^2 \\ &= \left[(\Delta\tau-1)^2\sum_{i=1}^{\bar\tau+1}1+2(\Delta\tau-1)\sum_{i=1}^{\bar\tau+1}i+\sum_{i=1}^{\bar\tau+1}i^2\right]\bar v^2 \\ &= (\bar\tau+1)\left[\Delta\tau^2+\Delta\tau\,\bar\tau+\frac{1}{3}\bar\tau^2+\frac{1}{6}\bar\tau\right]\bar v^2 \end{aligned} \tag{8.24}$$

with $\Delta\tau=\bar\tau-\tau_A$ and so

$$\alpha_{\mathcal{P}_3'} = \sqrt{\Delta\tau^2+\Delta\tau\,\bar\tau+\frac{1}{3}\bar\tau^2+\frac{1}{6}\bar\tau}\,. \tag{8.25}$$

Figure 8.18 shows the results for α_T and the corresponding ℓ_2 gains $\alpha_{\mathcal{P}_3'}$ for different acausal delays. Condition (8.25) reduces to

$$\alpha = \sqrt{\frac{\bar\tau}{6}(14\bar\tau+1)} \tag{8.26}$$

in causal case where $\Delta\tau=\bar\tau$ as indicated in Chapter 7. The presented delay pattern allows to reproduce additional points in Figure 8.18 as, e.g., for $\tau_A=0$ and $\tau_A=1$ as well as for different cases as shown in Appendix C.5.

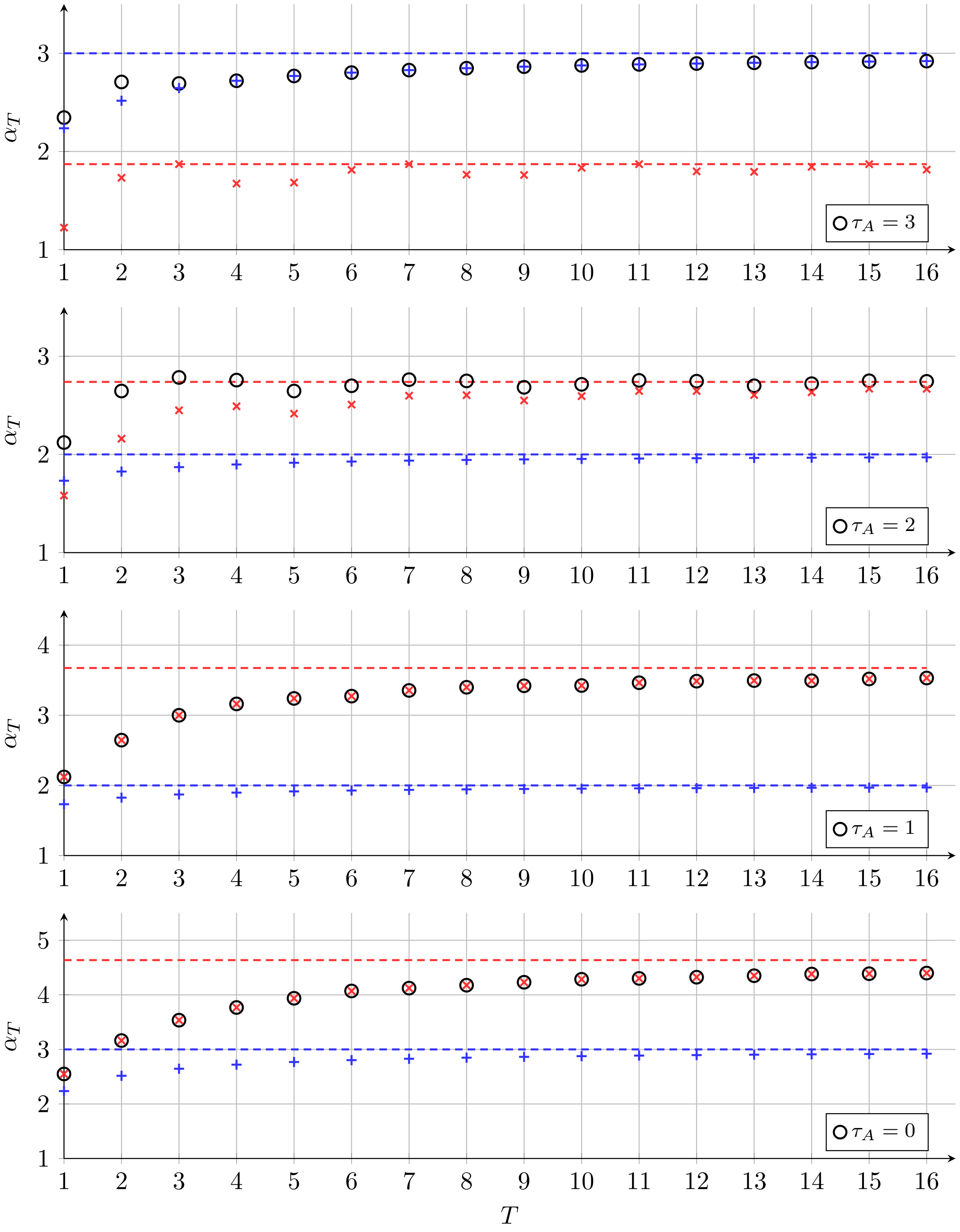

Figure 8.18: Gains α_T as a function of truncation times T, $\bar{\tau} = 3$ and different acausal delays τ_A: $\mathcal{P}_1$ (blue), $\mathcal{P}_3'$ (red). The dashed lines represent the corresponding ℓ_2 gains α.

Delay Pattern $\mathcal{P}_3''$

A second delay pattern follows by modifying the introductory part of $\mathcal{P}_3'$ such that

$$(\tau_j) = \Big((\bar{\tau} - \tau_A),\ \underbrace{-\tau_A, -\tau_A, \ldots, -\tau_A}_{\bar{\tau}\text{ times}},\ \underbrace{(\bar{\tau} - \tau_A)\,, (\bar{\tau} - \tau_A - 1)\,, \ldots, -\tau_A}_{\star},\ \star, \star, \ldots \Big)\,. \tag{8.27}$$

The resulting packet patterns and inner signals of the uncertainty are exemplified in Figure 8.19 for $\bar{\tau} = 3$, $T = 10$ and an acausal delay of $\tau_A = 2$.

k	-3	-2	-1	0	1	2	3	4	5	6	7	8	9	10	11	12	13	14	15	16
$b_k^{(-2)}$	0	1	2	3	4	5	6	7	8	9	10	11	11	11	11	11	11	11	11	11
$b_k^{(1)}$	0	0	1	2	3	4	5	6	7	8	9	10	11	11	11	11	11	11	11	11
$b_k^{(0)} = a_k$	0	0	0	1	2	3	4	5	6	7	8	9	10	11	11	11	11	11	11	11
$b_k^{(1)}$	0	0	0	0	1	2	3	4	5	6	7	8	9	10	11	11	11	11	11	11
$b_k^{(-2)}$	0	$\cancel{1}$	2	3	4	$\cancel{5}$	$\cancel{6}$	$\cancel{7}$	8	$\cancel{9}$	$\cancel{10}$	$\cancel{11}$	11	$\cancel{11}$	$\cancel{11}$	$\cancel{11}$	11	$\cancel{11}$	$\cancel{11}$	$\cancel{11}$
$b_k^{(-1)}$	0	0	$\cancel{1}$	$\cancel{2}$	$\cancel{3}$	$\cancel{4}$	$\cancel{5}$	$\cancel{6}$	7	$\cancel{8}$	$\cancel{9}$	$\cancel{10}$	11	$\cancel{11}$	$\cancel{11}$	$\cancel{11}$	11	$\cancel{11}$	$\cancel{11}$	$\cancel{11}$
$b_k^{(0)} = a_k$	0	0	0	$\cancel{1}$	$\cancel{2}$	$\cancel{3}$	$\cancel{4}$	$\cancel{5}$	6	$\cancel{7}$	$\cancel{8}$	$\cancel{9}$	10	$\cancel{11}$	$\cancel{11}$	$\cancel{11}$	11	$\cancel{11}$	$\cancel{11}$	$\cancel{11}$
$b_k^{(1)}$	0	0	0	0	1	$\cancel{2}$	$\cancel{3}$	$\cancel{4}$	5	$\cancel{6}$	$\cancel{7}$	$\cancel{8}$	9	$\cancel{10}$	$\cancel{11}$	$\cancel{11}$	11	$\cancel{11}$	$\cancel{11}$	$\cancel{11}$
$b_k^{(-2)} - a_k$	0	1	2	2	2	2	2	2	2	2	2	2	1	0	0	0	0	0	0	0
$b_k^{(-1)} - a_k$	0	0	1	1	1	1	1	1	1	1	1	1	1	0	0	0	0	0	0	0
$b_k^{(0)} - a_k$	0	0	0	0	0	0	0	0	0	0	0	0	0	0	0	0	0	0	0	0
$b_k^{(1)} - a_k$	0	0	0	-1	-1	-1	-1	-1	-1	-1	-1	-1	-1	-1	0	0	0	0	0	0
packet arr.	no	no	yes	yes	yes	no	no	no	yes	no	no	no	yes	no	no	no	yes	no	no	no
c_k	0	0	2	3	1	1	1	1	5	5	5	5	9	9	9	9	11	11	11	11
w_k	0	0	2	2	-1	-2	-3	-4	-1	-2	-3	-4	-1	-2	-2	-2	0	0	0	0
block			A$^-$	A$^+$	B	B	B	B	B	B	B	B	C	C	C	C	C	C	C	C
τ_j				1	-2	-2	-2	1	0	-1	-2	1	0	-1	-2	1	0	-1	-2	1

Figure 8.19: Packet pattern and inner signals of the uncertainty for $\mathcal{P}_3''$, $\bar{\tau} = 3$, $T = 10$ and $\tau_A = 2$.

Figures 8.20 and 8.21 illustrate the patterns for different $\bar{\tau}$, τ_A and truncation times T. More cases are considered in Appendix C.6.

$\bar{\tau}$	min	max	k	-4	-3	-2	-1	0	1	2	3	4	5	6	7	8	9	10	11	12	13	14	15	16	17	18
2	0	2	τ_j					2	0	0	2	1	0	2	1	0	2	1	0	2	1	0				
			w_k			0	0	-1	0	-2	-3	-4	-2	-3	-4	-2	-3	-4	-1	-1	-1	0				
2	-1	1	τ_j					1	-1	-1	1	0	-1	1	0	-1	1	0	-1	1	0	-1				
			w_k			0	0	1	-1	-2	-3	-1	-2	-3	-1	-2	-3	-1	-1	-1	0	0				
2	-2	0	τ_j					0	-2	-2	0	-1	-2	0	-1	-2	0	-1	-2	0	-1	-2				
			w_k			0	2	0	-1	-2	0	-1	-2	0	-1	-2	0	-1	-1	0	0	0				
3	0	3	τ_j					3	0	0	0	3	2	1	0	3	2	1	0	3	2	1	0	3		
			w_k		0	0	0	-1	0	0	-3	-4	-5	-6	-3	-4	-5	-6	-2	-2	-2	-2	0	0		
3	-1	2	τ_j					2	-1	-1	-1	2	1	0	-1	2	1	0	-1	2	1	0	-1	2		
			w_k		0	0	0	1	1	-2	-3	-4	-5	-2	-3	-4	-5	-2	-2	-2	-2	0	0	0		
3	-2	1	τ_j					1	-2	-2	-2	1	0	-1	-2	1	0	-1	-2	1	0	-1	-2	1		
			w_k		0	0	2	2	-1	-2	-3	-4	-1	-2	-3	-4	-1	-2	-2	-2	0	0	0	0		
3	-3	0	τ_j					0	-3	-3	-3	0	-1	-2	-3	0	-1	-2	-3	0	-1	-2	-3	0		
			w_k		0	2	3	0	-1	-2	-3	0	-1	-2	-3	0	-1	-2	-2	0	0	0	0	0		
4	0	4	τ_j					4	0	0	0	0	4	3	2	1	0	4	3	2	1	0	4	3	2	1
			w_k	0	0	0	0	-1	0	0	0	-4	-5	-6	-7	-8	-4	-5	-5	-5	-5	0	0	0	0	0
4	-1	3	τ_j					3	-1	-1	-1	-1	3	2	1	0	-1	3	2	1	0	-1	3	2	1	0
			w_k	0	0	0	0	1	1	1	-3	-4	-5	-6	-7	-3	-4	-5	-5	-5	0	0	0	0	0	0
4	-2	2	τ_j					2	-2	-2	-2	-2	2	1	0	-1	-2	2	1	0	-1	-2	2	1	0	-1
			w_k	0	0	0	2	2	2	-2	-3	-4	-5	-6	-2	-3	-4	-5	-5	0	0	0	0	0	0	0
4	-3	1	τ_j					1	-3	-3	-3	-3	1	0	-1	-2	-3	1	0	-1	-2	-3	1	0	-1	-2
			w_k	0	0	2	3	3	-1	-2	-3	-4	-5	-1	-2	-3	-4	-5	0	0	0	0	0	0	0	0
4	-4	0	τ_j					0	-4	-4	-4	-4	0	-1	-2	-3	-4	0	-1	-2	-3	-4	0	-1	-2	-3
			w_k	0	2	3	4	0	-1	-2	-3	-4	0	-1	-2	-3	-4	0	0	0	0	0	0	0	0	0

Figure 8.20: Resulting delay patterns (τ_j) and worst case output sequences (w_k) for $\mathcal{P}_3''$, $\bar{\tau} \in \{2, 3, 4\}$ and $T = 10$.

In contrast to (8.22), the introductory part A is split into A^+ for $k \geq 0$ and A^- for $k < 0$. All other parts remain the same as in $\mathcal{P}_3'$. According to Figures 8.20 and 8.21 and the tables in Appendix C.6, the modified introductory part can mathematically be

$\bar{\tau}$	min	max	k	−4	−3	−2	−1	0	1	2	3	4	5	6	7	8	9	10	11	12	13	14	15	16	17	18
2	0	2	τ_j					2	0	0	2	1	0	2												
			w_k			0	0	−1	0	−2	−2	−2	0	0												
2	−1	1	τ_j					1	−1	−1	1	0	−1	1												
			w_k			0	0	1	−1	−2	−2	0	0	0												
2	−2	0	τ_j					0	−2	−2	0	−1	−2	0												
			w_k			0	2	0	−1	−2	0	0	0	0												
3	0	3	τ_j					3	0	0	0	3	2	1	0	3										
			w_k		0	0	0	−1	0	0	−2	−2	−2	−2	0	0										
3	−1	2	τ_j					2	−1	−1	−1	2	1	0	−1	2										
			w_k		0	0	0	1	1	−2	−2	−2	−2	0	0	0										
3	−2	1	τ_j					1	−2	−2	−2	1	0	−1	−2	1										
			w_k		0	0	2	2	−1	−2	−2	−2	0	0	0	0										
3	−3	0	τ_j					0	−3	−3	−3	0	−1	−2	−3	0										
			w_k		0	2	3	0	−1	−2	−2	0	0	0	0	0										
4	0	4	τ_j					4	0	0	0	0	4	3	2	1	0	4								
			w_k	0	0	0	0	−1	0	0	0	−2	−2	−2	−2	−2	0	0								
4	−1	3	τ_j					3	−1	−1	−1	−1	3	2	1	0	−1	3								
			w_k	0	0	0	0	1	1	0	−2	−2	−2	−2	−2	0	0	0								
4	−2	2	τ_j					2	−2	−2	−2	−2	2	1	0	−1	−2	2								
			w_k	0	0	0	2	2	1	−2	−2	−2	−2	−2	0	0	0	0								
4	−3	1	τ_j					1	−3	−3	−3	−3	1	0	−1	−2	−3	1								
			w_k	0	0	2	3	2	−1	−2	−2	−2	−2	0	0	0	0	0								
4	−4	0	τ_j					0	−4	−4	−4	−4	0	−1	−2	−3	−4	0								
			w_k	0	2	3	3	0	−1	−2	−2	−2	0	0	0	0	0	0								

Figure 8.21: Resulting delay patterns (τ_j) and worst case output sequences (w_k) for $\mathcal{P}_3''$, $\bar{\tau} \in \{2,3,4\}$ and $T = 2$.

described by

$$A^+ = \begin{cases} \bar{v}^2 & \text{if} \qquad \tau_A = 0 \\ \sum\limits_{i=1}^{\bar{\tau}-\tau_A} \left(\min\Big\{T, \tau_A, \max\left\{0, T-i+1\right\}\Big\}\right)^2 \bar{v}^2 & \text{otherwise} \end{cases} \tag{8.28a}$$

and

$$A^- = \begin{cases} 0 & \text{if} \quad \tau_A \in \{0,1\} \\ \sum\limits_{i=2}^{\tau_A} \Big(\min\left\{i, T+1\right\}\Big)^2 \bar{v}^2 & \text{otherwise} \end{cases} . \tag{8.28b}$$

Relation (7.12) in combination with (8.22) and (8.28) allows to calculate α_T as presented in Figure 8.22. It can be observed that the limit of α_T for $T \to \infty$ is equal to $\mathcal{P}_3'$. However, larger vales

$$\alpha_{\mathcal{P}_3''} = \sup_T \alpha_{T,\mathcal{P}_3''} \tag{8.29}$$

result for smaller T, as, e.g. for $\tau_A = 2$ and $T = 3$ in Figure 8.22. This effect can also be observed for other parameter settings in Appendix C.7.

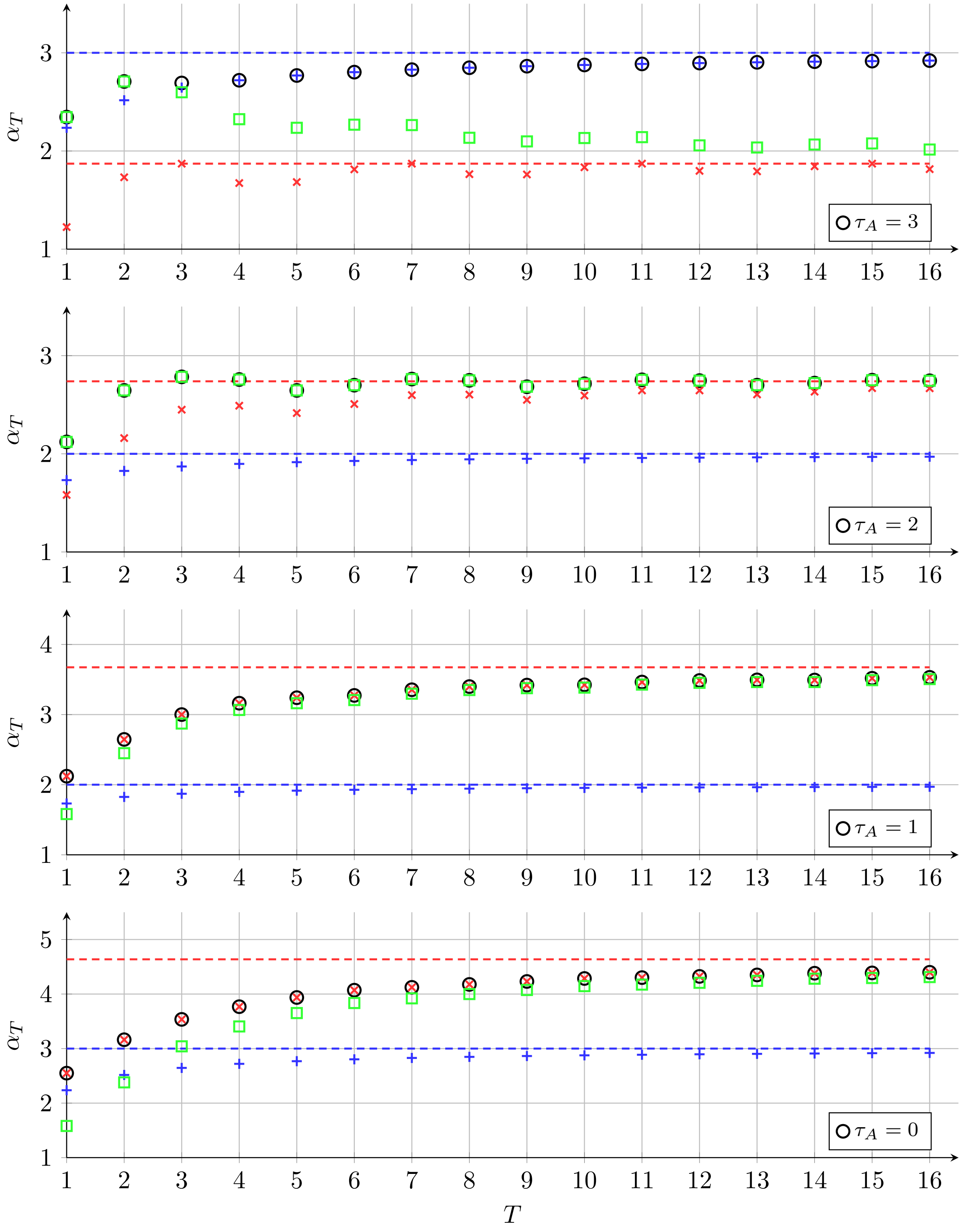

Figure 8.22: Gains α_T as a function of truncation times T, $\bar{\tau} = 3$ and different acausal delays τ_A: $\mathcal{P}_1$ (blue), $\mathcal{P}_3'$ (red), $\mathcal{P}_3''$ (green). The dashed lines represent the corresponding ℓ_2 gains α.

Delay Pattern $\mathcal{P}_3'''$

Almost all points in Figure 8.22 can be mathematically described by using either $\mathcal{P}_1$, $\mathcal{P}_3'$ or $\mathcal{P}_3''$. However, this is not true for, e.g., $\tau_A = 3$ and $T = 3$. Thus, the additional delay pattern

$$(\tau_j) = \big(\underbrace{-\tau_A, -\tau_A, \ldots, -\tau_A}_{T-\bar{\tau}+1\text{ elements}}, (\bar{\tau}-\tau_A), \underbrace{-\tau_A, -\tau_A, \ldots, -\tau_A}_{\bar{\tau}\text{ elements}}, (\bar{\tau}-\tau_A), (\bar{\tau}-\tau_A), \ldots\big) \tag{8.30}$$

for $T - \bar{\tau} + 1 \geq 0$, i.e. $T \geq \bar{\tau} - 1$ is utilized. The corresponding patterns and inner signals are shown in Figures 8.23 to 8.25 and in Appendix C.8 for different values of $\bar{\tau}$, τ_A, and T.

k	-3	-2	-1	0	1	2	3	4	5	6	7	8	9	10	11	12	13	14	15	16
$b_k^{(-2)}$	0	1	2	3	4	5	6	7	8	9	10	11	11	11	11	11	11	11	11	11
$b_k^{(1)}$	0	0	1	2	3	4	5	6	7	8	9	10	11	11	11	11	11	11	11	11
$b_k^{(0)} = a_k$	0	0	0	1	2	3	4	5	6	7	8	9	10	11	11	11	11	11	11	11
$b_k^{(1)}$	0	0	0	0	1	2	3	4	5	6	7	8	9	10	11	11	11	11	11	11
$b_k^{(-2)}$	0	1	2	3	4	5	6	7	8	~~9~~	10	11	11	~~11~~	~~11~~	~~11~~	~~11~~	~~11~~	~~11~~	~~11~~
$b_k^{(-1)}$	0	0	~~1~~	~~2~~	~~3~~	~~4~~	~~5~~	~~6~~	~~7~~	~~8~~	~~9~~	~~10~~	~~11~~	~~11~~	~~11~~	~~11~~	~~11~~	~~11~~	~~11~~	~~11~~
$b_k^{(0)} = a_k$	0	0	0	~~1~~	~~2~~	~~3~~	~~4~~	~~5~~	~~6~~	~~7~~	~~8~~	~~9~~	~~10~~	~~11~~	~~11~~	~~11~~	~~11~~	~~11~~	~~11~~	~~11~~
$b_k^{(1)}$	0	0	0	0	~~1~~	~~2~~	~~3~~	~~4~~	~~5~~	~~6~~	~~7~~	~~8~~	9	~~10~~	~~11~~	~~11~~	11	11	11	11
$b_k^{(-2)} - a_k$	0	1	2	2	2	2	2	2	2	2	2	2	1	0	0	0	0	0	0	0
$b_k^{(-1)} - a_k$	0	0	1	1	1	1	1	1	1	1	1	1	1	0	0	0	0	0	0	0
$b_k^{(0)} - a_k$	0	0	0	0	0	0	0	0	0	0	0	0	0	0	0	0	0	0	0	0
$b_k^{(1)} - a_k$	0	0	0	-1	-1	-1	-1	-1	-1	-1	-1	-1	-1	-1	0	0	0	0	0	0
packet arr.	no	yes	yes	yes	yes	yes	yes	yes	yes	no	yes	yes	yes	no	no	no	yes	yes	yes	yes
c_k	0	1	2	3	4	5	6	7	8	8	10	11	9	9	9	9	11	11	11	11
w_k	0	1	2	2	2	2	2	2	2	1	2	2	-1	-2	-2	-2	0	0	0	0
block	A	A	B	B	B	B	B	B	B	C	C	C	D	D	D	D				
τ_j				-2	-2	-2	-2	-2	-2	-2	-2	1	-2	-2	-2	1	1	1	1	1

Figure 8.23: Packet pattern and inner signals of the uncertainty for $\mathcal{P}_3'''$, $\bar{\tau} = 3$, $T = 10$ and $\tau_A = 2$.

$\bar{\tau}$	min	max	k	-4	-3	-2	-1	0	1	2	3	4	5	6	7	8	9	10	11	12	13	14	15	16	17	18
2	0	2	τ_j					0	0	0	0	0	0	0	0	0	2	0	0	2	2	2				
			w_k			0	0	0	0	0	0	0	0	0	0	0	-1	0	-1	-1	-1	0				
2	-1	1	τ_j					-1	-1	-1	-1	-1	-1	-1	-1	-1	1	-1	-1	1	1	1				
			w_k			0	1	1	1	1	1	1	1	1	1	0	1	-1	-1	-1	0	0				
2	-2	0	τ_j					-2	-2	-2	-2	-2	-2	-2	-2	-2	0	-2	-2	0	0	0				
			w_k			1	2	2	2	2	2	2	2	2	1	2	0	-1	-1	0	0	0				
3	-3	0	τ_j					0	0	0	0	0	0	0	0	3	0	0	0	3	3	3	3	3		
			w_k		0	0	0	0	0	0	0	0	0	0	0	-1	0	0	-2	-2	-2	-2	0	0		
3	-2	1	τ_j					-1	-1	-1	-1	-1	-1	-1	-1	2	-1	-1	-1	2	2	2	2	2		
			w_k		0	0	1	1	1	1	1	1	1	1	0	1	1	-2	-2	-2	-2	0	0	0		
3	-1	2	τ_j					-2	-2	-2	-2	-2	-2	-2	-2	1	-2	-2	-2	1	1	1	1	1		
			w_k		0	1	2	2	2	2	2	2	2	1	2	2	-1	-2	-2	-2	0	0	0	0		
3	0	3	τ_j					-3	-3	-3	-3	-3	-3	-3	-3	0	-3	-3	-3	0	0	0	0	0		
			w_k		1	2	3	3	3	3	3	3	2	3	3	0	-1	-2	-2	0	0	0	0	0		
4	-4	0	τ_j					0	0	0	0	0	0	0	4	0	0	0	0	4	4	4	4	4	4	4
			w_k	0	0	0	0	0	0	0	0	0	0	0	-1	0	0	0	-3	-3	-3	-3	-3	0	0	0
4	-3	1	τ_j					-1	-1	-1	-1	-1	-1	-1	3	-1	-1	-1	-1	3	3	3	3	3	3	3
			w_k	0	0	0	1	1	1	1	1	1	1	0	1	1	1	-3	-3	-3	-3	-3	0	0	0	0
4	-2	2	τ_j					-2	-2	-2	-2	-2	-2	-2	2	-2	-2	-2	-2	2	2	2	2	2	2	2
			w_k	0	0	1	2	2	2	2	2	2	1	2	2	2	-2	-3	-3	-3	-3	0	0	0	0	0
4	-1	3	τ_j					-3	-3	-3	-3	-3	-3	-3	1	-3	-3	-3	-3	1	1	1	1	1	1	1
			w_k	0	1	2	3	3	3	3	3	2	3	3	3	-1	-2	-3	-3	-3	0	0	0	0	0	0
4	0	4	τ_j					-4	-4	-4	-4	-4	-4	-4	0	-4	-4	-4	-4	0	0	0	0	0	0	0
			w_k	1	2	3	4	4	4	4	3	4	4	4	0	-1	-2	-3	-3	0	0	0	0	0	0	0

Figure 8.24: Resulting delay patterns (τ_j) and worst case output sequences (w_k) for $\mathcal{P}_3'''$, $\bar{\tau} \in \{2, 3, 4\}$ and $T = 10$.

Block A, C and D consist of $\bar{\tau} - 1$, $\bar{\tau}$ and $\bar{\tau} + 1$ samples, respectively. As a result, the length of (orange) block B is $T - \bar{\tau} - \tau_A + 2$. The worst case norm of output sequence

$\bar{\tau}$	min	max	k	-4	-3	-2	-1	0	1	2	3	4	5	6	7	8	9	10	11	12	13	14	15	16	17	18
2	0	2	τ_j					0	2	0	0	2	2	2												
			w_k			0	0	0	-1	0	-1	-1	-1	0												
2	-1	1	τ_j					-1	1	-1	-1	1	1	1												
			w_k			0	1	0	1	-1	-1	-1	0	0												
2	-2	0	τ_j					-2	0	-2	-2	0	0	0												
			w_k			1	1	2	0	-1	-1	0	0	0												
3	-3	0	τ_j					3	0	0	0	3	3	3	3	3										
			w_k		0	0	0	-1	0	0	-2	-2	-2	-2	0	0										
3	-2	1	τ_j					2	-1	-1	-1	2	2	2	2	2										
			w_k		0	0	0	1	1	-2	-2	-2	-2	0	0	0										
3	-1	2	τ_j					1	-2	-2	-2	1	1	1	1	1										
			w_k		0	0	2	2	-1	-2	-2	-2	0	0	0	0										
3	0	3	τ_j					0	-3	-3	-3	0	0	0	0	0										
			w_k		0	2	3	0	-1	-2	-2	0	0	0	0	0										
4	-4	0	τ_j																							
			w_k																							
4	-3	1	τ_j																							
			w_k																							
4	-2	2	τ_j																							
			w_k																							
4	-1	3	τ_j																							
			w_k																							
4	0	4	τ_j																							
			w_k																							

Figure 8.25: Resulting delay patterns (τ_j) and worst case output sequences (w_k) for $\mathcal{P}_3'''$, $\bar{\tau} \in \{2,3,4\}$ and $T = 2$.

(w_k) for $\mathcal{P}_3'''$ is given by

$$||(w_k)_T||_2^2 = A + B + C + D \tag{8.31}$$

with

$$A = \begin{cases} 0 & \text{if} \quad \tau_A \in \{0,1\} \\ \displaystyle\sum_{i=1}^{\tau_A - 1} \left(i - \delta^{(i)}\right)^2 \bar{v}^2 & \text{otherwise} \end{cases} \tag{8.32a}$$

$$\delta^{(i)} = \begin{cases} 1 & \text{if} \quad i = (T - \bar{\tau} + 2) \ \wedge \ (T < \bar{\tau} - 2 + \tau_A) \\ 0 & \text{otherwise} \end{cases} \tag{8.32b}$$

$$B = \begin{cases} (T - \bar{\tau} - \tau_A + 2)\tau_A^2 \bar{v}^2 & \text{if} \quad T \geq \bar{\tau} - 2 + \tau_A \\ (T - \tau_A + 2)\tau_A^2 \bar{v}^2 & \text{otherwise} \end{cases} \tag{8.32c}$$

$$C = \begin{cases} \displaystyle\sum_{i=\tau_A - 1}^{\tau_A + \bar{\tau} - 2} \left(\min\{i, \tau_A\}\right)^2 \bar{v}^2 & \text{if} \quad T \geq \bar{\tau} - 2 + \tau_A \\ 0 & \text{otherwise} \end{cases} \tag{8.32d}$$

and

$$D = \sum_{i=\bar{\tau}-\tau_A}^{2\bar{\tau}-\tau_A} \left(\min\{i, \bar{\tau} - 1\}\right)^2 \bar{v}^2 \tag{8.32e}$$

for $T \geq \bar{\tau} - 1$. The different cases in (8.32) allow to correctly calculate $\alpha_{T,\mathcal{P}_3'''}$ also for small truncation T as shown in Figure 8.26 and, in more detail, in Appendix C.9 as well as

$$\alpha_{\mathcal{P}_3'''} = \sup_T \alpha_{T,\mathcal{P}_3'''} \ . \tag{8.33}$$

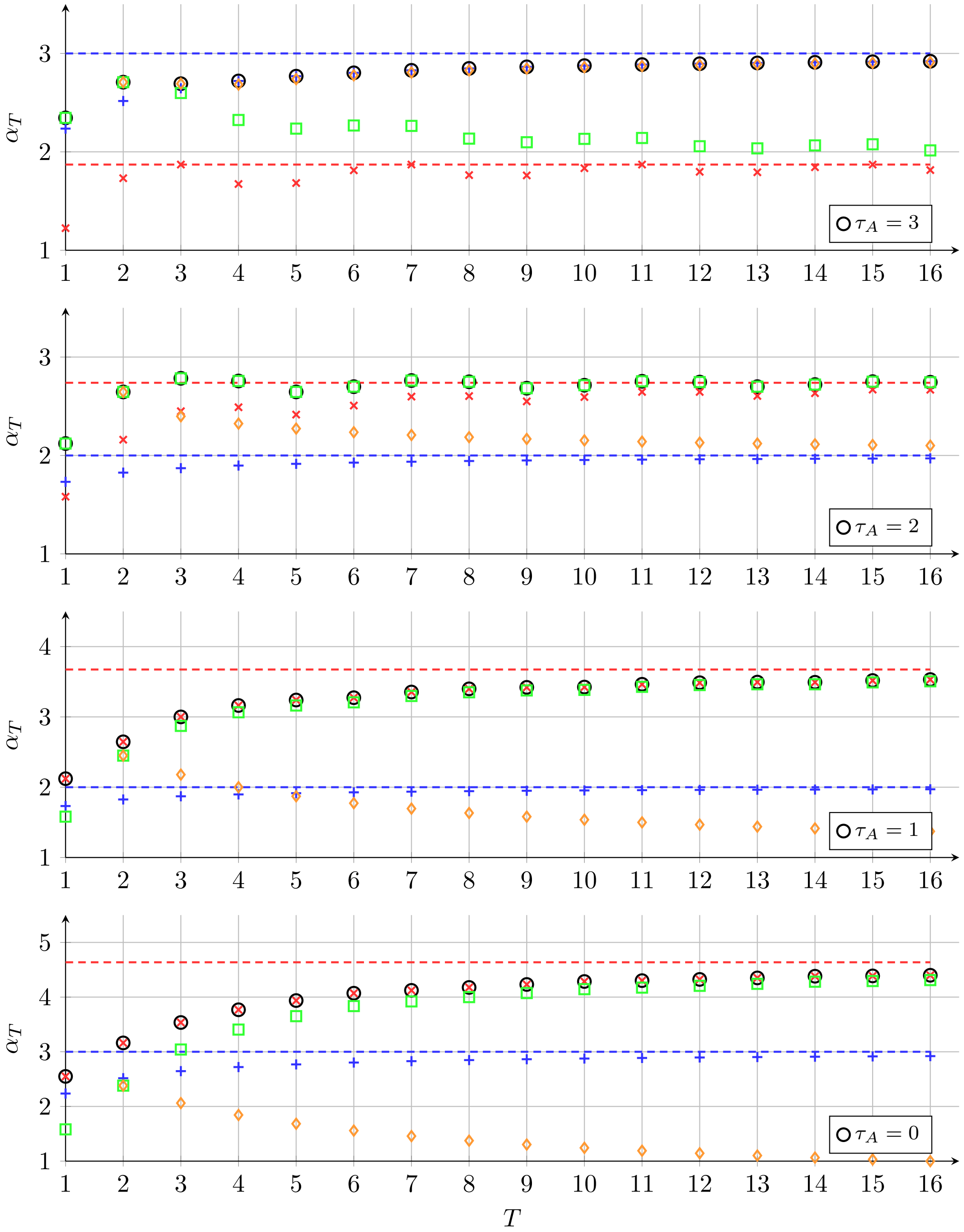

Figure 8.26: Gains α_T as a function of truncation times T, $\bar{\tau} = 3$ and different acausal delays τ_A: $\mathcal{P}_1$ (blue), $\mathcal{P}_3'$ (red), $\mathcal{P}_3''$ (green) and $\mathcal{P}_3'''$ (orange). The dashed lines represent the corresponding ℓ_2 gains α.

Protocol $\mathcal{P}_3$

To find the overall finite ℓ_2 gain for protocol $\mathcal{P}_3$ one has to combine the results for packet patterns $\mathcal{P}_1$, $\mathcal{P}_3'$, $\mathcal{P}_3''$ and $\mathcal{P}_3'''$.

Different gains that depend on the actual choice of the acausal delay τ_A follow for the considered delay patterns. Values for α_T that are found by direct variation of all possible combinations of packet delays τ_j are indicated as black circles in Figure 8.26 to show that the used mathematical description exactly reproduces all α_T. In Figures 8.27 and 8.28, the results for $T = \{1, 2, 3, 4\}$ are shown depending on acausal delay τ_A and truncation times T. Results for larger T are omitted for more clarity in the plots.

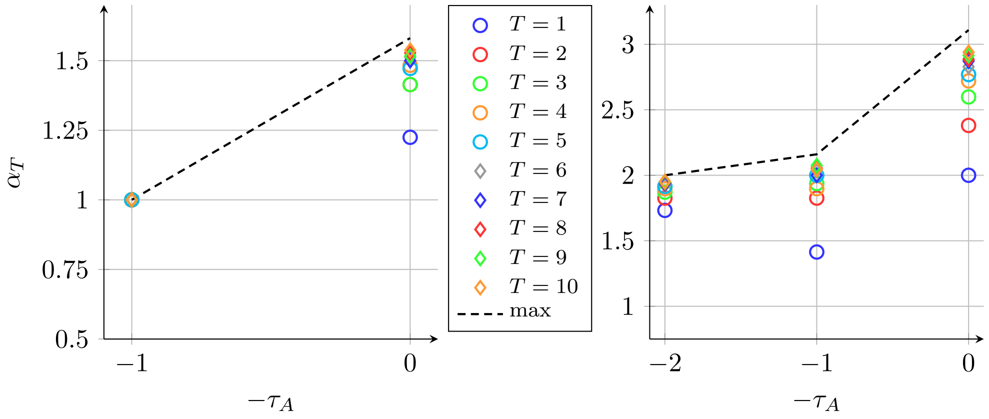

Figure 8.27: Gains α_T for different T and τ_A as well as ℓ_2 gains α (dashed lines) for $\mathcal{P}_3$, $\bar{\tau} = 1$ (left) and $\bar{\tau} = 2$ (right).

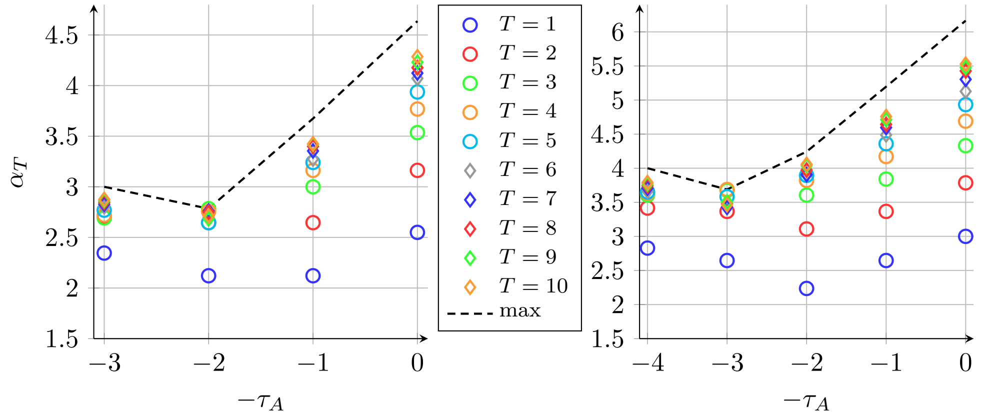

Figure 8.28: Gains α_T for different T and τ_A as well as ℓ_2 gains α (dashed lines) for $\mathcal{P}_3$, $\bar{\tau} = 3$ (left) and $\bar{\tau} = 4$ (right).

The optimal ℓ_2 gain α^* and the optimal acausal delay τ_A^* are found numerically as the minimum among the different patterns. Results for $\bar{\tau} \in \{1, 2, 3, 4, 10, 30, 50, 100\}$ are visualized in Figures 8.29 to 8.32 using black dots. In addition, the contribution of the individual packet patterns $\mathcal{P}_1$, $\mathcal{P}_3'$, $\mathcal{P}_3''$ and $\mathcal{P}_3'''$ are plotted in different colors.

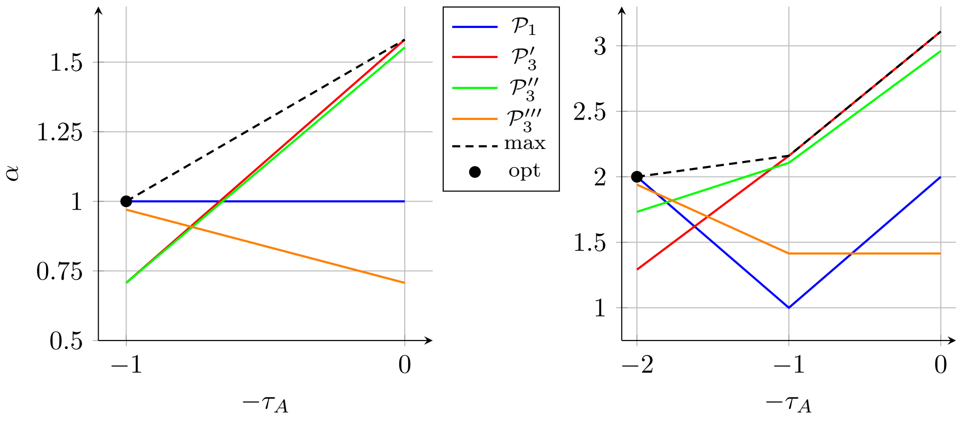

Figure 8.29: Finite ℓ_2 gain α (black dashed lines) and the optimal choice of the acausal delay τ_A (black dots) for $\mathcal{P}_3$, $\bar{\tau} = 1$ (left) and $\bar{\tau} = 2$ (right).

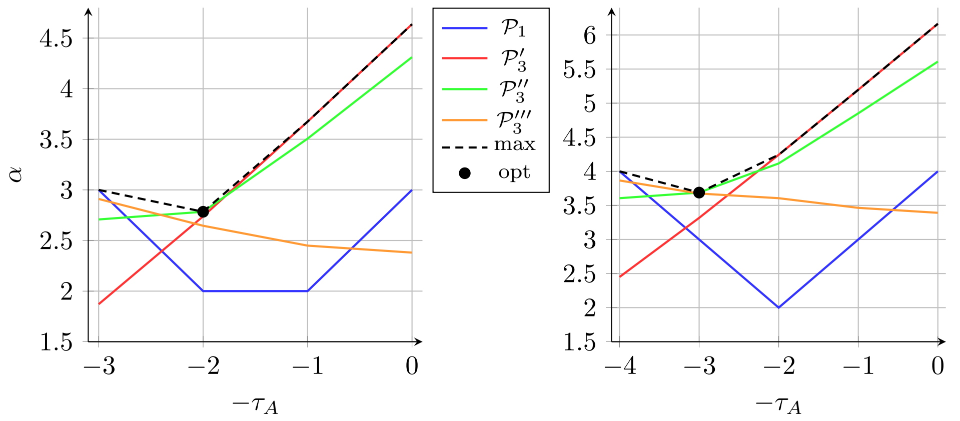

Figure 8.30: Finite ℓ_2 gain α (black dashed lines) and the optimal choice of the acausal delay τ_A (black dots) for $\mathcal{P}_3$, $\bar{\tau} = 3$ (left) and $\bar{\tau} = 4$ (right).

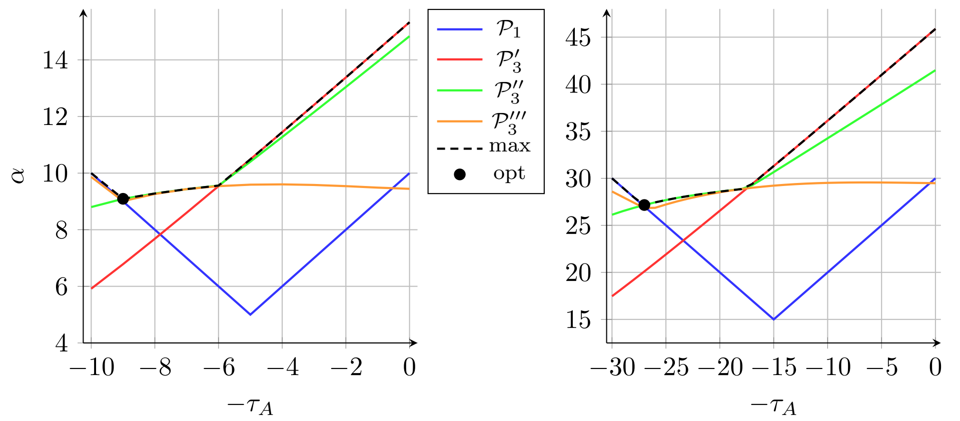

Figure 8.31: Finite ℓ_2 gain α (black dashed lines) and the optimal choice of the acausal delay τ_A (black dots) for $\mathcal{P}_3$, $\bar{\tau} = 10$ (left) and $\bar{\tau} = 30$ (right).

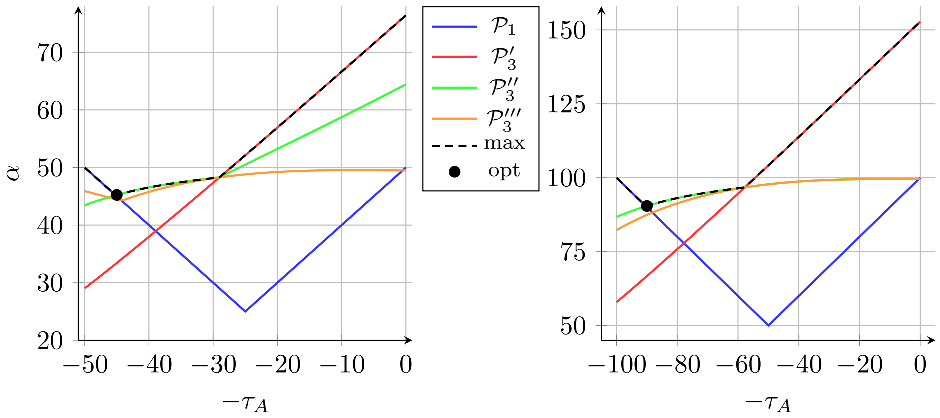

Figure 8.32: Finite ℓ_2 gain α (black dashed lines) and the optimal choice of the acausal delay τ_A (black dots) for $\mathcal{P}_3$, $\bar{\tau} = 50$ (left) and $\bar{\tau} = 100$ (right).

Consequently, the finite ℓ_2 gain follows as

$$\alpha^* = \min_{\tau_A} \left\{ \max_{\tau_A} \left\{ \alpha_{\mathcal{P}_1}, \alpha_{\mathcal{P}_3'}, \alpha_{\mathcal{P}_3''}, \alpha_{\mathcal{P}_3'''} \right\} \right\}, \tag{8.34}$$

with the corresponding optimal choice for the acausal delay

$$\tau_A^* = \operatorname*{argmin}_{\tau_A} \left\{ \max_{\tau_A} \left\{ \alpha_{\mathcal{P}_1}, \alpha_{\mathcal{P}_3'}, \alpha_{\mathcal{P}_3''}, \alpha_{\mathcal{P}_3'''} \right\} \right\}. \tag{8.35}$$

The numeric evaluation of (8.34) and (8.35) results in relation (8.10) in Theorem 8.2 and Table 8.1.

As pointed out directly below Theorem 8.2, it is possible to make use of the gain that follows for $\mathcal{P}_1$ evaluated at $\tau_A = \bar{\tau}$ as an over-estimation of α^* for protocol $\mathcal{P}_3$, cf. Figures 8.29 to 8.32.

This completes the proof. ■

8.4 Simulation Example

The example of a feedback loop with filtered Smith predictor is continued in this section. The LMI-based stability analysis can be found in Section 6.2.2 and the analysis using the basic version of the SGT-based Theorem 7.1 in Section 7.3.

An evaluation of the LMI conditions stated in Theorem 6.3 yields either 5 or 1 for the maximal admissible time-varying delay $\bar{\tau}$, see also Table 8.2. However, as shown in Chapter 6, there are sequences of packet delays that already lead to instability for $\bar{\tau} = 4$. This is because the packetized character of the transmissions is not explicitly considered in the analysis. This issue is overcome by using Theorem 7.1, where the SGT is utilized for the causal case. The maximum achievable $\bar{\tau} = 4$ for protocol $\mathcal{P}_1$ and $\bar{\tau} = 2$ for $\mathcal{P}_3$.

Next, Theorem 8.2 is evaluated for the simulation example. Conditions (8.9), and (8.10) are evaluated for $\underline{\tau}_N = 0$ and different $\bar{\tau}$. The optimal acausal delay τ_A^* is used in the predictor and relation (8.11) is checked by using Bode magnitude plots for $M(z)\alpha^*$ as shown in Figures 8.33 and 8.34.

Table 8.2: Simulation example: maximal admissible variable time delay $\bar{\tau}$ for conventional LMI approaches and SGT approaches that include the packetized nature of network transmissions.

approach	theorem	maximal $\bar{\tau}$
LMI	Theorem 6.3(i)	5
LMI	Theorem 6.3(ii)	1
SGT	Theorem 7.1 for $\mathcal{P}_1$	4
SGT	Theorem 7.1 for $\mathcal{P}_3$	2
SGT acausal	Theorem 8.2 for $\mathcal{P}_1$	6
SGT acausal	Theorem 8.2 for $\mathcal{P}_3$	3

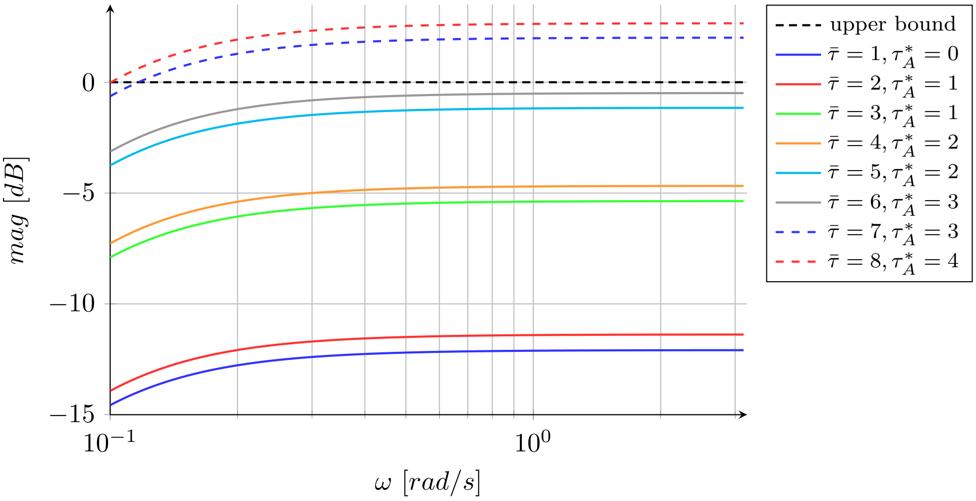

Figure 8.33: Simulation example: Bode magnitude plots of $M(z)\alpha$ in condition (8.11) for protocol $\mathcal{P}_1$.

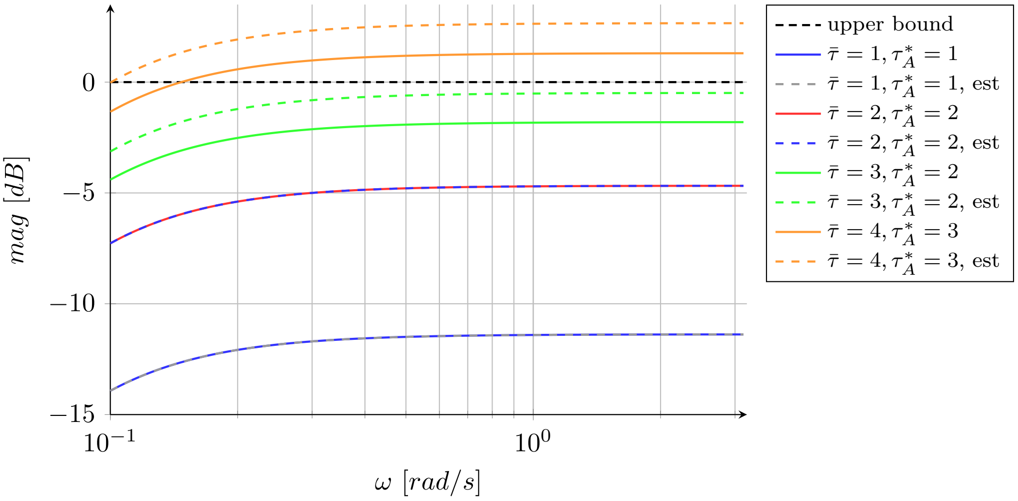

Figure 8.34: Simulation example: Bode magnitude plots of $M(z)\alpha$ in condition (8.11) for protocol $\mathcal{P}_3$.

Figure 8.33 reveals that one can show stability for a maximal value of $\bar{\tau} = 6$ with the proposed theorem for $\mathcal{P}_1$, which is larger than using the LMI-based approach.

A maximum $\bar{\tau} = 3$ is achieved for protocol $\mathcal{P}_3$ as depicted in Figure 8.34. Please note that one can find delay patterns for $\bar{\tau} = 4$ (see Figures 6.7 and 6.8) that lead to instability for the setting in the LMI-based approach in Section 6.2.2. Hence, the upper bound provided by Theorem 8.2 equals the largest achievable value for the admissible time-varying delay. An over-estimation of the gain as stated in (8.12) for $\mathcal{P}_3$ will often lead to a smaller admissible $\bar{\tau}$, which is not the case for the presented example, see green dashed line in Figure 8.34. Table 8.2 compares of the results for all considered approaches for the simulation example.

8.5 Laboratory Experiment

Theorem 8.2 is also evaluated for the mass-spring laboratory experiment introduced in Section 7.4. Figures 8.35 and 8.35 show the resulting Bode magnitude plots of $M(z)\alpha^*$ in Theorem 8.2. For the present lab setup, the choice of the acausal delay τ_A^* in terms of the use of the floor or ceiling-operator stated in (8.9a) for protocol $\mathcal{P}_1$ does not yield any differences.

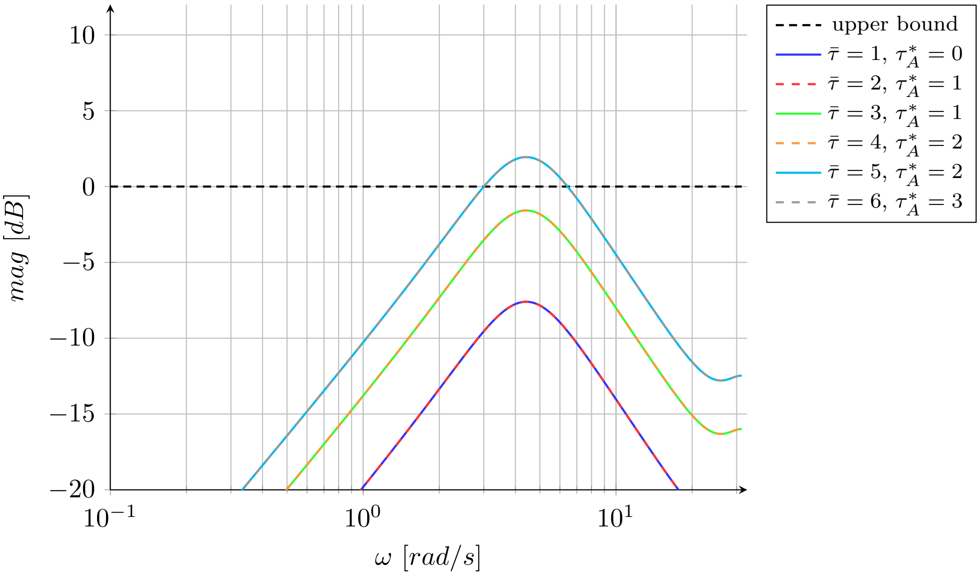

Figure 8.35: Experiment: Bode magnitude plots of $M(z)\alpha$ in condition (8.11) for protocol $\mathcal{P}_1$.

A maximal admissible time-varying delay of $\bar{\tau} = 4$ for $\mathcal{P}_1$ as well as $\bar{\tau} = 2$ for $\mathcal{P}_3$ follow the evaluation of Theorem 8.2. Hence, a less conservative stability result is obtained, when compared to the basic version of the SGT-based Theorem 7.1. This is also summarized in Table 8.3.

Figures 8.37 and 8.38 underpin that already $\bar{\tau} = 5$ and $\bar{\tau} = 3$ result in an unstable feedback loops for protocols $\mathcal{P}_1$ and $\mathcal{P}_2$, respectively. As a result, the experiment is stopped because the cord jumps out of the pulley. Please note that this was predicted by Theorem 8.2 as shown in Table 8.3.

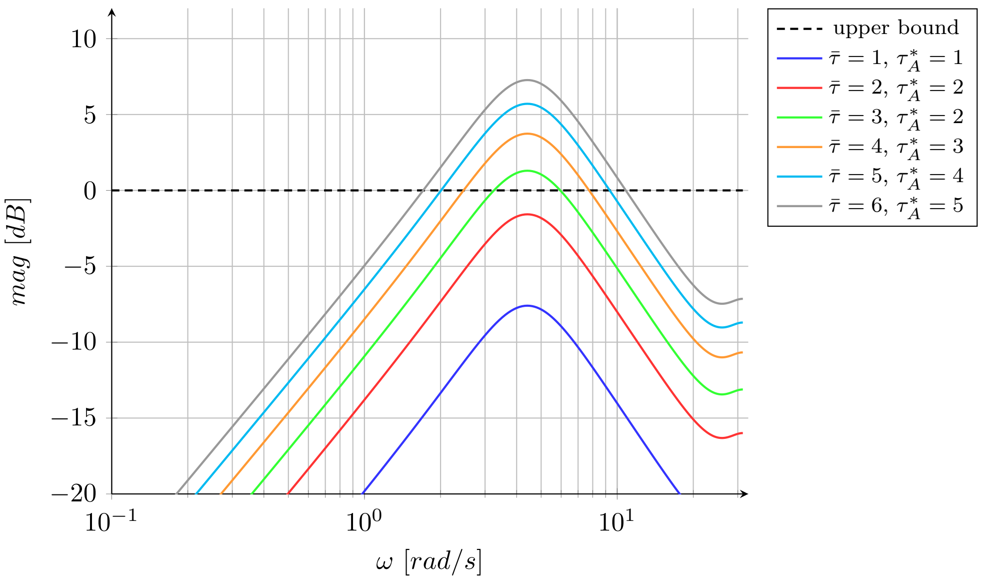

Figure 8.36: Experiment: Bode magnitude plots of $M(z)\alpha$ in condition (8.11) for protocol $\mathcal{P}_3$.

Table 8.3: Experiment: maximal admissible variable time delay $\bar{\tau}$ for the different SGT approaches that include the packetized nature of network transmissions.

approach	theorem	maximal $\bar{\tau}$
SGT	Theorem 7.1 with $\mathcal{P}_1$	2
SGT	Theorem 7.1 with $\mathcal{P}_3$	1
SGT acausal	Theorem 8.2 with $\mathcal{P}_1$	4
SGT acausal	Theorem 8.2 with $\mathcal{P}_3$	2

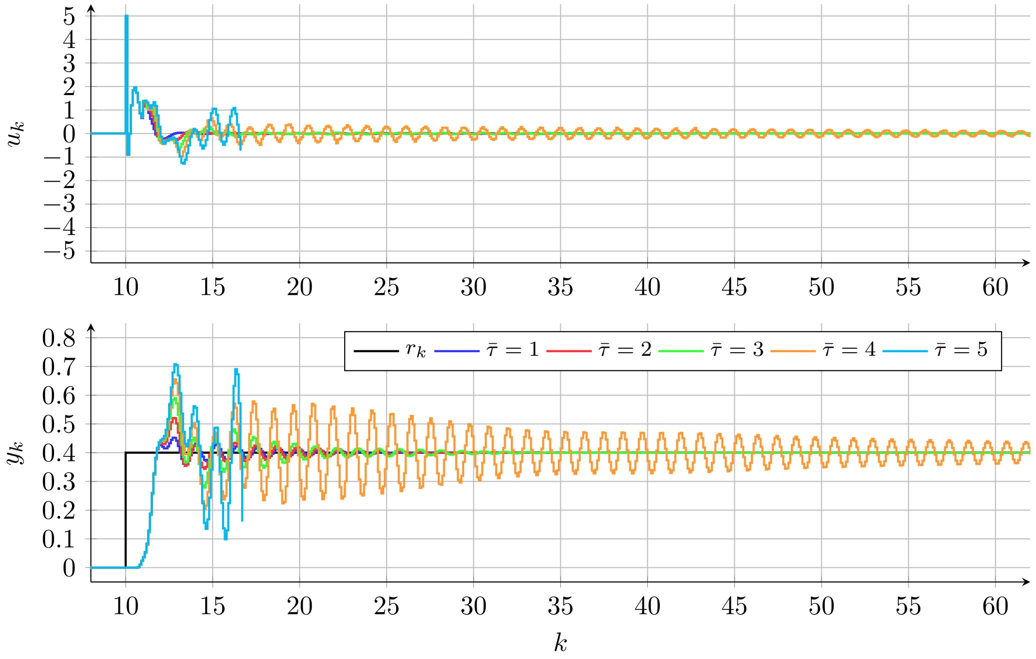

Figure 8.37: Experiment: step responses (y_k) and actuating signals (u_k) for different maximal admissible $\bar{\tau}$ utilizing protocol $\mathcal{P}_1$ for the acausal design and analysis approach.

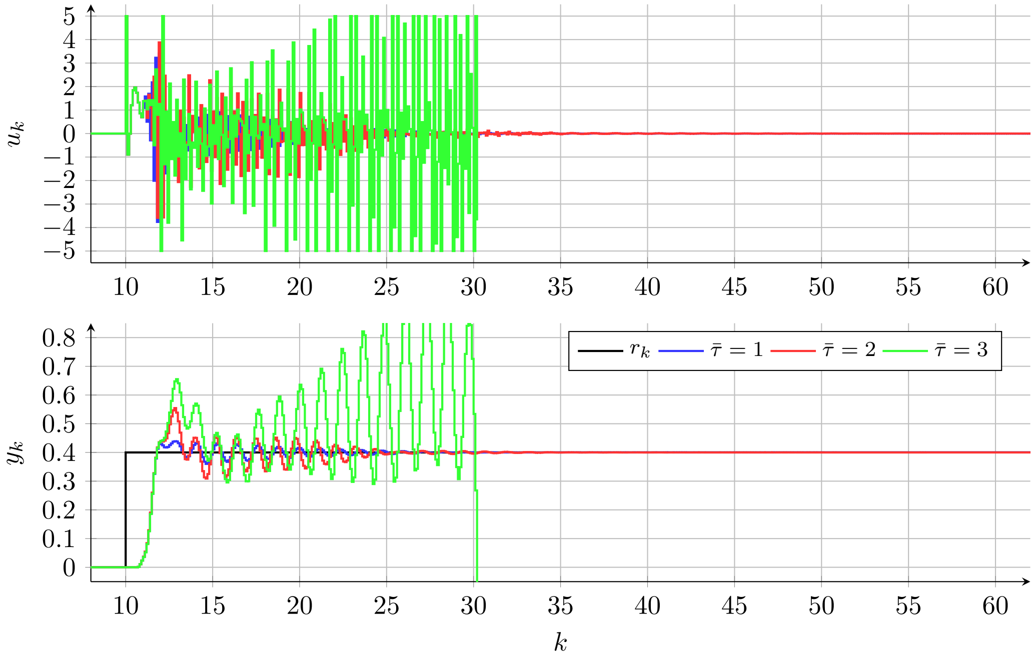

Figure 8.38: Experiment: step responses (y_k) and actuating signals (u_k) for different maximal admissible $\bar{\tau}$ utilizing protocol $\mathcal{P}_3$ for the acausal design and analysis approach.

Chapter 9

Outlook

This work focuses on various aspects that appear in networked control systems, where the data is sent in separate packets. The correct consideration of this packet-based characteristics is vital for the analysis and controller design.

The very basis is laid by an accurate modeling and simulation of data transmissions subject to time-varying packet delays. It is also shown in the present work that the analysis and design of packetized NCS is always a trade-off between the properties (and thus assumptions) on the network and the complexity for the controller design and stability analysis. This can be seen, e.g., by the proposed robust control approach for buffered networked systems as well as by the adaptive methods introduced in this thesis.

Novel stability criteria are proposed for NCS, where the data transmissions occur with time-varying packet delays while different protocols are in place. The considered protocols differ in their packet selection, packet skipping and hold mechanisms. It is pointed out that it is of utmost importance to include the packet-based characteristics of the data transmissions in the analysis, which is commonly not explicitly done in LMI-based approaches.

The goal of this thesis was to bridge the gap between classical methods from automatic control and novel networked control systems by incorporating the effects of packet-based data transmissions. An important aspect was to come up with methods, which are easy to apply and simple to implement. For example, the introduced SGT-based approaches are an extension of classical frequency domain techniques that preserves the easy-to-use and computationally inexpensive nature.

Various enhancements of the introduced criteria are possible such as, e.g., to focus on dedicated frequency ranges in the analysis. Further extensions may deal with the inclusion of additional protocols and the generalization to more complex networked structures, such as multi-loop systems. Also, an improved alleviation of the effects due to external perturbations and packet dropout are of interest for future research.

Appendix A

Filtered Smith Predictor

The classical Smith predictor [Smi59] is a structure to control a linear plant $P(z) = \hat{P}(z)z^{-\hat{d}}$ that includes a constant and known time delay $\hat{d}$. Figure A.1 shows a feedback loop with such a plant and a controller $\tilde{C}(z)$ that should be designed to track a reference sequence (r_k) and reduce the effect of a disturbance (d_k). The overall transfer function from the reference (r_k) to the output (y_k) is given by

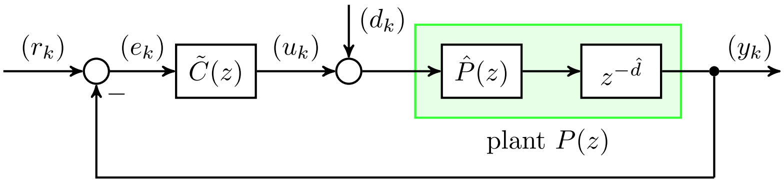

Figure A.1: Unity feedback loop with a nominal plant $\hat{P}(z)$, nominal plant delay $\hat{d}$ and controller $\tilde{C}(z)$. Sequences (r_k) and (d_k) represent the reference input and the disturbance, respectively.

$$\tilde{T}(z) = \frac{\tilde{C}(z)\hat{P}(z)z^{-\hat{d}}}{1 + \tilde{C}(z)\hat{P}(z)z^{-\hat{d}}} \tag{A.1}$$

The main idea of the Smith predictor is to design a controller $\tilde{C}(z)$ such that the feedback loop in Figure A.1 is equivalent to Figure A.2 with transfer function

$$T(z) = \frac{C(z)\hat{P}(z)}{1 + C(z)\hat{P}(z)}\, z^{-\hat{d}} \tag{A.2}$$

and, as a consequence, controller $C(z)$ can be designed for the nominal, delay-free case.

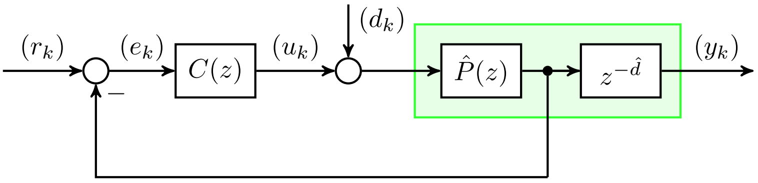

Figure A.2: Target setup for the classical Smith predictor.

The requirement $T(z) = \tilde{T}(z)$ yields a relation between the two controllers such that

$$\tilde{C}(z) = \frac{C(z)}{1 + C(z)\left(\hat{P}(z) - \hat{P}(z)z^{-\hat{d}}\right)}, \tag{A.3}$$

which can be graphically represented as in Figure A.3. For $F(z) = 1$, one gets the classical Smith predictor structure, where a copy of the nominal plant is used in parallel to the real-world plant to generate an additional error signal that is used by the nominal control loop formed by $C(z)$ and $\hat{P}(z)$. Consequently, the relation between (r_k) and (u_k) is given by

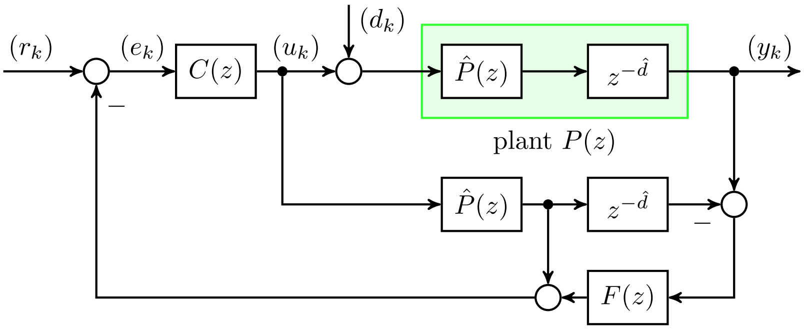

Figure A.3: Classical Smith predictor with additional filter transfer function $F(z)$.

$$\tilde{u}(z) = \mathcal{Z}\{(u_k)\} = \frac{C(z)}{1 + C(z)\hat{P}(z)}\tilde{r}(z) \tag{A.4}$$

with $\tilde{r}(z) = \mathcal{Z}\{(r_k)\}$ and between (d_k) and (y_k) one gets

$$\tilde{y}(z) = \hat{P}(z)z^{-\hat{d}}\left(\tilde{u}(z) + \tilde{d}(z)\right) = \hat{P}(z)z^{-\hat{d}}\,\tilde{d}(z) \tag{A.5}$$

with $\tilde{d}(z) = \mathcal{Z}\{(d_k)\}$ for the case that $r_k = 0$ for all k. Additionally, it is assumed in (A.5) that the plant model is identical to the model used in the predictor. In this case, $\tilde{u}(z) = -C(z)\hat{P}(z)\tilde{u}(z) + C(z)\hat{P}(z)z^{-\hat{d}}\tilde{u}(z) - C(z)\hat{P}(z)z^{-\hat{d}}\tilde{u}(z) + C(z)\tilde{r}(z)$ yields $\tilde{u}(z) = 0$ for $\tilde{r}(z) = 0$. The resulting effect of disturbance (d_k) on the output (y_k) in (A.5) makes it clear that the classical Smith predictor must only be used for stable plants.

Several modified (filtered) Smith predictors as, e.g., in [NRC09] are proposed to enable one to control unstable plants as well. The main idea here is to introduce an additional filter transfer function $F(z)$ as shown in Figure A.3 to weight the difference between the output of the physical plant and the predicted output. Thus the modified feedback loop can be described by

$$\begin{aligned}\tilde{y}(z) = &\frac{C(z)P(z)}{1 + C(z)\hat{P}(z) + C(z)F(z)\left(P(z) - \hat{P}(z)z^{-\hat{d}}\right)}\tilde{r}(z) \\ &+ \frac{P(z)\left(1 + C(z)\hat{P}(z) - C(z)F(z)\hat{P}(z)z^{-\hat{d}}\right)}{1 + C(z)\hat{P}(z) + C(z)F(z)\left(P(z) - \hat{P}(z)z^{-\hat{d}}\right)}\tilde{d}(z)\end{aligned} \tag{A.6}$$

and

$$\tilde{u}(z) = \frac{C(z)}{1 + C(z)\hat{P}(z) + C(z)F(z)\left(P(z) - \hat{P}(z)z^{-\hat{d}}\right)}\,\tilde{r}(z) \qquad \text{(A.7)}$$
$$\frac{C(z)F(z)P(z)}{1 + C(z)\hat{P}(z) + C(z)F(z)\left(P(z) - \hat{P}(z)z^{-\hat{d}}\right)}\,\tilde{d}(z)\,.$$

In the nominal case, i.e. $P(z) = \hat{P}(z)z^{-\hat{d}}$, the transfer functions between inputs (r_k), (d_k) and (y_k), (u_k) are given as

$$(r_k) \to (y_k) \qquad T(z) = \frac{C(z)P(z)}{1 + C(z)\hat{P}(z)}\,, \qquad \text{(A.8a)}$$

$$(d_k) \to (y_k) \qquad S(z) = P(z)\left[1 - \frac{C(z)F(z)P(z)}{1 + C(z)\hat{P}(z)}\right]\,, \qquad \text{(A.8b)}$$

$$(r_k) \to (u_k) \qquad T_u(z) = \frac{C(z)}{1 + C(z)\hat{P}(z)}\,, \qquad \text{(A.8c)}$$

$$(d_k) \to (u_k) \qquad S_u(z) = -\frac{C(z)P(z)F(z)}{1 + C(z)\hat{P}(z)}\,. \qquad \text{(A.8d)}$$

Transfer functions $T(z)$ and $T_u(z)$ are stable by design, e.g., using algebraic synthesis [Che06]. The feedback loop in Figure A.3 is internally stable [DFT09] if $P(z)$ and $F(z)$ are stable, see (A.8b) and (A.8d). To get rid of the limitation to stable plants, Figure A.3 is drawn in a different way in Figure A.4.

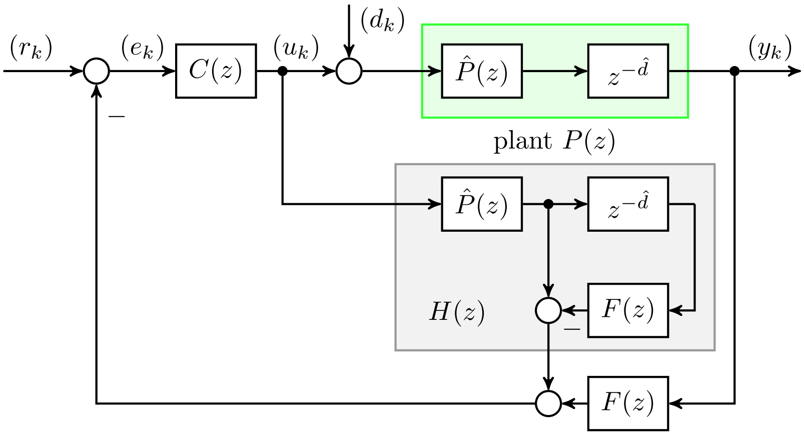

Figure A.4: Modified Figure A.3 to introduce transfer function $H(z)$.

An additional transfer function

$$H(z) = \hat{P}(z) - \hat{P}(z)z^{-\hat{d}}F(z) = \hat{P}(z)\left(1 - z^{-\hat{d}}F(z)\right) \qquad \text{(A.9)}$$

is introduced to get the final structure of the filtered Smith predictor depicted in Figure A.5 with the corresponding relations

$$\tilde{y}(z) = \frac{C(z)P(z)}{1 + C(z)H(z) + P(z)C(z)F(z)}\,\tilde{r}(z) \qquad \text{(A.10)}$$
$$+ \frac{P(z)\big(1 + C(z)H(z)\big)}{1 + C(z)H(z) + P(z)C(z)F(z)}\,\tilde{d}(z)$$

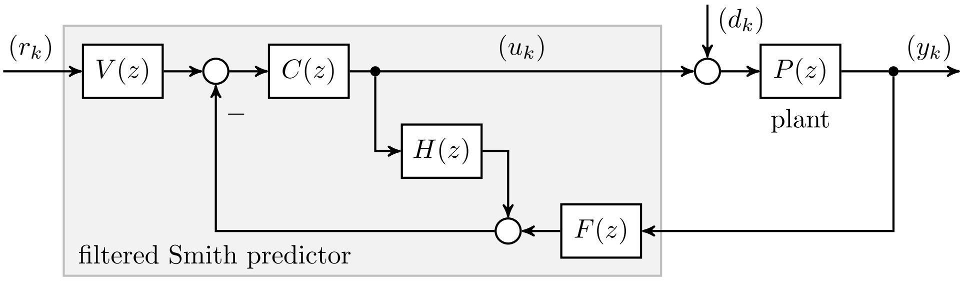

Figure A.5: Filtered Smith predictor.

and

$$\begin{aligned} \tilde{u}(z) = & \frac{C(z)}{1 + C(z)H(z) + P(z)C(z)F(z)} \tilde{r}(z) \\ & - \frac{C(z)F(z)P(z)}{1 + C(z)H(z) + P(z)C(z)F(z)} \tilde{d}(z) \,. \end{aligned} \tag{A.11}$$

The choice of $H(z)$ as in (A.9) in relations (A.10) and (A.11) yields transfer functions

$$(r_k) \to (y_k) \qquad T(z) = \frac{C(z)P(z)}{1 + C(z)\hat{P}(z)} \,, \tag{A.12a}$$

$$(d_k) \to (y_k) \qquad S(z) = \frac{P(z)}{1 + C(z)\hat{P}(z)} + \frac{P(z)C(z)H(z)}{1 + C(z)\hat{P}(z)} \,, \tag{A.12b}$$

$$(r_k) \to (u_k) \qquad T_u(z) = \frac{C(z)}{1 + C(z)\hat{P}(z)} \,, \tag{A.12c}$$

$$(d_k) \to (u_k) \qquad S_u(z) = -\frac{C(z)P(z)F(z)}{1 + C(z)\hat{P}(z)} \,, \tag{A.12d}$$

because $1 + C(z)H(z) + P(z)C(z)F(z) = 1 + C(z)\hat{P}(z)$ holds. Transfer functions $T(z)$ and $T_u(z)$ are again stable by the nominal controller design as for the classical Smith predictor. What about the stability of (A.12b) and (A.12d) that depend on the specific choice of $F(z)$ and the resulting $H(z)$ defined in (A.9)? A stable filter transfer function

$$F(z) = \frac{\mu_F(z)}{\nu_F(z)} \tag{A.13}$$

is designed [NRC09] such that

$$H(z) = \frac{\hat{\mu}(z)}{\hat{\nu}(z)} \left(1 - z^{-\hat{d}} \frac{\mu_F(z)}{\nu_F(z)} \right) = \frac{\hat{\mu}(z) \left(z^{\hat{d}} \nu_F(z) - \mu_F(z) \right)}{z^{\hat{d}} \hat{\nu}(z) \nu_F(z)} \tag{A.14}$$

with

$$z^{\hat{d}} \, \nu_F(z) - \mu_F(z) = 0 \qquad \forall z \quad | \quad \hat{\nu}(z) = 0 \quad \wedge \quad |z| \geq 1 \,. \tag{A.15}$$

to compensate all unstable poles in the denominator polynomial $\hat{\nu}(z)$ of plant

$$\hat{P}(z) = \frac{\hat{\mu}(z)}{\hat{\nu}(z)} \tag{A.16}$$

in $H(z)$, which is possible because all parts of (A.14) are exactly realized in the very same predictive controller. Hence, $H(z)$ is stable. This implies that

$$S(z) = \frac{T(z)}{C(z)} + T(z)H(z) \tag{A.17}$$

is stable, because $\frac{T(z)}{C(z)}$ is also stable by design since no unstable zeros are canceled between $\hat{P}(z)$ and $C(z)$. In addition, (A.12d) equals

$$S_u(z) = -T(z)F(z)\,, \tag{A.18}$$

which is stable as well. As a consequence, the filter Smith predictor in Figure A.5 is also internally stable for unstable plants.

For the example plant (1.2) in Chapters 1 and 6, one has to compensate one pole at $z_1 = 1.0513$. Therefore, (A.15) has to hold for z_1 and a chosen filter denominator polynomial $\nu_F(z) = z - \lambda$ with $\lambda = 0.95$, which is possible for a numerator polynomial $\mu_F(z) = z - f$ with $f = 0.968$. Consequently, the resulting filter transfer function

$$F(z) = \left(\frac{1-\lambda}{1-f}\right)\frac{z-f}{z-\lambda} \tag{A.19}$$

with a dc-gain equal to one is given as in (1.8) and

$$H(z) = \frac{0.0051271(z-1)\left(z^2+1.773z+1.199\right)\left(z^2-0.6713z+1.199\right)}{z^5(z-0.95)} \tag{A.20}$$

is the second transfer function needed for the filtered Smith predictor in Figure A.5. The corresponding zeros of $H(z)$ are $z_{1,2} = -0.8863 \pm j0.6431$, $z_{3,4} = 0.3357 \pm j1.0421$ and $z_5 = 1$.

Appendix B

Delay and Packet Patterns for the SGT in Chapter 7

B.1 Patterns for $\mathcal{P}_1$

k	-1	0	1	2	3	4	5	6
$b_k^{(0)} = a_k$	0	$\cancel{1}$	$\cancel{2}$	$\cancel{3}$	$\cancel{4}$	$\cancel{4}$	$\cancel{4}$	4
$b_k^{(1)}$	$\cancel{0}$	$\cancel{0}$	$\cancel{1}$	$\cancel{2}$	$\cancel{3}$	$\cancel{4}$	$\cancel{4}$	4
$b_k^{(2)}$	$\cancel{0}$	$\cancel{0}$	$\cancel{0}$	$\cancel{1}$	$\cancel{2}$	$\cancel{3}$	$\cancel{4}$	4
$b_k^{(3)}$	$\cancel{0}$	$\cancel{0}$	$\cancel{0}$	$\cancel{0}$	1	2	3	4
w_k	0	-1	-2	-3	-3	-2	-1	0
τ_j		3	3	3	3	≥ 2	≥ 1	≥ 0

(a) $T = 3$

k	-1	0	1	2	3	4	5	6	7
$b_k^{(0)} = a_k$	0	$\cancel{1}$	$\cancel{2}$	$\cancel{3}$	$\cancel{4}$	$\cancel{5}$	$\cancel{5}$	$\cancel{5}$	5
$b_k^{(1)}$	$\cancel{0}$	$\cancel{0}$	$\cancel{1}$	$\cancel{2}$	$\cancel{3}$	$\cancel{4}$	$\cancel{5}$	$\cancel{5}$	5
$b_k^{(2)}$	$\cancel{0}$	$\cancel{0}$	$\cancel{0}$	$\cancel{1}$	$\cancel{2}$	$\cancel{3}$	$\cancel{4}$	$\cancel{5}$	5
$b_k^{(3)}$	$\cancel{0}$	$\cancel{0}$	$\cancel{0}$	$\cancel{0}$	1	2	3	4	5
w_k	0	-1	-2	-3	-3	-3	-2	-1	0
τ_j		3	3	3	3	3	≥ 2	≥ 1	≥ 0

(b) $T = 4$

k	-1	0	1	2	3	4	5	6	7	8
$b_k^{(0)} = a_k$	0	$\cancel{1}$	$\cancel{2}$	$\cancel{3}$	$\cancel{4}$	$\cancel{5}$	$\cancel{6}$	$\cancel{6}$	$\cancel{6}$	6
$b_k^{(1)}$	$\cancel{0}$	$\cancel{0}$	$\cancel{1}$	$\cancel{2}$	$\cancel{3}$	$\cancel{4}$	$\cancel{5}$	$\cancel{6}$	$\cancel{6}$	6
$b_k^{(2)}$	$\cancel{0}$	$\cancel{0}$	$\cancel{0}$	$\cancel{1}$	$\cancel{2}$	$\cancel{3}$	$\cancel{4}$	$\cancel{5}$	$\cancel{6}$	6
$b_k^{(3)}$	$\cancel{0}$	$\cancel{0}$	$\cancel{0}$	$\cancel{0}$	1	2	3	4	5	6
w_k	0	-1	-2	-3	-3	-3	-3	-2	-1	0
τ_j		3	3	3	3	3	3	≥ 2	≥ 1	≥ 0

(c) $T = 5$

Figure B.1: $\mathcal{P}_1$, $\bar{\tau} = 3$ and $T \in \{3, 4, 5\}$.

k	-1	0	1	2	3	4	5	6	7	8	9
$b_k^{(0)} = a_k$	0	~~1~~	~~2~~	~~3~~	~~4~~	~~5~~	~~6~~	~~7~~	~~7~~	~~7~~	7
$b_k^{(1)}$	~~0~~	~~0~~	~~1~~	~~2~~	~~3~~	~~4~~	~~5~~	~~6~~	~~7~~	~~7~~	7
$b_k^{(2)}$	~~0~~	~~0~~	~~0~~	~~1~~	~~2~~	~~3~~	~~4~~	~~5~~	~~6~~	~~7~~	7
$b_k^{(3)}$	~~0~~	~~0~~	~~0~~	~~0~~	1	2	3	4	5	6	7
w_k	0	-1	-2	-3	-3	-3	-3	-3	-2	-1	0
τ_j		3	3	3	3	3	3	≥ 2	≥ 1	≥ 0	

(a) $T = 6$

k	-1	0	1	2	3	4	5	6	7	8	9	10
$b_k^{(0)} = a_k$	0	~~1~~	~~2~~	~~3~~	~~4~~	~~5~~	~~6~~	~~7~~	~~8~~	~~8~~	~~8~~	8
$b_k^{(1)}$	~~0~~	~~0~~	~~1~~	~~2~~	~~3~~	~~4~~	~~5~~	~~6~~	~~7~~	~~8~~	~~8~~	8
$b_k^{(2)}$	~~0~~	~~0~~	~~0~~	~~1~~	~~2~~	~~3~~	~~4~~	~~5~~	~~6~~	~~7~~	~~8~~	8
$b_k^{(3)}$	~~0~~	~~0~~	~~0~~	~~0~~	1	2	3	4	5	6	7	8
w_k	0	-1	-2	-3	-3	-3	-3	-3	-3	-2	-1	0
τ_j		3	3	3	3	3	3	3	3	≥ 2	≥ 1	≥ 0

(b) $T = 7$

k	-1	0	1	2	3	4	5	6	7	8	9	10	11
$b_k^{(0)} = a_k$	0	~~1~~	~~2~~	~~3~~	~~4~~	~~5~~	~~6~~	~~7~~	~~8~~	~~9~~	~~9~~	~~9~~	9
$b_k^{(1)}$	~~0~~	~~0~~	~~1~~	~~2~~	~~3~~	~~4~~	~~5~~	~~6~~	~~7~~	~~8~~	~~9~~	~~9~~	9
$b_k^{(2)}$	~~0~~	~~0~~	~~0~~	~~1~~	~~2~~	~~3~~	~~4~~	~~5~~	~~6~~	~~7~~	~~8~~	~~9~~	9
$b_k^{(3)}$	~~0~~	~~0~~	~~0~~	~~0~~	1	2	3	4	5	6	7	8	9
w_k	0	-1	-2	-3	-3	-3	-3	-3	-3	-3	-2	-1	0
τ_j		3	3	3	3	3	3	3	3	3	≥ 2	≥ 1	≥ 0

(c) $T = 8$

k	-1	0	1	2	3	4	5	6	7	8	9	10	11	12
$b_k^{(0)} = a_k$	0	~~1~~	~~2~~	~~3~~	~~4~~	~~5~~	~~6~~	~~7~~	~~8~~	~~9~~	~~10~~	~~10~~	~~10~~	10
$b_k^{(1)}$	~~0~~	~~0~~	~~1~~	~~2~~	~~3~~	~~4~~	~~5~~	~~6~~	~~7~~	~~8~~	~~9~~	~~10~~	~~10~~	10
$b_k^{(2)}$	~~0~~	~~0~~	~~0~~	~~1~~	~~2~~	~~3~~	~~4~~	~~5~~	~~6~~	~~7~~	~~8~~	~~9~~	~~10~~	10
$b_k^{(3)}$	~~0~~	~~0~~	~~0~~	~~0~~	1	2	3	4	5	6	7	8	9	10
w_k	0	-1	-2	-3	-3	-3	-3	-3	-3	-3	-3	-2	-1	0
τ_j		3	3	3	3	3	3	3	3	3	3	≥ 2	≥ 1	≥ 0

(d) $T = 9$

Figure B.2: $\mathcal{P}_1$, $\bar{\tau} = 3$ and $T \in \{6, 7, 8, 9\}$.

k	-1	0	1	2	3	4	5
$b_k^{(0)} = a_k$	0	~~1~~	~~2~~	~~3~~	~~4~~	~~4~~	4
$b_k^{(1)}$	~~0~~	~~0~~	~~1~~	~~2~~	~~3~~	~~4~~	4
$b_k^{(2)}$	~~0~~	~~0~~	~~0~~	1	2	3	4
w_k	0	-1	-2	-2	-2	-1	0
τ_j		2	2	2	2	≥ 1	≥ 0

(a) $T = 3$

Figure B.3: $\mathcal{P}_1$, $\bar{\tau} = 2$ and $T = 3$.

k	-1	0	1	2	3	4	5	6
$b_k^{(0)} = a_k$	0	~~1~~	~~2~~	~~3~~	~~4~~	~~5~~	~~5~~	5
$b_k^{(1)}$	~~0~~	~~0~~	~~1~~	~~2~~	~~3~~	~~4~~	~~5~~	5
$b_k^{(2)}$	~~0~~	~~0~~	~~0~~	1	2	3	4	5
w_k	0	-1	-2	-2	-2	-2	-1	0
τ_j		2	2	2	2	2	≥ 1	≥ 0

(a) $T = 4$

k	-1	0	1	2	3	4	5	6	7
$b_k^{(0)} = a_k$	0	~~1~~	~~2~~	~~3~~	~~4~~	~~5~~	~~6~~	~~6~~	6
$b_k^{(1)}$	~~0~~	~~0~~	~~1~~	~~2~~	~~3~~	~~4~~	~~5~~	~~6~~	6
$b_k^{(2)}$	~~0~~	~~0~~	~~0~~	1	2	3	4	5	6
w_k	0	-1	-2	-2	-2	-2	-2	-1	0
τ_j		2	2	2	2	2	2	≥ 1	≥ 0

(b) $T = 5$

k	-1	0	1	2	3	4	5	6	7	8
$b_k^{(0)} = a_k$	0	~~1~~	~~2~~	~~3~~	~~4~~	~~5~~	~~6~~	~~7~~	~~7~~	7
$b_k^{(1)}$	~~0~~	~~0~~	~~1~~	~~2~~	~~3~~	~~4~~	~~5~~	~~6~~	~~7~~	7
$b_k^{(2)}$	~~0~~	~~0~~	~~0~~	1	2	3	4	5	6	7
w_k	0	-1	-2	-2	-2	-2	-2	-2	-1	0
τ_j		2	2	2	2	2	2	2	≥ 1	≥ 0

(c) $T = 6$

k	-1	0	1	2	3	4	5	6	7	8	9
$b_k^{(0)} = a_k$	0	~~1~~	~~2~~	~~3~~	~~4~~	~~5~~	~~6~~	~~7~~	~~8~~	~~8~~	8
$b_k^{(1)}$	~~0~~	~~0~~	~~1~~	~~2~~	~~3~~	~~4~~	~~5~~	~~6~~	~~7~~	~~8~~	8
$b_k^{(2)}$	~~0~~	~~0~~	~~0~~	1	2	3	4	5	6	7	8
w_k	0	-1	-2	-2	-2	-2	-2	-2	-2	-1	0
τ_j		2	2	2	2	2	2	2	2	≥ 1	≥ 0

(d) $T = 7$

k	-1	0	1	2	3	4	5	6	7	8	9	10
$b_k^{(0)} = a_k$	0	~~1~~	~~2~~	~~3~~	~~4~~	~~5~~	~~6~~	~~7~~	~~8~~	~~9~~	~~9~~	9
$b_k^{(1)}$	~~0~~	~~0~~	~~1~~	~~2~~	~~3~~	~~4~~	~~5~~	~~6~~	~~7~~	~~8~~	~~9~~	9
$b_k^{(2)}$	~~0~~	~~0~~	~~0~~	1	2	3	4	5	6	7	8	9
w_k	0	-1	-2	-2	-2	-2	-2	-2	-2	-2	-1	0
τ_j		2	2	2	2	2	2	2	2	2	≥ 1	≥ 0

(e) $T = 8$

k	-1	0	1	2	3	4	5	6	7	8	9	10	11
$b_k^{(0)} = a_k$	0	~~1~~	~~2~~	~~3~~	~~4~~	~~5~~	~~6~~	~~7~~	~~8~~	~~9~~	~~10~~	~~10~~	10
$b_k^{(1)}$	~~0~~	~~0~~	~~1~~	~~2~~	~~3~~	~~4~~	~~5~~	~~6~~	~~7~~	~~8~~	~~9~~	~~10~~	10
$b_k^{(2)}$	~~0~~	~~0~~	~~0~~	1	2	3	4	5	6	7	8	9	10
w_k	0	-1	-2	-2	-2	-2	-2	-2	-2	-2	-2	-1	0
τ_j		2	2	2	2	2	2	2	2	2	2	≥ 1	≥ 0

(f) $T = 9$

Figure B.4: $\mathcal{P}_1$, $\bar{\tau} = 2$ and $T \in \{4, 5, 6, 7, 8, 9\}$.

B.2 Patterns for $\mathcal{P}_2$

k	-1	0	1	2	3	4	5	6	7	8
$b_k^{(0)} = a_k$	0	$\cancel{1}$	$\cancel{2}$	3	$\cancel{4}$	$\cancel{4}$	$\cancel{4}$	$\cancel{4}$	4	4
$b_k^{(1)}$	$\cancel{0}$	$\cancel{0}$	$\cancel{1}$	2	$\cancel{3}$	$\cancel{4}$	$\cancel{4}$	$\cancel{4}$	4	4
$b_k^{(2)}$	$\cancel{0}$	$\cancel{0}$	$\cancel{0}$	$\cancel{1}$	$\cancel{2}$	$\cancel{3}$	$\cancel{4}$	$\cancel{4}$	4	4
$b_k^{(3)}$	$\cancel{0}$	$\cancel{0}$	$\cancel{0}$	$\cancel{0}$	1	$\cancel{2}$	$\cancel{3}$	4	4	4
w_k	0	-1	-2	0	-3	-3	-3	0	0	0
τ_j		3	1	0	3	3	≥ 2	≥ 1	≥ 0	≥ 0

(a) $T = 3$

k	-1	0	1	2	3	4	5	6	7	8	9
$b_k^{(0)} = a_k$	0	$\cancel{1}$	$\cancel{2}$	3	$\cancel{4}$	$\cancel{5}$	$\cancel{5}$	$\cancel{5}$	5	5	5
$b_k^{(1)}$	$\cancel{0}$	$\cancel{0}$	$\cancel{1}$	2	$\cancel{3}$	$\cancel{4}$	$\cancel{5}$	$\cancel{5}$	5	5	5
$b_k^{(2)}$	$\cancel{0}$	$\cancel{0}$	$\cancel{0}$	$\cancel{1}$	$\cancel{2}$	$\cancel{3}$	$\cancel{4}$	$\cancel{5}$	5	5	5
$b_k^{(3)}$	$\cancel{0}$	$\cancel{0}$	$\cancel{0}$	$\cancel{0}$	1	$\cancel{2}$	$\cancel{3}$	4	5	5	5
w_k	0	-1	-2	0	-3	-4	-4	-1	0	0	0
τ_j		3	1	0	3	3	≥ 2	≥ 1	≥ 0	≥ 0	≥ 0

(b) $T = 4$

k	-1	0	1	2	3	4	5	6	7	8	9	10
$b_k^{(0)} = a_k$	0	$\cancel{1}$	$\cancel{2}$	3	$\cancel{4}$	$\cancel{5}$	$\cancel{6}$	$\cancel{6}$	$\cancel{6}$	6	6	6
$b_k^{(1)}$	$\cancel{0}$	$\cancel{0}$	$\cancel{1}$	2	$\cancel{3}$	$\cancel{4}$	$\cancel{5}$	$\cancel{6}$	$\cancel{6}$	6	6	6
$b_k^{(2)}$	$\cancel{0}$	$\cancel{0}$	$\cancel{0}$	$\cancel{1}$	$\cancel{2}$	$\cancel{3}$	$\cancel{4}$	$\cancel{5}$	$\cancel{6}$	6	6	6
$b_k^{(3)}$	$\cancel{0}$	$\cancel{0}$	$\cancel{0}$	$\cancel{0}$	1	$\cancel{2}$	$\cancel{3}$	4	5	6	6	6
w_k	0	-1	-2	0	-3	-4	-5	-2	-1	0	0	0
τ_j		3	1	0	3	3	3	≥ 2	≥ 1	≥ 0	≥ 0	≥ 0

(c) $T = 5$

k	-1	0	1	2	3	4	5	6	7	8	9	10	11
$b_k^{(0)} = a_k$	0	$\cancel{1}$	$\cancel{2}$	3	$\cancel{4}$	$\cancel{5}$	$\cancel{6}$	$\cancel{7}$	$\cancel{7}$	$\cancel{7}$	7	7	7
$b_k^{(1)}$	$\cancel{0}$	$\cancel{0}$	$\cancel{1}$	2	$\cancel{3}$	$\cancel{4}$	$\cancel{5}$	$\cancel{6}$	$\cancel{7}$	$\cancel{7}$	7	7	7
$b_k^{(2)}$	$\cancel{0}$	$\cancel{0}$	$\cancel{0}$	$\cancel{1}$	$\cancel{2}$	$\cancel{3}$	$\cancel{4}$	$\cancel{5}$	$\cancel{6}$	$\cancel{7}$	7	7	7
$b_k^{(3)}$	$\cancel{0}$	$\cancel{0}$	$\cancel{0}$	$\cancel{0}$	1	$\cancel{2}$	$\cancel{3}$	4	5	6	7	7	7
w_k	0	-1	-2	0	-3	-4	-5	-3	-2	-1	0	0	0
τ_j		3	1	0	3	3	3	3	≥ 2	≥ 1	≥ 0	≥ 0	≥ 0

(d) $T = 6$

k	-1	0	1	2	3	4	5	6	7	8	9	10	11	12
$b_k^{(0)} = a_k$	0	$\cancel{1}$	$\cancel{2}$	3	$\cancel{4}$	$\cancel{5}$	$\cancel{6}$	7	$\cancel{8}$	$\cancel{8}$	$\cancel{8}$	8	8	8
$b_k^{(1)}$	$\cancel{0}$	$\cancel{0}$	$\cancel{1}$	2	$\cancel{3}$	$\cancel{4}$	$\cancel{5}$	6	$\cancel{7}$	$\cancel{8}$	$\cancel{8}$	8	8	8
$b_k^{(2)}$	$\cancel{0}$	$\cancel{0}$	$\cancel{0}$	$\cancel{1}$	$\cancel{2}$	$\cancel{3}$	$\cancel{4}$	$\cancel{5}$	$\cancel{6}$	$\cancel{7}$	$\cancel{8}$	8	8	8
$b_k^{(3)}$	$\cancel{0}$	$\cancel{0}$	$\cancel{0}$	$\cancel{0}$	1	$\cancel{2}$	$\cancel{3}$	4	5	$\cancel{6}$	$\cancel{7}$	8	8	8
w_k	0	-1	-2	0	-3	-4	-5	0	-3	-3	-3	0	0	0
τ_j		3	1	0	3	3	1	0	3	≥ 2	≥ 1	≥ 0	≥ 0	≥ 0

(e) $T = 7$

Figure B.5: $\mathcal{P}_2$, $\bar{\tau} = 3$ and $T \in \{3, 4, 5, 6, 7\}$.

k	-1	0	1	2	3	4	5	6	7	8	9	10	11	12	13
$b_k^{(0)} = a_k$	0	$\cancel{1}$	$\cancel{2}$	3	$\cancel{4}$	$\cancel{5}$	$\cancel{6}$	7	$\cancel{8}$	$\cancel{9}$	$\cancel{9}$	$\cancel{9}$	9	9	9
$b_k^{(1)}$	$\cancel{0}$	$\cancel{0}$	$\cancel{1}$	2	$\cancel{3}$	$\cancel{4}$	$\cancel{5}$	6	$\cancel{7}$	$\cancel{8}$	$\cancel{9}$	$\cancel{9}$	9	9	9
$b_k^{(2)}$	$\cancel{0}$	$\cancel{0}$	$\cancel{0}$	$\cancel{1}$	$\cancel{2}$	$\cancel{3}$	$\cancel{4}$	$\cancel{5}$	$\cancel{6}$	$\cancel{7}$	$\cancel{8}$	$\cancel{9}$	9	9	9
$b_k^{(3)}$	$\cancel{0}$	$\cancel{0}$	$\cancel{0}$	$\cancel{0}$	1	$\cancel{2}$	$\cancel{3}$	4	5	$\cancel{6}$	$\cancel{7}$	8	9	9	9
w_k	0	-1	-2	0	-3	-4	-5	0	-3	-4	-4	-1	0	0	0
τ_j		3	1	0	3	3	1	0	3	3	≥ 2	≥ 1	≥ 0	≥ 0	≥ 0

(a) $T = 8$

k	-1	0	1	2	3	4	5	6	7	8	9	10	11	12	13	14
$b_k^{(0)} = a_k$	0	$\cancel{1}$	$\cancel{2}$	3	$\cancel{4}$	$\cancel{5}$	$\cancel{6}$	7	$\cancel{8}$	$\cancel{9}$	$\cancel{10}$	$\cancel{10}$	$\cancel{10}$	10	10	10
$b_k^{(1)}$	$\cancel{0}$	$\cancel{0}$	$\cancel{1}$	2	$\cancel{3}$	$\cancel{4}$	$\cancel{5}$	6	$\cancel{7}$	$\cancel{8}$	$\cancel{9}$	$\cancel{10}$	$\cancel{10}$	10	10	10
$b_k^{(2)}$	$\cancel{0}$	$\cancel{0}$	$\cancel{0}$	$\cancel{1}$	$\cancel{2}$	$\cancel{3}$	$\cancel{4}$	$\cancel{5}$	$\cancel{6}$	$\cancel{7}$	$\cancel{8}$	$\cancel{9}$	$\cancel{10}$	10	10	10
$b_k^{(3)}$	$\cancel{0}$	$\cancel{0}$	$\cancel{0}$	$\cancel{0}$	1	$\cancel{2}$	$\cancel{3}$	4	5	$\cancel{6}$	$\cancel{7}$	8	9	10	10	10
w_k	0	-1	-2	0	-3	-4	-5	0	-3	-4	-5	-2	-1	0	0	0
τ_j		3	1	0	3	3	1	0	3	3	3	≥ 2	≥ 1	≥ 0	≥ 0	≥ 0

(b) $T = 9$

Figure B.6: $\mathcal{P}_2$, $\bar{\tau} = 3$ and $T \in \{8, 9\}$.

k	-1	0	1	2	3	4	5	6
$b_k^{(0)} = a_k$	0	$\cancel{1}$	2	$\cancel{3}$	$\cancel{4}$	$\cancel{4}$	4	4
$b_k^{(1)}$	$\cancel{0}$	$\cancel{0}$	$\cancel{1}$	$\cancel{2}$	$\cancel{3}$	$\cancel{4}$	4	4
$b_k^{(2)}$	$\cancel{0}$	$\cancel{0}$	$\cancel{0}$	1	$\cancel{2}$	3	4	4
w_k	0	-1	0	-2	-3	-1	0	0
τ_j		2	0	2	2	≥ 1	≥ 0	≥ 0

(a) $T = 3$

k	-1	0	1	2	3	4	5	6	7
$b_k^{(0)} = a_k$	0	$\cancel{1}$	2	$\cancel{3}$	$\cancel{4}$	$\cancel{5}$	$\cancel{5}$	5	5
$b_k^{(1)}$	$\cancel{0}$	$\cancel{0}$	$\cancel{1}$	$\cancel{2}$	$\cancel{3}$	$\cancel{4}$	$\cancel{5}$	5	5
$b_k^{(2)}$	$\cancel{0}$	$\cancel{0}$	$\cancel{0}$	1	$\cancel{2}$	3	4	5	5
w_k	0	-1	0	-2	-3	-2	-1	0	0
τ_j		2	0	2	2	2	≥ 1	≥ 0	≥ 0

(b) $T = 4$

k	-1	0	1	2	3	4	5	6	7	8
$b_k^{(0)} = a_k$	0	$\cancel{1}$	2	$\cancel{3}$	$\cancel{4}$	$\cancel{5}$	$\cancel{6}$	$\cancel{6}$	6	6
$b_k^{(1)}$	$\cancel{0}$	$\cancel{0}$	$\cancel{1}$	$\cancel{2}$	$\cancel{3}$	$\cancel{4}$	$\cancel{5}$	$\cancel{6}$	6	6
$b_k^{(2)}$	$\cancel{0}$	$\cancel{0}$	$\cancel{0}$	1	$\cancel{2}$	3	4	5	6	6
w_k	0	-1	0	-2	-3	-2	-2	-1	0	0
τ_j		2	0	2	2	2	2	≥ 1	≥ 0	≥ 0

(c) $T = 5$

k	-1	0	1	2	3	4	5	6	7	8	9
$b_k^{(0)} = a_k$	0	$\cancel{1}$	2	$\cancel{3}$	$\cancel{4}$	5	$\cancel{6}$	$\cancel{7}$	$\cancel{7}$	7	7
$b_k^{(1)}$	$\cancel{0}$	$\cancel{0}$	$\cancel{1}$	$\cancel{2}$	$\cancel{3}$	$\cancel{4}$	$\cancel{5}$	$\cancel{6}$	$\cancel{7}$	7	7
$b_k^{(2)}$	$\cancel{0}$	$\cancel{0}$	$\cancel{0}$	1	$\cancel{2}$	3	4	$\cancel{5}$	6	7	7
w_k	0	-1	0	-2	-3	0	-2	-3	-1	0	0
τ_j		2	0	2	2	0	2	2	≥ 1	≥ 0	≥ 0

(d) $T = 6$

Figure B.7: $\mathcal{P}_2$, $\bar{\tau} = 2$ and $T \in \{3, 4, 5, 6\}$.

k	-1	0	1	2	3	4	5	6	7	8	9	10
$b_k^{(0)} = a_k$	0	$\cancel{1}$	2	$\cancel{3}$	$\cancel{4}$	5	$\cancel{6}$	$\cancel{7}$	$\cancel{8}$	$\cancel{8}$	8	8
$b_k^{(1)}$	$\cancel{0}$	$\cancel{0}$	$\cancel{1}$	$\cancel{2}$	$\cancel{3}$	$\cancel{4}$	$\cancel{5}$	$\cancel{6}$	$\cancel{7}$	$\cancel{8}$	8	8
$b_k^{(2)}$	$\cancel{0}$	$\cancel{0}$	$\cancel{0}$	1	$\cancel{2}$	3	4	$\cancel{5}$	6	7	8	8
w_k	0	-1	0	-2	-3	0	-2	-3	-2	-1	0	0
τ_j		2	0	2	2	0	2	2	2	≥ 1	≥ 0	≥ 0

(a) $T = 7$

k	-1	0	1	2	3	4	5	6	7	8	9	10	11
$b_k^{(0)} = a_k$	0	$\cancel{1}$	2	$\cancel{3}$	$\cancel{4}$	5	$\cancel{6}$	$\cancel{7}$	$\cancel{8}$	$\cancel{9}$	$\cancel{9}$	9	9
$b_k^{(1)}$	$\cancel{0}$	$\cancel{0}$	$\cancel{1}$	$\cancel{2}$	$\cancel{3}$	$\cancel{4}$	$\cancel{5}$	$\cancel{6}$	$\cancel{7}$	$\cancel{8}$	$\cancel{9}$	9	9
$b_k^{(2)}$	$\cancel{0}$	$\cancel{0}$	$\cancel{0}$	1	$\cancel{2}$	3	4	$\cancel{5}$	6	7	8	9	9
w_k	0	-1	0	-2	-3	0	-2	-3	-2	-2	-1	0	0
τ_j		2	0	2	2	0	2	2	2	2	≥ 1	≥ 0	≥ 0

(b) $T = 8$

k	-1	0	1	2	3	4	5	6	7	8	9	10	11	12
$b_k^{(0)} = a_k$	0	$\cancel{1}$	2	$\cancel{3}$	$\cancel{4}$	5	$\cancel{6}$	$\cancel{7}$	8	$\cancel{9}$	$\cancel{10}$	$\cancel{10}$	10	10
$b_k^{(1)}$	$\cancel{0}$	$\cancel{0}$	$\cancel{1}$	$\cancel{2}$	$\cancel{3}$	$\cancel{4}$	$\cancel{5}$	$\cancel{6}$	$\cancel{7}$	$\cancel{8}$	$\cancel{9}$	$\cancel{10}$	10	10
$b_k^{(2)}$	$\cancel{0}$	$\cancel{0}$	$\cancel{0}$	1	$\cancel{2}$	3	4	$\cancel{5}$	6	7	$\cancel{8}$	9	10	10
w_k	0	-1	0	-2	-3	0	-2	-3	0	-2	-3	-1	0	0
τ_j		2	0	2	2	0	2	2	0	2	2	≥ 1	≥ 0	≥ 0

(c) $T = 9$

Figure B.8: $\mathcal{P}_2$, $\bar{\tau} = 2$ and $T \in \{7, 8, 9\}$.

B.3 Patterns for $\mathcal{P}_3$

k	−1	0	1	2	3	4	5	6	7	8	9
$b_k^{(0)} = a_k$	0	~~1~~	~~2~~	~~3~~	4	~~4~~	~~4~~	~~4~~	4	~~4~~	~~4~~
$b_k^{(1)}$	~~0~~	~~0~~	~~1~~	~~2~~	3	~~4~~	~~4~~	~~4~~	4	~~4~~	~~4~~
$b_k^{(2)}$	~~0~~	~~0~~	~~0~~	~~1~~	2	~~3~~	~~4~~	~~4~~	4	~~4~~	~~4~~
$b_k^{(3)}$	~~0~~	~~0~~	~~0~~	~~0~~	1	~~2~~	~~3~~	~~4~~	4	~~4~~	~~4~~
w_k	0	−1	−2	−3	−3	−3	−3	−3	0	0	0
τ_j		3	2	1	0	3	2	1	0	3	2

(a) $T = 3$

k	−1	0	1	2	3	4	5	6	7	8	9	10
$b_k^{(0)} = a_k$	0	~~1~~	~~2~~	~~3~~	4	~~5~~	~~5~~	~~5~~	5	~~5~~	~~5~~	~~5~~
$b_k^{(1)}$	~~0~~	~~0~~	~~1~~	~~2~~	3	~~4~~	~~5~~	~~5~~	5	~~5~~	~~5~~	~~5~~
$b_k^{(2)}$	~~0~~	~~0~~	~~0~~	~~1~~	2	~~3~~	~~4~~	~~5~~	5	~~5~~	~~5~~	~~5~~
$b_k^{(3)}$	~~0~~	~~0~~	~~0~~	~~0~~	1	~~2~~	~~3~~	~~4~~	5	~~5~~	~~5~~	~~5~~
w_k	0	−1	−2	−3	−3	−4	−4	−4	0	0	0	0
τ_j		3	2	1	0	3	2	1	0	3	2	1

(b) $T = 4$

k	−1	0	1	2	3	4	5	6	7	8	9	10	11
$b_k^{(0)} = a_k$	0	~~1~~	~~2~~	~~3~~	4	~~5~~	~~6~~	~~6~~	6	~~6~~	~~6~~	~~6~~	6
$b_k^{(1)}$	~~0~~	~~0~~	~~1~~	~~2~~	3	~~4~~	~~5~~	~~6~~	6	~~6~~	~~6~~	~~6~~	6
$b_k^{(2)}$	~~0~~	~~0~~	~~0~~	~~1~~	2	~~3~~	~~4~~	~~5~~	6	~~6~~	~~6~~	~~6~~	6
$b_k^{(3)}$	~~0~~	~~0~~	~~0~~	~~0~~	1	~~2~~	~~3~~	~~4~~	5	~~6~~	~~6~~	~~6~~	6
w_k	0	−1	−2	−3	−3	−4	−5	−5	−1	−1	−1	−1	0
τ_j		3	2	1	0	3	2	1	0	3	2	1	0

(c) $T = 5$

k	−1	0	1	2	3	4	5	6	7	8	9	10	11	12
$b_k^{(0)} = a_k$	0	~~1~~	~~2~~	~~3~~	4	~~5~~	~~6~~	~~7~~	7	~~7~~	~~7~~	~~7~~	7	~~7~~
$b_k^{(1)}$	~~0~~	~~0~~	~~1~~	~~2~~	3	~~4~~	~~5~~	~~6~~	7	~~7~~	~~7~~	~~7~~	7	~~7~~
$b_k^{(2)}$	~~0~~	~~0~~	~~0~~	~~1~~	2	~~3~~	~~4~~	~~5~~	6	~~7~~	~~7~~	~~7~~	7	~~7~~
$b_k^{(3)}$	~~0~~	~~0~~	~~0~~	~~0~~	1	~~2~~	~~3~~	~~4~~	5	~~6~~	~~7~~	~~7~~	7	~~7~~
w_k	0	−1	−2	−3	−3	−4	−5	−6	−2	−2	−2	−2	0	0
τ_j		3	2	1	0	3	2	1	0	3	2	1	0	3

(d) $T = 6$

k	−1	0	1	2	3	4	5	6	7	8	9	10	11	12	13
$b_k^{(0)} = a_k$	0	~~1~~	~~2~~	~~3~~	4	~~5~~	~~6~~	~~7~~	8	~~8~~	~~8~~	~~8~~	8	~~8~~	~~8~~
$b_k^{(1)}$	~~0~~	~~0~~	~~1~~	~~2~~	3	~~4~~	~~5~~	~~6~~	7	~~8~~	~~8~~	~~8~~	8	~~8~~	~~8~~
$b_k^{(2)}$	~~0~~	~~0~~	~~0~~	~~1~~	2	~~3~~	~~4~~	~~5~~	6	~~7~~	~~8~~	~~8~~	8	~~8~~	~~8~~
$b_k^{(3)}$	~~0~~	~~0~~	~~0~~	~~0~~	1	~~2~~	~~3~~	~~4~~	5	~~6~~	~~7~~	~~8~~	8	~~8~~	~~8~~
w_k	0	−1	−2	−3	−3	−4	−5	−6	−3	−3	−3	−3	0	0	0
τ_j		3	2	1	0	3	2	1	0	3	2	1	0	3	2

(e) $T = 7$

Figure B.9: $\mathcal{P}_3$, $\bar{\tau} = 3$ and $T \in \{3, 4, 5, 6, 7\}$.

k	-1	0	1	2	3	4	5	6	7	8	9	10	11	12	13	14
$b_k^{(0)} = a_k$	0	$\cancel{1}$	$\cancel{2}$	$\cancel{3}$	4	$\cancel{5}$	$\cancel{6}$	$\cancel{7}$	8	$\cancel{9}$	$\cancel{9}$	$\cancel{9}$	9	$\cancel{9}$	$\cancel{9}$	$\cancel{9}$
$b_k^{(1)}$	$\cancel{0}$	$\cancel{0}$	$\cancel{1}$	$\cancel{2}$	3	$\cancel{4}$	$\cancel{5}$	$\cancel{6}$	7	$\cancel{8}$	$\cancel{9}$	$\cancel{9}$	9	$\cancel{9}$	$\cancel{9}$	$\cancel{9}$
$b_k^{(2)}$	$\cancel{0}$	$\cancel{0}$	$\cancel{0}$	$\cancel{1}$	2	$\cancel{3}$	$\cancel{4}$	$\cancel{5}$	6	$\cancel{7}$	$\cancel{8}$	$\cancel{9}$	9	$\cancel{9}$	$\cancel{9}$	$\cancel{9}$
$b_k^{(3)}$	$\cancel{0}$	$\cancel{0}$	$\cancel{0}$	$\cancel{0}$	1	$\cancel{2}$	$\cancel{3}$	$\cancel{4}$	5	$\cancel{6}$	$\cancel{7}$	$\cancel{8}$	9	$\cancel{9}$	$\cancel{9}$	$\cancel{9}$
w_k	0	-1	-2	-3	-3	-4	-5	-6	-3	-4	-4	-4	0	0	0	0
τ_j		3	2	1	0	3	2	1	0	3	2	1	0	3	2	1

(a) $T = 8$

k	-1	0	1	2	3	4	5	6	7	8	9	10	11	12	13	14	15
$b_k^{(0)} = a_k$	0	$\cancel{1}$	$\cancel{2}$	$\cancel{3}$	4	$\cancel{5}$	$\cancel{6}$	$\cancel{7}$	8	$\cancel{9}$	$\cancel{10}$	$\cancel{10}$	10	$\cancel{10}$	$\cancel{10}$	$\cancel{10}$	10
$b_k^{(1)}$	$\cancel{0}$	$\cancel{0}$	$\cancel{1}$	$\cancel{2}$	3	$\cancel{4}$	$\cancel{5}$	$\cancel{6}$	7	$\cancel{8}$	$\cancel{9}$	$\cancel{10}$	10	$\cancel{10}$	$\cancel{10}$	$\cancel{10}$	10
$b_k^{(2)}$	$\cancel{0}$	$\cancel{0}$	$\cancel{0}$	$\cancel{1}$	2	$\cancel{3}$	$\cancel{4}$	$\cancel{5}$	6	$\cancel{7}$	$\cancel{8}$	$\cancel{9}$	10	$\cancel{10}$	$\cancel{10}$	$\cancel{10}$	10
$b_k^{(3)}$	$\cancel{0}$	$\cancel{0}$	$\cancel{0}$	$\cancel{0}$	1	$\cancel{2}$	$\cancel{3}$	$\cancel{4}$	5	$\cancel{6}$	$\cancel{7}$	$\cancel{8}$	9	$\cancel{10}$	$\cancel{10}$	$\cancel{10}$	10
w_k	0	-1	-2	-3	-3	-4	-5	-6	-3	-4	-5	-5	-1	-1	-1	-1	0
τ_j		3	2	1	0	3	2	1	0	3	2	1	0	3	2	1	0

(b) $T = 9$

Figure B.10: $\mathcal{P}_3$, $\bar{\tau} = 3$ and $T \in \{8, 9\}$.

k	-1	0	1	2	3	4	5	6	7
$b_k^{(0)} = a_k$	0	$\cancel{1}$	$\cancel{2}$	3	$\cancel{4}$	$\cancel{4}$	4	$\cancel{4}$	$\cancel{4}$
$b_k^{(1)}$	$\cancel{0}$	$\cancel{0}$	$\cancel{1}$	2	$\cancel{3}$	$\cancel{4}$	4	$\cancel{4}$	$\cancel{4}$
$b_k^{(2)}$	$\cancel{0}$	$\cancel{0}$	$\cancel{0}$	1	$\cancel{2}$	$\cancel{3}$	4	$\cancel{4}$	$\cancel{4}$
w_k	0	-1	-2	-2	-3	-3	0	0	0
τ_j		2	1	0	2	1	0	2	1

(a) $T = 3$

k	-1	0	1	2	3	4	5	6	7	8
$b_k^{(0)} = a_k$	0	$\cancel{1}$	$\cancel{2}$	3	$\cancel{4}$	$\cancel{5}$	5	$\cancel{5}$	$\cancel{5}$	5
$b_k^{(1)}$	$\cancel{0}$	$\cancel{0}$	$\cancel{1}$	2	$\cancel{3}$	$\cancel{4}$	5	$\cancel{5}$	$\cancel{5}$	5
$b_k^{(2)}$	$\cancel{0}$	$\cancel{0}$	$\cancel{0}$	1	$\cancel{2}$	$\cancel{3}$	4	$\cancel{5}$	$\cancel{5}$	5
w_k	0	-1	-2	-2	-3	-4	-1	-1	-1	0
τ_j		2	1	0	2	1	0	2	1	0

(b) $T = 4$

k	-1	0	1	2	3	4	5	6	7	8	9
$b_k^{(0)} = a_k$	0	$\cancel{1}$	$\cancel{2}$	3	$\cancel{4}$	$\cancel{5}$	6	$\cancel{6}$	$\cancel{6}$	6	$\cancel{6}$
$b_k^{(1)}$	$\cancel{0}$	$\cancel{0}$	$\cancel{1}$	2	$\cancel{3}$	$\cancel{4}$	5	$\cancel{6}$	$\cancel{6}$	6	$\cancel{6}$
$b_k^{(2)}$	$\cancel{0}$	$\cancel{0}$	$\cancel{0}$	1	$\cancel{2}$	$\cancel{3}$	4	$\cancel{5}$	$\cancel{6}$	6	$\cancel{6}$
w_k	0	-1	-2	-2	-3	-4	-2	-2	-2	0	0
τ_j		2	1	0	2	1	0	2	1	0	2

(c) $T = 5$

k	-1	0	1	2	3	4	5	6	7	8	9	10
$b_k^{(0)} = a_k$	0	$\cancel{1}$	$\cancel{2}$	3	$\cancel{4}$	$\cancel{5}$	6	$\cancel{7}$	$\cancel{7}$	7	$\cancel{7}$	$\cancel{7}$
$b_k^{(1)}$	$\cancel{0}$	$\cancel{0}$	$\cancel{1}$	2	$\cancel{3}$	$\cancel{4}$	5	$\cancel{6}$	$\cancel{7}$	7	$\cancel{7}$	$\cancel{7}$
$b_k^{(2)}$	$\cancel{0}$	$\cancel{0}$	$\cancel{0}$	1	$\cancel{2}$	$\cancel{3}$	4	$\cancel{5}$	$\cancel{6}$	7	$\cancel{7}$	$\cancel{7}$
w_k	0	-1	-2	-2	-3	-4	-2	-3	-3	0	0	0
τ_j		2	1	0	2	1	0	2	1	0	2	1

(d) $T = 6$

Figure B.11: $\mathcal{P}_3$, $\bar{\tau} = 2$ and $T \in \{3, 4, 5, 6\}$.

k	-1	0	1	2	3	4	5	6	7	8	9	10	11
$b_k^{(0)} = a_k$	0	$\cancel{1}$	$\cancel{2}$	3	$\cancel{4}$	$\cancel{5}$	6	$\cancel{7}$	$\cancel{8}$	8	$\cancel{8}$	$\cancel{8}$	8
$b_k^{(1)}$	$\cancel{0}$	$\cancel{0}$	$\cancel{1}$	2	$\cancel{3}$	$\cancel{4}$	5	$\cancel{6}$	$\cancel{7}$	8	$\cancel{8}$	$\cancel{8}$	8
$b_k^{(2)}$	$\cancel{0}$	$\cancel{0}$	$\cancel{0}$	1	$\cancel{2}$	$\cancel{3}$	4	$\cancel{5}$	$\cancel{6}$	7	$\cancel{8}$	$\cancel{8}$	8
w_k	0	-1	-2	-2	-3	-4	-2	-3	-4	-1	-1	-1	0
τ_j		2	1	0	2	1	0	2	1	0	2	1	0

(a) $T = 7$

k	-1	0	1	2	3	4	5	6	7	8	9	10	11	12
$b_k^{(0)} = a_k$	0	$\cancel{1}$	$\cancel{2}$	3	$\cancel{4}$	$\cancel{5}$	6	$\cancel{7}$	$\cancel{8}$	9	$\cancel{9}$	$\cancel{9}$	9	$\cancel{9}$
$b_k^{(1)}$	$\cancel{0}$	$\cancel{0}$	$\cancel{1}$	2	$\cancel{3}$	$\cancel{4}$	5	$\cancel{6}$	$\cancel{7}$	8	$\cancel{9}$	$\cancel{9}$	9	$\cancel{9}$
$b_k^{(2)}$	$\cancel{0}$	$\cancel{0}$	$\cancel{0}$	1	$\cancel{2}$	$\cancel{3}$	4	$\cancel{5}$	$\cancel{6}$	7	$\cancel{8}$	$\cancel{9}$	9	$\cancel{9}$
w_k	0	-1	-2	-2	-3	-4	-2	-3	-4	-2	-2	-2	0	0
τ_j		2	1	0	2	1	0	2	1	0	2	1	0	2

(b) $T = 8$

k	-1	0	1	2	3	4	5	6	7	8	9	10	11	12	13
$b_k^{(0)} = a_k$	0	$\cancel{1}$	$\cancel{2}$	3	$\cancel{4}$	$\cancel{5}$	6	$\cancel{7}$	$\cancel{8}$	9	$\cancel{10}$	$\cancel{10}$	10	$\cancel{10}$	$\cancel{10}$
$b_k^{(1)}$	$\cancel{0}$	$\cancel{0}$	$\cancel{1}$	2	$\cancel{3}$	$\cancel{4}$	5	$\cancel{6}$	$\cancel{7}$	8	$\cancel{9}$	$\cancel{10}$	10	$\cancel{10}$	$\cancel{10}$
$b_k^{(2)}$	$\cancel{0}$	$\cancel{0}$	$\cancel{0}$	1	$\cancel{2}$	$\cancel{3}$	4	$\cancel{5}$	$\cancel{6}$	7	$\cancel{8}$	$\cancel{9}$	10	$\cancel{10}$	$\cancel{10}$
w_k	0	-1	-2	-2	-3	-4	-2	-3	-4	-2	-3	-3	0	0	0
τ_j		2	1	0	2	1	0	2	1	0	2	1	0	2	1

(c) $T = 9$

Figure B.12: $\mathcal{P}_3$, $\bar{\tau} = 2$ and $T \in \{7, 8, 9\}$.

Appendix C

Delay and Packet Patterns for the acausal SGT in Chapter 8

C.1 Patterns for $\mathcal{P}_1$

k	-3	-2	-1	0	1	2	3	4	5	6	7	8	9	10	11	12	13	14	15	16
$b_k^{(0)} = a_k$	0	0	0	1	2	3	4	5	6	7	8	9	10	11	11	11	11	11	11	11
$b_k^{(1)}$	0	0	0	0	1	2	3	4	5	6	7	8	9	10	11	11	11	11	11	11
$b_k^{(2)}$	0	0	0	0	0	1	2	3	4	5	6	7	8	9	10	11	11	11	11	11
$b_k^{(3)}$	0	0	0	0	0	0	1	2	3	4	5	6	7	8	9	10	11	11	11	11
$b_k^{(0)} = a_k$	0	0	0	~~1~~	~~2~~	~~3~~	~~4~~	~~5~~	~~6~~	~~7~~	~~8~~	~~9~~	~~10~~	~~11~~	~~11~~	~~11~~	~~11~~	~~11~~	~~11~~	~~11~~
$b_k^{(1)}k$	0	0	0	0	~~1~~	~~2~~	~~3~~	~~4~~	~~5~~	~~6~~	~~7~~	~~8~~	~~9~~	~~10~~	~~11~~	~~11~~	~~11~~	~~11~~	~~11~~	~~11~~
$b_k^{(2)}$	0	0	0	0	0	~~1~~	~~2~~	~~3~~	~~4~~	~~5~~	~~6~~	~~7~~	~~8~~	~~9~~	~~10~~	~~11~~	~~11~~	~~11~~	~~11~~	~~11~~
$b_k^{(3)}$	0	0	0	0	0	0	1	2	3	4	5	6	7	8	9	10	11	11	11	11
$b_k^{(0)} - a_k$	0	0	0	0	0	0	0	0	0	0	0	0	0	0	0	0	0	0	0	0
$b_k^{(1)} - a_k$	0	0	0	-1	-1	-1	-1	-1	-1	-1	-1	-1	-1	-1	0	0	0	0	0	0
$b_k^{(2)} - a_k$	0	0	0	-1	-2	-2	-2	-2	-2	-2	-2	-2	-2	-2	-1	0	0	0	0	0
$b_k^{(3)} - a_k$	0	0	0	-1	-2	-3	-3	-3	-3	-3	-3	-3	-3	-3	-2	-1	0	0	0	0
packet arr.	no	no	no	no	no	no	yes	yes	yes	yes	yes	yes	yes	yes	yes	yes	yes	yes	yes	yes
c_k	0	0	0	0	0	0	1	2	3	4	5	6	7	8	9	10	11	11	11	11
w_k	0	0	0	-1	-2	-3	-3	-3	-3	-3	-3	-3	-3	-3	-2	-1	0	0	0	0
block				A	A	B	B	B	B	B	B	B	B	B	C	C	0	0	0	0
τ_j				3	3	3	3	3	3	3	3	3	3	3	3	3	3	3	3	3

Figure C.1: $\mathcal{P}_1$, $\bar{\tau} = 3$, $T = 10$ and $\tau_A = 0$

k	-3	-2	-1	0	1	2	3	4	5	6	7	8	9	10	11	12	13	14	15	16
$b_k^{(-1)}$	0	0	1	2	3	4	5	6	7	8	9	10	11	11	11	11	11	11	11	11
$b_k^{(0)} = a_k$	0	0	0	1	2	3	4	5	6	7	8	9	10	11	11	11	11	11	11	11
$b_k^{(1)}$	0	0	0	0	1	2	3	4	5	6	7	8	9	10	11	11	11	11	11	11
$b_k^{(2)}$	0	0	0	0	0	1	2	3	4	5	6	7	8	9	10	11	11	11	11	11
$b_k^{(-1)}$	0	0	~~1~~	~~2~~	~~3~~	~~4~~	~~5~~	~~6~~	~~7~~	~~8~~	~~9~~	~~10~~	~~11~~	~~11~~	~~11~~	~~11~~	~~11~~	~~11~~	~~11~~	~~11~~
$b_k^{(0)} = a_k$	0	0	0	~~1~~	~~2~~	~~3~~	~~4~~	~~5~~	~~6~~	~~7~~	~~8~~	~~9~~	~~10~~	~~11~~	~~11~~	~~11~~	~~11~~	~~11~~	~~11~~	~~11~~
$b_k^{(1)}$	0	0	0	0	~~1~~	~~2~~	~~3~~	~~4~~	~~5~~	~~6~~	~~7~~	~~8~~	~~9~~	~~10~~	~~11~~	~~11~~	~~11~~	~~11~~	~~11~~	~~11~~
$b_k^{(2)}$	0	0	0	0	0	1	2	3	4	5	6	7	8	9	10	11	11	11	11	11
$b_k^{(-1)} - a_k$	0	0	1	1	1	1	1	1	1	1	1	1	1	0	0	0	0	0	0	0
$b_k^{(0)} - a_k$	0	0	0	0	0	0	0	0	0	0	0	0	0	0	0	0	0	0	0	0
$b_k^{(1)} - a_k$	0	0	0	-1	-1	-1	-1	-1	-1	-1	-1	-1	-1	-1	0	0	0	0	0	0
$b_k^{(2)} - a_k$	0	0	0	-1	-2	-2	-2	-2	-2	-2	-2	-2	-2	-2	-1	0	0	0	0	0
packet arr.	no	no	no	no	no	yes	yes	yes	yes	yes	yes	yes	yes	yes	yes	yes	yes	yes	yes	yes
c_k	0	0	0	0	0	1	2	3	4	5	6	7	8	9	10	11	11	11	11	11
w_k	0	0	0	-1	-2	-2	-2	-2	-2	-2	-2	-2	-2	-2	-1	0	0	0	0	0
block				A	B	B	B	B	B	B	B	B	B	B	C	0	0	0	0	0
τ_j				2	2	2	2	2	2	2	2	2	2	2	2	2	2	2	2	2

Figure C.2: $\mathcal{P}_1$, $\bar{\tau} = 3$, $T = 10$ and $\tau_A = 1$

k	-3	-2	-1	0	1	2	3	4	5	6	7	8	9	10	11	12	13	14	15	16
$b_k^{(-2)}$	0	1	2	3	4	5	6	7	8	9	10	11	11	11	11	11	11	11	11	11
$b_k^{(1)}$	0	0	1	2	3	4	5	6	7	8	9	10	11	11	11	11	11	11	11	11
$b_k^{(0)} = a_k$	0	0	0	1	2	3	4	5	6	7	8	9	10	11	11	11	11	11	11	11
$b_k^{(1)}$	0	0	0	0	1	2	3	4	5	6	7	8	9	10	11	11	11	11	11	11
$b_k^{(-2)}$	0	1	2	3	4	5	6	7	8	9	10	11	11	11	11	11	11	11	11	11
$b_k^{(-1)}$	0	0	~~1~~	~~2~~	~~3~~	~~4~~	~~5~~	~~6~~	~~7~~	~~8~~	~~9~~	~~10~~	~~11~~	~~11~~	~~11~~	~~11~~	~~11~~	~~11~~	~~11~~	~~11~~
$b_k^{(0)} = a_k$	0	0	0	~~1~~	~~2~~	~~3~~	~~4~~	~~5~~	~~6~~	~~7~~	~~8~~	~~9~~	~~10~~	~~11~~	~~11~~	~~11~~	~~11~~	~~11~~	~~11~~	~~11~~
$b_k^{(1)}$	0	0	0	0	~~1~~	~~2~~	~~3~~	~~4~~	~~5~~	~~6~~	~~7~~	~~8~~	~~9~~	~~10~~	~~11~~	~~11~~	~~11~~	~~11~~	~~11~~	~~11~~
$b_k^{(-2)} - a_k$	0	1	2	2	2	2	2	2	2	2	2	2	1	0	0	0	0	0	0	0
$b_k^{(-1)} - a_k$	0	0	1	1	1	1	1	1	1	1	1	1	1	0	0	0	0	0	0	0
$b_k^{(0)} - a_k$	0	0	0	0	0	0	0	0	0	0	0	0	0	0	0	0	0	0	0	0
$b_k^{(1)} - a_k$	0	0	-0	-1	-1	-1	-1	-1	-1	-1	-1	-1	-1	-1	0	0	0	0	0	0
packet arr.	no	yes	yes	yes	yes	yes	yes	yes	yes	yes	yes	yes	yes	yes	yes	yes	yes	yes	yes	yes
c_k	0	1	2	3	4	5	6	7	8	9	10	11	11	11	11	11	11	11	11	11
w_k	0	1	2	2	2	2	2	2	2	2	2	2	1	0	0	0	0	0	0	0
block		A	B	B	B	B	B	B	B	B	B	B	C	0	0	0	0	0	0	0
τ_j				-2	-2	-2	-2	-2	-2	-2	-2	-2	-2	-2	-2	-2	-2	-2	-2	-2

Figure C.3: $\mathcal{P}_1$, $\bar{\tau} = 3$, $T = 10$ and $\tau_A = 2$

k	-3	-2	-1	0	1	2	3	4	5	6	7	8	9	10	11	12	13	14	15	16
$b_k^{(-3)}$	1	2	3	4	5	6	7	8	9	10	11	11	11	11	11	11	11	11	11	11
$b_k^{(-2)}$	0	1	2	3	4	5	6	7	8	9	10	11	11	11	11	11	11	11	11	11
$b_k^{(-1)}$	0	0	1	2	3	4	5	6	7	8	9	10	11	11	11	11	11	11	11	11
$b_k^{(0)} = a_k$	0	0	0	1	2	3	4	5	6	7	8	9	10	11	11	11	11	11	11	11
$b_k^{(-3)}$	1	2	3	4	5	6	7	8	9	10	11	11	11	11	11	11	11	11	11	11
$b_k^{(-2)}$	0	~~1~~	~~2~~	~~3~~	~~4~~	~~5~~	~~6~~	~~7~~	~~8~~	~~9~~	~~10~~	~~11~~	~~11~~	~~11~~	~~11~~	~~11~~	~~11~~	~~11~~	~~11~~	~~11~~
$b_k^{(-1)}$	0	0	~~1~~	~~2~~	~~3~~	~~4~~	~~5~~	~~6~~	~~7~~	~~8~~	~~9~~	~~10~~	~~11~~	~~11~~	~~11~~	~~11~~	~~11~~	~~11~~	~~11~~	~~11~~
$b_k^{(0)} = a_k$	0	0	0	~~1~~	~~2~~	~~3~~	~~4~~	~~5~~	~~6~~	~~7~~	~~8~~	~~9~~	~~10~~	~~11~~	~~11~~	~~11~~	~~11~~	~~11~~	~~11~~	~~11~~
$b_k^{(-3)} - a_k$	1	2	3	3	3	3	3	3	3	3	3	2	1	0	0	0	0	0	0	0
$b_k^{(-2)} - a_k$	0	1	2	2	2	2	2	2	2	2	2	2	1	0	0	0	0	0	0	0
$b_k^{(-1)} - a_k$	0	0	1	1	1	1	1	1	1	1	1	1	1	0	0	0	0	0	0	0
$b_k^{(0)} - a_k$	0	0	0	0	0	0	0	0	0	0	0	0	0	0	0	0	0	0	0	0
packet arr.	yes	yes	yes	yes	yes	yes	yes	yes	yes	yes	yes	yes	yes	yes	yes	yes	yes	yes	yes	yes
c_k	1	2	3	4	5	6	7	8	9	10	11	11	11	11	11	11	11	11	11	11
w_k	1	2	3	3	3	3	3	3	3	3	3	2	1	0	0	0	0	0	0	0
block	A	A	B	B	B	B	B	B	B	B	B	C	C	0	0	0	0	0	0	0
τ_j				-3	-3	-3	-3	-3	-3	-3	-3	-3	-3	-3	-3	-3	-3	-3	-3	-3

Figure C.4: $\mathcal{P}_1$, $\bar{\tau} = 3$, $T = 10$ and $\tau_A = 3$

$\bar{\tau}$	min	max	k	-4	-3	-2	-1	0	1	2	3	4	5	6	7	8	9	10	11	12	13	14	15	16	17	18
2	0	2	τ_j					2	2	2	2	2	2	2	2	2	2	2	2	2						
			w_k			0	0	-1	-2	-2	-2	-2	-2	-2	-2	-2	-2	-2	-1	0						
2	-1	1	τ_j					1	1	1	1	1	1	1	1	1	1	1	1	1						
			w_k			0	0	-1	-1	-1	-1	-1	-1	-1	-1	-1	-1	-1	0	0						
2	-2	0	τ_j					-2	-2	-2	-2	-2	-2	-2	-2	-2	-2	-2	-2	-2						
			w_k			1	2	2	2	2	2	2	2	2	2	2	1	0	0	0						
3	0	3	τ_j					3	3	3	3	3	3	3	3	3	3	3	3	3	3					
			w_k		0	0	0	-1	-2	-3	-3	-3	-3	-3	-3	-3	-3	-3	-2	-1	0					
3	-1	2	τ_j					2	2	2	2	2	2	2	2	2	2	2	2	2	2					
			w_k		0	0	0	-1	-2	-2	-2	-2	-2	-2	-2	-2	-2	-2	-1	0	0					
3	-2	1	τ_j					-2	-2	-2	-2	-2	-2	-2	-2	-2	-2	-2	-2	-2	-2					
			w_k		0	1	2	2	2	2	2	2	2	2	2	2	1	0	0	0	0					
3	-3	0	τ_j					-3	-3	-3	-3	-3	-3	-3	-3	-3	-3	-3	-3	-3	-3					
			w_k		1	2	3	3	3	3	3	3	3	3	3	2	1	0	0	0	0					
4	0	4	τ_j					4	4	4	4	4	4	4	4	4	4	4	4	4	4	4				
			w_k	0	0	0	0	-1	-2	-3	-4	-4	-4	-4	-4	-4	-4	-4	-3	-2	-1	0				
4	-1	3	τ_j					3	3	3	3	3	3	3	3	3	3	3	3	3	3	3				
			w_k	0	0	0	0	-1	-2	-3	-3	-3	-3	-3	-3	-3	-3	-3	-2	-1	0	0				
4	-2	2	τ_j					2	2	2	2	2	2	2	2	2	2	2	2	2	2	2				
			w_k	0	0	0	0	-1	-2	-2	-2	-2	-2	-2	-2	-2	-2	-2	-1	0	0	0				
4	-3	1	τ_j					-3	-3	-3	-3	-3	-3	-3	-3	-3	-3	-3	-3	-3	-3	-3				
			w_k	0	1	2	3	3	3	3	3	3	3	3	3	2	1	0	0	0	0	0				
4	-4	0	τ_j					-4	-4	-4	-4	-4	-4	-4	-4	-4	-4	-4	-4	-4	-4	-4				
			w_k	1	2	3	4	4	4	4	4	4	4	4	3	2	1	0	0	0	0	0				

Figure C.5: $\mathcal{P}_1$, $\bar{\tau} \in \{2, 3, 4\}$ and $T = 10$

$\bar{\tau}$	min	max	k	−4	−3	−2	−1	0	1	2	3	4	5	6	7	8	9	10	11	12	13	14	15	16	17	18
2	0	2	τ_j					2	2	2	2	2	2	2	2	2	2	2	2							
			w_k			0	0	−1	−2	−2	−2	−2	−2	−2	−2	−2	−2	−1	0							
2	−1	1	τ_j					1	1	1	1	1	1	1	1	1	1	1	1							
			w_k			0	0	−1	−1	−1	−1	−1	−1	−1	−1	−1	−1	0	0							
2	−2	0	τ_j					−2	−2	−2	−2	−2	−2	−2	−2	−2	−2	−2	−2							
			w_k			1	2	2	2	2	2	2	2	2	2	1	0	0	0							
3	0	3	τ_j					3	3	3	3	3	3	3	3	3	3	3	3	3						
			w_k		0	0	0	−1	−2	−3	−3	−3	−3	−3	−3	−3	−3	−2	−1	0						
3	−1	2	τ_j					2	2	2	2	2	2	2	2	2	2	2	2	2						
			w_k		0	0	0	−1	−2	−2	−2	−2	−2	−2	−2	−2	−2	−1	0	0						
3	−2	1	τ_j					−2	−2	−2	−2	−2	−2	−2	−2	−2	−2	−2	−2	−2						
			w_k		0	1	2	2	2	2	2	2	2	2	2	1	0	0	0	0						
3	−3	0	τ_j					−3	−3	−3	−3	−3	−3	−3	−3	−3	−3	−3	−3	−3						
			w_k		1	2	3	3	3	3	3	3	3	3	2	1	0	0	0	0						
4	0	4	τ_j					4	4	4	4	4	4	4	4	4	4	4	4	4	4					
			w_k	0	0	0	0	−1	−2	−3	−4	−4	−4	−4	−4	−4	−4	−3	−2	−1	0					
4	−1	3	τ_j					3	3	3	3	3	3	3	3	3	3	3	3	3	3					
			w_k	0	0	0	0	−1	−2	−3	−3	−3	−3	−3	−3	−3	−3	−2	−1	0	0					
4	−2	2	τ_j					2	2	2	2	2	2	2	2	2	2	2	2	2	2					
			w_k	0	0	0	0	−1	−2	−2	−2	−2	−2	−2	−2	−2	−2	−1	0	0	0					
4	−3	1	τ_j					−3	−3	−3	−3	−3	−3	−3	−3	−3	−3	−3	−3	−3	−3					
			w_k	0	1	2	3	3	3	3	3	3	3	3	2	1	0	0	0	0	0					
4	−4	0	τ_j					−4	−4	−4	−4	−4	−4	−4	−4	−4	−4	−4	−4	−4	−4					
			w_k	1	2	3	4	4	4	4	4	4	4	3	2	1	0	0	0	0	0					

Figure C.6: $\mathcal{P}_1$, $\bar{\tau} \in \{2, 3, 4\}$ and $T = 9$

$\bar{\tau}$	min	max	k	−4	−3	−2	−1	0	1	2	3	4	5	6	7	8	9	10	11	12	13	14	15	16	17	18
2	0	2	τ_j					2	2	2	2	2	2	2	2	2	2	2								
			w_k			0	0	−1	−2	−2	−2	−2	−2	−2	−2	−2	−1	0								
2	−1	1	τ_j					1	1	1	1	1	1	1	1	1	1	1								
			w_k			0	0	−1	−1	−1	−1	−1	−1	−1	−1	−1	0	0								
2	−2	0	τ_j					−2	−2	−2	−2	−2	−2	−2	−2	−2	−2	−2								
			w_k			1	2	2	2	2	2	2	2	2	1	0	0	0								
3	0	3	τ_j					3	3	3	3	3	3	3	3	3	3	3	3							
			w_k		0	0	0	−1	−2	−3	−3	−3	−3	−3	−3	−3	−2	−1	0							
3	−1	2	τ_j					2	2	2	2	2	2	2	2	2	2	2	2							
			w_k		0	0	0	−1	−2	−2	−2	−2	−2	−2	−2	−2	−1	0	0							
3	−2	1	τ_j					−2	−2	−2	−2	−2	−2	−2	−2	−2	−2	−2	−2							
			w_k		0	1	2	2	2	2	2	2	2	2	1	0	0	0	0							
3	−3	0	τ_j					−3	−3	−3	−3	−3	−3	−3	−3	−3	−3	−3	−3							
			w_k		1	2	3	3	3	3	3	3	3	2	1	0	0	0	0							
4	0	4	τ_j					4	4	4	4	4	4	4	4	4	4	4	4	4						
			w_k	0	0	0	0	−1	−2	−3	−4	−4	−4	−4	−4	−4	−3	−2	−1	0						
4	−1	3	τ_j					3	3	3	3	3	3	3	3	3	3	3	3	3						
			w_k	0	0	0	0	−1	−2	−3	−3	−3	−3	−3	−3	−3	−2	−1	0	0						
4	−2	2	τ_j					2	2	2	2	2	2	2	2	2	2	2	2	2						
			w_k	0	0	0	0	−1	−2	−2	−2	−2	−2	−2	−2	−2	−1	0	0	0						
4	−3	1	τ_j					−3	−3	−3	−3	−3	−3	−3	−3	−3	−3	−3	−3	−3						
			w_k	0	1	2	3	3	3	3	3	3	3	2	1	0	0	0	0	0						
4	−4	0	τ_j					−4	−4	−4	−4	−4	−4	−4	−4	−4	−4	−4	−4	−4						
			w_k	1	2	3	4	4	4	4	4	4	3	2	1	0	0	0	0	0						

Figure C.7: $\mathcal{P}_1$, $\bar{\tau} \in \{2, 3, 4\}$ and $T = 8$

$\bar{\tau}$	min	max	k	−4	−3	−2	−1	0	1	2	3	4	5	6	7	8	9	10	11	12	13	14	15	16	17	18
2	0	2	τ_j					2	2	2	2	2	2	2	2	2	2									
			w_k			0	0	−1	−2	−2	−2	−2	−2	−2	−2	−1	0									
2	−1	1	τ_j					1	1	1	1	1	1	1	1	1	1									
			w_k			0	0	−1	−1	−1	−1	−1	−1	−1	−1	0	0									
2	−2	0	τ_j					−2	−2	−2	−2	−2	−2	−2	−2	−2	−2									
			w_k			1	2	2	2	2	2	2	2	1	0	0	0									
3	0	3	τ_j					3	3	3	3	3	3	3	3	3	3	3								
			w_k		0	0	0	−1	−2	−3	−3	−3	−3	−3	−3	−2	−1	0								
3	−1	2	τ_j					2	2	2	2	2	2	2	2	2	2	2								
			w_k		0	0	0	−1	−2	−2	−2	−2	−2	−2	−2	−1	0	0								
3	−2	1	τ_j					−2	−2	−2	−2	−2	−2	−2	−2	−2	−2	−2								
			w_k		0	1	2	2	2	2	2	2	2	1	0	0	0	0								
3	−3	0	τ_j					−3	−3	−3	−3	−3	−3	−3	−3	−3	−3	−3								
			w_k		1	2	3	3	3	3	3	3	2	1	0	0	0	0								
4	0	4	τ_j					4	4	4	4	4	4	4	4	4	4	4	4							
			w_k	0	0	0	0	−1	−2	−3	−4	−4	−4	−4	−4	−3	−2	−1	0							
4	−1	3	τ_j					3	3	3	3	3	3	3	3	3	3	3	3							
			w_k	0	0	0	0	−1	−2	−3	−3	−3	−3	−3	−3	−2	−1	0	0							
4	−2	2	τ_j					2	2	2	2	2	2	2	2	2	2	2	2							
			w_k	0	0	0	0	−1	−2	−2	−2	−2	−2	−2	−2	−1	0	0	0							
4	−3	1	τ_j					−3	−3	−3	−3	−3	−3	−3	−3	−3	−3	−3	−3							
			w_k	0	1	2	3	3	3	3	3	3	2	1	0	0	0	0	0							
4	−4	0	τ_j					−4	−4	−4	−4	−4	−4	−4	−4	−4	−4	−4	−4							
			w_k	1	2	3	4	4	4	4	4	3	2	1	0	0	0	0	0							

Figure C.8: $\mathcal{P}_1$, $\bar{\tau} \in \{2, 3, 4\}$ and $T = 7$

$\bar{\tau}$	min	max	k	−4	−3	−2	−1	0	1	2	3	4	5	6	7	8	9	10	11	12	13	14	15	16	17	18
2	0	2	τ_j					2	2	2	2	2	2	2	2	2										
			w_k			0	0	−1	−2	−2	−2	−2	−2	−2	−1	0										
2	−1	1	τ_j					1	1	1	1	1	1	1	1	1										
			w_k			0	0	−1	−1	−1	−1	−1	−1	−1	0	0										
2	−2	0	τ_j					−2	−2	−2	−2	−2	−2	−2	−2	−2										
			w_k			1	2	2	2	2	2	2	1	0	0	0										
3	0	3	τ_j					3	3	3	3	3	3	3	3	3	3									
			w_k		0	0	0	−1	−2	−3	−3	−3	−3	−3	−2	−1	0									
3	−1	2	τ_j					2	2	2	2	2	2	2	2	2	2									
			w_k		0	0	0	−1	−2	−2	−2	−2	−2	−2	−1	0	0									
3	−2	1	τ_j					−2	−2	−2	−2	−2	−2	−2	−2	−2	−2									
			w_k		0	1	2	2	2	2	2	2	1	0	0	0	0									
3	−3	0	τ_j					−3	−3	−3	−3	−3	−3	−3	−3	−3	−3									
			w_k		1	2	3	3	3	3	3	2	1	0	0	0	0									
4	0	4	τ_j					4	4	4	4	4	4	4	4	4	4	4								
			w_k	0	0	0	0	−1	−2	−3	−4	−4	−4	−4	−3	−2	−1	0								
4	−1	3	τ_j					3	3	3	3	3	3	3	3	3	3	3								
			w_k	0	0	0	0	−1	−2	−3	−3	−3	−3	−3	−2	−1	0	0								
4	−2	2	τ_j					2	2	2	2	2	2	2	2	2	2	2								
			w_k	0	0	0	0	−1	−2	−2	−2	−2	−2	−2	−1	0	0	0								
4	−3	1	τ_j					−3	−3	−3	−3	−3	−3	−3	−3	−3	−3	−3								
			w_k	0	1	2	3	3	3	3	3	2	1	0	0	0	0	0								
4	−4	0	τ_j					−4	−4	−4	−4	−4	−4	−4	−4	−4	−4	−4								
			w_k	1	2	3	4	4	4	4	3	2	1	0	0	0	0	0								

Figure C.9: $\mathcal{P}_1$, $\bar{\tau} \in \{2, 3, 4\}$ and $T = 6$

$\bar{\tau}$	min	max	k	−4	−3	−2	−1	0	1	2	3	4	5	6	7	8	9	10	11	12	13	14	15	16	17	18
2	0	2	τ_j					2	2	2	2	2	2	2	2											
			w_k			0	0	−1	−2	−2	−2	−2	−2	−1	0											
2	−1	1	τ_j					1	1	1	1	1	1	1	1											
			w_k			0	0	−1	−1	−1	−1	−1	−1	0	0											
2	−2	0	τ_j					−2	−2	−2	−2	−2	−2	−2	−2											
			w_k			1	2	2	2	2	2	1	0	0	0											
3	0	3	τ_j					3	3	3	3	3	3	3	3	3										
			w_k		0	0	0	−1	−2	−3	−3	−3	−3	−2	−1	0										
3	−1	2	τ_j					2	2	2	2	2	2	2	2	2										
			w_k		0	0	0	−1	−2	−2	−2	−2	−2	−1	0	0										
3	−2	1	τ_j					−2	−2	−2	−2	−2	−2	−2	−2	−2										
			w_k		0	1	2	2	2	2	2	1	0	0	0	0										
3	−3	0	τ_j					−3	−3	−3	−3	−3	−3	−3	−3	−3										
			w_k		1	2	3	3	3	3	2	1	0	0	0	0										
4	0	4	τ_j					4	4	4	4	4	4	4	4	4	4									
			w_k	0	0	0	0	−1	−2	−3	−4	−4	−4	−3	−2	−1	0									
4	−1	3	τ_j					3	3	3	3	3	3	3	3	3	3									
			w_k	0	0	0	0	−1	−2	−3	−3	−3	−3	−2	−1	0	0									
4	−2	2	τ_j					2	2	2	2	2	2	2	2	2	2									
			w_k	0	0	0	0	−1	−2	−2	−2	−2	−2	−1	0	0	0									
4	−3	1	τ_j					−3	−3	−3	−3	−3	−3	−3	−3	−3	−3									
			w_k	0	1	2	3	3	3	3	2	1	0	0	0	0	0									
4	−4	0	τ_j					−4	−4	−4	−4	−4	−4	−4	−4	−4	−4									
			w_k	1	2	3	4	4	4	3	2	1	0	0	0	0	0									

Figure C.10: $\mathcal{P}_1$, $\bar{\tau} \in \{2, 3, 4\}$ and $T = 5$

$\bar{\tau}$	min	max	k	−4	−3	−2	−1	0	1	2	3	4	5	6	7	8	9	10	11	12	13	14	15	16	17	18
2	0	2	τ_j					2	2	2	2	2	2	2												
			w_k			0	0	−1	−2	−2	−2	−2	−1	0												
2	−1	1	τ_j					1	1	1	1	1	1	1												
			w_k			0	0	−1	−1	−1	−1	−1	0	0												
2	−2	0	τ_j					−2	−2	−2	−2	−2	−2	−2												
			w_k			1	2	2	2	2	1	0	0	0												
3	0	3	τ_j					3	3	3	3	3	3	3	3											
			w_k		0	0	0	−1	−2	−3	−3	−3	−2	−1	0											
3	−1	2	τ_j					2	2	2	2	2	2	2	2											
			w_k		0	0	0	−1	−2	−2	−2	−2	−1	0	0											
3	−2	1	τ_j					−2	−2	−2	−2	−2	−2	−2	−2											
			w_k		0	1	2	2	2	2	1	0	0	0	0											
3	−3	0	τ_j					−3	−3	−3	−3	−3	−3	−3	−3											
			w_k		1	2	3	3	3	2	1	0	0	0	0											
4	0	4	τ_j					4	4	4	4	4	4	4	4	4										
			w_k	0	0	0	0	−1	−2	−3	−4	−4	−3	−2	−1	0										
4	−1	3	τ_j					3	3	3	3	3	3	3	3	3										
			w_k	0	0	0	0	−1	−2	−3	−3	−3	−2	−1	0	0										
4	−2	2	τ_j					2	2	2	2	2	2	2	2	2										
			w_k	0	0	0	0	−1	−2	−2	−2	−2	−1	0	0	0										
4	−3	1	τ_j					−3	−3	−3	−3	−3	−3	−3	−3	−3										
			w_k	0	1	2	3	3	3	2	1	0	0	0	0	0										
4	−4	0	τ_j					−4	−4	−4	−4	−4	−4	−4	−4	−4										
			w_k	1	2	3	4	4	3	2	1	0	0	0	0	0										

Figure C.11: $\mathcal{P}_1$, $\bar{\tau} \in \{2, 3, 4\}$ and $T = 4$

$\bar{\tau}$	min	max	k	−4	−3	−2	−1	0	1	2	3	4	5	6	7	8	9	10	11	12	13	14	15	16	17	18
2	0	2	τ_j					2	2	2	2	2	2													
			w_k			0	0	−1	−2	−2	−2	−1	0													
2	−1	1	τ_j					1	1	1	1	1	1													
			w_k			0	0	−1	−1	−1	−1	0	0													
2	−2	0	τ_j					−2	−2	−2	−2	−2	−2													
			w_k			1	2	2	2	1	0	0	0													
3	0	3	τ_j					3	3	3	3	3	3	3												
			w_k		0	0	0	−1	−2	−3	−3	−2	−1	0												
3	−1	2	τ_j					2	2	2	2	2	2	2												
			w_k		0	0	0	−1	−2	−2	−2	−1	0	0												
3	−2	1	τ_j					−2	−2	−2	−2	−2	−2	−2												
			w_k		0	1	2	2	2	1	0	0	0	0												
3	−3	0	τ_j					−3	−3	−3	−3	−3	−3	−3												
			w_k		1	2	3	3	2	1	0	0	0	0												
4	0	4	τ_j					4	4	4	4	4	4	4	4											
			w_k	0	0	0	0	−1	−2	−3	−4	−3	−2	−1	0											
4	−1	3	τ_j					3	3	3	3	3	3	3	3											
			w_k	0	0	0	0	−1	−2	−3	−3	−2	−1	0	0											
4	−2	2	τ_j					2	2	2	2	2	2	2	2											
			w_k	0	0	0	0	−1	−2	−2	−2	−1	0	0	0											
4	−3	1	τ_j					−3	−3	−3	−3	−3	−3	−3	−3											
			w_k	0	1	2	3	3	2	1	0	0	0	0	0											
4	−4	0	τ_j					−4	−4	−4	−4	−4	−4	−4	−4											
			w_k	1	2	3	4	3	2	1	0	0	0	0	0											

Figure C.12: $\mathcal{P}_1$, $\bar{\tau} \in \{2, 3, 4\}$ and $T = 3$

$\bar{\tau}$	min	max	k	−4	−3	−2	−1	0	1	2	3	4	5	6	7	8	9	10	11	12	13	14	15	16	17	18
2	0	2	τ_j					2	2	2	2	2														
			w_k			0	0	−1	−2	−2	−1	0														
2	−1	1	τ_j					1	1	1	1	1														
			w_k			0	0	−1	−1	−1	0	0														
2	−2	0	τ_j					−2	−2	−2	−2	−2														
			w_k			1	2	2	1	0	0	0														
3	0	3	τ_j					3	3	3	3	3	3													
			w_k		0	0	0	−1	−2	−3	−2	−1	0													
3	−1	2	τ_j					2	2	2	2	2	2													
			w_k		0	0	0	−1	−2	−2	−1	0	0													
3	−2	1	τ_j					−2	−2	−2	−2	−2	−2													
			w_k		0	1	2	2	1	0	0	0	0													
3	−3	0	τ_j					−3	−3	−3	−3	−3	−3													
			w_k		1	2	3	2	1	0	0	0	0													
4	0	4	τ_j					4	4	4	4	4	4	4												
			w_k	0	0	0	0	−1	−2	−3	−3	−2	−1	0												
4	−1	3	τ_j					3	3	3	3	3	3	3												
			w_k	0	0	0	0	−1	−2	−3	−2	−1	0	0												
4	−2	2	τ_j					2	2	2	2	2	2	2												
			w_k	0	0	0	0	−1	−2	−2	−1	0	0	0												
4	−3	1	τ_j					−3	−3	−3	−3	−3	−3	−3												
			w_k	0	1	2	3	2	1	0	0	0	0	0												
4	−4	0	τ_j					−4	−4	−4	−4	−4	−4	−4												
			w_k	1	2	3	3	2	1	0	0	0	0	0												

Figure C.13: $\mathcal{P}_1$, $\bar{\tau} \in \{2, 3, 4\}$ and $T = 2$

$\bar{\tau}$	min	max	k	-4	-3	-2	-1	0	1	2	3	4	5	6	7	8	9	10	11	12	13	14	15	16	17	18
2	0	2	τ_j					2	2	2	2															
			w_k			0	0	-1	-2	-1	0															
2	-1	1	τ_j					1	1	1	1															
			w_k			0	0	-1	-1	0	0															
2	-2	0	τ_j					-2	-2	-2	-2															
			w_k			1	2	1	0	0	0															
3	0	3	τ_j					3	3	3	3	3														
			w_k		0	0	0	-1	-2	-2	-1	0														
3	-1	2	τ_j					2	2	2	2	2														
			w_k		0	0	0	-1	-2	-1	0	0														
3	-2	1	τ_j					-2	-2	-2	-2	-2														
			w_k		0	1	2	1	0	0	0	0														
3	-3	0	τ_j					-3	-3	-3	-3	-3														
			w_k		1	2	2	1	0	0	0	0														
4	0	4	τ_j					4	4	4	4	4	4													
			w_k	0	0	0	0	-1	-2	-2	-2	-1	0													
4	-1	3	τ_j					3	3	3	3	3	3													
			w_k	0	0	0	0	-1	-2	-2	-1	0	0													
4	-2	2	τ_j					2	2	2	2	2	2													
			w_k	0	0	0	0	-1	-2	-1	0	0	0													
4	-3	1	τ_j					-3	-3	-3	-3	-3	-3													
			w_k	0	1	2	2	1	0	0	0	0	0													
4	-4	0	τ_j					-4	-4	-4	-4	-4	-4													
			w_k	1	2	2	2	1	0	0	0	0	0													

Figure C.14: $\mathcal{P}_1$, $\bar{\tau} \in \{2, 3, 4\}$ and $T = 1$

C.2 Gains for $\mathcal{P}_1$

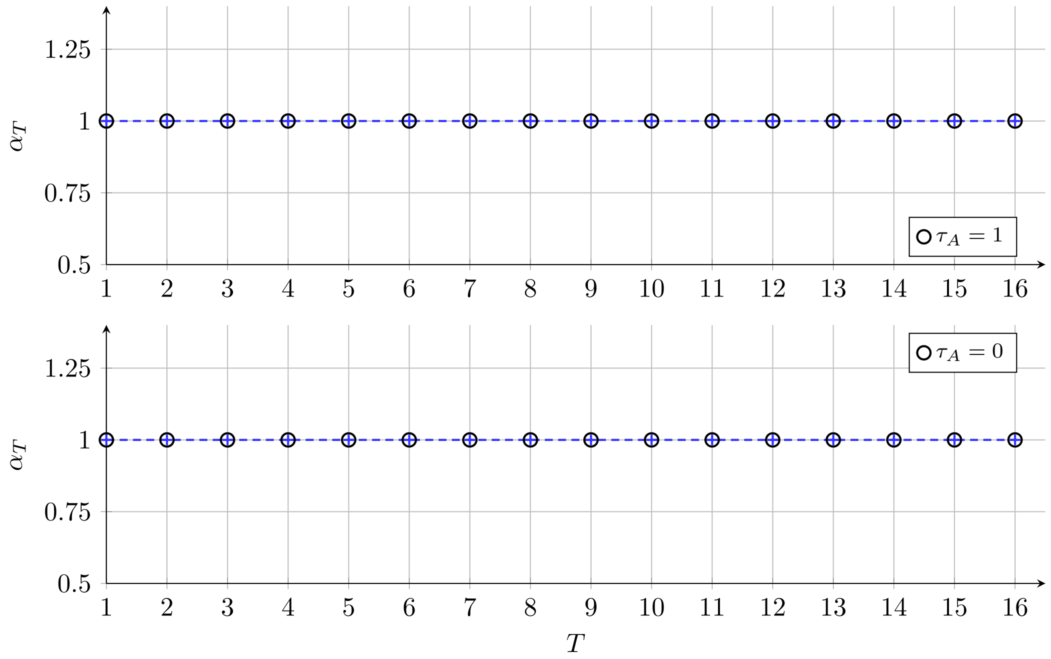

Figure C.15: $\mathcal{P}_1$, $\bar{\tau} = 1$

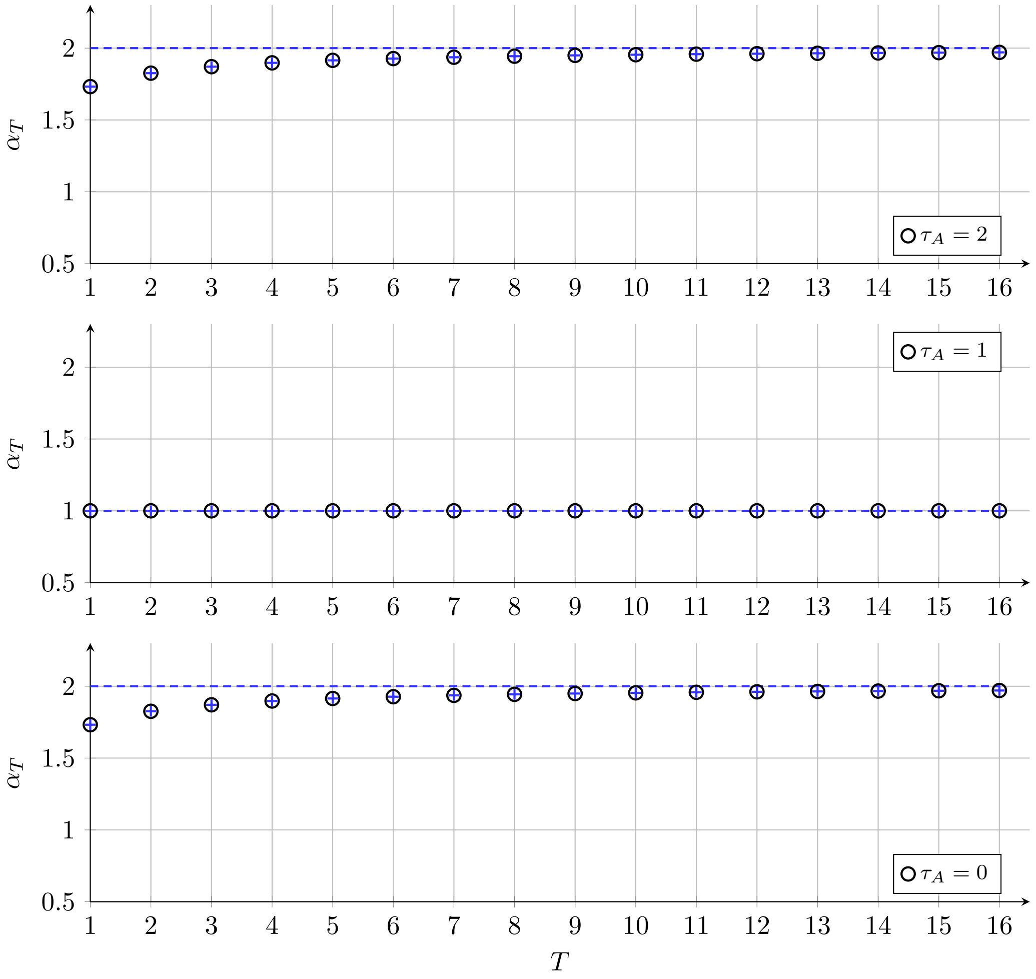

Figure C.16: $\mathcal{P}_1$, $\bar{\tau} = 2$

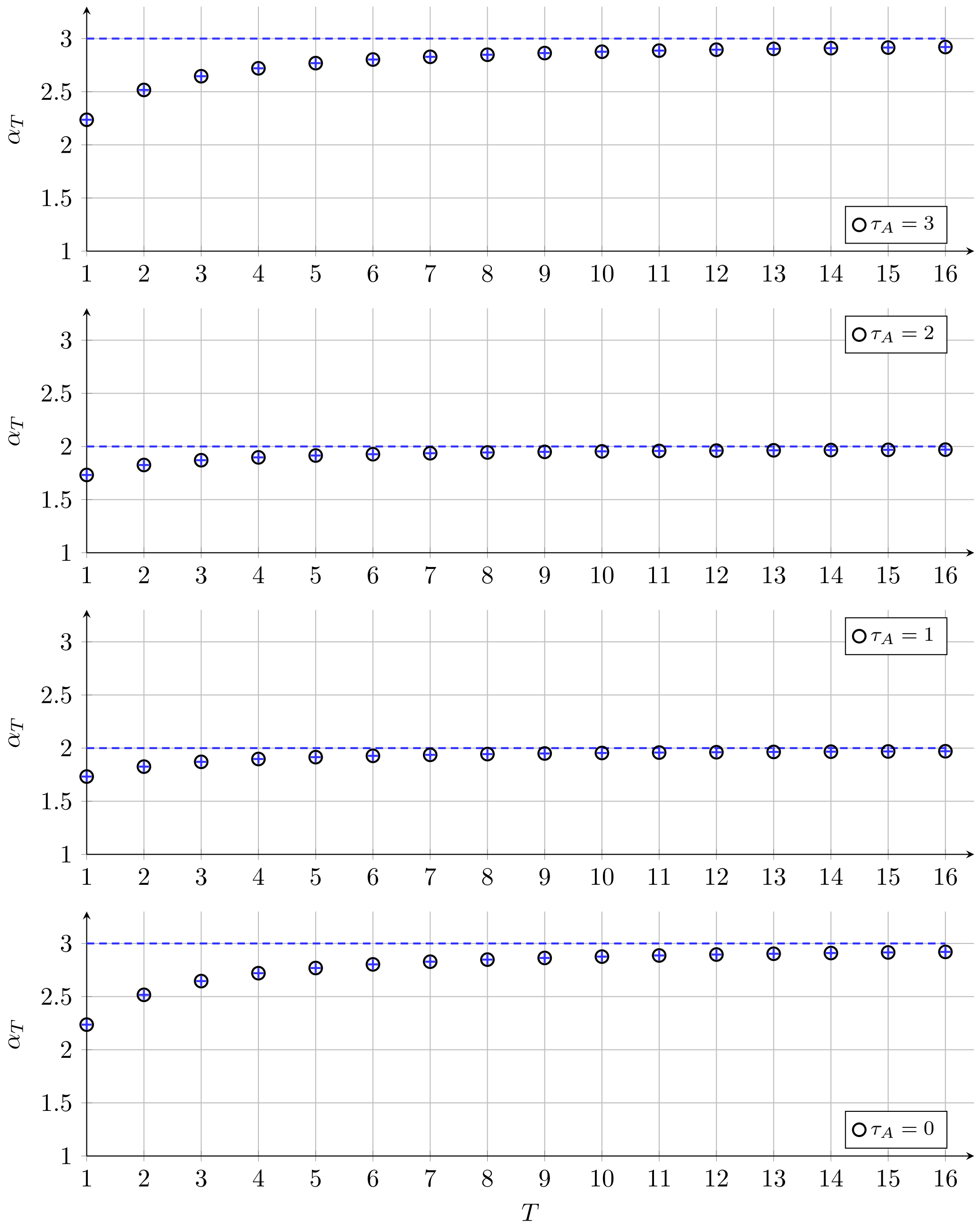

Figure C.17: $\mathcal{P}_1$, $\bar{\tau} = 3$

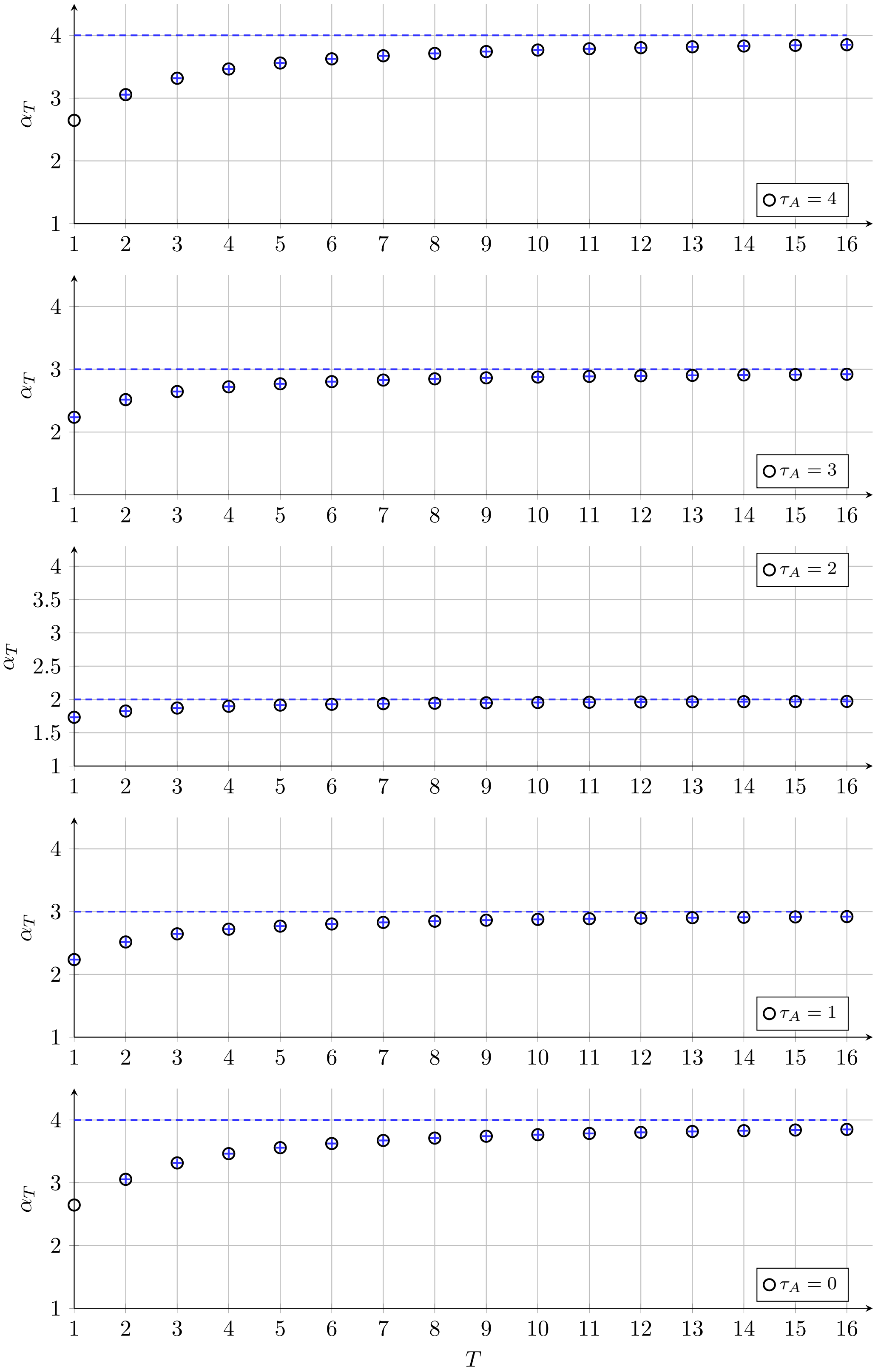

Figure C.18: $\mathcal{P}_1$, $\bar{\tau} = 4$

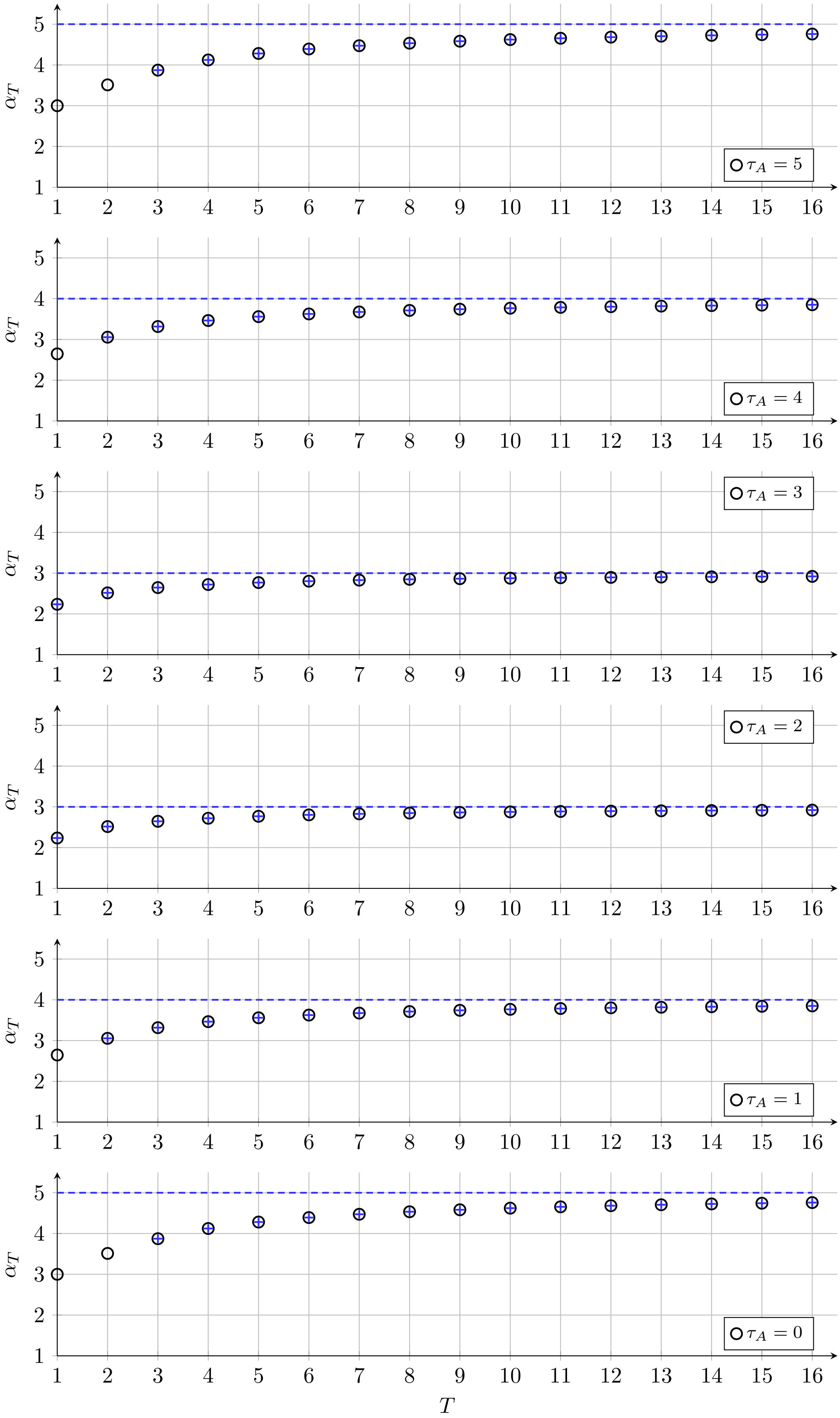

Figure C.19: $\mathcal{P}_1$, $\bar{\tau} = 5$

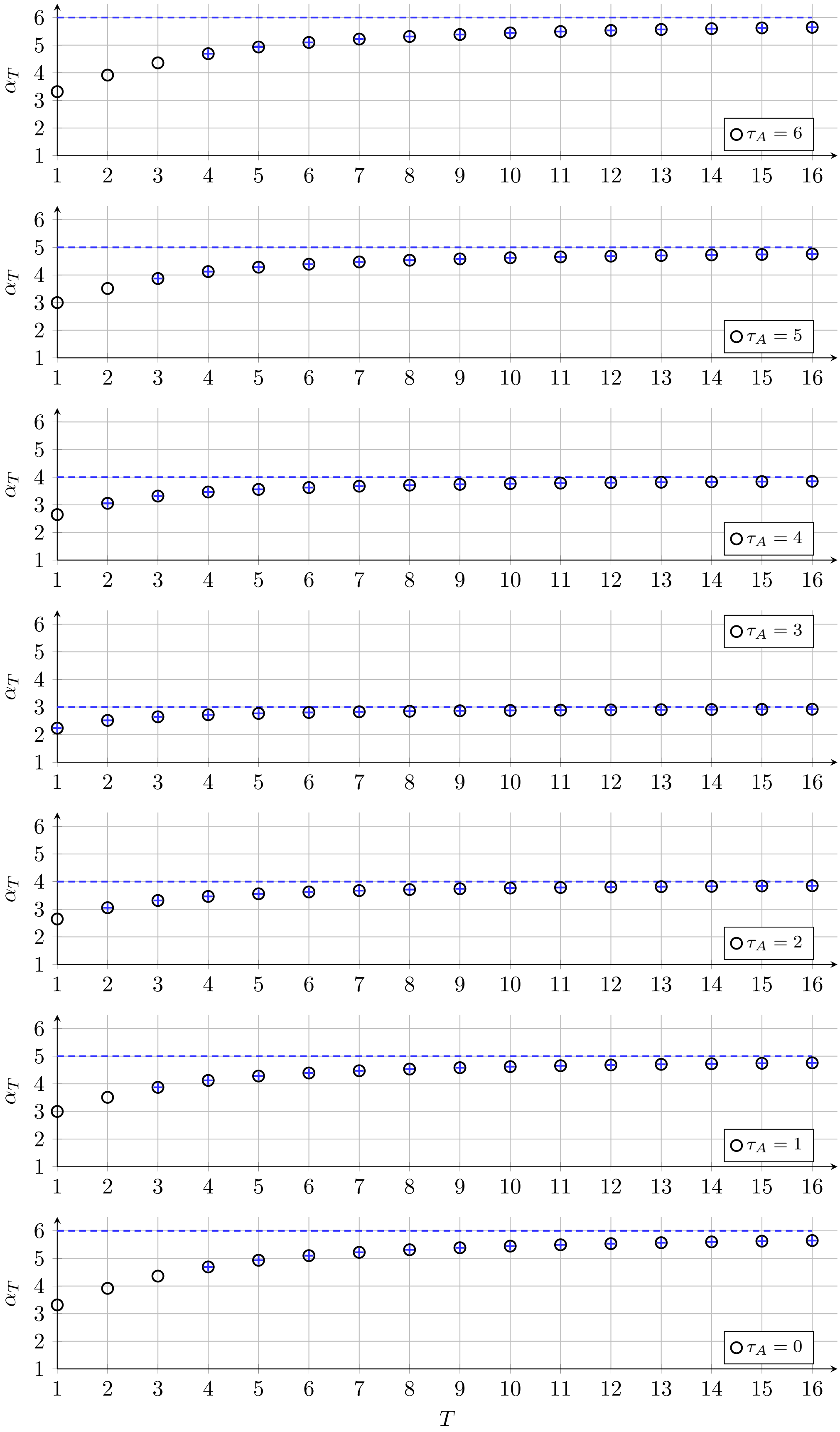

Figure C.20: $\mathcal{P}_1$, $\bar{\tau} = 6$

C.3 Calculated gains from $\mathcal{P}_1$ applied to data from $\mathcal{P}_3$

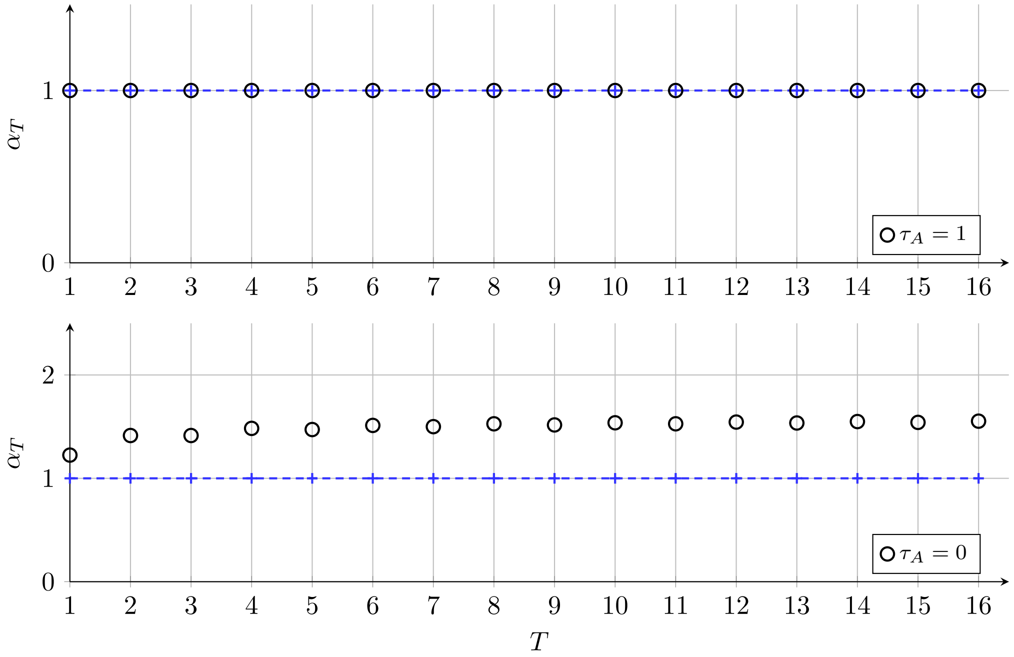

Figure C.21: $\mathcal{P}_3$, $\bar{\tau} = 1$: $\mathcal{P}_1$ (blue)

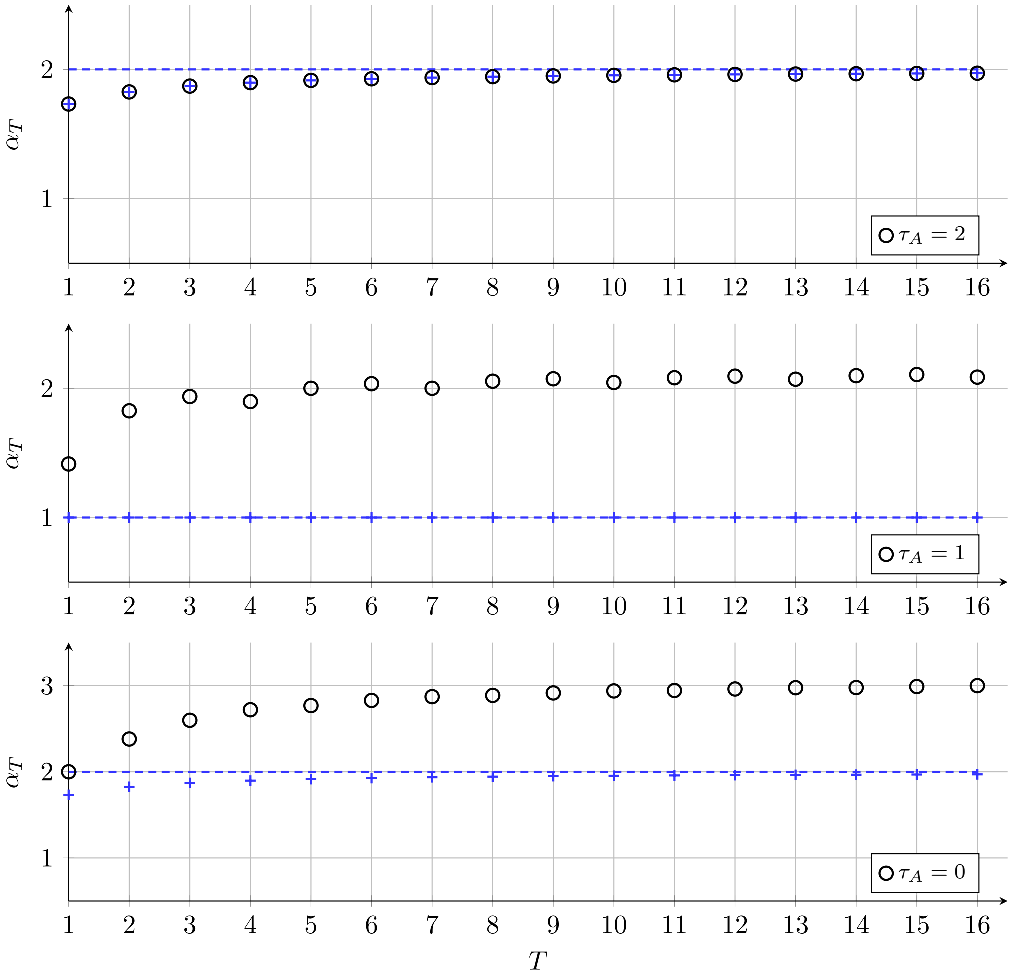

Figure C.22: $\mathcal{P}_3$, $\bar{\tau} = 2$: $\mathcal{P}_1$ (blue)

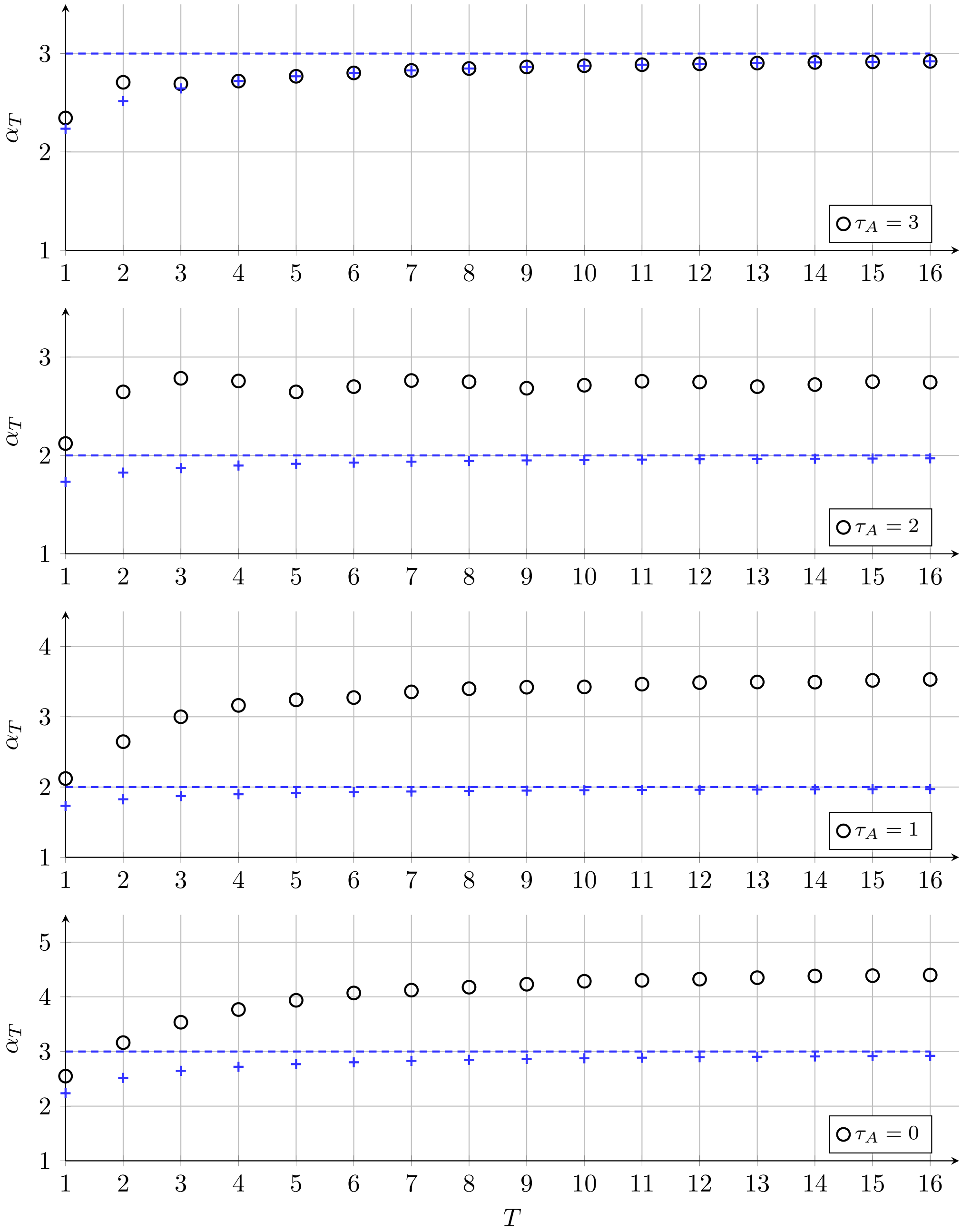

Figure C.23: $\mathcal{P}_3$, $\bar{\tau} = 3$: $\mathcal{P}_1$ (blue)

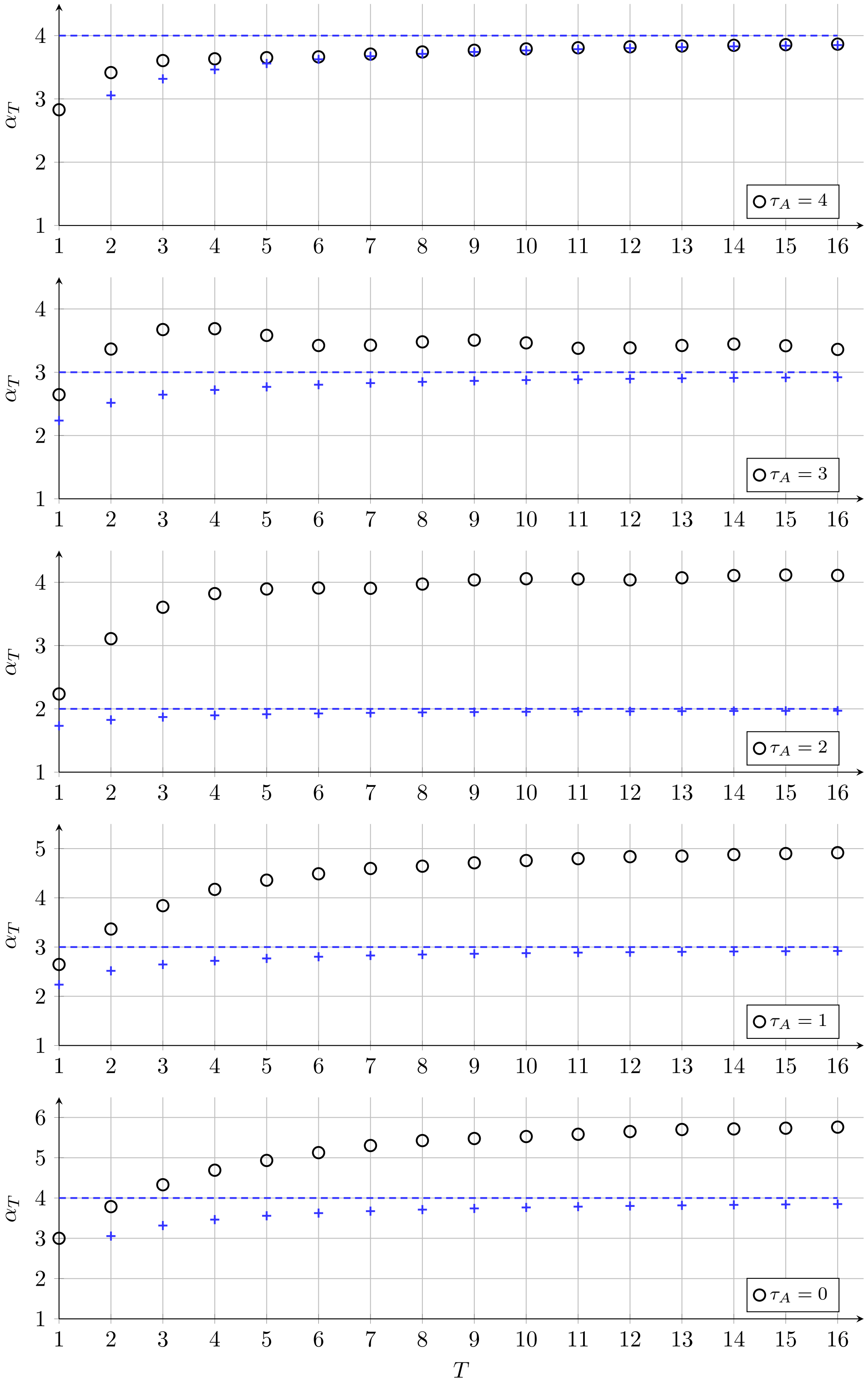

Figure C.24: $\mathcal{P}_3$, $\bar{\tau} = 4$: $\mathcal{P}_1$ (blue)

C.4 Patterns for $\mathcal{P}_3'$

k	-3	-2	-1	0	1	2	3	4	5	6	7	8	9	10	11	12	13	14	15	16
$b_k^{(0)} = a_k$	0	0	0	1	2	3	4	5	6	7	8	9	10	11	11	11	11	11	11	11
$b_k^{(1)}$	0	0	0	0	1	2	3	4	5	6	7	8	9	10	11	11	11	11	11	11
$b_k^{(2)}$	0	0	0	0	0	1	2	3	4	5	6	7	8	9	10	11	11	11	11	11
$b_k^{(3)}$	0	0	0	0	0	0	1	2	3	4	5	6	7	8	9	10	11	11	11	11
$b_k^{(0)} = a_k$	0	0	0	~~1~~	~~2~~	~~3~~	4	~~5~~	~~6~~	~~7~~	8	~~9~~	~~10~~	~~11~~	11	~~11~~	~~11~~	~~11~~	11	~~11~~
$b_k^{(1)}k$	0	0	0	0	~~1~~	~~2~~	3	~~4~~	~~5~~	~~6~~	7	~~8~~	~~9~~	~~10~~	11	~~11~~	~~11~~	~~11~~	11	~~11~~
$b_k^{(2)}$	0	0	0	0	0	~~1~~	2	~~3~~	~~4~~	~~5~~	6	~~7~~	~~8~~	~~9~~	10	~~11~~	~~11~~	~~11~~	11	~~11~~
$b_k^{(3)}$	0	0	0	0	0	0	1	~~2~~	~~3~~	~~4~~	5	~~6~~	~~7~~	~~8~~	9	~~10~~	~~11~~	~~11~~	11	~~11~~
$b_k^{(0)} - a_k$	0	0	0	0	0	0	0	0	0	0	0	0	0	0	0	0	0	0	0	0
$b_k^{(1)} - a_k$	0	0	0	-1	-1	-1	-1	-1	-1	-1	-1	-1	-1	-1	0	0	0	0	0	0
$b_k^{(2)} - a_k$	0	0	0	-1	-2	-2	-2	-2	-2	-2	-2	-2	-2	-2	-1	0	0	0	0	0
$b_k^{(3)} - a_k$	0	0	0	-1	-2	-3	-3	-3	-3	-3	-3	-3	-3	-3	-2	-1	0	0	0	0
packet arr.	no	no	no	no	no	no	yes	no	no	no	yes	no	no	no	yes	no	no	no	yes	no
c_k	0	0	0	0	0	0	1	1	1	1	5	5	5	5	9	9	9	9	11	11
w_k	0	0	0	-1	-2	-3	-3	-4	-5	-6	-3	-4	-5	-6	-2	-2	-2	-2	0	0
block				A	A	A	B	B	B	B	B	B	B	B	C	C	C	C	D	D
τ_j				3	2	1	0	3	2	1	0	3	2	1	0	3	2	1	0	3

Figure C.25: $\mathcal{P}_3'$, $\bar{\tau} = 3$, $T = 10$ and $\tau_A = 0$

k	-3	-2	-1	0	1	2	3	4	5	6	7	8	9	10	11	12	13	14	15	16
$b_k^{(-1)}$	0	0	1	2	3	4	5	6	7	8	9	10	11	11	11	11	11	11	11	11
$b_k^{(0)} = a_k$	0	0	0	1	2	3	4	5	6	7	8	9	10	11	11	11	11	11	11	11
$b_k^{(1)}$	0	0	0	0	1	2	3	4	5	6	7	8	9	10	11	11	11	11	11	11
$b_k^{(2)}$	0	0	0	0	0	1	2	3	4	5	6	7	8	9	10	11	11	11	11	11
$b_k^{(-1)}$	0	0	~~1~~	~~2~~	~~3~~	4	~~5~~	~~6~~	~~7~~	8	~~9~~	~~10~~	~~11~~	11	~~11~~	~~11~~	~~11~~	11	~~11~~	~~11~~
$b_k^{(0)} = a_k$	0	0	0	~~1~~	~~2~~	3	~~4~~	~~5~~	~~6~~	7	~~8~~	~~9~~	~~10~~	11	~~11~~	~~11~~	~~11~~	11	~~11~~	~~11~~
$b_k^{(1)}$	0	0	0	0	~~1~~	2	~~3~~	~~4~~	~~5~~	6	~~7~~	~~8~~	~~9~~	10	~~11~~	~~11~~	~~11~~	11	~~11~~	~~11~~
$b_k^{(2)}$	0	0	0	0	0	1	~~2~~	~~3~~	~~4~~	5	~~6~~	~~7~~	~~8~~	9	~~10~~	~~11~~	~~11~~	11	~~11~~	~~11~~
$b_k^{(-1)} - a_k$	0	0	1	1	1	1	1	1	1	1	1	1	1	0	0	0	0	0	0	0
$b_k^{(0)} - a_k$	0	0	0	0	0	0	0	0	0	0	0	0	0	0	0	0	0	0	0	0
$b_k^{(1)} - a_k$	0	0	0	-1	-1	-1	-1	-1	-1	-1	-1	-1	-1	-1	0	0	0	0	0	0
$b_k^{(2)} - a_k$	0	0	0	-1	-2	-2	-2	-2	-2	-2	-2	-2	-2	-2	-1	0	0	0	0	0
packet arr.	no	no	no	no	no	yes	no	no	no	yes	no	no	no	yes	no	no	no	yes	no	no
c_k	0	0	0	0	0	1	1	1	1	5	5	5	5	9	9	9	9	11	11	11
w_k	0	0	0	-1	-2	-2	-3	-4	-5	-2	-3	-4	-5	-2	-2	-2	-2	0	0	0
block				A	A	B	B	B	B	B	B	B	B	C	C	C	C	D	D	D
τ_j				2	1	0	-1	2	1	0	-1	2	1	0	-1	2	1	0	-1	2

Figure C.26: $\mathcal{P}_3'$, $\bar{\tau} = 3$, $T = 10$ and $\tau_A = 1$

k	-3	-2	-1	0	1	2	3	4	5	6	7	8	9	10	11	12	13	14	15	16
$b_k^{(-2)}$	0	1	2	3	4	5	6	7	8	9	10	11	11	11	11	11	11	11	11	11
$b_k^{(1)}$	0	0	1	2	3	4	5	6	7	8	9	10	11	11	11	11	11	11	11	11
$b_k^{(0)} = a_k$	0	0	0	1	2	3	4	5	6	7	8	9	10	11	11	11	11	11	11	11
$b_k^{(1)}$	0	0	0	0	1	2	3	4	5	6	7	8	9	10	11	11	11	11	11	11
$b_k^{(-2)}$	0	~~1~~	~~2~~	~~3~~	4	~~5~~	~~6~~	~~7~~	8	~~9~~	~~10~~	~~11~~	11	~~11~~	~~11~~	~~11~~	11	~~11~~	~~11~~	~~11~~
$b_k^{(-1)}$	0	0	~~1~~	~~2~~	3	~~4~~	~~5~~	~~6~~	7	~~8~~	~~9~~	~~10~~	11	~~11~~	~~11~~	~~11~~	11	~~11~~	~~11~~	~~11~~
$b_k^{(0)} = a_k$	0	0	0	~~1~~	2	~~3~~	~~4~~	~~5~~	6	~~7~~	~~8~~	~~9~~	10	~~11~~	~~11~~	~~11~~	11	~~11~~	~~11~~	~~11~~
$b_k^{(1)}$	0	0	0	0	1	~~2~~	~~3~~	~~4~~	5	~~6~~	~~7~~	~~8~~	9	~~10~~	~~11~~	~~11~~	11	~~11~~	~~11~~	~~11~~
$b_k^{(-2)} - a_k$	0	1	2	2	2	2	2	2	2	2	2	2	1	0	0	0	0	0	0	0
$b_k^{(-1)} - a_k$	0	0	1	1	1	1	1	1	1	1	1	1	1	0	0	0	0	0	0	0
$b_k^{(0)} - a_k$	0	0	0	0	0	0	0	0	0	0	0	0	0	0	0	0	0	0	0	0
$b_k^{(1)} - a_k$	0	0	0	-1	-1	-1	-1	-1	-1	-1	-1	-1	-1	-1	0	0	0	0	0	0
packet arr.	no	no	no	no	yes	no	no	no	yes	no	no	no	yes	no	no	no	yes	no	no	no
c_k	0	0	0	0	1	1	1	1	5	5	5	5	9	9	9	9	11	11	11	11
w_k	0	0	0	-1	-1	-2	-3	-4	-1	-2	-3	-4	-1	-2	-2	-2	0	0	0	0
block				A	B	B	B	B	B	B	B	B	C	C	C	C	C	C	C	C
τ_j				1	0	-1	-2	1	0	-1	-2	1	0	-1	-2	1	0	-1	-2	1

Figure C.27: $\mathcal{P}'_3$, $\bar{\tau} = 3$, $T = 10$ and $\tau_A = 2$

k	-3	-2	-1	0	1	2	3	4	5	6	7	8	9	10	11	12	13	14	15	16
$b_k^{(-3)}$	1	2	3	4	5	6	7	8	9	10	11	11	11	11	11	11	11	11	11	11
$b_k^{(-2)}$	0	1	2	3	4	5	6	7	8	9	10	11	11	11	11	11	11	11	11	11
$b_k^{(-1)}$	0	0	1	2	3	4	5	6	7	8	9	10	11	11	11	11	11	11	11	11
$b_k^{(0)} = a_k$	0	0	0	1	2	3	4	5	6	7	8	9	10	11	11	11	11	11	11	11
$b_k^{(-3)}$	~~1~~	~~2~~	~~3~~	4	~~5~~	~~6~~	~~7~~	8	~~9~~	~~10~~	~~11~~	11	~~11~~	~~11~~	~~11~~	11	~~11~~	~~11~~	~~11~~	11
$b_k^{(-2)}$	0	~~1~~	~~2~~	3	~~4~~	~~5~~	~~6~~	7	~~8~~	~~9~~	~~10~~	11	~~11~~	~~11~~	~~11~~	11	~~11~~	~~11~~	~~11~~	11
$b_k^{(-1)}$	0	0	~~1~~	2	~~3~~	~~4~~	~~5~~	6	~~7~~	~~8~~	~~9~~	10	~~11~~	~~11~~	~~11~~	11	~~11~~	~~11~~	~~11~~	11
$b_k^{(0)} = a_k$	0	0	0	1	~~2~~	~~3~~	~~4~~	5	~~6~~	~~7~~	~~8~~	9	~~10~~	~~11~~	~~11~~	11	~~11~~	~~11~~	~~11~~	11
$b_k^{(-3)} - a_k$	1	2	3	3	3	3	3	3	3	3	3	2	1	0	0	0	0	0	0	0
$b_k^{(-2)} - a_k$	0	1	2	2	2	2	2	2	2	2	2	2	1	0	0	0	0	0	0	0
$b_k^{(-1)} - a_k$	0	0	1	1	1	1	1	1	1	1	1	1	1	0	0	0	0	0	0	0
$b_k^{(0)} - a_k$	0	0	0	0	0	0	0	0	0	0	0	0	0	0	0	0	0	0	0	0
packet arr.	no	no	no	yes	no	no	no	yes	no	no	no	yes	no	no	no	yes	no	no	no	yes
c_k	0	0	0	1	1	1	1	5	5	5	5	9	9	9	9	11	11	11	11	11
w_k	0	0	0	0	-1	-2	-3	0	-1	-2	-3	0	-1	-2	-2	0	0	0	0	0
block	0	0	0	B	B	B	B	B	B	B	B	C	C	C	C	C	C	C	C	D
τ_j				0	-1	-2	-3	0	-1	-2	-3	0	-1	-2	-3	0	-1	-2	-3	0

Figure C.28: $\mathcal{P}'_3$, $\bar{\tau} = 3$, $T = 10$ and $\tau_A = 3$

$\bar{\tau}$	min	max	k	-4	-3	-2	-1	0	1	2	3	4	5	6	7	8	9	10	11	12	13	14	15	16	17	18
2	0	2	τ_j					2	1	0	2	1	0	2	1	0	2	1	0	2	1	0				
			w_k			0	0	-1	-2	-2	-3	-4	-2	-3	-4	-2	-3	-4	-1	-1	-1	0				
2	-1	1	τ_j					1	0	-1	1	0	-1	1	0	-1	1	0	-1	1	0	-1				
			w_k			0	0	-1	-1	-2	-3	-1	-2	-3	-1	-2	-3	-1	-1	-1	0	0				
2	-2	0	τ_j					0	-1	-2	0	-1	-2	0	-1	-2	0	-1	-2	0	-1	-2				
			w_k			0	0	0	-1	-2	0	-1	-2	0	-1	-2	0	-1	-1	0	0	0				
3	0	3	τ_j					3	2	1	0	3	2	1	0	3	2	1	0	3	2	1	0	3		
			w_k		0	0	0	-1	-2	-3	-3	-4	-5	-6	-3	-4	-5	-6	-2	-2	-2	-2	0	0		
3	-1	2	τ_j					2	1	0	-1	2	1	0	-1	2	1	0	-1	2	1	0	-1	2		
			w_k		0	0	0	-1	-2	-2	-3	-4	-5	-2	-3	-4	-5	-2	-2	-2	-2	0	0	0		
3	-2	1	τ_j					1	0	-1	-2	1	0	-1	-2	1	0	-1	-2	1	0	-1	-2	1		
			w_k		0	0	0	-1	-1	-2	-3	-4	-1	-2	-3	-4	-1	-2	-2	-2	0	0	0	0		
3	-3	0	τ_j					0	-1	-2	-3	0	-1	-2	-3	0	-1	-2	-3	0	-1	-2	-3	0		
			w_k		0	0	0	0	-1	-2	-3	0	-1	-2	-3	0	-1	-2	-2	0	0	0	0	0		
4	0	4	τ_j					4	3	2	1	0	4	3	2	1	0	4	3	2	1	0	4	3	2	1
			w_k	0	0	0	0	-1	-2	-3	-4	-4	-5	-6	-7	-8	-4	-5	-5	-5	-5	0	0	0	0	0
4	-1	3	τ_j					3	2	1	0	-1	3	2	1	0	-1	3	2	1	0	-1	3	2	1	0
			w_k	0	0	0	0	-1	-2	-3	-3	-4	-5	-6	-7	-3	-4	-5	-5	-5	0	0	0	0	0	0
4	-2	2	τ_j					2	1	0	-1	-2	2	1	0	-1	-2	2	1	0	-1	-2	2	1	0	-1
			w_k	0	0	0	0	-1	-2	-2	-3	-4	-5	-6	-2	-3	-4	-5	-5	0	0	0	0	0	0	0
4	-3	1	τ_j					1	0	-1	-2	-3	1	0	-1	-2	-3	1	0	-1	-2	-3	1	0	-1	-2
			w_k	0	0	0	0	-1	-1	-2	-3	-4	-5	-1	-2	-3	-4	-5	0	0	0	0	0	0	0	0
4	-4	0	τ_j					0	-1	-2	-3	-4	0	-1	-2	-3	-4	0	-1	-2	-3	-4	0	-1	-2	-3
			w_k	0	0	0	0	0	-1	-2	-3	-4	0	-1	-2	-3	-4	0	0	0	0	0	0	0	0	0

Figure C.29: $\mathcal{P}'_3$, $\bar{\tau} \in \{2, 3, 4\}$ and $T = 10$

$\bar\tau$	min	max	k	−4	−3	−2	−1	0	1	2	3	4	5	6	7	8	9	10	11	12	13	14	15	16	17	18
2	0	2	τ_j					2	1	0	2	1	0	2	1	0	2	1	0	2	1					
			w_k			0	0	−1	−2	−2	−3	−4	−2	−3	−4	−2	−3	−3	0	0	0					
2	−1	1	τ_j					1	0	−1	1	0	−1	1	0	−1	1	0	−1	1	0					
			w_k			0	0	−1	−1	−2	−3	−1	−2	−3	−1	−2	−3	0	0	0	0					
2	−2	0	τ_j					0	−1	−2	0	−1	−2	0	−1	−2	0	−1	−2	0	−1					
			w_k			0	0	0	−1	−2	0	−1	−2	0	−1	−2	0	0	0	0	0					
3	0	3	τ_j					3	2	1	0	3	2	1	0	3	2	1	0	3	2	1	0			
			w_k		0	0	0	−1	−2	−3	−3	−4	−5	−6	−3	−4	−5	−5	−1	−1	−1	−1	0			
3	−1	2	τ_j					2	1	0	−1	2	1	0	−1	2	1	0	−1	2	1	0	−1			
			w_k		0	0	0	−1	−2	−2	−3	−4	−5	−2	−3	−4	−5	−1	−1	−1	−1	0	0			
3	−2	1	τ_j					1	0	−1	−2	1	0	−1	−2	1	0	−1	−2	1	0	−1	−2			
			w_k		0	0	0	−1	−1	−2	−3	−4	−1	−2	−3	−4	−1	−1	−1	−1	0	0	0			
3	−3	0	τ_j					0	−1	−2	−3	0	−1	−2	−3	0	−1	−2	−3	0	−1	−2	−3			
			w_k		0	0	0	0	−1	−2	−3	0	−1	−2	−3	0	−1	−1	−1	0	0	0	0			
4	0	4	τ_j					4	3	2	1	0	4	3	2	1	0	4	3	2	1	0	4	3	2	
			w_k	0	0	0	0	−1	−2	−3	−4	−4	−5	−6	−7	−8	−4	−4	−4	−4	−4	0	0	0	0	
4	−1	3	τ_j					3	2	1	0	−1	3	2	1	0	−1	3	2	1	0	−1	3	2	1	
			w_k	0	0	0	0	−1	−2	−3	−3	−4	−5	−6	−7	−3	−4	−4	−4	−4	0	0	0	0	0	
4	−2	2	τ_j					2	1	0	−1	−2	2	1	0	−1	−2	2	1	0	−1	−2	2	1	0	
			w_k	0	0	0	0	−1	−2	−2	−3	−4	−5	−6	−2	−3	−4	−4	−4	0	0	0	0	0	0	
4	−3	1	τ_j					1	0	−1	−2	−3	1	0	−1	−2	−3	1	0	−1	−2	−3	1	0	−1	
			w_k	0	0	0	0	−1	−1	−2	−3	−4	−5	−1	−2	−3	−4	−4	0	0	0	0	0	0	0	
4	−4	0	τ_j					0	−1	−2	−3	−4	0	−1	−2	−3	−4	0	−1	−2	−3	−4	0	−1	−2	
			w_k	0	0	0	0	0	−1	−2	−3	−4	0	−1	−2	−3	−4	0	0	0	0	0	0	0	0	

Figure C.30: $\mathcal{P}'_3$, $\bar\tau \in \{2, 3, 4\}$ and $T = 9$

$\bar\tau$	min	max	k	−4	−3	−2	−1	0	1	2	3	4	5	6	7	8	9	10	11	12	13	14	15	16	17	18
2	0	2	τ_j					2	1	0	2	1	0	2	1	0	2	1	0	2						
			w_k			0	0	−1	−2	−2	−3	−4	−2	−3	−4	−2	−2	−2	0	0						
2	−1	1	τ_j					1	0	−1	1	0	−1	1	0	−1	1	0	−1	1						
			w_k			0	0	−1	−1	−2	−3	−1	−2	−3	−1	−2	−3	0	0	0						
2	−2	0	τ_j					0	−1	−2	0	−1	−2	0	−1	−2	0	−1	−2	0						
			w_k			0	0	0	−1	−2	0	−1	−2	0	−1	−2	0	0	0	0						
3	0	3	τ_j					3	2	1	0	3	2	1	0	3	2	1	0	3	2	1				
			w_k		0	0	0	−1	−2	−3	−3	−4	−5	−6	−3	−4	−4	−4	0	0	0	0				
3	−1	2	τ_j					2	1	0	−1	2	1	0	−1	2	1	0	−1	2	1	0				
			w_k		0	0	0	−1	−2	−2	−3	−4	−5	−2	−3	−4	−4	0	0	0	0	0				
3	−2	1	τ_j					1	0	−1	−2	1	0	−1	−2	1	0	−1	−2	1	0	−1				
			w_k		0	0	0	−1	−1	−2	−3	−4	−1	−2	−3	−4	0	0	0	0	0	0				
3	−3	0	τ_j					0	−1	−2	−3	0	−1	−2	−3	0	−1	−2	−3	0	−1	−2				
			w_k		0	0	0	0	−1	−2	−3	0	−1	−2	−3	0	0	0	0	0	0	0				
4	0	4	τ_j					4	3	2	1	0	4	3	2	1	0	4	3	2	1	0	4	3		
			w_k	0	0	0	0	−1	−2	−3	−4	−4	−5	−6	−7	−8	−3	−3	−3	−3	−3	0	0	0		
4	−1	3	τ_j					3	2	1	0	−1	3	2	1	0	−1	3	2	1	0	−1	3	2		
			w_k	0	0	0	0	−1	−2	−3	−3	−4	−5	−6	−7	−3	−3	−3	−3	−3	0	0	0	0		
4	−2	2	τ_j					2	1	0	−1	−2	2	1	0	−1	−2	2	1	0	−1	−2	2	1		
			w_k	0	0	0	0	−1	−2	−2	−3	−4	−5	−6	−2	−3	−3	−3	−3	0	0	0	0	0		
4	−3	1	τ_j					1	0	−1	−2	−3	1	0	−1	−2	−3	1	0	−1	−2	−3	1	0		
			w_k	0	0	0	0	−1	−1	−2	−3	−4	−5	−1	−2	−3	−3	−3	0	0	0	0	0	0		
4	−4	0	τ_j					0	−1	−2	−3	−4	0	−1	−2	−3	−4	0	−1	−2	−3	−4	0	−1		
			w_k	0	0	0	0	0	−1	−2	−3	−4	0	−1	−2	−3	−3	0	0	0	0	0	0	0		

Figure C.31: $\mathcal{P}'_3$, $\bar\tau \in \{2, 3, 4\}$ and $T = 8$

$\bar\tau$	min	max	k	−4	−3	−2	−1	0	1	2	3	4	5	6	7	8	9	10	11	12	13	14	15	16	17	18
2	0	2	τ_j					2	1	0	2	1	0	2	1	0	2	1	0							
			w_k			0	0	−1	−2	−2	−3	−4	−2	−3	−4	−1	−1	−1	0							
2	−1	1	τ_j					1	0	−1	1	0	−1	1	0	−1	1	0	−1							
			w_k			0	0	−1	−1	−2	−3	−1	−2	−3	−1	−1	−1	0	0							
2	−2	0	τ_j					0	−1	−2	0	−1	−2	0	−1	−2	0	−1	−2							
			w_k			0	0	0	−1	−2	0	−1	−2	0	−1	−1	0	0	0							
3	0	3	τ_j					3	2	1	0	3	2	1	0	3	2	1	0	3	2					
			w_k		0	0	0	−1	−2	−3	−3	−4	−5	−6	−3	−3	−3	−3	0	0	0					
3	−1	2	τ_j					2	1	0	−1	2	1	0	−1	2	1	0	−1	2	1					
			w_k		0	0	0	−1	−2	−2	−3	−4	−5	−2	−3	−3	−3	0	0	0	0					
3	−2	1	τ_j					1	0	−1	−2	1	0	−1	−2	1	0	−1	−2	1	0					
			w_k		0	0	0	−1	−1	−2	−3	−4	−1	−2	−3	−3	0	0	0	0	0					
3	−3	0	τ_j					0	−1	−2	−3	0	−1	−2	−3	0	−1	−2	−3	0	−1					
			w_k		0	0	0	0	−1	−2	−3	0	−1	−2	−3	0	0	0	0	0	0					
4	0	4	τ_j					4	3	2	1	0	4	3	2	1	0	4	3	2	1	0	4			
			w_k	0	0	0	0	−1	−2	−3	−4	−4	−5	−6	−7	−7	−2	−2	−2	−2	−2	0	0			
4	−1	3	τ_j					3	2	1	0	−1	3	2	1	0	−1	3	2	1	0	−1	3			
			w_k	0	0	0	0	−1	−2	−3	−3	−4	−5	−6	−7	−2	−2	−2	−2	−2	0	0	0			
4	−2	2	τ_j					2	1	0	−1	−2	2	1	0	−1	−2	2	1	0	−1	−2	2			
			w_k	0	0	0	0	−1	−2	−2	−3	−4	−5	−6	−2	−2	−2	−2	−2	0	0	0	0			
4	−3	1	τ_j					1	0	−1	−2	−3	1	0	−1	−2	−3	1	0	−1	−2	−3	1			
			w_k	0	0	0	0	−1	−1	−2	−3	−4	−5	−1	−2	−2	−2	−2	0	0	0	0	0			
4	−4	0	τ_j					0	−1	−2	−3	−4	0	−1	−2	−3	−4	0	−1	−2	−3	−4	0			
			w_k	0	0	0	0	0	−1	−2	−3	−4	0	−1	−2	−2	−2	0	0	0	0	0	0			

Figure C.32: $\mathcal{P}'_3$, $\bar\tau \in \{2, 3, 4\}$ and $T = 7$

$\bar{\tau}$	min	max	k	−4	−3	−2	−1	0	1	2	3	4	5	6	7	8	9	10	11	12	13	14	15	16	17	18
2	0	2	τ_j					2	1	0	2	1	0	2	1	0	2	1								
			w_k			0	0	−1	−2	−2	−3	−4	−2	−3	−3	0	0	0								
2	−1	1	τ_j					1	0	−1	1	0	−1	1	0	−1	1	0								
			w_k			0	0	−1	−1	−2	−3	−1	−2	−3	0	0	0	0								
2	−2	0	τ_j					0	−1	−2	0	−1	−2	0	−1	−2	0	−1								
			w_k			0	0	0	−1	−2	0	−1	−2	0	0	0	0	0								
3	0	3	τ_j					3	2	1	0	3	2	1	0	3	2	1	0	3						
			w_k		0	0	0	−1	−2	−3	−3	−4	−5	−6	−2	−2	−2	−2	0	0						
3	−1	2	τ_j					2	1	0	−1	2	1	0	−1	2	1	0	−1	2						
			w_k		0	0	0	−1	−2	−2	−3	−4	−5	−2	−2	−2	−2	0	0	0						
3	−2	1	τ_j					1	0	−1	−2	1	0	−1	−2	1	0	−1	−2	1						
			w_k		0	0	0	−1	−1	−2	−3	−4	−1	−2	−2	−2	0	0	0	0						
3	−3	0	τ_j					0	−1	−2	−3	0	−1	−2	−3	0	−1	−2	−3	0						
			w_k		0	0	0	0	−1	−2	−3	0	−1	−2	−2	0	0	0	0	0						
4	0	4	τ_j					4	3	2	1	0	4	3	2	1	0	4	3	2	1	0				
			w_k	0	0	0	0	−1	−2	−3	−4	−4	−5	−6	−6	−6	−1	−1	−1	−1	−1	0				
4	−1	3	τ_j					3	2	1	0	−1	3	2	1	0	−1	3	2	1	0	−1				
			w_k	0	0	0	0	−1	−2	−3	−3	−4	−5	−6	−6	−1	−1	−1	−1	−1	0	0				
4	−2	2	τ_j					2	1	0	−1	−2	2	1	0	−1	−2	2	1	0	−1	−2				
			w_k	0	0	0	0	−1	−2	−2	−3	−4	−5	−6	−1	−1	−1	−1	−1	0	0	0				
4	−3	1	τ_j					1	0	−1	−2	−3	1	0	−1	−2	−3	1	0	−1	−2	−3				
			w_k	0	0	0	0	−1	−1	−2	−3	−4	−5	−1	−1	−1	−1	−1	0	0	0	0				
4	−4	0	τ_j					0	−1	−2	−3	−4	0	−1	−2	−3	−4	0	−1	−2	−3	−4				
			w_k	0	0	0	0	0	−1	−2	−3	−4	0	−1	−1	−1	−1	0	0	0	0	0				

Figure C.33: $\mathcal{P}'_3$, $\bar{\tau} \in \{2,3,4\}$ and, $T = 6$

$\bar{\tau}$	min	max	k	−4	−3	−2	−1	0	1	2	3	4	5	6	7	8	9	10	11	12	13	14	15	16	17	18
2	0	2	τ_j					2	1	0	2	1	0	2	1	0	2									
			w_k			0	0	−1	−2	−2	−3	−4	−2	−2	−2	0	0									
2	−1	1	τ_j					1	0	−1	1	0	−1	1	0	−1	1									
			w_k			0	0	−1	−1	−2	−3	−1	−2	−2	0	0	0									
2	−2	0	τ_j					0	−1	−2	0	−1	−2	0	−1	−2	0									
			w_k			0	0	0	−1	−2	0	−1	−2	0	0	0	0									
3	0	3	τ_j					3	2	1	0	3	2	1	0	3	2	1	0							
			w_k		0	0	0	−1	−2	−3	−3	−4	−5	−5	−1	−1	−1	−1	0							
3	−1	2	τ_j					2	1	0	−1	2	1	0	−1	2	1	0	−1							
			w_k		0	0	0	−1	−2	−2	−3	−4	−5	−1	−1	−1	−1	0	0							
3	−2	1	τ_j					1	0	−1	−2	1	0	−1	−2	1	0	−1	−2							
			w_k		0	0	0	−1	−1	−2	−3	−4	−1	−1	−1	−1	0	0	0							
3	−3	0	τ_j					0	−1	−2	−3	0	−1	−2	−3	0	−1	−2	−3							
			w_k		0	0	0	0	−1	−2	−3	0	−1	−1	−1	0	0	0	0							
4	0	4	τ_j					4	3	2	1	0	4	3	2	1	0	4	3	2	1					
			w_k	0	0	0	0	−1	−2	−3	−4	−4	−5	−5	−5	−5	0	0	0	0	0					
4	−1	3	τ_j					3	2	1	0	−1	3	2	1	0	−1	3	2	1	0					
			w_k	0	0	0	0	−1	−2	−3	−3	−4	−5	−5	−5	0	0	0	0	0	0					
4	−2	2	τ_j					2	1	0	−1	−2	2	1	0	−1	−2	2	1	0	−1					
			w_k	0	0	0	0	−1	−2	−2	−3	−4	−5	−5	0	0	0	0	0	0	0					
4	−3	1	τ_j					1	0	−1	−2	−3	1	0	−1	−2	−3	1	0	−1	−2					
			w_k	0	0	0	0	−1	−1	−2	−3	−4	−5	0	0	0	0	0	0	0	0					
4	−4	0	τ_j					0	−1	−2	−3	−4	0	−1	−2	−3	−4	0	−1	−2	−3					
			w_k	0	0	0	0	0	−1	−2	−3	−4	0	0	0	0	0	0	0	0	0					

Figure C.34: $\mathcal{P}'_3$, $\bar{\tau} \in \{2,3,4\}$ and $T = 5$

$\bar{\tau}$	min	max	k	−4	−3	−2	−1	0	1	2	3	4	5	6	7	8	9	10	11	12	13	14	15	16	17	18
2	0	2	τ_j					2	1	0	2	1	0	2	1	0										
			w_k			0	0	−1	−2	−2	−3	−4	−1	−1	−1	0										
2	−1	1	τ_j					1	0	−1	1	0	−1	1	0	−1										
			w_k			0	0	−1	−1	−2	−3	−1	−1	−1	0	0										
2	−2	0	τ_j					0	−1	−2	0	−1	−2	0	−1	−2										
			w_k			0	0	0	−1	−2	0	−1	−1	0	0	0										
3	0	3	τ_j					3	2	1	0	3	2	1	0	3	2	1								
			w_k		0	0	0	−1	−2	−3	−3	−4	−4	−4	0	0	0	0								
3	−1	2	τ_j					2	1	0	−1	2	1	0	−1	2	1	0								
			w_k		0	0	0	−1	−2	−2	−3	−4	−4	0	0	0	0	0								
3	−2	1	τ_j					1	0	−1	−2	1	0	−1	−2	1	0	−1								
			w_k		0	0	0	−1	−1	−2	−3	−4	0	0	0	0	0	0								
3	−3	0	τ_j					0	−1	−2	−3	0	−1	−2	−3	0	−1	−2								
			w_k		0	0	0	0	−1	−2	−3	0	0	0	0	0	0	0								
4	0	4	τ_j					4	3	2	1	0	4	3	2	1	0	4	3	2						
			w_k	0	0	0	0	−1	−2	−3	−4	−4	−4	−4	−4	−4	0	0	0	0						
4	−1	3	τ_j					3	2	1	0	−1	3	2	1	0	−1	3	2	1						
			w_k	0	0	0	0	−1	−2	−3	−3	−4	−4	−4	−4	0	0	0	0	0						
4	−2	2	τ_j					2	1	0	−1	−2	2	1	0	−1	−2	2	1	0						
			w_k	0	0	0	0	−1	−2	−2	−3	−4	−4	−4	0	0	0	0	0	0						
4	−3	1	τ_j					1	0	−1	−2	−3	1	0	−1	−2	−3	1	0	−1						
			w_k	0	0	0	0	−1	−1	−2	−3	−4	−4	0	0	0	0	0	0	0						
4	−4	0	τ_j					0	−1	−2	−3	−4	0	−1	−2	−3	−4	0	−1	−2						
			w_k	0	0	0	0	0	−1	−2	−3	−4	0	0	0	0	0	0	0	0						

Figure C.35: $\mathcal{P}'_3$, $\bar{\tau} \in \{2,3,4\}$ and $T = 4$

$\bar{\tau}$	min	max	k	−4	−3	−2	−1	0	1	2	3	4	5	6	7	8	9	10	11	12	13	14	15	16	17	18
2	0	2	τ_j					2	1	0	2	1	0	2	1											
			w_k			0	0	−1	−2	−2	−3	−3	0	0	0											
2	−1	1	τ_j					1	0	−1	1	0	−1	1	0											
			w_k			0	0	−1	−1	−2	−3	0	0	0	0											
2	−2	0	τ_j					0	−1	−2	0	−1	−2	0	−1											
			w_k			0	0	0	−1	−2	0	0	0	0	0											
3	0	3	τ_j					3	2	1	0	3	2	1	0	3	2									
			w_k		0	0	0	−1	−2	−3	−3	−3	−3	−3	0	0	0									
3	−1	2	τ_j					2	1	0	−1	2	1	0	−1	2	1									
			w_k		0	0	0	−1	−2	−2	−3	−3	−3	0	0	0	0									
3	−2	1	τ_j					1	0	−1	−2	1	0	−1	−2	1	0									
			w_k		0	0	0	−1	−1	−2	−3	−3	0	0	0	0	0									
3	−3	0	τ_j					0	−1	−2	−3	0	−1	−2	−3	0	−1									
			w_k		0	0	0	0	−1	−2	−3	0	0	0	0	0	0									
4	0	4	τ_j					4	3	2	1	0	4	3	2	1	0	4	3							
			w_k	0	0	0	0	−1	−2	−3	−4	−3	−3	−3	−3	−3	0	0	0							
4	−1	3	τ_j					3	2	1	0	−1	3	2	1	0	−1	3	2							
			w_k	0	0	0	0	−1	−2	−3	−3	−3	−3	−3	−3	0	0	0	0							
4	−2	2	τ_j					2	1	0	−1	−2	2	1	0	−1	−2	2	1							
			w_k	0	0	0	0	−1	−2	−2	−3	−3	−3	−3	0	0	0	0	0							
4	−3	1	τ_j					1	0	−1	−2	−3	1	0	−1	−2	−3	1	0							
			w_k	0	0	0	0	−1	−1	−2	−3	−3	−3	0	0	0	0	0	0							
4	−4	0	τ_j					0	−1	−2	−3	−4	0	−1	−2	−3	−4	0	−1							
			w_k	0	0	0	0	0	−1	−2	−3	−3	0	0	0	0	0	0	0							

Figure C.36: $\mathcal{P}'_3$, $\bar{\tau} \in \{2, 3, 4\}$ and $T = 3$

$\bar{\tau}$	min	max	k	−4	−3	−2	−1	0	1	2	3	4	5	6	7	8	9	10	11	12	13	14	15	16	17	18
2	0	2	τ_j					2	1	0	2	1	0	2												
			w_k			0	0	−1	−2	−2	−2	−2	0	0												
2	−1	1	τ_j					1	0	−1	1	0	−1	1												
			w_k			0	0	−1	−1	−2	−2	0	0	0												
2	−2	0	τ_j					0	−1	−2	0	−1	−2	0												
			w_k			0	0	0	−1	−2	0	0	0	0												
3	0	3	τ_j					3	2	1	0	3	2	1	0	3										
			w_k		0	0	0	−1	−2	−3	−2	−2	−2	−2	0	0										
3	−1	2	τ_j					2	1	0	−1	2	1	0	−1	2										
			w_k		0	0	0	−1	−2	−2	−2	−2	−2	0	0	0										
3	−2	1	τ_j					1	0	−1	−2	1	0	−1	−2	1										
			w_k		0	0	0	−1	−1	−2	−2	−2	0	0	0	0										
3	−3	0	τ_j					0	−1	−2	−3	0	−1	−2	−3	0										
			w_k		0	0	0	0	−1	−2	−2	0	0	0	0	0										
4	0	4	τ_j					4	3	2	1	0	4	3	2	1	0	4								
			w_k	0	0	0	0	−1	−2	−3	−3	−2	−2	−2	−2	−2	0	0								
4	−1	3	τ_j					3	2	1	0	−1	3	2	1	0	−1	3								
			w_k	0	0	0	0	−1	−2	−3	−2	−2	−2	−2	−2	0	0	0								
4	−2	2	τ_j					2	1	0	−1	−2	2	1	0	−1	−2	2								
			w_k	0	0	0	0	−1	−2	−2	−2	−2	−2	−2	0	0	0	0								
4	−3	1	τ_j					1	0	−1	−2	−3	1	0	−1	−2	−3	1								
			w_k	0	0	0	0	−1	−1	−2	−2	−2	−2	0	0	0	0	0								
4	−4	0	τ_j					0	−1	−2	−3	−4	0	−1	−2	−3	−4	0								
			w_k	0	0	0	0	0	−1	−2	−2	−2	0	0	0	0	0	0								

Figure C.37: $\mathcal{P}'_3$, $\bar{\tau} \in \{2, 3, 4\}$ and $T = 2$

$\bar{\tau}$	min	max	k	−4	−3	−2	−1	0	1	2	3	4	5	6	7	8	9	10	11	12	13	14	15	16	17	18
2	0	2	τ_j					2	1	0	2	1	0													
			w_k			0	0	−1	−2	−1	−1	−1	0													
2	−1	1	τ_j					1	0	−1	1	0	−1													
			w_k			0	0	−1	−1	−1	−1	0	0													
2	−2	0	τ_j					0	−1	−2	0	−1	−2													
			w_k			0	0	0	0	0	0	0	0													
3	0	3	τ_j					3	2	1	0	3	2	1	0											
			w_k		0	0	0	−1	−2	−2	−1	−1	−1	−1	0											
3	−1	2	τ_j					2	1	0	−1	2	1	0	−1											
			w_k		0	0	0	−1	−2	−1	−1	−1	−1	0	0											
3	−2	1	τ_j					1	0	−1	−2	1	0	−1	−2											
			w_k		0	0	0	−1	−1	−1	−1	−1	0	0	0											
3	−3	0	τ_j					0	−1	−2	−3	0	−1	−2	−3											
			w_k		0	0	0	0	−1	−1	−1	0	0	0	0											
4	0	4	τ_j					4	3	2	1	0	4	3	2	1	0									
			w_k	0	0	0	0	−1	−2	−2	−2	−1	−1	−1	−1	−1	0									
4	−1	3	τ_j					3	2	1	0	−1	3	2	1	0	−1									
			w_k	0	0	0	0	−1	−2	−2	−1	−1	−1	−1	−1	0	0									
4	−2	2	τ_j					2	1	0	−1	−2	2	1	0	−1	−2									
			w_k	0	0	0	0	−1	−2	−1	−1	−1	−1	−1	0	0	0									
4	−3	1	τ_j					1	0	−1	−2	−3	1	0	−1	−2	−3									
			w_k	0	0	0	0	−1	−1	−1	−1	−1	−1	0	0	0	0									
4	−4	0	τ_j					0	−1	−2	−3	−4	0	−1	−2	−3	−4									
			w_k	0	0	0	0	0	−1	−1	−1	−1	0	0	0	0	0									

Figure C.38: $\mathcal{P}'_3$, $\bar{\tau} \in \{2, 3, 4\}$ and $T = 1$

C.5 Gains for $\mathcal{P}_3'$

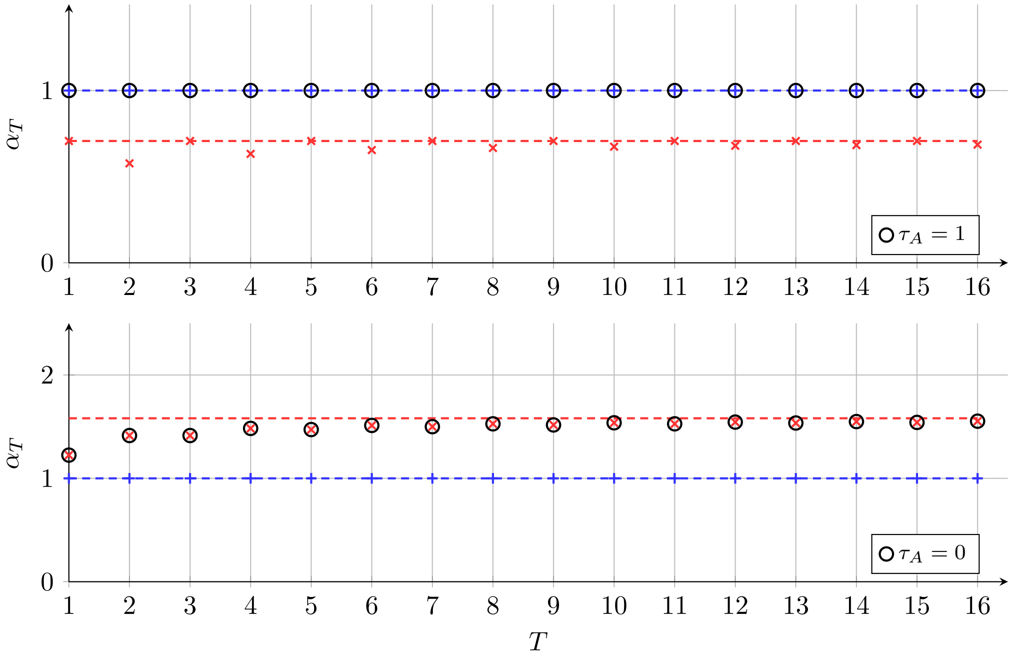

Figure C.39: $\mathcal{P}_3$, $\bar{\tau} = 1$: $\mathcal{P}_1$ (blue), $\mathcal{P}_3'$ (red)

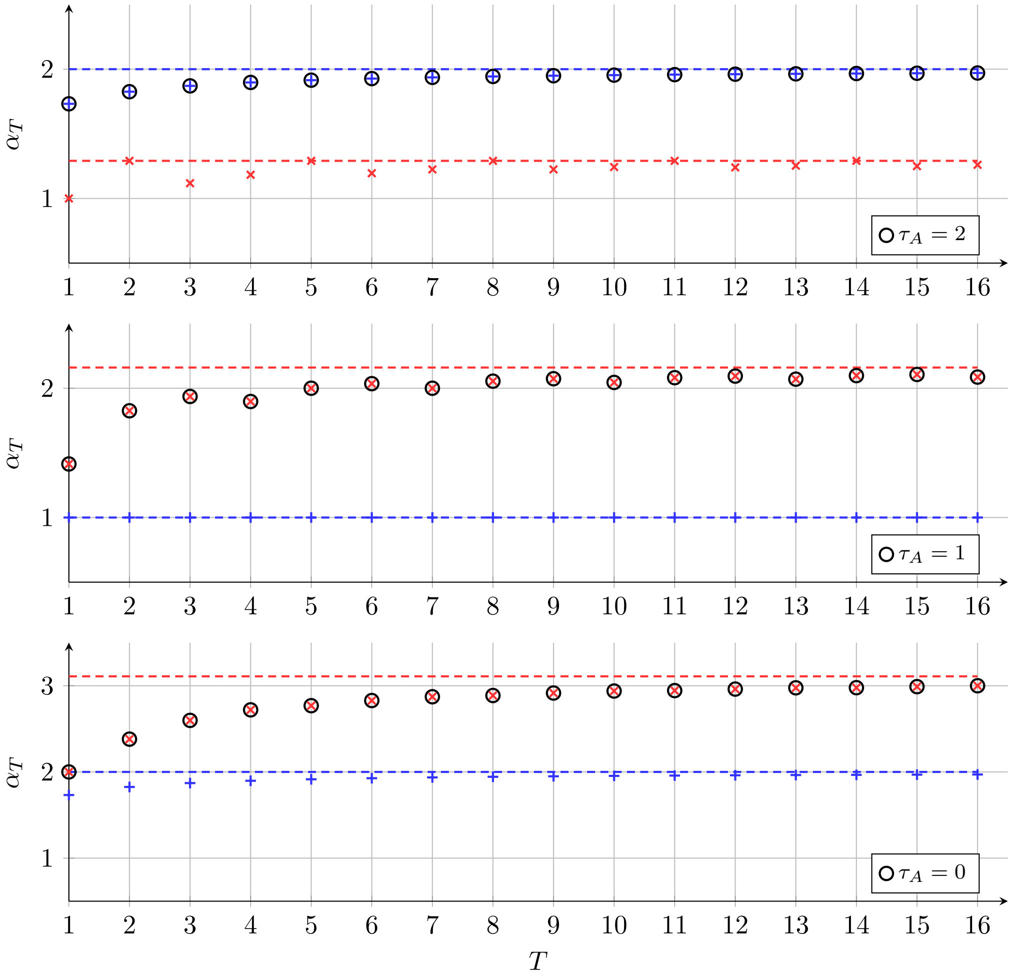

Figure C.40: $\mathcal{P}_3$, $\bar{\tau} = 2$: $\mathcal{P}_1$ (blue), $\mathcal{P}_3'$ (red)

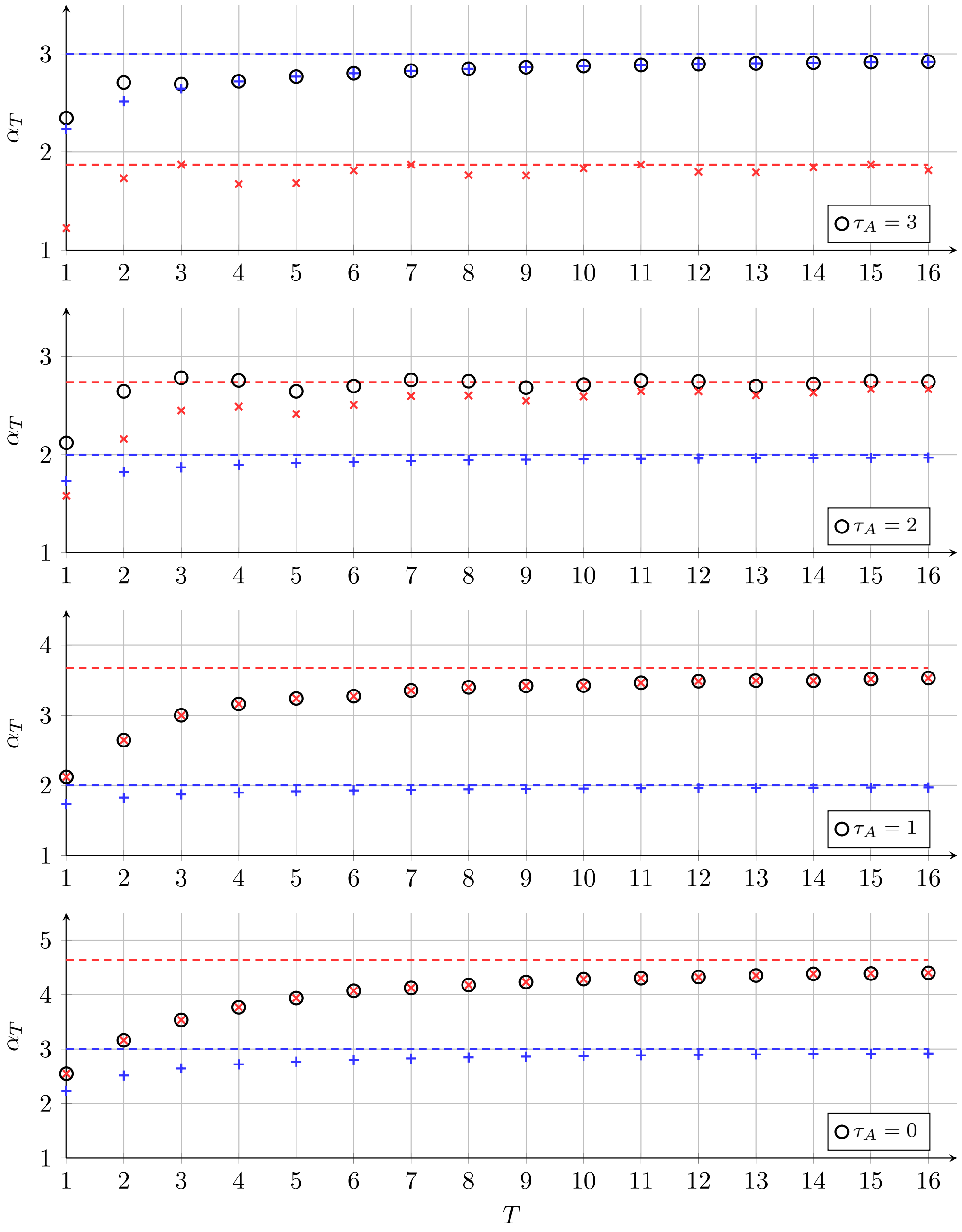

Figure C.41: $\mathcal{P}_3$, $\bar{\tau} = 3$: $\mathcal{P}_1$ (blue), $\mathcal{P}_3'$ (red)

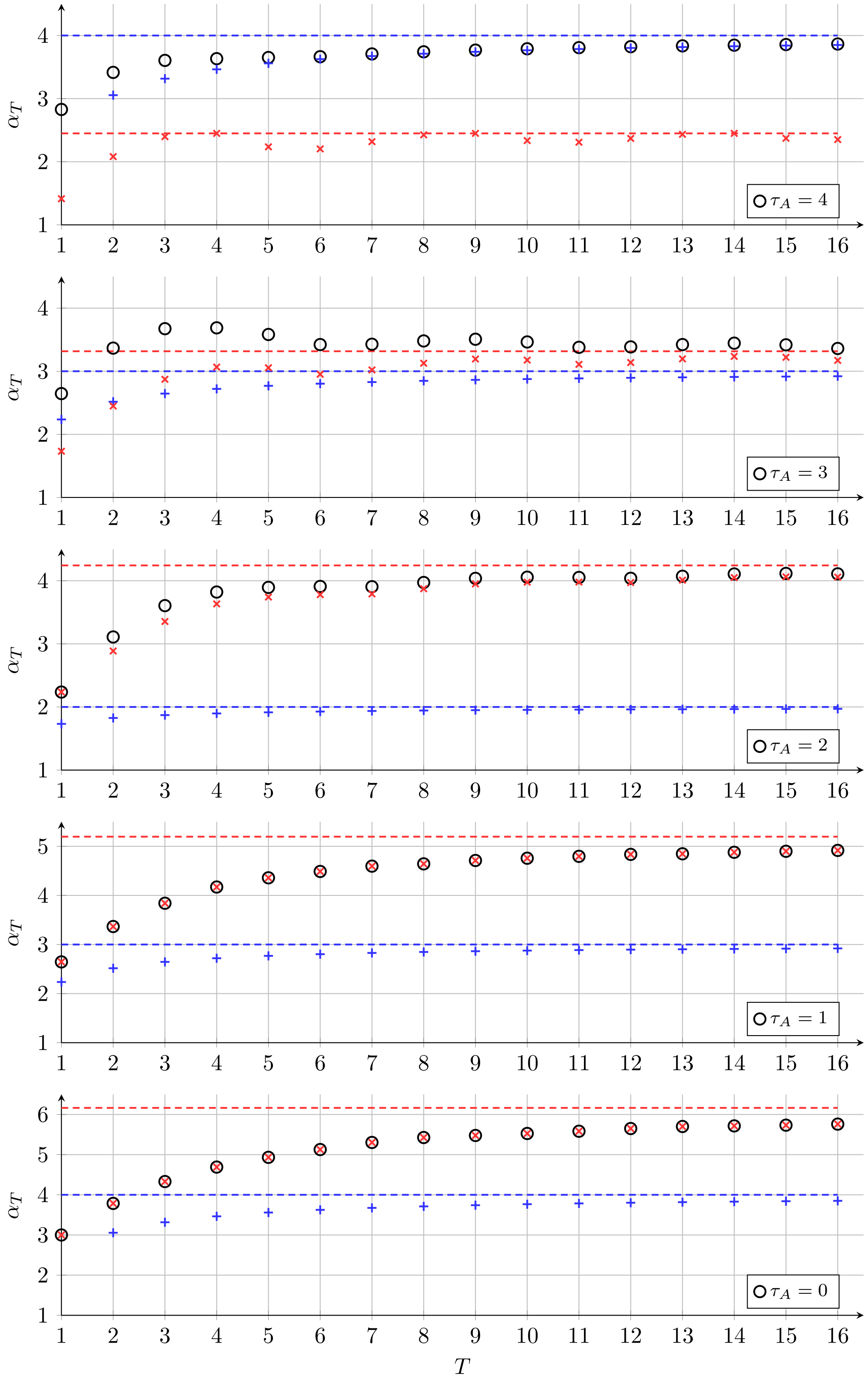

Figure C.42: $\mathcal{P}_3$, $\bar{\tau} = 4$: $\mathcal{P}_1$ (blue), $\mathcal{P}_3'$ (red)

C.6 Patterns for $\mathcal{P}_3''$

k	−3	−2	−1	0	1	2	3	4	5	6	7	8	9	10	11	12	13	14	15	16
$b_k^{(0)} = a_k$	0	0	0	1	2	3	4	5	6	7	8	9	10	11	11	11	11	11	11	11
$b_k^{(1)}$	0	0	0	0	1	2	3	4	5	6	7	8	9	10	11	11	11	11	11	11
$b_k^{(2)}$	0	0	0	0	0	1	2	3	4	5	6	7	8	9	10	11	11	11	11	11
$b_k^{(3)}$	0	0	0	0	0	0	1	2	3	4	5	6	7	8	9	10	11	11	11	11
$b_k^{(0)} = a_k$	0	0	0	~~1~~	2	3	4	~~5~~	~~6~~	~~7~~	8	~~9~~	~~10~~	~~11~~	11	~~11~~	~~11~~	~~11~~	11	~~11~~
$b_k^{(1)}k$	0	0	0	0	~~1~~	~~2~~	~~3~~	~~4~~	~~5~~	~~6~~	7	~~8~~	~~9~~	~~10~~	11	~~11~~	~~11~~	~~11~~	11	~~11~~
$b_k^{(2)}$	0	0	0	0	0	~~1~~	~~2~~	~~3~~	~~4~~	~~5~~	6	~~7~~	~~8~~	~~9~~	10	~~11~~	~~11~~	~~11~~	11	~~11~~
$b_k^{(3)}$	0	0	0	0	0	0	1	~~2~~	~~3~~	~~4~~	5	~~6~~	~~7~~	~~8~~	9	~~10~~	~~11~~	~~11~~	11	~~11~~
$b_k^{(0)} - a_k$	0	0	0	0	0	0	0	0	0	0	0	0	0	0	0	0	0	0	0	0
$b_k^{(1)} - a_k$	0	0	0	−1	−1	−1	−1	−1	−1	−1	−1	−1	−1	−1	0	0	0	0	0	0
$b_k^{(2)} - a_k$	0	0	0	−1	−2	−2	−2	−2	−2	−2	−2	−2	−2	−2	−1	0	0	0	0	0
$b_k^{(3)} - a_k$	0	0	0	−1	−2	−3	−3	−3	−3	−3	−3	−3	−3	−3	−2	−1	0	0	0	0
packet arr.	no	no	no	no	yes	yes	yes	no	no	no	yes	no	no	no	yes	no	no	no	yes	no
c_k	0	0	0	0	2	3	1	1	1	1	5	5	5	5	9	9	9	9	11	11
w_k block	0	0	0	−1 A$^+$	0 A$^+$	0 A$^+$	−3 B	−4 B	−5 B	−6 B	−3 B	−4 B	−5 B	−6 B	−2 C	−2 C	−2 C	−2 C	0 D	0 D
τ_j				3	0	0	0	3	2	1	0	3	2	1	0	3	2	1	0	3

Figure C.43: $\mathcal{P}_3''$, $\bar{\tau} = 3$, $T = 10$ and $\tau_A = 0$

k	−3	−2	−1	0	1	2	3	4	5	6	7	8	9	10	11	12	13	14	15	16
$b_k^{(-1)}$	0	0	1	2	3	4	5	6	7	8	9	10	11	11	11	11	11	11	11	11
$b_k^{(0)} = a_k$	0	0	0	1	2	3	4	5	6	7	8	9	10	11	11	11	11	11	11	11
$b_k^{(1)}$	0	0	0	0	1	2	3	4	5	6	7	8	9	10	11	11	11	11	11	11
$b_k^{(2)}$	0	0	0	0	0	1	2	3	4	5	6	7	8	9	10	11	11	11	11	11
$b_k^{(-1)}$	0	0	~~1~~	2	3	4	~~5~~	~~6~~	~~7~~	8	~~9~~	~~10~~	~~11~~	11	~~11~~	~~11~~	~~11~~	11	~~11~~	~~11~~
$b_k^{(0)} = a_k$	0	0	0	~~1~~	~~2~~	~~3~~	~~4~~	~~5~~	~~6~~	7	~~8~~	~~9~~	~~10~~	11	~~11~~	~~11~~	~~11~~	11	~~11~~	~~11~~
$b_k^{(1)}$	0	0	0	0	~~1~~	~~2~~	~~3~~	~~4~~	~~5~~	6	~~7~~	~~8~~	~~9~~	10	~~11~~	~~11~~	~~11~~	11	~~11~~	~~11~~
$b_k^{(2)}$	0	0	0	0	0	1	~~2~~	~~3~~	~~4~~	5	~~6~~	~~7~~	~~8~~	9	~~10~~	~~11~~	~~11~~	11	~~11~~	~~11~~
$b_k^{(-1)} - a_k$	0	0	1	1	1	1	1	1	1	1	1	1	1	0	0	0	0	0	0	0
$b_k^{(0)} - a_k$	0	0	0	0	0	0	0	0	0	0	0	0	0	0	0	0	0	0	0	0
$b_k^{(1)} - a_k$	0	0	0	−1	−1	−1	−1	−1	−1	−1	−1	−1	−1	−1	0	0	0	0	0	0
$b_k^{(2)} - a_k$	0	0	0	−1	−2	−2	−2	−2	−2	−2	−2	−2	−2	−2	−1	0	0	0	0	0
packet arr.	no	no	no	yes	yes	yes	no	no	no	yes	no	no	no	yes	no	no	no	yes	no	no
c_k	0	0	0	2	3	1	1	1	1	5	5	5	5	9	9	9	9	11	11	11
w_k block	0	0	0	1 A$^+$	1 A$^+$	−2 B	−3 B	−4 B	−5 B	−2 B	−3 B	−4 B	−5 B	−2 C	−2 C	−2 C	−2 C	0 D	0 D	0 D
τ_j				2	−1	−1	−1	2	1	0	−1	2	1	0	−1	2	1	0	−1	2

Figure C.44: $\mathcal{P}_3''$, $\bar{\tau} = 3$, $T = 10$ and $\tau_A = 1$

k	-3	-2	-1	0	1	2	3	4	5	6	7	8	9	10	11	12	13	14	15	16
$b_k^{(-2)}$	0	1	2	3	4	5	6	7	8	9	10	11	11	11	11	11	11	11	11	11
$b_k^{(1)}$	0	0	1	2	3	4	5	6	7	8	9	10	11	11	11	11	11	11	11	11
$b_k^{(0)} = a_k$	0	0	0	1	2	3	4	5	6	7	8	9	10	11	11	11	11	11	11	11
$b_k^{(1)}$	0	0	0	0	1	2	3	4	5	6	7	8	9	10	11	11	11	11	11	11
$b_k^{(-2)}$	0	$\cancel{1}$	2	3	4	$\cancel{5}$	$\cancel{6}$	$\cancel{7}$	8	$\cancel{9}$	$\cancel{10}$	$\cancel{11}$	11	$\cancel{11}$	$\cancel{11}$	$\cancel{11}$	11	$\cancel{11}$	$\cancel{11}$	$\cancel{11}$
$b_k^{(-1)}$	0	0	$\cancel{1}$	$\cancel{2}$	$\cancel{3}$	$\cancel{4}$	$\cancel{5}$	$\cancel{6}$	7	$\cancel{8}$	$\cancel{9}$	$\cancel{10}$	11	$\cancel{11}$	$\cancel{11}$	$\cancel{11}$	11	$\cancel{11}$	$\cancel{11}$	$\cancel{11}$
$b_k^{(0)} = a_k$	0	0	0	$\cancel{1}$	$\cancel{2}$	$\cancel{3}$	$\cancel{4}$	$\cancel{5}$	6	$\cancel{7}$	$\cancel{8}$	$\cancel{9}$	10	$\cancel{11}$	$\cancel{11}$	$\cancel{11}$	11	$\cancel{11}$	$\cancel{11}$	$\cancel{11}$
$b_k^{(1)}$	0	0	0	0	1	$\cancel{2}$	$\cancel{3}$	$\cancel{4}$	5	$\cancel{6}$	$\cancel{7}$	$\cancel{8}$	9	$\cancel{10}$	$\cancel{11}$	$\cancel{11}$	11	$\cancel{11}$	$\cancel{11}$	$\cancel{11}$
$b_k^{(-2)} - a_k$	0	1	2	2	2	2	2	2	2	2	2	2	1	0	0	0	0	0	0	0
$b_k^{(-1)} - a_k$	0	0	1	1	1	1	1	1	1	1	1	1	1	0	0	0	0	0	0	0
$b_k^{(0)} - a_k$	0	0	0	0	0	0	0	0	0	0	0	0	0	0	0	0	0	0	0	0
$b_k^{(1)} - a_k$	0	0	0	-1	-1	-1	-1	-1	-1	-1	-1	-1	-1	-1	0	0	0	0	0	0
packet arr.	no	no	yes	yes	yes	no	no	no	yes	no	no	no	yes	no	no	no	yes	no	no	no
c_k	0	0	2	3	1	1	1	1	5	5	5	5	9	9	9	9	11	11	11	11
w_k	0	0	2	2	-1	-2	-3	-4	-1	-2	-3	-4	-1	-2	-2	-2	0	0	0	0
block			A$^-$	A$^+$	B	B	B	B	B	B	B	B	C	C	C	C	C	C	C	C
τ_j				1	-2	-2	-2	1	0	-1	-2	1	0	-1	-2	1	0	-1	-2	1

Figure C.45: $\mathcal{P}_3''$, $\bar{\tau} = 3$, $T = 10$ and $\tau_A = 2$

k	-3	-2	-1	0	1	2	3	4	5	6	7	8	9	10	11	12	13	14	15	16
$b_k^{(-3)}$	1	2	3	4	5	6	7	8	9	10	11	11	11	11	11	11	11	11	11	11
$b_k^{(-2)}$	0	1	2	3	4	5	6	7	8	9	10	11	11	11	11	11	11	11	11	11
$b_k^{(-1)}$	0	0	1	2	3	4	5	6	7	8	9	10	11	11	11	11	11	11	11	11
$b_k^{(0)} = a_k$	0	0	0	1	2	3	4	5	6	7	8	9	10	11	11	11	11	11	11	11
$b_k^{(-3)}$	$\cancel{1}$	2	3	4	$\cancel{5}$	$\cancel{6}$	$\cancel{7}$	8	$\cancel{9}$	$\cancel{10}$	$\cancel{11}$	11	$\cancel{11}$	$\cancel{11}$	$\cancel{11}$	11	$\cancel{11}$	$\cancel{11}$	$\cancel{11}$	11
$b_k^{(-2)}$	0	$\cancel{1}$	$\cancel{2}$	$\cancel{3}$	$\cancel{4}$	$\cancel{5}$	$\cancel{6}$	7	$\cancel{8}$	$\cancel{9}$	$\cancel{10}$	11	$\cancel{11}$	$\cancel{11}$	$\cancel{11}$	11	$\cancel{11}$	$\cancel{11}$	$\cancel{11}$	11
$b_k^{(-1)}$	0	0	$\cancel{1}$	$\cancel{2}$	$\cancel{3}$	$\cancel{4}$	$\cancel{5}$	6	$\cancel{7}$	$\cancel{8}$	$\cancel{9}$	10	$\cancel{11}$	$\cancel{11}$	$\cancel{11}$	11	$\cancel{11}$	$\cancel{11}$	$\cancel{11}$	11
$b_k^{(0)} = a_k$	0	0	0	1	$\cancel{2}$	$\cancel{3}$	$\cancel{4}$	5	$\cancel{6}$	$\cancel{7}$	$\cancel{8}$	9	$\cancel{10}$	$\cancel{11}$	$\cancel{11}$	11	$\cancel{11}$	$\cancel{11}$	$\cancel{11}$	11
$b_k^{(-3)} - a_k$	1	2	3	3	3	3	3	3	3	3	3	2	1	0	0	0	0	0	0	0
$b_k^{(-2)} - a_k$	0	1	2	2	2	2	2	2	2	2	2	2	1	0	0	0	0	0	0	0
$b_k^{(-1)} - a_k$	0	0	1	1	1	1	1	1	1	1	1	1	1	0	0	0	0	0	0	0
$b_k^{(0)} - a_k$	0	0	0	0	0	0	0	0	0	0	0	0	0	0	0	0	0	0	0	0
packet arr.	no	yes	yes	yes	no	no	no	yes	no	no	no	yes	no	no	no	yes	no	no	no	yes
c_k	0	2	3	1	1	1	1	5	5	5	5	9	9	9	9	11	11	11	11	11
w_k	0	2	3	0	-1	-2	-3	0	-1	-2	-3	0	-1	-2	-2	0	0	0	0	0
block	0	A$^-$	A$^-$	B	B	B	B	B	B	B	B	C	C	C	C	C	C	C	C	D
τ_j				0	-3	-3	-3	0	-1	-2	-3	0	-1	-2	-3	0	-1	-2	-3	0

Figure C.46: $\mathcal{P}_3''$, $\bar{\tau} = 3$, $T = 10$ and $\tau_A = 3$

$\bar{\tau}$	min	max	k	-4	-3	-2	-1	0	1	2	3	4	5	6	7	8	9	10	11	12	13	14	15	16	17	18
2	0	2	τ_j					2	0	0	2	1	0	2	1	0	2	1	0	2	1	0				
			w_k			0	0	-1	0	-2	-3	-4	-2	-3	-4	-2	-3	-4	-1	-1	-1	0				
2	-1	1	τ_j					1	-1	-1	1	0	-1	1	0	-1	1	0	-1	1	0	-1				
			w_k			0	0	1	-1	-2	-3	-1	-2	-3	-1	-2	-3	-1	-1	-1	0	0				
2	-2	0	τ_j					0	-2	-2	0	-1	-2	0	-1	-2	0	-1	-2	0	-1	-2				
			w_k			0	2	0	-1	-2	0	-1	-2	0	-1	-2	0	-1	-1	0	0	0				
3	0	3	τ_j					3	0	0	0	3	2	1	0	3	2	1	0	3	2	1	0	3		
			w_k		0	0	0	-1	0	0	-3	-4	-5	-6	-3	-4	-5	-6	-2	-2	-2	-2	0	0		
3	-1	2	τ_j					2	-1	-1	-1	2	1	0	-1	2	1	0	-1	2	1	0	-1	2		
			w_k		0	0	0	1	1	-2	-3	-4	-5	-2	-3	-4	-5	-2	-2	-2	-2	0	0	0		
3	-2	1	τ_j					1	-2	-2	-2	1	0	-1	-2	1	0	-1	-2	1	0	-1	-2	1		
			w_k		0	0	2	2	-1	-2	-3	-4	-1	-2	-3	-4	-1	-2	-2	-2	0	0	0	0		
3	-3	0	τ_j					0	-3	-3	-3	0	-1	-2	-3	0	-1	-2	-3	0	-1	-2	-3	0		
			w_k		0	2	3	0	-1	-2	-3	0	-1	-2	-3	0	-1	-2	-2	0	0	0	0	0		
4	0	4	τ_j					4	0	0	0	0	4	3	2	1	0	4	3	2	1	0	4	3	2	1
			w_k	0	0	0	0	-1	0	0	0	-4	-5	-6	-7	-8	-4	-5	-5	-5	-5	0	0	0	0	0
4	-1	3	τ_j					3	-1	-1	-1	-1	3	2	1	0	-1	3	2	1	0	-1	3	2	1	0
			w_k	0	0	0	0	1	1	1	-3	-4	-5	-6	-7	-3	-4	-5	-5	-5	0	0	0	0	0	0
4	-2	2	τ_j					2	-2	-2	-2	-2	2	1	0	-1	-2	2	1	0	-1	-2	2	1	0	-1
			w_k	0	0	0	2	2	2	-2	-3	-4	-5	-6	-2	-3	-4	-5	-5	0	0	0	0	0	0	0
4	-3	1	τ_j					1	-3	-3	-3	-3	1	0	-1	-2	-3	1	0	-1	-2	-3	1	0	-1	-2
			w_k	0	0	2	3	3	-1	-2	-3	-4	-5	-1	-2	-3	-4	-5	0	0	0	0	0	0	0	0
4	-4	0	τ_j					0	-4	-4	-4	-4	0	-1	-2	-3	-4	0	-1	-2	-3	-4	0	-1	-2	-3
			w_k	0	2	3	4	0	-1	-2	-3	-4	0	-1	-2	-3	-4	0	0	0	0	0	0	0	0	0

Figure C.47: $\mathcal{P}_3''$, $\bar{\tau} \in \{2, 3, 4\}$ and $T = 10$

$\bar{\tau}$	min	max	k	−4	−3	−2	−1	0	1	2	3	4	5	6	7	8	9	10	11	12	13	14	15	16	17	18
2	0	2	τ_j					2	0	0	2	1	0	2	1	0	2	1	0	2	1					
			w_k			0	0	−1	0	−2	−3	−4	−2	−3	−4	−2	−3	−3	0	0	0					
2	−1	1	τ_j					1	−1	−1	1	0	−1	1	0	−1	1	0	−1	1	0					
			w_k			0	0	1	−1	−2	−3	−1	−2	−3	−1	−2	−3	0	0	0	0					
2	−2	0	τ_j					0	−2	−2	0	−1	−2	0	−1	−2	0	−1	−2	0	−1					
			w_k			0	2	0	−1	−2	0	−1	−2	0	−1	−2	0	0	0	0	0					
3	0	3	τ_j					3	0	0	0	3	2	1	0	3	2	1	0	3	2	1	0			
			w_k		0	0	0	−1	0	0	−3	−4	−5	−6	−3	−4	−5	−5	−1	−1	−1	−1	0			
3	−1	2	τ_j					2	−1	−1	−1	2	1	0	−1	2	1	0	−1	2	1	0	−1			
			w_k		0	0	0	1	1	−2	−3	−4	−5	−2	−3	−4	−5	−1	−1	−1	−1	0	0			
3	−2	1	τ_j					1	−2	−2	−2	1	0	−1	−2	1	0	−1	−2	1	0	−1	−2			
			w_k		0	0	2	2	−1	−2	−3	−4	−1	−2	−3	−4	−1	−1	−1	−1	0	0	0			
3	−3	0	τ_j					0	−3	−3	−3	0	−1	−2	−3	0	−1	−2	−3	0	−1	−2	−3			
			w_k		0	2	3	0	−1	−2	−3	0	−1	−2	−3	0	−1	−1	−1	0	0	0	0			
4	0	4	τ_j					4	0	0	0	0	4	3	2	1	0	4	3	2	1	0	4	3	2	
			w_k	0	0	0	0	−1	0	0	0	−4	−5	−6	−7	−8	−4	−4	−4	−4	−4	0	0	0	0	
4	−1	3	τ_j					3	−1	−1	−1	−1	3	2	1	0	−1	3	2	1	0	−1	3	2	1	
			w_k	0	0	0	0	1	1	1	−3	−4	−5	−6	−7	−3	−4	−4	−4	−4	0	0	0	0	0	
4	−2	2	τ_j					2	−2	−2	−2	−2	2	1	0	−1	−2	2	1	0	−1	−2	2	1	0	
			w_k	0	0	0	2	2	2	−2	−3	−4	−5	−6	−2	−3	−4	−4	−4	0	0	0	0	0	0	
4	−3	1	τ_j					1	−3	−3	−3	−3	1	0	−1	−2	−3	1	0	−1	−2	−3	1	0	−1	
			w_k	0	0	2	3	3	−1	−2	−3	−4	−5	−1	−2	−3	−4	−4	0	0	0	0	0	0	0	
4	−4	0	τ_j					0	−4	−4	−4	−4	0	−1	−2	−3	−4	0	−1	−2	−3	−4	0	−1	−2	
			w_k	0	2	3	4	0	−1	−2	−3	−4	0	−1	−2	−3	−4	0	0	0	0	0	0	0	0	

Figure C.48: $\mathcal{P}_3''$, $\bar{\tau} \in \{2,3,4\}$ and $T = 9$

$\bar{\tau}$	min	max	k	−4	−3	−2	−1	0	1	2	3	4	5	6	7	8	9	10	11	12	13	14	15	16	17	18
2	0	2	τ_j					2	0	0	2	1	0	2	1	0	2	1	0	2						
			w_k			0	0	−1	0	−2	−3	−4	−2	−3	−4	−2	−2	−2	0	0						
2	−1	1	τ_j					1	−1	−1	1	0	−1	1	0	−1	1	0	−1	1						
			w_k			0	0	1	−1	−2	−3	−1	−2	−3	−1	−2	−2	0	0	0						
2	−2	0	τ_j					0	−2	−2	0	−1	−2	0	−1	−2	0	−1	−2	0						
			w_k			0	2	0	−1	−2	0	−1	−2	0	−1	−2	0	−1	−2	0						
3	0	3	τ_j					3	0	0	0	3	2	1	0	3	2	1	0	3	2	1				
			w_k		0	0	0	−1	0	0	−3	−4	−5	−6	−3	−4	−4	−4	0	0	0	0				
3	−1	2	τ_j					2	−1	−1	−1	2	1	0	−1	2	1	0	−1	2	1	0				
			w_k		0	0	0	1	1	−2	−3	−4	−5	−2	−3	−4	−4	0	0	0	0	0				
3	−2	1	τ_j					1	−2	−2	−2	1	0	−1	−2	1	0	−1	−2	1	0	−1				
			w_k		0	0	2	2	−1	−2	−3	−4	−1	−2	−3	−4	0	0	0	0	0	0				
3	−3	0	τ_j					0	−3	−3	−3	0	−1	−2	−3	0	−1	−2	−3	0	−1	−2				
			w_k		0	2	3	0	−1	−2	−3	0	−1	−2	−3	0	0	0	0	0	0	0				
4	0	4	τ_j					4	0	0	0	0	4	3	2	1	0	4	3	2	1	0	4	3		
			w_k	0	0	0	0	−1	0	0	0	−4	−5	−6	−7	−8	−3	−3	−3	−3	−3	0	0	0		
4	−1	3	τ_j					3	−1	−1	−1	−1	3	2	1	0	−1	3	2	1	0	−1	3	2		
			w_k	0	0	0	0	1	1	1	−3	−4	−5	−6	−7	−3	−3	−3	−3	−3	0	0	0	0		
4	−2	2	τ_j					2	−2	−2	−2	−2	2	1	0	−1	−2	2	1	0	−1	−2	2	1		
			w_k	0	0	0	2	2	2	−2	−3	−4	−5	−6	−2	−3	−3	−3	−3	0	0	0	0	0		
4	−3	1	τ_j					1	−3	−3	−3	−3	1	0	−1	−2	−3	1	0	−1	−2	−3	1	0		
			w_k	0	0	2	3	3	−1	−2	−3	−4	−5	−1	−2	−3	−3	−3	0	0	0	0	0	0		
4	−4	0	τ_j					0	−4	−4	−4	−4	0	−1	−2	−3	−4	0	−1	−2	−3	−4	0	−1		
			w_k	0	2	3	4	0	−1	−2	−3	−4	0	−1	−2	−3	−3	0	0	0	0	0	0	0		

Figure C.49: $\mathcal{P}_3''$, $\bar{\tau} \in \{2,3,4\}$ and $T = 8$

$\bar{\tau}$	min	max	k	−4	−3	−2	−1	0	1	2	3	4	5	6	7	8	9	10	11	12	13	14	15	16	17	18
2	0	2	τ_j					2	0	0	2	1	0	2	1	0	2	1	0							
			w_k			0	0	−1	0	−2	−3	−4	−2	−3	−4	−1	−1	−1	0							
2	−1	1	τ_j					1	−1	−1	1	0	−1	1	0	−1	1	0	−1							
			w_k			0	0	1	−1	−2	−3	−1	−2	−3	−1	−1	−1	0	0							
2	−2	0	τ_j					0	−2	−2	0	−1	−2	0	−1	−2	0	−1	−2							
			w_k			0	2	0	−1	−2	0	−1	−2	0	−1	−1	0	0	0							
3	0	3	τ_j					3	0	0	0	3	2	1	0	3	2	1	0	3	2					
			w_k		0	0	0	−1	0	0	−3	−4	−5	−6	−3	−3	−3	−3	0	0	0					
3	−1	2	τ_j					2	−1	−1	−1	2	1	0	−1	2	1	0	−1	2	1					
			w_k		0	0	0	1	1	−2	−3	−4	−5	−2	−3	−3	−3	0	0	0	0					
3	−2	1	τ_j					1	−2	−2	−2	1	0	−1	−2	1	0	−1	−2	1	0					
			w_k		0	0	2	2	−1	−2	−3	−4	−1	−2	−3	−3	0	0	0	0	0					
3	−3	0	τ_j					0	−3	−3	−3	0	−1	−2	−3	0	−1	−2	−3	0	−1					
			w_k		0	2	3	0	−1	−2	−3	0	−1	−2	−3	0	0	0	0	0	0					
4	0	4	τ_j					4	0	0	0	0	4	3	2	1	0	4	3	2	1	0	4			
			w_k	0	0	0	0	−1	0	0	0	−4	−5	−6	−7	−7	−2	−2	−2	−2	−2	0	0			
4	−1	3	τ_j					3	−1	−1	−1	−1	3	2	1	0	−1	3	2	1	0	−1	3			
			w_k	0	0	0	0	1	1	1	−3	−4	−5	−6	−7	−2	−2	−2	−2	−2	0	0	0			
4	−2	2	τ_j					2	−2	−2	−2	−2	2	1	0	−1	−2	2	1	0	−1	−2	2			
			w_k	0	0	0	2	2	2	−2	−3	−4	−5	−6	−2	−2	−2	−2	−2	0	0	0	0			
4	−3	1	τ_j					1	−3	−3	−3	−3	1	0	−1	−2	−3	1	0	−1	−2	−3	1			
			w_k	0	0	2	3	3	−1	−2	−3	−4	−5	−1	−2	−2	−2	−2	0	0	0	0	0			
4	−4	0	τ_j					0	−4	−4	−4	−4	0	−1	−2	−3	−4	0	−1	−2	−3	−4	0			
			w_k	0	2	3	4	0	−1	−2	−3	−4	0	−1	−2	−2	−2	0	0	0	0	0	0			

Figure C.50: $\mathcal{P}_3''$, $\bar{\tau} \in \{2,3,4\}$ and $T = 7$

$\bar{\tau}$	min	max	k	−4	−3	−2	−1	0	1	2	3	4	5	6	7	8	9	10	11	12	13	14	15	16	17	18
2	0	2	τ_j					2	0	0	2	1	0	2	1	0	2	1								
			w_k			0	0	−1	0	−2	−3	−4	−2	−3	−3	0	0	0								
2	−1	1	τ_j					1	−1	−1	1	0	−1	1	0	−1	1	0								
			w_k			0	0	1	−1	−2	−3	−1	−2	−3	0	0	0	0								
2	−2	0	τ_j					0	−2	−2	0	−1	−2	0	−1	−2	0	−1								
			w_k			0	2	0	−1	−2	0	−1	−2	0	0	0	0	0								
3	0	3	τ_j					3	0	0	0	3	2	1	0	3	2	1	0	3						
			w_k		0	0	0	−1	0	0	−3	−4	−5	−6	−2	−2	−2	−2	0	0						
3	−1	2	τ_j					2	−1	−1	−1	2	1	0	−1	2	1	0	−1	2						
			w_k		0	0	0	1	1	−2	−3	−4	−5	−2	−2	−2	−2	0	0	0						
3	−2	1	τ_j					1	−2	−2	−2	1	0	−1	−2	1	0	−1	−2	1						
			w_k		0	0	2	2	−1	−2	−3	−4	−1	−2	−2	−2	0	0	0	0						
3	−3	0	τ_j					0	−3	−3	−3	0	−1	−2	−3	0	−1	−2	−3	0						
			w_k		0	2	3	0	−1	−2	−3	0	−1	−2	−2	0	0	0	0	0						
4	0	4	τ_j					4	0	0	0	0	4	3	2	1	0	4	3	2	1	0				
			w_k	0	0	0	0	−1	0	0	0	−4	−5	−6	−6	−6	−1	−1	−1	−1	−1	0				
4	−1	3	τ_j					3	−1	−1	−1	−1	3	2	1	0	−1	3	2	1	0	−1				
			w_k	0	0	0	0	1	1	1	−3	−4	−5	−6	−6	−1	−1	−1	−1	−1	0	0				
4	−2	2	τ_j					2	−2	−2	−2	−2	2	1	0	−1	−2	2	1	0	−1	−2				
			w_k	0	0	0	2	2	2	−2	−3	−4	−5	−6	−1	−1	−1	−1	−1	0	0	0				
4	−3	1	τ_j					1	−3	−3	−3	−3	1	0	−1	−2	−3	1	0	−1	−2	−3				
			w_k	0	0	2	3	3	−1	−2	−3	−4	−5	−1	−1	−1	−1	−1	0	0	0	0				
4	−4	0	τ_j					0	−4	−4	−4	−4	0	−1	−2	−3	−4	0	−1	−2	−3	−4				
			w_k	0	2	3	4	0	−1	−2	−3	−4	0	−1	−1	−1	−1	0	0	0	0	0				

Figure C.51: $\mathcal{P}_3''$, $\bar{\tau} \in \{2,3,4\}$ and $T = 6$

$\bar{\tau}$	min	max	k	−4	−3	−2	−1	0	1	2	3	4	5	6	7	8	9	10	11	12	13	14	15	16	17	18
2	0	2	τ_j					2	0	0	2	1	0	2	1	0	2									
			w_k			0	0	−1	0	−2	−3	−4	−2	−2	−2	0	0									
2	−1	1	τ_j					1	−1	−1	1	0	−1	1	0	−1	1									
			w_k			0	0	1	−1	−2	−3	−1	−2	−2	0	0	0									
2	−2	0	τ_j					0	−2	−2	0	−1	−2	0	−1	−2	0									
			w_k			0	2	0	−1	−2	0	−1	−2	0	0	0	0									
3	0	3	τ_j					3	0	0	0	3	2	1	0	3	2	1	0							
			w_k		0	0	0	−1	0	0	−3	−4	−5	−5	−1	−1	−1	−1	0							
3	−1	2	τ_j					2	−1	−1	−1	2	1	0	−1	2	1	0	−1							
			w_k		0	0	0	1	1	−2	−3	−4	−5	−1	−1	−1	−1	0	0							
3	−2	1	τ_j					1	−2	−2	−2	1	0	−1	−2	1	0	−1	−2							
			w_k		0	0	2	2	−1	−2	−3	−4	−1	−1	−1	−1	0	0	0							
3	−3	0	τ_j					0	−3	−3	−3	0	−1	−2	−3	0	−1	−2	−3							
			w_k		0	2	3	0	−1	−2	−3	0	−1	−1	−1	0	0	0	0							
4	0	4	τ_j					4	0	0	0	0	4	3	2	1	0	4	3	2	1					
			w_k	0	0	0	0	−1	0	0	0	−4	−5	−5	−5	−5	0	0	0	0	0					
4	−1	3	τ_j					3	−1	−1	−1	−1	3	2	1	0	−1	3	2	1	0					
			w_k	0	0	0	0	1	1	1	−3	−4	−5	−5	−5	0	0	0	0	0	0					
4	−2	2	τ_j					2	−2	−2	−2	−2	2	1	0	−1	−2	2	1	0	−1					
			w_k	0	0	0	2	2	2	−2	−3	−4	−5	−5	0	0	0	0	0	0	0					
4	−3	1	τ_j					1	−3	−3	−3	−3	1	0	−1	−2	−3	1	0	−1	−2					
			w_k	0	0	2	3	3	−1	−2	−3	−4	−5	0	0	0	0	0	0	0	0					
4	−4	0	τ_j					0	−4	−4	−4	−4	0	−1	−2	−3	−4	0	−1	−2	−3					
			w_k	0	2	3	4	0	−1	−2	−3	−4	0	0	0	0	0	0	0	0	0					

Figure C.52: $\mathcal{P}_3''$, $\bar{\tau} \in \{2,3,4\}$ and $T = 5$

$\bar{\tau}$	min	max	k	−4	−3	−2	−1	0	1	2	3	4	5	6	7	8	9	10	11	12	13	14	15	16	17	18
2	0	2	τ_j					2	0	0	2	1	0	2	1	0										
			w_k			0	0	−1	0	−2	−3	−4	−1	−1	−1	0										
2	−1	1	τ_j					1	−1	−1	1	0	−1	1	0	−1										
			w_k			0	0	1	−1	−2	−3	−1	−1	−1	0	0										
2	−2	0	τ_j					0	−2	−2	0	−1	−2	0	−1	−2										
			w_k			0	2	0	−1	−2	0	−1	−1	0	0	0										
3	0	3	τ_j					3	0	0	0	3	2	1	0	3	2	1								
			w_k		0	0	0	−1	0	0	−3	−4	−4	−4	0	0	0	0								
3	−1	2	τ_j					2	−1	−1	−1	2	1	0	−1	2	1	0								
			w_k		0	0	0	1	1	−2	−3	−4	−4	0	0	0	0	0								
3	−2	1	τ_j					1	−2	−2	−2	1	0	−1	−2	1	0	−1								
			w_k		0	0	2	2	−1	−2	−3	−4	0	0	0	0	0	0								
3	−3	0	τ_j					0	−3	−3	−3	0	−1	−2	−3	0	−1	−2								
			w_k		0	2	3	0	−1	−2	−3	0	0	0	0	0	0	0								
4	0	4	τ_j					4	0	0	0	0	4	3	2	1	0	4	3	2						
			w_k	0	0	0	0	−1	0	0	0	−4	−4	−4	−4	−4	0	0	0	0						
4	−1	3	τ_j					3	−1	−1	−1	−1	3	2	1	0	−1	3	2	1						
			w_k	0	0	0	0	1	1	1	−3	−4	−4	−4	−4	0	0	0	0	0						
4	−2	2	τ_j					2	−2	−2	−2	−2	2	1	0	−1	−2	2	1	0						
			w_k	0	0	0	2	2	2	−2	−3	−4	−4	−4	0	0	0	0	0	0						
4	−3	1	τ_j					1	−3	−3	−3	−3	1	0	−1	−2	−3	1	0	−1						
			w_k	0	0	2	3	3	−1	−2	−3	−4	−4	0	0	0	0	0	0	0						
4	−4	0	τ_j					0	−4	−4	−4	−4	0	−1	−2	−3	−4	0	−1	−2						
			w_k	0	2	3	4	0	−1	−2	−3	−4	0	0	0	0	0	0	0	0						

Figure C.53: $\mathcal{P}_3''$, $\bar{\tau} \in \{2,3,4\}$ and $T = 4$

$\bar{\tau}$	min	max	k	-4	-3	-2	-1	0	1	2	3	4	5	6	7	8	9	10	11	12	13	14	15	16	17	18
2	0	2	τ_j					2	0	0	2	1	0	2	1											
			w_k			0	0	-1	0	-2	-3	-3	0	0	0											
2	-1	1	τ_j					1	-1	-1	1	0	-1	1	0											
			w_k			0	0	1	-1	-2	-3	0	0	0	0											
2	-2	0	τ_j					0	-2	-2	0	-1	-2	0	-1											
			w_k			0	2	0	-1	-2	0	0	0	0	0											
3	0	3	τ_j					3	0	0	0	3	2	1	0	3	2									
			w_k		0	0	0	-1	0	0	-3	-3	-3	-3	0	0	0									
3	-1	2	τ_j					2	-1	-1	-1	2	1	0	-1	2	1									
			w_k		0	0	0	1	1	-2	-3	-3	-3	0	0	0	0									
3	-2	1	τ_j					1	-2	-2	-2	1	0	-1	-2	1	0									
			w_k		0	0	2	2	-1	-2	-3	-3	0	0	0	0	0									
3	-3	0	τ_j					0	-3	-3	-3	0	-1	-2	-3	0	-1									
			w_k		0	2	3	0	-1	-2	-3	0	0	0	0	0	0									
4	0	4	τ_j					4	0	0	0	0	4	3	2	1	0	4	3							
			w_k	0	0	0	0	-1	0	0	0	-3	-3	-3	-3	-3	0	0	0							
4	-1	3	τ_j					3	-1	-1	-1	-1	3	2	1	0	-1	3	2							
			w_k	0	0	0	0	1	1	1	-3	-3	-3	-3	-3	0	0	0	0							
4	-2	2	τ_j					2	-2	-2	-2	-2	2	1	0	-1	-2	2	1							
			w_k	0	0	0	2	2	2	-2	-3	-3	-3	-3	0	0	0	0	0							
4	-3	1	τ_j					1	-3	-3	-3	-3	1	0	-1	-2	-3	1	0							
			w_k	0	0	2	3	3	-1	-2	-3	-3	-3	0	0	0	0	0	0							
4	-4	0	τ_j					0	-4	-4	-4	-4	0	-1	-2	-3	-4	0	-1							
			w_k	0	2	3	4	0	-1	-2	-3	-3	0	0	0	0	0	0	0							

Figure C.54: $\mathcal{P}''_3$, $\bar{\tau} \in \{2, 3, 4\}$ and $T = 3$

$\bar{\tau}$	min	max	k	-4	-3	-2	-1	0	1	2	3	4	5	6	7	8	9	10	11	12	13	14	15	16	17	18
2	0	2	τ_j					2	0	0	2	1	0	2												
			w_k			0	0	-1	0	-2	-2	-2	0	0												
2	-1	1	τ_j					1	-1	-1	1	0	-1	1												
			w_k			0	0	1	-1	-2	-2	0	0	0												
2	-2	0	τ_j					0	-2	-2	0	-1	-2	0												
			w_k			0	2	0	-1	-2	0	0	0	0												
3	0	3	τ_j					3	0	0	0	3	2	1	0	3										
			w_k		0	0	0	-1	0	0	-2	-2	-2	-2	0	0										
3	-1	2	τ_j					2	-1	-1	-1	2	1	0	-1	2										
			w_k		0	0	0	1	1	-2	-2	-2	-2	0	0	0										
3	-2	1	τ_j					1	-2	-2	-2	1	0	-1	-2	1										
			w_k		0	0	2	2	-1	-2	-2	-2	0	0	0	0										
3	-3	0	τ_j					0	-3	-3	-3	0	-1	-2	-3	0										
			w_k		0	2	3	0	-1	-2	-2	0	0	0	0	0										
4	0	4	τ_j					4	0	0	0	0	4	3	2	1	0	4								
			w_k	0	0	0	0	-1	0	0	0	-2	-2	-2	-2	-2	0	0								
4	-1	3	τ_j					3	-1	-1	-1	-1	3	2	1	0	-1	3								
			w_k	0	0	0	0	1	1	0	-2	-2	-2	-2	-2	0	0	0								
4	-2	2	τ_j					2	-2	-2	-2	-2	2	1	0	-1	-2	2								
			w_k	0	0	0	2	2	1	-2	-2	-2	-2	-2	0	0	0	0								
4	-3	1	τ_j					1	-3	-3	-3	-3	1	0	-1	-2	-3	1								
			w_k	0	0	2	3	2	-1	-2	-2	-2	-2	0	0	0	0	0								
4	-4	0	τ_j					0	-4	-4	-4	-4	0	-1	-2	-3	-4	0								
			w_k	0	2	3	3	0	-1	-2	-2	-2	0	0	0	0	0	0								

Figure C.55: $\mathcal{P}''_3$, $\bar{\tau} \in \{2, 3, 4\}$ and $T = 2$

$\bar{\tau}$	min	max	k	-4	-3	-2	-1	0	1	2	3	4	5	6	7	8	9	10	11	12	13	14	15	16	17	18
2	0	2	τ_j					2	0	0	2	1	0													
			w_k			0	0	-1	0	-1	-1	-1	0													
2	-1	1	τ_j					1	-1	-1	1	0	-1													
			w_k			0	0	1	-1	-1	-1	0	0													
2	-2	0	τ_j					0	-2	-2	0	-1	-2													
			w_k			0	2	0	-1	-1	0	0	0													
3	0	3	τ_j					3	0	0	0	3	2	1	0											
			w_k		0	0	0	-1	0	0	-1	-1	-1	-1	0											
3	-1	2	τ_j					2	-1	-1	-1	2	1	0	-1											
			w_k		0	0	0	1	0	-1	-1	-1	-1	0	0											
3	-2	1	τ_j					1	-2	-2	-2	1	0	-1	-2											
			w_k		0	0	2	1	-1	-1	-1	-1	0	0	0											
3	-3	0	τ_j					0	-3	-3	-3	0	-1	-2	-3											
			w_k		0	2	2	0	-1	-1	-1	0	0	0	0											
4	0	4	τ_j					4	0	0	0	0	4	3	2	1	0									
			w_k	0	0	0	0	-1	0	0	0	-1	-1	-1	-1	-1	0									
4	-1	3	τ_j					3	-1	-1	-1	-1	3	2	1	0	-1									
			w_k	0	0	0	0	1	0	0	-1	-1	-1	-1	-1	0	0									
4	-2	2	τ_j					2	-2	-2	-2	-2	2	1	0	-1	-2									
			w_k	0	0	0	2	1	0	-1	-1	-1	-1	-1	0	0	0									
4	-3	1	τ_j					1	-3	-3	-3	-3	1	0	-1	-2	-3									
			w_k	0	0	2	2	1	-1	-1	-1	-1	-1	0	0	0	0									
4	-4	0	τ_j					0	-4	-4	-4	-4	0	-1	-2	-3	-4									
			w_k	0	2	2	2	0	-1	-1	-1	-1	0	0	0	0	0									

Figure C.56: $\mathcal{P}''_3$, $\bar{\tau} \in \{2, 3, 4\}$ and $T = 1$

C.7 Gains for $\mathcal{P}_3''$

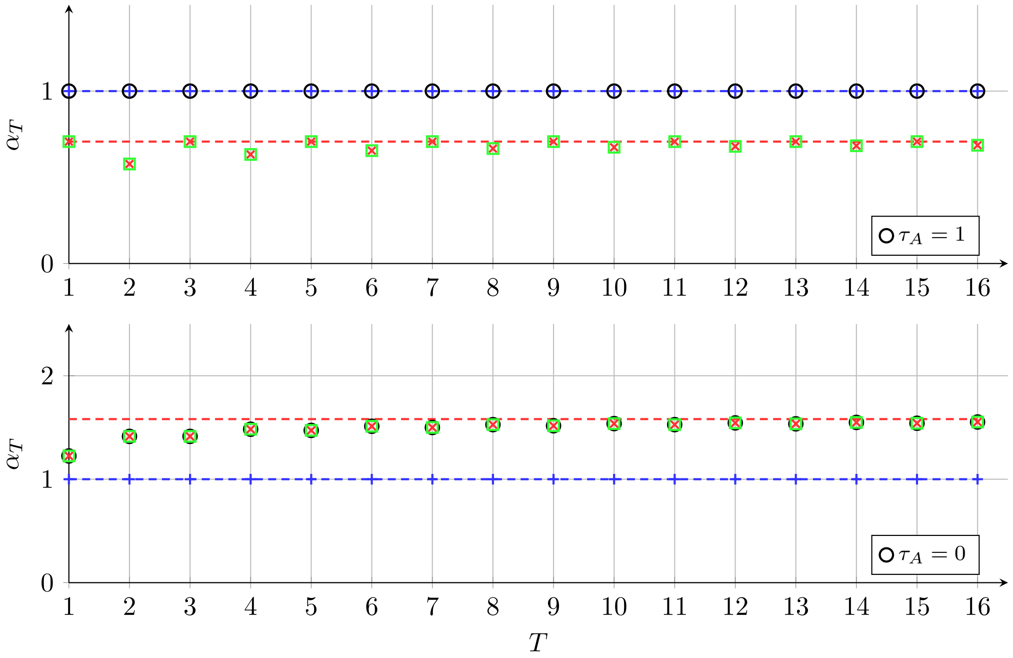

Figure C.57: $\mathcal{P}_3$, $\bar{\tau} = 1$: $\mathcal{P}_1$ (blue), $\mathcal{P}_3'$ (red), $\mathcal{P}_3''$ (green)

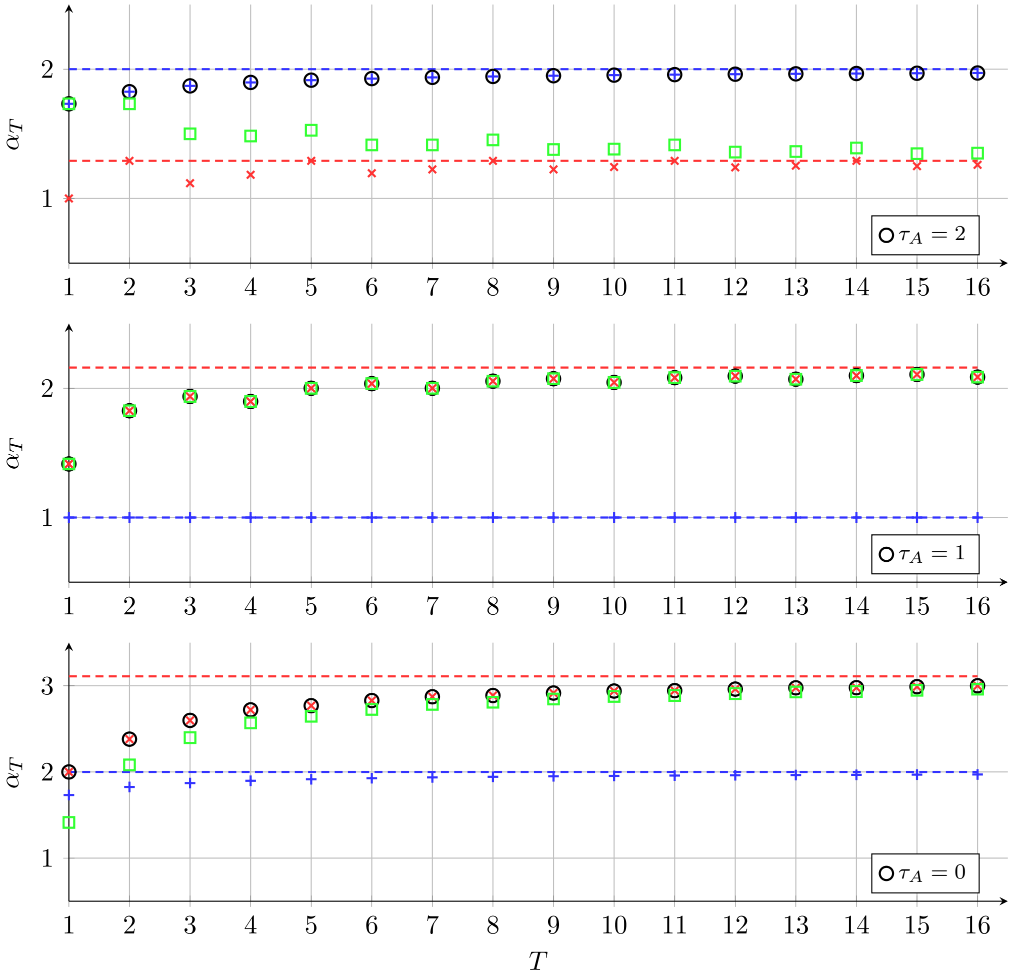

Figure C.58: $\mathcal{P}_3$, $\bar{\tau} = 2$: $\mathcal{P}_1$ (blue), $\mathcal{P}_3'$ (red), $\mathcal{P}_3''$ (green)

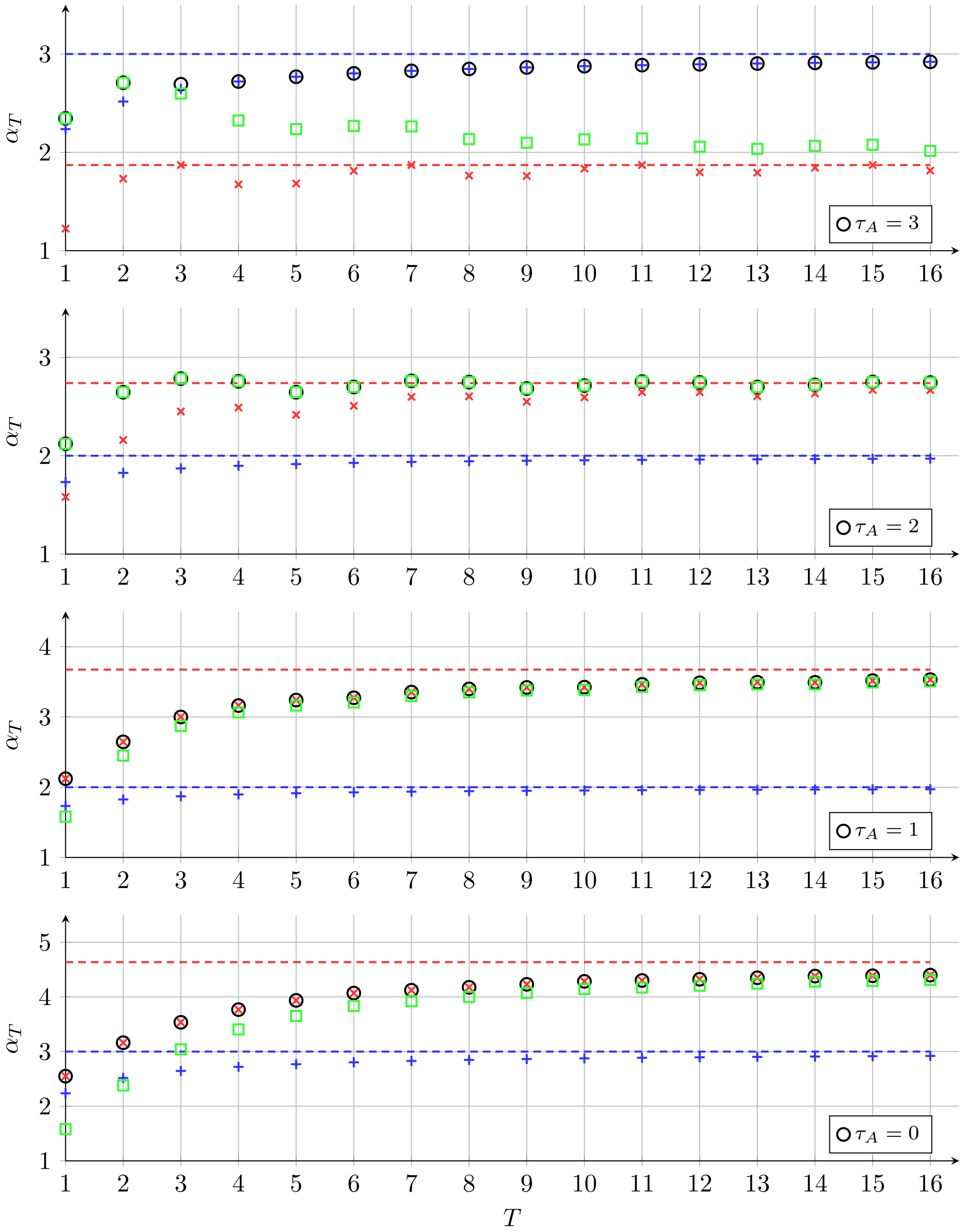

Figure C.59: $\mathcal{P}_3$, $\bar{\tau} = 3$: $\mathcal{P}_1$ (blue), $\mathcal{P}_3'$ (red), $\mathcal{P}_3''$ (green)

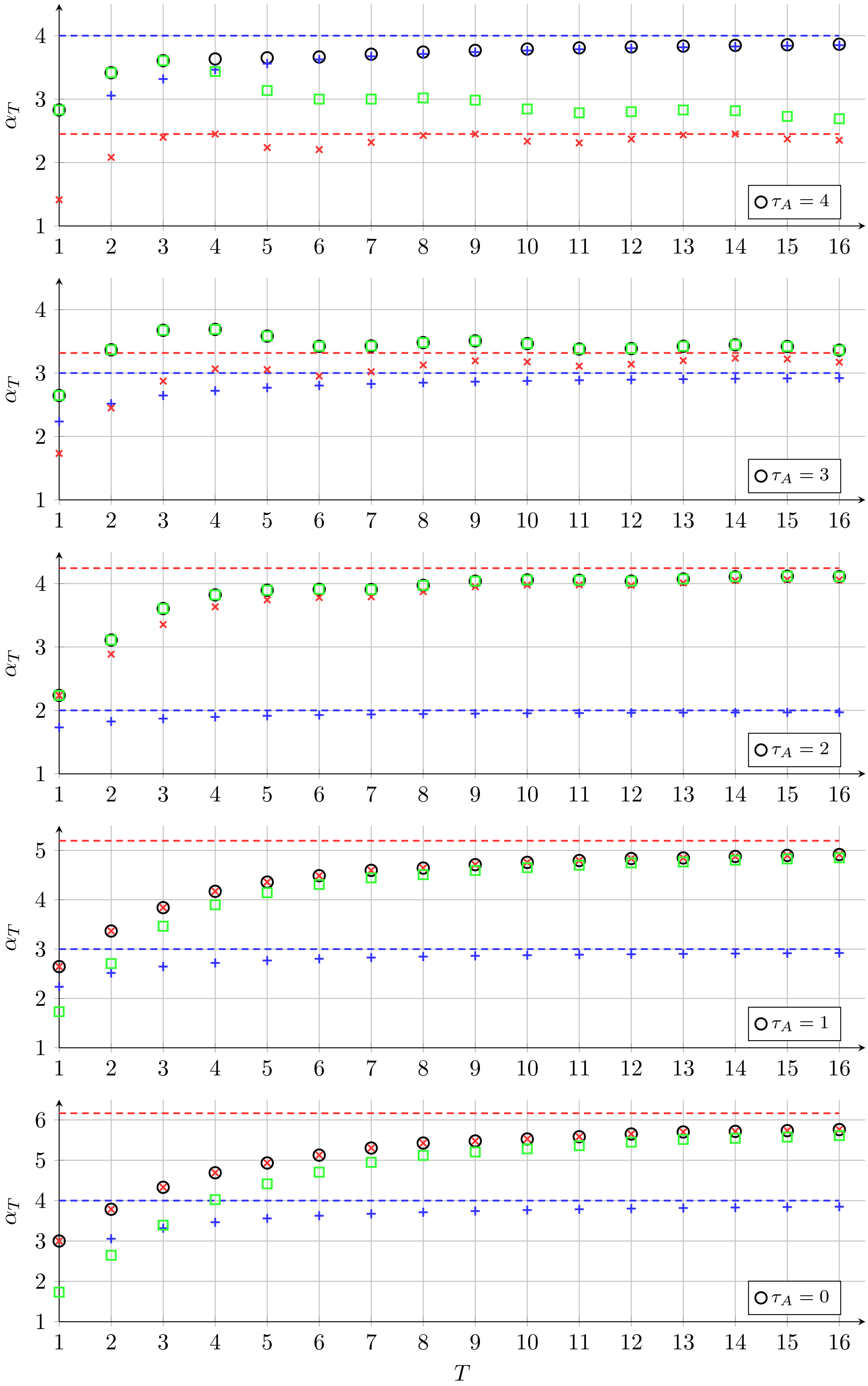

Figure C.60: $\mathcal{P}_3$, $\bar{\tau} = 4$: $\mathcal{P}_1$ (blue), $\mathcal{P}_3'$ (red), $\mathcal{P}_3''$ (green)

C.8 Patterns for $\mathcal{P}_3'''$

k	-3	-2	-1	0	1	2	3	4	5	6	7	8	9	10	11	12	13	14	15	16
$b_k^{(0)} = a_k$	0	0	0	1	2	3	4	5	6	7	8	9	10	11	11	11	11	11	11	11
$b_k^{(1)}$	0	0	0	0	1	2	3	4	5	6	7	8	9	10	11	11	11	11	11	11
$b_k^{(2)}$	0	0	0	0	0	1	2	3	4	5	6	7	8	9	10	11	11	11	11	11
$b_k^{(3)}$	0	0	0	0	0	0	1	2	3	4	5	6	7	8	9	10	11	11	11	11
$b_k^{(0)} = a_k$	0	0	0	1	2	3	4	5	6	7	8	~~9~~	10	11	11	~~11~~	~~11~~	~~11~~	~~11~~	~~11~~
$b_k^{(1)}k$	0	0	0	0	~~1~~	~~2~~	~~3~~	~~4~~	~~5~~	~~6~~	~~7~~	~~8~~	~~9~~	~~10~~	~~11~~	~~11~~	~~11~~	~~11~~	~~11~~	~~11~~
$b_k^{(2)}$	0	0	0	0	0	~~1~~	~~2~~	~~3~~	~~4~~	~~5~~	~~6~~	~~7~~	~~8~~	~~9~~	~~10~~	~~11~~	~~11~~	~~11~~	~~11~~	~~11~~
$b_k^{(3)}$	0	0	0	0	0	0	~~1~~	~~2~~	~~3~~	~~4~~	~~5~~	~~6~~	~~7~~	~~8~~	9	~~10~~	~~11~~	~~11~~	11	11
$b_k^{(0)} - a_k$	0	0	0	0	0	0	0	0	0	0	0	0	0	0	0	0	0	0	0	0
$b_k^{(1)} - a_k$	0	0	0	-1	-1	-1	-1	-1	-1	-1	-1	-1	-1	-1	0	0	0	0	0	0
$b_k^{(2)} - a_k$	0	0	0	-1	-2	-2	-2	-2	-2	-2	-2	-2	-2	-2	-1	0	0	0	0	0
$b_k^{(3)} - a_k$	0	0	0	-1	-2	-3	-3	-3	-3	-3	-3	-3	-3	-3	-2	-1	0	0	0	0
packet arr.	no	no	no	yes	yes	yes	yes	yes	yes	yes	yes	no	yes	yes	yes	no	no	no	yes	yes
c_k	0	0	0	1	2	3	4	5	6	7	8	8	10	11	9	9	9	9	11	11
w_k	0	0	0	0	0	0	0	0	0	0	0	-1	0	0	-2	-2	-2	-2	0	0
block	A	A	B	B	B	B	B	B	B	B	B	C	C	C	D	D	D	D		
τ_j				0	0	0	0	0	0	0	0	3	0	0	0	3	3	3	3	3

Figure C.61: $\mathcal{P}_3'''$, $\bar{\tau} = 3$, $T = 10$ and $\tau_A = 0$

k	-3	-2	-1	0	1	2	3	4	5	6	7	8	9	10	11	12	13	14	15	16
$b_k^{(-1)}$	0	0	1	2	3	4	5	6	7	8	9	10	11	11	11	11	11	11	11	11
$b_k^{(0)} = a_k$	0	0	0	1	2	3	4	5	6	7	8	9	10	11	11	11	11	11	11	11
$b_k^{(1)}$	0	0	0	0	1	2	3	4	5	6	7	8	9	10	11	11	11	11	11	11
$b_k^{(2)}$	0	0	0	0	0	1	2	3	4	5	6	7	8	9	10	11	11	11	11	11
$b_k^{(-1)}$	0	0	1	2	3	4	5	6	7	8	~~9~~	10	11	11	~~11~~	~~11~~	~~11~~	~~11~~	~~11~~	~~11~~
$b_k^{(0)} = a_k$	0	0	0	~~1~~	~~2~~	~~3~~	~~4~~	~~5~~	~~6~~	~~7~~	~~8~~	~~9~~	~~10~~	~~11~~	~~11~~	~~11~~	~~11~~	~~11~~	~~11~~	~~11~~
$b_k^{(1)}$	0	0	0	0	~~1~~	~~2~~	~~3~~	~~4~~	~~5~~	~~6~~	~~7~~	~~8~~	~~9~~	~~10~~	~~11~~	~~11~~	~~11~~	~~11~~	~~11~~	~~11~~
$b_k^{(2)}$	0	0	0	0	0	~~1~~	~~2~~	~~3~~	~~4~~	~~5~~	~~6~~	~~7~~	~~8~~	9	~~10~~	~~11~~	~~11~~	11	11	11
$b_k^{(-1)} - a_k$	0	0	1	1	1	1	1	1	1	1	1	1	1	0	0	0	0	0	0	0
$b_k^{(0)} - a_k$	0	0	0	0	0	0	0	0	0	0	0	0	0	0	0	0	0	0	0	0
$b_k^{(1)} - a_k$	0	0	0	-1	-1	-1	-1	-1	-1	-1	-1	-1	-1	-1	0	0	0	0	0	0
$b_k^{(2)} - a_k$	0	0	0	-1	-2	-2	-2	-2	-2	-2	-2	-2	-2	-2	-1	0	0	0	0	0
packet arr.	no	no	yes	yes	yes	yes	yes	yes	yes	yes	no	yes	yes	yes	no	no	no	yes	yes	yes
c_k	0	0	1	2	3	4	5	6	7	8	8	10	11	9	9	9	9	11	11	11
w_k	0	0	1	1	1	1	1	1	1	1	0	1	1	-2	-2	-2	-2	0	0	0
block	A	A	A	B	B	B	B	B	B	B	C	C	C	D	D	D	D			
τ_j				-1	-1	-1	-1	-1	-1	-1	-1	2	-1	-1	-1	2	2	2	2	2

Figure C.62: $\mathcal{P}_3'''$, $\bar{\tau} = 3$, $T = 10$ and $\tau_A = 1$

k	-3	-2	-1	0	1	2	3	4	5	6	7	8	9	10	11	12	13	14	15	16
$b_k^{(-2)}$	0	1	2	3	4	5	6	7	8	9	10	11	11	11	11	11	11	11	11	11
$b_k^{(1)}$	0	0	1	2	3	4	5	6	7	8	9	10	11	11	11	11	11	11	11	11
$b_k^{(0)} = a_k$	0	0	0	1	2	3	4	5	6	7	8	9	10	11	11	11	11	11	11	11
$b_k^{(1)}$	0	0	0	0	1	2	3	4	5	6	7	8	9	10	11	11	11	11	11	11
$b_k^{(-2)}$	0	1	2	3	4	5	6	7	8	~~9~~	10	11	11	~~11~~	~~11~~	~~11~~	~~11~~	~~11~~	~~11~~	~~11~~
$b_k^{(-1)}$	0	0	~~1~~	~~2~~	~~3~~	~~4~~	~~5~~	~~6~~	~~7~~	~~8~~	~~9~~	~~10~~	~~11~~	~~11~~	~~11~~	~~11~~	~~11~~	~~11~~	~~11~~	~~11~~
$b_k^{(0)} = a_k$	0	0	0	~~1~~	~~2~~	~~3~~	~~4~~	~~5~~	~~6~~	~~7~~	~~8~~	~~9~~	~~10~~	~~11~~	~~11~~	~~11~~	~~11~~	~~11~~	~~11~~	~~11~~
$b_k^{(1)}$	0	0	0	0	~~1~~	~~2~~	~~3~~	~~4~~	~~5~~	~~6~~	~~7~~	~~8~~	9	~~10~~	~~11~~	~~11~~	11	11	11	11
$b_k^{(-2)} - a_k$	0	1	2	2	2	2	2	2	2	2	2	2	1	0	0	0	0	0	0	0
$b_k^{(-1)} - a_k$	0	0	1	1	1	1	1	1	1	1	1	1	1	0	0	0	0	0	0	0
$b_k^{(0)} - a_k$	0	0	0	0	0	0	0	0	0	0	0	0	0	0	0	0	0	0	0	0
$b_k^{(1)} - a_k$	0	0	0	-1	-1	-1	-1	-1	-1	-1	-1	-1	-1	-1	0	0	0	0	0	0
packet arr.	no	yes	yes	yes	yes	yes	yes	yes	yes	no	yes	yes	yes	no	no	no	yes	yes	yes	yes
c_k	0	1	2	3	4	5	6	7	8	8	10	11	9	9	9	9	11	11	11	11
w_k	0	1	2	2	2	2	2	2	2	1	2	2	-1	-2	-2	-2	0	0	0	0
block	A	A	B	B	B	B	B	B	B	C	C	C	D	D	D	D				
τ_j				-2	-2	-2	-2	-2	-2	-2	-2	1	-2	-2	-2	1	1	1	1	1

Figure C.63: $\mathcal{P}_3'''$, $\bar{\tau} = 3$, $T = 10$ and $\tau_A = 2$

k	-3	-2	-1	0	1	2	3	4	5	6	7	8	9	10	11	12	13	14	15	16
$b_k^{(-3)}$	1	2	3	4	5	6	7	8	9	10	11	11	11	11	11	11	11	11	11	11
$b_k^{(-2)}$	0	1	2	3	4	5	6	7	8	9	10	11	11	11	11	11	11	11	11	11
$b_k^{(-1)}$	0	0	1	2	3	4	5	6	7	8	9	10	11	11	11	11	11	11	11	11
$b_k^{(0)} = a_k$	0	0	0	1	2	3	4	5	6	7	8	9	10	11	11	11	11	11	11	11
$b_k^{(-3)}$	1	2	3	4	5	6	7	8	~~9~~	10	11	11	~~11~~	~~11~~	~~11~~	~~11~~	~~11~~	~~11~~	~~11~~	~~11~~
$b_k^{(-2)}$	0	~~1~~	~~2~~	~~3~~	~~4~~	~~5~~	~~6~~	~~7~~	~~8~~	~~9~~	~~10~~	~~11~~	~~11~~	~~11~~	~~11~~	~~11~~	~~11~~	~~11~~	~~11~~	~~11~~
$b_k^{(-1)}$	0	0	~~1~~	~~2~~	~~3~~	~~4~~	~~5~~	~~6~~	~~7~~	~~8~~	~~9~~	~~10~~	~~11~~	~~11~~	~~11~~	~~11~~	~~11~~	~~11~~	~~11~~	~~11~~
$b_k^{(0)} = a_k$	0	0	0	~~1~~	~~2~~	~~3~~	~~4~~	~~5~~	~~6~~	~~7~~	~~8~~	9	~~10~~	~~11~~	~~11~~	11	11	11	11	11
$b_k^{(-3)} - a_k$	1	2	3	3	3	3	3	3	3	3	3	2	1	0	0	0	0	0	0	0
$b_k^{(-2)} - a_k$	0	1	2	2	2	2	2	2	2	2	2	2	1	0	0	0	0	0	0	0
$b_k^{(-1)} - a_k$	0	0	1	1	1	1	1	1	1	1	1	1	1	0	0	0	0	0	0	0
$b_k^{(0)} - a_k$	0	0	0	0	0	0	0	0	0	0	0	0	0	0	0	0	0	0	0	0
packet arr.	yes	yes	yes	yes	yes	yes	yes	yes	no	yes	yes	yes	no	no	no	yes	yes	yes	yes	yes
c_k	1	2	3	4	5	6	7	8	8	10	11	9	9	9	9	11	11	11	11	11
w_k	1	2	3	3	3	3	3	3	2	3	3	0	-1	-2	-2	0	0	0	0	0
block	A	A	B	B	B	B	B	B	C	C	C	D	D	D	D					
τ_j				-3	-3	-3	-3	-3	-3	-3	-3	0	-3	-3	-3	0	0	0	0	0

Figure C.64: $\mathcal{P}_3'''$, $\bar{\tau} = 3$, $T = 10$ and $\tau_A = 3$

$\bar{\tau}$	min	max	k	-4	-3	-2	-1	0	1	2	3	4	5	6	7	8	9	10	11	12	13	14	15	16	17	18
2	0	2	τ_j					0	0	0	0	0	0	0	0	0	2	0	0	2	2	2				
			w_k			0	0	0	0	0	0	0	0	0	0	0	-1	0	-1	-1	-1	0				
2	-1	1	τ_j					-1	-1	-1	-1	-1	-1	-1	-1	-1	1	-1	-1	1	1	1				
			w_k			0	1	1	1	1	1	1	1	1	1	0	1	-1	-1	-1	0	0				
2	-2	0	τ_j					-2	-2	-2	-2	-2	-2	-2	-2	-2	0	-2	-2	0	0	0				
			w_k			1	2	2	2	2	2	2	2	2	1	2	0	-1	-1	0	0	0				
3	-3	0	τ_j					0	0	0	0	0	0	0	0	3	0	0	0	3	3	3	3	3		
			w_k		0	0	0	0	0	0	0	0	0	0	0	-1	0	0	-2	-2	-2	-2	0	0		
3	-2	1	τ_j					-1	-1	-1	-1	-1	-1	-1	-1	2	-1	-1	-1	2	2	2	2	2		
			w_k		0	0	1	1	1	1	1	1	1	1	0	1	1	-2	-2	-2	-2	0	0	0		
3	-1	2	τ_j					-2	-2	-2	-2	-2	-2	-2	-2	1	-2	-2	-2	1	1	1	1	1		
			w_k		0	1	2	2	2	2	2	2	2	1	2	2	-1	-2	-2	-2	0	0	0	0		
3	0	3	τ_j					-3	-3	-3	-3	-3	-3	-3	-3	0	-3	-3	-3	0	0	0	0	0		
			w_k		1	2	3	3	3	3	3	3	2	3	3	0	-1	-2	-2	0	0	0	0	0		
4	-4	0	τ_j					0	0	0	0	0	0	0	4	0	0	0	0	4	4	4	4	4	4	4
			w_k	0	0	0	0	0	0	0	0	0	0	0	-1	0	0	0	-3	-3	-3	-3	-3	0	0	0
4	-3	1	τ_j					-1	-1	-1	-1	-1	-1	-1	3	-1	-1	-1	-1	3	3	3	3	3	3	3
			w_k	0	0	0	1	1	1	1	1	1	1	0	1	1	1	-3	-3	-3	-3	-3	0	0	0	0
4	-2	2	τ_j					-2	-2	-2	-2	-2	-2	-2	2	-2	-2	-2	-2	2	2	2	2	2	2	2
			w_k	0	0	1	2	2	2	2	2	2	1	2	2	2	-2	-3	-3	-3	-3	0	0	0	0	0
4	-1	3	τ_j					-3	-3	-3	-3	-3	-3	-3	1	-3	-3	-3	-3	1	1	1	1	1	1	1
			w_k	0	1	2	3	3	3	3	3	2	3	3	3	-1	-2	-3	-3	-3	0	0	0	0	0	0
4	0	4	τ_j					-4	-4	-4	-4	-4	-4	-4	0	-4	-4	-4	-4	0	0	0	0	0	0	0
			w_k	1	2	3	4	4	4	4	3	4	4	4	0	-1	-2	-3	-3	0	0	0	0	0	0	0

Figure C.65: $\mathcal{P}_3'''$ and $\bar{\tau} \in \{2, 3, 4\}$, $T = 10$

$\bar{\tau}$	min	max	k	−4	−3	−2	−1	0	1	2	3	4	5	6	7	8	9	10	11	12	13	14	15	16	17	18
2	0	2	τ_j					0	0	0	0	0	0	0	0	2	0	0	2	2	2					
			w_k			0	0	0	0	0	0	0	0	0	0	−1	0	−1	−1	−1	0					
2	−1	1	τ_j					−1	−1	−1	−1	−1	−1	−1	−1	1	−1	−1	1	1	1					
			w_k			0	1	1	1	1	1	1	1	1	0	1	−1	−1	−1	0	0					
2	−2	0	τ_j					−2	−2	−2	−2	−2	−2	−2	−2	0	−2	−2	0	0	0					
			w_k			1	2	2	2	2	2	2	2	1	2	0	−1	−1	0	0	0					
3	−3	0	τ_j					0	0	0	0	0	0	0	3	0	0	0	3	3	3	3	3			
			w_k		0	0	0	0	0	0	0	0	0	0	−1	0	0	−2	−2	−2	−2	0	0			
3	−2	1	τ_j					−1	−1	−1	−1	−1	−1	−1	2	−1	−1	−1	2	2	2	2	2			
			w_k		0	0	1	1	1	1	1	1	1	0	1	1	−2	−2	−2	−2	0	0	0			
3	−1	2	τ_j					−2	−2	−2	−2	−2	−2	−2	1	−2	−2	−2	1	1	1	1	1			
			w_k		0	1	2	2	2	2	2	2	1	2	2	−1	−2	−2	−2	0	0	0	0			
3	0	3	τ_j					−3	−3	−3	−3	−3	−3	−3	0	−3	−3	−3	0	0	0	0	0			
			w_k		1	2	3	3	3	3	3	2	3	3	0	−1	−2	−2	0	0	0	0	0			
4	−4	0	τ_j					0	0	0	0	0	0	4	0	0	0	0	4	4	4	4	4	4	4	
			w_k	0	0	0	0	0	0	0	0	0	0	−1	0	0	0	−3	−3	−3	−3	−3	0	0	0	
4	−3	1	τ_j					−1	−1	−1	−1	−1	−1	3	−1	−1	−1	−1	3	3	3	3	3	3	3	
			w_k	0	0	0	1	1	1	1	1	1	0	1	1	1	−3	−3	−3	−3	−3	0	0	0	0	
4	−2	2	τ_j					−2	−2	−2	−2	−2	−2	2	−2	−2	−2	−2	2	2	2	2	2	2	2	
			w_k	0	0	1	2	2	2	2	2	1	2	2	2	−2	−3	−3	−3	−3	0	0	0	0	0	
4	−1	3	τ_j					−3	−3	−3	−3	−3	−3	1	−3	−3	−3	−3	1	1	1	1	1	1	1	
			w_k	0	1	2	3	3	3	3	2	3	3	3	−1	−2	−3	−3	−3	0	0	0	0	0	0	
4	0	4	τ_j					−4	−4	−4	−4	−4	−4	0	−4	−4	−4	−4	0	0	0	0	0	0	0	
			w_k	1	2	3	4	4	4	3	4	4	4	0	−1	−2	−3	−3	0	0	0	0	0	0	0	

Figure C.66: $\mathcal{P}_3'''$ and $\bar{\tau} \in \{2, 3, 4\}$, $T = 9$

$\bar{\tau}$	min	max	k	−4	−3	−2	−1	0	1	2	3	4	5	6	7	8	9	10	11	12	13	14	15	16	17	18
2	0	2	τ_j					0	0	0	0	0	0	0	2	0	0	2	2	2						
			w_k			0	0	0	0	0	0	0	0	0	−1	0	−1	−1	−1	0						
2	−1	1	τ_j					−1	−1	−1	−1	−1	−1	−1	1	−1	−1	1	1	1						
			w_k			0	1	1	1	1	1	1	1	0	1	−1	−1	−1	0	0						
2	−2	0	τ_j					−2	−2	−2	−2	−2	−2	−2	0	−2	−2	0	0	0						
			w_k			1	2	2	2	2	2	2	1	2	0	−1	−1	0	0	0						
3	−3	0	τ_j					0	0	0	0	0	0	3	0	0	0	3	3	3	3	3				
			w_k		0	0	0	0	0	0	0	0	0	−1	0	0	−2	−2	−2	−2	0	0				
3	−2	1	τ_j					−1	−1	−1	−1	−1	−1	2	−1	−1	−1	2	2	2	2	2				
			w_k		0	0	1	1	1	1	1	1	0	1	1	−2	−2	−2	−2	0	0	0				
3	−1	2	τ_j					−2	−2	−2	−2	−2	−2	1	−2	−2	−2	1	1	1	1	1				
			w_k		0	1	2	2	2	2	2	1	2	2	−1	−2	−2	−2	0	0	0	0				
3	0	3	τ_j					−3	−3	−3	−3	−3	−3	0	−3	−3	−3	0	0	0	0	0				
			w_k		1	2	3	3	3	3	2	3	3	0	−1	−2	−2	0	0	0	0	0				
4	−4	0	τ_j					0	0	0	0	0	4	0	0	0	0	4	4	4	4	4	4	4		
			w_k	0	0	0	0	0	0	0	0	0	−1	0	0	0	−3	−3	−3	−3	−3	0	0	0		
4	−3	1	τ_j					−1	−1	−1	−1	−1	3	−1	−1	−1	−1	3	3	3	3	3	3	3		
			w_k	0	0	0	1	1	1	1	1	0	1	1	1	−3	−3	−3	−3	−3	0	0	0	0		
4	−2	2	τ_j					−2	−2	−2	−2	−2	2	−2	−2	−2	−2	2	2	2	2	2	2	2		
			w_k	0	0	1	2	2	2	2	1	2	2	2	−2	−3	−3	−3	−3	0	0	0	0	0		
4	−1	3	τ_j					−3	−3	−3	−3	−3	1	−3	−3	−3	−3	1	1	1	1	1	1	1		
			w_k	0	1	2	3	3	3	2	3	3	3	−1	−2	−3	−3	−3	0	0	0	0	0	0		
4	0	4	τ_j					−4	−4	−4	−4	−4	0	−4	−4	−4	−4	0	0	0	0	0	0	0		
			w_k	1	2	3	4	4	3	4	4	4	0	−1	−2	−3	−3	0	0	0	0	0	0	0		

Figure C.67: $\mathcal{P}_3'''$ and $\bar{\tau} \in \{2, 3, 4\}$, $T = 8$

$\bar{\tau}$	min	max	k	−4	−3	−2	−1	0	1	2	3	4	5	6	7	8	9	10	11	12	13	14	15	16	17	18
2	0	2	τ_j					0	0	0	0	0	0	2	0	0	2	2	2							
			w_k			0	0	0	0	0	0	0	0	−1	0	−1	−1	−1	0							
2	−1	1	τ_j					−1	−1	−1	−1	−1	−1	1	−1	−1	1	1	1							
			w_k			0	1	1	1	1	1	1	0	1	−1	−1	−1	0	0							
2	−2	0	τ_j					−2	−2	−2	−2	−2	−2	0	−2	−2	0	0	0							
			w_k			1	2	2	2	2	2	1	2	0	−1	−1	0	0	0							
3	−3	0	τ_j					0	0	0	0	0	3	0	0	0	3	3	3	3	3					
			w_k		0	0	0	0	0	0	0	0	−1	0	0	−2	−2	−2	−2	0	0					
3	−2	1	τ_j					−1	−1	−1	−1	−1	2	−1	−1	−1	2	2	2	2	2					
			w_k		0	0	1	1	1	1	1	0	1	1	−2	−2	−2	−2	0	0	0					
3	−1	2	τ_j					−2	−2	−2	−2	−2	1	−2	−2	−2	1	1	1	1	1					
			w_k		0	1	2	2	2	2	1	2	2	−1	−2	−2	−2	0	0	0	0					
3	0	3	τ_j					−3	−3	−3	−3	−3	0	−3	−3	−3	0	0	0	0	0					
			w_k		1	2	3	3	3	2	3	3	0	−1	−2	−2	0	0	0	0	0					
4	−4	0	τ_j					0	0	0	0	4	0	0	0	0	4	4	4	4	4	4	4			
			w_k	0	0	0	0	0	0	0	0	−1	0	0	0	−3	−3	−3	−3	−3	0	0	0			
4	−3	1	τ_j					−1	−1	−1	−1	3	−1	−1	−1	−1	3	3	3	3	3	3	3			
			w_k	0	0	0	1	1	1	1	0	1	1	1	−3	−3	−3	−3	−3	0	0	0	0			
4	−2	2	τ_j					−2	−2	−2	−2	2	−2	−2	−2	−2	2	2	2	2	2	2	2			
			w_k	0	0	1	2	2	2	1	2	2	2	−2	−3	−3	−3	−3	0	0	0	0	0			
4	−1	3	τ_j					−3	−3	−3	−3	1	−3	−3	−3	−3	1	1	1	1	1	1	1			
			w_k	0	1	2	3	3	2	3	3	3	−1	−2	−3	−3	−3	0	0	0	0	0	0			
4	0	4	τ_j					−4	−4	−4	−4	0	−4	−4	−4	−4	0	0	0	0	0	0	0			
			w_k	1	2	3	4	3	4	4	4	0	−1	−2	−3	−3	0	0	0	0	0	0	0			

Figure C.68: $\mathcal{P}_3'''$ and $\bar{\tau} \in \{2, 3, 4\}$, $T = 7$

$\bar{\tau}$	min	max	k	-4	-3	-2	-1	0	1	2	3	4	5	6	7	8	9	10	11	12	13	14	15	16	17	18
2	0	2	τ_j					0	0	0	0	0	2	0	0	2	2	2								
			w_k			0	0	0	0	0	0	0	-1	0	-1	-1	-1	0								
2	-1	1	τ_j					-1	-1	-1	-1	-1	1	-1	-1	1	1	1								
			w_k			0	1	1	1	1	1	0	1	-1	-1	-1	0	0								
2	-2	0	τ_j					-2	-2	-2	-2	-2	0	-2	-2	0	0	0								
			w_k			1	2	2	2	2	1	2	0	-1	-1	0	0	0								
3	-3	0	τ_j					0	0	0	0	3	0	0	0	3	3	3	3	3						
			w_k		0	0	0	0	0	0	0	-1	0	0	-2	-2	-2	-2	0	0						
3	-2	1	τ_j					-1	-1	-1	-1	2	-1	-1	-1	2	2	2	2	2						
			w_k		0	0	1	1	1	1	0	1	1	-2	-2	-2	-2	0	0	0						
3	-1	2	τ_j					-2	-2	-2	-2	1	-2	-2	-2	1	1	1	1	1						
			w_k		0	1	2	2	2	1	2	2	-1	-2	-2	-2	0	0	0	0						
3	0	3	τ_j					-3	-3	-3	-3	0	-3	-3	-3	0	0	0	0	0						
			w_k		1	2	3	3	2	3	3	0	-1	-2	-2	0	0	0	0	0						
4	-4	0	τ_j					0	0	0	4	0	0	0	0	4	4	4	4	4	4	4				
			w_k	0	0	0	0	0	0	0	-1	0	0	0	-3	-3	-3	-3	-3	0	0	0				
4	-3	1	τ_j					-1	-1	-1	3	-1	-1	-1	-1	3	3	3	3	3	3	3				
			w_k	0	0	0	1	1	1	0	1	1	1	-3	-3	-3	-3	-3	0	0	0	0				
4	-2	2	τ_j					-2	-2	-2	2	-2	-2	-2	-2	2	2	2	2	2	2	2				
			w_k	0	0	1	2	2	1	2	2	2	-2	-3	-3	-3	-3	0	0	0	0	0				
4	-1	3	τ_j					-3	-3	-3	1	-3	-3	-3	-3	1	1	1	1	1	1	1				
			w_k	0	1	2	3	2	3	3	3	-1	-2	-3	-3	-3	0	0	0	0	0	0				
4	0	4	τ_j					-4	-4	-4	0	-4	-4	-4	-4	0	0	0	0	0	0	0				
			w_k	1	2	3	3	4	4	4	0	-1	-2	-3	-3	0	0	0	0	0	0	0				

Figure C.69: $\mathcal{P}_3'''$ and $\bar{\tau} \in \{2, 3, 4\}$, $T = 6$

$\bar{\tau}$	min	max	k	-4	-3	-2	-1	0	1	2	3	4	5	6	7	8	9	10	11	12	13	14	15	16	17	18
2	0	2	τ_j					0	0	0	0	2	0	0	2	2	2									
			w_k			0	0	0	0	0	0	-1	0	-1	-1	-1	0									
2	-1	1	τ_j					-1	-1	-1	-1	1	-1	-1	1	1	1									
			w_k			0	1	1	1	1	0	1	-1	-1	-1	0	0									
2	-2	0	τ_j					-2	-2	-2	-2	0	-2	-2	0	0	0									
			w_k			1	2	2	2	1	2	0	-1	-1	0	0	0									
3	-3	0	τ_j					0	0	0	3	0	0	0	3	3	3	3	3							
			w_k		0	0	0	0	0	0	-1	0	0	-2	-2	-2	-2	0	0							
3	-2	1	τ_j					-1	-1	-1	2	-1	-1	-1	2	2	2	2	2							
			w_k		0	0	1	1	1	0	1	1	-2	-2	-2	-2	0	0	0							
3	-1	2	τ_j					-2	-2	-2	1	-2	-2	-2	1	1	1	1	1							
			w_k		0	1	2	2	1	2	2	-1	-2	-2	-2	0	0	0	0							
3	0	3	τ_j					-3	-3	-3	0	-3	-3	-3	0	0	0	0	0							
			w_k		1	2	3	2	3	3	0	-1	-2	-2	0	0	0	0	0							
4	-4	0	τ_j					0	0	4	0	0	0	0	4	4	4	4	4	4	4					
			w_k	0	0	0	0	0	0	-1	0	0	0	-3	-3	-3	-3	-3	0	0	0					
4	-3	1	τ_j					-1	-1	3	-1	-1	-1	-1	3	3	3	3	3	3	3					
			w_k	0	0	0	1	1	0	1	1	1	-3	-3	-3	-3	-3	0	0	0	0					
4	-2	2	τ_j					-2	-2	2	-2	-2	-2	-2	2	2	2	2	2	2	2					
			w_k	0	0	1	2	1	2	2	2	-2	-3	-3	-3	-3	0	0	0	0	0					
4	-1	3	τ_j					-3	-3	1	-3	-3	-3	-3	1	1	1	1	1	1	1					
			w_k	0	1	2	2	3	3	3	-1	-2	-3	-3	-3	0	0	0	0	0	0					
4	0	4	τ_j					-4	-4	0	-4	-4	-4	-4	0	0	0	0	0	0	0					
			w_k	1	2	2	4	4	4	0	-1	-2	-3	-3	0	0	0	0	0	0	0					

Figure C.70: $\mathcal{P}_3'''$ and $\bar{\tau} \in \{2, 3, 4\}$, $T = 5$

$\bar{\tau}$	min	max	k	-4	-3	-2	-1	0	1	2	3	4	5	6	7	8	9	10	11	12	13	14	15	16	17	18
2	0	2	τ_j					0	0	0	2	0	0	2	2	2										
			w_k			0	0	0	0	0	-1	0	-1	-1	-1	0										
2	-1	1	τ_j					-1	-1	-1	1	-1	-1	1	1	1										
			w_k			0	1	1	1	0	1	-1	-1	-1	0	0										
2	-2	0	τ_j					-2	-2	-2	0	-2	-2	0	0	0										
			w_k			1	2	2	1	2	0	-1	-1	0	0	0										
3	-3	0	τ_j					0	0	3	0	0	0	3	3	3	3	3								
			w_k		0	0	0	0	0	-1	0	0	-2	-2	-2	-2	0	0								
3	-2	1	τ_j					-1	-1	2	-1	-1	-1	2	2	2	2	2								
			w_k		0	0	1	1	0	1	1	-2	-2	-2	-2	0	0	0								
3	-1	2	τ_j					-2	-2	1	-2	-2	-2	1	1	1	1	1								
			w_k		0	1	2	1	2	2	-1	-2	-2	-2	0	0	0	0								
3	0	3	τ_j					-3	-3	0	-3	-3	-3	0	0	0	0	0								
			w_k		1	2	2	3	3	0	-1	-2	-2	0	0	0	0	0								
4	-4	0	τ_j					0	4	0	0	0	0	4	4	4	4	4	4	4						
			w_k	0	0	0	0	0	-1	0	0	0	-3	-3	-3	-3	-3	0	0	0						
4	-3	1	τ_j					-1	3	-1	-1	-1	-1	3	3	3	3	3	3	3						
			w_k	0	0	0	1	0	1	1	1	-3	-3	-3	-3	-3	0	0	0	0						
4	-2	2	τ_j					-2	2	-2	-2	-2	-2	2	2	2	2	2	2	2						
			w_k	0	0	1	1	2	2	2	-2	-3	-3	-3	-3	0	0	0	0	0						
4	-1	3	τ_j					-3	1	-3	-3	-3	-3	1	1	1	1	1	1	1						
			w_k	0	1	1	3	3	3	-1	-2	-3	-3	-3	0	0	0	0	0	0						
4	0	4	τ_j					-4	0	-4	-4	-4	-4	0	0	0	0	0	0	0						
			w_k	1	1	3	4	4	0	-1	-2	-3	-3	0	0	0	0	0	0	0						

Figure C.71: $\mathcal{P}_3'''$ and $\bar{\tau} \in \{2, 3, 4\}$, $T = 4$

$\bar{\tau}$	min	max	k	−4	−3	−2	−1	0	1	2	3	4	5	6	7	8	9	10	11	12	13	14	15	16	17	18
2	0	2	τ_j					0	0	2	0	0	2	2	2											
			w_k			0	0	0	0	−1	0	−1	−1	−1	0											
2	−1	1	τ_j					−1	−1	1	−1	−1	1	1	1											
			w_k			0	1	1	0	1	−1	−1	−1	0	0											
2	−2	0	τ_j					−2	−2	0	−2	−2	0	0	0											
			w_k			1	2	1	2	0	−1	−1	0	0	0											
3	−3	0	τ_j					0	3	0	0	0	3	3	3	3	3									
			w_k		0	0	0	0	−1	0	0	−2	−2	−2	−2	0	0									
3	−2	1	τ_j					−1	2	−1	−1	−1	2	2	2	2	2									
			w_k		0	0	1	0	1	1	−2	−2	−2	−2	0	0	0									
3	−1	2	τ_j					−2	1	−2	−2	−2	1	1	1	1	1									
			w_k		0	1	1	2	2	−1	−2	−2	−2	0	0	0	0									
3	0	3	τ_j					−3	0	−3	−3	−3	0	0	0	0	0									
			w_k		1	1	3	3	0	−1	−2	−2	0	0	0	0	0									
4	−4	0	τ_j					4	0	0	0	0	4	4	4	4	4	4	4							
			w_k	0	0	0	0	−1	0	0	0	−3	−3	−3	−3	−3	0	0	0							
4	−3	1	τ_j					3	−1	−1	−1	−1	3	3	3	3	3	3	3							
			w_k	0	0	0	0	1	1	1	−3	−3	−3	−3	−3	0	0	0	0							
4	−2	2	τ_j					2	−2	−2	−2	−2	2	2	2	2	2	2	2							
			w_k	0	0	0	2	2	2	−2	−3	−3	−3	−3	0	0	0	0	0							
4	−1	3	τ_j					1	−3	−3	−3	−3	1	1	1	1	1	1	1							
			w_k	0	0	2	3	3	−1	−2	−3	−3	−3	0	0	0	0	0	0							
4	0	4	τ_j					0	−4	−4	−4	−4	0	0	0	0	0	0	0							
			w_k	0	2	3	4	0	−1	−2	−3	−3	0	0	0	0	0	0	0							

Figure C.72: $\mathcal{P}_3'''$ and $\bar{\tau} \in \{2, 3, 4\}$, $T = 3$

$\bar{\tau}$	min	max	k	−4	−3	−2	−1	0	1	2	3	4	5	6	7	8	9	10	11	12	13	14	15	16	17	18
2	0	2	τ_j					0	2	0	0	2	2	2												
			w_k			0	0	0	−1	0	−1	−1	−1	0												
2	−1	1	τ_j					−1	1	−1	−1	1	1	1												
			w_k			0	1	0	1	−1	−1	−1	0	0												
2	−2	0	τ_j					−2	0	−2	−2	0	0	0												
			w_k			1	1	2	0	−1	−1	0	0	0												
3	−3	0	τ_j					3	0	0	0	3	3	3	3	3										
			w_k		0	0	0	−1	0	0	−2	−2	−2	−2	0	0										
3	−2	1	τ_j					2	−1	−1	−1	2	2	2	2	2										
			w_k		0	0	0	1	1	−2	−2	−2	−2	0	0	0										
3	−1	2	τ_j					1	−2	−2	−2	1	1	1	1	1										
			w_k		0	0	2	2	−1	−2	−2	−2	0	0	0	0										
3	0	3	τ_j					0	−3	−3	−3	0	0	0	0	0										
			w_k		0	2	3	0	−1	−2	−2	0	0	0	0	0										
4	−4	0	τ_j																							
			w_k																							
4	−3	1	τ_j																							
			w_k																							
4	−2	2	τ_j																							
			w_k																							
4	−1	3	τ_j																							
			w_k																							
4	0	4	τ_j																							
			w_k																							

Figure C.73: $\mathcal{P}_3'''$ and $\bar{\tau} \in \{2, 3, 4\}$, $T = 2$

$\bar{\tau}$	min	max	k	-4	-3	-2	-1	0	1	2	3	4	5	6	7	8	9	10	11	12	13	14	15	16	17	18
2	0	2	τ_j					2	0	0	2	2	2													
			w_k			0	0	-1	0	-1	-1	-1	0													
2	-1	1	τ_j					1	-1	-1	1	1	1													
			w_k			0	0	1	-1	-1	-1	0	0													
2	-2	0	τ_j					0	-2	-2	0	0	0													
			w_k			0	2	0	-1	-1	0	0	0													
3	-3	0	τ_j																							
			w_k																							
3	-2	1	τ_j																							
			w_k																							
3	-1	2	τ_j																							
			w_k																							
3	0	3	τ_j																							
			w_k																							
4	-4	0	τ_j																							
			w_k																							
4	-3	1	τ_j																							
			w_k																							
4	-2	2	τ_j																							
			w_k																							
4	-1	3	τ_j																							
			w_k																							
4	0	4	τ_j																							
			w_k																							

Figure C.74: $\mathcal{P}_3'''$ and $\bar{\tau} \in \{2, 3, 4\}$, $T = 1$

C.9 Gains for $\mathcal{P}_3'''$

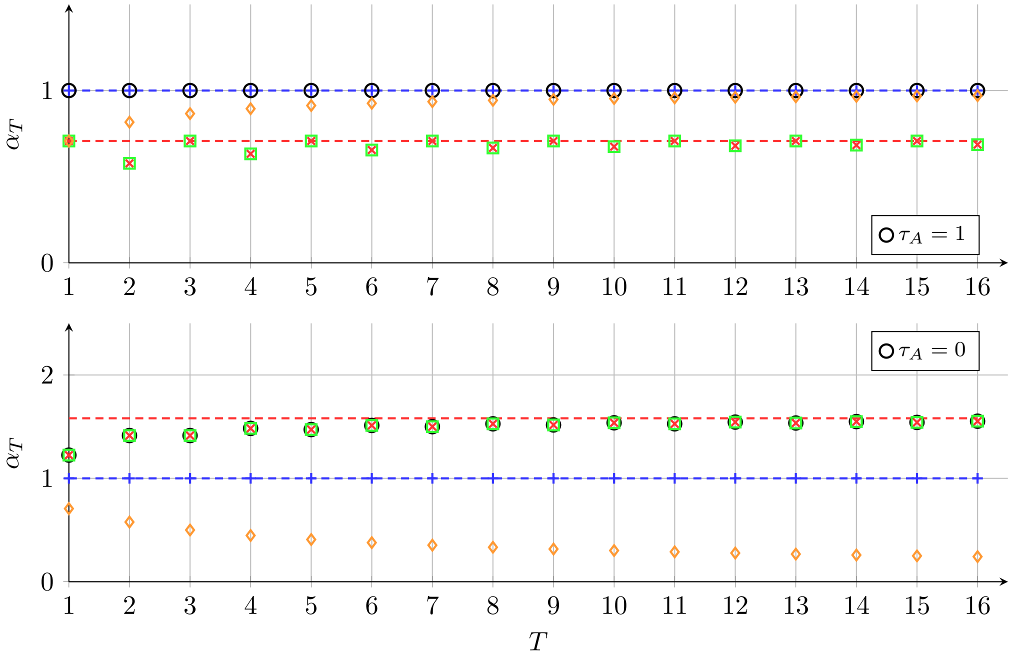

Figure C.75: $\mathcal{P}_3$, $\bar{\tau} = 1$: $\mathcal{P}_1$ (blue), $\mathcal{P}_3'$ (red), $\mathcal{P}_3''$ (green) and $\mathcal{P}_3'''$ (orange)

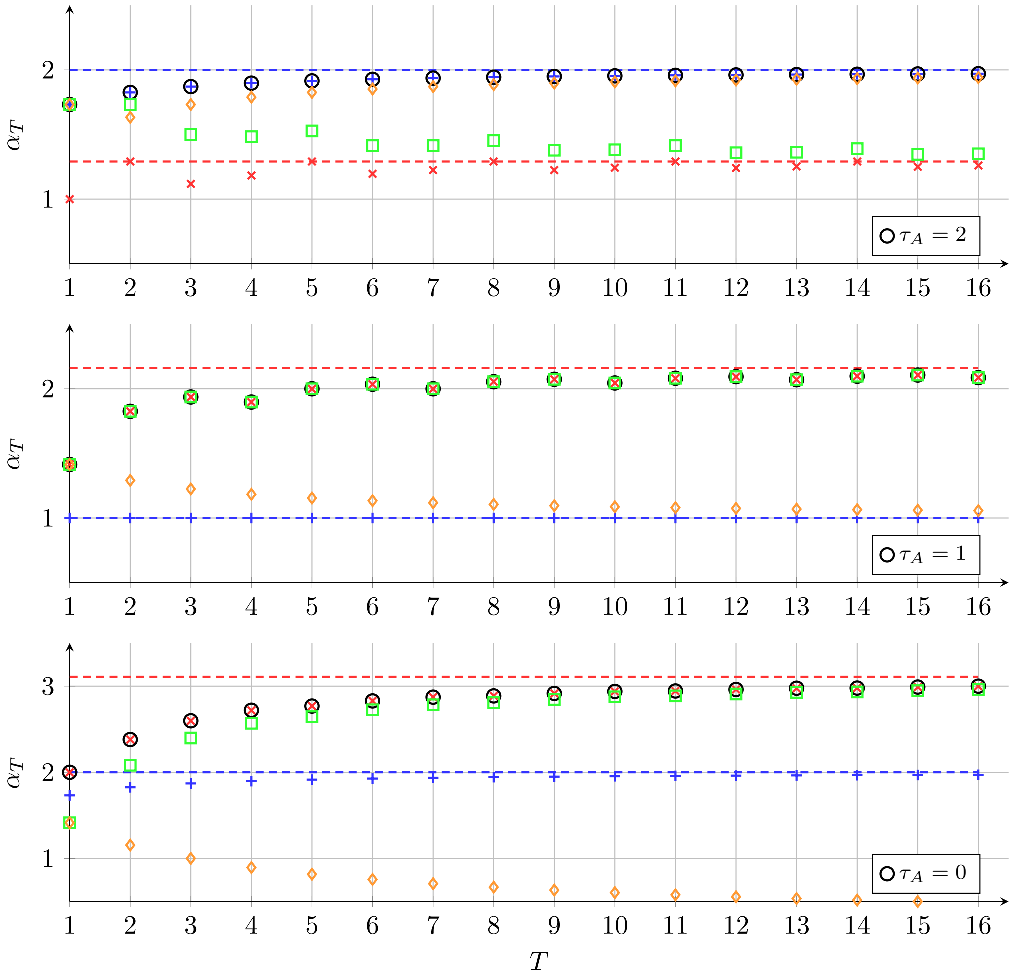

Figure C.76: $\mathcal{P}_3$, $\bar{\tau} = 2$: $\mathcal{P}_1$ (blue), $\mathcal{P}_3'$ (red), $\mathcal{P}_3''$ (green) and $\mathcal{P}_3'''$ (orange)

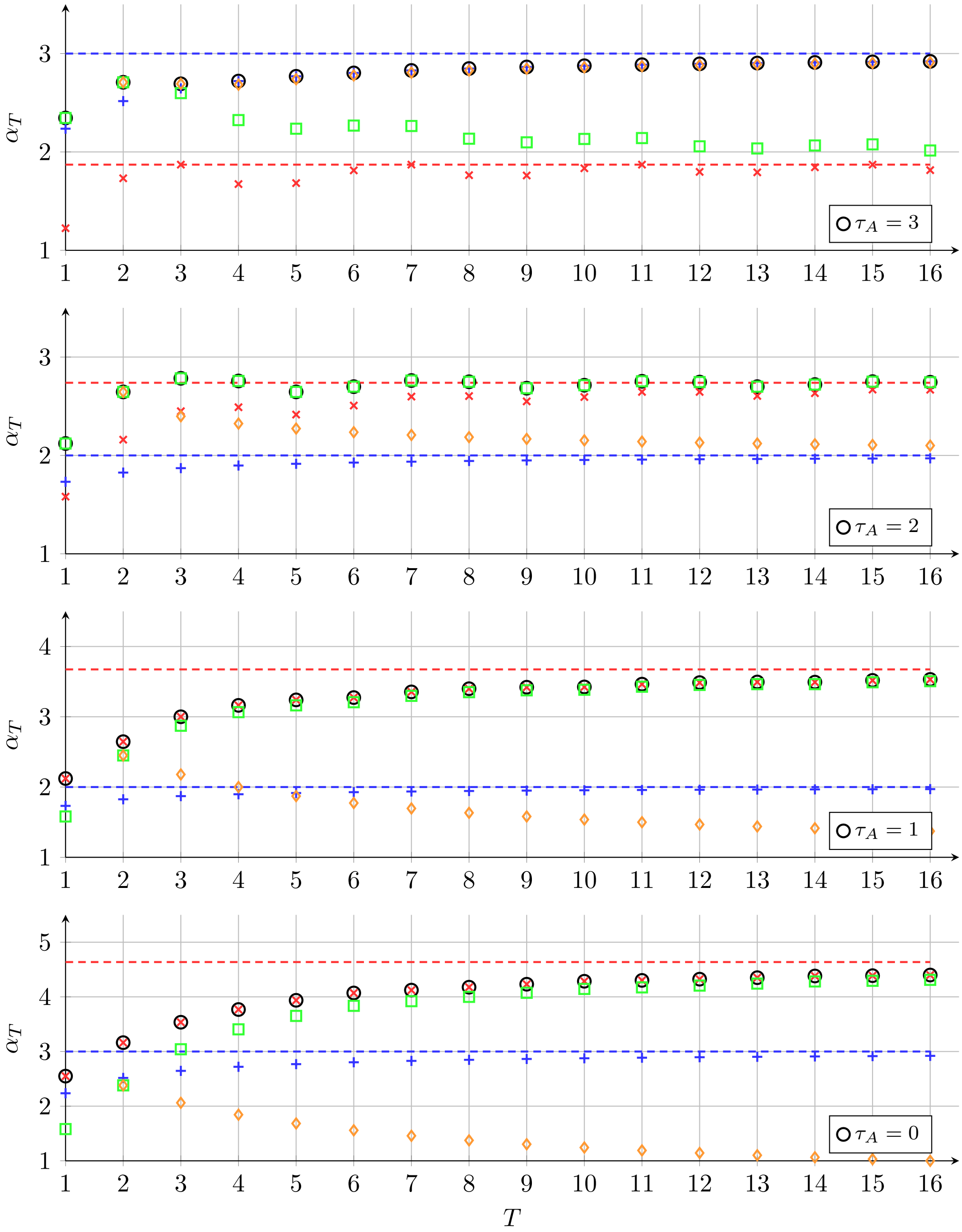

Figure C.77: $\mathcal{P}_3$, $\bar{\tau} = 3$: $\mathcal{P}_1$ (blue), $\mathcal{P}_3'$ (red), $\mathcal{P}_3''$ (green) and $\mathcal{P}_3'''$ (orange)

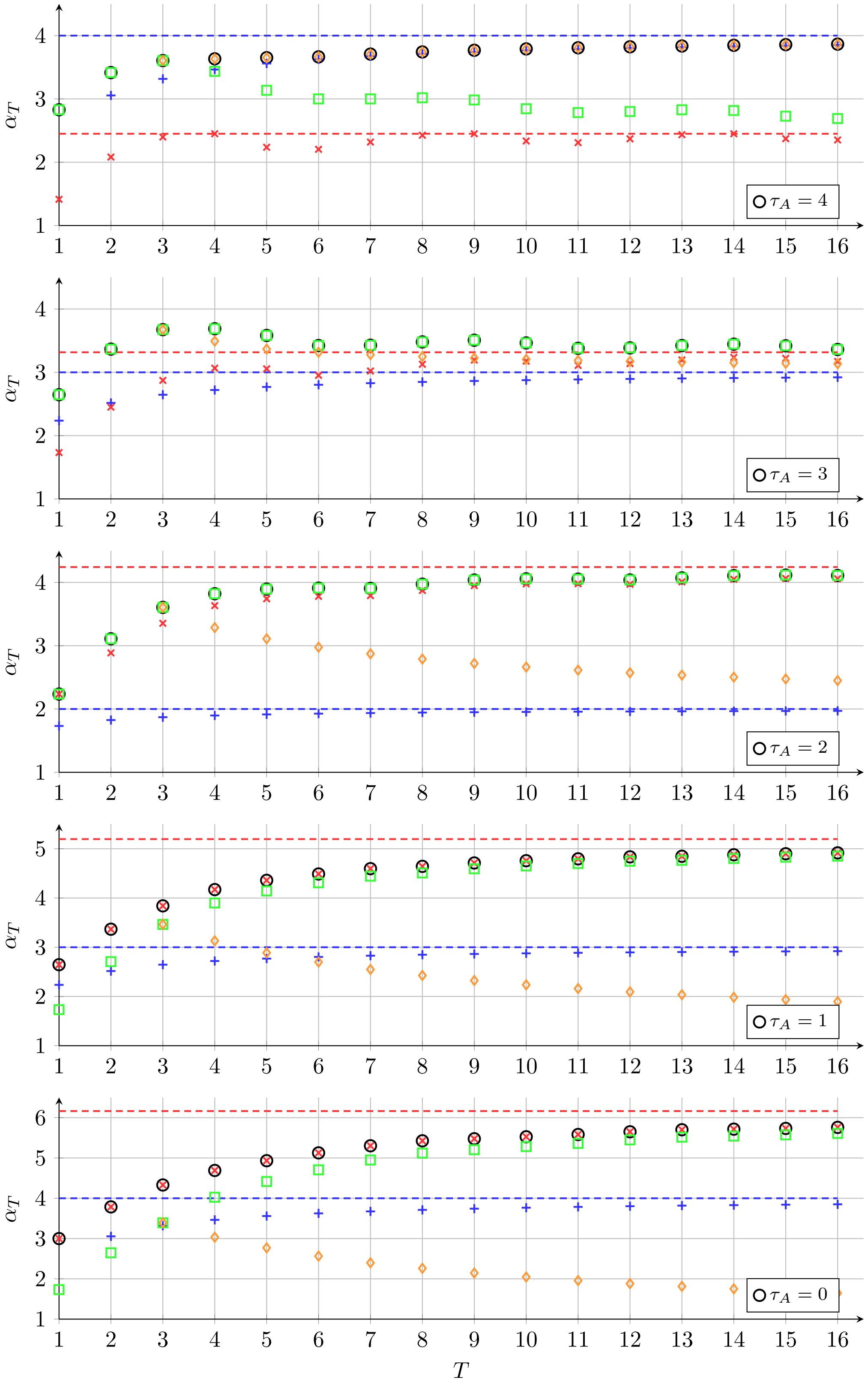

Figure C.78: $\mathcal{P}_3$, $\bar{\tau} = 4$: $\mathcal{P}_1$ (blue), $\mathcal{P}_3'$ (red), $\mathcal{P}_3''$ (green) and $\mathcal{P}_3'''$ (orange)

Bibliography

[ABL08] G. Alldredge, M. S. Branicky, and V. Liberatore. Play-back Buffers in Networked Control Systems: Evaluation and Design. In *IEEE American Control Conference*, pages 3106–3113, 2008.

[ACK19] S. Al Issa, A. Chakravarty, and I. Kar. Improved Event-Triggered Adaptive Control of Non-linear Uncertain Networked Systems. *IET Control Theory and Applications*, 13(13):2146–2152, 2019.

[AL06] L. Atzori and M. Lobina. Playout Buffering in IP Telephony: a Survey Discussing Problems and Approaches. *IEEE Communications Surveys & Tutorials*, 8(3):36–46, 2006.

[ASP20] K. Abidi, H. J. Soo, and I. Postlethwaite. Discrete-time Adaptive Control of Uncertain Sampled-data Systems with Uncertain Input Delay: A Reduction. *IET Control Theory and Applications*, 14(13):1681–1691, 2020.

[AW08] K. J. Aström and B. Wittenmark. *Adaptive Control.* Dover, second edition, 2008.

[Azi03] B. Azimi-Sadjadi. Stability of Networked Control Systems in the Presence of Packet Losses. In *IEEE International Conference on Decision and Control*, pages 676–681, 2003.

[Bar98] A. Bartoszewicz. Discrete-time Quasi-Sliding-Mode Control Strategies. *IEEE Transactions on Industrial Electronics*, 45(4):633–637, 1998.

[BB16] A. K. Behera and B. Bandyopadhyay. Event-triggered Sliding Mode Control for a Class of Nonlinear Systems. *International Journal of Control*, 89(9):1916–1931, 2016.

[Ber09] D. S. Bernstein. *Matrix Mathematics: Theory, Facts, and Formulas.* Princeton University Press, 2009.

[BFU95] G. Bartolini, A. Ferrara, and V. I. Utkin. Adaptive Sliding Mode Control in Discete-Time Systems. *Automatica*, 31(5):769—773, 1995.

[BJ18] A. P. Batista and P. G. Jota. Performance Improvement of an NCS closed over the Internet with an Adaptive Smith Predictor. *Control Engineering Practice*, 71:34–43, 2018.

[BLP$^+$13] G. Bartolini, A. Levant, F. Plestan, M. Taleb, and E. Punta. Adaptation of Sliding Modes. *IMA Journal of Mathematical Control and Identification*, 30(3):285–300, 2013.

[BSG17] S. Bonala, B. Subudhi, and S. Ghosh. On Delay Robustness Improvement using Digital Smith Predictor for Networked Control Systems. *European Journal of Control*, 34:59–65, 2017.

[CB16] S. Chakrabarty and A. Bartoszewicz. Improved Robustness and Performance of Discrete Time Sliding Mode Control Systems. *ISA Transactions*, 65:143–149, 2016.

[Cha97] C. Y. Chan. Discrete Adaptive Sliding-Mode Tracking Controller. *Automatica*, 33(5):999–1002, 1997.

[CHCL03] J. P. V. S. Cunha, L. Hsu, R. R. Costa, and F. Lizarralde. Output-Feedback Model-Reference Sliding Mode Control of Uncertain Multivariable Systems. *IEEE Transactions on Automatic Control*, 48(12):2245–2250, 2003.

[Che06] C.-T. Chen. *Analog & Digital Control System Design: Transfer-function, State-space, & Algebraic Methods.* Oxford University Press, 2006.

[CHL$^+$03] A. Cervin, D. Henriksson, B. Lincoln, J. Eker, and K. E. Arzen. How does Control Timing affect Performance? Analysis and Simulation of Timing using Jitterbug and TrueTime. *IEEE Control Systems Magazine*, 23(3):16–30, 2003.

[CHvdW$^+$10] M. B. G. Cloosterman, L. Hetel, N. van de Wouw, W. P. M. H. Heemels, J. Daafouz, and H. Nijmeijer. Controller Synthesis for Networked Control Systems. *Automatica*, 46(10):1584–1594, 2010.

[COC14] C. L. Coutinho, T. R. Oliveira, and J. P. V. S. Cunha. Output-feedback Sliding-Mode Control via Cascade Observers for Global Stabilisation of a Class of Nonlinear Systems with Output Time Delay. *International Journal of Control*, 87(11):2327–2337, 2014.

[DB01] J. Daafouz and J. Bernussou. Parameter Dependent Lyapunov Functions for Discrete Time Systems with Time Varying Parametric Uncertainties. *Systems & Control Letters*, 43(5):355–359, 2001.

[DFT09] J. C. Doyle, B. A. Francis, and A. R. Tannenbaum. *Feedback Control Theory.* Dover Publications, 2009.

[DH12] M. C. F. Donkers and W. P. M. H. Heemels. Output-Based Event-Triggered Control With Guaranteed $\mathcal{L}_\infty$-Gain and Improved and Decentralized Event-Triggering. *IEEE Transactions on Automatic Control*, 57(6):1362–1376, 2012.

[DLR$^+$20] Y. Deng, V. Lechappe, S. Rouquet, E. Moulay, and F. Plestan. Super-Twisting Algorithm-Based Time-Varying Delay Estimation With External Signal. *IEEE Transactions on Industrial Electronics*, 67(12):10663–10671, 2020.

[ES98] C. Edwards and S. Spurgeon. *Sliding Mode Control: Theory and Applications* . Taylor & Francis Ltd, 1998.

[ES16] C. Edwards and Y. B. Shtessel. Adaptive Continuous Higher Order Sliding Mode Control. *Automatica*, 65:183–190, 2016.

[FPB14] L. Fridman, A. Poznyak, and F. J. Bejarano. *Robust Output LQ Optimal Control via Integral Sliding Modes.* Birkhäuser, 2014.

[FPW97] G. F. Franklin, J. D. Powell, and M. L. Workman. *Digital Control of Dynamic Systems.* Addison-Wesley, 3. edition, 1997.

[Fri01] E. Fridman. New Lyapunov-Krasovskii Functionals for Stability of Llinear Retarded and Neutral Type Systems. *Systems & Control Letters*, 43(4):309–319, 2001.

[Fri14] E. Fridman. *Introduction to Time-Delay Systems.* Springer International Publishing Switzerland, 2014.

[FS03] E. Fridman and U. Shaked. Delay-dependent Stability and H_∞ Control: Constant and Time-Varying Delays. *International Journal of Control*, 76(1):48–60, 2003.

[FS16] E. Fridman and L. Shaikhet. Delay-induced Stability of Vector Second-Order Systems via simple Lyapunov Functionals. *Automatica*, 74:288–296, 2016.

[GC07] H. Gao and T. Chen. New Results on Stability of Discrete-Time Systems With Time-Varying State Delay. *IEEE Transactions on Automatic Control*, 52(2):328–334, 2007.

[GC10] R. A. Gupta and M.-Y. Chow. Networked Control System: Overview and Research Trends. *IEEE Transactions on Industrial Electronics*, 57(7):2527–2535, 2010.

[GJ18] W. Gao and Z.-P. Jiang. Adaptive Optimal Output Regulation of Discrete-time Linear Systems subject to Input Time-delay. In *2018 Annual American Control Conference*, pages 4484–4489, 2018.

[GN01] K. Gu and S.-I. Niculescu. Further Remarks on Additional Dynamics in various Model Transformations of Linear Delay Systems. *IEEE Transactions on Automatic Control*, 46(3):497–500, 2001.

[GS84] G. C. Goodwin and K. S. Sin. *Adaptive Filtering Prediction and Control.* Dover, 1984.

[GSRA16] M. Gamal, N. Sadek, M. R. Rizk, and A. K. Abou-elSaoud. Delay Compensation using Smith Predictor for Wireless Network Control System. *Alexandria Engineering Journal*, 55(2):1421–1428, 2016.

[HFO$^+$17] L. Hetel, C. Fiter, H. Omran, A. Seuret, E. Fridman, J.-P. Richard, and S. I. Niculescu. Recent Developments on the Stability of Systems with Aperiodic Sampling: An Overview. *Automatica*, 76:309–335, 2017.

[HJT12] W. P. M. H. Heemels, K. H. Johansson, and P. Tabuada. An Introduction to Event-Triggered and Self-Triggered Control. In *IEEE Conference on Decision and Control*, pages 3270–3285, 2012.

[HLD97] L. Hsu, F. Lizarralde, and A. D. De Araujo. New Results on Output-Feedback Variable Structure Model-Reference Adaptive Control: Design and Stability Analysis. *IEEE Transactions on Automatic Control*, 42(3):386–393, 1997.

[HNX07] J. P. Hespanha, P. Naghshtabrizi, and Y. Xu. A Survey of Recent Results in Networked Control Systems. *Proceedings of the IEEE*, 95(1):138–162, 2007.

[HvdW10] W. P. M. H. Heemels and N. van de Wouw. Stability and Stabilization of Networked Control Systems. In A. Bemporad, W. P. M. H. Heemels, and M. Johansson, editors, *Networked Control Systems*, volume 406 of *Lecture Notes in Control and Information Sciences*, pages 203–253. Springer, London, 2010.

[IEE08] IEEE. IEEE Standard for a Precision Clock Synchronization Protocol for Networked Measurement and Control Systems. *IEEE Std 1588-2008 (Revision of IEEE Std 1588-2002)*, pages 1–300, 2008.

[IF16] G. P. Incremona and A. Ferrara. Adaptive Model-based Event-Triggered Sliding Mode Control. *International Journal of Adaptive Control and Signal Processing*, 30(8-10, SI):1298–1316, 2016.

[IFM17] G. P. Incremona, A. Ferrara, and L. Magni. Asynchronous Networked MPC with ISM for Uncertain Nonlinear Systems. *IEEE Transactions on Automatic Control*, 62(9):4305–4317, 2017.

[KHN63] R. Kalman, B. L. Ho, and N. Narendra. Controllability of Linear Dynamical Systems. *Contributions to Differential Equations*, 1:198–213, 1963.

[KL04] C.-Y. Kao and B. Lincoln. Simple Stability Criteria for Systems with Time-Varying Delays. *Automatica*, 40(8):1429–1434, 2004.

[KR99] V. B. Kolmanovskii and J.-P. Richard. Stability of some Linear Systems with Delays. *IEEE Transactions on Automatic Control*, 44(5):984–989, 1999.

[KR19] S. Koch and M. Reichhartinger. Discrete-time equivalents of the super-twisting algorithm. *Automatica*, 107:190–199, 2019.

[Lev93] A. Levant. Sliding Order and Sliding Accuracy in Sliding Mode Control. *International Journal of Control*, 58(6):1247–1263, 1993.

[LF12] K. Liu and E. Fridman. Networked-based Stabilization via Discontinuous Lyapunov Functionals. *International Journal of Robust and Nonlinear Control*, 22(4):420–436, 2012.

[LFH12] K. Liu, E. Fridman, and L. Hetel. Network-based Control via a novel Analysis of Hybrid Systems with Time-Varying Delays. In *IEEE Conference on Decision and Control*, pages 3886–3891, 2012.

[LG11] X. Li and H. Gao. A New Model Transformation of Discrete-Time Systems With Time-Varying Delay and Its Application to Stability Analysis. *IEEE Transactions on Automatic Control*, 56(9):2172–2178, 2011.

[LH10] C.-L. Lai and P.-L. Hsu. Design the Remote Control System With the Time-Delay Estimator and the Adaptive Smith Predictor. *IEEE Transactions on Industrial Electronics*, 6(1):73–80, 2010.

[Lib06] V. Liberatore. Integrated Play-Back, Sensing, and Networked Control. In *IEEE International Conference on Computer Communications*, pages 1–12, 2006.

[Liu10] G. P. Liu. Predictive Controller Design of Networked Systems With Communication Delays and Data Loss. *IEEE Transactions on Circuits and Systems II: Express Briefs*, 57(6):481–485, 2010.

[LL10] J. Lunze and D. Lehmann. A state-feedback Approach to Event-Based Control. *Automatica*, 46(1):211–215, 2010.

[LL14] M. Livne and A. Levant. Proper Discretization of Homogeneous Differentiators. *Automatica*, 50(8):2007–2014, 2014.

[LLL15] S. Li, D.-P. Li, and Y.-J. Liu. Adaptive Neural Network Tracking Design for a Class of Uncertain Nonlinear Discrete-time Systems with Unknown Time-Delay. *Neurocomputing*, 168:152–159, 2015.

[LMRC06] G. P. Liu, J. X. Mu, D. Rees, and S. C. Chai. Design and Stability Analysis of Networked Control Systems with Random Communication Time Delay using the Modified MPC. *International Journal of Control*, 79(4):288–297, 2006.

[LN80] Y.-H. Lin and K. S. Narandra. A New Error Model for Adaptive Systems. *IEEE Transactions on Automatic Control*, 25(3):585–587, 1980.

[LO98] P. M. Lee and J. H. Oh. Improvements on VSS-type Self-tuning Control for a Tracking Controller. *IEEE Transactions on Industial Electronics*, 45(2):319–325, 1998.

[LRSH19] J. Ludwiger, M. Reichhartinger, M. Steinberger, and M. Horn. Discrete-Time Super Twisting Controller for Networked Control Systems. *IFAC-PapersOnLine, IFAC Symposium on Nonlinear Control Systems*, 52(16):789–794, 2019.

[LSCS11] H. Li, Z. Sun, M.-Y. Chow, and F. Sun. Gain-Scheduling-Based State Feedback Integral Control for Networked Control Systems. *IEEE Transactions on Industrial Electronics*, 58(6):2465–2472, 2011.

[LSH$^+$18] J. Ludwiger, M. Steinberger, M. Horn, G. Kubin, and A. Ferrara. Discrete Time Sliding Mode Control Strategies for Buffered Networked Systems. In *IEEE Conference on Decision and Control*, pages 6735–6740, Miami, 2018.

[LSH19] J. Ludwiger, M. Steinberger, and M. Horn. Spatially Distributed Networked Sliding Mode Control. *IEEE Control Systems Letters*, 3(4):972–977, 2019.

[LSR$^+$17] J. Ludwiger, M. Steinberger, M. Rotulo, M. Horn, A. Luppi, G. Kubin, and A. Ferrara. Towards Networked Sliding Mode Control. In *IEEE Conference on Decision and Control*, pages 6021–6026, 2017.

[Lud20] J. Ludwiger. *Discrete Time Sliding Mode Controller Design for Networked Control Systems.* PhD thesis, Graz University of Technology, 2020.

[LZL18] B. Lian, Q. Zhang, and J. Li. Sliding Mode Control and Sampling Rate Strategy for Networked Control Systems with Packet Disordering via Markov Chain Prediction. *ISA Transactions*, 83:1–12, 2018.

[LZS09] G. Liu, A. Zinober, and Y. B. Shtessel. Second-Order SM Approach to SISO Time-Delay System Output Tracking. *IEEE Transactions on Industrial Electronics*, 56(9):3638–3645, 2009.

[LZY$^+$15] A. Liu, W. Zhang, L. Yu, S. Liu, and M. Z. Q. Chen. New results on Stabilization of Networked Control Systems with Packet Disordering. *Automatica*, 52:255–259, 2015.

[MAT] MATLAB/Simulink. *www.mathworks.com.* accessed on 08.03.2021.

[MKSL04] M. Maróti, B. Kusy, G. Simon, and A. Lédeczi. The Flooding Time Synchronization Protocol. In *International Conference on Embedded Networked Sensor Systems*, pages 39–49, 2004.

[MLR05] J. X. Mu, G. P. Liu, and D. Rees. Design of Robust Networked Predictive Control Systems. In *IEEE American Control Conference*, pages 638–643, 2005.

[MNTF16] J. A. Moreno, D. Y. Negrete, V. Torres-Gonzalez, and L. Fridman. Adaptive Continuous Twisting Algorithm. *International Journal of Control*, 89(9):1798–1806, 2016.

[MOS] MOSEK. *https://www.mosek.com.* accessed on 08.03.2021.

[NA12] K. S. Narendra and A. M. Annaswamy. *Stable Adaptive Systems.* Dover, 2012.

[NKMP05] M. Narbutt, A. Kelly, L. Murphy, and P. Perry. Adaptive VoIP Playout Scheduling: Assessing User Satisfaction. *IEEE Internet Computing*, 9(4):28–34, 2005.

[NL80] K. S. Narendra and Y.-H. Lin. *Applications of Adaptive Control*, chapter Design of Stable Model Reference Adaptive Controllers, pages 69–130. Academic Press, 1980.

[NRC09] J. E. Normey-Rico and E. F. Camacho. Unified Approach for Robust Dead-time Compensator Design. *Journal of Process Control*, 19(1):38–47, 2009.

[NRGG12] J. E. Norrney-Rico, P. Garcia, and A. Gonzalez. Robust Stability Analysis of filtered Smith Predictor for Time-Varying Delay Processes. *Journal of Process Control*, 22(10):1975–1984, 2012.

[OCH16] T. R. Oliveira, J. P. V. S. Cunha, and L. Hsu. Adaptive Sliding Mode Control for Disturbances with unknown Bounds. In *14th International Workshop on Variable Structure Systems*, pages 59–64, 2016.

[OFLH18] H. Obeid, L. M. Fridman, S. Laghrouche, and M. Harmouche. Barrier function-based Adaptive Sliding Mode Control. *Automatica*, 93:540–544, 2018.

[OMN] OMNet++. *https://omnetpp.org/intro/.* accessed on 08.03.2021.

[ORF18] T. R. Oliveira, V. H. P. Rodrigues, and L. Fridman. Generalized Model Reference Adaptive Control by means of Global HOSM Differentiators. *IEEE Transactions on Automatic Control*, 64(5):2053–2060, 2018.

[PEF$^+$18] P. Park, S. C. Ergen, C. Fischione, C. Lu, and K. H. Johansson. Wireless Network Design for Control Systems: A Survey. *IEEE Communications Surveys and Tutorials*, 20(2):978–1013, 2018.

[Pos80] J. Postel. *Transmission Control Protocol.* Internet Engineering Task Force, Request for Comments 768, 1980.

[Pos81] J. Postel. *User Datagram Protocol.* Internet Engineering Task Force, Request for Comments 793, 1981.

[PSH21] M. Palmisano, M. Steinberger, and M. Horn. Optimal Finite-Horizon Control for Networked Control Systems in the Presence of Random Delays and Packet Losses. *IEEE Control Systems Letters*, 5(1):271–276, 2021.

[QN11] D. E. Quevedo and D. Nesic. Input-to-State Stability of Packetized Predictive Control Over Unreliable Networks Affected by Packet-Dropouts. *IEEE Transactions on Automatic Control*, 56(2):370–375, 2011.

[QUA] Quanser QUARC. *http://www.quanser.com.* accessed on 08.03.2021.

[Ric03] J.-P. Richard. Time-delay Systems: An Overview of some Recent Advances and Open Problems. *Automatica*, 39(10):1667–1694, 2003.

[RKTS94] R. Ramjee, J. Kurose, D. Towsley, and H. Schulzrinne. Adaptive Playout Mechanisms for Packetized Audio Applications in Wide-Area Networks. In *Conference on Computer Communications*, pages 680–688, 1994.

[RMQF14] L. Repele, R. Muradore, D. Quaglia, and P. Fiorini. Improving Performance of Networked Control Systems by Using Adaptive Buffering. *IEEE Transactions on Industrial Electronics*, 61(9):4847–4856, 2014.

[RRFM11] M. Rubagotti, D. M. Raimondo, A. Ferrara, and L. Magni. Robust Model Predictive Control With Integral Sliding Mode in Continuous-Time Sampled-Data Nonlinear Systems. *IEEE Transactions on Automatic Control*, 56(3):556–570, 2011.

[RRJ$^+$15] D. M. Raimondo, M. Rubagotti, C. N. Jones, L. Magni, A. Ferrara, and M. Morari. Multirate Sliding Mode Disturbance Compensation for Model Predictive Control. *International Journal of Robust and Nonlinear Control*, 25(16):2984–3003, 2015.

[Sas99] S. Sastry. *Nonlinear Systems: Analysis, Stability and Control.* Springer New York, 1999.

[SCHF20] M. Steinberger, I. Castillo, M. Horn, and L. Fridman. Robust Output Tracking of Constrained Perturbed Linear Systems via Model Predictive Sliding Mode Control. *International Journal of Robust and Nonlinear Control*, 30(3):1258–1274, 2020.

[SEFL15] Y. Shtessel, C. Edwards, L. Fridman, and A. Levant. *Sliding Mode Control and Observation.* Birkhäuser, 2015.

[SGF15] A. Seuret, F. Gouaisbaut, and E. Fridman. Stability of Discrete-Time Systems With Time-Varying Delays via a Novel Summation Inequality. *IEEE Transactions on Automatic Control*, 60(10):2740–2745, 2015.

[SH17] R. Seeber and M. Horn. Stability Proof for a well-established Super-Twisting Parameter Setting. *Automatica*, 84:241–243, 2017.

[SH20] M. Steinberger and M. Horn. From classical to Networked Control: Retrofitting the Concept of Smith Predictors. *arXiv:2010.05486, submitted for journal publication*, 2020.

[SH21a] M. Steinberger and M. Horn. A Less-Conservative Stability Criterion for Networked Control Systems with Time-varying Packet Delays. *arxiv:2103.16514, revised version submitted for journal publication*, 2021.

[SH21b] M. Steinberger and M. Horn. A Stability Criterion for Networked Control Systems with Packetized Transmissions. *IEEE Control Systems Letters*, 5(3):911–916, 2021.

[SHF19] M. Steinberger, M. Horn, and A. Ferrara. Discrete-time Model Reference Adaptive Sliding Mode Control for Systems in State-Space Representation. In *IEEE Conference on Decision and Control*, pages 6007–6012, Nice, 2019.

[SHF21] M. Steinberger, M. Horn, and A. Ferrara. Adaptive Control of Multivariable Networked Systems with Uncertain Time Delays. *IEEE Transactions on Automatic Control*, early access, doi 10.1109/TAC.2021.3083563, 2021.

[Smi59] O. Smith. Closer Control of Loops with Dead Time. *Chemical Engineering Progress*, 53(5):217–219, 1959.

[SSF$^+$07] L. Schenato, B. Sinopoli, M. Franceschetti, K. Poolla, and S. S. Sastry. Foundations of Control and Estimation Over Lossy Networks. *Proceedings of the IEEE*, 95(1):163–187, 2007.

[SSGH20] A. Sarjaš, M. Steinberger, D. Gleich, and M. Horn. Event-Triggered Sliding Mode Control Strategies for Positioning Systems: An Experimental Assessment. In *IEEE International Workshop on Advanced Motion Control*, pages 191–197, 2020.

[SSLH21] K. Stanojevic, M. Steinberger, J. Ludwiger, and M. Horn. Robust Control of Multivariable Buffered Networked Systems. *submitted*, 2021.

[STHJ20] M. Steinberger, M. Tranninger, M. Horn, and K. H. Johansson. How to Simulate Networked Control Systems with Variable Time Delays? *21st IFAC World Congress, IFAC-PapersOnLine*, 53(2):3098–3103, 2020.

[STNR16] T. L. M. Santos, B. C. Torrico, and J. E. Normey-Rico. Simplified Filtered Smith Predictor for MIMO Processes with multiple Time Delays. *ISA Transactions*, 65:339–349, 2016.

[SXLC15] A. Saifullah, Y. Xu, C. Lu, and Y. Chen. End-to-End Communication Delay Analysis in Industrial Wireless Networks. *IEEE Transactions on Computers*, 64(5):1361–1374, 2015.

[Tab07] P. Tabuada. Event-Triggered Real-Time Scheduling of Stabilizing Control Tasks. *IEEE Transactions on Automatic Control*, 52(9):1680–1685, 2007.

[Tao14] Gang Tao. Multivariable Adaptive Control: A Survey. *Automatica*, 50(11):2737–2764, 2014.

[TC04] Y. Tipsuwan and M. Y. Chow. Gain Scheduler Middleware: A Methodology to enable existing Controllers for Networked Control and Teleoperation - Part I: Networked Control. *IEEE Transactions on Industrial Electronics*, 51(6):1218–1227, 2004.

[Td06] P. L. Tang and C. W. de Silva. Compensation for Transmission Delays in an Ethernet-based Control Network using Variable-Horizon Predictive Control. *IEEE Transactions on Control Systems Technology*, 14(4):707–718, 2006.

[Tru] TrueTime. *http://www.control.lth.se/research/tools-and-software/truetime/.* accessed on 08.03.2021.

[TTY18] C. Tan, G. Tao, and H. Yang. A Multiple-Model MRAC Scheme for Discrete-time Multivariable Systems with Uncertain Actuation Delays. In *IEEE Conference on Decision and Control*, pages 6283–6288, 2018.

[UI08] H. U. Ünal and A. Iftar. A Small Gain Theorem for Systems with Noncausal Subsystems. *Automatica*, 44(11):2950–2953, 2008.

[UP13] V. I. Utkin and A. S. Poznyak. Adaptive Sliding Mode Control with Application to Super-Twist Algorithm: Equivalent Control Method. *Automatica*, 49(1):39–47, 2013.

[US96] V. Utkin and J. Shi. Integral Sliding Mode in Systems Operating under Uncertainty Conditions. In *IEEE Conference on Decision and Control*, pages 4591–4596, 1996.

[Utk92] V. I. Utkin. *Sliding Modes in Control and Optimization.* Springer Berlin Heidelberg, 1992.

[vDHv10] J. J. C. van Schendel, M. C. F. Donkers, W. P. M. H. Heemels, and N. van de Wouw. On Dropout Modelling for Stability Analysis of Networked Control Systems. In *IEEE American Control Conference*, pages 555–561, 2010.

[Vid02] M. Vidyasagar. *Nonlinear Systems Analysis.* SIAM: Society for Industrial and Applied Mathematics, 2002.

[WZ18] W. Wu and Y. Zhang. Event-triggered fault-tolerant Control and Scheduling Codesign for Nonlinear Networked Control Systems with Medium-Access Constraint and Packet Disordering. *International Journal of Robust and Nonlinear Control*, 28(4):1182–1198, 2018.

[XJL12] Hao Xu, S. Jagannathan, and F. L. Lewis. Stochastic Optimal Control of Unknown Linear Networked Control System in the presence of Random delays and Packet Losses. *Automatica*, 48(6):1017–1030, 2012.

[XL07] J. Xiong and J. Lam. Stabilization of Linear Systems over Networks with Bounded Packet Loss. *Automatica*, 43(1):80–87, 2007.

[XZL$^+$10] Y. Xia, Z. Zhu, C. Li, H. Yang, and Q. Zhu. Robust Adaptive Sliding Mode Control for Uncertain discrete-time Systems with Time Delay. *Journal of the Franklin Institute - Engineering and Applied Mathematics*, 347(1):339–357, 2010.

[YAL] YALMIP. *https://yalmip.github.io.* accessed on 08.03.2021.

[ZHY16] X.-M. Zhang, Q.-L. Han, and X. Yu. Survey on Recent Advances in Networked Control Systems. *IEEE Transactions on Industrial Informatics*, 12(5):1740–1752, 2016.

[ZMW19] L. Zhao, X. Ma, and J. Wang. Networked Predictive Control for Linear Systems with Quantizers by an event-driven Strategy. *Journal of the Franklin Institute*, 356(6):3245–3269, 2019.

[ZSWY17] D. Zhang, P. Shi, Q.-G. Wang, and L. Yu. Analysis and Synthesis of Networked Control Systems: A Survey of Recent Advances and Challenges. *ISA Transactions*, 66:376–392, 2017.

[ZY12] F. Zhang and M. Yeddanapudi. Modeling and Simulation of time-varying Delays. In *Symposium on Theory of Modeling and Simulation*, pages 1–9, 2012.